Evaluating the Efficacy of Current and Novel Chemotherapeutic Agents for the Treatment of Glioma

by

Joud Sabouni

A thesis submitted in partial fulfilment for the requirements for the degree of PhD at the University of Central Lancashire

Vol. 1 of 2

June 2019

Evaluating the Efficacy of Current and Novel Chemotherapeutic Agents for the Treatment of Glioma

by

Joud Sabouni

A thesis submitted in partial fulfilment for the requirements for the degree of PhD at the University of Central Lancashire

Vol. 2 of 2

June 2019

DECLARATION FORM

Type of Award: Doctor of philosophy (PhD)
School: Pharmacy and Biomedical Sciences

I declare that while registered as a candidate for the research degree, I have not been a registered candidate or enrolled student for another award of the University or other academic or professional intuition.

I declare that no material contained in the thesis has been used in any other submission award and is solely my own work

Signature of candidate ……Joud Sabouni……

Date ……24/01/2020……

ABSTRACT

Glioblastoma (GBM) is the most common and aggressive tumour of the central nervous system. Currently, GBM remains an incurable tumour characterized by a poor prognosis with a median survival time of 15 months. Both hypoxia and inflammation are central hallmarks of the GBM microenvironment leading to therapy resistance, however, research studies on GBM are rarely undertaken in hypoxic conditions. A lack of progress in the development of novel treatments has led to repurposing of existing licensed drugs as an alternative option. Research has suggested a role for aspirin, a non-steroidal anti-inflammatory drug, in the treatment and prevention of GBM. However, widespread aspirin usage is challenging due to side effects which has led to the development of several novel aspirin analogues with the aim of producing the same or better anti-cancer effects accompanied with safer toxicity profiles.

This study has investigated the effects of one such analogue, PN517, in addition to aspirin, cisplatin, and temozolomide either as monotherapy or combined therapy on the U87-MG glioblastoma and non-cancerous SVG-p12 cell lines under normoxic and hypoxic conditions. Multiple assays were performed including cell viability assay, proliferation and cell cycle analysis, wound healing assay, mitopotential and cell death assays, metabolic activity assays as well as western blot analysis for several proteins. In addition, U87-MG hypoxia-adapted cell lines and 3D spheroid models were generated and employed to examine the effect of the drug treatments in models that better mimic the GBM microenvironment.

Results found that PN517 and aspirin decreased cell viability under normoxia and hypoxia in a time and concentration dependent manner with similar efficacy to cisplatin in the U87-MG glioblastoma cell line. Interestingly, data suggested different mechanism of actions for PN517 and aspirin, with PN517 being consistently more efficacious. PN517 significantly inhibited cell proliferation, wound healing and GAPDH enzymatic activity. Additionally, PN517 induced significant alterations in the metabolic network of the cells by simultaneously reducing glycolytic and mitochondrial activities leading ultimately to apoptosis. Furthermore, PN517 significantly enhanced the efficacy of cisplatin and

temozolomide where the combination of PN517 and temozolomide always produced the greatest efficacy among all drug treatments. Most importantly, the enhanced therapeutic efficacy of the combined therapy as compared to the monotherapy was also observed in the hypoxia-adapted cell lines and 3D spheroid cultures, and the combination of PN517 and temozolomide remained the most effective drug treatment.

In conclusion, these results have suggested possible mechanisms of action for the effects of PN517 and aspiring in GBM and highlighted PN517 as an effective and potentially well-tolerated treatment which could have potential therapeutic value for the future treatment of GBM by enhancing temozolomide efficacy and increasing the patients' tolerance to the chemotherapy. Therefore, this study supports the further investigation of the combined therapy of PN517 with standard drugs *in vivo* using animal models of GBM in order to confirm its efficacy and ability to cross the blood brain barrier.

TABLE OF CONTENTS

ACKNOWLEDGEMENTS

First and foremost, I want to thank God Almighty for guiding me through and giving me the opportunity, knowledge, ability and strength to complete this project. Without his blessings, this achievement would not have been possible.

This work would not have been possible without the assistance and support of CARA organisation, the funders and all wonderful people there. Thank you for helping me to take this opportunity and for continuous support. Also, I would like to acknowledge the School of Pharmacy and Biomedical Sciences in the University of Central Lancashire for funding this research.

I would like to express my most sincere gratitude and appreciation for my supervisor Dr. Philip Welsby for providing his heartfelt support, concern and guidance and for giving me invaluable expertise, inspiration and suggestions in my quest for knowledge. I want also to thank my Co-supervisor, Dr. Gail Welsby, for sharing her knowledge, invaluable advice and expertise when needed. Thank you both for your patience, constant encouragement and friendly attitude throughout this journey. I could not have imagined better supervisors for my PhD study and will always be grateful to you.

I would also like to thank Dr. Tim Snape for his contribution to the supervisory team for my project and for always being there to provide any help and support when needed. I am also grateful to Dr. Iain Nicholl for providing us with the compounds I have tested. I have great pleasure in acknowledging all the academic staff who have taken some time to enrich my work. Special thanks to Dr. Sarah Dennison and Dr. Julie Burrow for providing me with the necessary training on the equipment, being around for troubleshooting and all other help you have offered.

I owe profound gratitude to my parents who have been the reason behind my successes. Thanks, from the bottom of my heart, for your constant encouragement, endless love, unconditional support and great sacrifice that allowed me to complete this PhD project and thesis. This accomplishment would not have been possible without you. Thanks to my siblings and entire family for your encouragement and prayers and always showing how proud you are of me.

My deepest and most sincere gratitude is due to my husband and my best friend Murhaf. You were always around at times when I thought that it is impossible to continue, and you always believed in me. The last word goes to my beautiful son Majed who have been the light of my life and who his smile and love continue to be a powerful source of inspiration, motivation, love and hope.

This work is heartily dedicated to all patients suffering from cancer or who lost the battle with cancer because they could not afford the treatment in my home country Syria or any other place in the world.

LIST OF FIGURES

Chapter 1

Chapter 3

Chapter 4

Chapter 5

Chapter 6

Chapter 7

Chapter 9

LIST OF TABLES

LIST OF ABBREVIATIONS

2-HG	2-Hydroxyglutarate
7-AAD	7-Aminoactinomycin D
AIC	5-amino-imidazole-4-carboxamide
AIF	Apoptosis-inducing factor
AKT	Protein kinase B
AP-1	Activator protein 1
Asp	Aspirin
ATGs	Autophagy related proteins
BAX	BCL2 associated X
BBB	Blood brain barrier
Bcl-2	B-cell lymphoma 2
BCS	Bis(2-carboxyphenyl)succinate
BPG	1,3-Biphosphate Glycerate
CAIX	Carbonic Anhydrase IX
CAXII	Carbonic Anhydrase XII
CCCP	Carbonyl Cyanide 3-ChloroPhenyl-hydrazone
CCND1	Cyclin D1
CDKN2A	Cyclin-dependent kinase Inhibitor 2A
CDKs	Cyclin-dependant kinases
CFDA-SE	Carboxyfluorescein diacetate - succinimidyl ester
Cis	Cisplatin
CK	Cytokinesis
CKIs	Cyclin-dependent kinase inhibitors
CLQ	Chloroquine
CNS	Central nervous system
COX	Cyclooxygenase
DISC	Death-inducing signalling complex
DSBs	DNA double-strand breaks
ECAR	Extracellular acidification rate
EGF	Epidermal growth factor
EGFR	Epidermal growth factor receptor
EMT	Epithelial-mesenchymal transition
ETC	Electron transport chain
Ex/Em	Excitation / Emission
FADD	Fas associated via death domain

FasL	Fas Ligand
FasR	Fas Receptor
FBS	Foetal Bovine Serum
FIH	Asparaginyl hydroxylase
FITC	Fluorescein isothiocyanate
GAP	Glyceraldehyde-3-Phosphate
GAPDH	Glyceraldehyde-3-Phosphate Dehydrogenase
GBM	Glioblastoma
GLUT	Glucose transporter
GSCs	Glioma stem cells
HIF	Hypoxia-inducible factors
HK2	Hexokinase-2
IAPs	inhibitors of apoptosis proteins
IARC	International Agency for Research on Cancer
IC_{25}, IC_{50}	Inhibitory Concentrations at 25% and 50%
ICAD	Inhibitor of Caspase Activated DNAae
IDH	Isocitrate dehydrogenase
IKKβ	I kappaB Kinase beta
IL-6	Interleukin 6
IMRT	Intensity-modulated radiotherapy
JC-1	Tetraethylbenzimidazolylcarbocyanine iodide
JNK	c-Jun N-terminal kinase
LDH	Lactate dehydrogenase
MAPK	Mitogen-activated protein kinase
MCT	Monocarboxylate transporter
MDR	Multiple-drug resistance
MGMT	O6-methylguanine-DNA methyltransferase
MMP	Metalloproteinases
MPTP	Mitochondrial permeability transition pores
MTIC	5-(3-methyltriazen-1-yl)imidazole-4-carboxamide
mTOR	Mammalian target of rapamycin
MTT	3-(4,5-dimethyethiazol-2-yl)-2,5-diphenyltetrazolium bromide
Myc	Myelocytomatosis oncogene cellular homolog
NF-κB	Nuclear factor kappa B
NSAIDs	Nonsteroidal anti-inflammatory drugs
OCR	Oxygen consumption rate
PARP	Poly(ADP-ribose) polymerase

PB	PrestoBlue
PC	Pyruvate carboxylase
PDK1	3-phosphoinositide-dependent protein kinase-1
PGE2	Prostaglandin E2
PGF2α	Prostaglandin F2α
PGG2	Prostaglandin G2
PGH2	Prostaglandin H2
PGI2	Prostaglandin I2
PHD	Prolyl hydroxylase domain
PI	Propidium iodide
PI3K	Phosphoinositide 3-kinases
PIK3R4	Phosphoinositide-3-Kinase Regulatory Subunit 4
PtdSer	Phosphatidylserine
PTEN	Phosphatase and tensin homolog gene
PTPC	Permeability transition pore complexs
Raf	Rapidly accelerated fibrosarcoma
Rap	Rapamycin
Ras	Proto-oncogene protein p21
RB	Retinoblastoma protein
RONS	Reactive oxygen and nitrogen species
ROS	Reactive oxygen species
RRAD	Ras-related associated with diabetes
SAPK/JNK	Stress-activated protein kinase/c-Jun NH2-terminal kinase
SDS-PAGE	SDS-Polyacrylamide gel electrophoresis
STAT3	Signal transducer and activator of transcription 3
TCF	T-cell factor
TMZ	Temozolomide
TNF	Tumour necrosis factor
TP53	Tumour protein 53 gene
TRAIL	Tumour necrosis factor-related apoptosis inducing ligand
TTFs	Tumour Treating Fields
VEGF	Vascular endothelial factor
VEGFR	Vascular endothelial growth factor receptor
VHL	Von Hippel-Lindau tumour suppressor protein
WHO	World Health Organization
α-KG	α-ketoglutarate
Δψm	Mitochondrial Membrane Potential

CHAPTER 1: INTRODUCTION

1.1. Cancer

Cancer is among the leading causes of morbidity and mortality worldwide and affects all ages and populations (Siegel *et al.*, 2016). More than 70% of all cancer deaths occur in low- and middle-income countries and these regions are projected to account for two-thirds of all cases of cancer worldwide by 2050 (Bray and Møller, 2006). The statistics published by the International Agency for Research on Cancer (IARC) declared 17 million new cases of cancer worldwide in 2018 (52% males and 48% females). The four most common types of cancer worldwide are lung, breast, bowel and prostate cancers, and account for more than 43% of all new cases. IARC has predicted there will be 27.5 million new cancer cases worldwide each year by 2040.

In the UK, more than 360,000 new cancer cases are diagnosed every year with around 164,000 cancer deaths which accounts for more than 28% of all deaths (Cancer Research UK; World Cancer Factsheet 2016). The UK incidence rate for all cancers combined is ranked higher than 90% of the world countries with the same four most common types as those worldwide (IARC, accessed 2018). However, the World Health Organization (WHO) has highlighted that cancer mortality could be effectively reduced by strategies for prevention, early detection, improved diagnosis and enhanced treatment (Torre *et al.*, 2016).

1.2. Brain cancer

Annually, there are around 11,500 people diagnosed with a brain, other central nervous system (CNS), or intracranial tumour in the UK with around 5,200 deaths (Cancer Research UK, 2016). According to data collected by Cancer Research UK in 2016, the incidence rates of brain, other CNS and intracranial tumours have increased by around 15% in the UK over the last decade, with most malignant tumours occurring in the brain and much smaller proportions in the meninges, endocrine glands and other parts of the CNS, with these rates are projected to rise by 6% between 2014 and 2035. In contrast to most cancer types, the brain, other CNS and intracranial tumours occur relatively frequently at younger ages and the incidence rates are similar between males and females in most age groups as shown in figure 1.1. (Cancer Research UK, 2016).

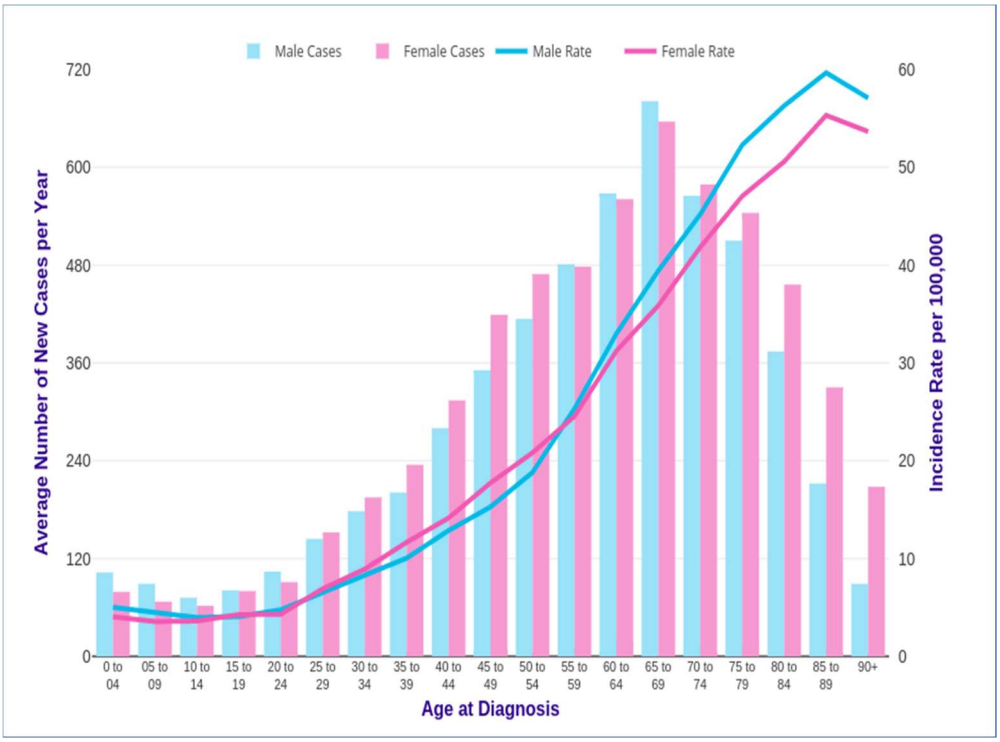

Figure 1. 1 Average number of brain, other CNS, and intracranial tumours cases per year and age-specific incidence rates per 100,000 population in the UK (Cancer Research UK, 2013-2015).

Although brain tumours are considered some of the rarest cancer types (representing 3% of all new cancer diagnosis), they were also the cause of 3% of cancer mortalities, and survival has barely improved over the last 40 years (Cancer Research UK).

1.3. Glioma

There are more than 130 different types of tumour which can occur in the brain, other CNS, or intracranial region (Louis *et al.*, 2007). Gliomas are the most common type of these tumours which arise from the supporting non-neuronal glial cells and can be divided histologically into astrocytomas, oligodendrogliomas and mixed groups (Laws *et al.*, 2003; Louis *et al.*, 2016). Gliomas were originally classified by WHO into grades I through IV based on the histological criteria and malignancy degree (Louis *et al.*, 2007) where grade IV tumours display the most aggressive features including angiogenesis, large-scale necrosis, infiltration of adjacent tissues as well as being refractory to radio and chemotherapy (Kleihues *et al.*, 1995; Furnari *et al.*, 2007).

Recently, WHO classification was revised to rely more on molecular analysis subtyping. The updated stratification of glioma incorporated molecular biomarkers such as isocitrate dehydrogenase IDH1/2 status, O6-methylguanine-DNA methyltransferase (MGMT)-promoter methylation, and 1p/19q co-deletion allowing for a better prognostic grading of gliomas which in turn leads to more personalized treatments (Reifenberger *et al.*, 2017) (Table.1.1). Recent advances in understanding the biological features of gliomas have led to vital changes in the classification, prognostic identification, and therapeutic management of newly diagnosed gliomas.

Table 1. 1. Grading of different glioma tumours according to WHO classification of central nervous system tumours (Louis *et al.*, 2016).

Diffuse astrocytic and oligodendroglial tumours	Grade
Diffuse astrocytoma, IDH-mutant	II
Anaplastic astrocytoma, IDH-mutant	III
Glioblastoma, IDH-wildtype	IV
Glioblastoma, IDH-mutant	IV
Diffuse midline glioma, H3K27M-mutant	IV
Oligodendroglioma, IDH-mutant and 1p/19q-codeleted	II
Anaplastic oligodendroglioma, IDH-mutant and 1p/19q-codeleted	III
Other astrocytic tumours	
Pilocytic astrocytoma	I
Subependymal giant cell astrocytoma	I
Pleomorphic xanthoastrocytoma	II
Anaplastic pleomorphic xanthoastrocytoma	III

Approximately 50-60% of all primary brain tumours are malignant gliomas, and they constitute about 2% of all diagnosed cancers annually in the UK (Braganhol *et al.*, 2006; Hervey-Jumper and Berger, 2014). The most common morphological types recorded in England in 2006-2010 were astrocytomas (34%) of which ~80% were the very aggressive subtype glioblastoma (Zhou *et al.*, 2013). The emergence of large-scale genomic and epigenomic studies has provided deeper

insights into molecular neuropathology of gliomas and shown promise for better diagnosis of the tumours (Fig 1.2) (Louis *et al.*, 2016; Park *et al.*, 2017).

Glioblastoma is histologically diagnosed by neoplastic cells with astrocytic features, endothelial proliferation and/or necrosis which may resemble a pseudopalisading form (Hambardzumyan and Bergers, 2015). Due to its aggressiveness and highly proliferative progression, glioblastoma is categorized as grade IV astrocytoma and the patients are further classified into primary or secondary glioblastoma based on the absence or presence of mutations in the *IDH1* or *IDH2* genes (Reifenberger *et al.*, 2017). Most glioblastomas are *IDH* wild-type and correspond to the description of primary glioblastoma that develop rapidly without any clinical, radiological, or morphological evidence. Up to 10% of glioblastoma patients have a mutation in the *IDH1* or *IDH2* genes and often arise from lower grade gliomas and are classified as secondary glioblastoma that may look histologically similar but affect different age groups (Ohgaki *et al.*, 2004).

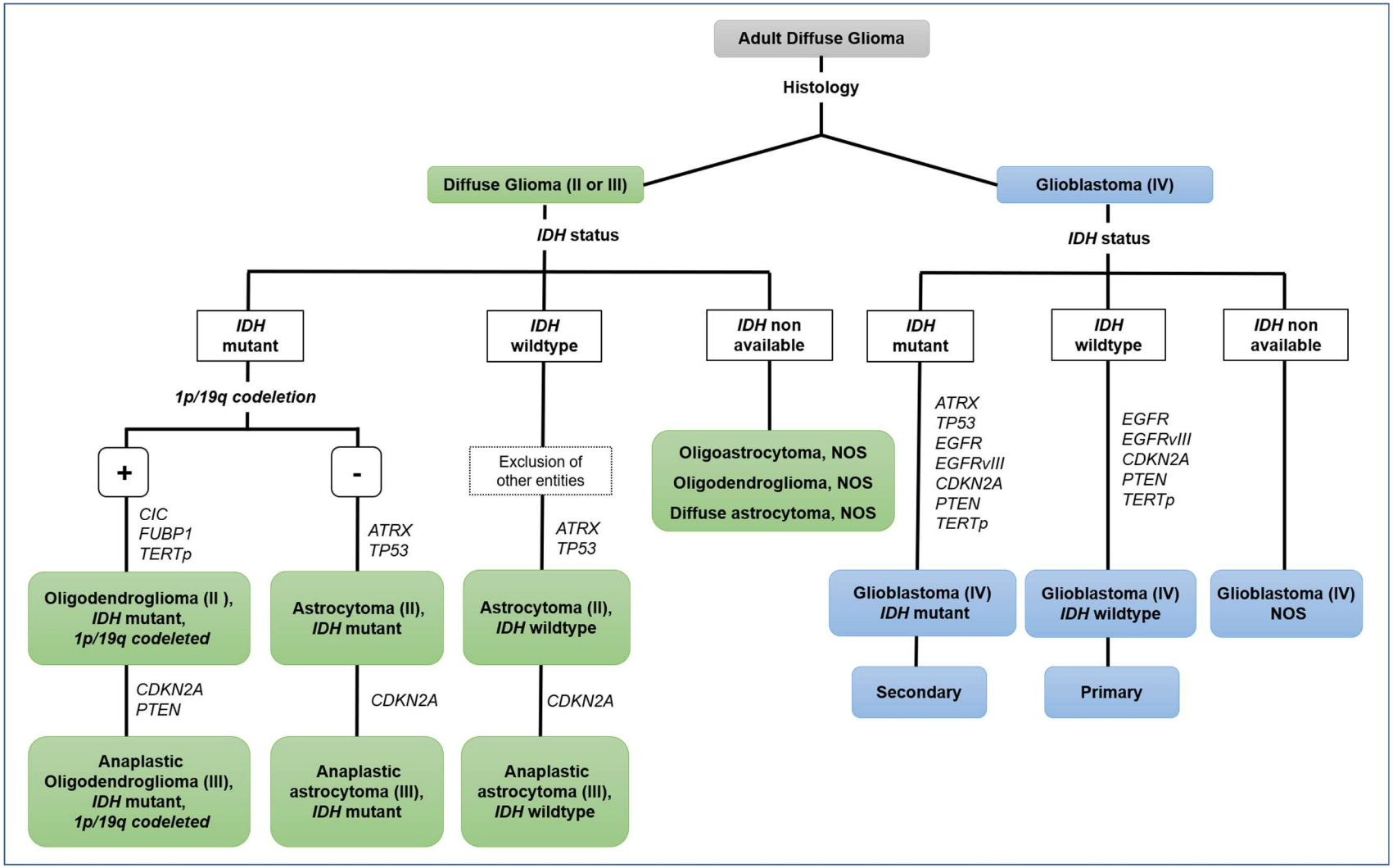

Figure 1. 2. Schematic algorithm for the classification of adult diffuse glioma according to histological and key genetic features. Modified from (Louis *et al.*, 2016; Park *et al.*, 2017). *IDH*, Isocitrate dehydrogenase gene; *EGFR*, Epidermal growth factor receptor gene; *CDKN2A,* Cyclin dependent kinase inhibitor gene; *PTEN*, Phosphatase and tensin homolog gene; $TERT_p$, Telomerase reverse transcriptase promoter; *ATRX*, X-linked gene of α-thalassemia and mental retardation syndrome; *TP53*, Tumour protein 53; *CIC*, Capicua transcriptional repressor; *FUBP1*, Far upstream element-binding protein 1 gene; NOS, not otherwise specified.

1.4. Glioblastoma

Glioblastoma (GBM), grade IV astrocytoma, is the most aggressive primary brain tumour in adults, and is characterized by having a highly mitotic rate, necrotic areas, and increased vascularization around the tumour (Senbabaoglu *et al.*, 2016). GBM tumours are polymorphic meaning that, even within the same tumour, the cells are highly heterogenous and display mixed histological features (Burger and Kleihues, 1989; Kleihues *et al.*, 1995; Miller and Perry, 2007).

Clinically, symptoms of GBM include headache that might not be considered seriously by the patient leading to late diagnosis. Fatigue, mood disturbances, and anxiety are also frequent complaints reported by the patients (Boele *et al.*, 2014). Other prominent symptoms include increased intracranial pressure, epilepsy, memory loss, confusion, cognitive dysfunction and focal neurological deficits which may arise in any stage of the disease (Preusser *et al.*, 2011; Boele *et al.*, 2014). Diagnosis is confirmed through computed tomography (CT or CAT scan) and magnetic resonance imaging (MRI) (Sizoo *et al.*, 2010).

Although GBM diagnosis is rare, its occurrence is universally and rapidly fatal with the potential of approximately 20 years of life lost after diagnosis, the highest among any other adult tumour type studied in different surveys (Burnet *et al.*, 2005; Rouse *et al.*, 2015). Despite clinical and technological advances in the understanding and treatment of brain tumours over the last three decades, the survival of patients with GBM has not notably improved with a nearly certain recurrence (Zhou *et al.*, 2012). At present, the standard care of GBM still results in poor prognosis, with a median survival time of less than 16 months, even after optimal treatment (Stupp *et al.*, 2005; Joseph *et al.*, 2015) and tumours eventually recur after multimodal treatments (Furnari *et al.*, 2007; Stupp *et al.*, 2009) with only 0.05% to 4.7% of patients surviving five years following diagnosis (Ostrom *et al.*, 2014).

GBM is currently classified into two categories namely IDH wild-type and IDH mutant which are associated with primary and secondary GBMs, respectively (Figure 1.2.). GBM tumours originate as primary tumours in more than 90% of cases with no clinical or histological evidence of a less malignant precursor and

rapidly progress to a malignant state in elderly patients. Secondary tumours usually advance from lower grade astrocytomas and more appear in younger patients (Ohgaki and Kleihues, 2007; Ohgaki and Kleihues, 2013).

There are several factors and challenges leading to the failure of treatment of glioblastoma (Lawson *et al.*, 2007). First, the diffuse infiltrative nature of these tumours (namely Scherer's structures) and invasion of the surrounding healthy tissue enables it to escape complete surgical resection (Cuddapah *et al.*, 2014). Another major obstacle in glioblastoma treatment is the presence of the blood brain barrier (BBB) which restricts the systemic-delivery of many molecules and hinders crossing into the brain (Neuwelt *et al.*, 1980; Halperin *et al.*, 1989). Additionally, the complex microenvironment and conditions of pro-tumoural inflammation in the extracellular matrix can make way for cancer cells, facilitating tumour invasion (Cuddapah *et al.*, 2014; Nørøxe *et al.*, 2016). Due to these complicated features of GBM with no distinct risk factors and lack of knowledge of cellular origins, it has become crucial to consider the biology of GBM especially whilst designing new targeted therapies (Zong *et al.*, 2012; Zong *et al.*, 2015).

Pathophysiological features of GBM

Despite aggressive chemoradiotherapy in GBM, the survival of patients has not significantly improved. The GBM microenvironment is extremely complex, involving a plethora of cell types and signalling pathways which enable GBM to thrive and adapt to therapies (Persano *et al.*, 2011; Meyer *et al.*, 2015). More specifically, these tumours are often presented with nuclear atypia, cellular pleomorphism, high mitotic activity, microvascular proliferation as well as pseudopalisading necrotic areas which altogether distinguish GBM from gliomas of lower grades (Hambardzumyan and Bergers, 2015). Therefore, advancements in understanding complex biology underling GBM tumorigenesis and especially in the area of tumour microenvironment have highlighted the urgency of considering the biological features of GBM at a molecular level when developing novel therapies.

1.4.1. Heterogeneity

GBMs are characterized as having a high degree of genetic, transcriptomic and functional heterogeneity that normally leads them to display different inter- and intra-tumoural phenotypes and diverse molecular profiles (Meyer et al., 2015). Studies have revealed that individual cells within the same tumour can show diverse expression patterns of two or more different subtypes at the same time relating to different cellular processes, such as proliferation, immune response, hypoxia and oncogenic signalling (Patel *et al.*, 2014). These multiple subclonal populations can either respond to or escape therapy regenerating as a treatment-refractory tumour which in turn can explain the poor prognosis and inevitable tumour recurrence of GBM (Qazi *et al.*, 2017). Therefore, regional variances in morphology and genetics of GBM have rendered the tumour mass to be highly resistant to both radiotherapy and chemotherapy with the ability to develop multiple resistance pathways, and made effective treatment regimens of gliomas massively challenging (Zhang and Barres, 2010).

Another factor contributing to the complexity of resistance in GBM is the subpopulation of glioma stem cells (GSCs) within tumours. These cells are tumorigenic due to their unlimited proliferative and self-renewal capacities, and are capable of differentiating into multiple heterogeneous glial tumours (Singh *et al.*, 2003; Park and Rich, 2009). Recent study proposed that intra-tumoural heterogeneity in glioblastoma is the expected outcome of fate decisions made by GSCs and their progeny (Lan *et al.*, 2017). GSC populations are highly resistant to the cytotoxic effects of radiation and chemotherapy. They can survive the initial therapy and overcome the induced damage through both innate properties like genetic heterogeneity and adaptive resistance pathways (Osuka and Van Meir, 2017). These findings have led many to conclude that GSCs offer a potential target in order to achieve complete responses (Altaner, 2008; Hambardzumyan *et al.*, 2008).

1.4.2. Hypoxic microenvironment

Role of hypoxia in GBM progression and resistance to treatment

As a consequence of GBM's aggressiveness, rapid proliferation and growth, the tumour initially has poor vascularisation and subsequently an extremely low

oxygen supply i.e. hypoxic conditions. The extended periods of hypoxia cause the hallmark necrotic regions found in GBM, tightly surrounded by hypoxic tumour cells (Figure 1.3) (Joseph *et al.*, 2015).

Remarkably, different grades of gliomas outlined by WHO classification present with differing levels of hypoxia, generally the more severe the tumour, the more hypoxic it is (Evans *et al.*, 2004). Hypoxia was measured in one study with the 2-nitroimidazole imaging agent EF5 and indicated that the physiological conditions of the brain and grade II tumours have a modest level of hypoxia of 10% pO_2, whereas grade III tumours ranged from 2.5-10% pO_2, and grade IV tumours were characterised by moderate to severe hypoxia ranging from 0.1-2.5% pO_2 (Evans *et al.*, 2004). Ten years later, a review study has indicated that while median oxygenation in healthy brain tissue is ~4.6% O_2, it drops to less than 1.7% in the high grade brain tumour (Muz *et al.*, 2015).

It has been postulated that hypoxia is involved in a large number of pathways leading to the growth of gliomas and plays a central role in the pathophysiology and progression of GBM tumours (Jawhari *et al.*, 2016). Studies have shown that hypoxia can trigger a complicated series of heterogeneous tissue events by multiple signalling pathways which affect GSCs self-renewal, cell proliferation, cell death, energetic metabolism, invasion and angiogenesis (Binello and Germano, 2011; Ho and Shim, 2017), promoting the malignant phenotype and tumour heterogeneity (Jawhari *et al.*, 2016).

The necrotic foci in GBM are typically surrounded by hypercellular zones called pseudopalisades, another constant feature for GBM (Barker *et al.*, 1996). Cells with pseudopalisades are hypoxic and may serve to promote the onset of aggressive growth and angiogenesis of the tumour by secreting vascular endothelial factor (VEGF) (Pilkington, 2001; Rong *et al.*, 2006; Jain *et al.*, 2007). Additionally, GSCs are enriched in the necrotic and hypoxic regions of GBM and characterized by reduced oxygen tension and activation of the hypoxia-inducible factors HIF-1 and HIF-2 (Brat *et al.*, 2004). The differential hypoxic environment in the different regions of the tumour activates a stem cell programme and favours an invasive phenotype (Manini *et al.*, 2018).

Tumour hypoxia is a critically important parameter associated with impairment of therapeutic efficacy and encouragement of rapid development of the drug resistance phenomenon (Binello and Germano, 2011). It has a substantial effect on responses across most types of cancer treatments irrespective of their mode of action (Mckeown, 2014). In regard to chemotherapy, resistance has been directly linked to the level of hypoxia present within the tumour (Persano *et al.*, 2012). Additionally, antiangiogenic therapy resistance, and radiation resistance may have hypoxic mechanisms (Jensen, 2009). For instance, the upregulation of LIVIN expression, a member of inhibitors of apoptosis proteins (IAPs), and downregulation of caspase activity were observed under cycling and chronic hypoxia in glioblastoma cells, associated with increased resistance to radiation and temozolomide (Hsieh *et al.*, 2015). In addition, the low level of oxygen in tumour tissue (Xu *et al.*, 2012) activates *MDR1* (Multiple-drug Resistance Gene 1) which encodes for P-glycoprotein (P-gp), and hinders the free radicals generated by radiation therapy (Liu *et al.*, 2016).

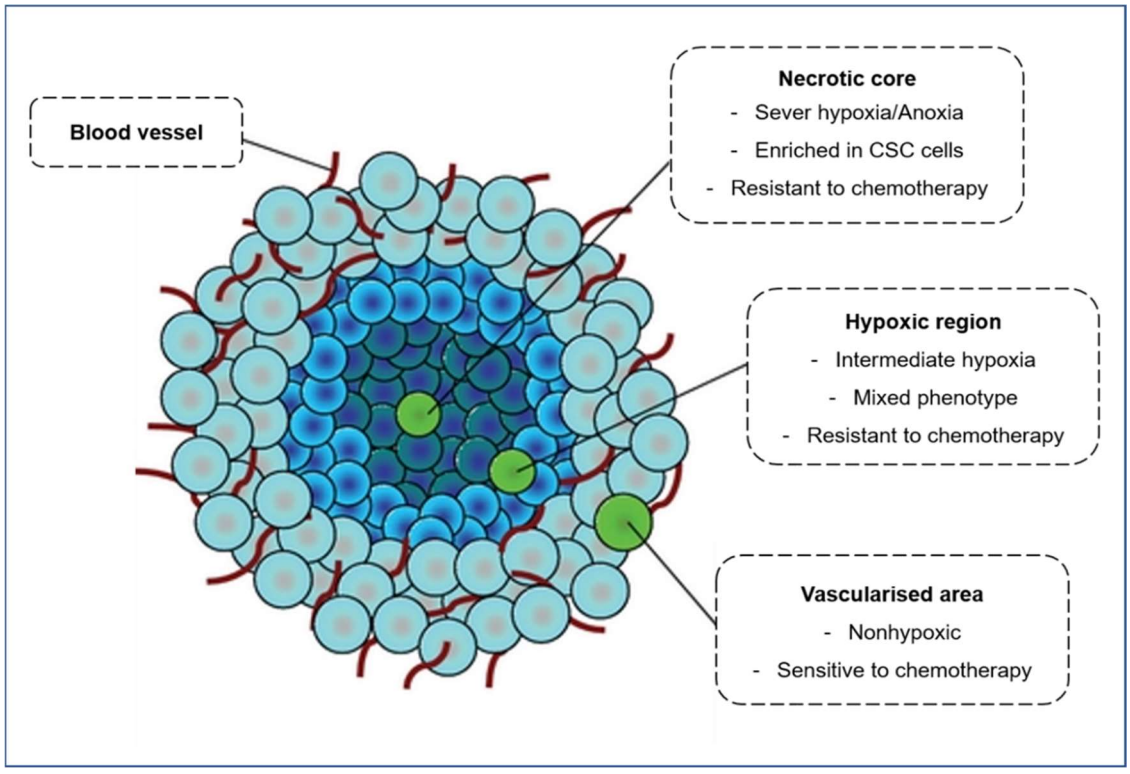

Figure 1. 3. Phenotypic and molecular characteristics of the three concentric layers model of GBM (Persano *et al.*, 2011).

Hypoxia signalling pathways

Hypoxia induces several complex intracellular signalling pathways. The key regulator of cellular responses to hypoxia is the hypoxia-inducible factor (HIF) pathway which grants cellular adaptation to hypoxia (Semenza *et al.*, 1991). Other hypoxia-associated pathways include phosphoinositide 3-kinases (PI3Ks)/ Protein kinase B (AKT)/ Mammalian target of rapamycin (mTOR), Mitogen-activated protein kinases (MAPK) and the nuclear factor NF-κB. These pathways are involved in cell survival, proliferation, apoptosis, metabolism, migration, and inflammation (Koong *et al.*, 1994; Seta *et al.*, 2002; Courtnay *et al.*, 2015).

The HIF transcriptional factor is a heterodimeric complex consisting of α and β subunits (Maxwell *et al.*, 2001; Melillo, 2004). The α subunit exists as multiple isoforms (HIF-1α, HIF-2α and HIF-3α) and only functions as a mediator in the hypoxic response, whereas the β-subunit, also known as the aryl hydrocarbon receptor nuclear translocator (ARNT), serves as a heterodimeric partner with the aryl hydrocarbon receptor, and it is constitutively expressed in most cells (Liu and Simon, 2004; Loboda *et al.*, 2010). HIF-1α is ubiquitously expressed and the protein level is upregulated in the majority of tumours and plays a pivotal role by signalling the presence of hypoxia, while the expression of HIF-2α and HIF-3α is more controlled and play more specialised roles in oxygen homeostasis (Semenza, 2000), however, their role in tumour hypoxia has not been widely studied (Rosenberger *et al.*, 2002; Holmquist-Mengelbier *et al.*, 2006; Gordan *et al.*, 2007).

<u>Oxygen dependent regulation of HIF:</u>

HIF-1 activity is reliant on limiting expression of the α-subunit. HIF-α is constitutively transcribed, and the protein continuously translated whose stability is mediated by a region known as the oxygen-dependent degradation domain (ODDD) (Semenza *et al.*, 1991; Semenza and Wang, 1992). The protein stabilization of HIF-α subunits after hypoxia induction is regulated by oxygen sensors, including prolyl hydroxylase domain (PHD) and asparaginyl hydroxylase (FIH-1) enzymes and their activity is oxygen-dependent as well (Bruick and Mcknight, 2001).

Under normal oxygen conditions, α subunits are rapidly degraded by the ubiquitin-26S proteasome system. This oxygen-dependent degradation is catalysed by PHD and FIH-1 enzymes which hydroxylate HIF-α in the ODDD, and facilitates the recognition of HIF-α by the von Hippel-Lindau tumour suppressor protein (VHL), which promotes the proteasomal degradation of HIF-α subunits (Kamura *et al.*, 2000; Semenza, 2000; Giaccia *et al.*, 2003; Liu and Simon, 2004).

In contrast to this, under hypoxic conditions, the α subunits are not degraded as the PHD containing proteins lack the oxygen required to hydroxylate HIF-α, and are hence not recognised by VHL and escape degradation. The stabilization of HIF-α allows it to translocate to the nucleus and heterodimerize with HIF-β (Huang *et al.*, 1996). Once HIF dimerized, and by interacting with co-activators p300/CBP (p300-binding protein/CREB-binding protein), it binds to hypoxia response elements (HREs) and initiates active transcription for wide array of genes. (Figure 1.4) (Kamura et al., 2000, Liu and Simon, 2004).

<u>Non-oxygen dependent regulation of HIF:</u>

HIF-α stabilization and activity could be modulated in a hypoxia-independent manner where its regulation occurs in response to other agents such as cytokines, lipopolysaccharides, chemokines, and growth factors mediated by PI3K/AKT/mTOR, MAPK, and NF-κB pathways which eventually may also lead to HIF-1α activation (Seta *et al.*, 2002; Salmena *et al.*, 2008; Courtnay *et al.*, 2015). Additionally, mitochondrial reactive oxygen species (ROS) and nitric oxide (NO) were found to up- or downregulate HIF-1α accumulation (Chandel *et al.*, 2000; Movafagh *et al.*, 2015). HIF is also affected by epigenetic changes and pathways, mutations in which can result in loss of tumour-suppressor functions (p53, PTEN, VHL) and acquisition of oncogene functions (proto-oncogene protein p21 (Ras), rapidly accelerated fibrosarcoma (Raf), proto-oncogene tyrosin-protein kinase (Src), Myelocytomatosis oncogene cellular homolog (Myc) and mTOR) causing uncontrollable cancer cell growth (Figure 1.4) (Van Uden *et al.*, 2008; Kilic-Eren *et al.*, 2013).

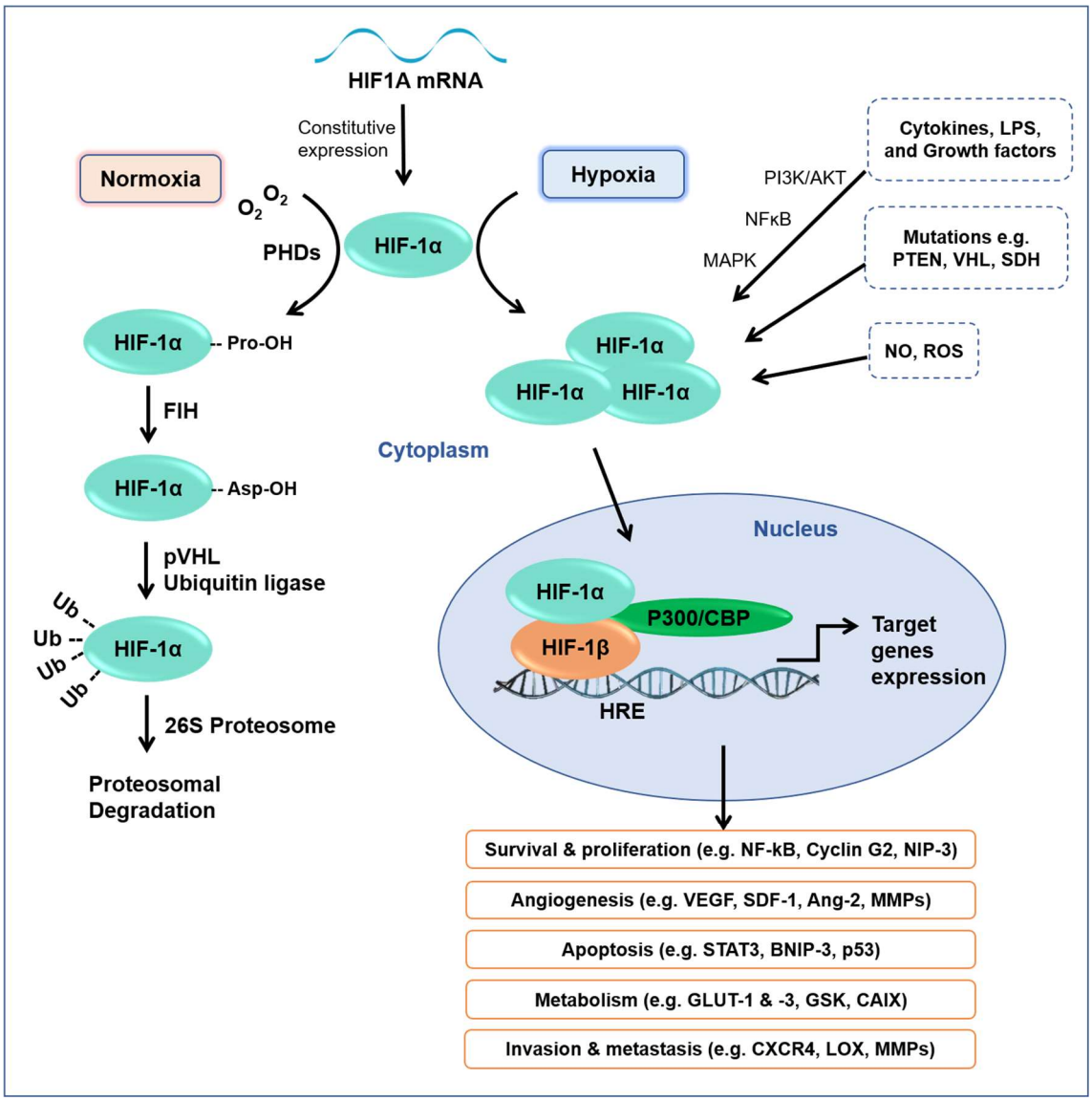

Figure 1. 4. Regulation of HIF-1α under normoxia and hypoxia and transcriptionally activated target genes expression. Modified from (Hong *et al.*, 2004; Walsh *et al.*, 2014). LPS, lipopolysaccharide; PTEN, phosphatase and tensin homolog gene; VHL, von Hippel-Lindau tumour suppressor protein; SDH, succinate dehydrogenase; ROS, reactive oxygen species; NO, nitric oxide.

1.4.3. Angiogenesis and invasion

To maintain high rates of growth, solid tumours rely on angiogenesis which is the formation of new blood vessels from rerouting and remodelling of pre-existing vessels to increase blood supply and provide nutrients and oxygen for the growing cells (Rahman *et al.*, 2010). Among solid tumours, GBM is one of the most vascularised tumour types and displays the highest degree of microvascular proliferation and endothelial cell hyperplasia, thus, angiogenesis is a key pathologic feature of GBM (Brem *et al.*, 1972). Such processes are controlled by

the homeostatic balance between pro-angiogenic and anti-angiogenic factors by both cellular sources and environmental stimuli (e.g. hypoxia) resulting in activation of the pro-angiogenic signalling pathway. Notably, large amounts of VEGFs are produced to initiate and promote angiogenesis (Brem *et al.*, 1972; Soda *et al.*, 2013). The essential role of HIFs in vascular protection will lead to recovery of tumour blood and nutrient supply rendering GBM treatment challenging with developing resistance in radiotherapy, chemotherapy and immunotherapy (Zeng *et al.*, 2015). Anti-angiogenesis drugs are expected to play a role as part of combination therapies and are currently being combined with other treatments in clinical trials (Zirlik and Duyster, 2018). Bevacizumab is an anti-angiogenesis drug that has had success in reducing tumour growth and increasing progression-free survival (Narita, 2015). However, patients are developing resistance to the drug after several treatments and the impact on overall patient survival is minimal (Lu and Bergers, 2013).

Another significant biological events of GBM that precludes successful therapy is invasion, the process by which tumour cells infiltrate the surrounding normal brain tissue, thereby rendering local control of GBM difficult with either surgery or radiation therapy (Bellail *et al.*, 2004). Invasive pathways involve complex interactions regulated by over 140 genes. Various components, including growth factor, cell adhesion molecules, proteases, extracellular matrix (ECM) components are involved in this multi-step process and are studied as parameters of brain tumour invasion (Ohka *et al.*, 2011). Hypoxic GBM cells *in vitro* were shown to secrete metalloproteinases (MMP), essential for ECM degradation, in high levels and migratory properties increased by up to 60% more than normoxic cells (Brat and Van Meir, 2004). This behaviour of being highly infiltrative and invasive is the most important contributing factor for the poor prognosis of GBM, despite the multimodal treatment with surgery, radiotherapy and chemotherapy (Waqas *et al.*, 2018).

1.4.4. Immunosuppression and inflammatory microenvironment

GBM microenvironment is highly immunosuppressive and thus reduces the effectiveness of immunotherapies. The microenvironmental factors, which result in GBM evasion from the immune system, can be derived from the tumour mass and as a result of the chronic inflammation found in the GBM microenvironment

(Ha *et al.*, 2014). Inflammation is a simple but powerful defence mechanism induced to stop tissue damage and promote repair (Munn, 2017), and has been reported to stimulate progression of the other hallmarks of cancer due to increased levels of NF-κB, reactive oxygen and nitrogen species (RONS), cytokines, prostaglandins and microRNAs (Schetter *et al.*, 2009).

The rapid growth rate of GBM does not lead just to hypoxia and aberrant vascular proliferation, but also to the infiltration of immune cells including macrophages, eosinophils, neutrophils, and T lymphocytes (Balkwill and Mantovani, 2001; Colotta *et al.*, 2009). The interaction between these cell populations promote abnormal activation or suppression of multiple signalling pathways by several cytokines that function in both a paracrine and autocrine manner and take part in the complex inflammatory microenvironment within the tumour (Balkwill and Mantovani, 2001; Colotta *et al.*, 2009). While these multiple components can help tissue repair after injury, the availability of activated inflammatory cells and the excretion of inflammatory mediators plays an important role in tumour cell proliferation, angiogenesis, and invasion (Figure 1.5) (Murat *et al.*, 2009; Charles *et al.*, 2012). For example, Cyclooxygenase-2 (COX-2) is released by cancer-associated fibroblasts, macrophage type 2 (M2) cells, and cancer cells to the tumour microenvironment and has been shown to play an essential role in tumour inflammation (Gurpinar *et al.*, 2013; Mostofa *et al.*, 2017). The resultant cytokines secreted during the inflammatory response stimulate tumour growth by activating NF-κB and the signal transducer and activator of transcription 3 (STAT3), which in turn activate proliferative and anti-apoptotic signals (Yu *et al.*, 2009; Didonato *et al.*, 2012; Nørøxe *et al.*, 2016). Furthermore, Interleukin 6 (IL-6) gene amplification in GBM tumours has been shown to correlate with the tumour aggressiveness and the reduced survival of the patients (Tchirkov *et al.*, 2007).

The chronically active inflammatory microenvironment in GBM has been supposed to encourage molecular evolution of tumour cells by either driving the first malignant-conferring genetic mutations and/or promoting them as a result of oncogene expression (Mantovani *et al.*, 2008). In fact, chronic inflammation in the GBM microenvironment is expected to play a critical role in triggering tumour initiation. This chronic inflammation may then drive GBM promotion, the next stage after tumour initiation, and progression, last stage of the disease which

loops back increasing the intensity of the underlying inflammation (Ha *et al.*, 2014).

Within the inflammatory GBM microenvironment, reactive oxygen, nitrogen and halogen species produced through activated macrophages, neutrophils, and eosinophils are expected to result in further mutations and epigenetic changes as GBM cells progress. These changes can alter cellular metabolism in a way can be exploited for the future targeted therapy focused against metabolism (Sowers *et al.*, 2014).

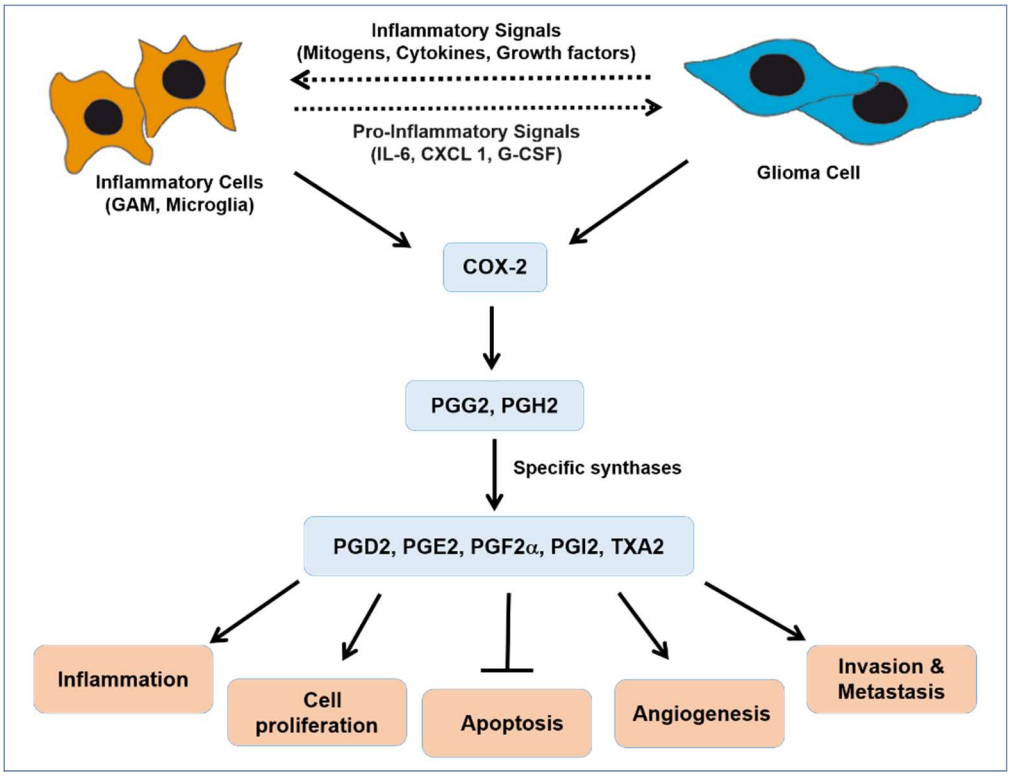

Figure 1. 5. The role of inflammation-induced cyclooxygenase in glioblastoma development (Gurpinar *et al.*, 2013; Mostofa *et al.*, 2017). GAM, glioma associated macrophages; IL-6, interleukin 6; CXCL 1, chemokine ligand 1; G-CSF, granulocyte colony-stimulating factor; Cox-2, cyclooxygenase-2; PGG2, prostaglandin G2; PGH2, prostaglandin H2; PGD2, prostaglandin D2; PGE2, prostaglandin E2; PGF2α, prostaglandin F2α; PGI2, prostaglandin I2; TXA2, thromboxane A2.

Generally, understanding the potential roles of inflammation in causing GBM initiation and progression and how the immune system and gliomas interact could help to develop more effective therapeutic approaches to treat gliomas (Sowers *et al.*, 2014).

1.4.5. Alterations in gene expression and cellular processes

The accumulation of gene mutations in cancer cells can eventually lead to uncontrolled cell proliferation and the different hallmarks of cancer (Hanahan and Weinberg, 2000; Garraway and Lander, 2013). GBM, like all human cancers, possess various chromosomal abnormalities, nucleotide substitutions and different epigenetic alterations, all of which are responsible for deregulation of multiple signalling pathways in GBM involved in cell proliferation, cell cycle, metabolism, survival and evading cell death (Network, 2008; Sturm *et al.*, 2012).

1.4.5.1. Sustaining cell proliferation

Cell replication is a tightly regulated process causes an irreversible and unidirectional changes in the state of the cell and loss of this regulation could lead to the uncontrolled expansion in the cell population found in cancer (Van Schaeybroeck *et al.*, 2005). Cell cycle progression plays a vital role in eukaryotic cell proliferation.

The eukaryotic cell cycle can be divided into two major stages; interphase and mitosis. Interphase is further divided into two gap phases: G1 and G2 and the S phase. Cells can also enter a quiescent state, the G0 phase (temporarily or permanently out of cycle) and in response to growth or mitotic signals, the cells move out of G0 through the early part of G1. In G1 phase, cells initiate RNA and protein synthesis to induce growth. The S phase is defined by synthesis of genomic DNA and the replication of chromosome. This is followed by the G2 phase where the cells undergo rapid growth and protein synthesis in order to prepare for division, or it is known to function as a time of DNA damage repair. The mitotic phase (M phase) is the process of nuclear division where a mother cell divides and produces two daughter cells. M phase is also sub-divided into stages defined by nuclear morphology – prophase, prometaphase, metaphase, anaphase A and B, and telophase. A final phase, division of the cytoplasm that overlaps telophase, is cytokinesis (CK) (Nojima, 1997; Crosio *et al.*, 2002; Tyson *et al.*, 2002; Rieder, 2011) (Figure 1.6). In the absence of mitotic signalling, the cell may undergo differentiation, apoptosis, or enter the quiescent state (G0).

Cell cycle progression is highly regulated by complexes composed of cyclin-dependant kinases (CDKs) and their corresponding cyclin regulatory subunits (cyclin -A, -B, -D, -E). CDKs induce downstream signals and major cellular events such as chromosome condensation, DNA replication, and spindle assembly by the phosphorylation of selected proteins. The levels of CDKs during the cell cycle remain constant, as opposed to the levels of cyclins which increase and decrease thus periodically activating their respective CDKs (Tyson *et al.*, 2002; Vermeulen *et al.*, 2003).

In turn, the regulation of cyclin/CDK complexes activity is controlled via multiple checkpoints during different phases of cell cycle by cyclin binding and cyclin-dependent kinase inhibitors (CKIs) to ensure integrity of daughter cells and prevent the cell from progressing to the next stage in the event of genomic damage, hence the cycle may be delayed or abandoned (Shackelford *et al.*, 1999; Vermeulen *et al.*, 2003).

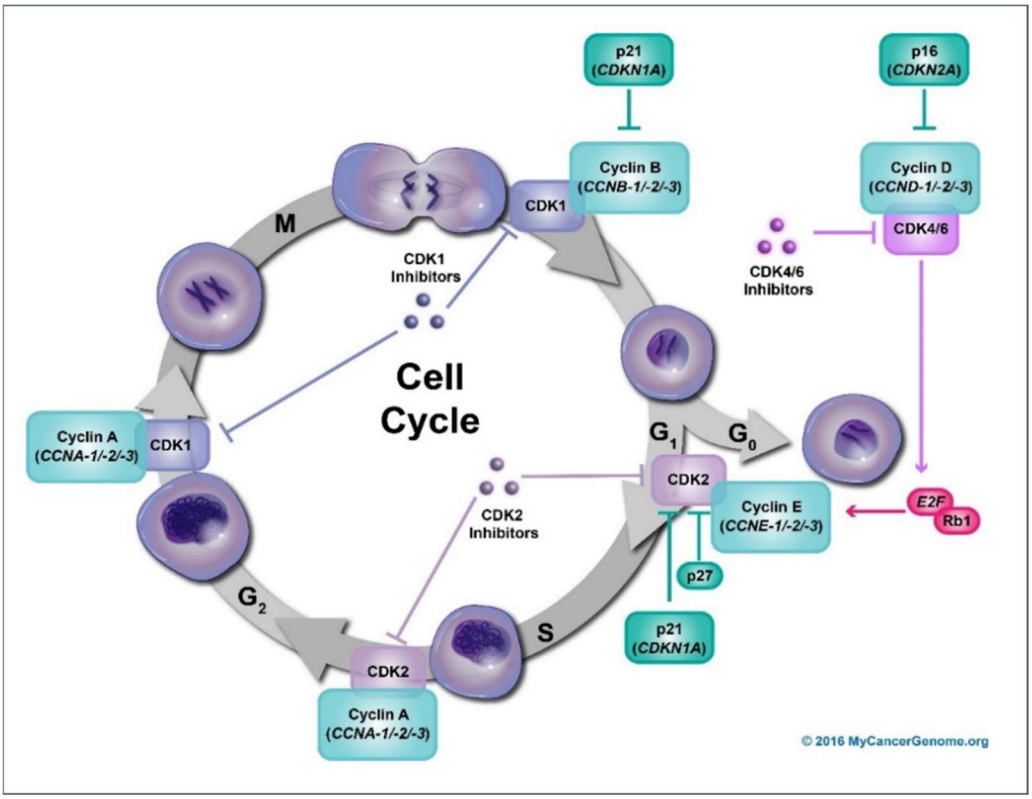

Figure 1. 6. Cyclins, cyclin dependent kinases and checkpoints involved in cell cycle regulation. The cycle begins in G1 with increased expression of the D cyclins (D1, D2, D3). The D cyclins associate with CDK4 and CDK6; formation of the cyclin/CDK complexes results in phosphorylation and activation of the CDKs. The activated CDKs then phosphorylate the retinoblastoma (RB) protein. The RB protein has a critical role in regulating G1 progression through the restriction point (Source: My Cancer Genome).

In GBM, several signalling pathways including p53, retinoblastoma protein (RB) and cyclin-dependent kinase Inhibitor 2A (CDKN2A) are dysregulated, all of which can play role in cell cycle regulation and sustaining cell proliferation (Network, 2008). In addition, while cyclin D1 expression is observed in normal brain tissue, it has shown to be overexpressed in glioma (Zhang *et al.*, 2005) leading to increased proliferation and invasion, while inhibiting apoptosis (Wang *et al.*, 2012). Cumulative evidence has shown that cyclin D1 overexpression in tumour cells is dependent in part on the mitogenic effects of EGF signalling through the EGFR in many cancers (Perry *et al.*, 1998; Poch *et al.*, 2001; Rieber and Rieber, 2006), and it is known to be amplified in 40% of GBM tumours leading to increases in cellular proliferation and resistance to radiotherapy (Barker Ii *et al.*, 2001).

1.4.5.2. Reprogramming cellular metabolism

Metabolic reprogramming is a hallmark of cancer and critical driver of all other hallmarks (Hanahan and Weinberg, 2000). Therefore, cancer has been considered a metabolic disease where the link between cancer and altered metabolism is well recognized (Cairns *et al.*, 2011; Soga, 2013). It has been expected that early metabolic changes inside tumour initiating cells increase intracellular oxidative stress, hence, increase oxidative DNA damage which can cause, combined with reduced DNA repair, subsequent mutations (Sowers *et al.*, 2014). Many of these mutations such as Myc, Ras, and Raf have a clear role in directing the metabolic transformation of tumour cells (Godlewski *et al.*, 2010)

Even with the great genetic and histological heterogeneity between tumours, malignant cells have shown to induce common metabolic pathways usually perturbed in cancer cells to support fundamental functions including anabolism, catabolism, and redox balance (Fig 1.7) (Cantor and Sabatini, 2012; Deberardinis and Chandel, 2016). Malignant cells may have abnormal activation of mTORC1 which induces an anabolic growth programme leading to nucleotide, protein, and lipid synthesis (Yuan and Cantley, 2008). Additionally, loss of tumour suppressors like p53 or activation of oncogenes like Myc promotes anabolism by transcriptional regulation of metabolic genes, hence playing a role as regulator of metabolism (Maddocks *et al.*, 2013; Stine *et al.*, 2015).

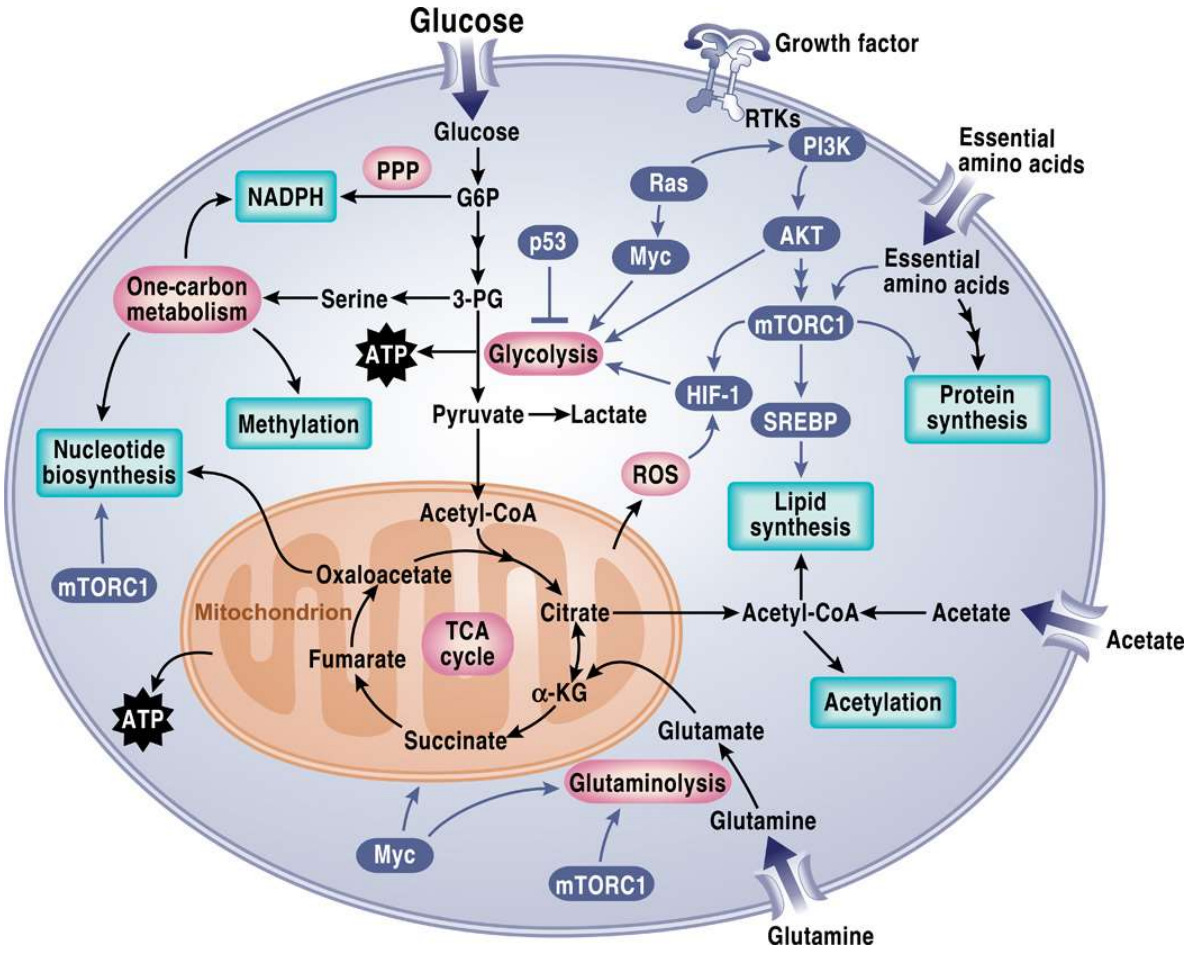

Figure 1. 7. The different signalling pathways regulating tumour cell metabolism. The two major energy producing pathways are mitochondrial respiration and glycolysis. Metabolism controls signalling through regulating reactive oxygen species (ROS), acetylation, and methylation. PPP, pentose phosphate pathway; G6P, glucose-6-phosphate; 3-PG, 3-phosphoglycerate; ATP, adenosine 5´-triphosphate; mTORC1, mTOR complex 1; a-KG, a-ketoglutarate; RTK, receptor tyrosine kinase (DeBerardinis and Chandel, 2016)

Cancer cells often redirect their energy metabolism to an aerobic glycolysis to meet the needs of rapidly dividing cells (Vander Heiden *et al.*, 2009; Cairns *et al.*, 2011; Soga, 2013). Aerobic glycolysis is the metabolic process that converts glucose into lactate even under aerobic conditions, while normal cells completely oxidise glucose in the mitochondria. This metabolic phenomenon of cancer cells was first noticed by Warburg and was initially thought to be caused by inherent mitochondrial dysfunction in tumour cells (Warburg, 1925; Warburg, 1956). However, accumulating evidence has indicated that tumour cells do not display

overt defects in oxidative metabolism and that mitochondria can contributes to Adenosine triphosphate (ATP) synthesis and cooperate with aerobic glycolysis to support anabolic reactions (Zu and Guppy, 2004; Vyas *et al.*, 2016). Furthermore, glutamine oxidation in the mitochondria is another major source of ATP production in tumour cells which contributes to the anabolic precursors synthesis (Fan *et al.*, 2013).

GBM cells, like other cancer cells, have been reported to exhibit the Warburg effect (Deberardinis *et al.*, 2008; Jones and Thompson, 2009; Poteet *et al.*, 2013; Xing *et al.*, 2017). Hypoxia, which is a hallmark for GBM as already mentioned, can cause stimulate the Warburg effect and induce acidosis through a shift in cellular metabolism from oxidative phosphorylation to glycolysis that generates a high acid load in the tumour microenvironment (Semenza, 2003; Pouysségur *et al.*, 2006). However, tumour cells can adapt to this excess in acidosis by inducing the activity of HIF which in turn enhances the expression of a number of pH regulating pathways that cope with acidosis such as carbonic anhydrase IX (CAIX), carbonic anhydrase XII (CAXII) and monocarboxylate transporter 4 (MCT4) which acts to maintain the extracellular pH environment of tumour cells and allows for adaptation to hypoxia (Chiche *et al.*, 2009). Due to the fundamental role of metabolic reprogramming in GBM progression, current research is focusing on targeting cell metabolism in GBM tumours as attractive potential therapy (Poteet *et al.*, 2013; Hujber *et al.*, 2018; Su *et al.*, 2018; Crunkhorn, 2019; Shi *et al.*, 2019; Sun *et al.*, 2019).

1.4.5.3. Promoting survival and resisting cell death

Resisting programmed cell death is a main contributing factor in GBM development and progression, and that occur by deregulation of multiple key signalling pathways including PI3K/AKT/mTOR pathway, NF-κB pathway, B-cell lymphoma 2 (BCL-2) family and IAPs (Wang *et al.*, 2004; Verhaak *et al.*, 2010; Qiu *et al.*, 2012). Cell death could occur as a result of apoptosis, necrosis or autophagy (Leist and Jäättelä, 2001).

Apoptosis

Apoptosis is an essential mechanism of programmed cell death, which is responsible for the destruction and elimination of the cells in controlled steps (Elmore, 2007). Apoptosis plays an important role in tissue homeostatic balance between cell proliferation and cell death to maintain the cell population. In addition, apoptosis functions as a defence mechanism such as in immune reactions or when cells are damaged by diseases (Elmore, 2007; Fulda *et al.*, 2010; Cheung *et al.*, 2012).

The apoptosis mechanism acts in a very complex and sophisticated manner including an energy dependent cascade of molecular events that mainly involve two apoptotic pathways, the extrinsic and the intrinsic pathway (Fig 1.8) (Elmore, 2007; Chen *et al.*, 2013). However, there is a relationship between the two pathways and the agents in one pathway can affect the others (Elmore, 2007). Another pathway of apoptosis involves T–cell mediated cytotoxicity as well as perforin-granzyme-dependent killing of the cell that is mediated by granzyme-B or granzyme-A (Brunner *et al.*, 2003). All these pathways meet on the same terminal or execution pathway, which is initiated by the cleavage of caspase-3 and leads to DNA fragmentation, cellular degradation, apoptotic bodies formation and ligands expression in order to be recognised by phagocytic cells (Elmore, 2007; Andoniou *et al.*, 2014).

a) Extrinsic pathway

This pathway involves transmembrane receptor-mediated interactions. It triggers apoptosis following binding of death ligands with a member of the tumour necrosis factor (TNF) receptor gene family (Locksley *et al.*, 2001). These receptors contain cysteine-rich extracellular domains and an 80 amino acid cytoplasmic domain (namely “death domain”), which are essential in transmitting death signal from cell surface to intracellular pathways (Ashkenazi and Dixit, 1998). The best characterised sequence of events defining the extrinsic pathway are FasL/FasR and TNF-*α*/TNFR1 models (Elmore, 2007). Following ligand binding, some cytoplasmic adapter proteins are employed which contain death domains that bind with the receptors. Binding Fas ligand to its receptor leads to the binding of the adapter protein FADD (Fas associated via death domain) while

binding TNF ligand to its receptor leads to the binding of the adapter protein TRADD (TNFR1-associated death domain protein) with recruiting FADD and RIP (receptor-interacting protein) (Hsu *et al.*, 1995; Wajant, 2002). Dimerization of the death effector domain leads to the association of FADD with procaspase-8 leading to the formation of a death-inducing signalling complex (DISC) and the auto-catalytic activation of procaspase-8. The execution phase of apoptosis is then induced directly when caspase-8 is activated (Kischkel *et al.*, 1995).

b) Intrinsic pathway

This signal pathway induces apoptosis through a different array of non-receptor-mediated stimuli that releases intracellular signals functioning directly on intracellular targets (Elmore, 2007). The Bcl-2 family of proteins regulate the apoptotic mitochondrial events. Bcl-2 family can directs mitochondrial membrane permeability either by the pro-apoptotic proteins (e.g., Bax, Bak, Bad, Bcl-Xs, Bid, Bik, Bim and Hrk) or the anti-apoptotic proteins (e.g. Bcl-2, Bcl-XL, Bcl-W, Bfl-1 and Mcl-1) (Fulda *et al.*, 2010; Wong, 2011). Stimuli triggering the intrinsic pathway can be attributed to the absence of particular growth factors, hormones and cytokines that can result in loss of death suppression, hence inducing apoptosis. Other stimuli of the intrinsic pathway includes, but not limited to, radiation, toxins, hypoxia, severe oxidative stress, viral infections and free radicals (Elmore, 2007; Wong, 2011).

In response to these stimuli, changes occur in the mitochondrial membrane leading to opening of the mitochondrial permeability transition pores (MPTP), loss of mitochondrial membrane potential and release two important groups of pro-apoptotic proteins into the cytosol (Saelens *et al.*, 2004). The first group includes cytochrome *c*, Smac (secondary mitochondria-derived activator of caspase), DIABLO (direct IAP Binding protein with Low pI) and the serine protease Omi/high temperature requirement protein A (HtrA2), which trigger the caspase-dependent mitochondrial pathway (Du *et al.*, 2000; Van Loo *et al.*, 2002; Garrido *et al.*, 2006). Cytochrome *c* can activate caspase-3 by forming the apoptosome complex by its binging to Apaf-1 and procaspase-9, whereas Smac/DIABLO and HtrA2/Omi trigger apoptosis by binding to IAP leading to disruption the interaction of IAP with caspase-3 or -9 resulting their activation (Kroemer *et al.*, 2007; Lacasse *et al.*, 2008; Wong, 2011). The second group of pro-apoptotic proteins produced from

mitochondria in late stage of apoptosis are apoptosis-inducing factor (AIF), endonuclease G and CAD. Both AIF and endonuclease G translocate to the nucleus, and act in a caspase-independent manner and lead to DNA fragmentation and chromatin condensation. However, caspase-activated DNase functions in a caspase-dependent manner and results in oligonucleoosomal DNA fragmentation and greater degree of chromatin condensation (Susin *et al.*, 2000; Joza *et al.*, 2001).

c) Perforin/granzyme pathway

Cytotoxic T lymphocytes (CTLs) can produce cytotoxic effects on tumour cells and virus-infected cells, involving secretion of the transmembrane pore-forming perforin with following insertion of cytoplasmic molecules into the target tissue (Pardo *et al.*, 2004). The most pivotal components within these molecules are the serine proteases granzyme A and granzyme B (Pardo *et al.*, 2004; Elmore, 2007). Granzyme B activates apoptosis by direct or indirect caspase activation (caspases-3 and -8) leading to disruption of mitochondrial membrane integrity though cleavage agents like ICAD (Inhibitor of Caspase Activated DNAase) (Brunner *et al.*, 2003; Pardo *et al.*, 2004; Elmore, 2007). It also has been shown that granzyme B can employ the mitochondrial pathway to amplify death signal by cleavage of Bid and promoting cytochrome c release (Barry and Bleackley, 2002). Additionally, direct activation of caspase-3 can occur by granzyme B and both mitochondrial and direct activation of caspase-3 have been suggested to be essential for granzyme B-induced killing (Goping *et al.*, 2003). Another component affecting cytotoxic T cell induced apoptosis and activation of caspase independent pathways is granzyme A. The granzyme-A pathway induces apoptosis though damage of single stranded DNA (Martinvalet *et al.*, 2005). Granzyme A activates DNA fragmentation by DNase NM23-H1, a tumour suppressor gene product which plays a vital role in immune surveillance through inducing apoptosis in tumour cells (Fan *et al.*, 2003).

d) Execution pathway

This is the final pathway of apoptosis that occurs by the activation of the execution caspases. Within this pathway, nuclear material and cytoskeletal proteins are degraded by cytoplasmic endonuclease and proteases. The set of caspases 3, 6 and 7 are the main effectors, leading to cleavage of various substrates including

cytokeratins, poly(ADP-ribose) polymerase (PARP), the nuclear protein NuMA and others, which eventually results in the morphological and biochemical changes observed in apoptotic cells (Slee *et al.*, 2001). The most effective caspase is caspase-3 which is activated by initiator caspases-8, -9 or -10, leading to cleavages ICAD, hence activating the endonuclease, caspase-activated DNase, which in turn degrades chromosomal DNA in the nuclei and leads to chromatin condensation (Sakahira *et al.*, 1998; Yang *et al.*, 1998).

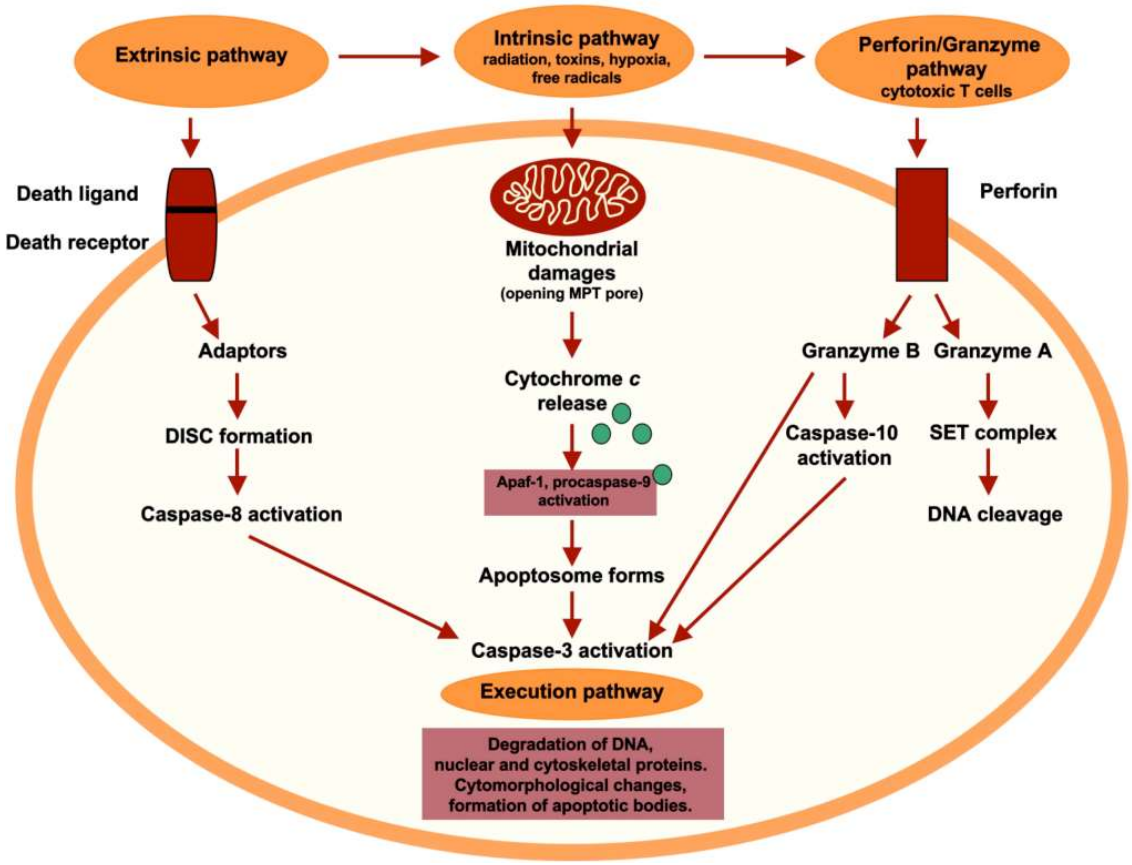

Figure 1. 8. Schematic representation of the three apoptotic pathways, intrinsic, extrinsic and perforin/granzyme. Each pathway requires specific triggering signals to commence an energy-dependent cascade of molecular events. All three pathways merge in the end to activate the executioner caspase-3 leading to cytoskeletal reorganization, chromatin condensation, and nuclear fragmentation and ultimately leading to formation of apoptotic bodies and cell death. However, granzyme A works in a caspase-independent fashion. Adapted from (Elmore, 2007).

Tumour protein 53 (P53) gene has an important link to apoptosis and is known as the most common mutation found in all human cancers (Kandoth *et al.*, 2013). Mutations or deficiencies in p53 genes leads to reduced apoptosis and is associated with tumour development and poor patient prognosis (Lowe and Lin,

2000). In GBM, P53 has been reported to be mutated 25-30% in primary tumours and 60-70% in secondary tumours (England *et al.*, 2013).

Necrosis

Necrosis is an alternative but less regulated process of cell death when compared to apoptosis. Necrosis is considered a toxic process where the cell is exposed to killing in an energy-independent mechanism unlike apoptosis (Majno and Joris, 1995). Apoptosis is controlled and an energy dependent mechanism that can influence individual or groups of cells, whereas necrosis is a passive uncontrolled process and can affect a wide range of cells. Necrosis is mediated by two main mechanisms including the interference with the energy supply of the cell and the direct damage to cell membranes (Majno and Joris, 1995). Several stress stimuli have been reported to trigger necrotic cell death such as ischemia, hypoxia, hypoglycaemia and exposure to DNA alkylating agents (Vanlangenakker *et al.*, 2008; Fulda *et al.*, 2010). However, reactive oxygen species and calcium are considered the main stimuli of a necrotic cell death (Vanlangenakker *et al.*, 2008). Although the mechanisms of necrosis and apoptosis differ, there is an overlap and crosstalk between the two processes. For example, factors such as depletion of intracellular ATP and decrease in the availability of caspases can convert an on-going apoptotic process into a necrotic process (Levin *et al.*, 1999; Denecker *et al.*, 2001; Elmore, 2007).

Autophagy

Autophagy is classified as another form of cell death alongside apoptosis and necrosis, yet is also considered as protective mechanism under specific stress conditions (Azad *et al.*, 2009). Macroautophagy (usually referred to as autophagy) is the process of the engulfment and degradation of intracellular damaged organelles, protein aggregates and other cytoplasmic contents inside vesicles known as autophagosomes resulting in amino acids, ATP and other small biomolecules recycled for reuse (Fig 1.9) (Levine and Kroemer, 2008; Mizushima *et al.*, 2008).

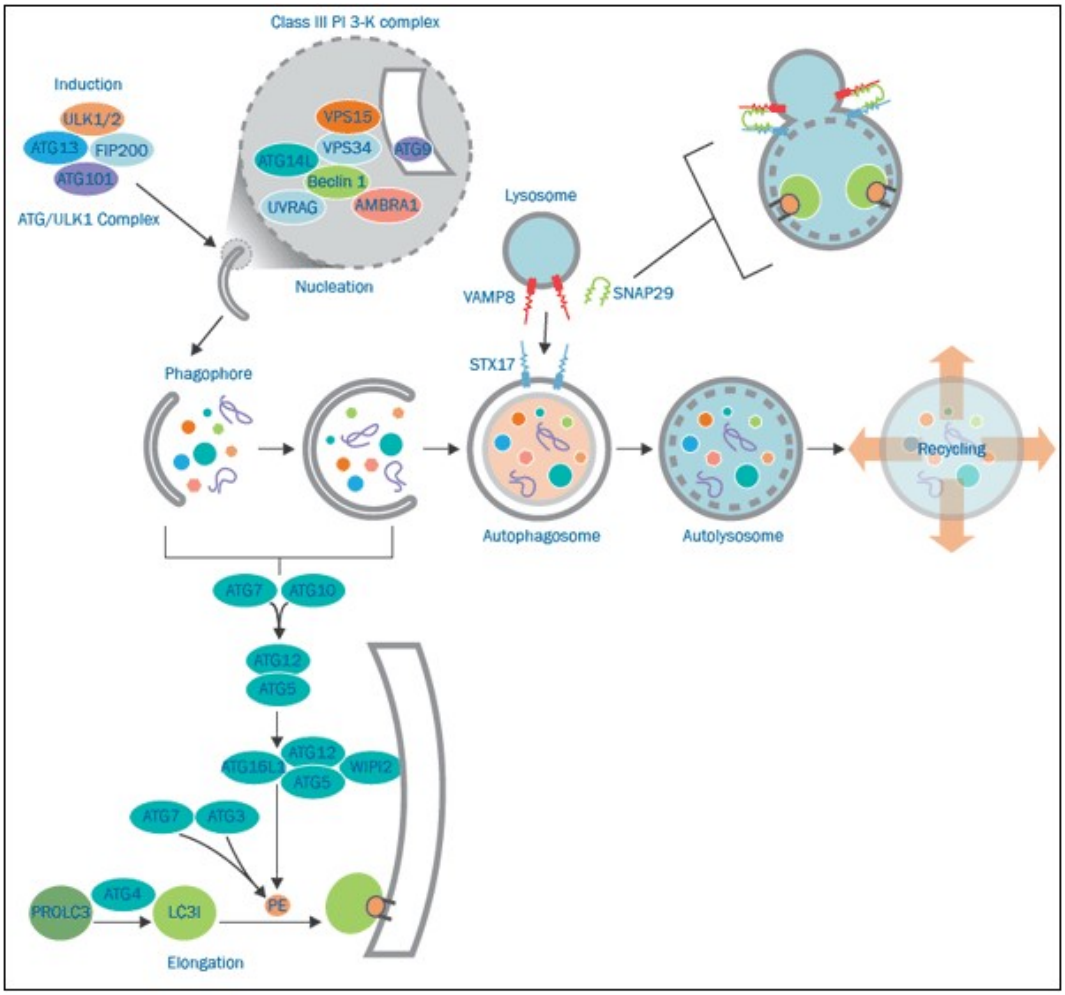

Figure 1. 9. Autophagy signalling pathways. The process of autophagy involves a series of events including induction, nucleation (Phagophore formation), elongation (Autophagosome formation), fusion with lysosome and degradation in the autolysosome. ATGs; autophagy related proteins, ULK1; unc-51-like kinase 1, RB1CC1; RB1-inducible coiled-coil 1, VSP; vacuolar protein sorting, PI 3-K; phosphatidylinositol 3-kinase, LC3; light protein chain 3, PE; phosphatidylethanolamine, STX17; syntaxin 17, VAMP8; vesicle associated membrane protein 8, SNAP29; synaptosome associated protein 29. (Source: Novus Biologicals).

Different factors can induce the autophagic process such as starvation, nutrient deprivation, growth factor depletion, innate immune signals, pharmacological agents, hypoxia, infection, and disease (Apel *et al.*, 2008; Azad *et al.*, 2009; Ravikumar *et al.*, 2009). Any of these conditions is able to initiate the first step in the autophagy process; nucleation step which requires ULK1/ATG1 kinase complex and the VPS34/Beclin-1 complex to form the PI3-K (phosphatidylinositol 3-kinase Class lll) complex including ATG14, VPS15 and VPS34 (Fig 1.9). This complex phosphorylates lipids and recruits ATGs to the new membrane and form a small vesicular sac known as phagophore. The elongation of the phagophore requires the majority of ATG proteins to promote the lipidation of LC3-II.

Phagophore membranes expand resulting in a double-membrane vesicle (autophagosome) and enclose a part of cytoplasm along with organelles and proteins placed in the inner phagophore membrane. LC3 is considered one of the few ATG proteins to remain with the autophagosome after its completely formed making it a suitable marker the number of autophagosomes (Levine and Kroemer, 2008; Mizushima *et al.*, 2010). Upon forming the autophagosome, the maturation stage takes place by fusion of the completed phagosome with the lysosome, acidic pH single membrane vesicle, forming the autolysosome where degradation of the captured content occurs by acidic hydrolases (Ravikumar *et al.*, 2009). There are different types of autophagy which can be selective or nonselective. Selective autophagy includes, but not limited to, peroxisomes (pexophagy), mitochondria (mitophagy), ubiquitinated proteins aggregates (aggrephagy) and others (Weidberg *et al.*, 2011; Lee *et al.*, 2012; Till *et al.*, 2012).

Autophagy is an important process in cancer where it is known to play two roles. The first role is preventing cancer through immunesurveillance, which represents the immune system elimination of potential tumorigenic cells before occurrence of malignant lesions (Ma *et al.*, 2013). In addition, proteins present in the pre-malignant cells that prevent malignant transformation induce autophagic responses. Alternatively, proteins having oncogenic potential inhibit the autophagy process (Morselli *et al.*, 2011). On the other hand, autophagy sustains tumour cell survival and proliferation when exposed to stress conditions promoting tumour growth (Guo *et al.*, 2013). Although autophagy is considered cytoprotective of tumour cells, excessive autophagy has been involved in autophagic cell death (Su *et al.*, 2013). As stated earlier, autophagy is activated as a result of intracellular and environmental stress, therefore, GBM therapies including radio and chemotherapy have been shown to upregulate cytoprotective autophagy most likely due to stress induced by damaged DNA, proteins and organelles (Amaravadi *et al.*, 2011). Consequently, recent studies have extensively investigated the effects of autophagy inhibition in combination with the standard and novel therapies of GBM (Palumbo *et al.*, 2012; Ma *et al.*, 2017; Buccarelli *et al.*, 2018; Lohitesh *et al.*, 2018).

1.5. Current Treatment of GBM

The standard treatment for newly diagnosed GBM patients includes maximal surgical resection of the tumour followed by radiotherapy and/or adjuvant chemotherapy (Stupp *et al.*, 2005; Stupp *et al.*, 2015). Surgical removal represents the first therapeutic approach to reduce the tumour mass and perform a histopathological and molecular diagnosis, with longer overall survival observed in patients with a greater extent of resection (Mcgirt *et al.*, 2009). However, as mentioned earlier, the extremely infiltrative nature and the finger-like tentacles of glioblastoma make it difficult for many surgeons to determine the tumour's margins and completely remove the tumour with common surgical techniques (Lonardi *et al.*, 2005). In fact, the extent of surgery and intensity of therapy is considered carefully as the brain has nearly terminally differentiated cells that could be damaged irreversibly which adversely affect the neurological and cognitive functioning of the patients (Lara-Velazquez *et al.*, 2017). As a result, advances in surgical approaches have been developed aiming to achieve optimal safe resection, and some tools have shown promising results in preclinical experiments for brain cancer (Lara-Velazquez *et al.*, 2017).

After surgery, most GBM patients will undergo ionizing radiation therapy for 6 weeks as well as concurrent chemotherapy with temozolomide (TMZ), where radiotherapy/temozolomide followed by maintenance temozolomide has become the worldwide standard of care for patients with newly diagnosed GBM (Stupp *et al.*, 2009; Paolillo *et al.*, 2018). Treatment begins with a 75 mg/m^2 dose of TMZ daily while patients are receiving radiation and increases to 150-200 mg/m^2 for five consecutive days, every four weeks, for a total of 6 months (Grossman *et al.*, 2011). This has shown only a moderate increase in survival rates, between 12.1 and 14.6 months with the majority of patients suffering treatment failure, largely due to therapeutic resistance (Stupp *et al.*, 2005).

Despite aggressive surgical resection and chemotherapy, almost all (90%) of GBM patients undergo tumour recurrence within 2 cm of the original tumour (Wen and Kesari, 2008; Milano *et al.*, 2010). Most patients with recurrent GBM are unable to undergo further surgical resection and options include systemic chemotherapy: retreatment with TMZ or other alkylating agents (carmustine,

lomustine), platinum drugs (cisplatin), or the VEGF inhibitor, bevacizumab (Aapro and Alberts, 1981, Goldberg et al., 2004,). However, the treatments are not curative and are usually linked to strong side effects that negatively affect patient wellbeing (Aapro and Alberts, 1981; Goldberg *et al.*, 2004; Hesketh, 2008), and ultimately patients die of this disease (Alifieris and Trafalis, 2015).

1.5.1. Radiotherapy

In addition to surgery, radiotherapy remains the most effective treatment option for GBM as it is proven to prolong survival of the GBM patients (Grossman and Batara, 2004; Preusser *et al.*, 2011). The advances in the technical delivery systems of radiotherapy have led to additional successful clinical outcomes with decreased toxicity and helped to retain the radiotherapy as a cornerstone of GBM treatment regime (Suzuki *et al.*, 2003).

As early as the 1940s, radiotherapy was used to treat brain tumours with kilovoltage X-rays (Walker *et al.*, 1979), and by the 1960s the treatment relied on exposing the whole brain to megavoltages of X-ray or cobalt teletherapy at a dose of 45-60 gray (Gy) with an improved survival from 4 to 6 months (Edland *et al.*, 1971). Radiotherapy techniques then developed into a two-phase technique with an initial phase of whole brain radiotherapy to 30-46 Gy followed by a boost to the tumour of an extra 20-30 Gy, showing 12 months survival (Brisman *et al.*, 1976). In the 2000s, the radiotherapy technique using single-phase (MV) 60 Gy followed by TMZ improved the survival to 14 months (Stupp *et al.*, 2005).

Afterward, in the 2010s, the discovery of intensity-modulated radiotherapy (IMRT) has allowed delivery of a high dose of radiation to a target while sparing surrounding critical structures (Reddy *et al.*, 2012). This technique was conducted by delivering various beamlets of radiation from many angles incident on a target. All locations within the target can receive different doses of radiation simultaneously. This technique achieves better standard aims of radiotherapy, when compared to the conventional 3D conformal radiotherapy, by delivering a high dose of radiation to the target and protecting the normal tissues. The benefits of IMRT including better target coverage, dose conformity with complex shape and reduced toxicity, can only be achieved in combination with the use of image-

guided radiotherapy (IGRT) in the purpose of accurate targeting (Burnet *et al.*, 2014). An innovative radiotherapy technique, volumetric-modulated arc therapy (VMAT), has emerged in the same period and is increasingly being used in the treatment of GBM because of the advantages of short treatment time over IMRT while keeping excellent dosimetry. Both radiotherapy techniques IMRT/VMAT (MV) 60 Gy + TMZ have shown 19-22 months survival of glioblastoma patients (Panet-Raymond *et al.*, 2012).

Despite this development in radiotherapy strategies, it is still producing poor prognosis where the high preponderance of hypoxic areas in GBM has been revealed to highly increase resistance to radiotherapy and requires a higher dose of radiation compared with the well-oxygenated cells in order to achieve cell death. Therefore, the hypoxic tumour cells may persist after radiation and divide leading to the development of an even more aggressive tumour phenotype. Furthermore, radiotherapy has been shown to be accompanied with some drawbacks such as causing learning difficulties in children or leading to additional tumours such as meningioma (Merchant *et al.*, 2010). Also, radiotherapy has not been recommended for elderly patients since it can put their life under higher risk, and it can only be applied when the tumour is growing rapidly and damaging the normal brain cells (Combs *et al.*, 2008). In order to improve patients' survival and reduce the toxicity related to treatment, radiation oncology needs to continue to develop the delivery, target definition and dose of radiotherapy to GBM patients.

1.5.2. Temozolomide

Temozolomide is an orally available DNA alkylating agent that was first licensed in 1999 and became the frontline treatment for GBM in 2005 where it remains to this day (Omar and Mason, 2009; Stupp *et al.*, 2015). It is used widely because of its ease of administration, excellent uptake and distribution behaviour, synergism with adjunctive radiotherapy, and low toxicity profile compared to other chemotherapy drugs on the market. On top of that, temozolomide shows excellent penetration of the blood brain barrier due to its small size and lipophilic properties with direct evidence of tumour localization (Agarwala and Kirkwood, 2000; Spiro *et al.*, 2001).

TMZ is an imidazotetrazine prodrug that undergoes hydrolytic ring opening at neutral or alkaline pH under purely chemical non-hepatic dependant control producing the active alkylating agent, MTIC, which is then hydrolysed to AIC and diazomethane (Fig 1.10) (Wheelhouse and Stevens, 1993). The therapeutic action of TMZ depends on its ability to add methyl groups to the purine bases of DNA by diazomethane causing lesions at different positions of DNA. The majority (70%) of the methyl groups transferred appear at N7-Guanine (N7-MG) sites with only about 10% at N3-Adenine (N3-MA) and 5% at O6-Guanine (O6-MG) (Denny *et al.*, 1994; Zhang *et al.*, 2012). This methylation damages the DNA and triggers a cascade of processes resulting in apoptosis of the GBM cell (Patel *et al.*, 2014).

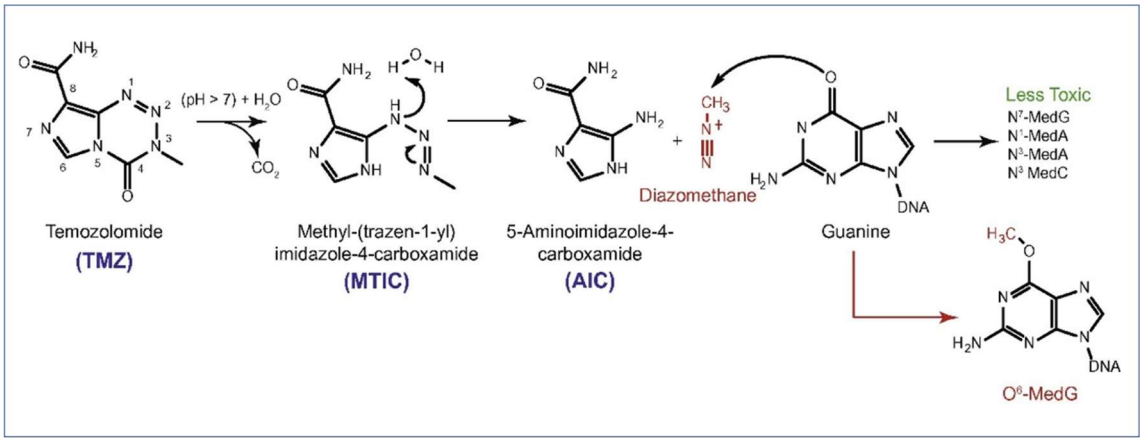

Figure 1. 10. Mechanism of action of TMZ. (Rai *et al.*, 2016).

Although TMZ is the most widely used treatment for GBM, it has a critical disadvantage since the tumour becomes resistant to TMZ and treatment is no longer efficacious (Yung *et al.*, 2000; Hegi *et al.*, 2004). The DNA repair in the malignant cells could happen through the MGMT methylation gene which encodes the O_6-alklyguanine DNA alkly transferase protein, and is critical for repair of methylated guanine residues protecting cells (particularly GSCs) from alkylating agents and limiting their efficacy (Liu *et al.*, 2006; Melguizo *et al.*, 2012). The methylation status of the MGMT promoter is common in GBM (~45%) and indicates increased efficacy of the treatment and more favourable patient survival (Hegi *et al.*, 2005). The methylation and silencing of MGMT has been long proposed as a prognostic marker, however, the accuracy of this as the independent predictive factor for GBM has frequently been debated (Fietkau *et al.*, 2013). Recent methods employing IDH1 status with MGMT has shown

improvements in predictive accuracy and personalized treatment strategies in glioblastoma (Thon *et al.*, 2013; Molenaar *et al.*, 2014).

1.5.3. Cisplatin

Cisplatin or cis-diamminedichloroplatinum (CDDP) is considered one of the most potent and widely utilised chemotherapeutic drugs, which has been used as a first-line treatment for a wide spectrum of solid tumours, such as ovarian, lung, bladder, testicular and colon cancer (Frezza *et al.*, 2010). It has been also used in childhood brain and CNS tumours and as adjuvant therapy in gliomas (Van Den Bent *et al.*, 2006; Singh *et al.*, 2010; Calogero *et al.*, 2011). Although it is widely used for the treatment of brain tumours, however, it represents a standard protocol for medulloblastoma but not glioblastoma, despite the fact that it is also efficacious against glioblastoma *in vitro* (Pérez *et al.*, 2019). In the past 10 years, a plethora of phase I and II studies have explored the safety and efficacy of TMZ combined with conventional chemotherapeutics including cisplatin for progressive or recurrent GBM (Brandes *et al.*, 2004; Silvani *et al.*, 2004; Capdevila *et al.*, 2014).

The mechanism of cisplatin action arises mainly from DNA intercalation (Fig 1.11). Cisplatin enters cells by both passive diffusion and active uptake and then undergoes a spontaneous aquation reaction whereby a chloride ion is replaced by a water molecule (Holzer *et al.*, 2006; Seo *et al.*, 2007). This results in binding to the nitrogen in the N7 position on purine bases with loss of the water molecule forming DNA-protein and DNA-DNA inter-strand and intra-strand cross-links (Eastman, 1987). The cross-linking in the DNA interferes with DNA replication and transcription causing cell cycle arrest leading to activation of DNA repair pathways which ultimately triggers apoptosis of the malignant cell (Dasari and Tchounwou, 2014).

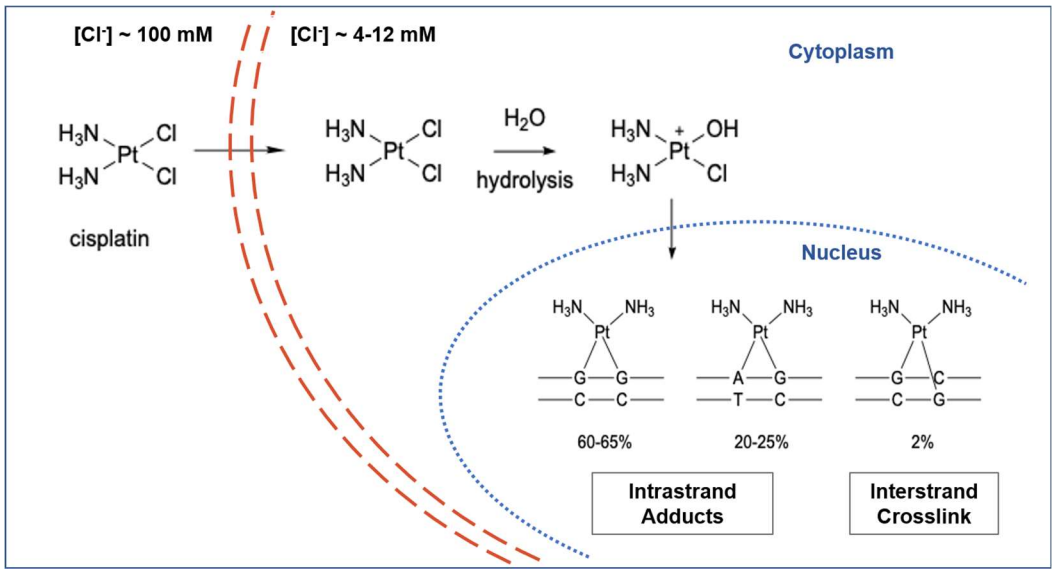

Figure 1. 11. Cisplatin activation and mechanism of action. Adapted from (Rocha *et al.*, 2018).

Though the efficacy of cisplatin is high, its clinical use is limited because of the dose-dependent toxicity on normal tissue. Systematic administration of cisplatin produces considerable side effects including severe kidney problems, allergic reactions, decreased immunity to infections, gastrointestinal disorders, haemorrhage, and hearing loss especially in younger patients. To lessen these effects, cisplatin is often given as a combination with other therapies to reduce the side-effect profile of the treatment, however cisplatin resistance remains a significant challenge (Mori *et al.*, 2003; Momekov *et al.*, 2006).

Patients develop relatively rapid cellular resistance to cisplatin with different mechanisms of resistance being described and typically with multiple forms being found at a same tumour site (Dasari and Tchounwou, 2014). In fact, cancer cells may lose their sensitivity to cisplatin cytotoxicity as a result of different genetic or epigenetic defects. These defects can cause a reduction in cisplatin accumulation within the cells either by affecting the actual binding of cisplatin to its targets, hence reducing its uptake, or by promoting its efflux from the cells (Mamenta *et al.*, 1994; Miyashita *et al.*, 2003). Additionally, cell resistance can occur due to an increased ability to repair the DNA damage or by impaired transmission of signals induced by cisplatin leading to a failure of apoptotic pathways (Mamenta *et al.*, 1994; Miyashita *et al.*, 2003; Siddik, 2003). Notably, cisplatin resistance is generally multifactorial. This explains, in part, why efficient strategies to increase

the sensitivity of malignant cells to cisplatin are still lacking despite a prolonged and intense wave of investigation.

Due to the highly toxic nature of cisplatin and the cellular resistance, other platinum-containing drugs have been developed in an attempt to reduce the side effects and enhance treatment efficacy (Fig 1.12) (Dasari and Tchounwou, 2014). For example, oxaliplatin has been evaluated for the treatment of GBM, but only marginally improved the overall survival of patients and caused significant side effects (Charest *et al.*, 2012). Further platinum-based drugs, nedaplatin, lobaplatin and eptaplatin, have gained regionally limited approval in Japan, China and South Korea, respectively, for the treatment of specific forms of cancer (Momekov *et al.*, 2005). Different cisplatin analogues have been evaluated in several clinical trials, but only one, carboplatin, has provided a definite advantage over cisplatin and achieved worldwide approval (Dasari and Tchounwou, 2014). Although carboplatin has eliminated nephrotoxicity, the reduced cytotoxicity means that 4-fold dose increase is required to match cisplatin's efficacy (Browning *et al.*, 2017).

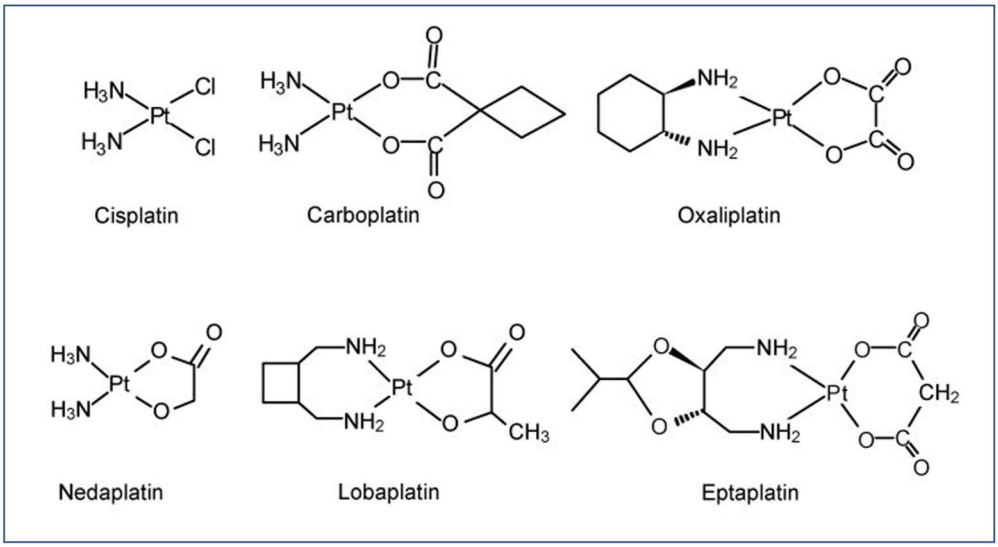

Figure 1. 12. Platinum-based drugs currently in clinical use (Yu *et al.*, 2008).

1.6. New approaches for GBM treatment

As the current standards of treatment for GBM still result in a very poor prognosis for patients, researchers are continuously looking for novel therapies in order to combat this. New techniques are being developed to work alongside and enhance existing treatments with a variety of strategies ranging from exploiting electromagnetic energy fields to developing personalised patient treatments (Carlsson *et al.*, 2014). Additionally, novel treatment methodologies and several pharmacological drugs have been developed against GBM and some are currently in, or have completed, clinical trials. The new strategies include mechanical solutions, immunotherapy, inhibition of DNA repair mechanisms, or repurposing existing medications. Although some of these drugs have shown promising efficacy, the clinical outcome still remains dismal (Wen and Kesari, 2008; Paolillo *et al.*, 2018). However, developing new therapeutic approaches for GBM requires more sophisticated approaches which consider the complex microenvironmental architecture of GBM, the multiple signalling, and cross communications between cells, and potentially targeting these features for GBM treatment.

1.6.1. Tumour Treating Fields (TTFs)

TTFs have been approved to be used as an effective, antimitotic treatment with limited toxicity in patients with newly diagnosed and recurrent GBM (Chaudhry *et al.*, 2015; Burri *et al.*, 2018). This technique is applied by the Novocure Optune device that delivers intermediate frequency (100-200 KHz), low intensity (1-2 V/cm), alternating electric fields within the patients' tumours through disposable ceramic transducer arrays located on the patients's shaved scalp (Salzberg *et al.*, 2008; Pless *et al.*, 2013). TTFs have shown antiproliferative characteristics *in vitro* and *in vivo* (Kirson *et al.*, 2007; Giladi *et al.*, 2015), where it significantly influences cells undergoing mitosis, leading to apoptosis, whereas no significant effect is present on nondividing cells (Kirson *et al.*, 2004; Stupp *et al.*, 2012). This impact on replication is considered the basis for TTFs in cancer therapy due to the greater replication rate in tumour tissues than that in normal tissues (Kirson *et al.*, 2007). It is expected that two mechanisms of action of TTFs are involved: microtubule subunit misalignment and dielectrophoretic motion of organelles and macromolecules (Kirson *et al.*, 2007; Stupp *et al.*, 2012). Being that the effect of

TTFs is via physical rather than biological or chemical reactions, the resultant effect is less likely reliant on specific cellular properties, which in turn makes TTFs effective against several tumour types and less susceptible to mutation immunity (Kirson *et al.*, 2007; Mittal *et al.*, 2018). TTFs have recently been added as a new standard of care for GBM patients to maintenance temozolomide chemotherapy (Nabors *et al.*, 2017; Stupp *et al.*, 2017), however, their true therapeutic efficacy has yet to be conclusively established.

1.6.2. Immunotherapy

Immunotherapy has emerged potentially as an attractive and effective strategy for cancer treatment. This treatment approach attempts to reprogramme the innate immune system of the patient to attack and destroy tumour cells by recognising specific antigens found on the tumour cells. Several potential effectors can be targeted through immunotherapy strategies including monoclonal antibodies, vaccination and immunomodulation through pathway inhibitors (Reardon *et al.*, 2014). Overall, early phase clinical trials of immunotherapy have shown encouraging results in GBM, and larger randomized trials are ongoing (Chuang and Lin, 2019).

Monoclonal antibodies (Mabs)

The objective of this type of immunotherapy is to disturb receptor signalling through targeting growth factors receptors like the vascular endothelial growth factor receptor (VEGFR), epidermal growth factor receptor (EGFR), platelet-derived growth factor receptors (PDGFR), or mast/stem cell growth factor receptor (SCFR), which will prevent activation of the downstream signalling pathways (Melstrom and Sentovich, 2017; Sousa *et al.*, 2018). Bevacizumab is a monoclonal antibody that binds to VEGF and inhibits the growth of tumour blood vessels, hence reducing angiogenesis (Diaz *et al.*, 2017). It was utilised in phase II clinical trials as a monotherapy to treat recurrent GBM. Moreover, it showed a median overall survival of 8-10 months resulting in FDA approval (Friedman *et al.*, 2009). However, the addition of bevacizumab to initial chemoradiation did not change the overall survival of the patients (Lai *et al.*, 2011). Additionally, it was observed that the nutritious depletion occurred by VEGF reduction may activate

a tumour escape response and increase the number of invasive cells (De Groot *et al.*, 2010).

Cediranib, another compound with more activity against PDGFR and SCFR, showed similar response rates in initial phase II clinical studies in patients with recurrent GBM to that of bevacizumab. However, in phase III clinical studies, cediranib did not significantly improve the progression-free survival as a monotherapy strategy or when combined with lomustine (Batchelor *et al.*, 2013). Another example is cetuximab, anti-EGFR Mab, which did not demonstrate effectiveness in treatment of recurrent GBM despite its approval for the treatment of other cancers (Jain, 2018).

Ipilimumab, antibody of cytotoxic T lymphocyte-associated antigen-4 (CTLA-4), is also an example of the antibody-based immunotherapy. This drug has been shown to improve the overall survival in patients with advanced stage malignant melanoma (Hodi *et al.*, 2010). Blocking CTLA-4 binding releases T cells from negative regulation allowing activity of immune effectors. The activity of CTLA-4 against malignant glioma as a monotherapy or when combining with cellular vaccination has been reported (Agarwalla *et al.*, 2012). Ipilimumab immunotherapy is in trial in recently diagnosed glioblastoma (Mcgranahan *et al.*, 2019).

Vaccines for GBM

These vaccines were prepared from patients' own tumour tissue. Although some vaccines showed promising findings, none has shown potential curative treatment of GBM (Jain, 2018). DCVax, is a dendritic cell (DC)–based personalised cancer vaccine produced using purified tumour-specific antigen or tumour cell extracts obtained from tumour (Phuphanich *et al.*, 2013). After the DCs with glioma cell antigens are administered to the patient, they present the glioma antigens, activate cytotoxic CD8+ cells and CD4+ T helper cells, and induce tumour cell death (Selznick *et al.*, 2008; Cohn and Delamarre, 2014). Results of the trials on GBM showed that addition of DCVax-L to standard therapy is feasible and safe in GBM patients, and may extend survival (Liau *et al.*, 2018; Johanns *et al.*, 2019). Another vaccine type is recombinant non-pathogenic polio-

rhinovirus chimera (PVSRIPO), which targets the neurotropic poliovirus receptor CD155 that is abundantly expressed on glioblastoma cells and enters these cells. This in turn leads to lysis and production of tumour antigens in addition to molecules recognised by the natural immune cells (Longo and Baden, 2018). As a result, an influx of macrophages, monocytes and DCs into the tumour tissue is occurred to scavenge cellular debris. Additionally, released molecules present a pattern for natural killer (NK) cells and tumour antigens to induce effector T cells to kill more cells. While the preclinical and early clinical studies of (PVSRIPO) have shown significant promise for improved care in GBM, causes of concern remain (Carpenter, 2019).

1.6.3. PARP inhibitors

Being that one of the GBM mechanisms to invade treatment efficacy is the resistance to apoptotic cell death, restoring apoptotic sensitivity can be an important approach to render GBM cells sensitive to drug therapy (Ghobrial *et al.*, 2005). Due to the fact that DNA repair enzyme poly(ADP-ribose) polymerase (PARP) is found at greater levels in tumour cells when compared to normal cells (Galia *et al.*, 2012), PARP may therefore represent a tumour specific therapeutic target (Von Minckwitz *et al.*, 2011). Moreover, PARP-1 specific siRNA, as well as, PJ34 (Hastak *et al.*, 2010) another PARP inhibitor, have shown increased extrinsic apoptosis in GBM cells *in vitro* and *in vivo*. This supports the interference with PARP by RNA silencing or PARP inhibitors to render tumour tissues more sensitive to the cytotoxicity of DNA-damage induced by standard treatment modalities including radiation or alkylating reagents such as temozolomide (Russo *et al.*, 2009; Murai *et al.*, 2014; Gupta *et al.*, 2018).

One of the most effective PARP inhibitors is olaparib, which crosses the blood-brain barrier and has already shown successful outcomes in GBM patients (Karpel-Massler *et al.*, 2014). This type of therapy is able to overcome apoptotic resistance and improve the sensitivity of GBM cells for death receptor-mediated apoptosis caused by TRAIL (Tumour necrosis factor-related apoptosis inducing ligand) through up-regulation of TRAIL receptor 2 (DR5) independent of their *TP*53 status. To obtain an ideal drug combination treatment with limited side effects, a combination therapy of PARP inhibitors with TRAIL agonist, which is

known for its tumour cells specificity, can be used (Karpel-Massler *et al.*, 2014). Olaparib and other targeted therapies are in ongoing clinical trials in adult patients with GBM (Chuang and Lin, 2019).

1.6.4. Repurposing existing medication

Chemotherapy drug development for the treatment of GBM has been associated with significant limitations concerning drug variety and efficacy, with only carmustine, temozolomide and bevacizumab being approved by the FDA and European Medicines Agency (EU) (Fig 1.13) (Basso *et al.*, 2018). Due to the high cost and long time required for production and approval of novel chemotherapeutic agents, in addition to the lack of effective options in GBM treatment, an alternative approach of repurposing currently licenced drugs has been widely considered (Hong *et al.*, 2011; Abbruzzese *et al.*, 2017; Massey and Robertson, 2018). The strategy of drug repurposing has recently emerged as an attractive approach to overcome these challenges by reusing FDA-approved drugs, applying new combinations of drug treatments or making modifications in the formulation of the original drug (Murteira *et al.*, 2014; Abbruzzese *et al.*, 2017). Furthermore, this approach considers the available data about pharmacokinetic, pharmacodynamic, toxicity and safety properties of existing drugs, and allows for faster and less expensive development processes (Murteira *et al.*, 2014). Accordingly, there have been numerous options for drug repurposing against GBM which have shown potential activity to treat GBM *in vitro* and *in vivo* such as antipsychotic drugs, antidiabetic drugs and nonsteroidal anti-inflammatory drugs (NSAIDs) (Thun *et al.*, 2002; Liu *et al.*, 2012; Chae *et al.*, 2016).

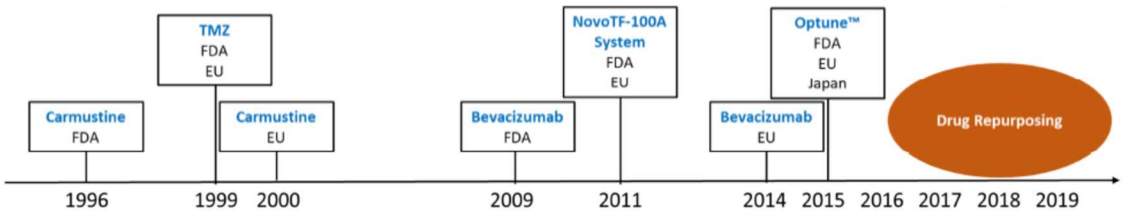

Figure 1. 13. Development of GBM treatment approaches over the last two decades (Basso *et al.*, 2018).

Antipsychotic drugs

Recently, various studies have shown that particular antipsychotics could have anti-tumour effects and have therapeutic potential in GBM. Antipsychotic drugs including pimozide, N-methyl-D-aspartate receptor agonists/antagonists, γ-aminobutyric acid inhibitors and valproic acids show a long clinical utility, tolerable safety in humans, and easily cross the BBB, which is of high importance for GBM therapy (Foster and Kemp, 2006; Rosenberg, 2007; Lapidus *et al.*, 2013).

Valproic acid, an approved drug for treatment of psychiatric disorders, was suggested to be a promising drug for GBM therapy (Driever *et al.*, 1999). Valproic acid has the ability to inhibit glioma cell growth by blocking angiogenesis (Osuka *et al.*, 2012) and promoting differentiation (Berendsen *et al.*, 2012). Furthermore, it can increase the susceptibility of glioma cells to conventional GBM treatment, including TMZ and γ-radiation (Van Nifterik *et al.*, 2012). Another important group of drugs that may have therapeutic potential in GBM is the dopamine receptor antagonists which have been reported to significantly inhibit the tumour formation capability of cancer stem cells (Sachlos *et al.*, 2012). The phenothiazine group including thioridazine, fluphenazine or perphenazine that is known to antagonize dopamine signalling, have shown anti-cancer properties in many glioma cell lines (Gil-Ad *et al.*, 2004).

Additionally, tricyclic neuroleptic drugs such as chlorpromazine induced autophagic cell death in the PTEN-null U87-MG glioblastoma cell line by inhibiting the PI3K/AKT/mTOR pathway (Shin *et al.*, 2013). Another group of antipsychotics includes the selective 5-HT_7 inhibitors such as paliperidone, pimozide and risperidone, which have been reported for their potential utility as an adjuvant chemotherapy in the treatment of GBM (Kast, 2010). However, the disadvantages associated with the use of antipsychotics are the common CNS side effects, such as sedation, dizziness, diarrhoea (Leucht *et al.*, 2013) and more seriously, the extrapyramidal side effects such as akathisia, dystonia and drug-induced secondary parkinsonism (Blair and Dauner, 1992).

Antidiabetic drugs

There have been several antidiabetic agents that have shown potential anti-tumour activity against GBM with recent focus on metformin (Gritti *et al.*, 2014; Sesen *et al.*, 2015). Metformin represent a low toxicity, low cost drug suitable as a repurposed agent, and can readily penetrate the BBB and reach brain cells (Bromage and Yellon, 2015). Repurposing metformin as a cancer treatment option has been already evaluated in a variety of clinical trials for various cancers where it showed adverse effects in tumour cells metabolism by inhibited fatty acid oxidation and mitochondrial gene expression in tumour cells but not normal cells (Lord *et al.*, 2016). In GBM, metformin showed several anticancer activities such as inducing apoptosis and autophagy, inhibiting cell proliferation, reducing angiogenesis and migration (Al Hassan *et al.*, 2018). It also produced adverse effects in the mitochondrial function of GBM cells (Gerthofer *et al.*, 2018). Furthermore, it has reduced TMZ resistance *in vitro* and *in vivo* (Lee *et al.*, 2018) suggesting the potential use of metformin to enhance standard therapy of GBM tumours. Metformin has been shown promising results in grade III glioma but not grade IV glioma and clinical trials are still ongoing (Seliger *et al.*, 2019).

1.7. Non-Steroidal Anti-Inflammatory Drugs

Nonsteroidal anti-inflammatory drugs (NSAIDs) are a family of drugs that can alleviate pain and reduce fevers and inflammatory responses. Most NSAIDs can reversibly inhibit cyclooxygenase (COX) enzyme activity of both COX-1 and COX-2 (Knights *et al.*, 2010). While COX-1 is constitutively expressed in many tissues, COX-2 expression occurs during inflammation and can be induced by extracellular and intracellular stimuli, such as epidermal growth factor (EGF), and this induction is transient (Hirst *et al.*, 1995; Kargman *et al.*, 1996).

Aspirin, also known as acetylsalicylic acid, is unique compared to other NSAIDs, as it is a non-selective COX inhibitor, which irreversibly inhibits both COX-1 and COX-2 iso-enzymes. Aspirin has been used as analgesic, antipyretic, anti-inflammatory and antirheumatic treatment, and it still seems to be the best and first choice among the different types of NSAIDs in recent years (Wennogle *et al.*, 1995; Zhang *et al.*, 2018).

Research has suggested that the regular intake of NSAIDs including aspirin, is associated with a reduction of many types of cancer including colorectal cancer, adenomatous polyps, stomach cancer, prostate cancer, breast cancer as well as promoting their regression (Thun *et al.*, 2002). Additionally, there was observed a significant dose-response relationship between NSAID use and CNS tumours risk (Zhang *et al*., 2017). With respect to brain tumours, epidemiological studies have shown that individuals with a history of NSAID use have decreased risk of developing glioma, whereas use of anti-histamines has the opposite association, and that was attributed to a suggested link between inflammation and gliomagenesis (Scheurer et al., 2011). Several *in vitro* studies on human glioblastoma and rat glioma cell lines have also reported a cytotoxic effect of NSAIDs and aspirin (Kim *et al.*, 2009). More recently meta-analysis study has found that increasing NSAID use, including non-aspirin and aspirin-NSAIDs, associated with significant lower risk of glioblastoma but not meningioma (Zhang *et al.*, 2017).

In fact, it has been assumed that NSAIDs can remove inflammatory factors from the surrounding inflammatory microenvironment of the tumour, thus exposing tumour cells directly to immune cells (Sivak-Sears *et al.*, 2004; Linos *et al.*, 2007; Scheurer *et al.*, 2008; Scheurer *et al.*, 2011). However, there have been multiple mechanisms of action reported for NSAIDs in inhibiting tumours including cyclooxygenase-dependent and independent ways (Gottfried *et al.*, 2013; Xu *et al.*, 2014).

1.7.1. Cyclooxygenase-dependent mechanism

While COX-2 expression is negligible in normal cells, it is frequently expressed in various types of cancers exerting many roles in promoting carcinogenesis, increasing the rate of cancer recurrence (Montezuma *et al.*, 2018) and reducing survival in affected patients (Sharma *et al.*, 2005; Höing *et al.*, 2018), in addition to increasing tumour resistance to chemo and radiotherapy (Wang *et al.*, 2017). In fact, the tumour microenvironment is the main inducer of COX-2 overexpression which exerts multiple signals mostly through prostaglandin E2 and promotes proliferation, angiogenesis, inflammation, invasion, apoptotic resistance and metastasis of cancer cells (Figure 1.5) (Noda *et al.*, 2002;

Hashemi Goradel *et al.*, 2019). For that reason, inhibition of COX-2 may provide a high possibility to exert therapeutic outcomes in cancer.

Notably, administration of COX-2 inhibitors in a preoperative setting could reduce the risk of metastasis in cancer patients (Hashemi Goradel *et al.*, 2019). In addition, COX-2 inhibition sensitizes cancer cells to treatments like radiotherapy and chemotherapy, and antitumor drugs and NSAIDs in combination can produce a better prognosis in tumour therapy (Zhang *et al.*, 2018). The combination of temozolomide and celecoxib was proposed to inhibit glioma progression through anti-angiogenic mechanisms, reducing tumour oedema (Kerschbaumer *et al.*, 2015). Such combinations have been reported to synergistically increase the antitumoral effect for chemotherapeutic agents and improved the overall response when administered before radiotherapy. One study for example has demonstrated a new technique by using nucleophilic substitution to combine cisplatin and aspirin in one molecule which can significantly reduce the drug resistance of cisplatin in tumour therapy (Cheng *et al.*, 2014).

1.7.2. cyclooxygenase-independent mechanism

There are numerous mechanisms by which NSAIDs can exert their anti-proliferative effects via COX-independent activity which include: 1) inhibition or activation of the transcription factor NF-κB (Kopp and Ghosh, 1994; Stark *et al.*, 2001); 2) activation of the p38 MAP kinase pathway with subsequent cyclin D1 degradation (Thoms et al., 2007); 3) activation of p53 and p21 dependent on the ATM serine/threonine kinase checkpoint kinase (Luciani *et al.*, 2007); 4) downregulation of Bcl-2 expression (Yu *et al.*, 2002); 5) upregulation of BCL2 associated X (BAX) or X-Ray Repair Cross Complementing 3 (XRCC3) expression (Dibra *et al.*, 2010); 6) inhibition of protein phosphatase 2A; 7) upregulation of 15-lipoxygenase-1 (Shureiqi *et al.*, 2000); 8) induction of expression of pro-apoptotic DNA repair proteins (Goel *et al.*, 2003); 9) inhibition of epidermal growth factor activation (Pangburn *et al.*, 2010); and 10) selection for microsatellite stability (Ruschoff *et al.*, 1998).

For instance, studies have shown that both diclofenac and ibuprofen repressed cell proliferation and migration of glioma cells; however, although both drugs

inhibited STAT3, only diclofenac reduced extracellular lactate, c-myc and activity of lactate dehydrogenase (LDH)-A (Leidgens *et al.*, 2015). Aspirin, as well, may suppress the growth of cancer cells via mechanisms independent of COX-2 (Henry *et al.*, 2017). Studies have indicated that aspirin may induce apoptosis in GBM cell lines by down-regulating STAT3 signalling dependent on interleukin-6 (Kim *et al.*, 2009). More recent research has shown that aspirin reduces invasiveness and inhibits GBM cell proliferation as well as the induction of apoptosis (Lan *et al.*, 2011).

The data collected from various large epidemiological studies has shown that aspirin reduces the risk of developing multiple cancer types, especially colon cancer and stomach cancer, (Smith *et al.*, 2000; Retsky *et al.*, 2012; Kleinstein *et al.*, 2013). A randomised controlled trial of Lynch syndrome patients revealed that ingestion of a 600 mg daily dose of aspirin for about 2 years was capable of substantially reducing colorectal cancer incidence (Burn *et al.*, 2011). Studies found that long-term use of low-dose aspirin (75–300 mg/daily) can effectively inhibit a variety of cancer incidence, malignant cancer metastasis rate, and provide patients with a high survival rate (Zhang *et al.*, 2018). Aspirin has been also proposed to suppress tumour metastasis mainly by eliminating platelet aggregation proving advantages to secondary tumour development (Jacobs *et al.*, 2007; Algra and Rothwell, 2012). It has been found that regular aspirin use after non-metastatic colorectal diagnosis is associated with a reduced mortality, especially when the primary tumour overexpressed COX-2 (Chan *et al.*, 2009). However, the mechanism of NSAIDs on preventing cancer is still not clear (Zhang *et al.*, 2018).

According to all previous findings, the US Preventive Services Working Group issued primary prevention guidelines on the use of NSAIDs, especially aspirin, for cardiovascular disease and colorectal cancer in 2017, and formally established the role of aspirin in cancer prevention. Inclusive consideration in the guidelines is given that aspirin should be taken at 50–325 mg/ day with emphasis on the need for balancing and individualization between aspirin-induced risks and benefits (Zhang *et al.*, 2018).

1.8. Aspirin analogues

Despite the substantial evidence of the preventative and therapeutic effectiveness of aspirin, its universal usage in cancer prevention and treatment is still controversial due to its potential side effects which cannot be ignored, especially when used for long-term or at higher doses (Lowe, 2001; Deb *et al.*, 2011). These side effects include increased risk of bleeding, increased uric acid, coagulation inhibition, allergic asthma, and both gastrointestinal and renal disturbances (Laine, 2002). Consequently, there has been an overwhelming rationale to identify aspirin-related compounds to improve upon the efficacy of aspirin whilst limiting its side effects.

Efforts have been made to produce a number of salicylate/aspirin derivatives which have been tested for toxicity to cancer cells such as mesalazine (5-aminosalicylic acid) which inhibits the growth of HCT-116 colorectal cancer cells (Gasche *et al.*, 2005; Campregher *et al.*, 2010). Moreover, nitro-derivatives of aspirin (NCX-4016 and NCX-4040) were able to inhibit tumour growth in ovarian cancer xenografts (Selvendiran *et al.*, 2008) and sensitise human colon cancer cells to oxaliplatin (Tesei *et al.*, 2008), respectively. Nitroxyl releasing aspirin prodrugs also exhibited significantly enhanced cytotoxicity compared to aspirin toward non-small cell lung carcinoma cells (A549) in addition to protection against stomach ulceration (Deb *et al.*, 2011; Basudhar *et al.*, 2013).

Perry and Nicholl managed to formulate novel aspirin analogues which have shown promising outcomes and retained the potent antineoplastic effects with reduced adverse effects (Deb *et al.*, 2011). They gained the patent for their invention which related to the use of diaspirin (bis(2-carboxyphenyl)succinate) (BCS) and its derivatives in the treatment of colon and colorectal cancer. It also related to novel derivatives of diaspirin and to a method of synthesising the di-aspirin and its derivatives. Initially, they sought to investigate the capacity of several modified salicylates to inhibit the growth of the colorectal cancer cells as an introduction to examination of any possible structure/activity relationships (Deb *et al.*, 2011). Four categories of compounds with varying degrees of structural similarity to acetylsalicylic acid were synthesised and tested (Figure.1.14).

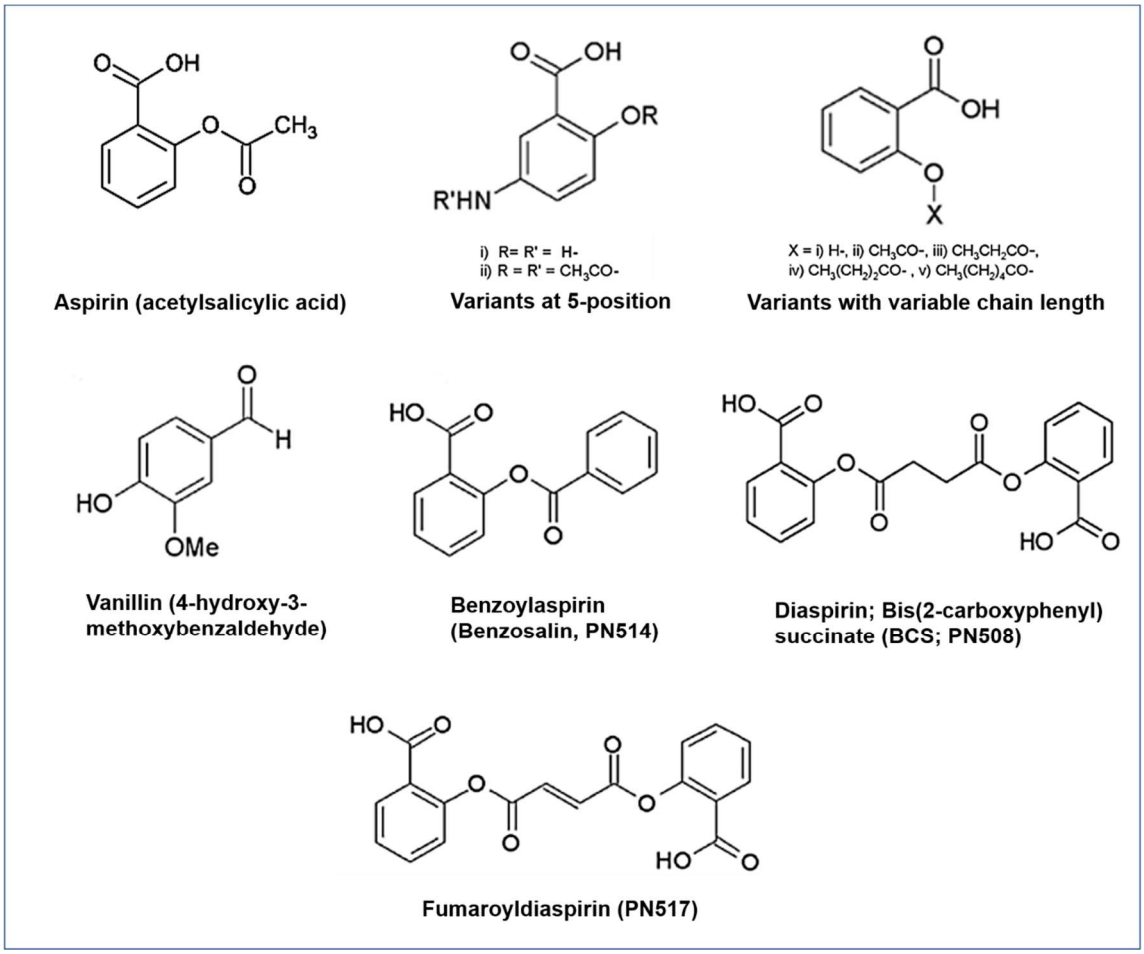

Figure 1. 14. Structure of aspirin analogues compounds. Adapted from (Deb *et al.*, 2011).

Following their preliminary screening, it was found that salicylate compounds with amino and acetamido substituents at 5-position were less toxic than aspirin against SW480 human colorectal cancer cell line. In addition, further extending the hydrocarbon chain length in the acyl groups did not enhance the inhibitory effect of aspirin. However, BCS and other diaspirins derivatives; fumaroyldiaspirin (PN517) and benzoylaspirin (PN514) exhibited significantly greater toxicity than aspirin against SW480 cell line, and this may suggest that the presence of a second nearby aromatic ring is beneficial to a binding relationship in the cytotoxicity of salicylates (Deb *et al.*, 2011). BCS and aspirin were toxic to SW480 cells through initiation of necrotic and apoptotic pathways, indicating that compounds containing two ring structures appeared to induce a greater degree of apoptosis than aspirin. However, aspirin and BCS exhibited substantially less toxicity in the human MCF7 breast cancer and U373 glioma cell line at the conditions studied (Deb *et al.*, 2011).

Later, they generated more novel compounds and extended their investigation on the diaspirins demonstrating that these aspirin analogues had more potent antitumour activity against colorectal cancer cells than aspirin. Additionally, using a syngeneic colorectal tumour model in mice, they found that these agents significantly inhibited tumour growth *in vivo* with no overt side effects being observed. Their mechanistic studies also helped to elucidate structure-function relationships for the aspirin molecule and diaspirins (Claudius *et al.*, 2014).

More recently, their studies aimed to explore the mechanism by which aspirin and its analogues exhibit toxicity to colorectal cancer cells. Additionally, the toxicity of aspirin and aspirin derivatives to oesophageal cancer and colorectal cancer cell lines was investigated in the presence and absence of platins, and they were able to define some derivatives which synergised with cisplatin or oxaliplatin when tested against both cell lines (Kilari *et al.*, 2018; Bashir *et al.*, 2019).

1.9. Rationale

While there is insufficient clinical data to currently support the use of aspirin or its analogues in glioma, further studies on this topic are warranted. Evaluating the efficacy of these novel compounds is also of interest in glioma as it is still relatively new and not fully understood, in comparison to the more extensively researched chemotherapeutic agents TMZ and cisplatin.

In a previously completed project in the lab, the effects of novel aspirin analogues in malignant glioma were initially described. Three glioma cell lines were used in the study; a grade I astrocytoma (1321N1), grade II/III astrocytoma/ oligodendroglioma (GOS-3), and grade IV glioblastoma (U87-MG) in addition to primary glioblastoma cell cultures, BTNW911 and BTNW 914. The effects on cell viability, proliferation, and apoptosis and of four aspirin derivatives (PN508, PN517, PN526 and PN529) was tested. The data from this study showed fumaroyldiaspirin, PN517, to be the most potent analogue of all tested compounds, and in some cases with greater efficacy than cisplatin, suggesting that PN517 represents a novel aspirin analogue with significant therapeutic potential for the treatment of glioma and warranting further investigation (Petinou

et al., 2014). Although high efficacy of the aspirin analogue PN517 was observed in various experiments, it is still essential to further characterise the mechanisms involved in its effects in addition to examining the efficacy of the combinations with another chemotherapeutics.

On the other hand, studies conducted on GBM and its drug therapies rarely consider or maintain the hypoxic conditions which are normally present *in vivo*. As hypoxia is a key regulator in progression of tumours and contributes to therapeutic resistance, it is important that any *in vitro* research is conducted with this in mind. Trying to simulate the GBM tumour microenvironment by keeping the levels of hypoxia consistent with that of the actual *in vivo* environment is crucial to obtaining results which are valid and reflect the activity in GBM tumours. For this reason, the current study is directed towards drug treatments of GBM maintained in various levels of hypoxia in order to observe any changes or differences between drug actions when pO_2 levels are altered.

In summary, this project aimed to evaluate the efficacy of the current and novel chemotherapeutic agents for glioblastoma treatments under normoxic and hypoxic conditions using different cell culture model systems.

Experimental models:

Established cancer cell lines are the main controlled method for long-term research projects in the development of new therapies despite the concern of not inevitably representing what is occurring *in vivo*. Cell lines are considered standard for biological research and preferred by many scientists because of their ease to use and longer life span than primary cells (Kaur and Dufour, 2012). The U87-MG cell line was employed in this study, which is an adherent cell line with an epithelial like morphology, was originally harvested from 44-year-old male patient in 1966 and classified as a grade IV glioblastoma using the 2007 WHO grading (Clark *et al.*, 2010). There are several studies investigating different experimental therapies in U87-MG cells which provide opportunity for comparison and extrapolation. Additionally, the embryonic cell line SVG-p12 served as control in this study. SVG-p12 is an immortalised human foetal glial cell line generated in 1985 by transfecting primary foetal brain cells with a plasmid containing an origin-defective mutant of simian virus 40 (SV40). SVG-p12 cells are adherent

brain cells with a fibroblast morphology (Henriksen *et al.*, 2014; Lou *et al.*, 2014). Both cell lines were investigated under normoxia and hypoxia.

Additionally, most studies examine hypoxia using only short term (24-72 hr) exposure to reduced oxygen levels. However, this may not be representative of tumour cells that have undergone adaptation to the low oxygen environment. For this reason, it was planned to complete cell acclimatisation to hypoxia where the cells can be exposed to decreasing levels of oxygen gradually over a period of approximately 10-12 weeks in order to generate hypoxia adapted cell lines in which the efficacy of the drug treatments could be examined.

On the other hand, the three-dimensional (3D) nature of spheroid cultures more closely replicates the *in vivo* tumour environment than the classical two-dimensional (2D) monolayer cultures, and produces a natural oxygen gradient dropping to lower levels in the spheroid core. With similar cellular and molecular features to that of GBM, 3D spheroids have stolen the spotlight in GBM research and become a priority in order to develop novel targeted therapies against this deadly disease. Therefore, this study also planned to use 3D U87-MG spheroid model that better simulates the various characterises of the real tumour *in vivo*.

Research aim and working hypothesis:

The aim of this research was to assess the effects of PN517, aspirin, temozolomide, and cisplatin both as monotherapies and combination therapies on grade IV glioblastoma tumour using standard cell culture models and applying a variety of experimental conditions. Hence, this project will more closely simulate the GBM tumour microenvironment which is crucial to obtaining results that are valid and reflect potential activity *in vivo*, leading to a better translation of findings in basic research to the clinic. Two key questions were raised: Do aspirin or its analogue PN517 enhance the efficiency of current chemotherapeutic treatments of glioma cell cultures? Does the level of hypoxia during drug treatment *in vitro* affect the efficacy of cisplatin, temozolomide, aspirin, or PN517 on glioma cell cultures?

CHAPTER 2: MATERIALS AND METHODS

2.1. Materials

Aspirin analogue (PN517) was supplied by Dr. Iain Nicholl (Wolverhampton University, UK). All other chemicals used were of the highest grade commercially available and obtained from the following suppliers:

Abcam (Cambridge, UK)

7-aminoactinomycin D (7-AAD), glyceraldehyde-3-phosphate dehydrogenase activity assay kit.

Agilent Technologies (Cheshire, UK)

Seahorse XFp fluxpak containing sensor cartridges, miniplates, and calibrant, Seahorse XFp cell mito stress test kit, Seahorse XFp glycolysis stress test kit, XF base medium.

American Type Culture Collection (ATCC) (Manassas, VA, USA)

SVG-p12 human foetal astroglial cell line.

BD Biosciences (Plymouth, UK)

Purified mouse anti-human HIF-1α, purified mouse anti-HIF-1β/ARNT1

Bioassay Systems (Hayward, CA) or VWR (Leicestershire, UK)

EnzyFluo™ L-lactate assay kit.

Cayman Chemical (Michigan, USA)

Temozolomide.

Cell Signalling, New England Biolabs (Hitchin, UK)

Cyclin D1 rabbit mAb, phospho-cyclin D1 (Thr286) XP® rabbit mAb, anti-rabbit IgG HRP-linked antibody, anti-mouse IgG HRP-linked antibody, autophagy vesicle nucleation antibody sampler kit, stress and apoptosis antibody sampler kit.

EMD Millipore (Watford, UK)

Guava® instrument cleaning fluid (ICF), Guava EasyCyte™ mitopotential kit, tetraethylbenzimidazolylcarbocyanine iodide (JC-1).

Enzo Life Sciences (Exeter, UK)

CYTO-ID® autophagy detection kit.

European Collection of Authenticated Cell Cultures (ECACC) (Porton Down, UK)

U87-MG grade IV human glioblastoma cell line.

Fisher Scientific (Loughborough, UK)

Methanol, phosphate buffered saline tablets, tris base, tris hydrochloride, glycine, sodium dodecyl sulphate (SDS), glycerol, bromophenol blue, dithiothreitol (DTT), triton X-100, sodium hydroxide, sodium chloride, HEPES, ammonium persulfate, amido black 10B, D-(+)-glucose, cell scrapers, gel loading pipet tips.

GE Healthcare Life Sciences (Buckinghamshire, UK)

Amersham ECL prime western blotting detection reagent, Protran nitrocellulose blotting membrane (0.45 µm pore size), PVDF blotting membrane (0.45 µm pore size).

Life Technologies (Paisley, UK)

PrestoBlue® cell viability reagent, Alexa Fluor® 488 annexin V/dead cell apoptosis kit, foetal bovine serum (FBS), carboxyfluorescein diacetate - succinimidyl ester (CFDA-SE), magicMark XP western protein standard, SimplyBlue™ safestain, anti-mouse IgG secondary antibody HRP conjugate, anti- β-actin mouse monoclonal antibody.

Lonza (Slough, UK)

Eagle's minimum essential medium (EMEM, 12-125F), non-essential amino acids (100X), L-glutamine (200mM), trypsin/EDTA (10X), sodium pyruvate (100mM).

Sigma-Aldrich® (Poole, UK)

Trypan blue, ribonuclease A from bovine pancreas, propidium Iodide, cisplatin, aspirin, dimethyl sulfoxide (DMSO), phosphatase inhibitor cocktail 2, protease inhibitor cocktail, carbonyl cyanide 3-chlorophenyl-hydrazone (CCCP), bovine serum albumin (BSA), ethylenediaminetetraacetic acid disodium salt dehydrate (EDTA), copper sulphate, acrylamide/bis-acrylamide (30%(w/v) solution), sodium azide, N,N,N′,N′-tetramethylethylenediamine (TEMED), ponceau-S, 2-deoxy-D-glucose, sodium deoxycholate.

Thermo Scientific (Paisley, Scotland)

Pierce BCA protein assay reagent A, western blotting filter paper, restore western blot stripping buffer, Nunclon Delta surface multi-well plates and flasks, Nunclon Sphera 96-well flat bottom plates, 8-well Lab-Tek® II chambered coverglass, serological pipettes, conical centrifuge tubes.

2.2. Methods

2.2.1. Cell Culture

U87-MG (Grade IV human glioblastoma) and SVG-p12 (human foetal astroglial cells) cell lines were maintained in T75 cm^2 flasks containing Eagles minimum essential media, supplemented with 10%(v/v) foetal bovine serum, L-glutamine (2mM), non-essential amino acids (1%(v/v)), sodium pyruvate (1mM) in a humidified incubator at 37^oC and normal atmosphere (21% O_2) containing 5% CO_2.

2D Monolayer Cultures

When a maximum confluence of 80% was reached, U87-MG and SVG-p12 cells monolayers were washed with phosphate buffered saline (PBS) solution. Trypsin-

EDTA (1X) was added and the flasks were returned to the incubator to allow cells to detach. After detachment, supplemented media was added to neutralise the trypsin and cells were triturated gently to ensure a single cell suspension. Cells were either passaged into freshly prepared flasks to maintain the cell line or seeded into cell culture - treated plates for experimental analysis under both normoxic and hypoxic conditions (21% and 1% O_2, respectively).

For experiments under hypoxic conditions, both cell lines were cultured, treated and maintained at 1% O_2 (unless otherwise stated) using Baker Ruskinn Invivo$_2$ 400 hypoxic workstation which accurately maintains and controls temperature, humidity, oxygen and carbon dioxide with nitrogen balance. Cells were exposed to the hypoxic environment for the whole duration of the experiment to eliminate any perfusion effect except at stages that had to be performed in normoxia such as reading fluorescence in a microplate reader.

Hypoxia-Adapted Cell Lines

For generating hypoxia-adapted cell lines, U87-MG and SVG-p12 cell monolayers were firstly cultured in normoxic incubator (95% air/ 5% CO_2, ~21% O_2) until reached ~80% confluency. Cells were then split and transferred to the hypoxic workstation set at 5% O_2/ 5% CO_2. Media was replaced every other day with hypoxic-equilibrated media and cells were maintained by regular passaging for 3 weeks under these conditions. Cells were then given new passage number (P1, 5% O_2) and either frozen at -80°C and stored in liquid nitrogen for subsequent analysis or split and moved on to the second stage by reducing the O_2 level to 1% with 5% CO_2. Cells were maintained for another three weeks then frozen and stored as (P1, 1% O_2). Some of these cells were split to continue to the third stage by reducing the O_2 to 0.1%. However, the cells were not able to survive longer than one week under these severe hypoxic conditions.

To monitor cell growth of the stored hypoxia-adapted cells, one cryovial of U87-MG and SVG-p12 (P1, 1% O_2) was defrosted directly inside the hypoxic chamber in T75 cm^2 flasks containing 15 ml hypoxic-equilibrated media and maintained to assess cell health and viability. Images were taken with a light microscope after each passage to detect any morphological changes.

3D Spheroid Cultures

The production and characterisation of uniform and reproducible multicellular U87-MG spheroids was established using Thermo Scientific™ Nunclon™ Sphera™ plates. These Flat-bottom 96-well plates have a polymer-coated culture surface that inhibits the binding of extracellular matrix proteins, which mediate cell adhesion.

U87-MG cells were seeded using different numbers of cells (250, 500, 1000, 2500, 5000 cells/well) in 200 µl of complete EMEM media into Nunclon Sphera 96-well plates. Plates were briefly centrifuged at 250 xg for 5 min and then incubated in a humidified incubator at 37°C and 5% CO_2 to monitor spheroid growth over 7 days under normoxia and hypoxia. Cells were re-fed after 72 hr by carefully removing 100µL of medium from each well and replenishing with 100 µl fresh growth medium. The spheroid formation, size, and growth were assessed using an inverted light microscope. After 7 days of spheroid culture, 20 µl of PrestoBlue reagent was added to each well of the plates which were then incubated at 37°C and 5% CO_2 for an additional 1-6 hr before reading on the microplate reader.

Unless otherwise stated, experiments were performed using monolayer cell cultures.

2.2.2. Growth curves

To determine the growth rate and the doubling time for each cell line, growth curve analysis was performed over a period of seven days. U87-MG and SVG-p12 cells were seeded in 6-well plates at a density of 2 x 10^4 cells/1 ml media per well. An extra 2 ml of media was added to each well and the cells were incubated in humified incubator at 37°C under normoxia or hypoxia. Every day post-seeding, cells were harvested by washing three wells with PBS then adding trypsin and allowing cells to detach in the incubator. The trypsin was then neutralised with media and cell suspension was collected from each well and transferred into microcentrifuge tube. The cells were counted manually using haemocytometer and Trypan blue exclusion test using an inverted light microscope. This procedure was repeated every day for 7 days after initial

seeding and the whole experiment was repeated three times with each experiment performed in triplicate, in normoxia, 1% O_2 hypoxia, and 0.1% O_2 hypoxia.

2.2.3. PrestoBlue® Linearity assay

PrestoBlue is a resazurin-based cell permeable viability indicator that is quickly reduced by metabolically active cells changing in colour from blue to red and becoming highly fluorescent providing a quantitative measure of viability and cytotoxicity by changing fluorescence.

As the greatest variable in viability assays is cell number, linearity of fluorescence versus cell number was determined in order to establish suitable working range of cell density. For this purpose, cells were seeded at 50, 100, 250, 500, 1000, and 5000 cells/well in a 100 µl volume of media in 96-well plates and incubated at 37°C overnight under normoxia or hypoxia. Cells were left in the incubator for another 24, 48, or 72 hr before adding PrestoBlue (1:10) for one hour at 37ºC in the dark and measuring the fluorescence by Tecan GENius PRO microplate reader at wavelength Ex/Em= 535/612 nm. This experiment was repeated three times, with each experiment performed in triplicate, both in normoxia and hypoxia.

2.2.4. Drug preparation

Compounds were prepared as stock solutions in media, saline or DMSO, and stored appropriately for the subsequent experimental treatments, then were diluted in complete media prior addition to the cells. Aspirin and PN517 were dissolved in complete media with NaOH (1M) added gradually to adjust the pH until the drug was fully dissolved to produce a stock concentration of 100mM which was stored at -20ºC. Cisplatin was prepared in saline (0.9%(w/v) NaCl) and sonicated for 15 min to achieve solubility and give stock concentration of 3mM which was stored at 4ºC to be used within one month. Temozolomide was solubilised in 100% DMSO to give stock solution of 100mM and stored at -20ºC.

For experimental analysis, drugs were prepared fresh on the day at 10X concentration with media and added at 1:10 dilution to the cells. Vehicle control treatments were included for all experiments by adding equivalent amount of the

final concentration of the solvent. All other drugs were prepared as per manufacturer's instructions unless otherwise stated.

2.2.5. Cell viability assay for mono-therapy.

Concentration - response curves for each drug treatment were generated following 24, 48 and 72 hr of drug treatment in order to assess the concentration and time course dependent effects and to determine the 50% and 25% inhibitory concentrations (IC_{50} and IC_{25}) of aspirin, PN517, cisplatin and temozolomide in both U87-MG and SVP-p12 cell lines under normoxic and hypoxic conditions.

The cytotoxic effect of these compounds was evaluated by PrestoBlue® viability assay. Briefly, cells were seeded at density of 10^3 cells/100 µl media per well in 96-well plates and incubated at 37ºC overnight under normoxia or hypoxia. On the next day, drugs were added to obtain final concentrations of aspirin, PN517 (30µM, 100µM, 300µM, 1mM, 3mM, and 10mM), cisplatin (1µM, 3µM, 10µM, 30µM, 100µM, and 300µM), and temozolomide (3µM, 10µM, 30µM, 100µM, 300µM, and 1mM). Cell viability was tested at each timepoint (as described in section 2.2.3). This experiment was repeated six times with each experiment performed in triplicate, both in normoxia and hypoxia, and concentration-response curves were established and analysed using GraphPad Prism Software.

While generating the hypoxia-adapted cells, concentration - response curves for aspirin were established at the last week of each oxygen stage and prior to reducing O_2 level to the next stage to compare the IC_{50} values after 48 hr of drug treatment for these cells.

2.2.6. Cell viability assay for combination-therapy

The cytotoxic effect of aspirin or its analogue PN517 in combination with temozolomide or cisplatin was tested to examine any possible synergistic effects with the conventional anticancer drugs in comparison to the mono-therapy.

Combination studies were performed by seeding both U87-MG and SVG-p12 cell lines at 10^3 cells/100 µl media per well in 96-well plates and culturing overnight

in a humified incubator at 37°C with 5% CO_2 under normoxia or hypoxia. The combination drug treatments were added by pairing aspirin or PN517 with each of cisplatin or temozolomide at IC_{50} concentrations as determined by the mono-therapy concentration-response curves after 48 hours of drug treatment (different values between normoxia and hypoxia), in addition to applying the mono-therapy for comparison. Cell viability was evaluated by PrestoBlue® assay following 24, 48 and 72 hr of adding drugs (as described in section 2.2.3). This experiment was repeated three times with each experiment performed in triplicate, both in normoxia and hypoxia.

For hypoxia-adapted cells, combination studies were performed using U87-MG and SVG-p12 adapted cells at 1% O_2 hypoxia. This experiment was repeated six times for U87-MG cells and three times for SVG-p12 cells, with each experiment performed in triplicate.

To evaluate the effect of the drug combinations on U87-MG spheroids viability after drug treatment, PrestoBlue viability assay was performed with modification. U87-MG cells were seeded at density of 2500 cell/200 µl media per well in Nunclon Sphera 96-Well plates. The plates were then centrifuged at 250 xg for 5 min and incubated overnight at 37°C and 5% CO_2 under normoxia or hypoxia to form spheroids of 300-350µm diameter. Drug treatments were added on the next day separately or in combination at IC_{50} concentrations as determined by the mono-therapy concentration-response curves after 48 hours. cell viability was assessed after 48 and 72 hr of drug treatment by adding Prestoblue reagent (1:10) and incubating 4 hours at 37°C in the dark and measuring the fluorescence by microplate reader at wavelength Ex/Em= 535/612 nm. This experiment was repeated four times, with each experiment performed in triplicate, both in normoxia and hypoxia.

2.2.7. Live/Dead Fluorescence staining assay

U87-MG spheroids cell viability was evaluated using Live/Dead Viability/Cytotoxicity assay which detects plasma membrane integrity and intracellular esterase activity. U87-MG cells were seeded at density of 2500 cell/200 µl media per well in Nunclon Sphera 96-Well plates. The plates were

then centrifuged at 250 xg for 5 min and incubated overnight at 37°C and 5% CO_2 under normoxia or hypoxia to form spheroids with diameter of 300-350 µm. Drug treatments were added the next day separately or in combinations at IC_{50} concentrations (as determined by the mono-therapy concentration-response curves after 48 hr) for 48 and 72 hr.

At the end of the treatment period, CFDA-SE (50µM) and PI (10µg/ml) stains were added to each well and incubated at 37°C for 30 min, protected from light. After staining, spheroids were rinsed at least three times with half-volume change of PBS and transferred to 8- well chambered coverglass with 1000 µl pipette tip and imaged on fluorescence microscope using 20x lens objective. Z-stack imaging was performed for each spheroid using FITC filter (Ex/Em= 492/517 nm) for CFSE staining and PI filter (Ex/Em= 305/617 nm) for PI staining. This experiment was repeated three times under normoxia and hypoxia.

2.2.8. Cell proliferation and cell cycle assay

The effect of drug treatments on cell proliferation was quantified using the proliferation marker CFDA-SE, which is non-fluorescent until it enters the cells where it is hydrolysed to the green fluorescent dye CFSE. As cells proliferate, the dye passes to each daughter cell halving the amount of fluorescence detected per cell. This assay was combined with cell cycle analysis using propidium iodide (PI) staining, a DNA intercalating agent, which allows for visualisation of cells at each phase of cell cycle by flow cytometry.

Following optimisation process, both the U87-MG and SVG-p12 cells were seeded at a density of 10^5 cells/1 ml media per well in 6-well plates for day 0 non-treated controls, and at 2 x 10^4 cells/1 ml per well in 12-well plates for drug treatments samples then placed in a humidified incubator at 37°C and 5 % CO_2 overnight under normoxia or hypoxia. Prior to drug treatment, cells were treated with CFDA-SE solution (5µM) in PBS for 30 min in the dark, then PBS-CFDA-SE solution was aspirated and replaced with fresh media and incubated for another 2 hours.

The non-treated control CFDA-SE treated cells in the 6-well plates were harvested on ice to establish day 0 staining (as described in section 2.2.2) and centrifuged at 100 xg for 5 min at 4°C. The supernatant was removed, and cell pellets were resuspended in 0.5 ml ice-cold PBS and centrifuged again. PBS was removed, and cells were fixed by adding 0.5 ml of ice-cold 70% (v/v) methanol in PBS. The tubes were mixed well and stored at -20°C for at least 48 hr prior to analysis.

Drug treatments were added to the cells seeded in the 12-well plates, separately or in combinations at IC_{25} concentrations (as determined by the mono-therapy concentration-response curves after 48 hr), and plates were incubated for a further 24, 48, 72, 96 and 120 hours under normoxia or hypoxia. At the end of each timepoint, cells were harvested, fixed and stored in -20ºC.

To conduct cell proliferation and cell cycle analysis, fixed samples were centrifuged at 100 xg for 5 min at 4°C, and washed with ice-cold PBS. Cells were then resuspended in 250 µl of PBS solution containing PI (10 µg/ml) and RNAase (250 µg/ml), vortexed briefly, and incubated for 2 hr at 37°C in the dark as determined by optimisation. On completion of incubation, samples were transferred to a non-adherent 96-well plate/ V-shaped or U- shaped to be analysed by flow cytometry.

Flow cytometric analysis was performed using the Guava EasyCyte™-12HT (Merck Millipore, Darmstadt, Germany) flow cytometer. Samples were gated on forward scatter (FS) versus side scatter (SS) to include the appropriately stained cell population and exclude debris or cell aggregates. Detection was performed using appropriate channels at wavelength of Ex/Em= 492/517 nm for CFSE and 535/617 nm for PI, and a total of 5,000 gated events were acquired for each treatment. This experiment was repeated six times, both in normoxia and hypoxia.

2.2.9. Apoptosis assay

The induction of apoptosis following drug treatment was quantified using a commercially available kit (Alexa Fluor® 488 annexin V/Dead Cell Apoptosis Kit) which allows to identify viable, early apoptotic, late apoptotic, or necrotic cells through differences in phosphatidyl serine (PtdSer) expression and plasma membrane integrity and permeability. Annexin V labelled with a fluorophore can identify apoptotic cells by binding to PtdSer exposed on the outer leaflet. In addition, the kit includes the propidium iodide (PI) nucleic acid binding dye which is impermeable to live cells and apoptotic cells, but stains dead cells with red fluorescence, binding tightly to the nucleic acids in the cell.

According to the manufacturer's instructions and following optimisation processes, U87-MG and SVG-p12 cells were seeded at a density of 25 x 10^3 cells/0.5 ml media per well in 24-well plates and incubated overnight in a humified incubator at 37°C, 5% CO_2 under normoxia or hypoxia. Drug treatments were added to the cells, separately or in combinations at IC_{50} (as determined by the mono-therapy concentration-response curves after 48 hr) and induction of apoptosis was examined after 24, 48 and 72 hr of drug treatment.

At the end of each timepoint, cells were harvested on ice (as described in section 2.2.2) and centrifuged at 100 xg for 5 min at 4°C. The supernatant was removed, and cell pellets were resuspended in 1X binding buffer containing PI (100µg/ml) and annexin-V (1:80) and incubated at room temperature for 15 min. Cells were then centrifuged to remove unbound dye and resuspended with 200 µl of 1X assay buffer and transferred to a non-adherent 96-well plate/V-shaped or U-shaped to be analysed.

Flow cytometry analysis was performed as soon as possible on the Guava flow cytometer. Samples were gated on forward scatter (FS) versus side scatter (SS) to include the appropriately stained cell population and exclude debris or cell aggregates. Detection was performed with appropriate channels at Ex/Em= 494/518 nm for annexin-V and 535/617 nm for PI, and a total of 5,000 gated events were acquired for each treatment. This experiment was repeated six times both in normoxia and hypoxia.

2.2.10. Autophagy assay

The ability of drug treatments to induce autophagy was tested using a commercially available kit (CYTO-ID® Autophagy Detection Kit) which monitors autophagic flux in live cells using a novel dye that selectively labels accumulated autophagic vacuoles.

For flow cytometry application and according to the manufacturer's instructions, U87-MG and SVG-p12 cells were seeded in 24-well plate at density of 5 x 10^4 cells/0.5 ml media per well and incubated overnight in a humified incubator at 37°C and 5% CO_2 under normoxia or hypoxia. On the following day, drug treatments were added, separately or in combinations at IC_{25} and IC_{50} concentrations (as determined by the mono-therapy concentration-response curves after 48 hr) for 24 hr. Positive control cells were treated with Rapamycin (500nM) and Chloroquine (10μM) for 16~18 hr.

At the end of the treatment period, cells were harvested on ice (as described in section 2.2.2), and centrifuged at 100 xg for 5 min at 4°C. The supernatant was removed, and cell pellets were washed by resuspending in 500 µL cell culture medium and centrifuged again. The supernatant was removed, and each sample was resuspended in 250 µL of media. The diluted stain solution was prepared (by diluting CYTO-ID® Green Detection Reagent 0.5 µl/ml assay buffer supplemented with 5% (v/v) FBS) and added (250 µL/well). Samples were mixed well by gently pipetting up and down repeatedly to achieve a mono-disperse cell suspension and incubated for 30 min at 37°C in the dark. Cells were then collected by centrifugation, supernatant removed, and cell pellets resuspended in 250 µL of PBS and transferred to non-adherent 96-well plates/V-shaped or U-shaped to be analysed by the flow cytometer.

Samples were gated on forward scatter (FS) versus side scatter (SS) to include the appropriately stained cell population and exclude debris or cell aggregates. The CYTO-ID® Green detection reagent was detected with a FITC filter using appropriate channel at Ex/Em=480/530 nm. This experiment was repeated five times, under both normoxia and hypoxia.

For fluorescence microscopy application, U87-MG cells were seeded in 8-well chambered coverglass at density of 3 x 10^4/0.5 ml media per well overnight in a humified incubator at 37°C and 5% CO_2 under normoxia. On the following day, cells were treated for 24 hr, separately or in combinations at IC_{50} concentrations (as determined by the mono-therapy concentration-response curves after 48 hr). Post-treatment, medium with the testing reagents was carefully removed and the cells were washed twice with 300 µL of 1X assay buffer supplemented with 5% (v/v) FBS to preserve the cells. A sufficient amount of microscopy dual detection reagent was prepared (2 µL of CYTO-ID® Green Detection Reagent and 0.5 µL of Hoechst 33342 Nuclear Stain were added for every 1 mL of media) and 200 µL was dispensed to cover each well. Cells were incubated for 30 min at 37°C in the dark. On the completion of incubation, cells were washed carefully with 300 µL 1X Assay buffer supplemented with 5%(v/v) FBS and excess buffer was removed, and replaced with media.

The stained cells were visualised by fluorescence microscopy and Z-stack imaging performed for each well using 40X oil objective lens. FITC filter set was used for imaging the autophagic signal (Ex/Em= 480/530 nm) and DAPI filter set for imaging the nuclear signal (Ex/Em= 340/480 nm) in addition to TL-DIC channel. Autophagy assay was also performed using U87-MG and SVG-p12 1% O_2 hypoxia-adapted cells, and the experiment was repeated three times, with each experiment performed in triplicate.

2.2.11. Mitochondrial membrane potential assay

The Guava EasyCyte™ MitoPotential Kit was used to evaluate any changes in mitochondrial membrane potential ($\Delta\psi_m$) after drug treatment. This assay uses JC-1, a cationic dye that accumulates in energized mitochondria and fluoresces either green or orange depending upon mitochondrial membrane potential. A second dye, 7-AAD, a cell-impermeant DNA intercalator was used to simultaneously monitor cell membrane permeability changes observed later in apoptosis and in necrotic cell death.

Following optimization processes and according to the manufacturer's instructions, U87-MG and SVG-p12 cells were seeded in 24-well plates at density

of 5 x 10^4 cell/ 0.5 ml media per well and incubated overnight in a humified incubator at 37°C and 5% CO_2 under normoxia or hypoxia. Next day, drug treatments were added, separately or in combinations at IC_{25} and IC_{50} concentrations (as determined by the mono-therapy concentration-response curves after 48 hr) for 24 and 48 hr.

At each timepoint, cells were harvested (as described in section 2.2.1.3) and centrifuged at 100 xg for 5 min at 4°C. The supernatant was removed, and cell pellets were resuspended in 500 µl PBS staining solution containing both dyes (2µM JC-1 and 2µM 7-AAD). For the positive control samples, CCCP was added (50µM) to the tube which directly disrupts the mitochondrial membrane potential.

Cells were incubated for 30-60 min at 37°C in the dark then mixed well and transferred to non-adherent 96-well plate to be analysed on Guava flow cytometer. Events to be analysed were gated on forward scatter (FS) versus side scatter (SS) to include the appropriately stained cell population and exclude debris or cell aggregates. The fluorescence change was monitored at Ex/Em= 490/525 nm and 490/590 nm for JC-1 and at Ex/Em= 488/647 nm for 7-AAD. This experiment was repeated five times, under both normoxia and hypoxia.

For fluorescence microscopy application, U87-MG cells were seeded in 8-well chambered coverglass at density of 10^5 cell/0.5 ml media per well and incubated in humified incubator at 37°C with 5% CO_2 overnight under normoxia. Next day, cells were treated and left for a further 24 and 48 hr in the incubator. At the end of the treatment period, the media was aspirated and replaced with 300 µl of fresh media containing JC-1 (2µM) and 7-AAD (2µM) into each well. CCCP positive control was added to one well (50µM) then cells were incubated for 60 min at 37°C in the dark.

On the completion of incubation, media was changed to remove the unbound dyes, and cells were visualised using fluorescence microscopy to monitor the fluorescence change at Ex/Em= 490/525 nm with FITC filter, and at 490/590 nm with JC-1 filters whereas Texas red filter was used for 7-AAD dye (Ex/Em= 488/647 nm). Z-stack imaging was performed for each well using 40X oil objective lens and TL-DIC channel.

2.2.12. Metabolic activity assay

Using the Seahorse XFp Flux Analyser, the effect of mono and combination therapies on cellular metabolism was assessed by commercially available kits. The XF Cell Mito and Glycolysis Stress Tests enable to identify any alterations in the mitochondrial and glycolytic functions in live cells by directly measuring the oxygen consumption rate (OCR) and the extracellular acidification rate (ECAR), respectively.

According to the manufacturer's instructions and following optimization processes, U87-MG and SVG-p12 cells were seeded in XFp miniplates at density of 5 $x10^3$ cell/80 µl of growth media per well. The first and last well of the plate were filled with media for blank samples. Plates were incubated in a humified incubator overnight at 37°C and 5% CO_2 under normoxia or hypoxia. On next day, cells were treated, separately or in combinations at IC_{50} (as determined by the mono-therapy concentration-response curves after 48 hr) for 24 hr. One sensor cartridge was hydrated for each miniplate with XF calibrant and incubated at 37°C in a humified non-CO_2 incubator overnight.

At the end of the treatment period, glycolysis assay media was prepared by adding L-glutamate (2mM) to XF base media, while Mito stress assay media was supplemented with L-glutamate (2mM), sodium pyruvate (1mM) and glucose (1mM). All kit reagents were reconstituted with the prepared assay medium to be loaded in the hydrated sensor cartridge. The growth media was removed from the wells in the miniplate and replaced with warmed assay media (180 µl/well) and incubated in non-CO_2 incubator for one hour prior to the assay. The loaded assay cartridge was placed in the instrument to do calibration then XFp miniplate was placed to run the assay and all test parameters were calculated using Wave Software and Assay Report Generator. This experiment was repeated five times under normoxia and three times under hypoxia.

Metabolic activity was also examined for the U87-MG hypoxia-adapted cells at 1% O_2. This experiment was repeated three times, with each experiment performed in triplicate.

2.2.13. L-Lactate excretion rate assay

Lactate production was measured using a commercially available kit (EnzyFluoTM L-lactate assay kit) which is based on lactate dehydrogenase catalysed oxidation of lactate, in which the formed NADH reduces a probe into a highly fluorescent product. The fluorescence intensity of this product is proportional to the lactate concentration in the cell media samples.

Following optimization processes, U87-MG cells were seeded at density of 5x 10^3 cell/100 µl of media/well in 96-well plates and incubated overnight at 37°C and 5% CO_2 in humified incubator under normoxia or hypoxia. On the next day, drug treatments were added separately or in combination at IC_{50} concentrations (as determined by the mono-therapy concentration-response curves after 48 hr) for 24 hr. At the end of the treatment period, the growth media was replaced with 100 µl Seahorse XF media (supplemented with glutamate 2mM) per well, per-warmed at 37°C. Cells were allowed to excrete lactate by incubation for 210 min at 37°C in 5% CO_2. On completion of incubation, media was collected and centrifuged at 100 xg for 5 min. Supernatant was transferred to a clean tube and diluted 5-fold with d.H_2O and stored at -20°C for subsequent analysis. This experiment was repeated five times with each experiment performed in triplicate, both in normoxia and hypoxia.

For measuring lactate levels according to the manufacturer's instructions, lactate standards diluted in the assay media were prepared for quantification. 50 µl of each standard dilution and sample were transferred into wells of a black non-tissue culture 96-well plate. Working reagent solution was prepared and 50 µl was added per reaction well. After mixing, the plate was incubated for 60 min at room temperature protected from light, then fluorescence was measured at Ex/Em= 530/585 nm using microplate reader.

Lactate assay was also performed for U87-MG spheroids after optimization processes. Briefly, cells were seeded at density of 5 x 10^3 cell/200 µl media per well in Nunclon Sphera 96-Well plates. The plates were then centrifuged at 250 xg for 5 min and incubated overnight at 37°C and 5% CO_2 incubator under normoxia or hypoxia to allow spheroid formation. On the following day, drug

treatments were added separately or in combination at IC_{50} concentrations (as determined by the mono-therapy concentration-response curves after 48 hr) for 24hr. Growth media was then replaced by washing six times with half-volume of Seahorse XF media supplemented with glutamate (2mM) and cells were allowed to excrete lactate by incubation with 100 µl assay media for 210 min at 37°C in 5% CO_2. Samples were prepared for lactate assay as mentioned earlier. This experiment was repeated three times under normoxia and hypoxia.

2.2.14. Glyceraldehyde-3-Phosphate Dehydrogenase activity assay

The commercially available kit, Glyceraldehyde-3-Phosphate Dehydrogenase Activity Assay Kit, was used to measure GAPDH enzymatic activity in U87-MG cells after drug treatment. In this colorimetric assay, GAPDH catalyses the conversion of glyceraldehyde-3-phosphate (GAP) into 1,3-biphosphate glycerate (BPG) and intermediate, which reacts with a developer to form a coloured product that absorbs maximally at 450 nm.

Following optimization processes, U87-MG cells were cultured in T25 cm^2 flasks under at 37°C and 5% CO_2 under normoxia or hypoxia. When cells reached at ~60% confluency, the media was changed, and drug treatments were added at IC_{50} concentrations (as determined by the mono-therapy concentration-response curves after 48 hr) for 24 hr and GAPDH assay was performed according to the manufacturer's instructions. Briefly, cells were scraped on ice and transferred to 15 ml conical tubes, centrifuged and washed with ice-cold PBS and resuspended in 100 µL of ice-cold GAPDH Assay Buffer. The cell suspension was homogenized quickly by pipetting and transferred into microcentrifuge tubes and incubated on ice for 10 min. Samples were then centrifuged at 10,000 xg for 5 min at 4°C, and supernatant was collected and transferred to a pre-chilled tube.

All working standards, samples, background and positive controls were prepared and added into a clear flat bottom 96-well plate and brought to final volume of 50µl with assay buffer. After optimisation processes using a range of dilutions to ensure readings are within the standard curve range, unknown samples were diluted at 1:100. Then, 50 µl of reaction mix was added into each standard, sample and positive control wells, whereas 50 µl of background reaction mix was

added to the background control wells and mixed well. Absorbance was measured at 450 nm on a microplate reader in a kinetic mode, every 30 sec, for 60 min at 37°C protected from light. This experiment was repeated twice, both in normoxia and hypoxia.

2.2.15. Wound healing assay

To determine the migratory capacity of U87-MG and SVG-p12 cells before and after drug treatment, the *in vitro* wound-healing assay (scratch assay) was performed. Live cell imaging was employed to examine wound healing after drug treatment and monitor the rate of gap closure, which is a measure of the speed of the collective motion of the cells.

U87-MG and SVG-p12 cells were seeded in 8-well chambered coverglass at a density of 9 x 10^4 cells/0.5 ml media per well and incubated for 48 hr at 37°C and 5% CO_2 under normoxia or hypoxia. On the following day and prior to drug treatment, a sterile cocktail stick was used to make a vertical scratch across the well, and media was changed to remove any dislodged cells. Then drug treatments were added separately or in combinations at IC_{50} concentrations (as determined by the mono-therapy concentration-response curves after 48 hr) for 24 hr.

Plates were transferred to the light microscope chamber set at 37°C and 5% CO_2 to follow the wound closure progress. Microscopic Images were taken with 20x lens objective every two hours over a period of 18 hr and the scratch size was measured using Zeiss ZEN software. For hypoxic plates, images were taken only at 0 and 18 hr timepoints. This experiment was repeated eight times, both in normoxia and hypoxia for U87-MG cells and four times for SVG-p12 cells.

2.2.16. SDS-PAGE and Western blotting

To determine the potential mechanisms of action for the drugs treatment, western blotting analysis was performed to detect changes in protein expression or phosphorylation.

Sample preparation

For protein analysis, U87-MG and SVG-p12 cells were maintained in T75 cm^2 flasks under normoxia and hypoxia. At ~60% confluency, cells were treated with IC_{25} concentrations (as determined by the mono-therapy concentration-response curves after 48 hr) for 24 hr. Cells were scraped and washed with 5 ml of ice-cold PBS then centrifuged at 179 xg for 5 min. The supernatant was removed, and cell pellets were frozen at -20°C.

Whole cells extracts were obtained by resuspending cell pellets in 250-500 µl of RIPA buffer (50mM HEPES at pH 7.5, 150mM NaCl, 1% (v/v) triton X-100, 0.5% (w/v) sodium deoxycholate, 0.1% (w/v) SDS) in the presence of protease and phosphatase inhibitors (1:200) by rotation at 4°C for 1 hr. The resulting cell lysates were centrifuged at 13000 xg for 15 min at 4°C and the resulting supernatant was transferred to pre-chilled tubes to perform protein quantification.

Bicinchoninic Acid (BCA) protein assay

BSA standard curve (0 to 2 mg/ml) was prepared were prepared in RIPA buffer. Unknown lysate samples dilutions (1, 1:2, 1:5, 1:10 and 1:20) were prepared to ensure values were within the linear range of the standard curve. 10 µl of each dilution was added per well in triplicate to a clear flat bottom 96- well plate. BCA working reagent was prepared by adding 4% (w/v) copper sulphate (reagent B) to BCA reagent A (1:50), mixing well, then 200 µl of the prepared working reagent was added per well and incubated for 30 min at room temperature. Absorbance was measured at 485 nm and unknown lysate protein concentration was calculated by interpolation to the BSA standard curve using linear regression with GraphPad Prism. Cell lysates were aliquoted afterwards and stored at -80°C for subsequent western blotting analysis.

SDS-Polyacrylamide gel electrophoresis

Cell lysates containing 20-40 µg protein for each sample were thawed on ice and 4x sample loading buffer (12% (w/v) SDS, 10% (v/v) glycerol, 50mM tris at pH 6.8, and few grains of bromophenol blue) was prepared by adding DTT (10 mM) prior to mixing with the sample. Samples were diluted with 1X sample buffer to

give an equal final volume for all samples, then were heated at 95^{o}C for 5 min prior to loading.

Samples were resolved on 8, 10, or 12% mini gels using a standard protocol depending on the protein of interest. Briefly, the resolving gel mix was prepared (table 9.1) and poured upon the addition of TEMED, overlaid with 1 ml of 0.1% (w/v) SDS solution, and left to polymerise for ~45 min. The overlaying solution was discarded, and the stacking gel was added using appropriate comb size and allowed ~30 min for polymerization. The comb and excess un-polymerized stacker were removed, and samples were wet-loaded and separated by electrophoresis using 100 V constant current until dye front ran off bottom of the gel.

Western blotting

Gels, nitrocellulose membranes, sponges and filter papers were equilibrated in transfer buffer for 10 min (or 100% methanol then transfer buffer for PVDF membrane). Resolved proteins were transferred onto the membrane by wet-transfer method using the Bio-Rad Trans-Blot kit assembled as described in kit guide with a constant 400 mA applied for 2 hr at room temperature.

After blotting, membranes were washed briefly in PBS then blocked with PBS-T (0.2% (v/v) triton-X in PBS) containing 5% (w/v) skimmed milk for 1 hour at room temperature. Membranes were then exposed to diluted primary antibody in PBS-T with 5% (w/v) skimmed milk or BSA depending on the antibody used (table 9.2) and incubated at 4^{o}C with gentle shaking overnight. On the following day, membranes were washed with PBS-T (3 x 10-minute washes) and incubated for 1 hour with the appropriate horseradish peroxidase-conjugated secondary antibody (1:3000 in 5% (w/v) skimmed milk in PBS-T). Finally, the membranes were washed three times for 10 min each with PBS-T and exposed to ECL reagent for 2 min prior to visualisation using a BioRad ChemiDoc system.

To illustrate equal band loading, membranes were stripped with Restore Western Blot stripping buffer as per manufacturer's instructions and probed for β-actin protein levels using a monoclonal anti-β-actin antibody following same procedure

as a loading control. Specific bands were identified using enhanced chemiluminescence and development using CCD camera and band density was quantified by densitometric analysis. This experiment was repeated six times for each antibody, for both normoxic and hypoxic samples.

Hypoxia-adapted cells lysates were also prepared and stored to detect any changes in HIF-1α and HIF-1β/ARNT1 in comparison to the normoxic and hypoxic cells following same western blotting protocol.

2.2.17. Statistical Analysis

Unless otherwise indicated, results of each assay were expressed as a percentage of untreated control cell populations. Data were expressed as average ± the standard error of mean (SEM) of at least three independent experiments with different cell passages. Statistical analyses were performed using Microsoft Excel 2013, GraphPad Prism 5 and IBM SPSS Statistics Version 22. Comparison between experimental groups was performed using either two-way or one-way ANOVA tests with Bonferroni's or Tukey's Post-Hoc test. P-values ≤ 0.05 were considered as statistically significant.

CHAPTER 3: EFFECTS OF DRUG TREATMENT ON CELL VIABILITY, PROLIFERATION, AND MIGRATION.

3.1. Introduction

The discovery of a positive effect of aspirin in decreasing the risk of developing colorectal cancer by Kune and colleagues in 1988 was a stepping-stone for instigating the study of the effects of aspirin on various other cancers. Evidence later demonstrated that indeed the daily intake of aspirin reduced mortality, incidence and metastasis of different cancers (Rothwell *et al.*, 2011; Algra and Rothwell, 2012; Nan *et al.*, 2015; Thorat and Cuzick, 2015; Drew *et al.*, 2016). Importantly, some studies showed a significant inverse association between aspirin or NSAID use and GBM risk (Sivak-Sears *et al.*, 2004; Ferris *et al.*, 2012).

To date, the majority of literature examining the cytotoxicity of NSAIDs and aspirin has made use of different established cancer cell lines (Aas *et al.*, 1995; Amin *et al.*, 2003; Lee *et al.*, 2005; Annabi *et al.*, 2009; Kambe *et al.*, 2009; Kang *et al.*, 2009; Kim *et al.*, 2009; Lo *et al.*, 2010; Lan *et al.*, 2011; Gomes and Colquhoun, 2012; White *et al.*, 2013). In this project, U87-MG cells, an adherent cell line derived from human glioma, were used to evaluate the anti-tumour activity of aspirin and fumaroyldiaspirin (PN517). Additionally, SVG-p12 cells, an immortalised human foetal glial cell line, were used as a control. Both these cell lines are well characterised and used widely for research purposes.

Cell Viability

Currently, *in vitro* cell viability and cytotoxicity assays are considered the best approach and most important screening tool to start evaluating the novel compounds on cultured cells. They are efficient indicators of general cell health and widely used as a primary method for drug screening to determine if a drug has effects on cell proliferation or shows direct cytotoxic effects that eventually lead to cell death (Riss *et al.*, 2004). Cell viability assays are based on several cell functions such as cell membrane permeability, enzyme activity, cell adherence, ATP production, co-enzyme production, and nucleotide uptake activity (Rampersad, 2012).

There are a wide variety of assays available to estimate the number of viable eukaryotic cells including tetrazolium salts such as 3-(4,5-dimethyethiazol-2-yl)-2, 5-diphenyltetrazolium bromide (MTT) and PrestoBlue assays which measure

some aspects of general metabolism or enzymatic activity as a marker of viable cells. They are cheap, reliable and reproducible short-term assays, each with their advantages and disadvantages (Mosmann, 1983; Lu *et al.*, 2012).

Direct comparison of the PrestoBlue and MTT assays was performed previously in the lab using primary (from grade IV glioblastoma tumours) and established glioma cell lines including U87-MG and SVG-p12 and examined both the relative sensitivity of the assays, in terms of its ability to detect changes in cell number and in terms of IC_{50} value determined for the drugs (unpublished data). Results have shown an equal ability to detect large cell numbers but that the sensitivity of the PrestoBlue assay was greater at low cell numbers and was in fact able to detect as few as 10 cells. In addition, the PrestoBlue assay appeared more sensitive to drug induced changes in viability. Based on these results, the PB assay was chosen in this project for subsequent testing, and several optimisation processes for untreated control and vehicle samples were established in order to detect the appropriate conditions for both cell lines studied.

Combination studies

It is well established that cancer biology includes the disruption of numerous molecular pathways which are all linked and typically better tackled with combined action of two or more drugs (Zimmermann *et al.*, 2007; Podolsky and Greene, 2011). Bearing in mind the heterogeneity of GBM tumours, it is not surprising that mono-drug treatments in clinical tests are often unsuccessful, and resistance to therapies usually results from the parallel activation of signalling pathways (Qazi *et al.*, 2017). Hence, interest in the development of combination therapies has focused on choosing more than on drug with different mechanisms of action targeting different pathways at once (Devita *et al.*, 1975; Shah and Schwartz, 2001). Targeting multiple binding sites and compensatory activation of alternative signalling pathways during combination therapies may be useful to overcome resistance problem due to the additive or synergistic effects (Thaker and Pollack, 2009).

Additionally, the increased interest in the development of combination therapies can be attributed also to the desire of achieving therapeutic effects at reduced doses, which will result in toxicity reduction and may delay or minimize the

induction of drug resistance (Chou, 2010). Since aspirin and aspirin analogues showed synergistic effects with chemotherapy of colon and stomach cancers (Tesei *et al.*, 2008; Basudhar *et al.*, 2013; Kilari *et al.*, 2018), this project aimed to investigate whether aspirin or PN517 can be used as a more affordable adjunct or in combination with other current chemotherapeutic agents in the prevention, maintenance and possible cure for glioma.

Cell proliferation and cell cycle analysis

Effects on cell viability reflect the overall health of a cell population and could be affected by a range of parameters including cell proliferation, cell death, and metabolic activity. Therefore, more specific assays are required in order to more precisely characterise drug effects on cancer cells.

Generally, cancer cells show increased rates of proliferation due to genetic mutations. The continuous cell division and high proliferative activity are essential for malignant cell survival (Kanu *et al.*, 2009; Minniti *et al.*, 2009). Hence, interfering with cell proliferation and/or cell cycle progression is an important factor in the assessment drug induced cytotoxicity, and numerous probes have been used for tracking and measuring cell division flow cytometrically including CFDA-SE, PHK26, and Violet Cell Trace, enabling easy monitoring of the proliferation rate. Among fluorochromes, CFDA-SE has been the most useful cell labelling dye in terms of long-term cell tracking and quantifying proliferation rate (Chen *et al.*, 2003). The non-fluorescent CFDA compound diffuses passively across the plasma membrane into the cytoplasm where nonspecific esterases remove its acetate substituents forming the fluorescent product (CFSE) which react with free primary amines of intracellular proteins to create a stable, covalent bond and is retained in the cytosol of cells. As CFSE-labelled cells divide, the number of CFSE-tagged molecules is distributed equally between the two daughter cells, having half the fluorescence of the parents. As a result, each successive division is assessed by measuring the corresponding decrease of the cellular fluorescence intensity by flow cytometry which allows distinguishing each cell generation (Fig 3.1).

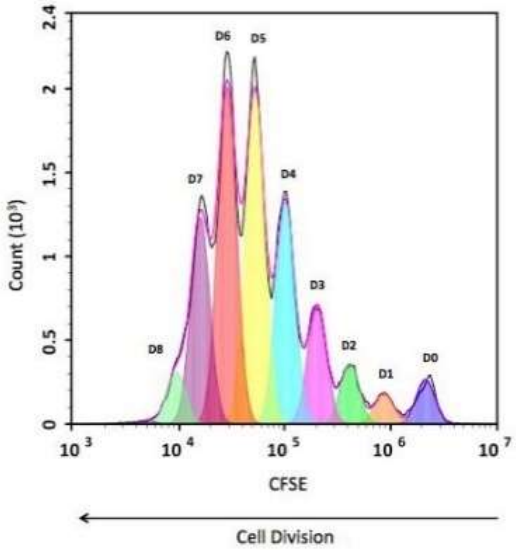

Figure 3. 1. Histogram plot for cell proliferation analysis. Peripheral blood mononuclear cells stained with 1µM CFSE before culturing for 8 days and analysing by flow cytometery (Source: Biocompare).

Although CFSE may has several disadvantages including leakage from the cell and cell toxicity at high concentrations, CFSE remains the most popular reagent used for monitoring cell proliferation with choosing the optimal labeling conditions which may vary with specific cell types (Wang *et al.*, 2005; Quah and Parish, 2010; Aslantürk, 2018). Therefore, following results obtained from viability assays it was decided to determine the drug treatment effects on cell proliferation rate using the fluorescent proliferation marker CFDA-SE and flow cytometry following control optimisation experiments to detect the optimum dye staining conditions.

On the other hand, consecutive cell proliferation also depends on well-organized cell cycle progression. The most common method for assessing the cell cycle is to use flow cytometry to measure cellular DNA content. The major cell cycle phases, G0/G1, S, G2/M can be quickly and accurately determined by direct quantitative measurement of the DNA content based on staining of DNA with fluorescence dye such as propidium iodide (PI) (Cecchini *et al.*, 2012).

PI is the most frequently used dye for cell cycle analysis. It is a red-fluorescent nuclear dye that intercalates stoichiometrically between DNA bases producing a highly fluorescent signal with a broad emission around 600 nm (Life Technologies UK, 2014). This property of PI has been exploited to determine the cell cycle phase distribution of a population. Cells preparing for division will contain

increasing amounts of DNA and display proportionally increased fluorescence. Differences in fluorescence intensity are used to determine the percentage of cells in each phase of the cell cycle (Fig 3.2).

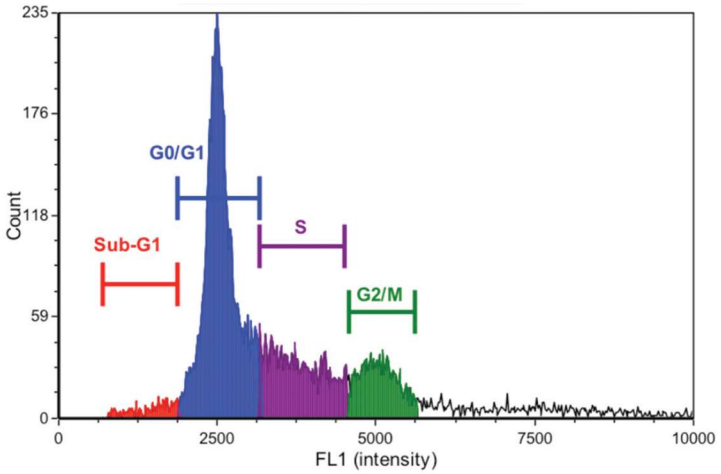

Figure 3. 2. Histogram plot of cell cycle analysis. Cell count versus PI staining plot generated using flow cytometer showing the four populations of cell cycle phases with increasing fluorescence intensity. (Source: cellometer)

In this project, CFSE proliferation studies were combined with cell cycle analysis throughout a time course study of several days to further characterise the effect of drug treatments can have on cell cycle progression using flow cytometry and propidium iodide staining.

Moreover, aberrant cell cycle progression and proliferation in cancer can occur due to changes in different cell cycle regulatory proteins. Increasing evidence has demonstrated that cyclin D1 is overexpressed in tumour cells including glioma and is partly dependent on the mitogenic effect of EGF signalling through EGFR (Perry *et al.*, 1998; Poch *et al.*, 2001; Rieber and Rieber, 2006) which in turn is frequently upregulated in a number of cancers including GBM (Yarden, 2001; Lo and Hung, 2006). Therefore, establishing cyclin D1 expression and the impact of drug treatment on its degradation is important in the development of novel therapies for GBM. Previous studies suggested that aspirin could affect the expression and activation of cyclin D1 in tumour cell lines like colorectal cancer (Claudius *et al.*, 2014), hence the effect of the studied drug treatment on cyclin D1 expression and phosphorylation was determined by western blotting.

Cell migration

As discussed earlier, GBM is characterized by rapid and highly infiltrative growth with cell invasion and migration being the main features of tumour spreading associated with therapeutic resistance and recurrence. Collective cell migration is a hallmark of many physiological and pathological processes such as tissue repair and cancer invasion and metastasis, immune responses and angiogenesis (Grada *et al.*, 2017).

The EGFR has been found to be responsible for the growth progression in many cancers, particularly in primary glioblastomas (Mendelsohn and Baselga, 2000). The EGFR signalling pathway is complicated and results in reduced apoptosis, increased cell proliferation, angiogenesis and metastasis (Mitsudomi and Yatabe, 2010). Also, cell migration is regulated by EGFR expression and abnormal wound healing is a characteristic of tumour cells and an important factor determining the malignancy of tumour cells (Lalloo *et al.*, 2006; Natarajan *et al.*, 2006; Gough *et al.*, 2011). For that reason, analysis of cell migration *in vitro* is a valuable assay to quantify any alteration in cell migratory capacity in response to drug treatment.

Several methods are described in the literature to study cell migration (such as Boyden chamber assay, barrier assays, and microfluidics-based assays), however, the wound healing assay, also known as the “scratch assay”, is a straightforward, versatile, convenient and economical method to assess and quantify collective cell migration and wound healing (Grada *et al.*, 2017). This assay is based on creating an artificial gap “scratch, wound” in a confluent cell monolayer. The exposure to the cell-free area induces the cells to migrate into the gap and microscopic images are captured at the beginning and regular intervals to monitor closing the scratch and determine the rate of cell migration (Liang *et al.*, 2007).

The wound healing assay is a standard *in vitro* technique for probing collective cell migration in two dimensions. When a cell monolayer is wounded or scratched, it responds to the cell-cell disruption by an increased amount of growth factors at the wound site and ultimately results in healing of the wound through cell proliferation and migration. The type of collective cell migration probed by the wound healing assay is known as sheet migration wherein epithelial and

endothelial monolayers move in two dimensions while maintaining their intercellular junctions, Sheet migration occurs in diverse processes such as cancer metastasis (Ilina and Friedl, 2009).

Given the role of EGF signalling in tissue repair, it has been suggested a role for aspirin as a chemopreventive agent and its inhibitory effect on wound healing (Bashir *et al.*, 2019). Therefore, this project aimed to study the effects of drug treatment on cell migration by performing a wound healing assay over a period of 18 hours using live- cell microscopy (Fig 3.3).

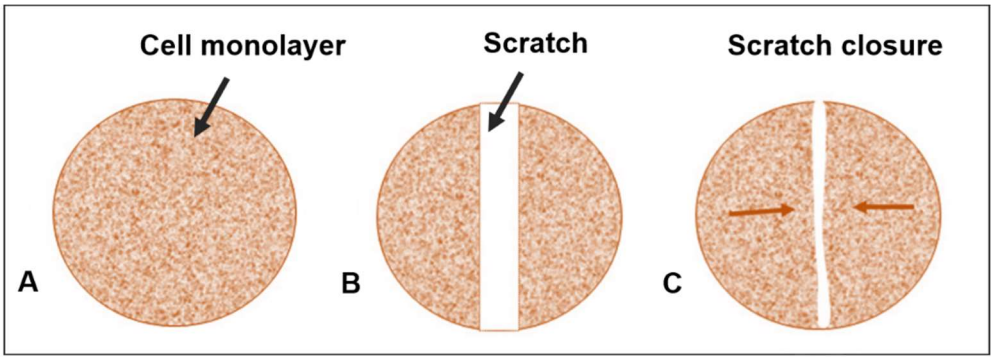

Figure 3. 3. Diagrammatic representation for *in vitro* scratch assay. Cells are seeded and incubated to form a confluent monolayer (A). linear thin scratch “wound” is made with a cocktail stick (B), and the free-cell area is imaged to measure the boundary of the wound at pre-migration (B) and after cells have migrated inward to fill the resulting space at different timepoints (C).

Consequently, the first chapter of this thesis aimed initially to examine the effect of aspirin and the aspirin analogue PN517 on U87-MG and SVG-p12 cell viability as a general indicator for the cell heath to approve the cytotoxicity of these drugs towards GBM cells. The next aim was to find the IC_{50} and IC_{25} values and apply the tested drugs in combination with the standard chemotherapeutic agents to explore any antagonism or synergism between the drugs. Afterthought, it was planned to treat the cells with either mono or combined therapy to investigate the effect of the drug treatment on cell proliferation, cell cycle and migration as major factors can influence cell viability.

3.2. Results

3.2.1. Growth curves

It is important to know and record the growth characteristics of the cell line in use before starting any experiments because any alteration in cellular growth can have significant effects on experimental results. Cell growth might be affected by hypoxia- associated genetic alteration, therefore, growth curves were performed to study the growth pattern for each individual cell line, identify any lag or stationary phase, and detect the population doubling time under both normoxic and hypoxic conditions.

Both cell lines expressed an exponential growth over a period of seven days under normoxia, displaying signs of a lag phase for approximately 1-2 days for both cell types and a decreased proliferation rate was noticed with lower O_2 levels (Fig 3.4). In the U87-MG cell line, the population doubling time was identified to be ~24 hr in normoxia, ~34 hr in 1% O_2 hypoxia, whereas in 0.1% O_2 hypoxia it took ~96 hr for the cells to double and they reached a plateau at day 6. A significant difference in growth rate was found between the incubation conditions of normoxia and hypoxia on day 5 onwards (p<0.0001). When total proliferation over seven days was examined, approximately a 50% reduction was observed by day 7 in U87-MG with each change in O_2 concentration ($8x10^5$ under normoxia, $4x10^5$ under 1% and $2x10^5$ under 0.1%).

With regards the SVG-p12 cell line, the growth pattern was similar under the different conditions. The population doubling time was found to be ~40 hours in normoxia, ~72 hours in hypoxia, while under severe hypoxia the cells exhibited a very low proliferation rate with a decrease in cell number after day 6 (Fig 3.4). In addition, SVG-p12 proliferation was found to be lower than in U87-MG cells, with a significant difference observed between the rates of growth of the two cell lines from day 5 ($p<0.001$) until day 7 ($p<0.0001$) under normoxia, and on day 6 ($p<0.05$) under hypoxia.

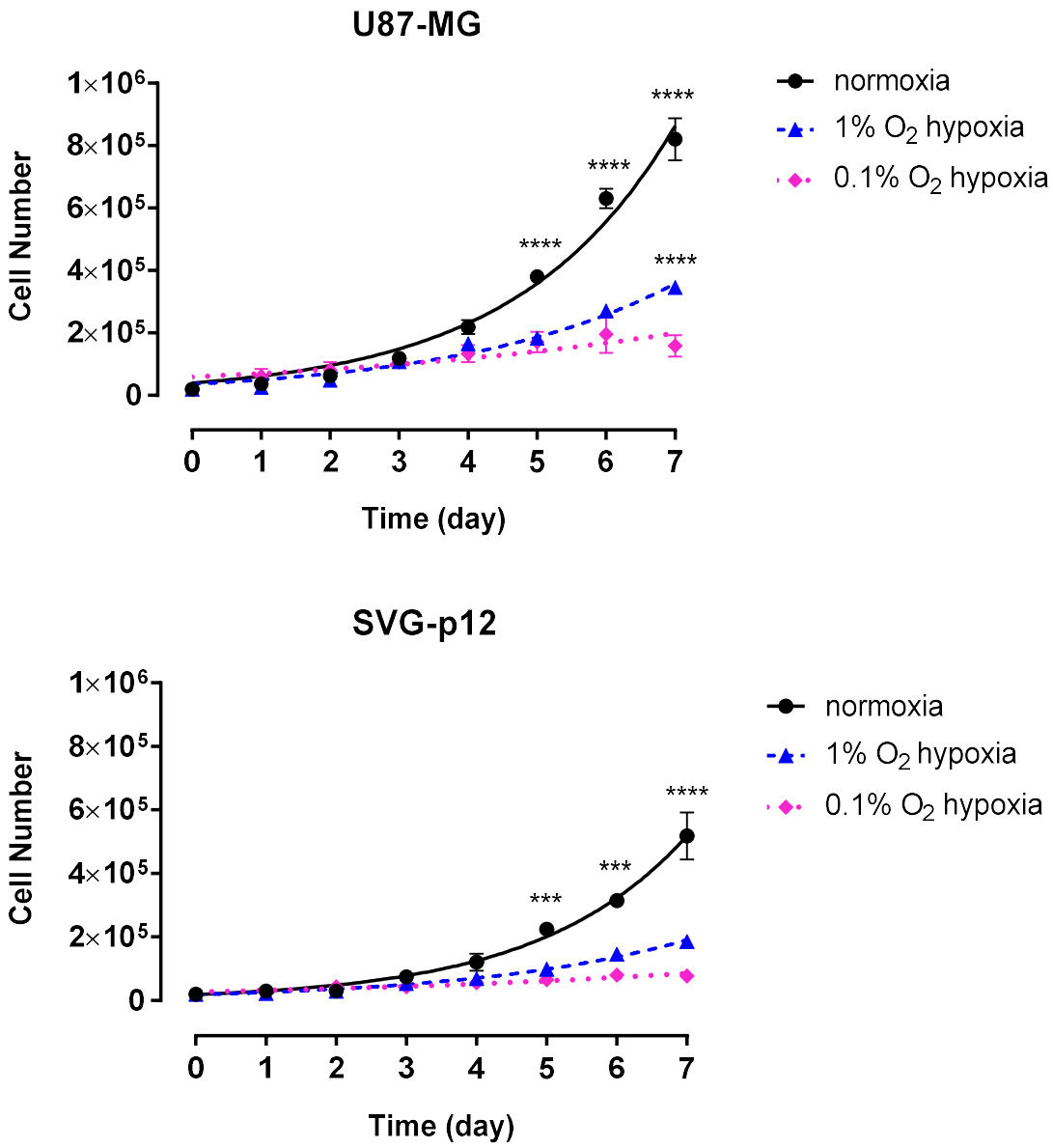

Figure 3. 4. Growth curves over seven days of U87-MG and SVG-p12 cell lines in different conditions. Upon initial seeding of 2x 10^4 cells per well, cell number was subsequently determined every 24 hours by haemocytometer analysis and Trypan blue exclusion over a seven-day period of incubation. Values represent mean ±SEM of three independent experiments. A two-way ANOVA was used to identify significant effects, with Bonferroni's multiple comparison test, *P < 0.05; **P < 0.01; ***P < 0.001; ****P < 0.0001. The experimental procedure was performed as described in Materials and Methods section 2.2.2.

3.2.2. PrestoBlue® linearity assay and control optimisation

In order to conduct cell viability analysis during the project, the PrestoBlue® reagent was used which is an enhanced version of the commonly available resazurin-based assays. Viable cells convert the dark blue oxidized form of the dye (resazurin) into a red-fluorescent reduced form (resorufin) and cell viability is determined by measuring the resulting fluorescent signal using a microplate reader. Optimisation to establish a suitable incubation period was performed previously in the lab and found that 60 minutes proved to be appropriate for cytotoxicity analysis (unpublished data).

In addition, the relationship between fluorescence and cell number was studied in order to establish the saturation point of the dye using increasing cell densities in a 96- well plate. The data obtained from both cell lines showed fluorescence readings were directly proportional to the seeding density at least up to 1000 cells/well and up to 5000 cells/well in some cases, and resulted in strong linearity and high R-square values under normoxia and hypoxia (Fig 3.5).

In normoxia, U87-MG and SVG-p12 cell lines displayed a linear relationship between the cell number and fluorescence after 24, 48 and 72 hours of incubation across the initial seeding density range of 0 – 1000 cell/well (R^2 = 0.992, 0.993 and 0.9144, respectively) for U87-MG and (R^2 = 0.9988, 0.9983 and 0.9976 respectively) for SVG-p12. In hypoxia both cell lines displayed a linear relationship between the cell number and fluorescence over three days across the initial seeding density range of 0 – 1000 cell/well (R^2 = 0.9767, 0.9728 and 0.9895, respectively) for U87-MG and (R^2 =0.9884, 0.9916 and 0.9965, respectively).

From the previous results, it was clear that the fit is linear up to 1000 cells under all studied conditions, hence the subsequent cell viability experiments were performed using a maximum cell density of 1000 cell/well in 96-well plate for both cell lines with incubation times up to 72 hours.

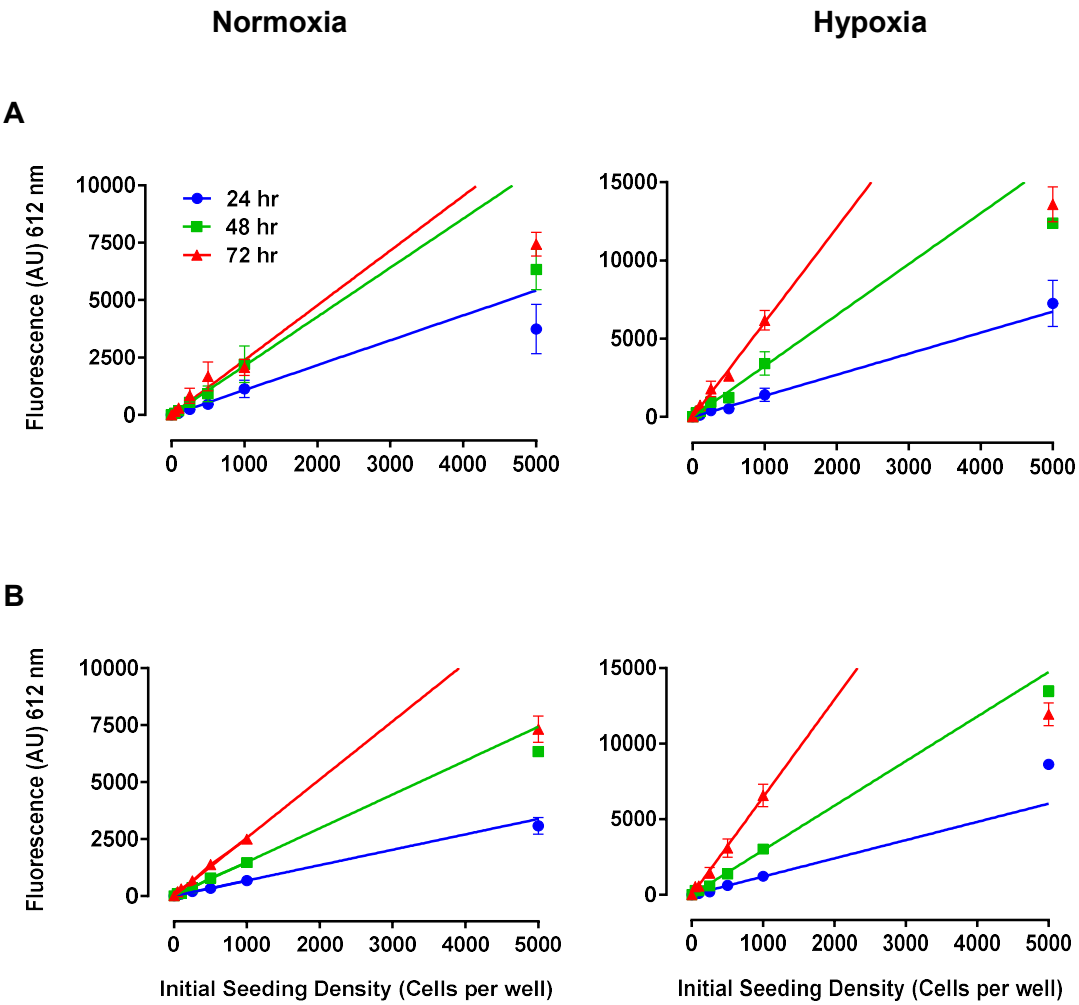

Figure 3. 5. The relationship between fluorescence and initial seeding density. The linearity assay was performed under normoxia and hypoxia with increasing cell number after 24, 48, and 72 hours of incubation using the Presto Blue® reagent for U87-MG cell line (A) and SVG-p12 cells (B). Values represents mean± SEM of three independent experiments. A two-way ANOVA was used to identify significant effects, with Tukey's multiple comparison test, *P < 0.05; **P < 0.01; ***P < 0.001; ****P < 0.0001. The experimental procedure was performed as described in Materials and Methods section 2.2.3.

Prior to analysing cell viability after drug treatment, the effect of the dissolution solvents of the drugs was tested. DMSO is generally considered as the universal solvent for biological experiments due to its ability to dissolve most molecules at high concentrations of up to 100mM (Pereira and Williams, 2007) and it was used for preparing TMZ stock solution. However, dissolution with DMSO was avoided in cisplatin as DMSO can react with platinum compounds thereby decreasing its cytotoxic effect (Hall et al., 2014). Therefore, cisplatin was dissolved using

physiological saline solution (0.9%(w/v) NaCl) as suggested by Hall (Hall *et al.*, 2014) which did not show any effect on cell viability (data not shown).

To test the cytotoxicity of DMSO, it was added at the highest concentration used in preparing TMZ (1%(v/v)) and cell viability was assessed by PrestoBlue® reagent over three days both in normoxia and hypoxia. The viable cells were calculated as a percentage relative to the negative control cells. Data showed no significant effect on cell viability under any condition (p>0.05) (Fig 3.6).

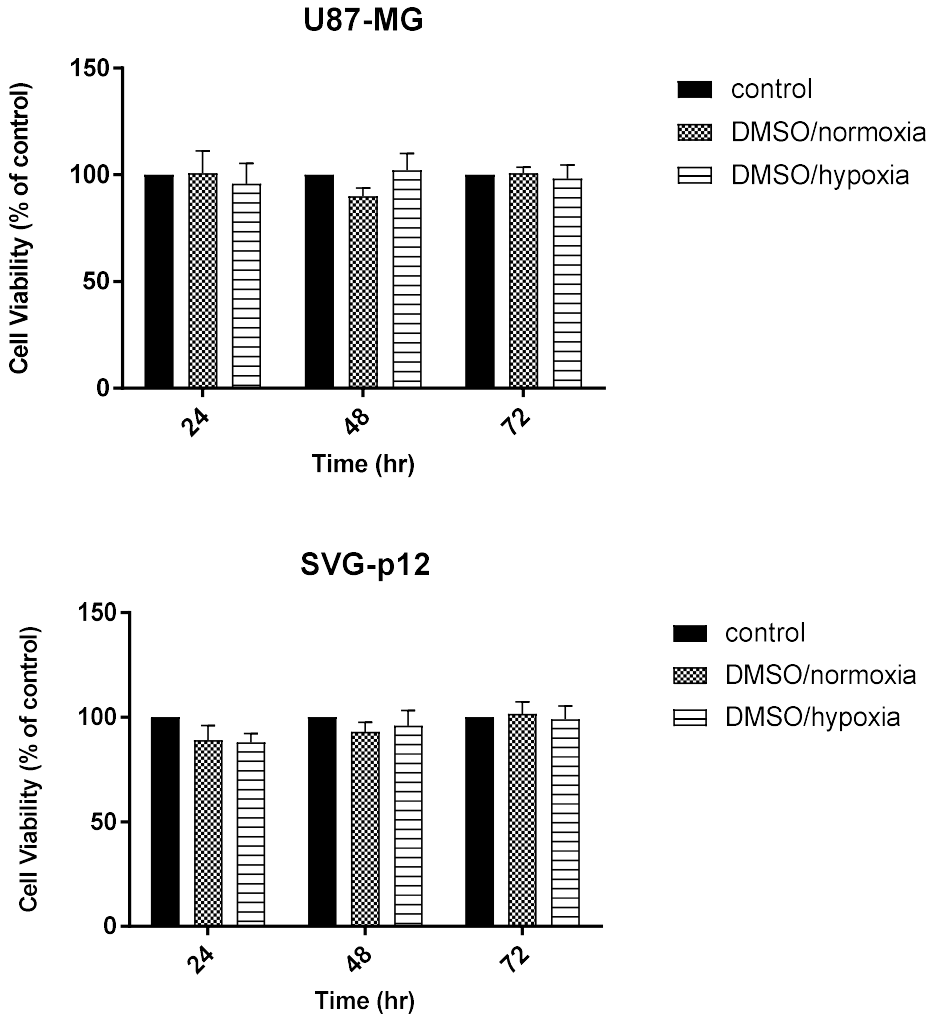

Figure 3. 6. Effects of DMSO on cell viability in U87-MG and SVG-p12 cell lines under normoxia and hypoxia. Cell viability was performed after adding the highest concentration used of DMSO (1%(v/v)) using the PrestoBlue® reagent over 24, 48 and 72 hours under normoxia and hypoxia. Values represents mean ± SEM generated from six independent experiments. A two-way ANOVA was used to identify significant effects, with Tukey's multiple comparison test, *P < 0.05; **P < 0.01; ***P < 0.001; ****P < 0.0001. The experimental procedure was performed as described in Materials and Methods section 2.2.5.

3.2.3. Effects of drug treatment on cell viability

Concentration-response assays were undertaken to characterise the effects of aspirin and its novel analogue PN517 on cell viability in comparison to the standard chemotherapeutic agents, TMZ and cisplatin, using glioblastoma U87-MG cell line and the control SVG-p12 cell line. Cells were treated with aspirin or PN517 at concentration between 30μM and 10mM, cisplatin at concentrations between 1μM and 300μM, and TMZ between 3μM and 1mM. The IC_{50} and IC_{25} values for each drug treatment were established from the concentration-response curves in order to obtain a standard for direct comparison, and to apply the appropriate drug concentration in the subsequent experiments. The IC_{50} and IC_{25} values were calculated using GraphPad Prism and presented in Table 3.1 and 3.2, respectively.

In U87-MG cell line, all treatments reduced cell viability in a concentration dependent manner under normoxia and hypoxia. All treatments produced their maximum reduction in viability at the highest concentration used, with the exception of cisplatin where a small but consistent rise in viability was observed at the highest concentration used (Fig 3.7).

Under normoxia, aspirin and PN517 were found to reduce cell viability in a time dependent manner. Cells treated with aspirin resulted in an inhibitory concentration of 50% of 9 ±1.4, 5 ±0.8 and 3 ±0.4 mM at 24, 48, and 72 hr, respectively. The aspirin analogue PN517 appeared to be slightly more cytotoxic that aspirin itself with IC_{50} values of 5 ±0.7, 3 ±0.6 and 2 ±0.2 mM. The effect of PN517 at 24 hr on cell viability was significantly greater the aspirin at this timepoint, $p<0.05$. At 48 and 72 hr, there were no significant differences between aspirin and PN517. However, drug treatment with aspirin or PN517 showed a trend towards greater efficacy under hypoxia with IC_{50} ~2mM for both drugs, although a time dependent effect was not observed, $p>0.05$.

In contrast, cisplatin which appeared to be the most cytotoxic drug under normoxia with IC_{50} values of 6 ±1.7, 4 ± 0.8, and 3 ±0.6 μM at 24, 48, and 72 hr, respectively, showed a trend towards lower efficacy under hypoxia and resulted in IC_{50} values of 17 ± 6.2, 8 ± 1.5, and 5 ± 0.6μM, respectively. Interestingly,

cisplatin under normoxia was significantly more effective at 24 hr than aspirin (p<0.05) and TMZ (p<0.001) but not than PN517 (p>0.05). Importantly, at this timepoint under hypoxia, cisplatin was highly significantly more effective than TMZ (p<0.0001) but not more effective than aspirin or PN517 (p>0.05). However, cisplatin showed significantly more cytotoxic effect than all other drug treatments at 48 hr under both conditions (p<0.0001), with an exception for PN517 where no significant difference was observed under hypoxia compared to cisplatin at 48 hr (p>0.05). At 72 hr of drug treatment, cisplatin was again significantly more effective than other drug treatments under both normoxia and hypoxia (p<0.0001, except for PN517 under normoxia p<0.01).

Concentration response assays were also conducted with the standard chemotherapeutic drug, temozolomide, but it had little effect on cell viability over the period studied especially under hypoxia in both cells lines apart from at the highest concentration used, with estimated IC_{50} of 1mM (Figs 3.7 & 3.8, Table 3.1). At 24 and 48 hr of drug treatment, TMZ was significantly less effective than aspirin and PN517 under normoxia (p<0.05) and hypoxia (p<0.0001). Also, at 72 hr, TMZ showed significantly less efficacy than the both drugs under normoxia (p<0.01) and hypoxia (p<0.0001).

In the SVG-p12 cell line, observations of drugs efficacy on cell viability were very similar to U87-MG. A reduction in cell viability was observed under normoxia and hypoxia following treatment with cisplatin in a time and concentration dependent manner (Fig 3.8). Also, aspirin and PN517 were similar in efficacy while showing a trend towards better efficacy under hypoxia. However, cisplatin had similar efficacy under both conditions in this cell line. At 24 hr, there was no significant differences between cisplatin, aspirin or PN517 under normoxia, whereas TMZ was significantly less effective than PN517 (p<0.05) and cisplatin (p<0.0001) under normoxia, and all other drugs under hypoxia (p<0.0001). At 48 hr, cisplatin showed significantly better efficacy than all other treatments (p<0.0001) under normoxia. This difference sustained under hypoxia compared to TMZ but to less extent compared to aspirin and PN517 (p<0.01). The cell viability reduction following the treatment with cisplatin was highly significantly greater than other drugs under both conditions (p<0.0001).

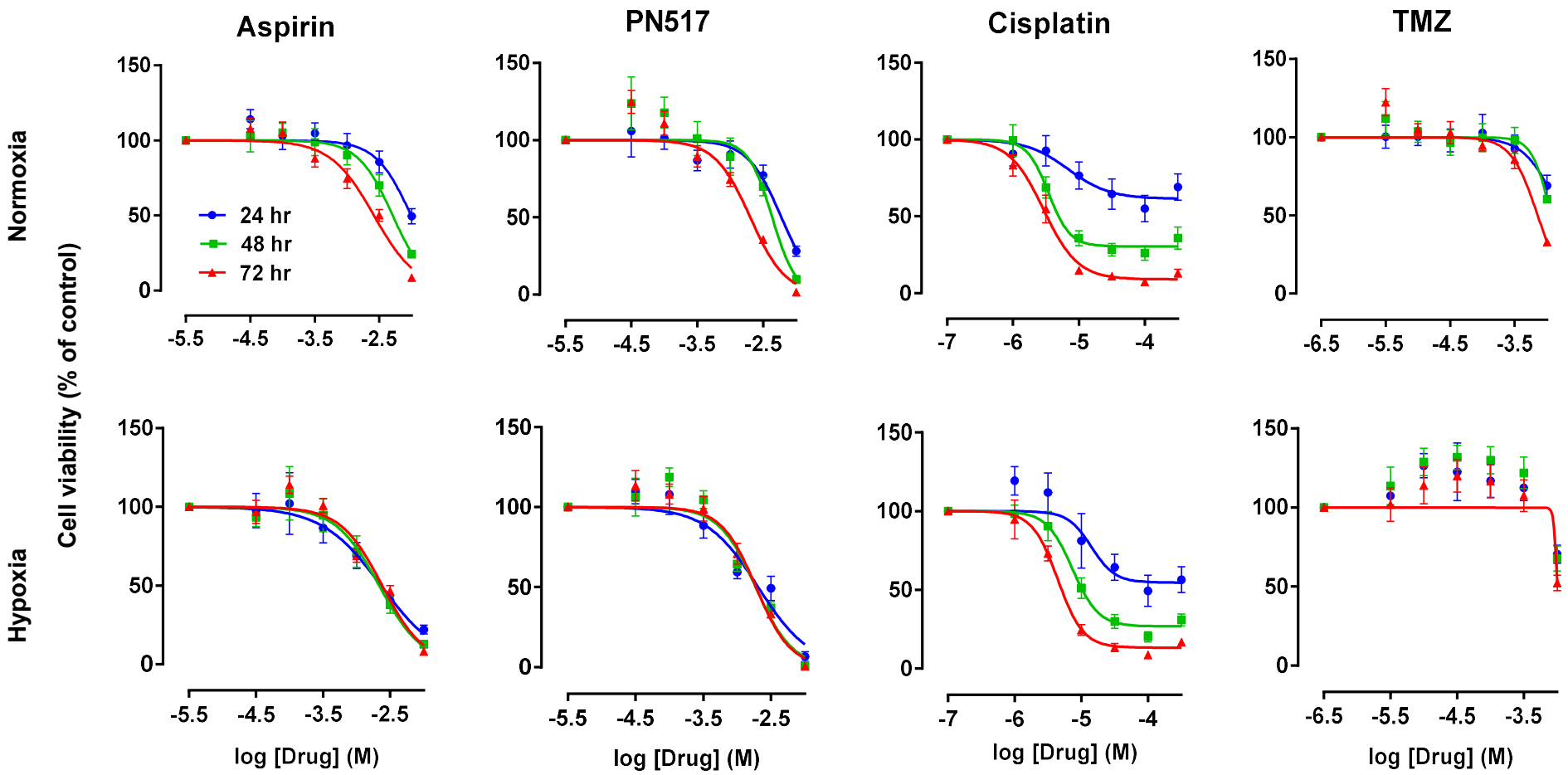

Figure 3. 7. Data illustrating the effect of drug treatment on cell viability in U87-MG cell line. The concentration-response curve of the drug treatment was established under normoxia and hypoxia using the PrestoBlue® reagent over 24, 48 and 72 hours of treatment. Values represents mean ± SEM of six independent experiments. A two-way ANOVA was used to identify significant effects, with Tukey's multiple comparison test. The experimental procedure was performed as described in Materials and Methods section 2.2.5.

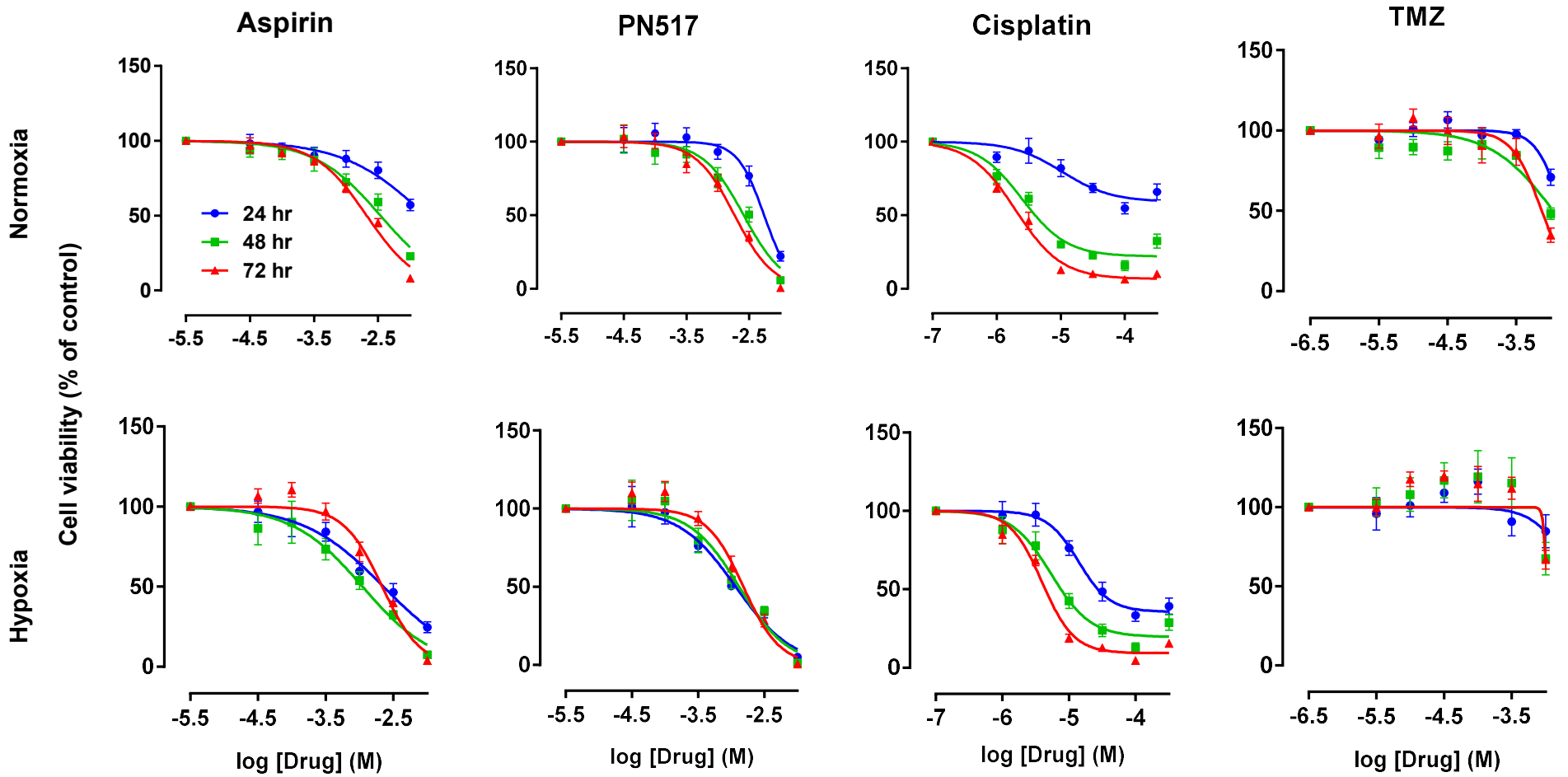

Figure 3. 8. Data illustrating the effect of drug treatment on cell viability in SVG-p12 cell line. The concentration-response curve of the drug treatment was established under normoxia and hypoxia using the PrestoBlue® reagent over 24, 48 and 72 hours of treatment. Values represents mean ± SEM of six independent experiments. A two-way ANOVA was used to identify significant effects, with Tukey's multiple comparison test. The experimental procedure was performed as described in Materials and Methods section 2.2.5.

Table 3. 1. IC_{50} values for U87-MG and SVG-p12 cell lines following 24, 48 and 72 hours of treatment, under normoxia and hypoxia.

Cell line	Condition	Time (hr)	Aspirin (mM)	PN517 (mM)	Cisplatin (μM)	TMZ (mM)
U87-MG	Normoxia	24	9 ± 1.4	5 ± 0.7	6 ± 1.7	1 ± 0.1
		48	5 ± 0.8	3 ± 0.6	4 ± 0.8	1 ± 0.1
		72	3 ± 0.4	2 ± 0.2	3 ± 0.6	1 ± 0.1
	Hypoxia	24	2 ± 0.5	2 ± 0.6	17 ± 6.2	-
		48	2 ± 0.4	2 ± 0.2	8 ± 1.5	-
		72	2 ± 0.3	2 ± 0.3	5 ± 0.6	1 ± 0.1
SVG-p12	Normoxia	24	16 ± 3.5	6 ± 0.9	19 ± 13	3 ± 1.8
		48	3 ± 0.8	4 ± 0.7	3 ± 0.4	2 ± 1.2
		72	2 ± 0.2	2 ± 0.3	2 ± 0.3	1 ± 0.1
	Hypoxia	24	2 ± 0.6	1 ± 0.2	17 ± 3.2	1 ± 0.4
		48	1 ± 0.3	1 ± 0.3	6 ± 1.1	1 ± 0.1
		72	2 ± 0.2	2 ± 0.3	4 ± 0.2	0.8 ± 0.3

Table 3. 2. IC_{25} values for U87-MG and SVG-p12 cell lines following 24, 48 and 72 hours of treatment, under normoxia and hypoxia.

Cell line	Condition	Time (hr)	Aspirin (mM)	PN517 (mM)	Cisplatin (μM)	TMZ (mM)
U87-MG	Normoxia	24	4 ± 1.1	2 ± 0.8	1 ± 0.8	1 ± 0.3
		48	3 ± 0.8	2 ± 0.6	2 ± 0.3	0.7 ± 0.2
		72	1 ± 0.3	1 ± 0.2	2 ± 0.5	0.4 ± 0.1
	Hypoxia	24	1 ± 0.4	1 ± 0.5	13 ± 5	-
		48	1 ± 0.3	1 ± 0.2	5 ± 1.3	-
		72	1 ± 0.2	1 ± 0.2	3 ± 0.5	-
SVG-p12	Normoxia	24	4 ± 1.4	3 ± 0.7	13 ± 5.8	1 ± 0.3
		48	1 ± 0.5	1 ± 0.4	1 ± 0.2	0.3 ± 0.1
		72	1 ± 0.1	1 ± 0.3	1 ± 0.1	0.3 ± 0.1
	Hypoxia	24	1 ± 0.2	0.4 ± 0.1	9 ± 1.8	3 ± 0.9
		48	1 ± 0.2	1 ± 0.2	2 ± 0.6	-
		72	1 ± 0.2	1 ± 0.2	2 ± 0.2	-

3.2.4. Drug combination studies

The IC_{50} values generated from the concentration response curves were used in the subsequent combination treatment assays to study any synergistic effects that may be involved following drug treatment of the two cell lines. The initial assays tested these IC_{50} concentrations on their own or in combination, with treatments being added simultaneously at IC_{50} concentrations obtained from dose-response curves at 48 hr and incubated for 24, 48, and 72 hours prior to determine viability using the PrestoBlue assay under normoxia and hypoxia. The same IC_{50} values were applied for both cell lines but were different under normoxia and hypoxia.

In U87-MG cell line, all treatments (mono or combination) reduced cell viability in a time dependent manner and all viability percentages were significantly different from the control ($P < 0.0001$) except cisplatin at 24 hr/normoxia (Fig 3.9). When adding the same concentration of aspirin or PN517 (3mM in normoxia and 1mM in hypoxia), PN517 was found to be more efficacious than aspirin at all timepoint and conditions and even more efficacious than cisplatin in some cases (Fig 3.10). With regards the control drug treatments, TMZ showed better efficacy than cisplatin in reducing cell viability under normoxia but the opposite was observed under hypoxia.

Cisplatin in combination with aspirin further reduced cell viability over cisplatin alone but the effect was not significantly different ($p>0.05$). However, the combination of cisplatin with PN517 was significantly different from cisplatin alone at all timepoints under normoxia (53±5% vs. 84±7.5% at 24 hr $p<0.001$, 32±5.7% vs. 61±4.9% at 48 hr $p<0.001$, and 18±0.6% vs. 38±1.5% at 72 hr $p<0.05$) and at 24 hr under hypoxia.

Additionally, both aspirin and PN517 enhanced the efficacy of TMZ while the greatest combination effect was found in TMZ in combination with PN517 which was greater than all the other combinations, but just with significant difference compared to cisplatin and PN517 combination at 24 hr ($p<0.05$). The cell viability reduction by TMZ and PN517 in combination was significantly greater than TMZ alone (33±4.6% vs. 54±8.3%, $p<0.05$) following 24 hours of treatment. A similar

pattern of effect was observed under hypoxia, where PN517 combinations typically showed the greatest effect and TMZ in combination with PN517 was significantly different from TMZ alone at all timepoints (37±0.6% vs. 77±7.1% at 24 hr $p<0.0001$, 24±2.1% vs. 55±3.8% at 48 hr $p<0.0001$, and 19±1.2% vs. 37±2.6% at 72 hr $p<0.05$) (Fig 3.10).

A similar pattern of effect was observed in SVG-p12 cells, with all drug combinations in normoxia reducing cell viability to a greater extent in comparison to the mono-treatments and showing a time dependent effect (Fig 3.11). All viability percentages were significantly different from the control under normoxia ($P< 0.0001$) except cisplatin at 24 and 48hr, and aspirin at 24 and 72hr in hypoxia.

The combination of aspirin or PN517 with cisplatin produced a significant further decrease in cell viability over cisplatin alone at all timepoints under normoxia and that was larger with PN517 (46±1% vs. 91±2.7% at 24 hr $p<0.0001$, 27±5.2% vs. 80±5.3% at 48 hr $p<0.0001$, and 13±2.3% vs. 56±5.2 % at 72 hr $p<0.0001$) (Fig 3.12). Again, the greatest effect was the combination of TMZ and PN517 which was significantly different from TMZ alone following 24 and 48 hours of drug treatment (25±3.2% vs. 52±5% at 24 hr $p<0.01$, 10±1.1% vs. 34±6.1% at 48 hr $p<0.05$). However, that was not the case under hypoxia where it appeared to have lower efficacy and the combination of TMZ and PN517 was significantly different from TMZ only following 24 hours of drug treatment (48±2.3% vs. 83±5.6% at 24 hr, $p<0.001$) (Fig 3.12).

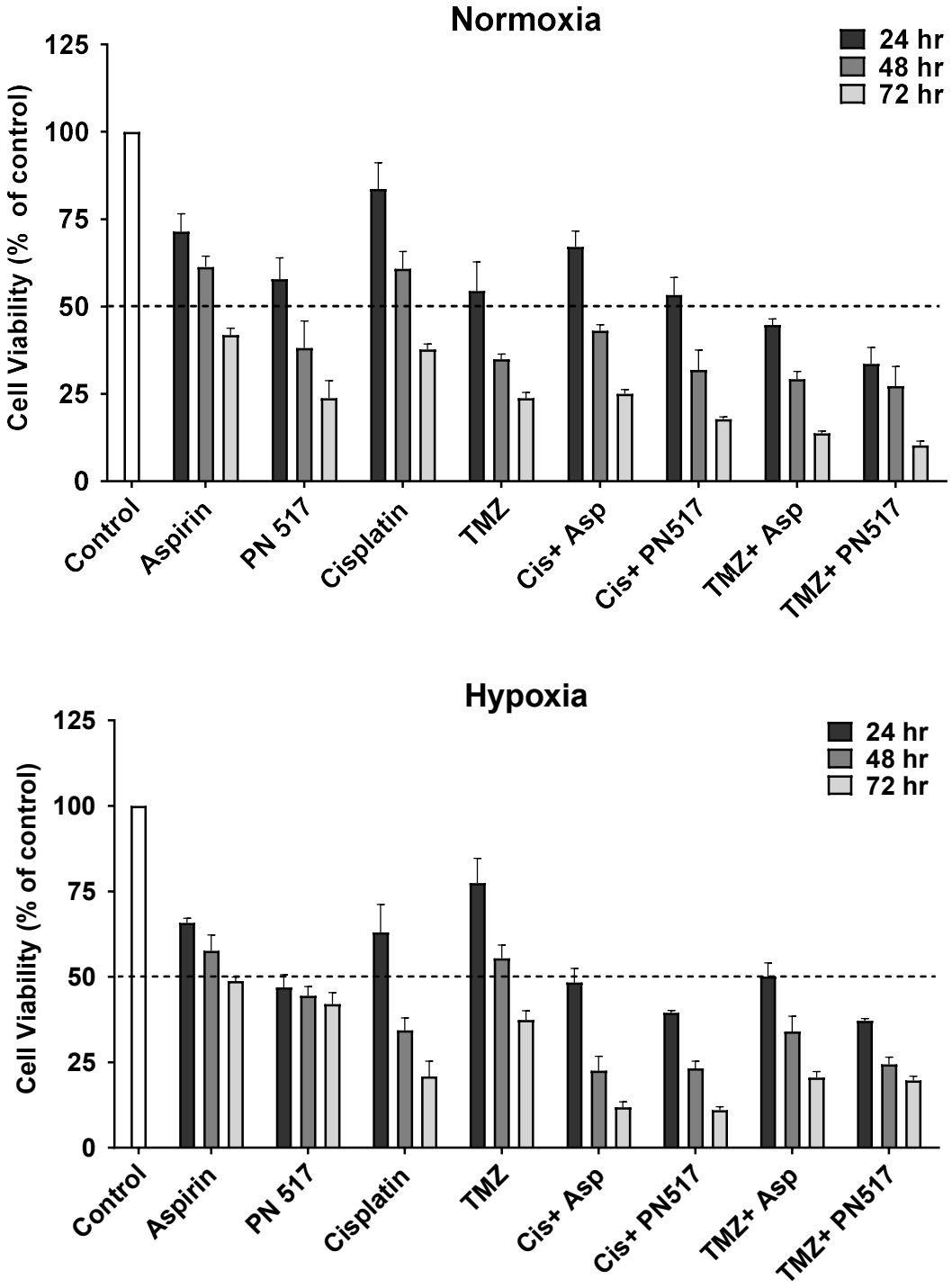

Figure 3. 9. Effect of combined therapy on cell viability of U87-MG cell line. Cell viability assay was performed under normoxia and hypoxia using the PrestoBlue reagent over 24, 48 and 72 hours of drug treatment at IC_{50} as determined by concentration-response curves at 48 hr. Values represents mean ± SEM of three independent experiments. A two-way ANOVA was used to identify significant effects, with Tukey's multiple comparison test, *P < 0.05; **P < 0.01; ***P < 0.001; ****P < 0.0001. The experimental procedure was performed as described in Materials and Methods section 2.2.6.

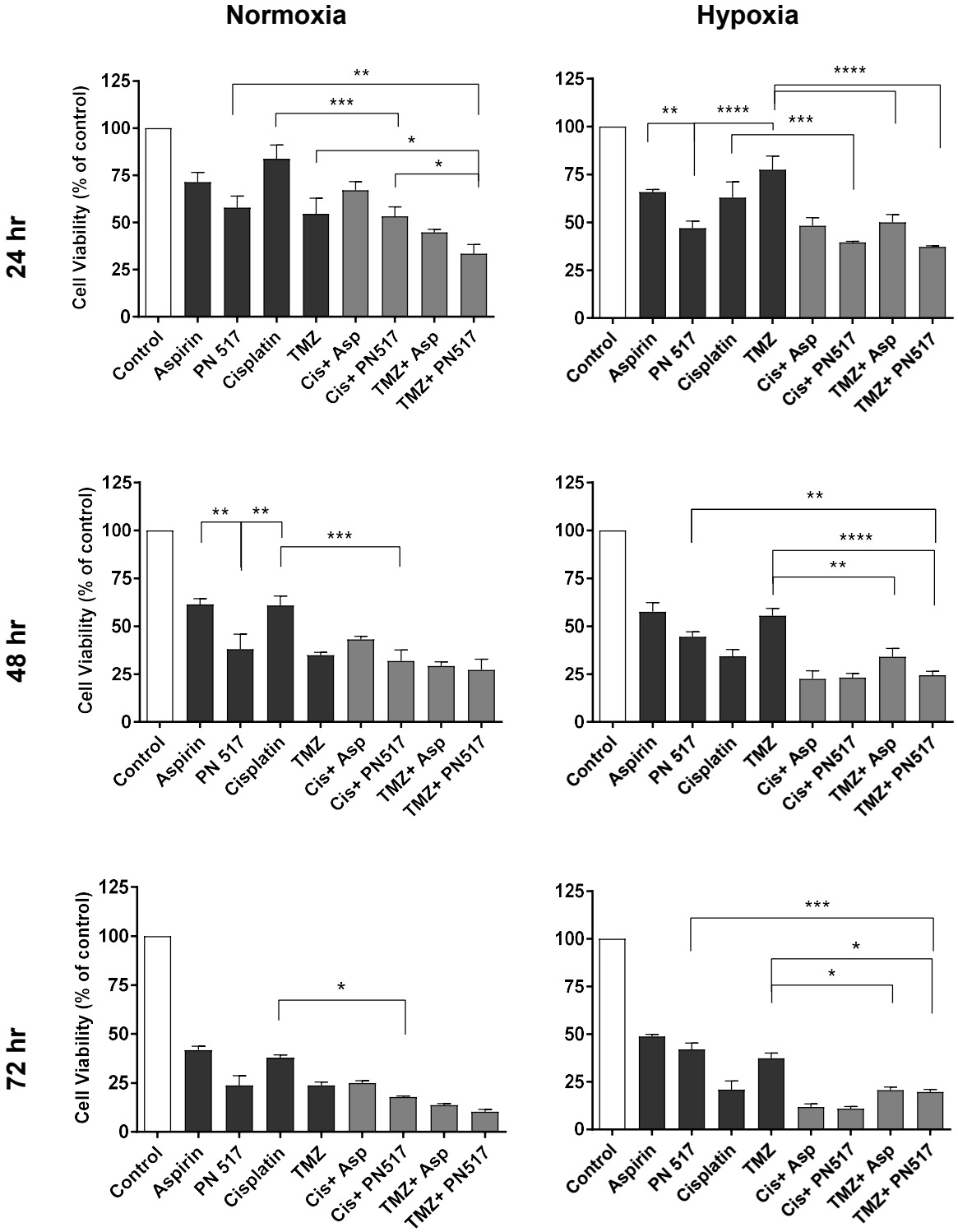

Figure 3. 10. The efficacy of cisplatin or TMZ when in combination compared to monotherapy in U87-MG cell line. Cell viability assay was performed under normoxia and hypoxia using the PrestoBlue reagent over 24, 48 and 72 hours of drug treatment at IC_{50} as determined by concentration-response curves at 48 hr. Values represents mean ± SEM of three independent experiments. A two-way ANOVA was used to identify significant effects, with Tukey's multiple comparison test, *P < 0.05; **P < 0.01; ***P < 0.001; ****P < 0.0001. The experimental procedure was performed as described in Materials and Methods section 2.2.6.

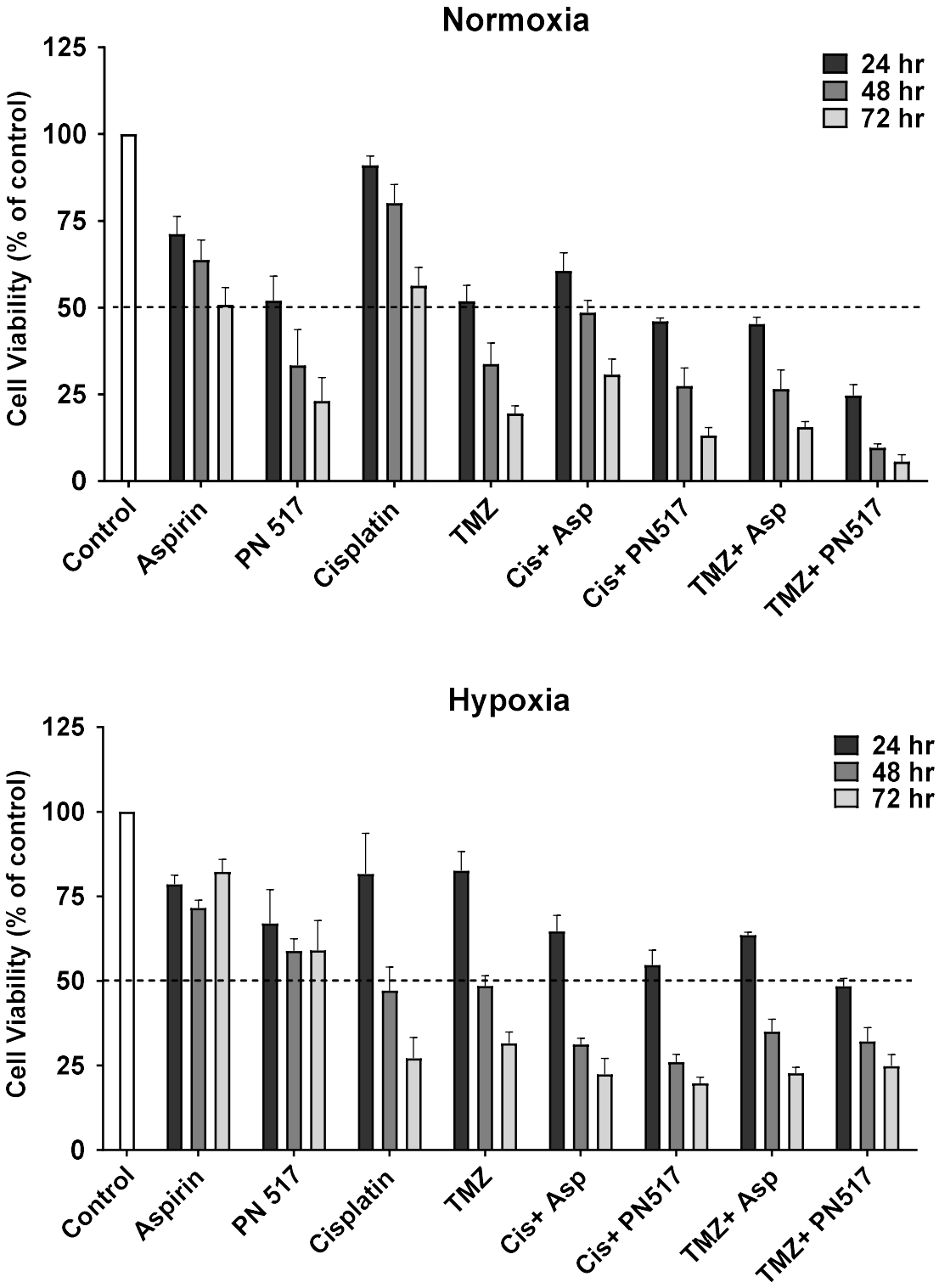

Figure 3. 11. Effect of combined therapy on cell viability of SVG-p12 cell line. Cell viability assay was performed under normoxia and hypoxia using the PrestoBlue reagent over 24, 48 and 72 hours of drug treatment at IC_{50} as determined by concentration-response curves at 48 hr. Values represents mean ± SEM of three independent experiments. A two-way ANOVA was used to identify significant effects, with Tukey's multiple comparison test, *P < 0.05; **P < 0.01; ***P < 0.001; ****P < 0.0001. The experimental procedure was performed as described in Materials and Methods section 2.2.6.

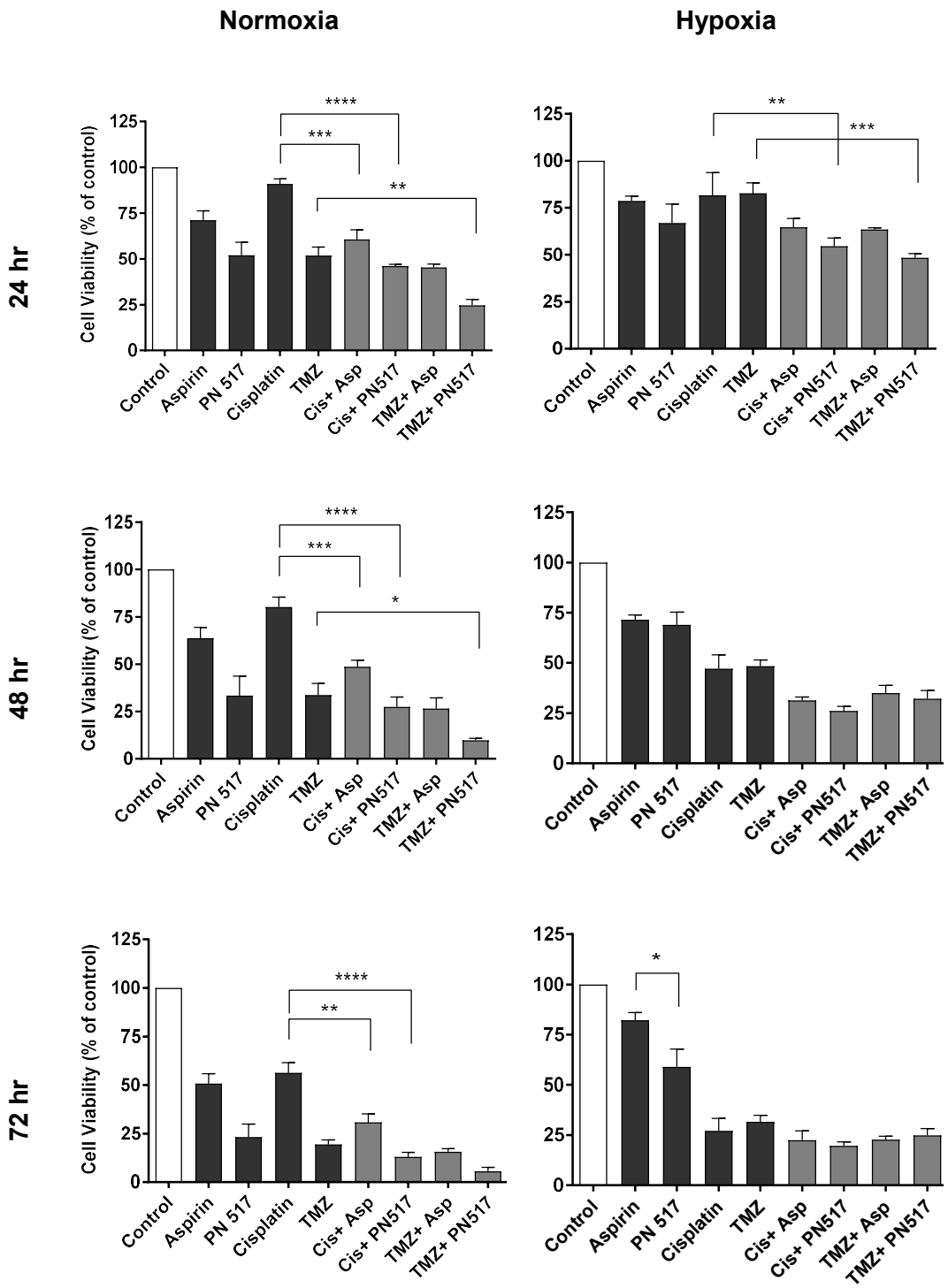

Figure 3. 12. The efficacy of cisplatin or TMZ when in combination compared to monotherapy in SVG-p12 cell line. Cell viability assay was performed under normoxia and hypoxia using the PrestoBlue reagent over 24, 48 and 72 hours of drug treatment at IC_{50} as determined by concentration-response curves at 48 hr. Values represents mean ± SEM of three independent experiments. A two-way ANOVA was used to identify significant effects, with Tukey's multiple comparison test, *P < 0.05; **P < 0.01; ***P < 0.001; ****P < 0.0001. The experimental procedure was performed as described in Materials and Methods section 2.2.6.

3.2.5. Effects of drug treatment on cell proliferation

Since cell proliferation can affect cell viability and is an important factor in determining cytotoxicity of the drugs, initial investigations aimed to examine any changes following drug treatment using the fluorescent proliferation marker CFDA-SE. The rate of cell proliferation was assessed in both cell lines after over five days of drug treatment, either separately or in combination, in normoxia and hypoxia. IC_{25} values determined from concentration-response curves at 48 hr were used for all drugs and the same values were applied for both cell lines under both conditions.

In the U87-MG cell line, under normoxia, control reduction in CFSE fluorescence was observed to 55±2.6, 38±3.8, 18±2.6, 14±3.2 and 8±2.5% at day 1,2,3,4 and 5, respectively (Fig 3.13). All monotherapy treatments reduced the proliferation rate in a time dependent manner (Aspirin $p<0.05$, PN517 $p<0.01$, cisplatin $p<0.0001$ and TMZ $p<0.001$) with the greatest effect following cisplatin treatment where a reduction in CFSE fluorescence was noticed to 67±9.9, 68±8.4, 63±11.1, 53±12 and 21±2.8% through the five days. However, when comparison was made between normoxia and hypoxia, it was clear that hypoxic conditions reduced cisplatin efficacy $p<0.05$. Similarly, TMZ had less of an effect under hypoxia compared to normoxia $p<0.05$, whereas, the effect of PN517 was largely unchanged, $p>0.05$.

With regards the effects of combinations (Fig 3.14), the biggest effect on proliferation rate was observed following treatment with the combination of cisplatin and PN517 under normoxia with a significant inhibition of the proliferation at day 2 (73±6%, $p<0.001$), day 3 (69±9.5%, $p<0.0001$), day 4 (65±4.5%, $p<0.0001$), and day 5 (38±4.9%, $p<0.01$) (Fig 3.15), but again the effect was reduced under hypoxia but remained significantly different from the control at day 4, $p<0.05$. Interestingly, aspirin and PN517 appeared to have a stronger combination effect with TMZ, where TMZ and PN517 combination effect was also maintained in hypoxia with a reduction just to 52±4.2% at day 5 (Fig 3.14 and 3.16). Significant statistically differences are summarised in Figures 3.15 and 3.16.

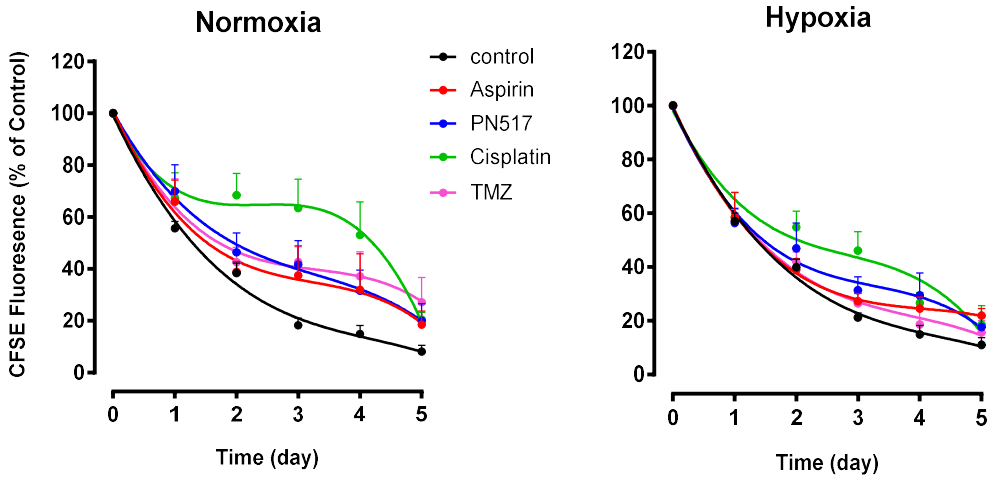

Figure 3. 13. The effect of drug treatment on cell proliferation of U87-MG cell line under normoxia and hypoxia. Data illustrates the effect of the monotherapy on U87-MG cells proliferation using CFDA-SE assay following drug treatment at IC_{25} as determined by concentration-response curves at 48 hr, where a decrease in CFSE fluorescence indicates cell proliferation. Values represent mean ± SEM of six independent experiments. A two-way ANOVA was used to identify significant effects, with Tukey's multiple comparison test. The experimental procedure was performed as described in Materials and Methods section 2.2.8.

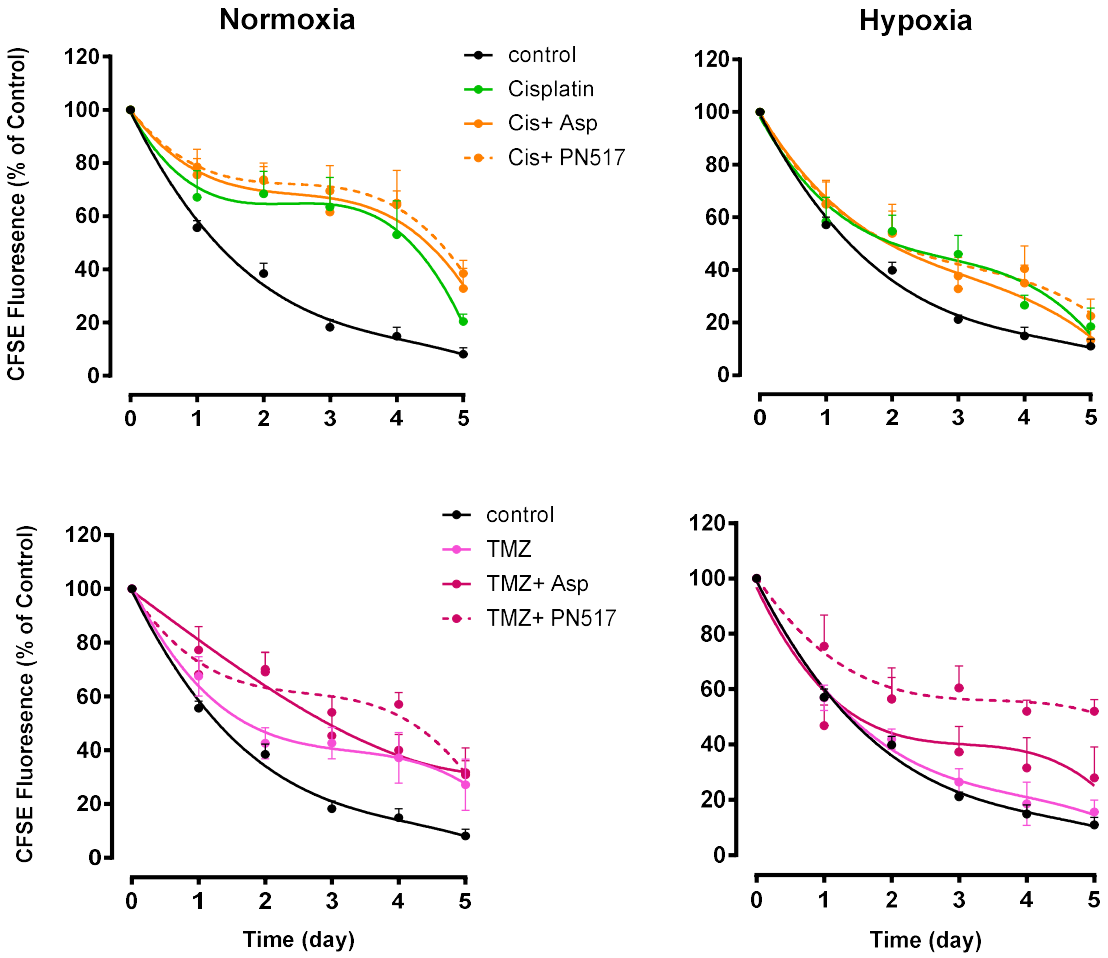

Figure 3. 14. The effect of combined therapy on cell proliferation of U87-MG cell line under normoxia and hypoxia. Data illustrates the effect of the combination therapy on U87-MG cells proliferation using CFDA-SE assay over five days, under normoxia and hypoxia, following drug treatment at IC_{25} as determined by concentration-response curves at 48 hr, where a decrease in CFSE fluorescence indicates cell proliferation. Values represent mean ± SEM of six independent experiments. A two-way ANOVA was used to identify significant effects, with Tukey's multiple comparison test. The experimental procedure was performed as described in Materials and Methods section 2.2.8.

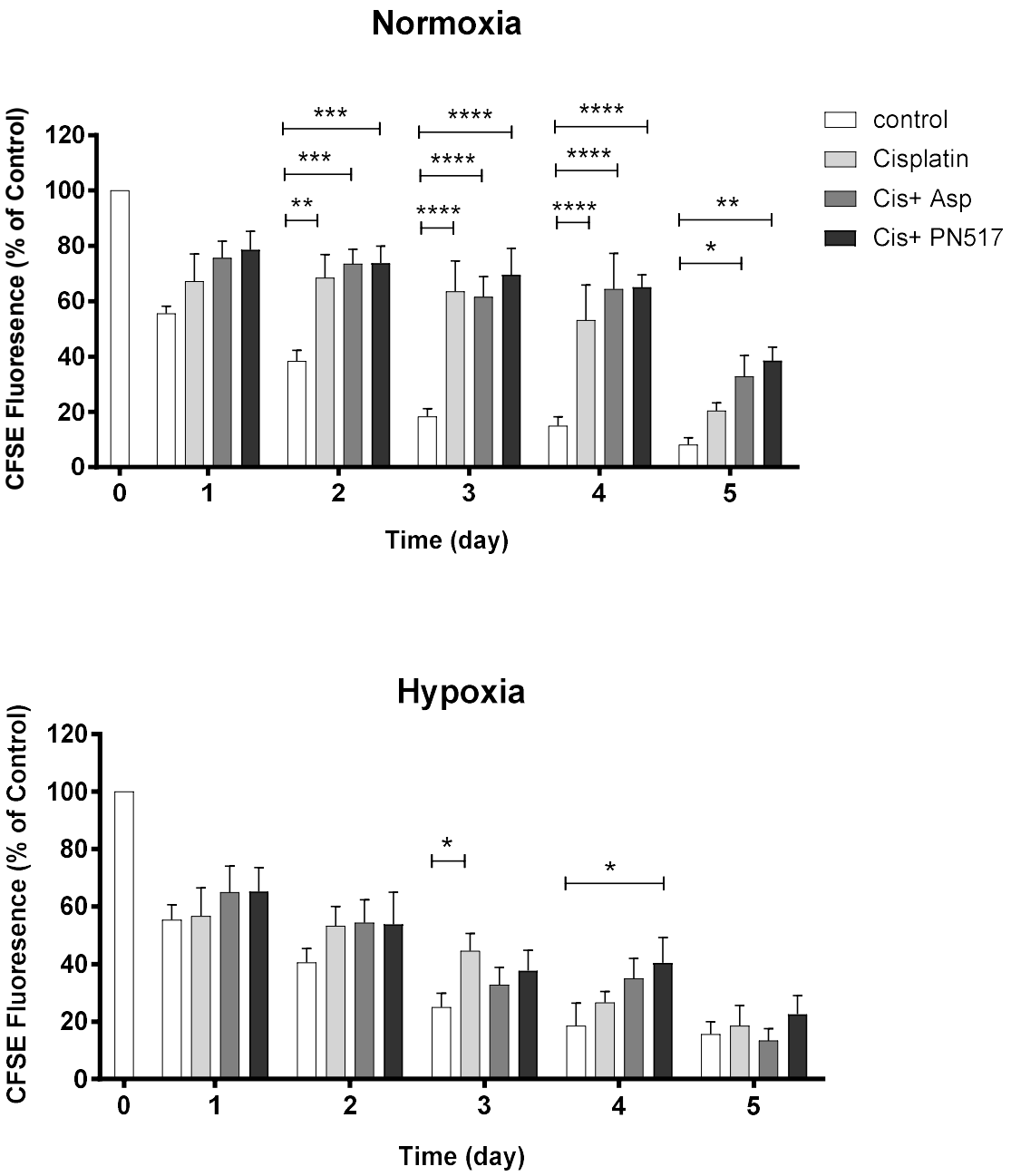

Figure 3. 15. Data illustrates the effect of the cisplatin combined therapy on U87-MG cells proliferation under normoxia and hypoxia. Assay performed using CFDA-SE over a period of 5 days following drug treatment at IC_{25} as determined by concentration-response curves at 48 hr, where a decrease in CFSE fluorescence indicates cell proliferation. Values represent mean ± SEM of six independent experiments. A two-way ANOVA was used to identify significant effects, with Tukey's multiple comparison test, *P < 0.05; **P < 0.01; ***P < 0.001; ****P < 0.0001. The experimental procedure was performed as described in Materials and Methods section 2.2.8.

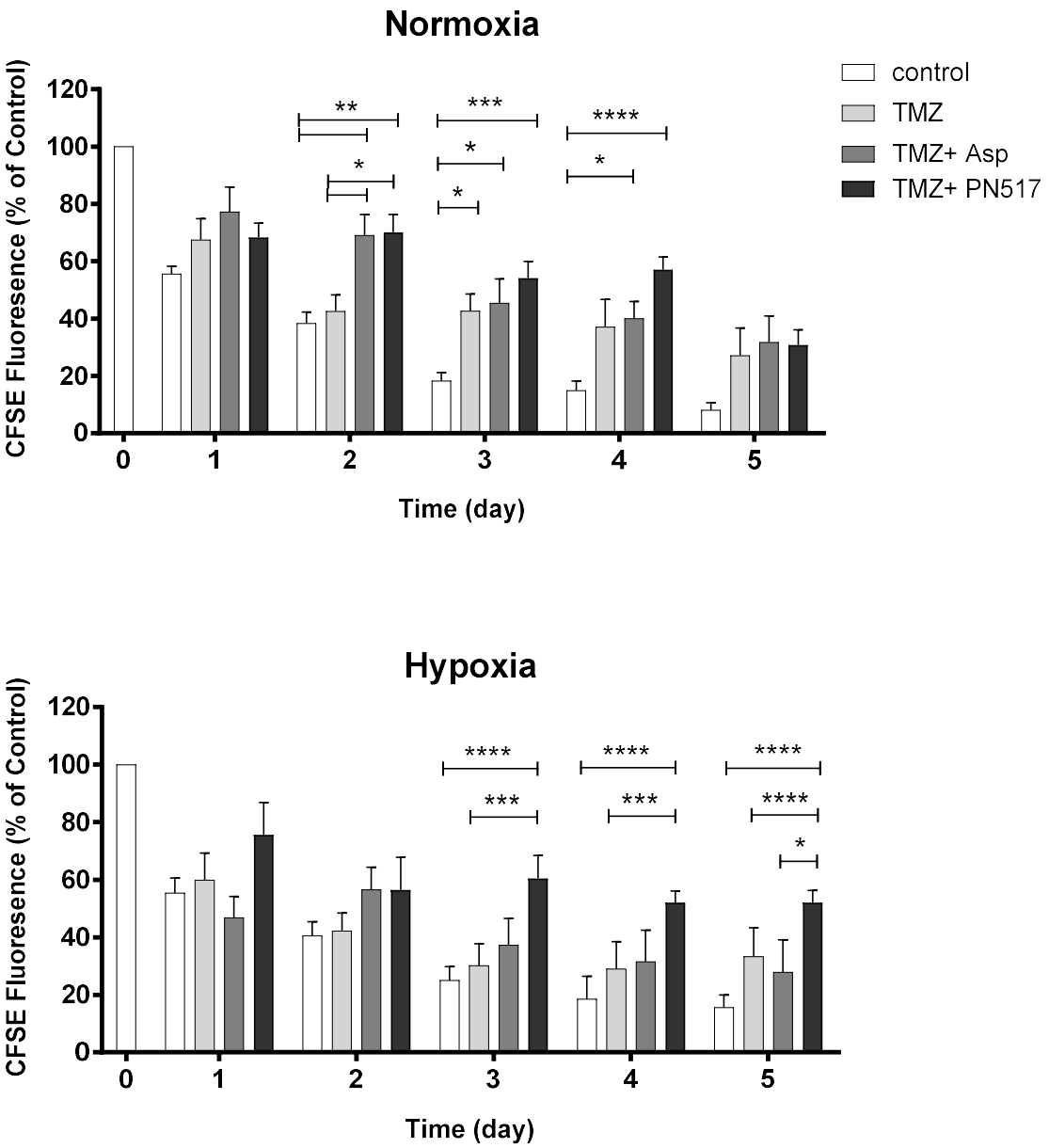

Figure 3. 16. Data illustrates the effect of the temozolomide combined therapy on U87-MG cells proliferation under normoxia and hypoxia. Assay performed using CFDA-SE assay over a period of 5 days following drug treatment at IC_{25} as determined by concentration-response curves at 48 hr, where a decrease in CFSE fluorescence indicates cell proliferation. Values represent mean ± SEM of six independent experiments. A two-way ANOVA was used to identify significant effects, with Tukey's multiple comparison test, *P < 0.05; **P < 0.01; ***P < 0.001; ****P < 0.0001. The experimental procedure was performed as described in Materials and Methods section 2.2.8.

When cell proliferation in SVG-p12 cell line was examined under normoxia, similar results to the U87-MG cell line were observed. A reduction in the control CFSE fluorescence was found in normoxia to 62±7.2, 43±6, 24±2.6, 16±3.3 and 14±2.2% at day 1,2,3,4 and 5, respectively (Fig 3.17). The combination of the drugs seemed to affect the U87-MG proliferation more than in SVG-p12 particularly under hypoxia (Fig 3.18). It is interesting that none of the treatments appeared to have had a particularly large effect on SVG-p12 proliferation and neither mono-therapy nor combinations produced significant changes in fluorescence compared to control (p>0.05) other than aspirin combinations on just day 2 under normoxia (Fig 3.19 and 3.20). Compared to the control fluorescence value at day 2 (43.8 ±6%), the combination of aspirin with cisplatin or TMZ produced a reduction in the fluorescence just to 69.6 ±9.3% (p>0.01) or 83.1 ±7.4% (p>0.001), respectively. Representative histogram plots for the proliferation data acquired by flow cytometry are shown in figures 9.1-9.4 (U87-MG), and figures 9.5-9.8 (SVG-p12), where a shift in peak to the left indicates cell proliferation, with each colour indicating a different timepoint of analysis. The vehicle (1% DMSO) did not show any significant effect on cell proliferation in either cell line (p>0.05).

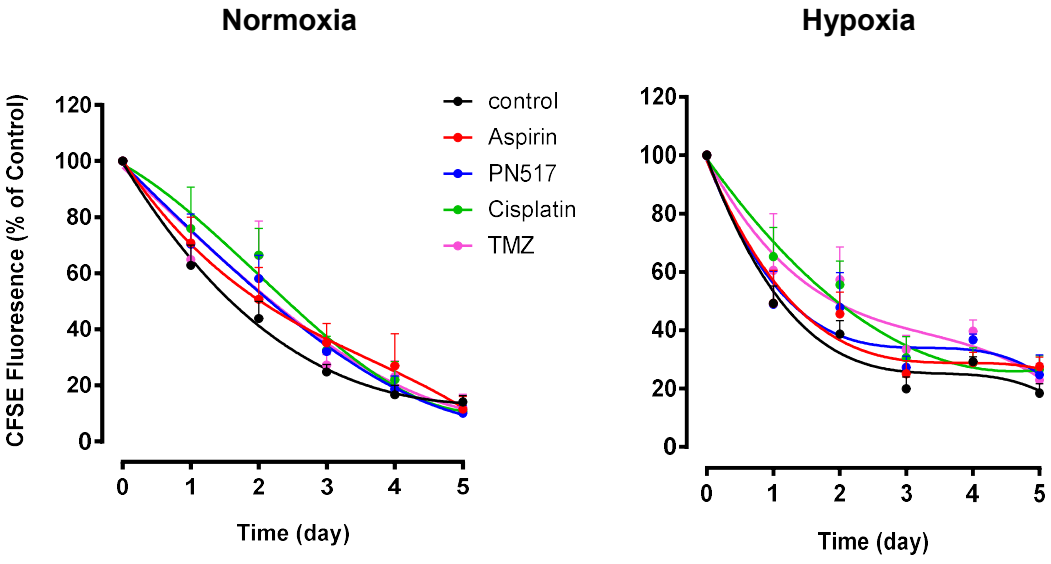

Figure 3. 17. The effect of drug treatment on cell proliferation of SVG-p12 cell line under normoxia and hypoxia. Data illustrates the effect of the monotherapy on SVG-p12 cells proliferation using CFDA-SE assay following drug treatment at IC_{25} as determined by concentration-response curves at 48 hr, where a decrease in CFSE fluorescence indicates cell proliferation. Values represent mean ± SEM of six independent experiments. A two-way ANOVA was used to identify significant effects, with Tukey's multiple comparison test. The experimental procedure was performed as described in Materials and Methods section 2.2.8.

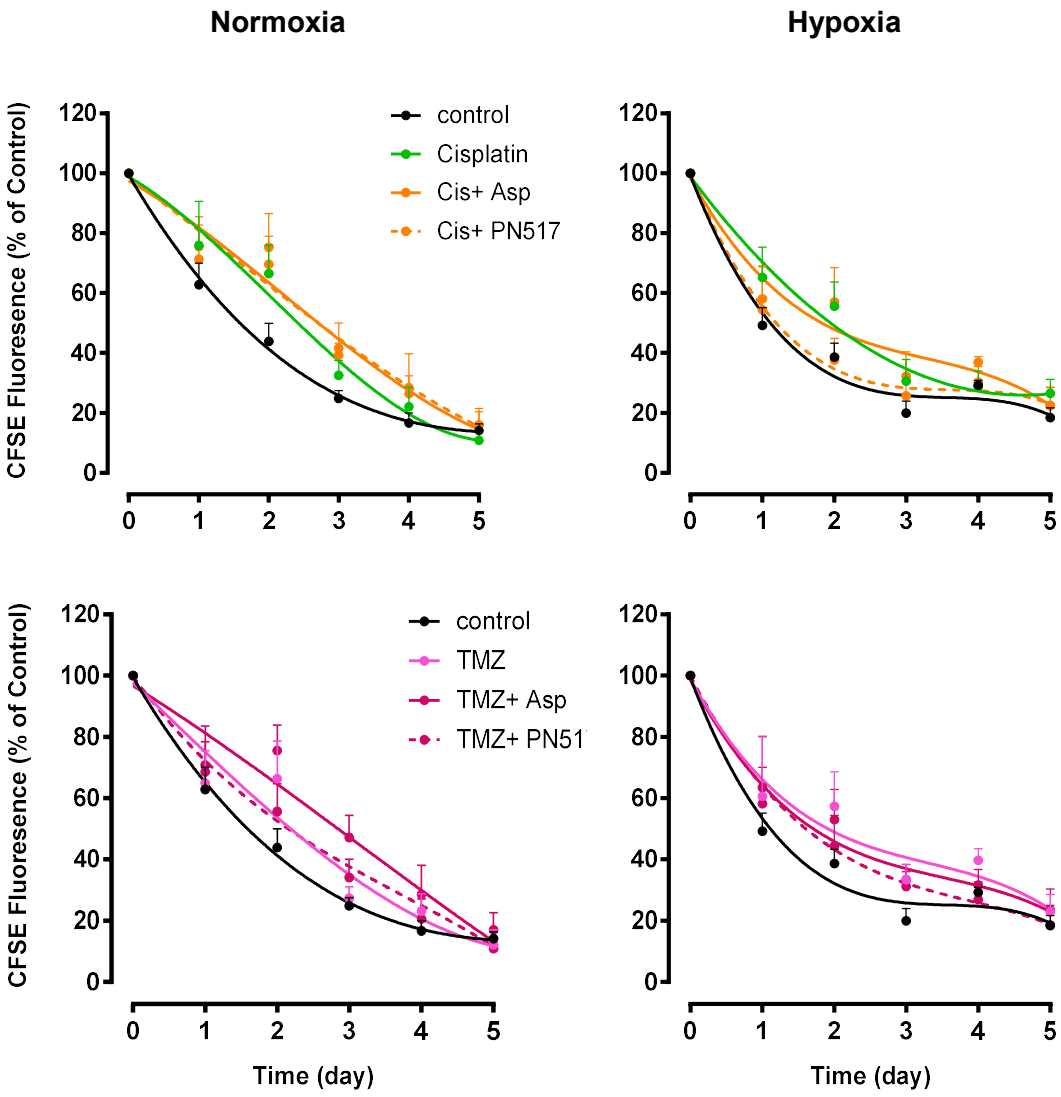

Figure 3. 18. The effect of combined therapy on cell proliferation of SVG-p12 cell line under normoxia and hypoxia. Data illustrates the effect of the combination therapy on SVG-p12 cells proliferation using CFDA-SE assay following drug treatment at IC_{25} as determined by concentration-response curves at 48 hr, where a decrease in CFSE fluorescence indicates cell proliferation. Values represent mean ± SEM of six independent experiments. A two-way ANOVA was used to identify significant effects, with Tukey's multiple comparison test**.** The experimental procedure was performed as described in Materials and Methods section 2.2.8.

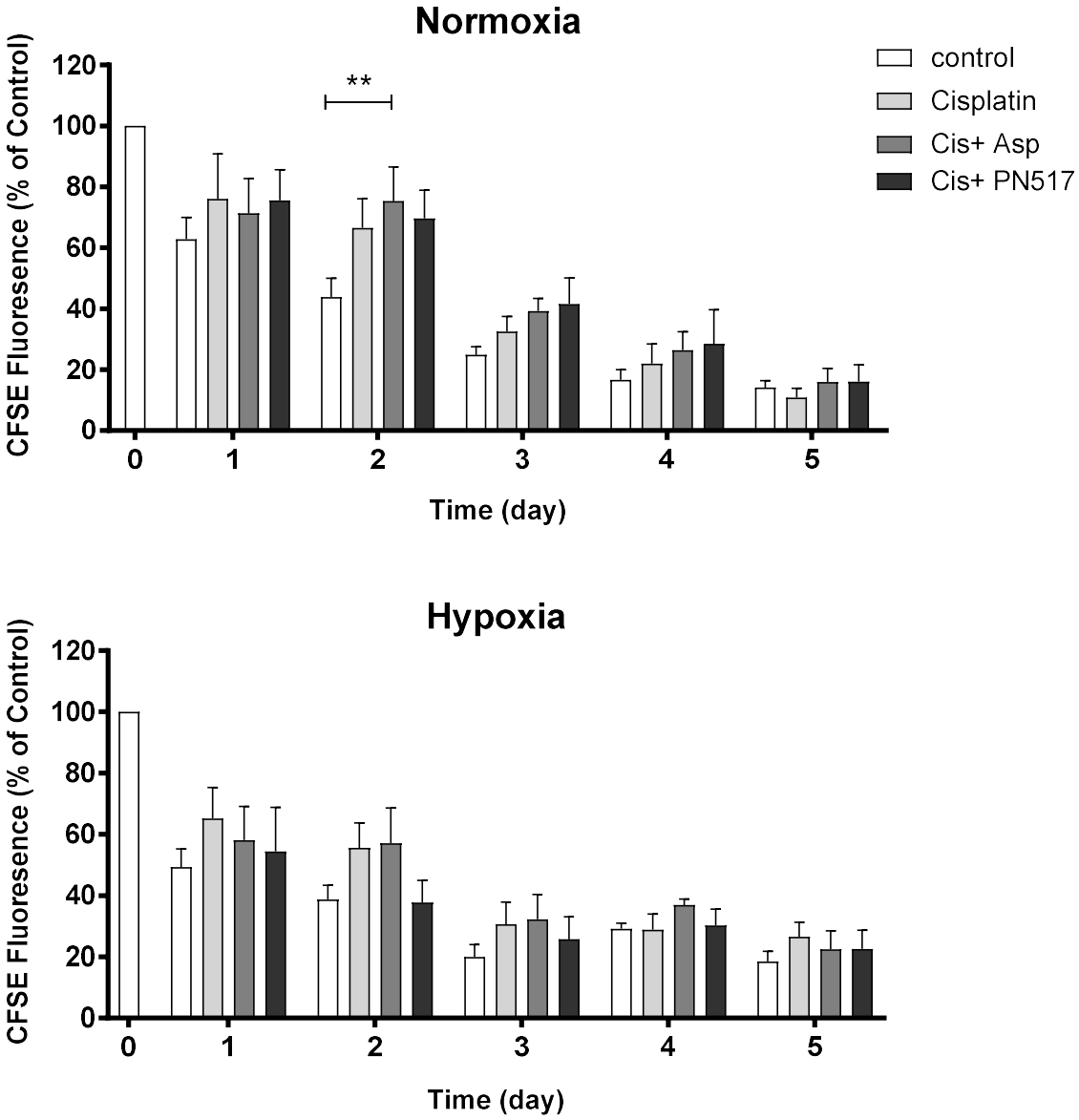

Figure 3. 19. Data illustrates the effect of the cisplatin combined therapy on SVG-p12 cells proliferation under normoxia and hypoxia. Assay performed using CFDA-SE assay following drug treatment at IC_{25} as determined by concentration-response curves at 48 hr, where a decrease in CFSE fluorescence indicates cell proliferation. Values represent mean ± SEM of six independent experiments. A two-way ANOVA was used to identify significant effects, with Tukey's multiple comparison test, *P < 0.05; **P < 0.01; ***P < 0.001; ****P < 0.0001. The experimental procedure was performed as described in Materials and Methods section 2.2.8.

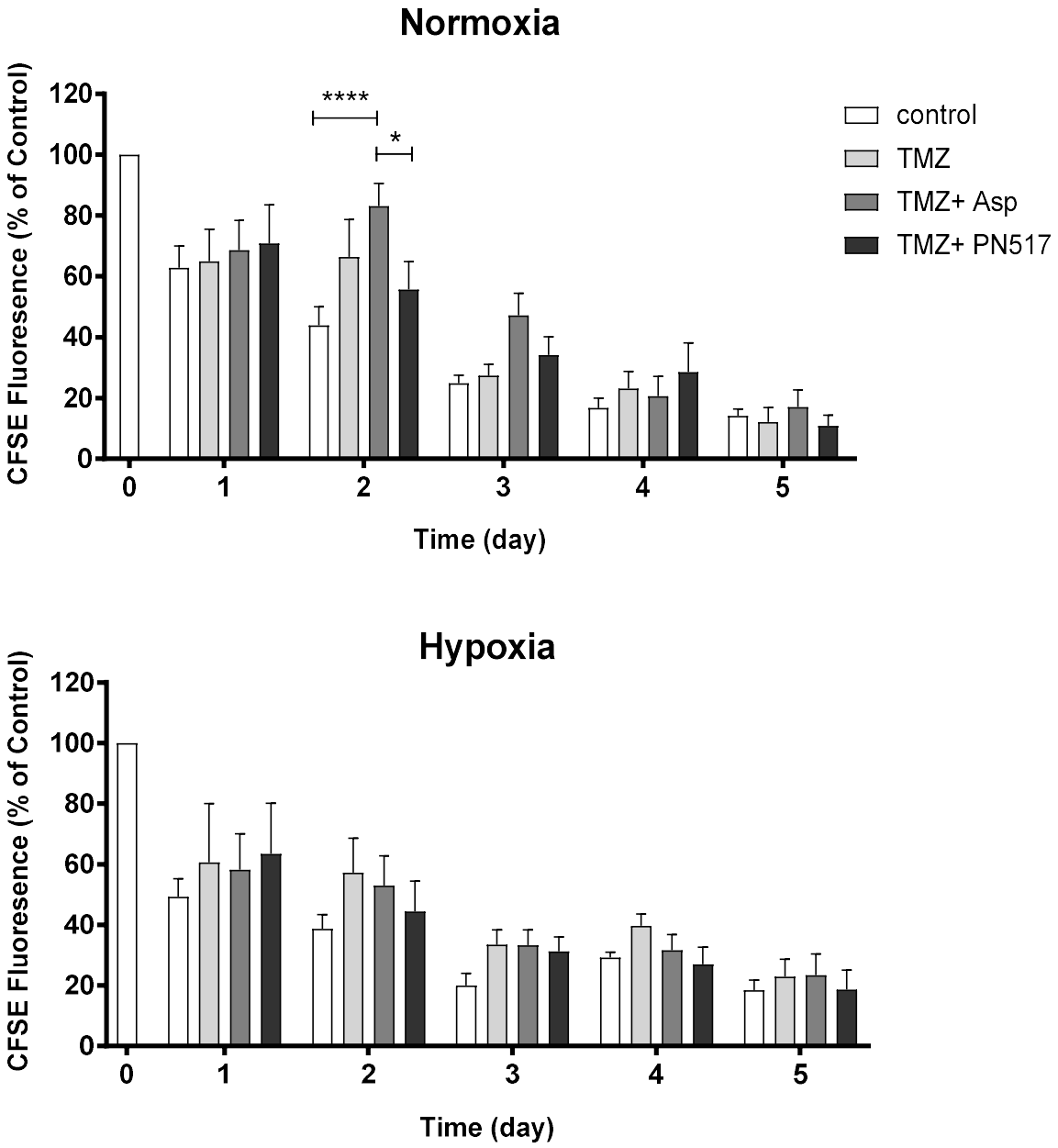

Figure 3. 20. Data illustrates the effect of the temozolomide combined therapy on SVG-p12 cells proliferation under normoxia and hypoxia. Assay performed using CFDA-SE assay following drug treatment at IC_{25} as determined by concentration-response curves at 48 hr, where a decrease in CFSE fluorescence indicates cell proliferation. Values represent mean ± SEM of six independent experiments. A two-way ANOVA was used to identify significant effects, with Tukey's multiple comparison test, *P < 0.05; **P < 0.01; ***P < 0.001; ****P < 0.0001. The experimental procedure was performed as described in Materials and Methods section 2.2.8.

3.2.6. Effects of drug treatment on cell cycle

Cell cycle progression is a highly controlled process and essential for the regulation of cell proliferation. Since cell death because of drug treatment can take place due to cell cycle arrest, initial investigations aimed to assess any effects of the drug treatments, either separately or in combination, on cell cycle in both cell lines using PI staining to quantify the amount of DNA present in cell population, under normoxia and hypoxia. IC_{25} values determined from concentration-response curves at 48 hr were used for all drugs and the same values applied for both cell lines under different conditions.

Cell cycle analysis of the U87-MG cell line showed controls remained largely unchanged across the five days under both conditions and without no significant difference between normoxia and hypoxia (Figure 3.21). Aspirin and PN517 alone did not appear to affect proliferation over the five days under any condition with no significant differences in cell cycle phases ($p>0.05$).

Cisplatin, however, produced an anticipated change in cell cycle distribution over time with lower cell populations in the G0/Gl phase and higher populations in the G2/M phase as well as increase in the apoptotic cell population (Sub G0). The decreases in G0/Gl population was significantly lower than the control at all timepoints ($p<0.0001$ for day 1 to 4, and $p<0.01$ for day 5) and the increases in G2/M population was significantly higher than the control at days 1 to 4 ($p<0.001$ for day 1, $p<0.0001$ for day 2 and 3, and $p<0.001$ for day 4). However, the effects were smaller under hypoxia (Fig 3.21).

TMZ also produced significant changes in the distribution of cell cycle phases under normoxia, decreasing the G0/G1 population with significant difference at day 1, 2 ($p<0.01$) and 3 ($p<0.05$), and increasing the G2/M population with significant difference at day 2 ($p<0.01$), but this did not change over time and the changes in the phases populations were not significantly different compared to the control at days 4 and 5, $p>0.05$ (Fig 3.21).

Interestingly, in contrast to the cell proliferation assay, neither PN517, nor aspirin enhanced the effect of cisplatin with no significant differences observed

compared to cisplatin alone (Fig 3.22). Also, it was noted that the cells may be recovering from drug treatment by day 5 under normoxia because reverse effect was observed by increasing G0/G1 populations and decreasing G2/M, but this effect was not observed with the combination of Cis and PN517 under hypoxia. In contrast, TMZ combination with PN517 clearly enhanced the effect of TMZ under normoxia with significant changes at day 3 and 4 (p<0.001) but no significant enhancement under hypoxia (Fig 2.23). The apoptotic population was observed to increase with cisplatin and TMZ treatment and their combinations at day 3 and it continues to increase over day 4 and 5 under hypoxia but not under normoxia. However, no significant differences were observed (p>0.05).

A similar pattern of cell cycle distribution was observed for the SVG-p12 cell line, where control remains largely unchanged under normoxia (Fig 3.24), but a small increase in the G2/M population of the control was found over time under hypoxia. Aspirin and PN517 treated samples were largely unchanged compared to the control under either condition over 5 days (p>0.05). Following the first day of drug treatment under normoxia, there was a significant decrease in the G0/G1 population (p<0.01) and increase in G2/M population (p<0.05) in cells treated with cisplatin and TMZ. Next day, both drugs sustained a significant decrease in the G0/G1 population (p<0.05) but only cisplatin showed significant increase in the G2/M population (p<0.01).

Similarly, at day 1 of drug treatment under hypoxia, cisplatin and TMZ showed significant decrease in the G0/G1 population (p<0.01). At day 2, only TMZ showed significant decrease in the G0/G1 population (p<0.01). However, no significant effect on G0/G1 and G2/M phases was found after day 2 under both conditions (Fig 3.24). Although cisplatin and TMZ effects were less pronounced over time, there was a remarkable increase in the apoptotic population over time under both conditions, with significance increase under hypoxia at day 4 with cisplatin (p<0.05) and at day 5 with TMZ (p<0.05) compared to the control. Also, no obvious effect on cell cycle distribution of combination treatment was observed in the SVG-p12 cells in comparison to the monotherapy, p>0.05 (Fig 3.25, and 3.26).

Representative histogram plots for cell cycle phase distribution acquired by flowcytometry with PI staining following drug treatment are presented in figures 9.9 & 9.10 (U87-MG) and figures 9.11 & 9.12 (SVG-p12). The vehicle (1% DMSO) did not show any significant change in cell cycle distribution in either cell line (p>0.05)

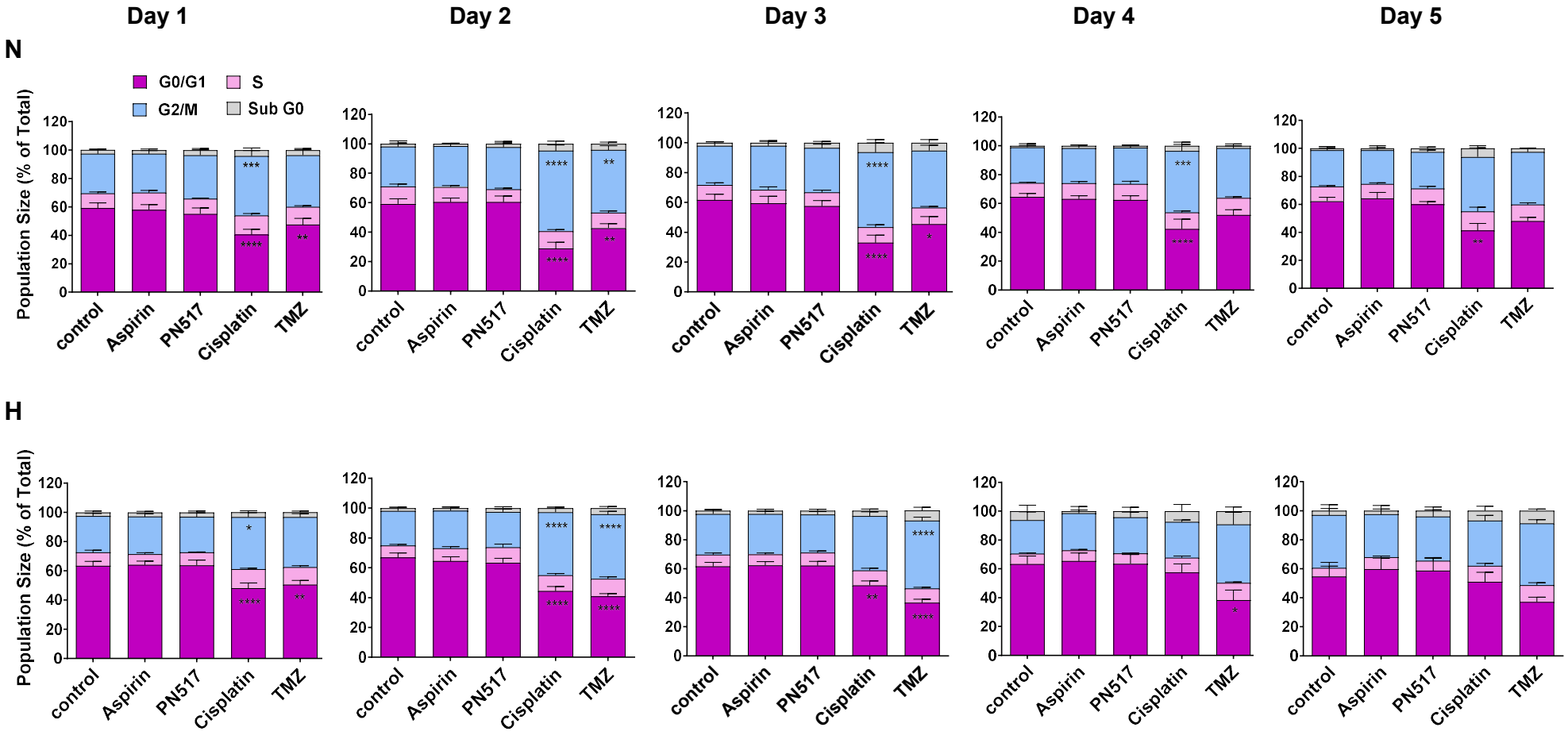

Figure 3. 21. The effect of drug treatment on cell cycle progression in U87-MG cell line under normoxia and hypoxia. Data shows relative proportion of cells in G0/G1 phase, S phase, G2/M phase and Sub G0 (apoptotic) population using PI staining after five days of treatment at IC_{25} as determined by concentration-response curves at 48 hr. N; Normoxia, H; Hypoxia. Values represent mean ±SEM of six independent experiment. A two-way ANOVA was used to identify significant effects, with Tukey's multiple comparison test, *P < 0.05; **P < 0.01; ***P < 0.001; ****P < 0.0001. The experimental procedure was performed as described in Materials and Methods section 2.2.8.

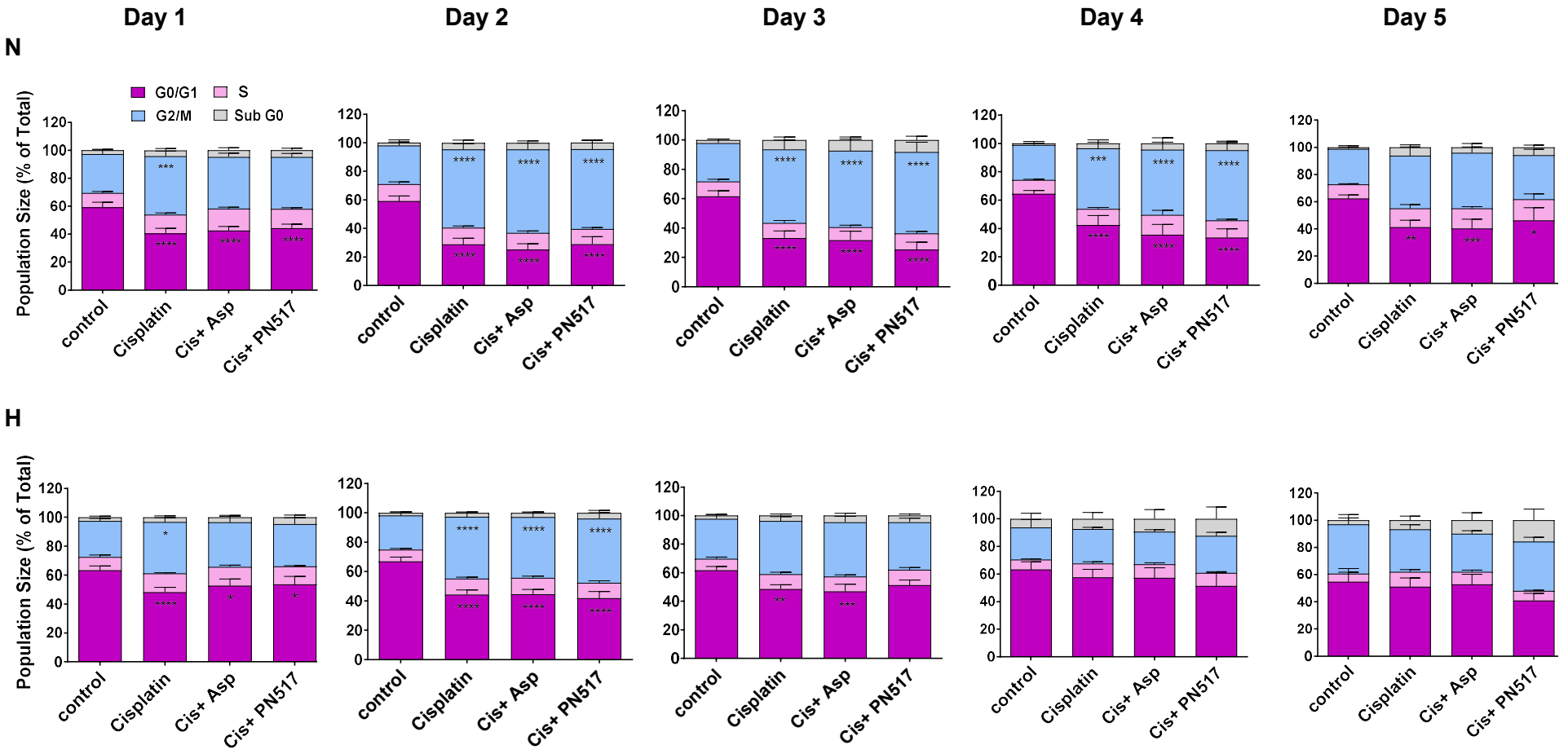

Figure 3. 22. The effect of cisplatin combinations on cell cycle progression in U87-MG cell line under normoxia and hypoxia. Data shows relative proportion of cells in G0/G1 phase, S phase, G2/M phase and Sub G0 (apoptotic) population using PI staining after five days of treatment at IC_{25} as determined by concentration-response curves at 48 hr. N; Normoxia, H; Hypoxia. Values represent mean ±SEM of six independent experiment. A two-way ANOVA was used to identify significant effects, with Tukey's multiple comparison test, *P < 0.05; **P < 0.01; ***P < 0.001; ****P < 0.0001. The experimental procedure was performed as described in Materials and Methods section 2.2.8.

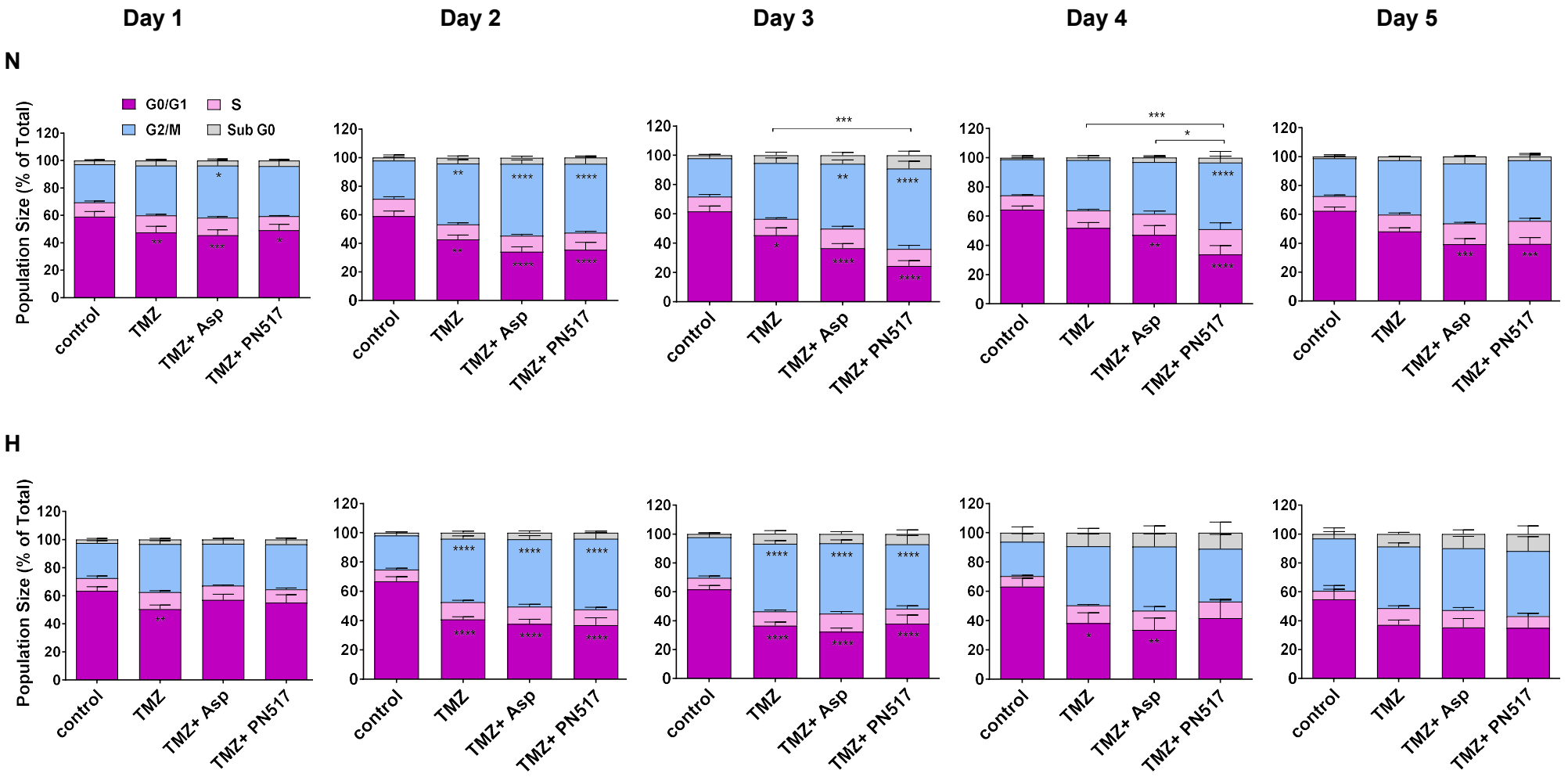

Figure 3. 23. The effect of temozolomide combinations on cell cycle progression in U87-MG cell line under normoxia. Data shows relative proportion of cells in G0/G1 phase, S phase, G2/M phase and Sun G0 (apoptotic) population using PI staining after five days of treatment at IC_{25} as determined by concentration-response curves at 48 hr. N; Normoxia, H; Hypoxia. Values represent mean ±SEM of six independent experiment. A two-way ANOVA was used to identify significant effects, with Tukey's multiple comparison test, *P < 0.05; **P < 0.01; ***P < 0.001; ****P < 0.0001. The experimental procedure was performed as described in Materials and Methods section 2.2.8.

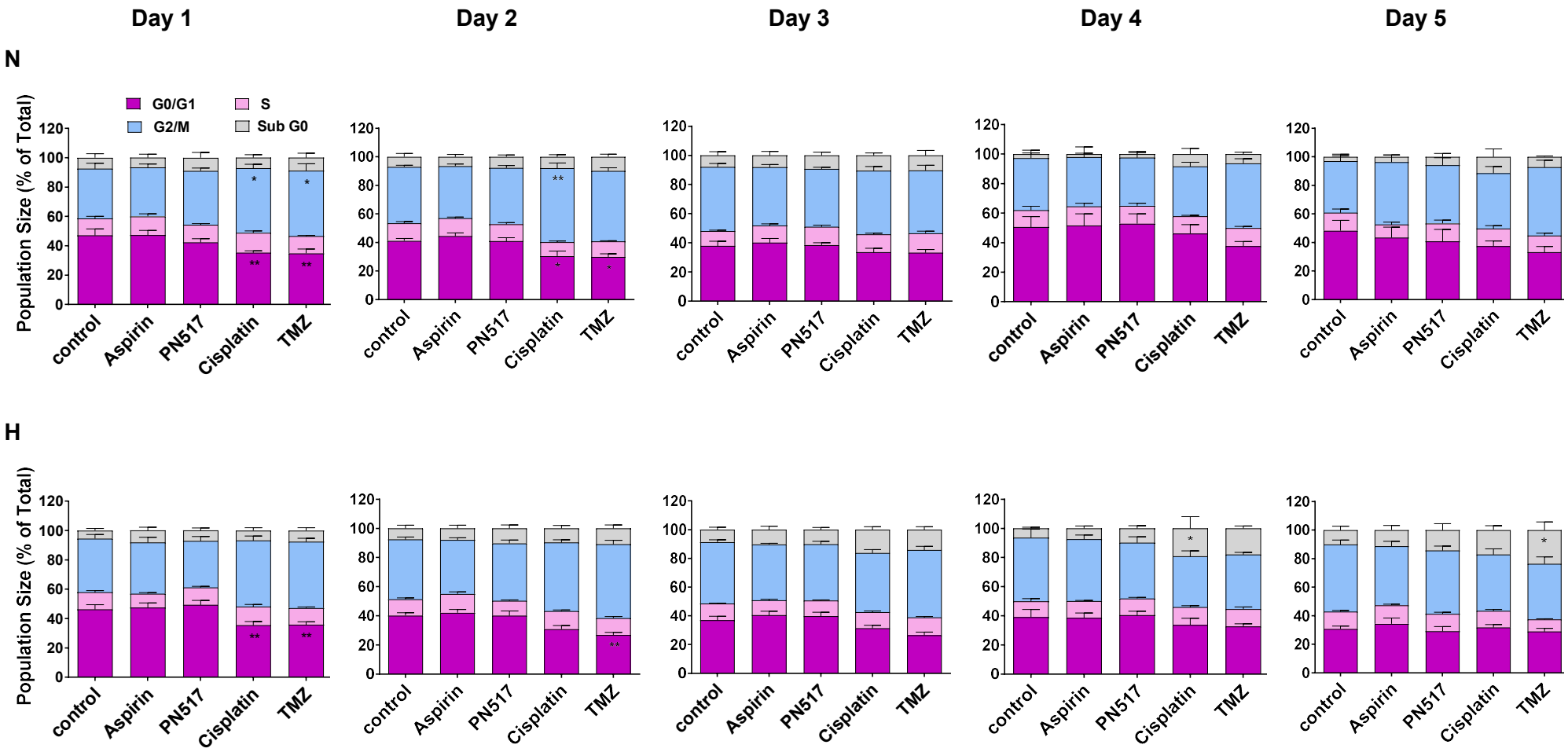

Figure 3. 24. The effect of drug treatment on cell cycle progression in SVG-p12 cell line under normoxia and hypoxia. Data shows relative proportion of cells in G0/G1 phase, S phase, G2/M phase and Sub G0 (apoptotic) population using PI staining after five days of treatment at IC_{25} as determined by concentration-response curves at 48 hr. N; Normoxia, H; Hypoxia. Values represent mean ±SEM of six independent experiment. A two-way ANOVA was used to identify significant effects, with Tukey's multiple comparison test, *P < 0.05; **P < 0.01; ***P < 0.001; ****P < 0.0001. The experimental procedure was performed as described in Materials and Methods section 2.2.8.

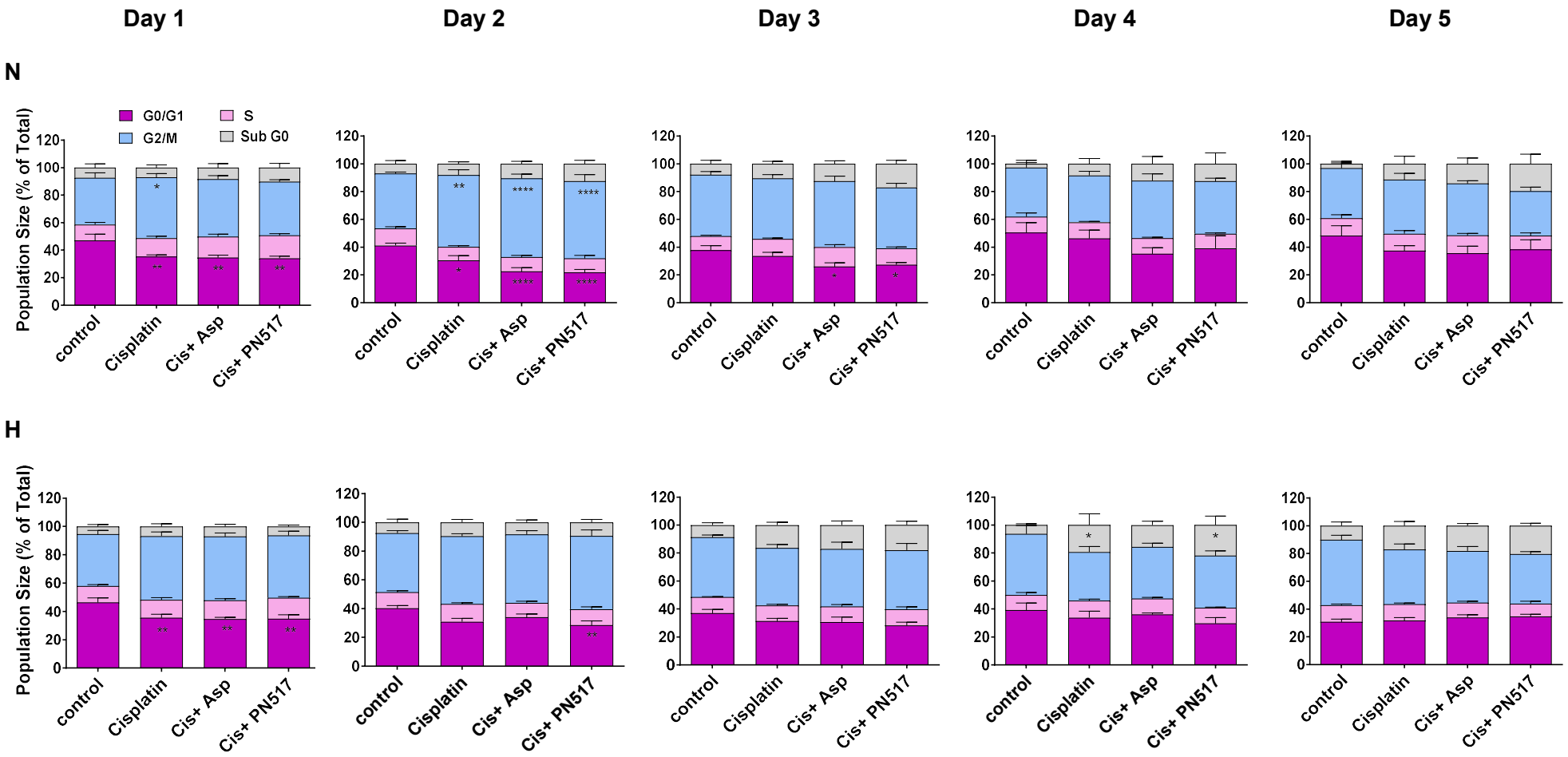

Figure 3. 25. The effect of cisplatin combinations on cell cycle progression in SVG-p12 cell line under normoxia and hypoxia. Data shows relative proportion of cells in G0/G1 phase, S phase, G2/M phase and Sub G0 (apoptotic) population using PI staining after five days of treatment at IC_{25} as determined by concentration-response curves at 48 hr. N; Normoxia, H; Hypoxia. Values represent mean ±SEM of six independent experiment. A two-way ANOVA was used to identify significant effects, with Tukey's multiple comparison test, *P < 0.05; **P < 0.01; ***P < 0.001; ****P < 0.0001. The experimental procedure was performed as described in Materials and Methods section 2.2.8.

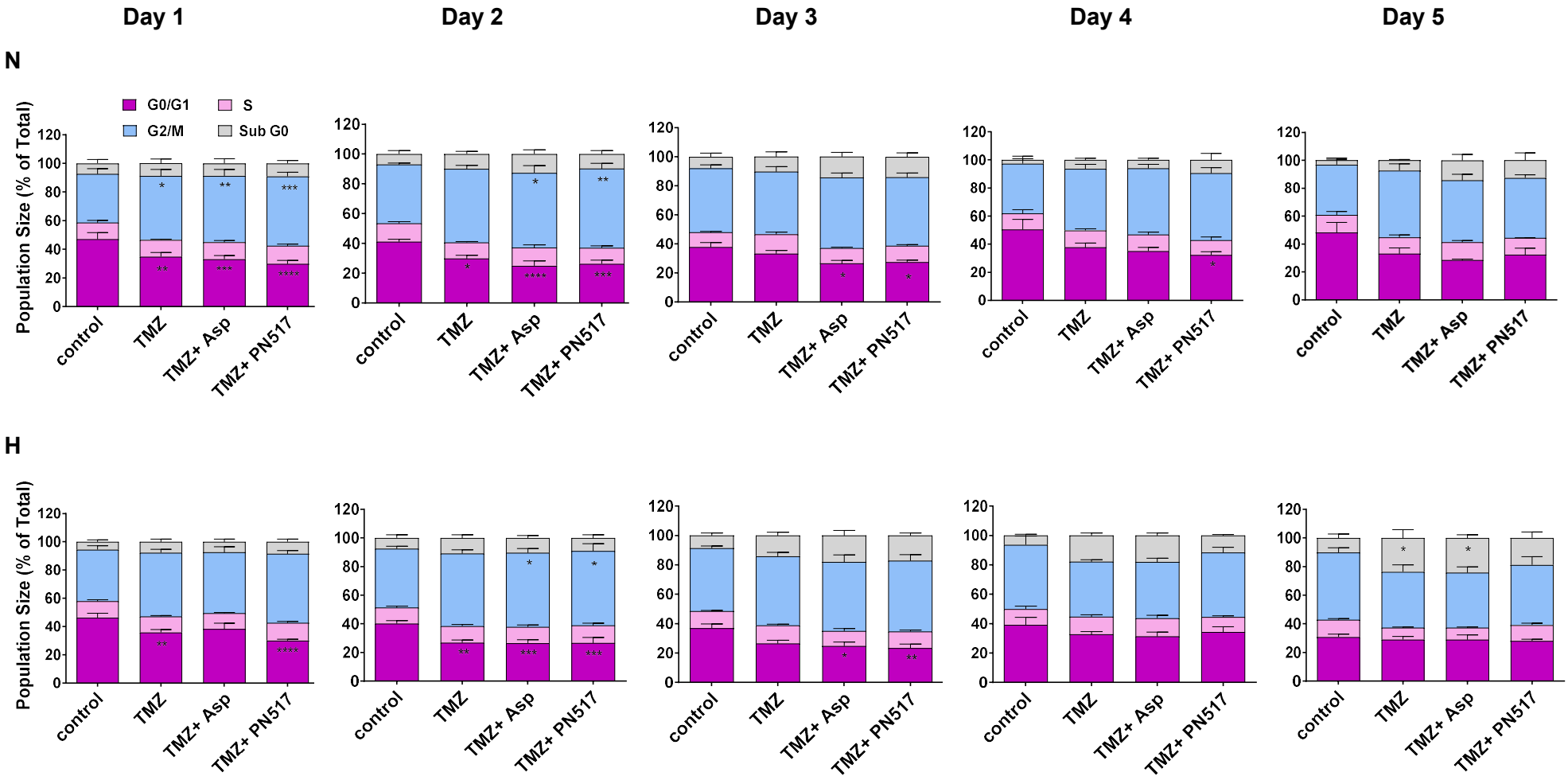

Figure 3. 26. The effect of temozolomide combinations on cell cycle progression in SVG-p12 cell line under normoxia and hypoxia. Data shows relative proportion of cells in G0/G1 phase, S phase, G2/M phase and Sub G0 (apoptotic) population using PI staining after five days of treatment at IC_{25} as determined by concentration-response curves at 48 hr. N; Normoxia, H; Hypoxia. Values represent mean ±SEM of six independent experiment. A two-way ANOVA was used to identify significant effects, with Tukey's multiple comparison test, *P < 0.05; **P < 0.01; ***P < 0.001; ****P < 0.0001. The experimental procedure was performed as described in Materials and Methods section 2.2.8.

Cyclin D1 assessment

The effect of drug treatment on cyclin D1 regulation in the U87-MG and SVG-p12 cell lines was examined after 24 hour of drug treatment at same concentrations used for cell proliferation and cell cycle analysis (IC_{25}) under normoxia and hypoxia. Total cyclin D1 expression was determined for each sample using immunoblotting and densitometry and quantified as a fold change of the untreated cells. Additionally, cyclin D1 degradation indicated by phosphorylation at Thr286, was also determined and normalised to the total protein level of each sample. The housekeeping β-actin protein was used for normalisation of all samples to correct any loading differences between lanes. The experimental conditions applied can be found in the appendix (Table 9.2).

In the U87-MG cell line, although cisplatin and TMZ were the only treatment to show a trend towards a decrease in total cyclin D1 level under normoxia but no significant difference was observed between control and any of the treatments at the timepoint tested (p>0.05), and all other treatments appeared to increase its level but again with no significant difference (Fig 3.27). Under hypoxia, all drug treatments showed a trend toward increasing the expression levels but with no statistically significant differences (p>0.05). Additionally, when assessing the phosphorylation levels of cyclin D1 at Thr286 site, it was found that none of the drug treatments resulted in significant changes in cyclin D1 phosphorylation at the conditions tested with overall lower values under hypoxia (p>0.05) (Fig 3. 28).

Similar results were found in the SVG-p12 control cell line. Total cyclin D1 expression levels remained unchanged following drug treatment. Cisplatin and TMZ showed a small decrease in cyclin D1 expression under both normoxia and hypoxia, however, no significant change was observed with any of the treatments under both conditions (p>0.05) (Fig 3.29). Likewise, phosphorylation levels of cyclin D1 did not show significant alterations following drug treatment compared to the control under both normoxia and hypoxia (p>0.05) (Fig 3.30).

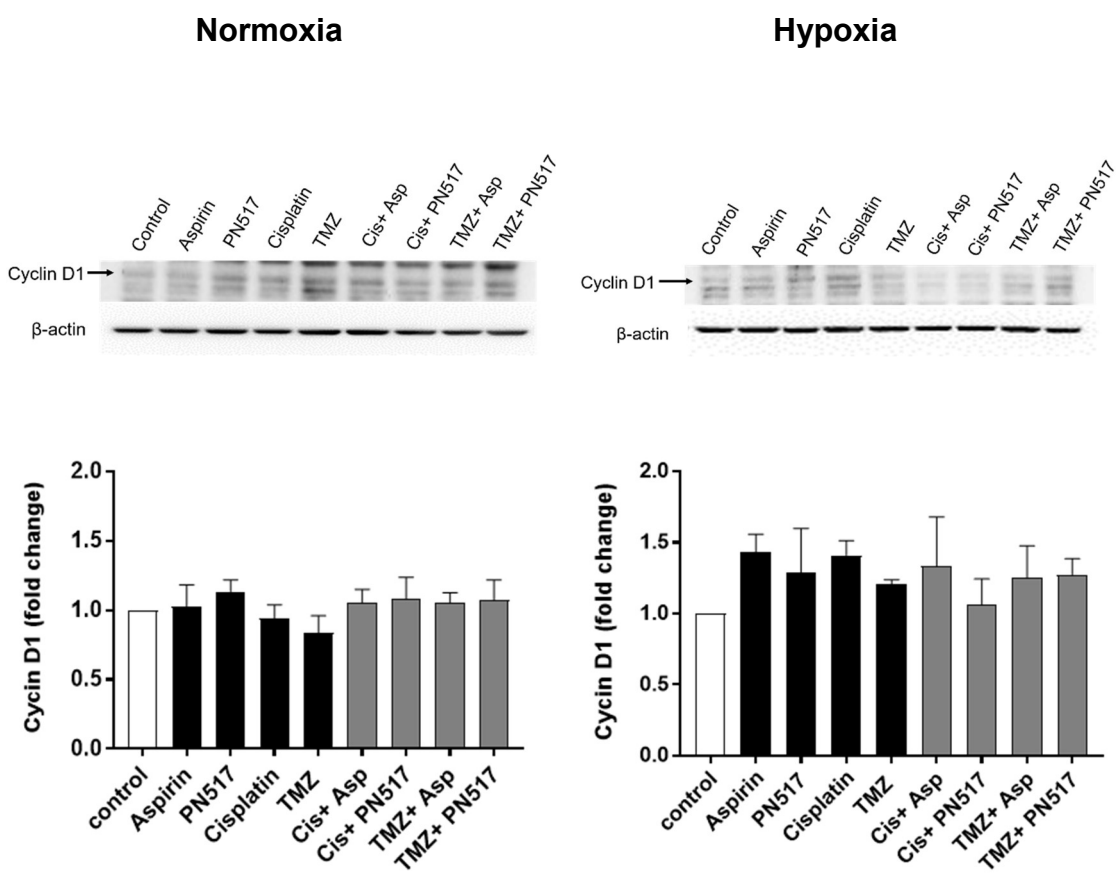

Figure 3. 27. Representative immunoblots and densitometric analysis of cyclin D1 protein levels in U87-MG cell line under normoxia and hypoxia. Data indicate the fold change of total cyclin D1 compared to the control following 24 hr of drug treatment with mono and combination therapy as determined by densitometry. Values represent mean ±SEM of at four independent experiment at least. A two-way ANOVA was used to identify significant effects, with Tukey's multiple comparison test, *P < 0.05; **P < 0.01; ***P < 0.001; ****P < 0.0001. The experimental procedure was performed as described in Materials and Methods section 2.2.16.

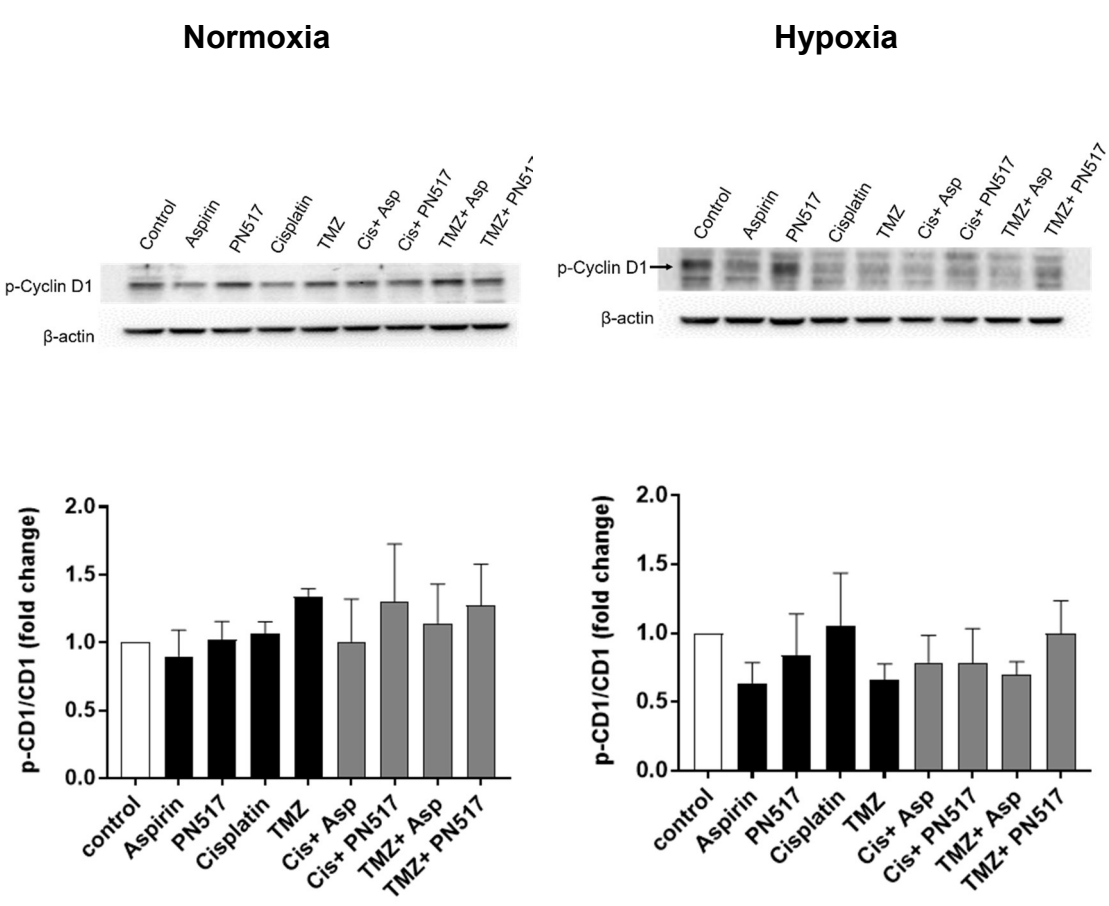

Figure 3. 28. Representative immunoblots and densitometric analysis of phosphorylation levels of cyclin D1 in U87-MG cell line under normoxia and hypoxia. Data indicate the fold change of the p-CD1/CD1 ratio compared to the control following 24 hr of drug treatment as determined by densitometry. Values represent mean ±SEM of at four independent experiment at least. A two-way ANOVA was used to identify significant effects, with Tukey's multiple comparison test, *P < 0.05; **P < 0.01; ***P < 0.001; ****P < 0.0001. The experimental procedure was performed as described in Materials and Methods section 2.2.16.

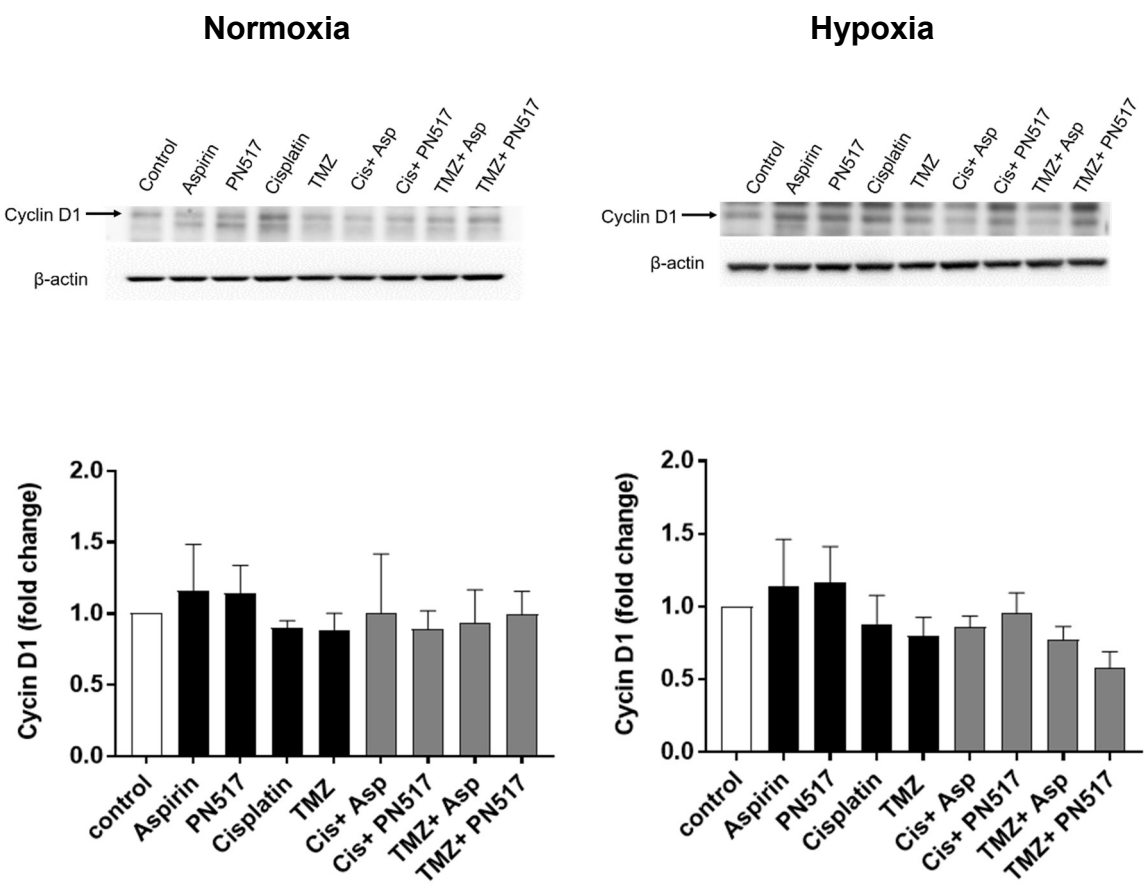

Figure 3. 29. Representative immunoblots and densitometric analysis of cyclin D1 protein levels in SVG-p12 cell line under normoxia and hypoxia. Data indicate the fold change of total cyclin D1 following 24 hr of drug treatment compared to control with mono and combination therapy as determined by densitometry. Values represent mean ±SEM of at four independent experiment at least. A two-way ANOVA was used to identify significant effects, with Tukey's multiple comparison test, *P < 0.05; **P < 0.01; ***P < 0.001; ****P < 0.0001. The experimental procedure was performed as described in Materials and Methods section 2.2.16.

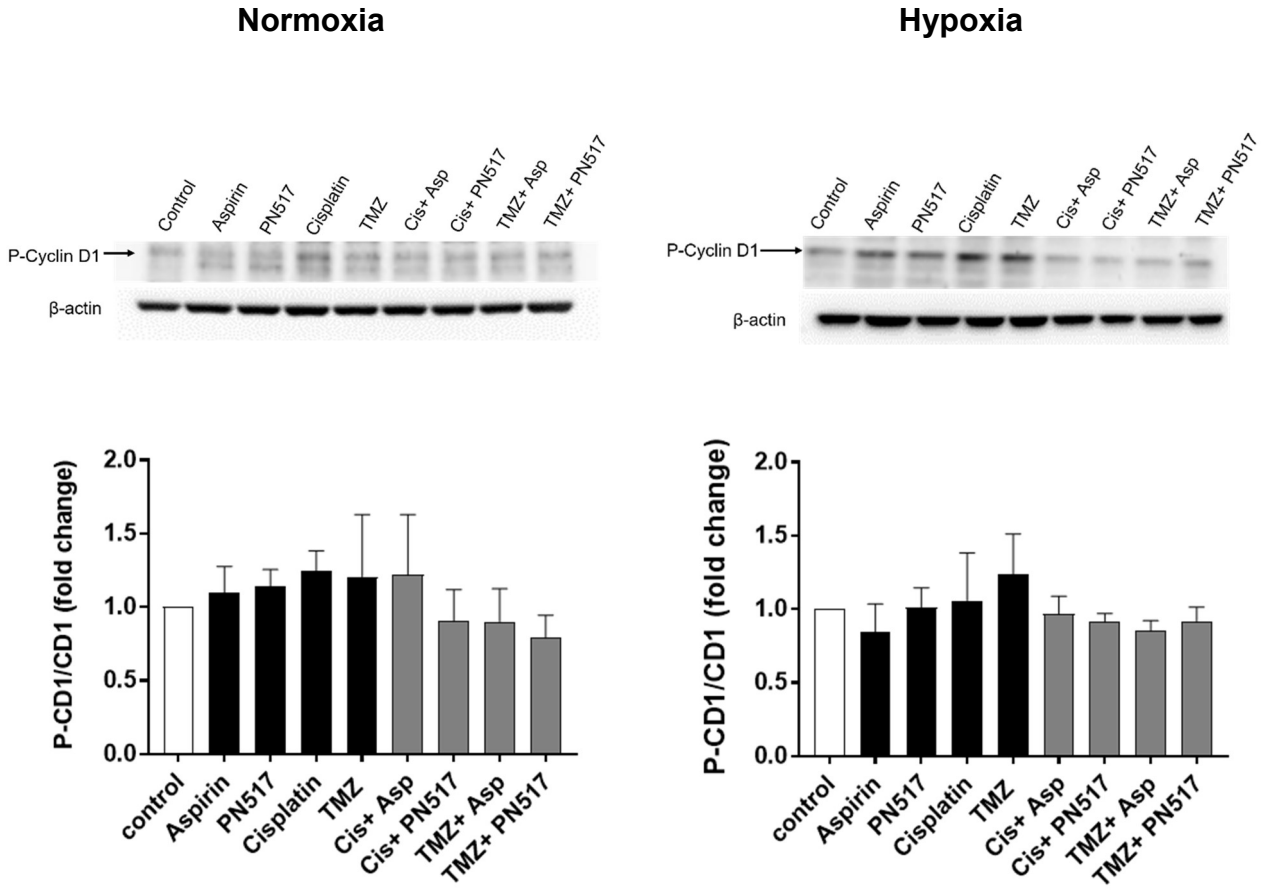

Figure 3. 30. Representative immunoblots and densitometric analysis of phosphorylation levels of cyclin D1 in SVG-p12 cell line under normoxia and hypoxia. Data indicate the fold change of the p-CD1/CD1 ratio following 24 hr of drug treatment compared to control as determined by densitometry. Values represent mean ±SEM of at four independent experiment at least. A two-way ANOVA was used to identify significant effects, with Tukey's multiple comparison test, *P < 0.05; **P < 0.01; ***P < 0.001; ****P < 0.0001. The experimental procedure was performed as described in Materials and Methods section 2.2.16.

3.2.7. Effects of drug treatment on wound healing

In order to examine the effect of drug treatment on cell migration, the *in vitro* scratch assay was performed. Both U87-MG and SVG-p12 cell monolayers were scratched, and treated with all drugs, separately or in combination at IC_{25} and imaged every two hours over a period of 18 hours in normoxia. With regards to hypoxia, images were taken directly after adding drug treatment and following 18 hours incubation. Images were analysed, and gap closure was monitored and expressed as the percentage of 0 hr timepoint. Representative images are shown in Figures 3.31- 3.34.

The scratch assay in the non-treated U87-MG cell line showed almost complete closure of the wound over 18 hours under normoxia (~90%). Aspirin, cisplatin and TMZ showed similar patterns to the control over the time period studied (p>0.05). However, following treatment with PN517, the closing rate was clearly slower and largely distinguished among the single drug treatments (Fig 3.35). Furthermore, the combinations of PN517 with cisplatin or TMZ largely enhanced the effect of cisplatin and TMZ on their own at all the timepoints while aspirin seemed to produce a smaller decrease in the closure rate in combination when compared to the PN517 combinations (Fig 3.35).

The percentages of scratch closure following 18 hours of incubation with each monotherapy showed overall lower values compared to the control, however, no significant differences observed except for PN517 which significantly decreased wound healing under normoxia (87±1.3% vs. 59 ±10%, p<0.05) and hypoxia (74±1.9 vs. 50±7.4, p<0.05) (Fig 3.36). Additionally, the combinations of standard drugs with PN517 produced the greatest reduction in wound healing and had a significantly slower rate than cisplatin alone (76.5±2.6% vs. 47.5 ±6.4%, p<0.05) or TMZ alone (77.8±2.1 vs. 44.8±4.9, p<0.01) under normoxia (Fig 3.37).

With respect to SVG-p12 cells, representative images are shown in Figures 3.38-3.41. Similar effects were observed following drug treatment when compared to U87-MG results (Fig 3.42). In control cultures, the scratch did not completely close over the 18-hour period (~80%). Cisplatin and TMZ showed a trend towards slower closure rate, whereas aspirin did not appear to have an effect on wound

healing at all with no significant differences for any of these drugs compared to the control (p>0.05). Treatment with PN517 showed more remarkable trend towards slower closure rate and reduced migration compared to control and aspirin, however, no significant differences with PN517 monotherapy were observed under normoxia or hypoxia, p>0.05. Compared to the control, only the combinations of PN517 with cisplatin or TMZ significantly slowed down wound healing under normoxia, p<0.05 and p<0.01, respectively (Fig 3.43 and 3.44).

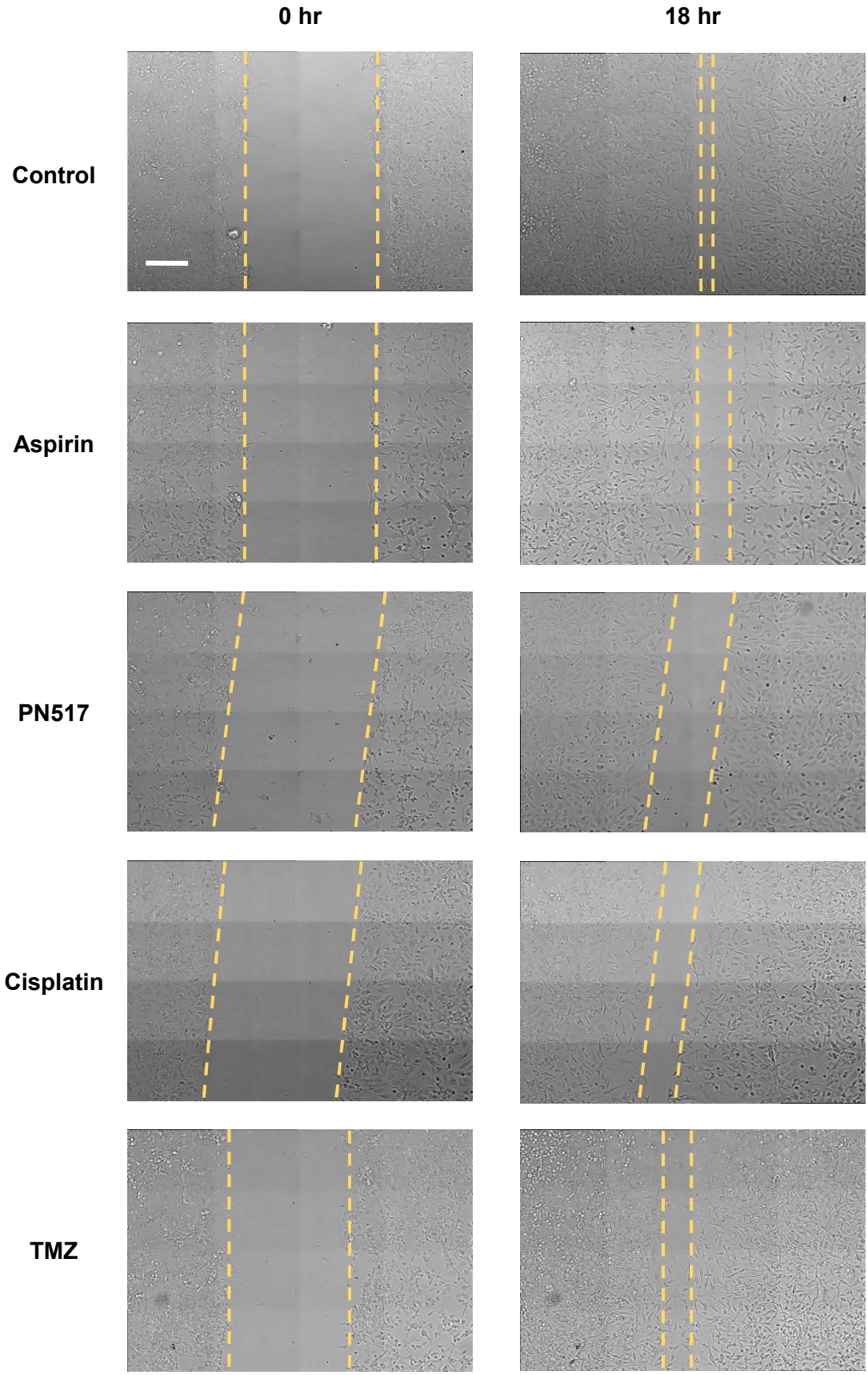

Figure 3. 31. Representative microscopic images showing the effect of monotherapy on wound healing in U87-MG cell line under normoxia. Images taken at scratching and after 18 hr of drug treatment (20X magnification). Dotted lines used for illustrative purposes to indicate cell boundary. Scale bar: 200μm. The experimental procedure was performed as described in Materials and Methods section 2.2.15.

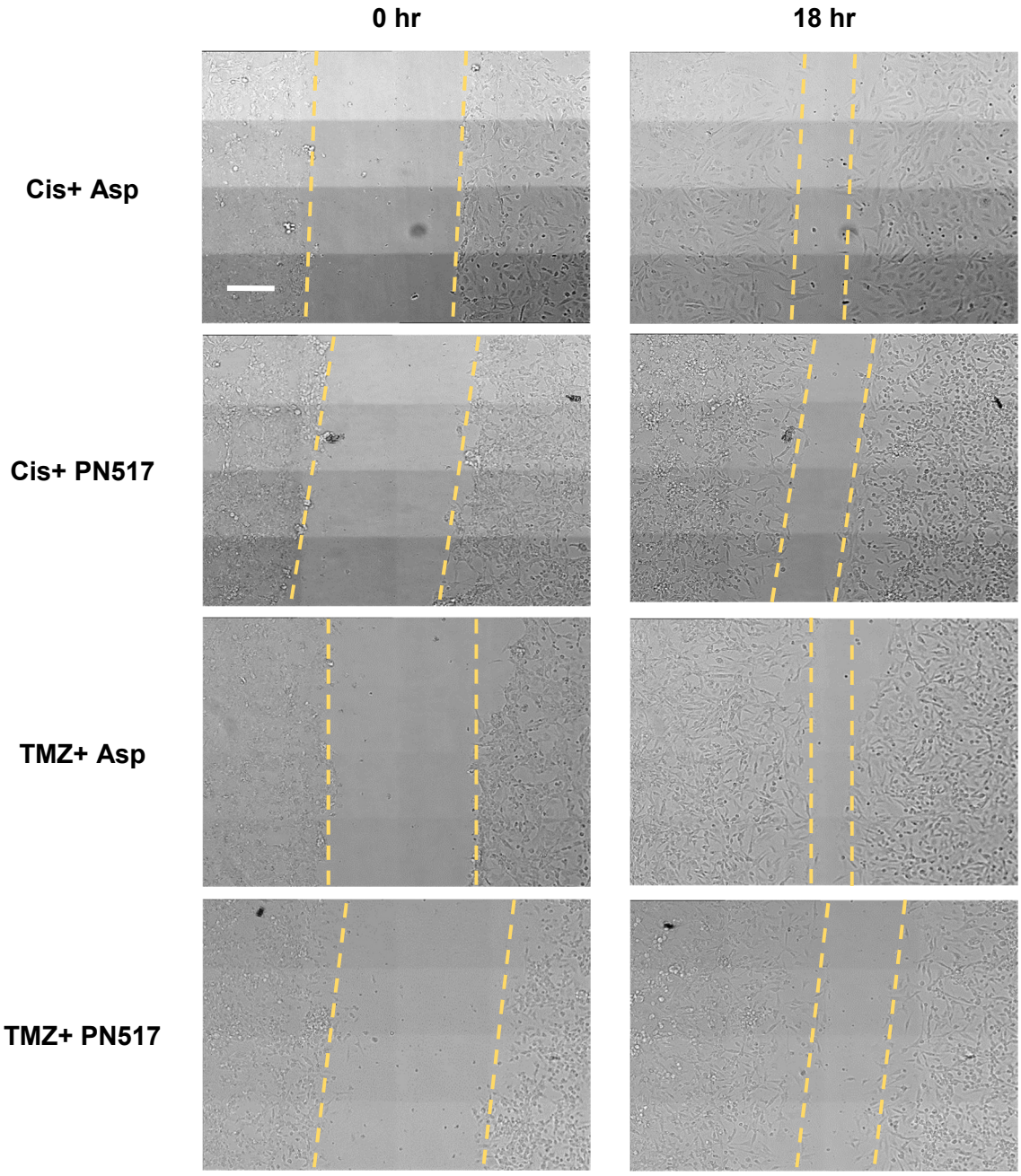

Figure 3. 32. Representative microscopic images showing the effect of combination therapy on wound healing in U87-MG cell line under normoxia. Images taken at scratching and after 18 hr of drug treatment (20X magnification). Dotted lines used for illustrative purposes to indicate cell boundary. Scale bar: 200µm. The experimental procedure was performed as described in Materials and Methods section 2.2.15.

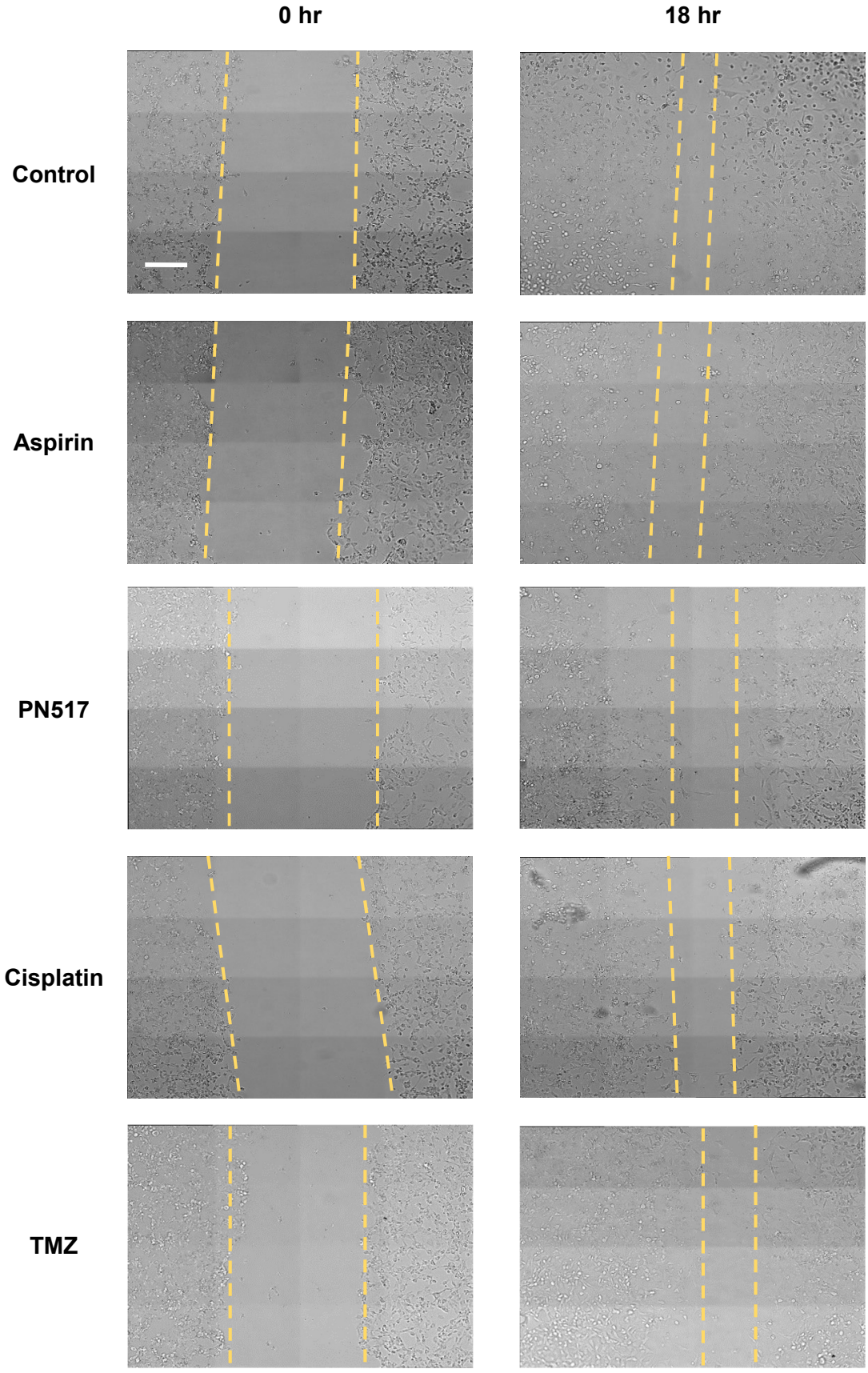

Figure 3. 33. Representative microscopic images showing the effect of monotherapy on wound healing in U87-MG cell line under hypoxia. Images taken at scratching and after 18 hr of drug treatment (20X magnification). Dotted lines used for illustrative purposes to indicate cell boundary. Scale bar: 200µm. The experimental procedure was performed as described in Materials and Methods section 2.2.15.

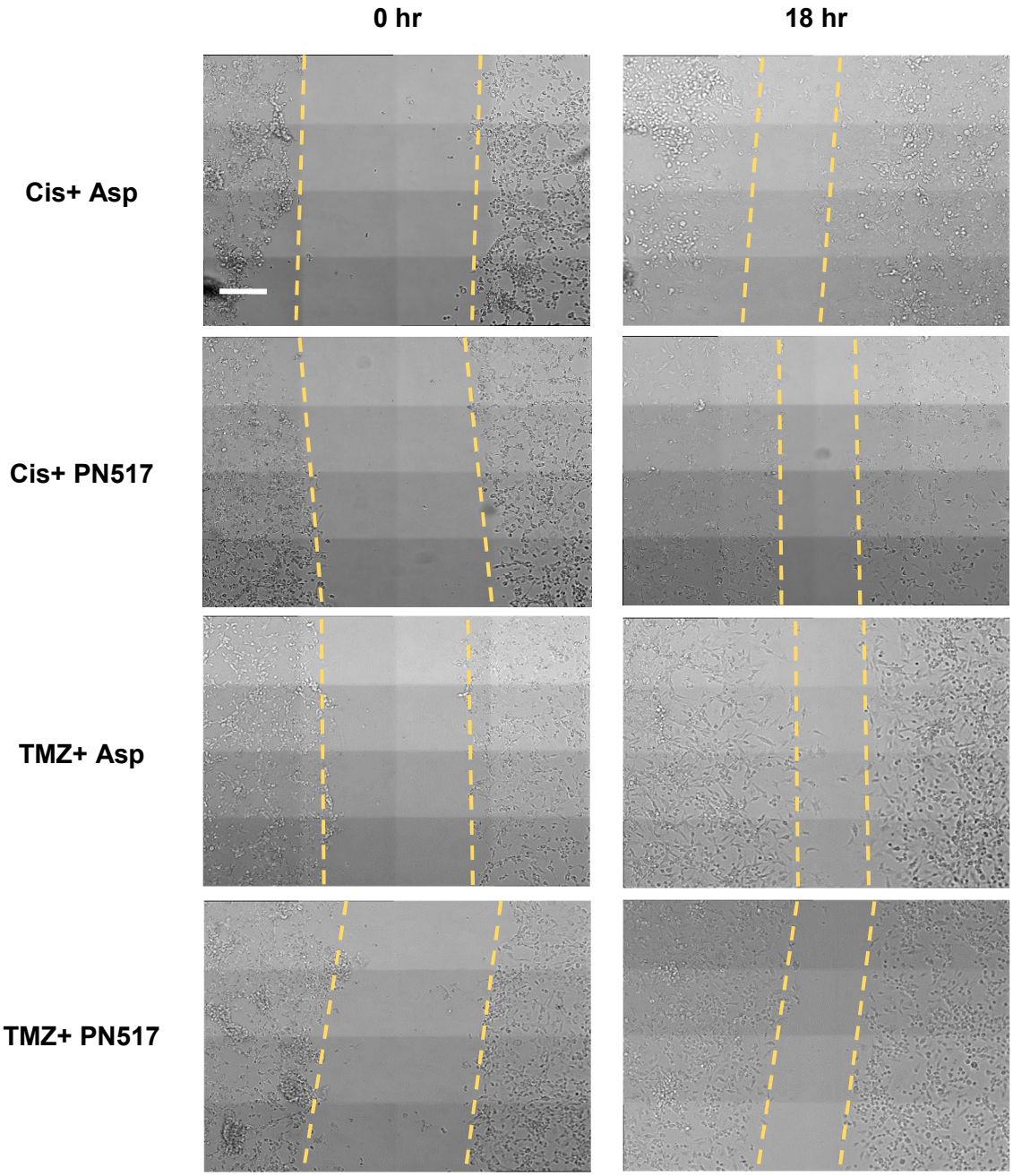

Figure 3. 34. Representative microscopic images showing the effect of combination therapy on wound healing in U87-MG cell line under hypoxia. Images taken at scratching and after 18 hr of drug treatment (20X magnification). Dotted lines used for illustrative purposes to indicate cell boundary. Scale bar: 200µm. The experimental procedure was performed as described in Materials and Methods section 2.2.15.

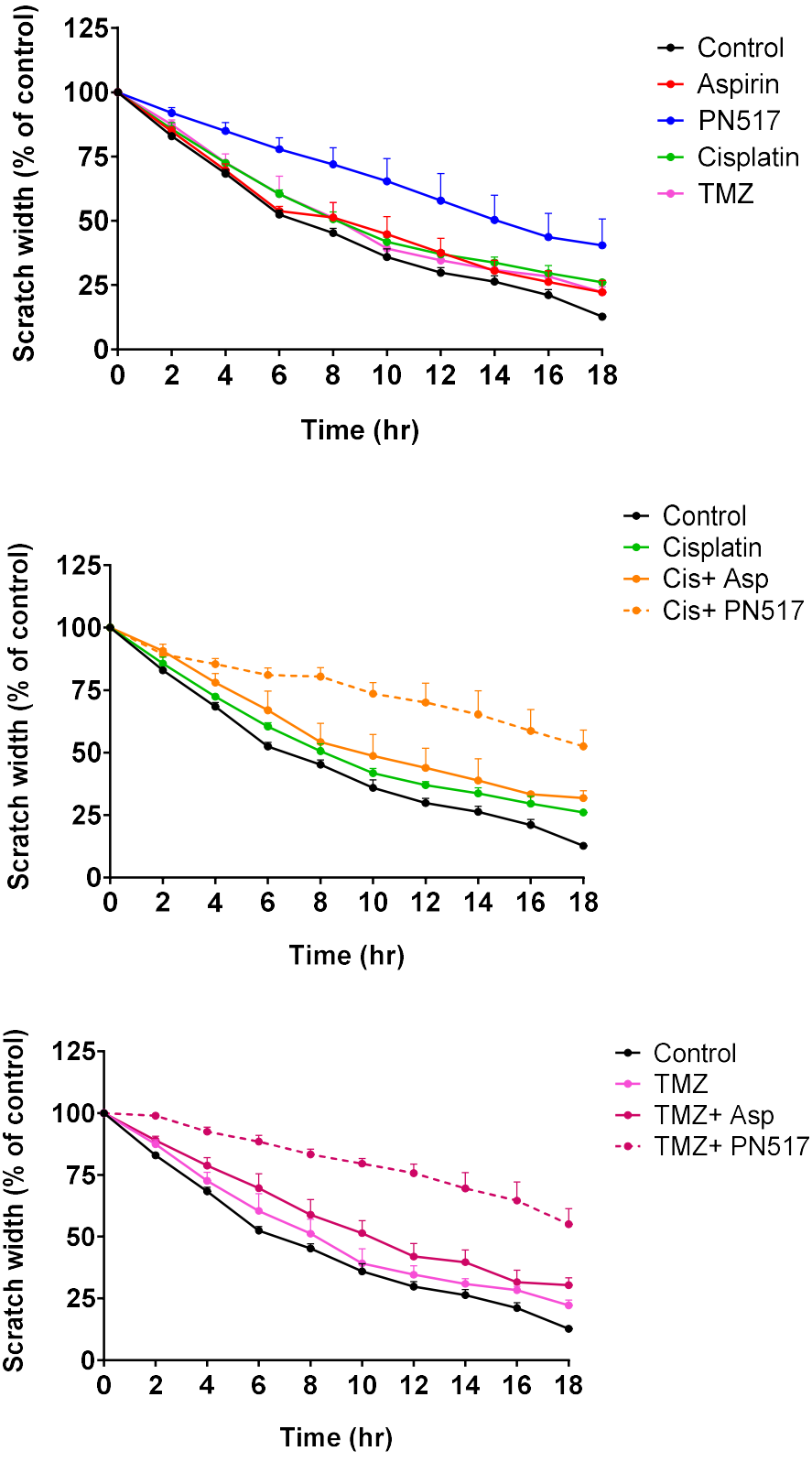

Figure 3. 35. The effect of mono and combined therapy on wound healing in U87-MG cell line under normoxia. Data shows the scratch width as % of control of the initial scratch width and measured every 2 hours over 18 hours. Values represent mean ± SEM for eight independent experiments. A two-way ANOVA was used to identify significant effects, with Tukey's multiple comparison test. The experimental procedure was performed as described in Materials and Methods section 2.2.15.

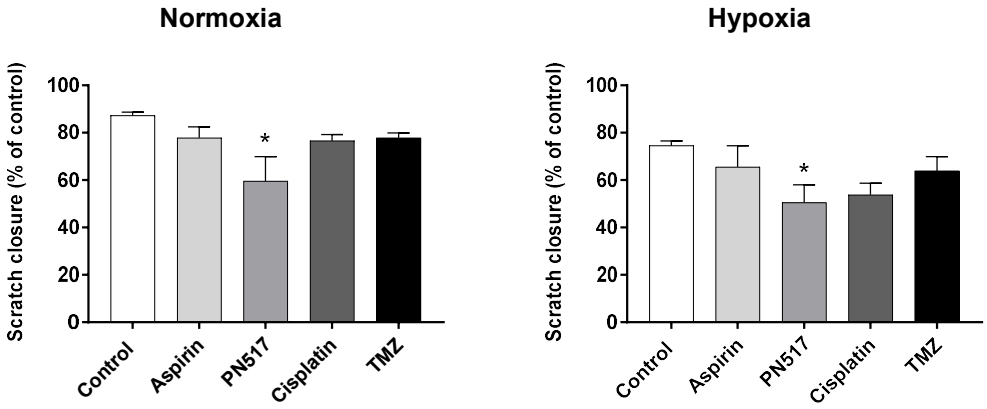

Figure 3. 36. The effect of drug treatment on scratch closure in U87-MG cell line under normoxia and hypoxia. Data shows the scratch closure as % of the initial scratch width after 18 hours under normoxia and hypoxia. Values represent mean ± SEM for eight independent experiments for normoxia and three for hypoxia. A two-way ANOVA was used to identify significant effects, with Tukey's multiple comparison test, *P < 0.05; **P < 0.01; ***P < 0.001; ****P < 0.0001. The experimental procedure was performed as described in Materials and Methods section 2.2.15.

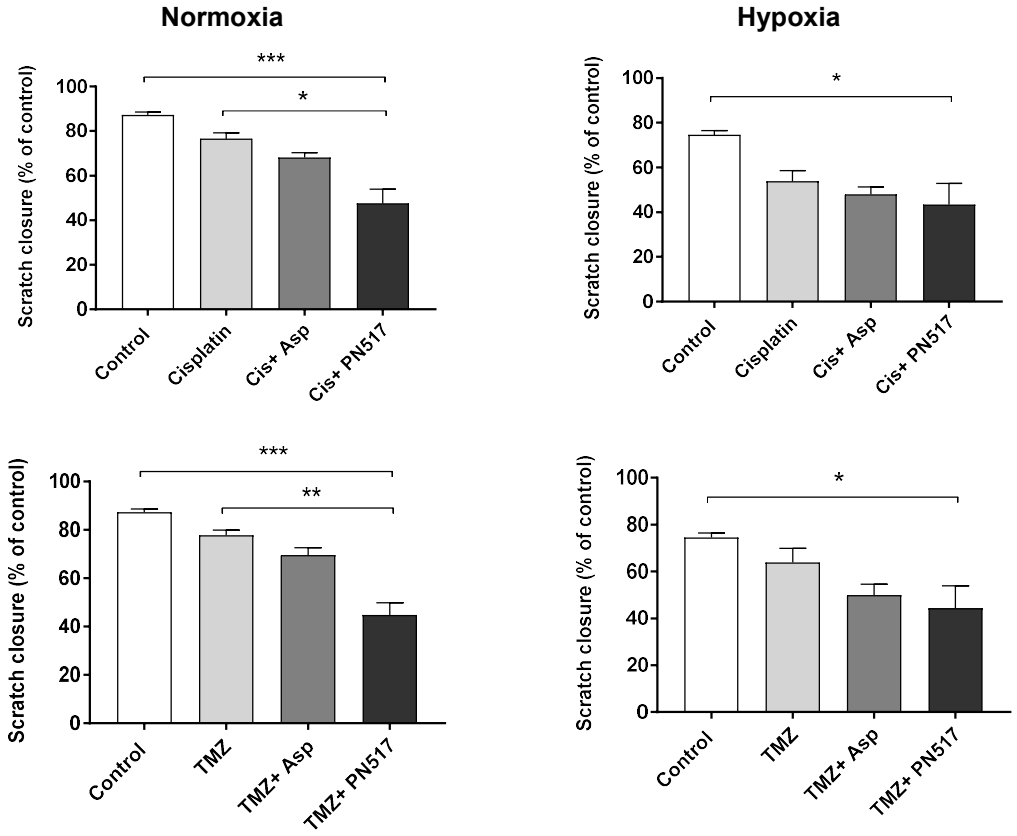

Figure 3. 37. The effect of combined therapy on scratch closure in U87-MG cell line. Data shows the scratch closure as % of the initial scratch width after 18 hours normoxia and hypoxia. Values represent mean ± SEM for eight independent experiments for normoxia and three for hypoxia. A two-way ANOVA was used to identify significant effects, with Tukey's multiple comparison test, *P < 0.05; **P < 0.01; ***P < 0.001; ****P < 0.0001. The experimental procedure was performed as described in Materials and Methods section 2.2.15.

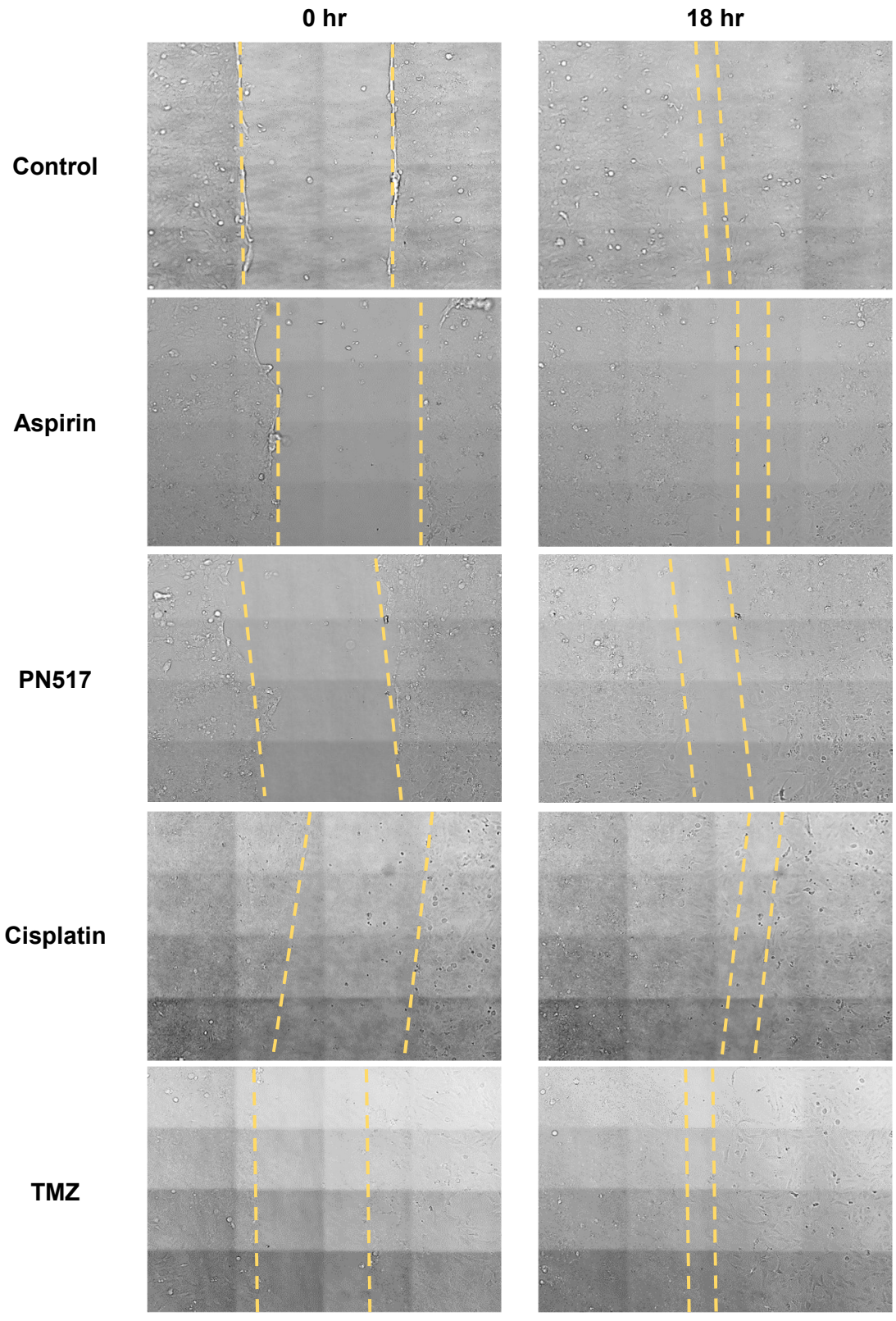

Figure 3. 38. Representative microscopic images showing the effect of monotherapy on wound healing in SVG-p12 cell line under normoxia. Images taken at scratching and after 18 hr of drug treatment (20X magnification). Dotted lines used for illustrative purposes to indicate cell boundary. The experimental procedure was performed as described in Materials and Methods section 2.2.15.

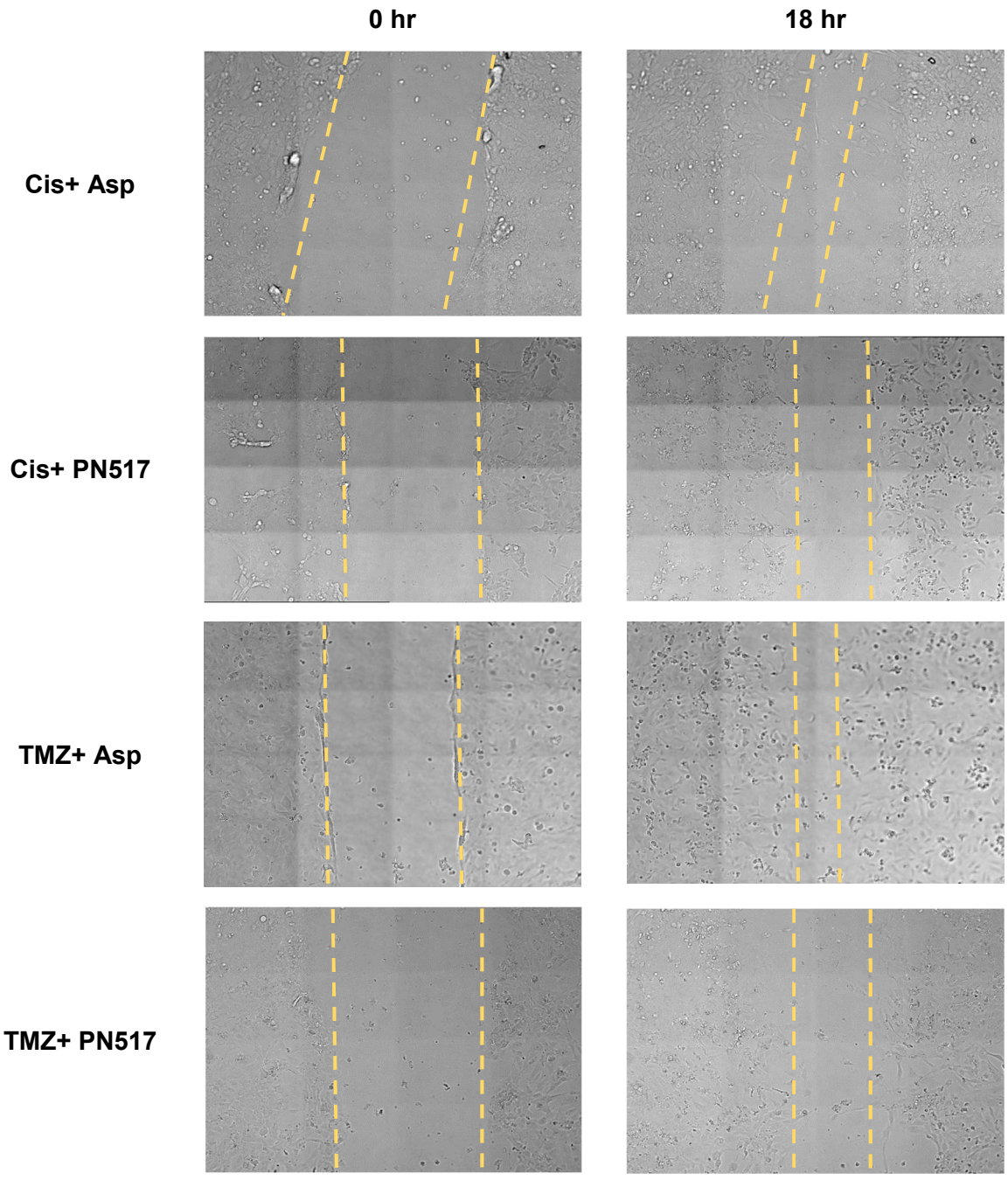

Figure 3. 39. Representative microscopic images showing the effect of combination therapy on wound healing in SVG-p-12 cell line under normoxia. Images taken at scratching and after 18 hr of drug treatment (20X magnification). Dotted lines used for illustrative purposes to indicate cell boundary. The experimental procedure was performed as described in Materials and Methods section 2.2.15.

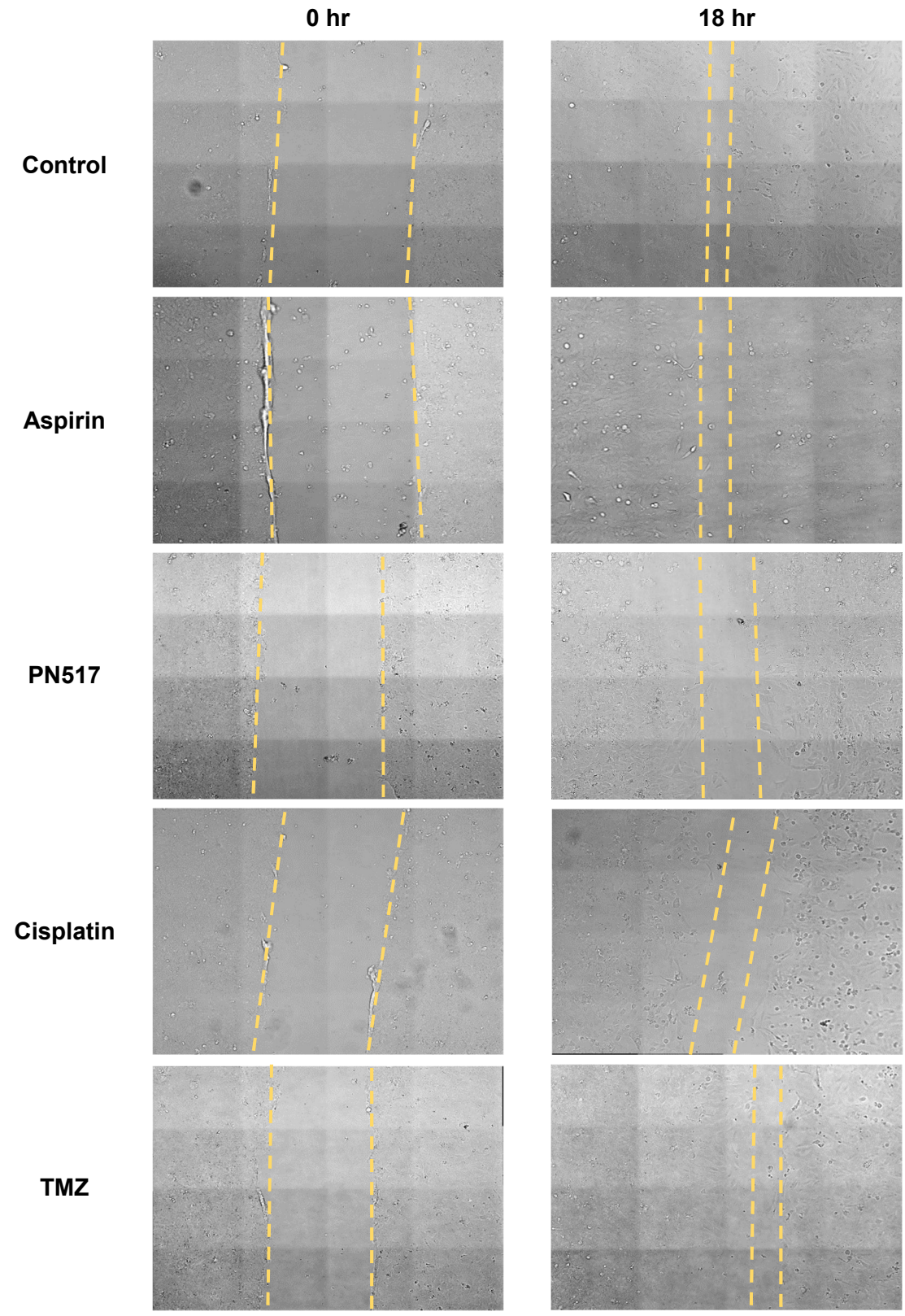

Figure 3. 40. Representative microscopic images showing the effect of monotherapy on wound healing in SVG-p12 cell line under hypoxia. Images taken at scratching and after 18 hr of drug treatment (20X magnification). Dotted lines used for illustrative purposes to indicate cell boundary. The experimental procedure was performed as described in Materials and Methods section 2.2.15.

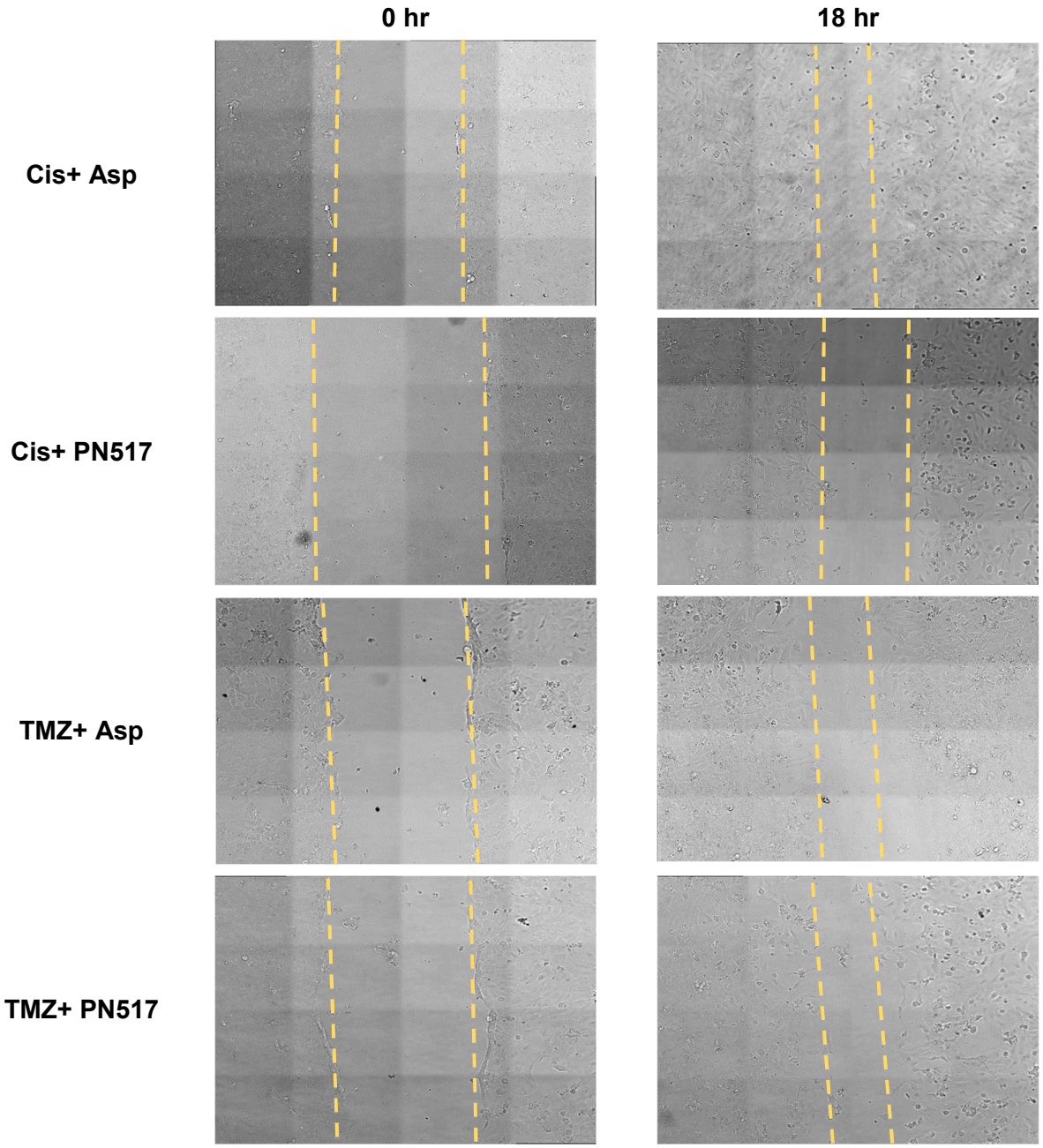

Figure 3. 41. Representative microscopic images showing the effect of combination therapy on wound healing in SVG-p12 cell line under hypoxia. Images taken at scratching and after 18 hr of drug treatment (20X magnification). Dotted lines used for illustrative purposes to indicate cell boundary. The experimental procedure was performed as described in Materials and Methods section 2.2.15.

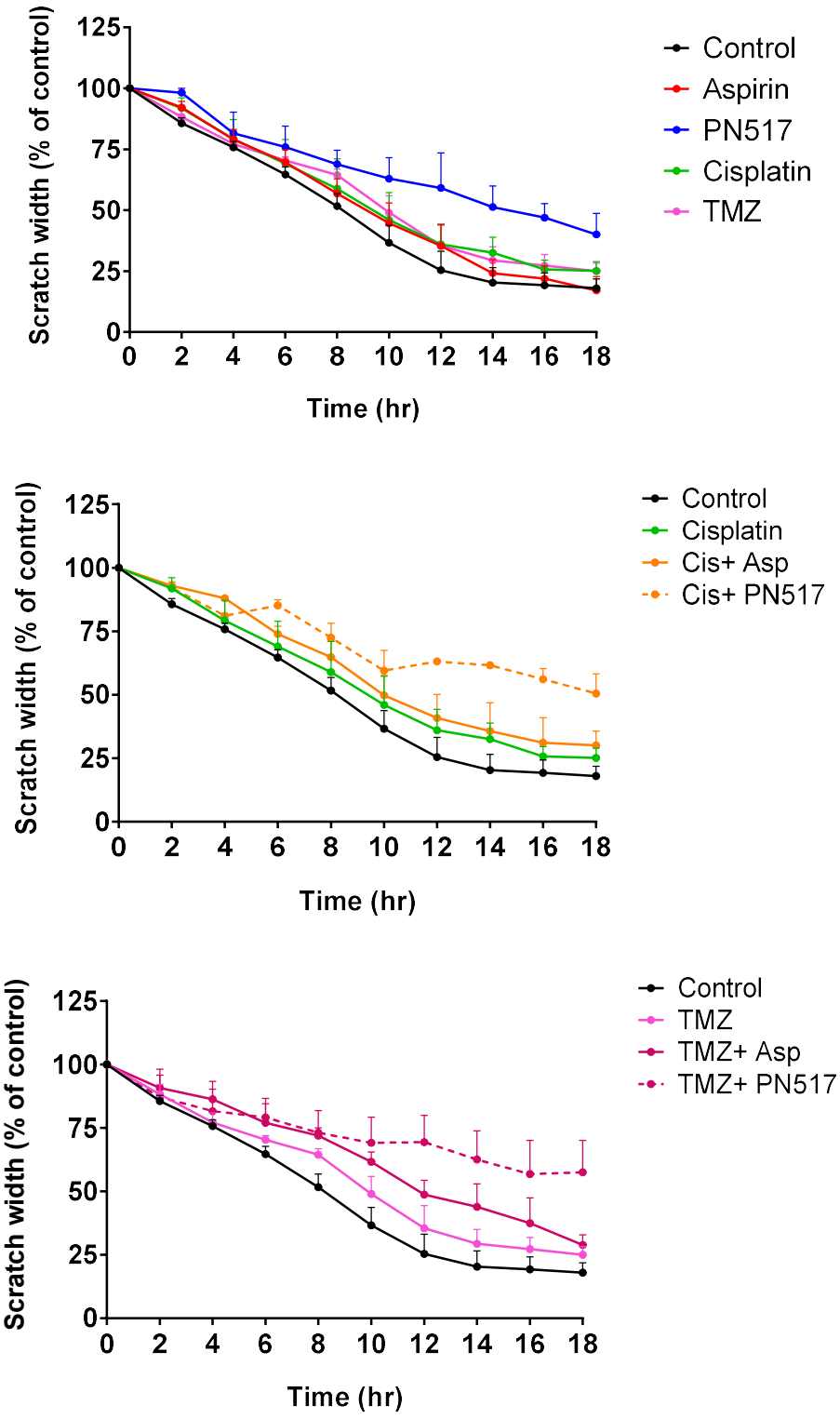

Figure 3. 42. The effect of mono and combined therapy on wound healing in SVG-p12 cell line under normoxia. Data shows the scratch width as % of control of the initial scratch width and measured every 2 hours over 18 hours. Values represent mean ± SEM for eight independent experiments. A two-way ANOVA was used to identify significant effects, with Tukey's multiple comparison test. The experimental procedure was performed as described in Materials and Methods section 2.2.15.

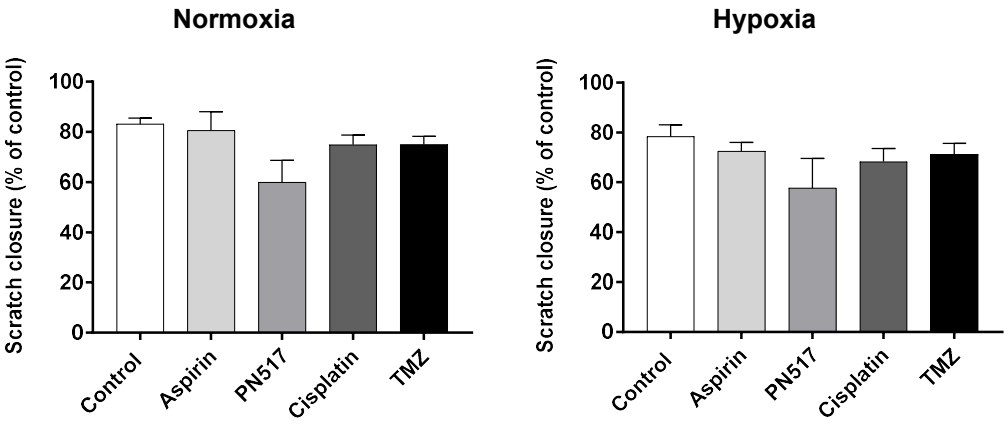

Figure 3. 43. The effect of drug treatment on scratch closure in SVG-p12 cell line under normoxia and hypoxia. Data shows the scratch closure as % of the initial scratch width after 18 hours. Values represent mean ± SEM for three independent experiments. A two-way ANOVA was used to identify significant effects, with Tukey's multiple comparison test, *P < 0.05; **P < 0.01; ***P < 0.001; ****P < 0.0001. The experimental procedure was performed as described in Materials and Methods section 2.2.15.

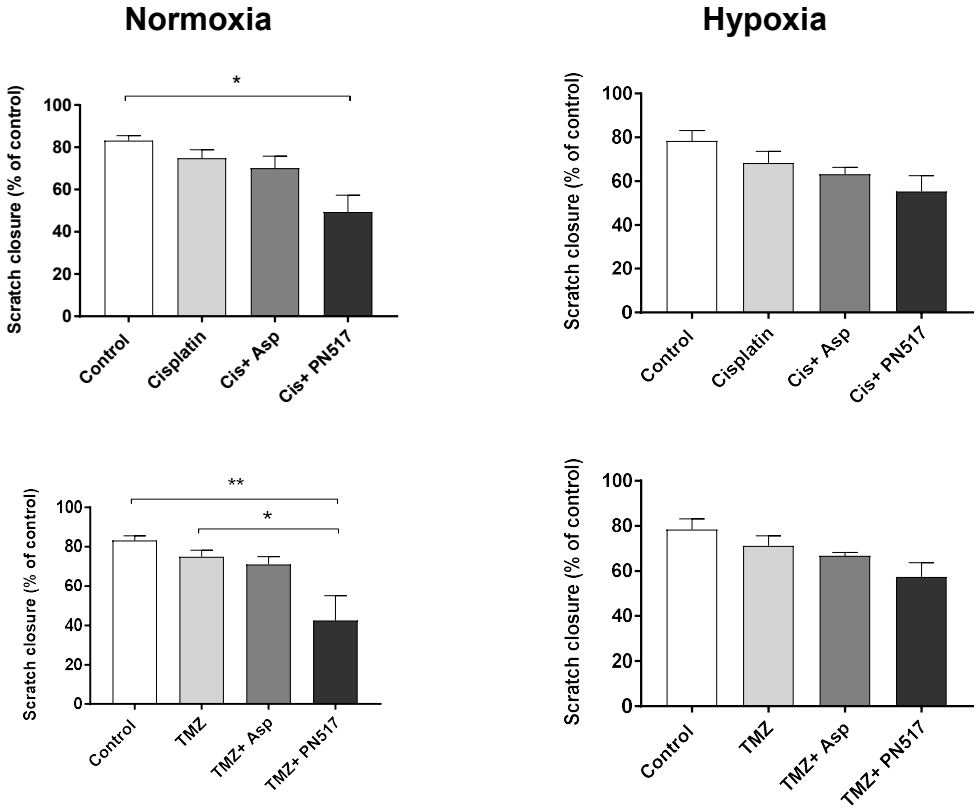

Figure 3. 44. The effect of combined therapy on scratch closure in SVG-p12 cell line. Data shows the scratch closure as % of the initial scratch width after 18 hours under normoxia and hypoxia. Values represent mean ± SEM for three independent experiments. A two-way ANOVA was used to identify significant effects, with Tukey's multiple comparison test, *P < 0.05; **P < 0.01; ***P < 0.001; ****P < 0.0001. The experimental procedure was performed as described in Materials and Methods section 2.2.15.

3.3. Discussion

The initial aim of the current study is to characterize the effects of aspirin and its newly synthesized analogue PN517, separately or combined with the standard chemotherapeutics, on glioma cell viability. For that purpose, the established U87-MG cell line (a grade IV glioblastoma) was used in addition to an experimental control, the SVG-p12 foetal glial cell line. Nevertheless, different cell types exhibit different growth durations and patterns, and the cytotoxic effect of the drugs depend upon the growth pattern of the cells. Therefore, to confirm the validity of the obtained results and correctly drug treat the cells, the first step was to study the growth pattern of both cell lines. It is important to provide information about lag phase, log phase and stationary phase among the different culturing conditions considered.

The lag phase is the time needed for cell recovery after subculturing to attach and spread, the log phase is normally the phase where the number of cells increase and the better stage to define the doubling time of a cell line. A cell population is considered to be the most viable during the log phase of growth, hence, it is the best stage to assess cellular functions. Stationary phase or plateau is where the cell growth rate slows down due to cell population becoming confluent where afterwards cell death can occur with a reduction in the number of viable cells (Mather and Roberts, 1998).

Growth curve analysis of the two cell lines demonstrated U87-MG cells to have a higher proliferation rate compared to the non-cancerous foetal SVG-p12 cell line (Fig 3.4). That would be expected of a cancer cell line due to the deregulation of the systems responsible for controlling the production and release of growth promoting molecules which lead to sustained and chronic proliferation (Hanahan and Weinberg, 2011; Macheret and Halazonetis, 2015). Growth pattern analysis under hypoxia showed significantly slower growth rate for both cell lines when decreasing oxygen levels. However, the growth rate for U87-MG cells was still significantly higher than SVG-p12 under hypoxia (Fig 3.4). That is may be due to the stress caused by sustained lack of oxygen which stimulates cell death in non-cancerous cells and select for gene mutations and resistance to hypoxia- induced

apoptosis in many tumour cells leading them adapt to the hypoxic microenvironment and support tumour growth and survival (Li *et al.*, 2004).

Interestingly, even after high neovascularization in GBM, oxygen supply stays behind the demands of the tumour and hypoxic areas remain a constant feature of this tumour (Helmlinger *et al.*, 1997). Hypoxic cells are generally distant from blood vessels and this distance causes a reduction in the rate of cell proliferation (Brown and William, 2004). This effect is the result of increased expression of specific proteins, e.g., the tumour suppressor p53 and the cyclin-dependent kinase inhibitors p21 $^{WAF/Cip1}$, $p27^{Kip1}$, which are induced under hypoxic conditions (Wartenberg *et al.*, 2003). Cell proliferation under hypoxia can be inhibited by the cyclin-dependent kinase inhibitor $p27^{Kip1}$ which inhibits the activation of cyclin E-Cdk2 or cyclin D-Cdk4 complexes thus controlling cell cycle progression at G1. Some cell lines like the human mesenchymal stem cells hMSC undergo an initial acclimatisation period where they do not proliferate, thus extending their lag phase (Grayson *et al.*, 2006). These findings match our results where a significantly slower growth of cells under hypoxia is observed resulting in an increase in the doubling time for both cell lines. The molecular responses to hypoxia exposure will be discussed further in detail in chapter 6.

3.3.1. Cell viability

As mentioned earlier, the cytotoxicity of aspirin and its analogues has been reported in various cancers (Din *et al.*, 2004; Gurpinar *et al.*, 2013; Claudius *et al.*, 2014). This study aimed to determine whether aspirin and its synthesised novel analogue PN517 have cytotoxic effects on the glioblastoma U87-MG cell line using the PrestoBlue (PB) viability assay. This assay relies on the reducing environment of the living cells as an indication of viability and provides the first evidence about therapeutic potential of the drugs. However, when measuring the fluorescence upon adding the reagent to cells, the largest variable impacting factor is the cell number (Riss *et al.*, 2004; Kumar *et al.*, 2018). Therefore, an assay was conducted to study the relationship between PB fluorescence and seeding density, and it established that over the period of incubation and with the given doubling time, fluorescence was directly proportional to cell density (Fig 3.5). Taking together the results from growth curves and linearity assay, it was

possible to identify the appropriate seeding density for subsequent experimental tests.

Tested drugs were prepared as stocks in suitable dissolution solvents that have the least cytotoxicity effects and diluted with culture media freshly on the experiment day. It is worth noting that although concentrations of aspirin and PN517 used may appear high compared to other chemotherapeutic drugs, it is not uncommon to use such values in investigating the molecular action of aspirin and salicylate *in vitro* and *in vivo* where concentrations of 1-5 mM or above were used (Din *et al.*, 2004; Hawley *et al.*, 2012; Shirakawa *et al.*, 2016). Also, levels of 0.5-2mM have been reported to be physiologically or pharmacologically relevant and achievable with a typically prescribed dose for aspirin (Borthwick *et al.*, 2006).

Aspirin and PN517 demonstrated their cytotoxic effects by reducing the cell viability of both cell lines in a concentration dependent manner (Fig 3.7), showing similar efficacy to that found in previous studies (Kim *et al.*, 2009; Deb *et al.*, 2011). Although aspirin has shown antiproliferative effect in a large diversity of cancers, the IC_{50} values for aspirin varies between different cell lines. For example, it was higher in the human glioblastoma A172 cells, 5 mM at 48 hr (Kim *et al.*, 2009), but lower in the SW480 colorectal cancer cell line, being about 1.5 mM at 24 hr (Din *et al.*, 2004). The effects of aspirin or its analogues on cell viability could involve a number of mechanisms, including the Wnt/β-catenin/ T-cell factor (TCF) pathway. The signalling of this pathway has been previously shown to be highly dysregulated in several cancers, like glioma (Logan and Nusse, 2004; Cadigan and Peifer, 2009; Pu *et al.*, 2009). The pathway is activated by the β-catenin/TCF complex and activates several effectors like Stat3, AKT1 and AKT2 (Huang *et al.*, 2009; Yue *et al.*, 2010; Chen *et al.*, 2011). Aspirin has been shown to antagonize the activity of the β-catenin/TCF complex in U87-MG, thereby exerting its anti-neoplastic activity (Lan *et al.*, 2011).

Furthermore, the anti-cancer effects of aspirin have been largely linked to its ability to inhibit the cyclooxygenase enzymes and reduce the production of prostaglandins. The expression of COX-2 protein is varied, and is found in both

normal brain and glioma specimens, but significantly higher in high-grade glioma than lower grade or normal brain cells (Joki *et al.*, 2000). The U87-MG cell line is both high grade and relatively slow growing, both characteristics associated with high COX-2 expression which leads to excessive production of prostaglandins (Kardosh *et al.*, 2004). COX-2 prostaglandins promote cell division, angiogenesis and metastasis while inhibiting apoptosis, which all lead to growth of the tumour (Grosch *et al.*, 2006). This provides a potential explanation for the high efficacy of aspirin and PN517 in this cell type and warrants further investigation as it could contribute to future patient specific treatment based on COX expression.

PN517 displayed a trend towards greater efficacy than aspirin, an observation consistent with several previous studies where PN517 was found to be more cytotoxic than aspirin towards different cancer cell lines (Deb *et al.*, 2011; Claudius *et al.*, 2014; Kilari *et al.*, 2018). Furthermore, there was significant reduction in cell viability for PN517 compared to aspirin at early timepoint (24 hr) suggesting that PN517 induce its cytotoxic effects earlier than aspirin, this is despite PN517 lacking some structural features that could contribute to the side effects seen with aspirin (Table 3.1). Consequently, this enhanced effect could be attributed to several reasons including structural differences. The analogue fumaroyldiaspirin PN517 was prepared by modifying bis (2-carboxyphenyl) succinate (PN508), which is effectively a double aspirin molecule, meaning that PN517 resembles two aspirin structures joined together by a double carbon bond (alkene grouping) (Fig 1.14). It has been suggested that this double carbon bond provides the molecule with rigidity when compared to PN508 (Deb *et al.*, 2011). In addition, a treatment equivalent to a double dose of aspirin was used as a control as the structures of the analogue PN517, but rarely replicated the potency of PN517 in cell viability assay suggesting that PN517 efficacy is due to other structural characteristics and not simply because it resembles two aspirin molecules (unpublished data).

Similar to aspirin, the analogues were also suggested to have antiproliferative effects through supressing cyclooxygenase enzymes. It is well known that aspirin can inhibit both COX-1 and COX-2 where the inhibition of COX-2 accounts for the anti-inflammatory effect of the drugs while the inhibition of COX-1 can lead to

toxicity and associated side effects (Schwitalla *et al.*, 2013). Aspirin produces greater inhibition of COX-1 than COX-2 and that was the main reason for synthesising analogues that display greater selectivity for COX-2 to reduce undesirable side effects (Deb *et al.*, 2011). Previous completed studies in the lab examined COX enzyme inhibition in order to identify the inhibitory activity against COX enzyme isoforms by aspirin and different analogues by using the COX fluorescent inhibitor screening assay kit. Results of this study showed that aspirin analogues inhibited the enzymes in a concentration dependent manner while indicating that PN517 more efficacious than aspirin. PN517 produced larger inhibition of COX-2 activity and lower inhibition of COX-1 activity than aspirin which also give an advantage for PN517 over aspirin and provide a potential antiproliferative mechanism for the activity of the analogue.

However, little further decrease in viability was observed over the three-timepoints examined with either aspirin or PN517 (Fig 3.7& 3.8). The simplest explanation for this finding is that these drugs are rapidly undergoing metabolism to form inactive metabolites by cytochrome P450 enzymes. The major two enzymes involved in the metabolism of aspirin are CYP2C9 (Miners and Birkett, 1998; Takahashi *et al.*, 2004), and UGT1A6 (Ciotti *et al.*, 1997). Both enzymes are polymorphic, and produce fast or slow-metabolizing enzymes, which cause the quick metabolism of aspirin and hence could also affect the metabolism of aspirin analogues in the different cell lines. Significantly, the CYP2C9 enzyme is expressed in glioma, with higher expression levels being observed with higher grades of cancer (Knupfer *et al.*, 2006). As U87-MG cell line was derived from high grade glioblastoma, this provides a potential explanation as to why the IC_{50} for aspirin and PN517 did not decrease significantly over time, especially in this cell line.

The efficacy of aspirin and PN517 was compared to temozolomide *in vitro*, the leading drug in the treatment of glioblastoma (Ding *et al.*, 2011; Zhang *et al.*, 2012). TMZ is a prodrug which is converted into the active alkylating agent MTIC under physiological conditions (Friedman *et al.*, 2000). However, temozolomide does not display reproducible effects *in vitro* due to its prodrug nature, so is commonly replaced in research with other standard chemotherapeutic drugs

such as cisplatin. This could explain its poor efficacy against cell viability of both cell lines and failure to reduce viability below 50% of control (Fig 3.7 &3.8).

Cisplatin has proven to be one of the more efficient anticancer chemotherapeutic agents due to targeting of multiple intracellular sites to induce cell death (Florea and Busselberg, 2011). In this study, cisplatin produced a decrease in cell viability of the two cell lines in a concentration and time dependent manner. Cisplatin mainly works by intercalation with DNA to form intrastrand crosslinks and adducts that cause changes in the conformation of the DNA and affect DNA replication. Other mechanisms of cisplatin cytotoxicity include mitochondrial damage, decreased ATPase activity, and altered cellular transport mechanisms. The cell death may occur due to the inhibition of DNA synthesis and repair resulting in cell cycle arrest at the G1, S or G2/M phase, thus inducing apoptosis (Florea and Busselberg, 2011).

Cisplatin displayed a concentration and time dependent efficacy *in vitro*, and its effect on cell viability increased significantly over time, an effect easily explained by its mechanism of action where it mainly causes DNA damage by affecting its replication, ultimately inducing apoptosis (Qin and Ng, 2002; Jiang *et al.*, 2004; Wang and Lippard, 2005; Florea and Busselberg, 2011). While cisplatin is not selective for cancer cells over healthy cells, it will affect rapidly growing cells more quickly and cell death will occur at a faster rate (Sancho-Martinez *et al.*, 2011). Thus, its mechanism of action also explains why U87-MG showed lower IC_{50} value in the first 24 hours following treatment with cisplatin as compared to SVG-p12 (Table 3.1).

Based on IC_{50} values obtained from the concentration-response curves, aspirin and PN517 showed a trend towards same or greater efficacy under hypoxia, whereas cisplatin showed a trend towards lower efficacy, as well as TMZ showed reduced cytotoxicity under hypoxia (Table 3.1). This effect of hypoxia on the drug efficacy can be largely related to its mechanism of action. It is well known that cisplatin and TMZ mechanisms of action is highly dependent on cell proliferation which is suppressed by the lower oxygen levels, as noticed earlier from both cell lines growth curves, resulting in less efficacy under hypoxia. As cell growth is

important for the cytotoxic effects of drugs, the cytotoxic effect of drugs was reduced. These results were consistent with previous studies where cisplatin was less effective in low oxygen environment (Koch *et al.*, 2003). On the other hand, earlier studies have revealed contradictive results showing hypoxic cells to be more sensitive to cisplatin in some cell lines within the same period of exposure or less (Strese *et al.*, 2013), showing also cisplatin to be a HIF-1 inhibitor (Duyndam *et al.*, 2007). However, the anti-cancer activity of a drug under hypoxia depends largely on the cell type and may increase or decrease accordingly (Koch *et al.*, 2003; Yao *et al.*, 2005).

In addition, numerous studies investigating the hypoxia- induced resistance to chemotherapy in glioma have demonstrated a reduced efficacy for TMZ under hypoxia, and the varied response of glioma cells to cytotoxic action of temozolomide in different oxygen conditions is a complex problem (Lan *et al.*, 2014; Bielecka and Obuchowicz, 2017). It has been shown that HIF-1α activity is associated with GBM responsiveness to TMZ, hence, its downregulation improves the response of TMZ-resistant cells (Lo Dico *et al.*, 2018). Hypoxia is not just leading to slower proliferation rate, but also to many molecular changes such as inducing acidosis through a shift in cellular metabolism that generates a high acid load in the tumour microenvironment (Chiche *et al.*, 2010). Since activation of TMZ prodrug occurs in slightly alkaline environment (PH>7), this acidosis under hypoxia condition could also prevent the prodrug hydrolysis to the active metabolite.

The combination studies have shown significant differences between monotherapy and combination therapy suggesting additive or synergistic action between the drugs (Fig 3.9). Aspirin and PN517 in combination with cisplatin significantly reduced the viability of the glioblastoma cells as compared to cisplatin on its own with the combination of PN517 being more potent than aspirin (Fig 3.10). Previous studies have revealed similar effects for the combination of aspirin and its analogues with platinum compounds with different levels of synergism being reported (Kilari *et al.*, 2018). In gastric cancer cells, cell growth was significantly inhibited when cisplatin was used in combination with aspirin (Dong *et al.*, 2014). Combinations of cisplatin and aspirin were also seen to have

synergistic effects in human cervical carcinoma HeLa cells (Yueling *et al.*, 2010) In the OE33 oesophageal cancer cells however, platinum compounds did not synergise with aspirin (Kilari *et al.*, 2018).

With respect to PN517, strong synergy was observed when cisplatin was combined with PN517 with a 5-fold decrease in IC_{50} for cisplatin in SW480 colorectal cancer cells (Kilari *et al.*, 2018). In addition, the synergistic effects of these combinations increased at higher concentrations, which is advantageous in chemotherapy (Chou, 2010). PN517 maintained the synergistic effects in the OE33 oesophageal cancer cell line with cisplatin but had an antagonistic effect with oxaliplatin and carboplatin (Kilari *et al.*, 2018). The differences in outcomes for each drug combination in different cell lines may be due to differences in specific targets by different compounds (Din *et al.*, 2004). With the prominent side effects of cisplatin, a reduction in its effective dose IC_{50} as a result of the combinations with aspirin or PN517 may reduce or totally alleviate this side effects because a reduction in drug concentration will result in reduced toxicity and delay or minimize the induction of drug resistance (Chou, 2010).

One possible reported explanation for this combined effect could be due to aspirin effectively inhibiting Cox-2 activity and prostaglandin E2 synthesis which are vastly up-regulated in glioblastoma (Joki *et al.*, 2000; Zhao *et al.*, 2017). Many reports has demonstrated that aspirin or other NSAIDs can decrease the glioma-mediated immunosuppression and inflammation observed in patient with brain tumours mainly due to their ability to inhibit prostaglandin production via cyclooxygenase (Hwang *et al.*, 2004; Pathak *et al.*, 2014). Furthermore, research has found that the exposure to aspirin exerts a priming effect on tumour cells rendering them susceptible to induction of cell death by cisplatin. This priming action was found to be dependent on an altered constitution of tumour microenvironment and modulation in the expression of survival regulatory molecules (Kumar and Singh, 2012).

It was also frequently noticed in this study that incubation of the glioblastoma cells with PN517 and temozolomide caused the most significant reduction in cell viability when compared to TMZ alone or other combinations (Fig 3.10). This

indicates that PN517 is augmenting the effect of TMZ and a lower dose of TMZ when combined with aspirin analogue can cause higher level of cytotoxic effect and the reasons for this combined effect will be studied further in this project.

3.3.2. Cell proliferation and cell cycle

To understand the effects and underlying mechanisms of monotherapy and combination therapy seen on U87-MG cell line, cell proliferation and cell cycle analysis was performed. Findings of this chapter showed moderate effect for aspirin and PN517 on cell proliferation but with no significant difference to control, like TMZ (Fig 3.13). This effect could be in part due to their COX-2 inhibition mechanism which has been shown to decrease prostaglandin levels and inhibit proliferation in many colon, prostate and pancreatic cancer cell lines (Tsujii *et al.*, 1998; Tucker *et al.*, 1999; Elder *et al.*, 2000; Liu *et al.*, 2000). Also, aspirin and other NSAIDs were shown to inhibit proliferation in glioma cell lines where elevated PGE2 and arachidonic acid levels have been found (Casper *et al.*, 2000). This suggestion could explain the less efficacy for aspirin and PN517 in the normal control cell line SVG-p12 since it was suggested to express lower levels of COX enzymes compared to U87-MG (Joki *et al.*, 2000; Zhao *et al.*, 2017). However, cell viability effects showed no significant effect between the two cell lines suggesting non-COX-2 dependent pathways. For example, pancreatic adenocarcinomas, cell lines negative for COX-2 expression were found to respond similarly to selective COX-2 inhibitor treatment as cell lines expressing the enzyme (Molina *et al.*, 1999).

Nevertheless, neither aspirin nor PN517 alone inhibited cell cycle progression of both the cell lines (Fig 3.21 &3.24). These findings correlate well with data obtained from western blotting where no significant effect for aspirin or PN517 on regulation of cyclin D1 levels was observed. In the literature, conflicting results were described regarding the effects of aspirin and NSAIDs on cell cycle progression and their impact on regulators of the cell cycle in variety of cancer cell lines. Early findings reported no effect for the selective COX-2 inhibitor NS-398 on cell cycle distribution in both COX-2 positive and negative colorectal cancer cell lines (Elder *et al.*, 1996). In contrast, another publication showed

accumulation in the G0/G1 phase seen following treatment with selective NSAIDs in colorectal cancer cell lines (Shiff *et al.*, 1995; Elder *et al.*, 1996).

More recent studies have reported G0/G1 arrest following aspirin treatment in different cell lines like in human hepatoma HepG2 cells (Raza *et al.*, 2011), oesophageal squamous carcinoma cells (Li *et al.*, 2009) and cholangiocarcinoma cells (Boueroy *et al.*, 2017). Another common finding among several studies is that NSAIDs treatment associate with downregulation of cyclin D1. However, exposing human pancreatic neuroendocrine cells BON1 and human bronchopulmonary NCI-H727 cells to aspirin led to reduced expression of the cyclin dependent kinase 4 (CDK4) and cyclin D3 (Spampatti *et al.*, 2014). The effect of aspirin treatment for 24 or 48 hours on cyclin D1 expression was examined in a range of colon cancer cell lines finding a significant decrease in all cases at concentrations higher than the concentrations used in this study (10mM) (Pathi *et al.*, 2012). However, the effect of a number of COX inhibitors on cyclins was determined by Yip-Schneider and colleagues who reported that sulindac, indomethacin and NS-398 decreased cyclin D1 expression in PaCa-2 and BxPC-3 pancreatic carcinoma cells (G1/S phase) whereas NS-398 was found to decrease the expression of cyclin A in both cell lines (S/G2 phase) (Yip-Schneider *et al.*, 2001). Another study on colorectal cancer cells has suggested that aspirin causes inhibition of cyclin D1/CDK4 through the p38 MAPK pathway and found that decreased cyclin D1 levels were accompanied by cell cycle arrest with a substantial increase in S phase population and G2/M, shifted from G0-G1, after aspirin exposure (Thoms *et al.*, 2007). Additionally, treatment with aspirin analogue NO-ASA on wide range of human carcinoma cell lines results in a decrease in the expression of cyclin D1, and an increase in the expression of cyclin B1 resulting in G2/M arrest in the SW480 colon cancer cell line (Gao and Williams, 2012).

Interestingly, the current data suggest that the mechanism of action of aspirin or PN517 is not linked as closely to cell proliferation. It was previously reported that treatment using relatively low concentrations (0.1-2mM) of aspirin does not affect the cell growth of leiomyoma cells or colon cancer cell (Kodela *et al.*, 2013) in a significant way. With respect to brain tumours, studies showed that aspirin could

induce G0/G1 arrest in U87-MG cell line and this may be due to the higher concentration of aspirin (10mM) (Lan *et al.*, 2011) than used in this study (1mM). The absence of effect on cell cycle and cyclin D1 protein levels in aspirin and PN517 samples in this study might be due to the low concentration (IC_{25}) of each drug in the assay, shorter exposure of drug treatment, or to different responses and mechanism of action in different cell lines (Fig 3.27-3.28). As already mentioned, the mechanism of action of aspirin or PN517 may not be linked as closely to cell proliferation. For instance, one publication found that the concentration of NS-398 required to inhibit cell proliferation was ten times higher than the concentration required to inhibit PGE2 production, suggesting prostaglandin independent pathway (Zhi *et al.*, 2006). While PN517 displayed equivalent efficacy to cisplatin in reducing cell viability in the U87-MG cell line, this was not replicated in cell cycle analysis, where cisplatin disturbed the cell cycle to a much greater degree suggesting a difference in the signalling pathways altered by analogue treatment in cell viability and proliferation (Fig 3.15). Findings by Claudius et al., (2014) reported that the analogue PN517 failed to induce nucleolar translocation of the transcription factor RelA or cell cycle arrest.

Another suggestion to explain why aspirin and PN517 did not show an effect on cell cycle and cyclin D1 regulation is that expression levels in the cell line. Cyclin D1 (CCND1) is frequently overexpressed in malignant gliomas reported and its expression was positively associated with the pathological grade and proliferative activity of astrocytomas, as CCND1 expresses more significantly in grade IV astrocytomas than in grades II and III astrocytomas (Zhang *et al.*, 2018). Data obtained by immunohistochemistry found a correlation between high grade glioma and the expression of p53 and p21, while p14 and p16 more frequently present in low grade tumours (Zolota *et al.*, 2008).These differences in expression supported the previous observation in earlier study in the lab about PN517 being able to alter the cell cycle distribution and proliferation of the 1321N1 and GOS-3 (grade II and III) cell lines at an earlier timepoint and at the lower drug concentration than was found in the U87 MG (grade IV) cell line. Taken together, these contradictory reports in the literature suggest that there is a large degree of variation in cell specific responses to NSAID treatment and

each drug may possess a unique efficacy pattern where COX inhibition is not the definite mechanism of action.

On the other hand, low concentration cisplatin had an inhibitory effect on the cell proliferation and cell cycle progression, an effect that appeared to be overcome with longer incubation at 72 hours. This effect was expected as explained, the mechanism of action of cisplatin involves the impedance of cell cycle and DNA replication (Siddik, 2003). Cisplatin causes transient cell cycle arrest in the early S phase leading to a final G2/M phase arrest and ultimately apoptosis (Sorenson *et al.*, 1990). Hence, as the cells proliferate, an additive cytotoxic effect is seen, which in turn reduces the rate of proliferation of cisplatin treated cells. Similarly, cell cycle analysis of cisplatin treated cells showed a G2/M phase arrest, as would be expected of cisplatin (O'brien and Brown, 2006). The findings of one study demonstrated that cisplatin can cause transient increase in the level of cyclin D1 which is likely to be a cellular response to survive the attack by cisplatin, however cisplatin eventually decreases cyclin D1 as part of its killing mechanism (El-Kady *et al.*, 2011). Also, cisplatin did not show a significant reduction in cyclin D1 expression alone but the effect was enhanced with butein, a polyphenolic compound, when tested on HeLa human cervical carcinoma cells (Zhang *et al.*, 2015).

In addition, TMZ caused cell cycle arrest in G2/M phase (Fig 3.21 &3.24). The proposed hypothesis is that when the cell repair process targeted to the DNA strand opposite the O^6-MG, it cannot find a correct partner, thus resulting in long-lived nicks in the DNA. These nicks accumulate and persist into the subsequent cell cycle, where they ultimately inhibit initiation of replication in the daughter cells, blocking the cell cycle at the G2/M phase (Karran *et al.*, 1993; Roos *et al.*, 2007). The G2 cell cycle arrest or early mitosis was associated with low levels of cyclin D1 and high levels of cyclin B1 (Filippi-Chiela *et al.*, 2013).

Interestingly, the combinations of aspirin and PN517 significantly enhance the effect TMZ which was most obvious under hypoxia, particularly with the combination of TMZ and PN517 (Fig 3.16 &3.23). This could be attributed to the efficacy of aspirin and PN517 under hypoxia and not being affected largely by the

low levels of oxygen. Although there was no combined effect in cell cycle distribution with cisplatin or TMZ, no antagonism effect was observed which implicates that low dose of aspirin or PN517 can be of beneficial use. Effects of hypoxia on cell proliferation and cell cycle, migration and all other processes will be discussed in detail in the final chapter.

3.3.3. Cell migration

As mentioned previously, cell migration and invasion represent key features of GBM tumours hence the effect of the drug treatment on cell migration in this project has been established via wound healing assay. PN517 was noticed to be the most efficacious treatment, even more than cisplatin, in inhibiting wound healing (3.25). Therefore, it was not surprising to see enhancement in the combinations of PN517 with both cisplatin and TMZ. Effects on cell migration were similar between cell lines which is one of the few times that it was consistent across both cell types suggesting this process to be very conserved (3.27 & 3.44).

A large amount of evidence in the literature has supported the role of aspirin and NSAIDs in the inhibition of migration, invasion and metastasis (Rothwell *et al.*, 2011; Algra and Rothwell, 2012). For example, inhibition of invasion in U87-MG cells by the NSAID sulindac was observed using transwell Boyden chambers and scratch assay and associated with a downregulation of MMP-2 (Lee *et al.*, 2005). Similar results were reported in HN4, HN12, HT29 and HCT116 colorectal cancer cell lines in addition to demonstrating a downregulation of MMP-9 (Koontongkaew *et al.*, 2010).

One pathway which some studies have demonstrated that aspirin and NSAIDs may affect is the EGFR axis, hence disturbing its regulation of cell proliferation and migration. Sulindac, for example, can inhibit EGFR signalling through the inhibition of EGFR phosphorylation and decreased EGFR expression in HT29 cell (Pangburn *et al.*, 2005). Also, NCX-4016, a nitro-derivative of aspirin was shown to inhibit EGFR signalling in cisplatin-resistance human ovarian cancer cells (Selvendiran *et al.*, 2008).

EGFR activation results in multiple signalling pathways like MAPK and PI3/Akt, and triggers changes in NF-κB and c-Myc, leading to regulation of various biological processes associated with tumour growth such as cell cycle progression and proliferation, invasion, metastasis, angiogenesis, migration and differentiation (Paul *et al.*, 2013). Thus, a down-regulation of EGFR activity would be considered as a potential target while developing new therapeutics for treating tumours (Pore *et al.*, 2006; Taylor *et al.*, 2012).

EGFR gene amplification and overexpression has been reported in high grade glioblastoma (e.g. U87 MG) but is rare in low-grade glioma (e.g. 1321N1 and GOS-3) (Mestre *et al.*, 1997; Hatanpaa *et al.*, 2010). Glioblastoma displays an increased rate of EGFR gene mutation and amplification (20-40% of cases). Moreover, EGFR expression is also amplified under hypoxia, in a HIF-2α dependent manner (Franovic *et al.*, 2007). Thus, even in the absence of EGFR gene mutation, an upregulation in EGFR expression would be expected under hypoxia. This cell type specific expression of EGFR could provide an explanation for the effects of aspirin and its analogues, where EGFR expression would correlate with correspondent reduction of cell proliferation and migration. Another previous study in the lab tested ERFR levels in the U87-MG cell line by western blotting and found that treatment with aspirin or PN517 significantly decreased EGFR expression over 24 hours. Additionally, it observed reduced cell migration by scratch assay following PN517 exposure, and also after aspirin treatment to a lesser extent in different glioma cell lines.

A recent study published in 2019 has investigated the role of aspirin and its analogues on critical molecules in the EGF pathway and hypothesized that the protective activity of aspirin and aspirin analogues may be explained in part by disturbed EGFR internalisation and activation which also may help in understating the inhibitory effect on wound healing (Bashir *et al.*, 2019). It was previously reported that diaspirins can supress NF-κB signalling in SW480 cells (Claudius *et al.*, 2014) and that salicylates can potentially antagonise wound healing since that EGFR and NF-κB signalling are intimately linked (Bashir *et al.*, 2019). The authors proposed that aspirin and diaspirins may rapidly perturb EGF and EGFR internalisation and endocytosis (within minutes) at modest

concentrations, and that EGF internalisation pathway was substantially altered in the presence of PN517 in comparison to aspirin. Additionally, it was noticed upon longer incubations that diaspirins may inhibit EGFR phosphorylation at Tyr1045 and Tyr1173, an effect was weak with aspirin. The effect of aspirin and its analogues on total EGFR levels expression in SW480 cells was further investigated following 24 hr incubation and found a higher reduction with PN517 than aspirin. EGF internalisation may also be perturbed in oesophageal cell lines, suggestive of an effect not only restricted to colorectal cancer cells (Bashir *et al.*, 2019). Depending on their findings, it was suggested that aspirin and salicylates may be useful in cancer treatment, where EGFR amplification, overexpression and constitutive activation in a cancer is notable, like in glioblastoma. With respect to the results obtained from the current study with aspirin and PN517 using scratch assay support previous findings and further confirm the therapeutic potential of PN517 for the treatment of glioma.

Previous studies in the lab demonstrated that cisplatin treatment lead to a partial closure of the scratch in different glioma cell lines and cisplatin-treated U87-MG cells showed a decrease in EGFR expression under normoxia and hypoxia, but differences were not significant. Cisplatin impact on cell migration of oral squamous carcinoma cell lines was evaluated by scratch assay where cisplatin caused significant reduction in cell migration after 20 hr of creating the scratch. However, drug treatment was done for 24 hrs before the scratches. In addition, cisplatin-resistant cell lines were enriched with the stem cell-like characteristics mediated drug-resistance through inducing epithelial-mesenchymal transition (EMT) and cell migration (Ghosh *et al.*, 2016). Another study on MCF-7 breast cancer cells assessed wound healing and showed that cisplatin inhibited the migration of the cells which was further inhibited in combination with Berberine, a natural isoquinoline alkaloid (Zhao *et al.*, 2016). It has been suggested that cisplatin activates pro-apoptotic pathways through mitochondrial and Fas-associated mechanisms (Friesen *et al.*, 1999; Cullen *et al.*, 2007), and exert anti-invasive mechanisms which are still not totally understood (Ramer *et al.*, 2007). The expression levels of MMP2, TIMP1 and TIMP2 are decreased by cisplatin and the inhibition of PI3K/Akt/mTOR pathway (Karam *et al.*, 2010). In contrast, one study showed that cisplatin can induce EGFR phosphorylation and could

result in its nuclear translocation and lead to interaction with DNA protein kinase, mediating DNA repair (Benhar *et al.*, 2002). Thus, cisplatin mediated EGFR activation is a survival mechanism by the cell, that in turn, reduces the efficacy of cisplatin (Ahsan *et al.*, 2010). However, most of the studies have seen an enhanced effect of cisplatin on cell migration and invasion when in combination with other chemotherapy.

In comparison, temozolomide as the standard chemotherapeutic agent for the treatment of GBM did not show significant effects in wound healing in many studies, while enhancing its effects on cell migration when combined with other drugs. For example, TMZ did not cause any alterations in the migration of LN18 glioblastoma cells (Bien-Moller *et al.*, 2016). The invasion of GBM8401 cells was inhibited by 500μM TMZ however that was after incubation for 48 hr (Chou *et al.*, 2015). TMZ at 400μM reduced cell migration with respect to control after 48 hr but more inhibition was observed when combined with panobinostat by reversing the epithelial–mesenchymal transition in LN405 glioblastoma cell line (Urdiciain *et al.*, 2018).

To summarise, a decrease in both cell viability and proliferation following treatment with the aspirin and its novel analogue PN517 was observed. Furthermore, the enhancement in the effect of the combinations of PN517 with standard drugs was very clear, particularly with TMZ. A highly important observation was that these compounds were also effective under hypoxia, a condition usually associated with chemotherapy resistance. Although aspirin and PN517 did not have a significant effect on cell cycle progression or cyclin D1 regulation on their own or, an effect that may be concentration dependent, they enhanced the inhibition of cell cycle progression by cisplatin and TMZ. Importantly, PN517 was the most effective drug in inhibiting cell migration and wound healing. Taken together, the results obtained so far support the therapeutic potential of PN517 for the treatment of glioma and justify more investigation into the underlying mechanisms for the combined effect.

CHAPTER 4: EFFECT OF DRUG TREATMENT ON CELL DEATH INDUCTION

4.1. Introduction

One important factor which can affect cell viability following drug treatment is cell death induction. Assessing cell death has become a basic part of evaluating the efficacy of chemotherapeutic drugs since the inability to effectively induce cell death can contribute to treatment failure and resistance (Shah and Schwartz, 2001; Elmore, 2007; Vanlangenakker *et al.*, 2008; Fulda *et al.*, 2010). Cell death takes place either via apoptosis, necrosis or autophagy (Leist and Jäättelä, 2001). However, it is clear that the processes occurring in cell death are extremely complex and involve pathway crosstalk, hence it is not always easy to distinguish between the different mechanisms (Edinger and Thompson, 2004).

Due to its controlled and self-contained nature, apoptosis is the preferred process for drug-induced cell death, whereas the leaked cell contents resulting from necrosis cause damage to neighbouring cells in an uncontrolled manner (Edinger and Thompson, 2004). However, more often these forms of cell death occur simultaneously, and although the classical form of cell death measured is apoptosis, the additional cell death pathways should also be considered (Edinger and Thompson, 2004).

Overall, there are a wide range of features of apoptotic cell death that can be assessed including morphological changes, caspase activation, DNA cleavage, Bcl-2 family, PARP cleavage, loss of cell membrane integrity and mitochondrial changes (e.g. disruption of membrane potential, cytochrome c release and mitochondrial calcium perturbations). These apoptotic events occur in different stages of apoptosis; early, intermediate and late stage, with various methods and reagents developed to identify the each apoptotic stage, and to clearly distinguish them from necrotic or autophagic processes (Wlodkowic *et al.*, 2011).

One of the most widely used approaches to measure apoptosis induction following drug treatment is the Annexin V and PI assay which depends on alterations in the plasma membrane integrity of cells. In live intact cells, phosphatidylserine (PtdSer), a negatively charged membrane phospholipid, is normally found exclusively in the inner leaflet of the plasma membrane. During the early-mid stages of apoptosis, the charge ratio of the cellular membrane

becomes disrupted, and PtdSer translocates to the extracellular side of the membrane and becomes exposed to the cell surface (Kawasaki *et al.*, 2000). This translocation of PtdSer can be detected using Annexin-V, a phospholipid and calcium binding protein of unclear function (Van Heerde *et al.*, 1995), conjugated to fluorescein isothiocyanate (FITC) or an alternative fluorochrome. Usually, this assay is combined with cell permeable dyes such as PI or 7-AAD due to their ability to interact with DNA and detect the late stage of apoptosis, characterised by DNA fragmentation, or dead cells, allowing the differentiation of early apoptosis from late apoptosis or necrosis (Chou *et al.*, 1987). Flow cytometry is used to sort the populations of cells undergoing apoptosis and necrosis according to their relative fluorescent staining (Fig 4.1).

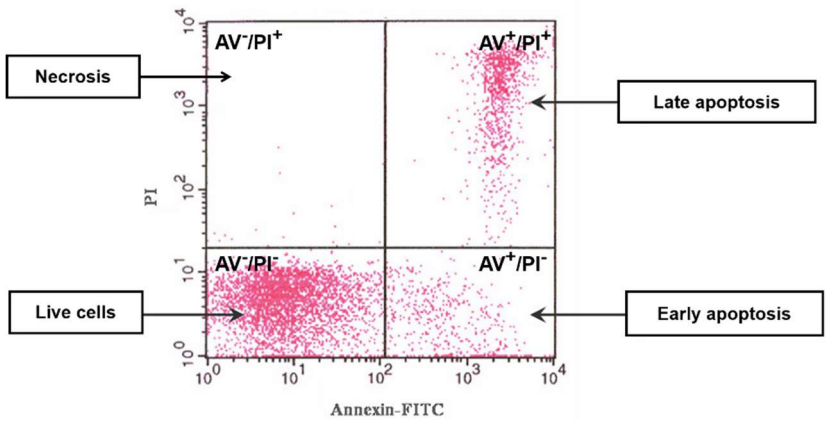

Figure 4. 1. Flow cytometry gating for a population of cells stained with Annexin V and PI. Cells that have little or very low binding of the dyes are identified as live healthy cells (lower left quadrant); cells that bind Annexin V dye only are identified as undergoing early apoptosis (lower right quadrant); cells that bind both dyes are identified as undergoing late apoptosis (upper right quadrant); and cells only binding the PI dye are identified either as necrotic or dead cells (upper left quadrant) (Adapted from Abnova & MyBioSource).

Several studies have suggested a complex crosstalk existing between autophagy and apoptosis (Maiuri *et al.*, 2007; Chaabane *et al.*, 2013; Nikoletopoulou *et al.*, 2013). As mentioned previously, autophagy may have two roles, the first being a pro-death role where autophagy serves as an alternative mechanism of cell death, autophagic cell death, which is classified as type II programmed cell death (Gozuacik and Kimchi, 2004). Conversely, autophagy can also play a pro-survival role, as autophagy inhibitors may enhance apoptotic cell death (Hara *et al.*, 2006). Therefore, monitoring cellular autophagy is another important factor when studying cell death following drug treatment.

Several methods have been developed for monitoring the autophagy pathway and the steps involved in autophagosome formation and the maturation of autophagosomes to autolysosomes (Mizushima *et al.*, 2010). Microscopy is a widely used technique that visualizes the autophagosomes in small populations of cells at a specific timepoint, however flow cytometry offers a high-throughput analysis of the autophagosomes detection.

A conventional fluorescent probe, monodansylcadaverine (MDC), has been used for the analysis of lysosomal/autophagic vacuoles (Vazquez and Colombo, 2009). MDC is known to generate weak a fluorescent signal with high background, and requires UV illumination that is not compatible with excitation sources commonly implemented in flow cytometry. However, a recently developed dye for monitoring autophagy activity at the cellular level, Cyto-ID, does not show background fluorescence under control conditions, and has a signal that responds to well-known autophagy modulators. This dye has been used relatively commonly in several studies to monitor autophagy induction (Shang *et al.*, 2017; Hwang *et al.*, 2018; Zhang *et al.*, 2018; Zhao *et al.*, 2018).

Cyto-ID assay is based on the usage of a fluorescent probe that selectively stains the various autophagic compartments (pre-autophagosomes, autophagosomes, and autophagolysosomes) in live cells and allows determination of autophagic flux as accumulation of stained compartments under basic or activated conditions (Stankov *et al.*, 2014). As opposed to lysomotrophic dyes which mainly detect lysosomes, it is suggested that Cyto-ID may prove more selective for autophagic vacuoles since it is serving as a selective marker of autolysosomes and earlier autophagic compartments while only weakly staining lysosomes (Klionsky *et al.*, 2016). An enhancement in the fluorescence emission intensity of the CYTO-ID dye occurs upon compartmentalization with the lamellar membrane structures associated with autophagic vesicles. This allows for detection of autophagy in live cells by fluorescence microscopy, flow cytometry and fluorescence microplate assay.

Additionally, the disruption of active mitochondria is a distinctive feature of the early stages of apoptosis with changes in the mitochondrial membrane potential

(Δψm) (Green and Reed, 1998; Ly *et al.*, 2003).These alterations in the membrane potential are presumed to be caused by either the formation of pores by members of the Bcl-2 family, or the opening of the inner membrane permeability transition pore complex (PTPC) allowing passage of ions and small molecules leading to the release of cytochrome c into the cytosol which then triggers the downstream events in the apoptotic cascade (Green and Reed, 1998).

On the other hand, it has been speculated that alterations in mitochondrial membrane potential appear to precede the mitophagy process and there is a crosstalk between the mitochondrial health, autophagy and oxidative cellular stress (Lee *et al.*, 2012). Therefore, the mitochondrial membrane potential is an important parameter of mitochondrial function and cell health, and alterations in the mitochondrial membrane potential can be assessed in live cells to study mitochondrial behaviour in a variety of conditions and following exposure to different cytotoxic treatments (Choi and Lim, 2014; Wheaton *et al.*, 2014).

Different fluorescent probes can be used to measure the mitochondrial membrane potential with a variety of fluorescent techniques including rhodamine 123 (2-(6-amino-3-imino-3H-xanthen-9-yl) benzoic acid methyl ester), TMRE (tetramethylrhodamine, ethyl ester) and JC-1 (tetraethylbenzimidazolylcarbocyanine iodide). These dyes are typically lipophilic and positively charged, hence, the polarized healthy mitochondria with a more negative Δψm will accumulate more dye than the depolarized unhealthy mitochondria (Lemasters and Ramshesh, 2007).

TMRE and Rhod123 are commonly used for slow and fast resolving acute studies, respectively (Perry *et al.*, 2011). The JC-1 dye is a membrane-permeable fluorochrome able to penetrate cellular and mitochondrial membranes and is widely used in apoptosis studies to monitor mitochondrial health and assess Δψm leading to apoptosis (Cossarizza *et al.*, 1993). Unlike other mitochondrial dyes, JC-1 depends only on the membrane potential and it is not affected by other factors such as mitochondrial size, shape, and density, which may influence single-component fluorescence signals.

At low concentrations, JC-1 exists as monomers, whereas at high concentrations it can aggregate into larger structures. Due to this property, the emission spectra of JC-1 varies based on its relative concentration within the cells and provides an accurate reflection of Δψm. In healthy cells, JC-1 is taken up as monomers and accumulate within the mitochondria because of the polarised membrane and forms red/orange aggregates. However, if the membrane is depolarised JC-1 is unable to penetrate the mitochondria and remains as green monomers in the cytoplasm of the cells. Therefore, when accumulated in mitochondria, JC-1 exhibits a shift in fluorescence emission from green to red. This allows mitochondrial depolarization to be measured by a decrease in the red/green fluorescence intensity ratio, which can be assessed by fluorescence microscopy or flowcytometry (Fig 4.2).

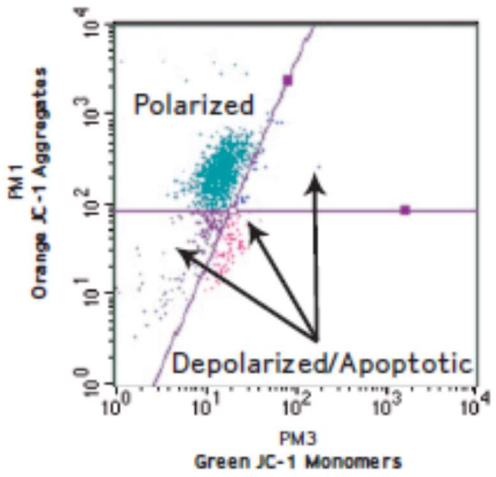

Figure 4. 2. Flow cytometry dot plot showing the gating of JC1 (orange)-aggregates and JC1 (green)-monomer (Source: Guava Technologies).

Having established that the drug treatment with aspirin or PN517 decreased cell viability and suggesting that the mechanism of action is not linked closely to cell proliferation, one potential factor contributing to this result is the induction of cell death Therefore, the work in this chapter aimed to investigate whether aspirin, PN517, or the combinations induce apoptosis, necrosis, autophagy or a mixture of them.

For that purpose, cells were stained with Annexin V and PI following drug treatment to assess apoptosis and necrosis contribution. Autophagy induction was monitored with the CYTO-ID reagent using flowcytometry and fluorescence microscopy, and the JC-1 dye was used as a mitochondrial membrane potential indicator which correlates with both early stages of apoptosis and autophagy. Additionally, the effect of the drug treatments on activation of different proteins that play a role in stress response, apoptosis or autophagy was tested using SDS-PAGE and western blot analysis. The autophagic proteins PI3K Class III, PIK3R4 (Phosphoinositide-3-Kinase Regulatory Subunit 4) and Atg14 were tested as well as the heat shock protein 27 (Hsp27) and c-Jun which is a component of the transcription factor activator protein 1 (AP-1).

4.2. Results

4.2.1. Evaluating Induction of Apoptosis following drug treatment

The initial investigations aimed to assess the relative percentage of U87-MG cells undergoing apoptosis or necrosis following drug treatment for 24, 48, and 72 hours using Annexin-V/PI dual staining. IC_{50} values determined from mono-treatment cell viability for 48 hr were used for all drugs either separately or in combination, under normoxia and hypoxia. Experimental controls included the SVG-p12 foetal glial cell line and the standard chemotherapeutic drugs cisplatin and temozolomide.

In the U87-MG glioblastoma cell line, in control cells under normoxia and hypoxia, no significant differences were found for any of the cell populations between timepoints or between normoxia and hypoxia ($p>0.05$) (Fig.4.3). Each drug treatment appeared to increase total apoptosis levels in a time dependent manner under both normoxia and hypoxia (Fig 4.3). In almost all cases, both early and late apoptosis levels were higher for all treatments compared to control across all timepoints and both conditions. At 24 hr, only PN517 and its combination with cisplatin and TMZ induced significant increase in total apoptosis (18.7 ±2% and 17.1 ±1.6%, respectively, compared to 8 ±0.3% in the control, $p<0.05$).

Following 48 hours of incubation under normoxia, treatment with PN517 alone or in combination with cisplatin or TMZ resulted in a significant proportion of early and total apoptotic cells compared to control and numbers were also higher than those with the two combinations of aspirin. While early apoptosis values were of 6.5 ±0.7% for control at 48 hr, they increased up to 14.5 ±1.7% ($p<0.01$), 13.6 ±1.2% ($p<0.01$) and 15.6 ±1.8% ($p<0.001$) with PN517, Cis +PN517 and TMZ+ PN517, respectively. Accordingly, these treatments showed also an increase in total apoptosis values to 19.8 ±2.2%, 21±2.2% and 26.6 ±2.5 vs. 9.6 ±0.8% in control (Fig 4.3). However, the TMZ and PN517 combination showed the greatest induction of late apoptosis with a significant difference compared to the control (11 ±1.5% vs. 3 ±0.7%, $p<0.01$).

The same combination treatment was also significantly different from control in inducing late apoptosis after 72 hours of treatment (28.6 ±5.7% vs. 3.3 ±0.5%, $p<0.001$) and it produced significant differences compared to all other drug treatments in the late apoptotic population ($p<0.0001$). As for total apoptosis results at this timepoint, only PN517 combinations showed a significant increase over control (9.9 ±0.8% vs. 22.5 ±2.7% for Cis +PN517, $p<0.05$ and 43.3 ±5.1% for TMZ +PN517 $p<0.0001$).

In hypoxia, a significant increase in total apoptosis was observed after 24 hours for aspirin and PN517 compared to control (17.3 ±2.3% and 20.2 ±3.2% vs. 8.3±1.1%) (Fig 4.3). Following 48 hours of incubation, only the treatment with PN517 and its combination with cisplatin resulted in a significant proportion of total apoptotic cells (23.4 ±3.2% and 25.5 ±4.6%, respectively) compared to the control at 13 ±1%. Following 72 hours, only PN517 combinations were showed a significant induction of apoptosis compared to the control ($p<0.01$ for cisplatin and PN517 and $p<0.05$ for TMZ and PN517).

Over the three days of drug treatment, the most effective monotherapy was consistently PN517, which was more effective than the positive control cisplatin with an exception at 72 hours under normoxia where cisplatin resulted in a greater overall level of apoptosis, but not significantly greater than PN517 ($p>0.05$). Additionally, the efficacy of all combinations increased over time under normoxia and hypoxia and the most effective combination under normoxia was TMZ and PN517 at 48 and 72 hr. However, this enhancement over TMZ alone was observed to a lesser extent under hypoxia ($p>0.05$).

In the SVG-p12 cell line, a small increase in the induction of apoptosis over time was observed in the control cells under normoxia and hypoxia. However, no significant differences were found for any of the cell populations between timepoints or between normoxia and hypoxia ($p>0.05$) (Fig.4.4). Data showed overall higher levels of apoptosis compared to U87-MG cells (Fig 4.3), and in general, all treatments increased early apoptosis compared to control apart from 72 hours hypoxia. However, only TMZ and its combination with aspirin and PN517 showed a significant increase in early apoptosis percentage over control

at 48 hr under normoxia (p<0.05). Additionally, TMZ was the sole monotherapy which produced a significant effect on SVG-p12 cells at 48 hr compared to the control under normoxia (11.2 ±1.1% vs. 28 ±6%, p<0.05).

Total apoptosis induction appeared to increase in response to all treatments compared to control at all timepoints and under both conditions, although not all changes were significant. Interestingly, PN517 did not show significant effect at 24 and 48 hr in contrast to U87-MG cells, under both conditions. However, it increased apoptosis induction significantly at 72 hr (p<0.05). Also, TMZ showed significant increase in total apoptosis compared to the control under normoxia at 72 hr (p<0.05). Moreover, the most effect combination was TMZ with PN517, and this was the most effective treatment at all timepoints under both conditions with significant differences in both late and total apoptosis compared to control (p<0.05) (Fig 4.4).

Both cell lines showed small proportions of cells undergoing necrosis which increased after 72 hours especially with combination treatments. Of particular note was an apparent increase in necrosis at 72 hr in SVG-p12 cells following cisplatin treatment. However, no significant effects were found between necrosis values under any condition (p>0.05).

Representative dot plots acquired by flow cytometry for the Annexin V/PI staining following drug treatment can be found in the appendix figures 9.13 & 9.14 (U87-MG) and figures 9.15 & 9.16 (SVG-p12). The vehicle (1%(v/v) DMSO) did not show any significant change in apoptosis in both cell lines under normoxia or hypoxia (p>0.05).

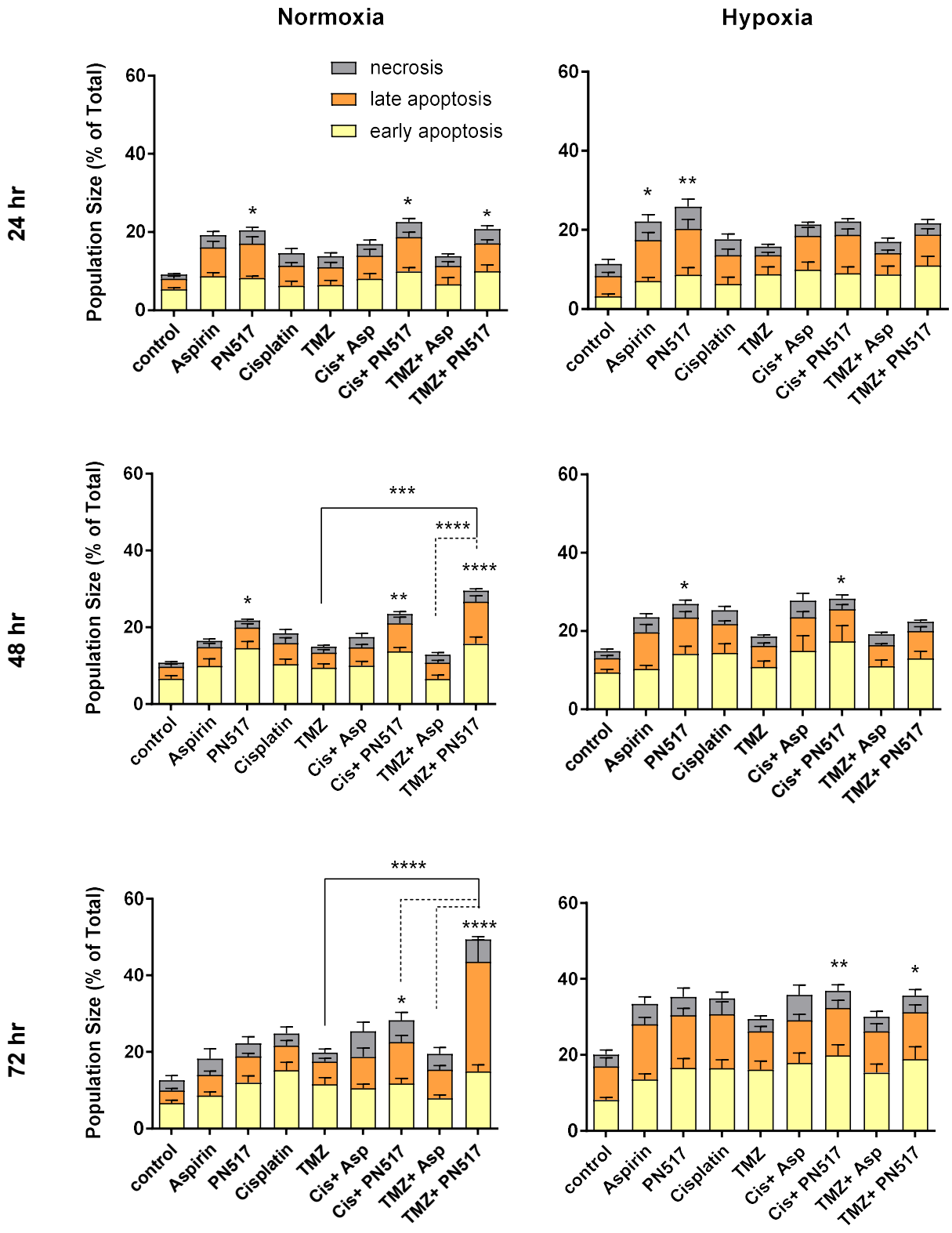

Figure 4. 3. The effect of drug treatment on inducing apoptosis and necrosis in the U87-MG cell line under normoxia and hypoxia. Data shows the relative proportions of early and late apoptotic cells, and necrotic cells observed using Annexin-V and PI staining after 24, 48, and 72 hours of drug treatment. Values represent mean ±SEM of six independent experiments. A two-way ANOVA was used to detect significant differences in total apoptosis, with Tukey's multiple comparison test, *P < 0.05; **P < 0.01; ***P < 0.001; ****P < 0.0001. The experimental procedure was performed as described in Materials and Methods section 2.2.9.

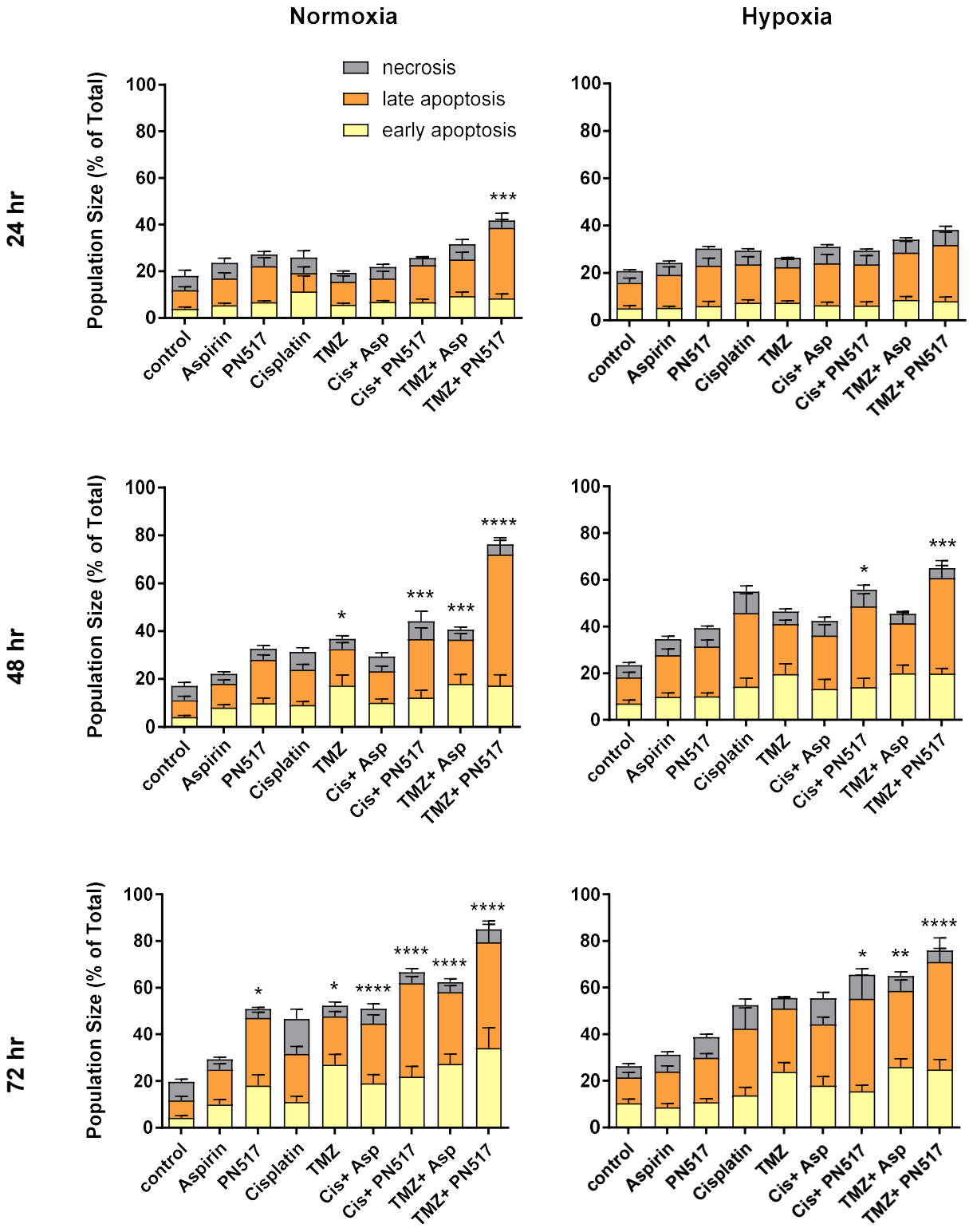

Figure 4. 4. The effect of drug treatment on inducing apoptosis and necrosis in the SVG-p12 cell line under normoxia and hypoxia**.** Data shows the relative proportions of early and late apoptotic cells, and necrotic cells observed using Annexin-V and PI staining after 24, 48, and 72 hours of drug treatment. Values represent mean ±SEM of six independent experiments. A two-way ANOVA was used to detect significant differences in total apoptosis, with Tukey's multiple comparison test, *P < 0.05; **P < 0.01; ***P < 0.001; ****P < 0.0001. The experimental procedure was performed as described in Materials and Methods section 2.2.9.

4.2.2. Evaluating induction of autophagy following drug treatment

Autophagy induction was monitored in U87-MG and SVG-p12 cells following 24 hr of drug treatment using Cyto-ID staining and flow cytometry with supporting qualitative images from fluorescence microscopy. IC_{50} values determined from mono-treatment cell viability for 48 hr were used for all drugs either separately or in combination, under normoxia and hypoxia. Rapamycin (Rap; an autophagy inducer by inhibiting mTOR) and Chloroquine (CLQ; a lysosomal inhibitor) were included as positive control (Rap+CLQ).

When assessing autophagic activity in U87-MG cells, all treatments appeared to induce autophagy compared to control under normoxia, although no all increases were statistically significant (Fig 4.5). Interestingly, aspirin appeared to induce more autophagic activity than its analogue PN517, and aspirin in combination with cisplatin or temozolomide showed the greatest effect with a significant difference between the combinations and control. When aspirin was combined with cisplatin or TMZ, an increase in the percentage of autophagy to 170 ±14.6% and 168 ±20% was observed, respectively ($p<0.01$) compared to the control. The addition of PN517 to cisplatin and TMZ did not appear to produce any additional effect over monotherapy with cisplatin or TMZ alone, with no significant differences compared to the control ($p>0.05$).

Under hypoxia, all treatments appeared to induce autophagy compared to control apart from PN517 (Fig 4.5). TMZ alone produced the largest percentage increase in autophagy among monotherapies (163 ±5.4%, $p<0.05$). PN517 did not produce an additional effect when in combination with cisplatin or TMZ ($p>0.05$). Similarly, to normoxia, combinations of cisplatin or TMZ with aspirin exhibited the largest overall induction of autophagy in U87-MG cells. An increase in the percentage of autophagy to 166.7 ±12.5% ($p<0.01$) and 158.5 ±14.4% ($p<0.05$) was observed with aspirin combination with cisplatin and TMZ, respectively.

In SVG-p12 cells, a general trend towards a lesser effect of all drug treatments was observed compared to U87-MG cells (Fig 4.6). The patterns of monotherapy effect on autophagy induction were very similar to U87-MG but with consistently lower levels of induction, under both culture conditions. Combinations of aspirin

or PN517 did not appear to enhance the autophagic activity for cisplatin and TMZ. However, there were no significant differences for any of the treatments under any condition (p>0.05).

The positive control (Rap+ CLQ) significantly induced autophagy detected with Cyto-ID in both cell lines and under different conditions (p<0.05). Additionally, the effects of drug treatment on autophagy activity was assessed in U87-MG cells under normoxia using fluorescence microscopy to confirm the formation of autophagy vacuoles (Fig 4.7). The green autophagic vacuoles were clearly observed with the positive control.

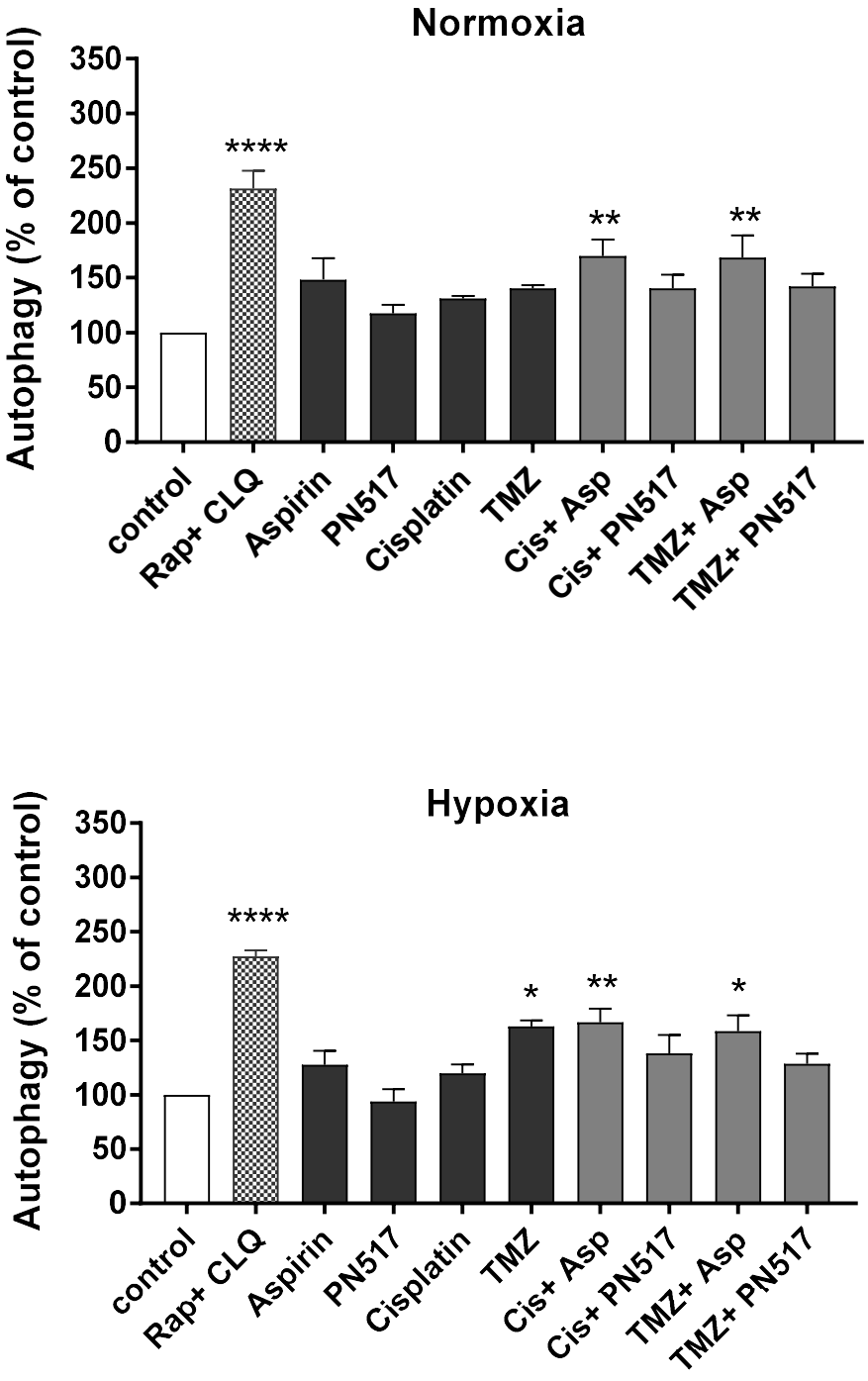

Figure 4. 5. The effect of drug treatment on inducing autophagy in the U87-MG cell line under normoxia and hypoxia. Data illustrates autophagy induction observed using Cyto-ID staining after 24 hours of drug treatment as percentage of control. Values represent mean ±SEM of six independent experiments. A two-way ANOVA was used to identify significant effects, with Tukey's multiple comparison test, *P < 0.05; **P < 0.01; ***P < 0.001; ****P < 0.0001. The experimental procedure was performed as described in Materials and Methods section 2.2.10.

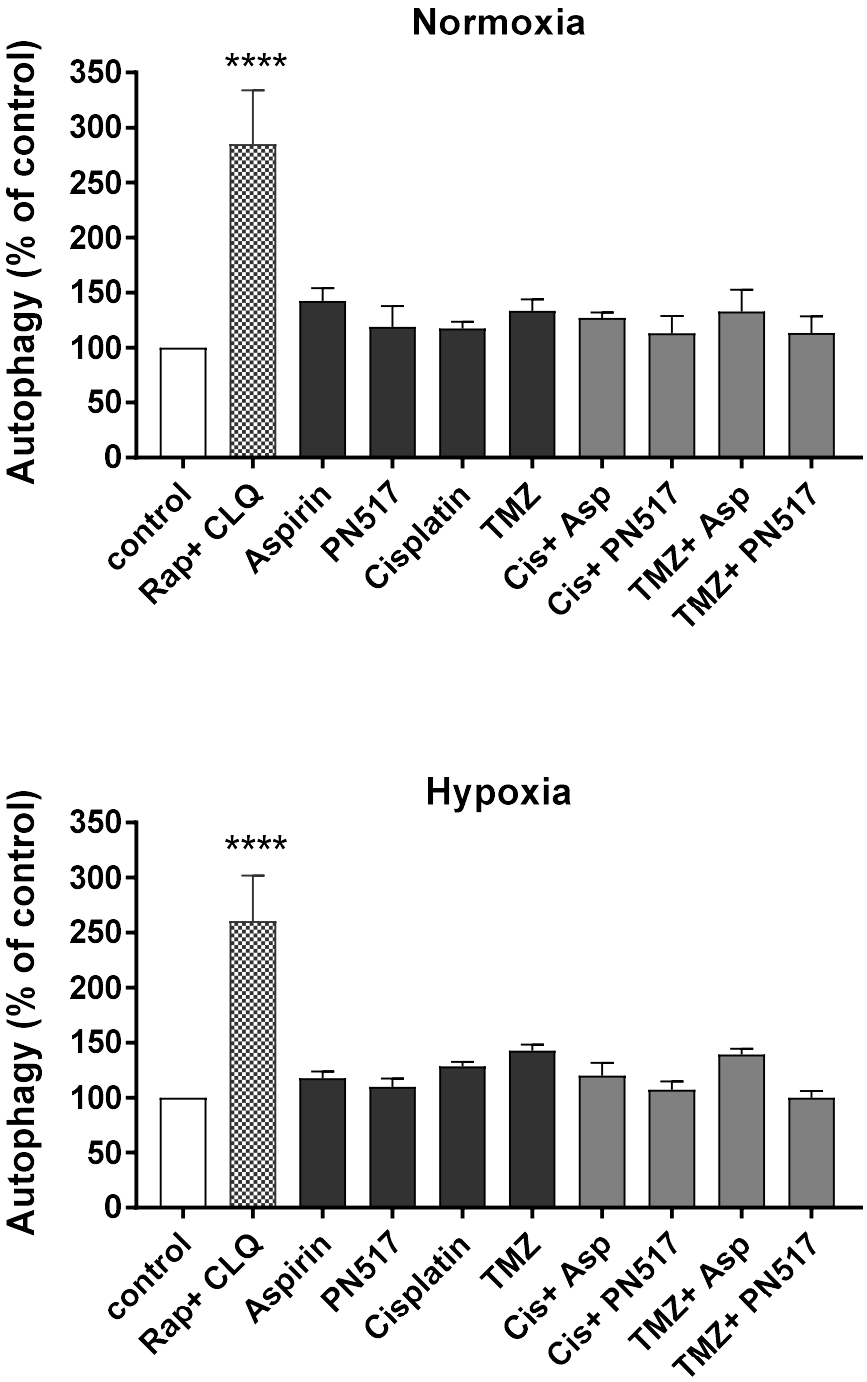

Figure 4. 6. The effect of drug treatment on inducing autophagy in the SVG-p12 cell line under normoxia and hypoxia. Data illustrates autophagy induction observed using Cyto-ID staining after 24 hours of drug treatment as percentage of control. Values represent mean ±SEM of six independent experiments. A two-way ANOVA was used to identify significant effects, with Tukey's multiple comparison test, *P < 0.05; **P < 0.01; ***P < 0.001; ****P < 0.0001. The experimental procedure was performed as described in Materials and Methods section 2.2.10.

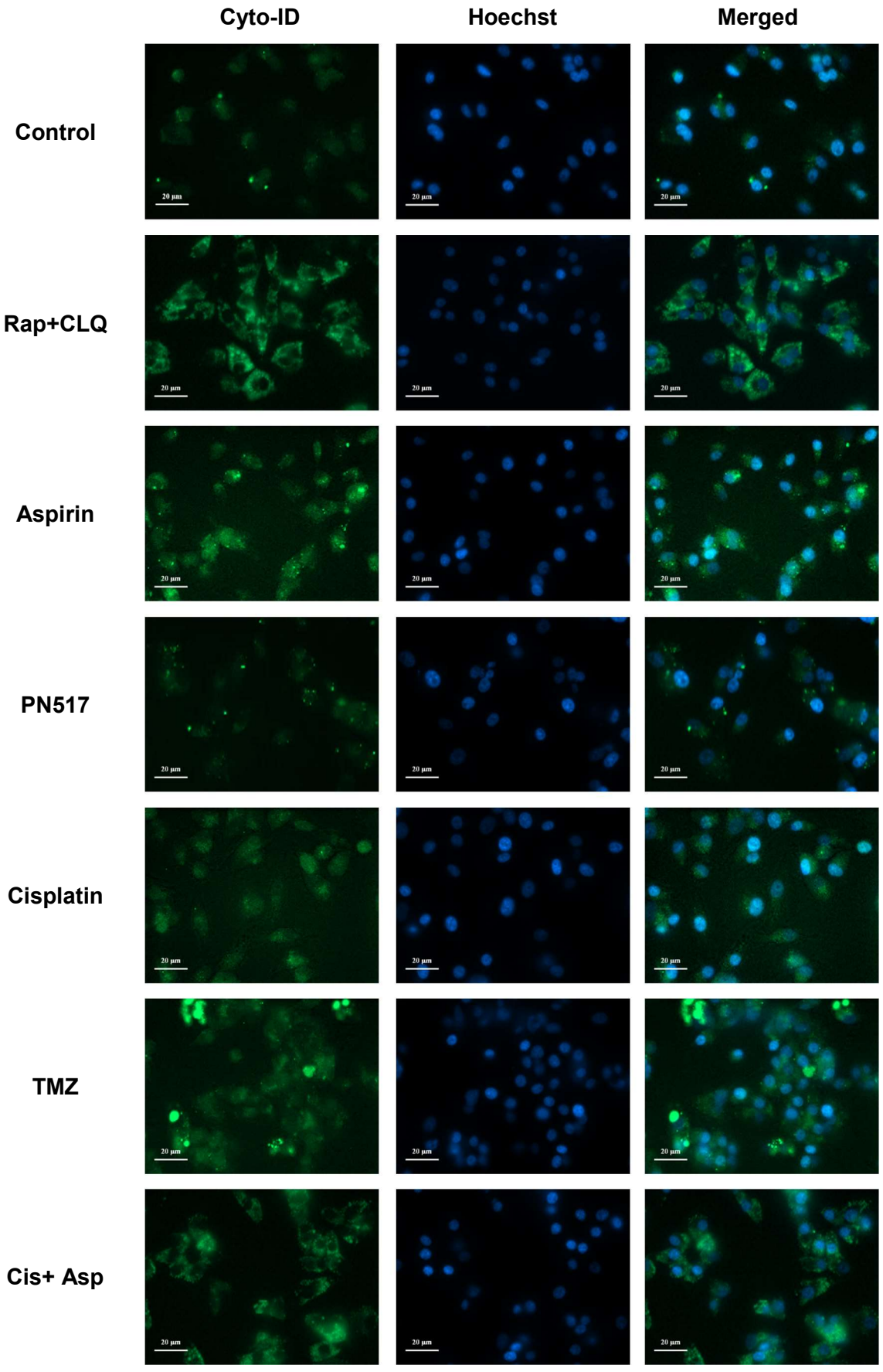
Cyto-ID
Hoechst
Merged
Control
Rap+CLQ
Aspirin
PN517
Cisplatin
TMZ
Cis+ Asp
20 μm

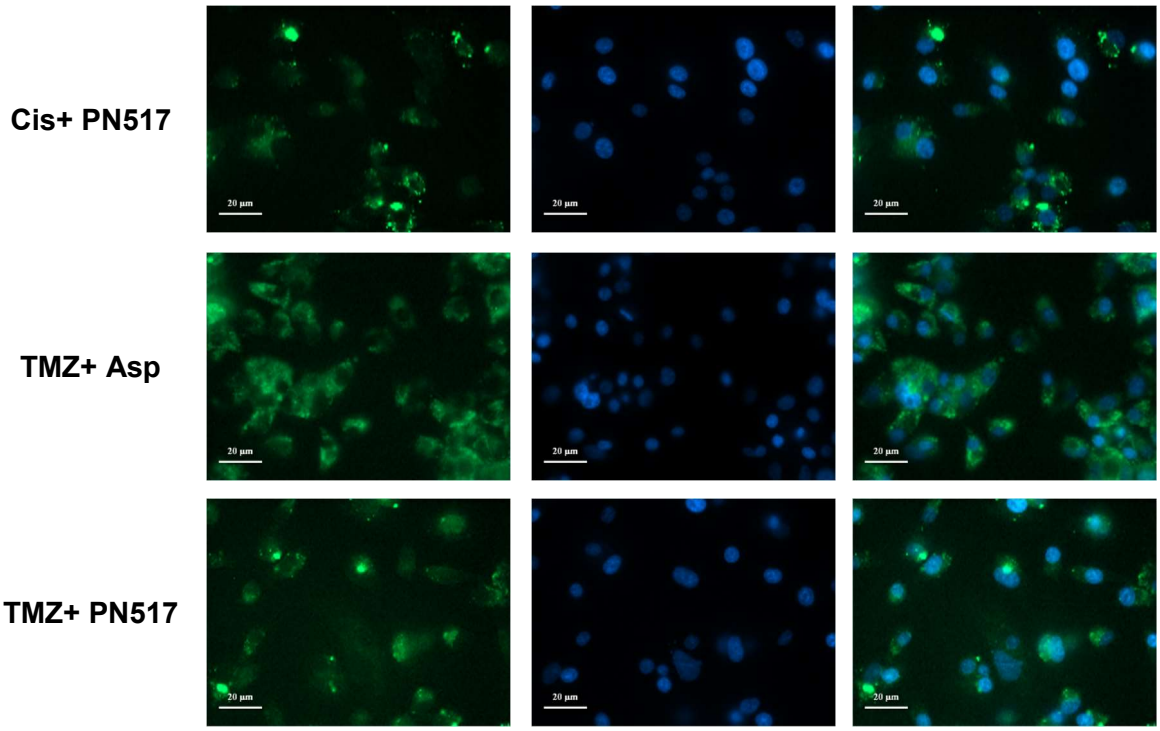

Figure 4. 7. Representative fluorescent microscopy images illustrating autophagy induction in U87-MG cells under normoxia. Cells were stained with the CYTO-ID autophagy dye (green) plus Hoechst 33342 nuclear dye (blue) after 24 hr of drug treatment. Autophagosome formation was observed by the appearance of punctate structures in the cells and an increase in green fluorescence (Scale bar: 20 µm). The experimental procedure was performed as described in Materials and Methods section 2.2.10.

Autophagy regulatory proteins assessment:

To further characterise the effect of drug treatment on autophagy pathways, western blotting analysis was performed to detecting changes in different essential proteins involved in autophagy regulation. Changes in the regulation of PI3K Class III, PIK3R4 and Atg14 were examined after 24 hour of drug treatment at same concentrations used for cell proliferation and cell cycle analysis (IC_{25}) in the U87-MG cell line, under normoxia and hypoxia. Effects on protein expression and regulation were determined using specific antibodies for immunoblotting and quantified as a fold change over the untreated cells by densitometry. The housekeeping β-actin protein was used for normalisation of all samples to correct any loading differences between lanes. The experimental conditions applied can be found in the appendix (Table 9.2).

When assessing the levels of PI3K Class III following drug treatment, a trend towards an upregulation in PI3K Class III following aspirin treatment was observed that was greater than that observed for PN517 under both culture conditions (Fig 4.8). In addition, a trend towards higher levels of protein expression was observed under hypoxia especially following combination treatments. However, no significant differences were found compared to the control under either condition ($p>0.05$).

A similar pattern was noted when assessing the cellular levels of a subunit of the PI3K complex; PIK3R4. A trend towards elevated levels was observed following aspirin treatment, an effect greater than that of PN517. In addition, higher levels of protein expression were observed under hypoxia, but with no significant differences under either condition ($p>0.05$) (Fig 4.9). Again, a trend towards increased Atg14 protein expression was observed following aspirin treatment compared to PN517, but no significant differences were found under either culture condition ($p>0.05$) (Fig 4.10).

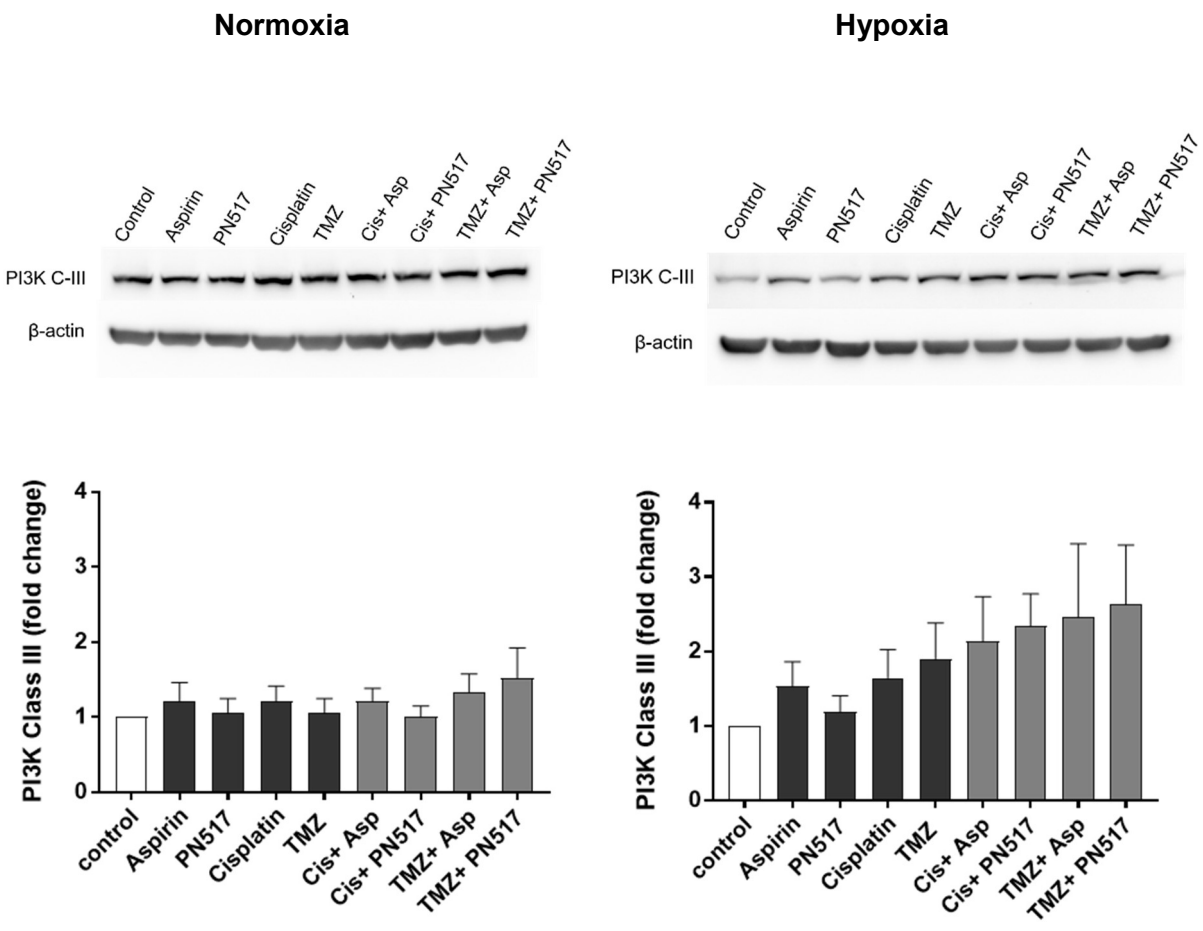

Figure 4. 8. Representative immunoblots and densitometric analysis of PI3K Class III levels in the U87-MG cell line under normoxia and hypoxia. Data indicate the fold change of phospho-I3Kinase levels following 24 hr of drug treatment compared to control as determined by densitometry. Values represent mean ±SEM of six independent experiments. A two-way ANOVA was used to identify significant effects, with Tukey's multiple comparison test, *P < 0.05; **P < 0.01; ***P < 0.001; ****P < 0.0001. The experimental procedure was performed as described in Materials and Methods section 2.2.16.

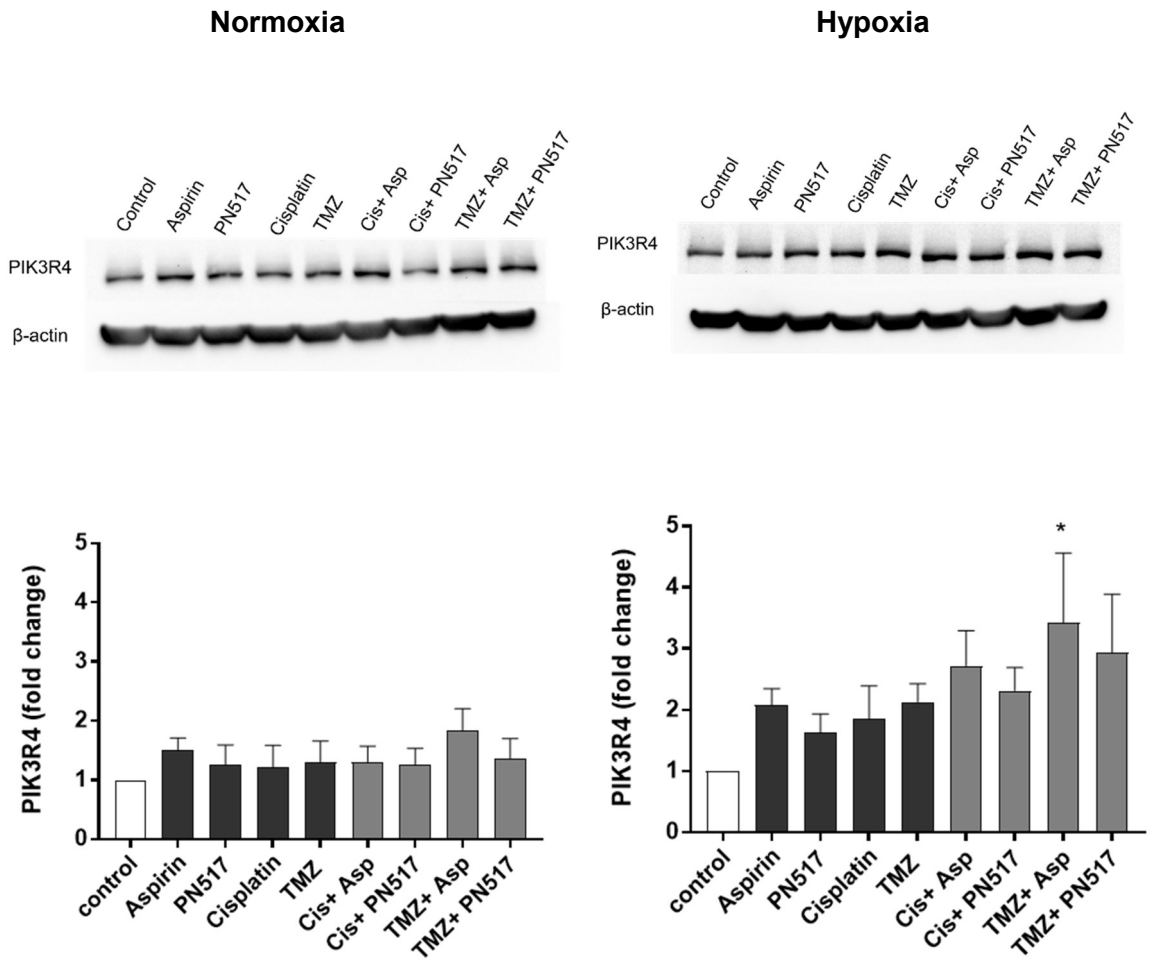

Figure 4. 9. Representative immunoblots and densitometric analysis of PIK3R4 levels in the U87-MG cell line under normoxia and hypoxia. Data indicate the fold change of PIK3R4 levels following 24 hr of drug treatment compared to control as determined by densitometry. Values represent mean ±SEM of six independent experiments. A two-way ANOVA was used to identify significant effects, with Tukey's multiple comparison test, *P < 0.05; **P < 0.01; ***P < 0.001; ****P < 0.0001. The experimental procedure was performed as described in Materials and Methods section 2.2.16.

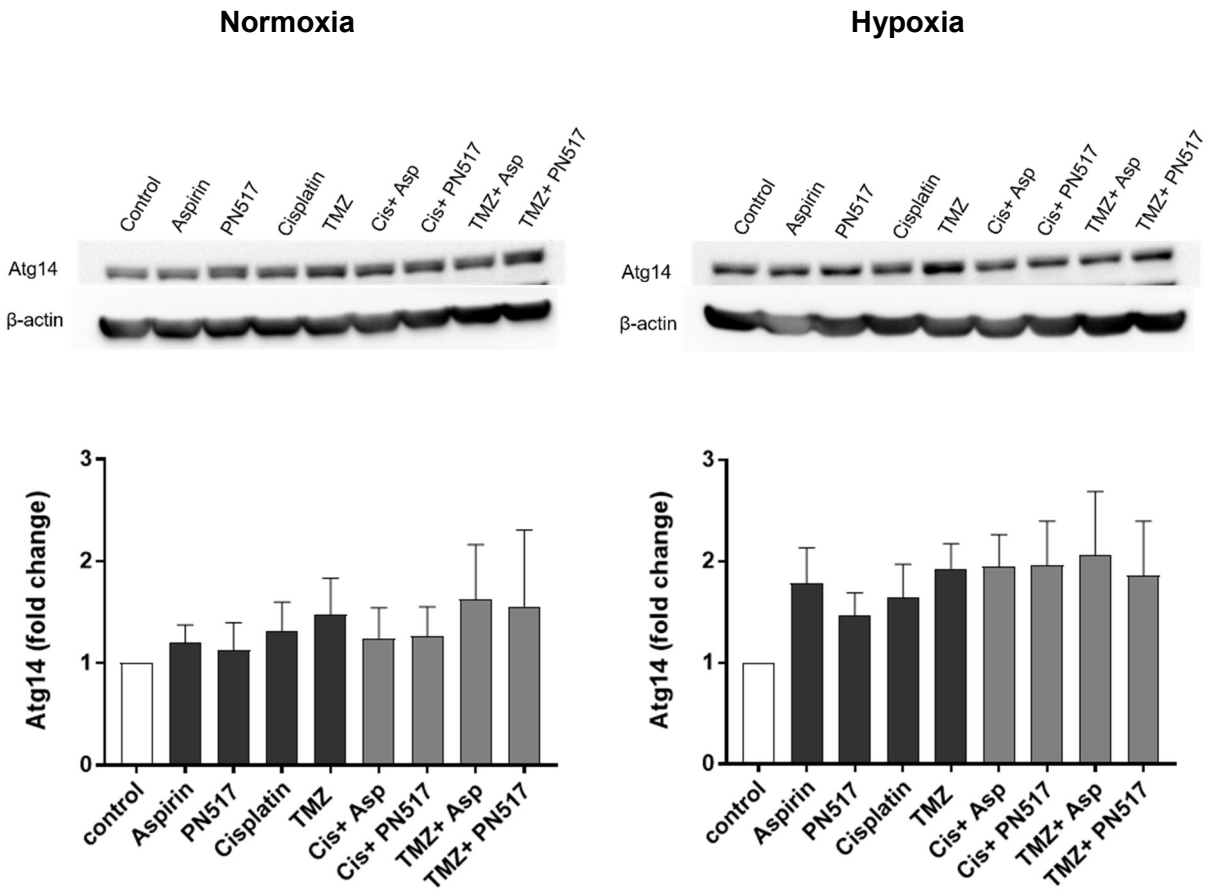

Figure 4. 10. Representative immunoblots and densitometric analysis of Atg14 levels in the U87-MG cell line under normoxia and hypoxia. Data indicate the fold change in Atg14 levels following 24 hr of drug treatment compared to control as determined by densitometry. Values represent mean ±SEM of six independent experiments. A two-way ANOVA was used to identify significant effects, with Tukey's multiple comparison test, *P < 0.05; **P < 0.01; ***P < 0.001; ****P < 0.0001. The experimental procedure was performed as described in Materials and Methods section 2.2.16.

4.2.3. Effects of drug treatment on mitochondrial membrane potential.

To investigate whether drug treatment can induce apoptosis or autophagic cell death by affecting mitochondrial function, U87-MG and SVG-p12 cells were assessed for depolarisation of the mitochondrial membrane potential using JC-1 and 7-AAD dual staining following drug treatment for 24 and 48 hours. IC_{50} values determined from mono-treatment cell viability for 48 hr were used for all drugs either separately or in combination, under normoxia and hypoxia. CCCP was used as positive control which is potent mitochondrial oxidative phosphorylation uncoupler that renders mitochondrial inner membrane permeable to protons and induces apoptosis. Positive depolarisation was defined by a shift from red/orange fluorescence (aggregate population) to green fluorescence (monomer population) using flow cytometer and fluorescence microscope.

In U87-MG cells, drug treatment produced a similar pattern of effect to the apoptosis assay with less of an overall effect of treatment under hypoxia compared to normoxia. The greatest effect at 24 hr of drug treatment was observed with PN517, larger than that of cisplatin, with an increase in the percentage of depolarised cells from 13.6 ±2.1% to 31.8 ±7.3%. However, no significant differences were found under either culture condition (p<0.05) (Fig 4.11).

There were greater increases in the depolarised cell populations for all treatments at 48 hr, under both conditions. The PN517 effect observed at 24 hours was sustained to 48 hours under normoxia and again produced the largest percentage of depolarised cells (51.4 ±4.8% vs. 11.4 ±1.1% in the control, p<0.001). TMZ treatment also resulted in a significant increase in the relative proportion of depolarised cells at 48 hr compared to control under normoxia (40.5 ±6.4%, p<0.05). With regards the combination treatment effects, the highest levels of depolarised cell populations were observed with PN517 combined with cisplatin or TMZ (45.6 ±3.2%, p<0.01 and 50.6 ±1.9%, p<0.001 compared to control, respectively). These combinations enhanced the effects of the single drug treatments of both cisplatin and TMZ but were no greater than PN517 alone (Fig 4.11).

At 48 hours under hypoxia, all treatments depolarised the mitochondrial membrane potential. PN517 was significantly efficacious compared to the control (40 ±9.1% vs. 18.4 ±4%, $p<0.05$). It is also worth noting that the effect of TMZ was not significant under hypoxia ($p>0.05$) whereas cisplatin produced a significant depolarisation compared to control (47 ±12.8%, $p>0.05$).

Levels of depolarisation of the mitochondrial membrane potential in SVG-p12 cells were greater compared to U87-MG cells under both conditions, as with apoptosis results. In similar way to effects observed in the U87-MG cells, no significant effect of treatment was found at 24 hours under either culture condition, $p>0.05$ (Fig 4.12). Under normoxia, combinations with PN517 appeared to produce the highest levels of depolarisation but were similar to PN517 alone. Combinations with aspirin did not show any increase in the effect of the monotherapy of cisplatin or TMZ. After 48 hr, all treatments showed similar efficacy under hypoxia. Importantly, there was no significant effect for any drug treatment compared to control under either condition and at both timepoints ($p>0.05$) (Fig. 4.12).

To support the results observed in the U87-MG cells, fluorescence microscope was used to visualise JC-1 and 7-AAD staining following drug treatment for 48 hr under normoxia. The effects of the drug treatment on the mitochondrial membrane potential and fluorescence shift of JC-1 was monitored (Fig 4.13). The positive control (CCCP) significantly induced depolarisation defined by a shift from red/orange fluorescence (aggregate population) to green fluorescence (monomer population) in both cell lines and under different conditions ($p<0.0001$).

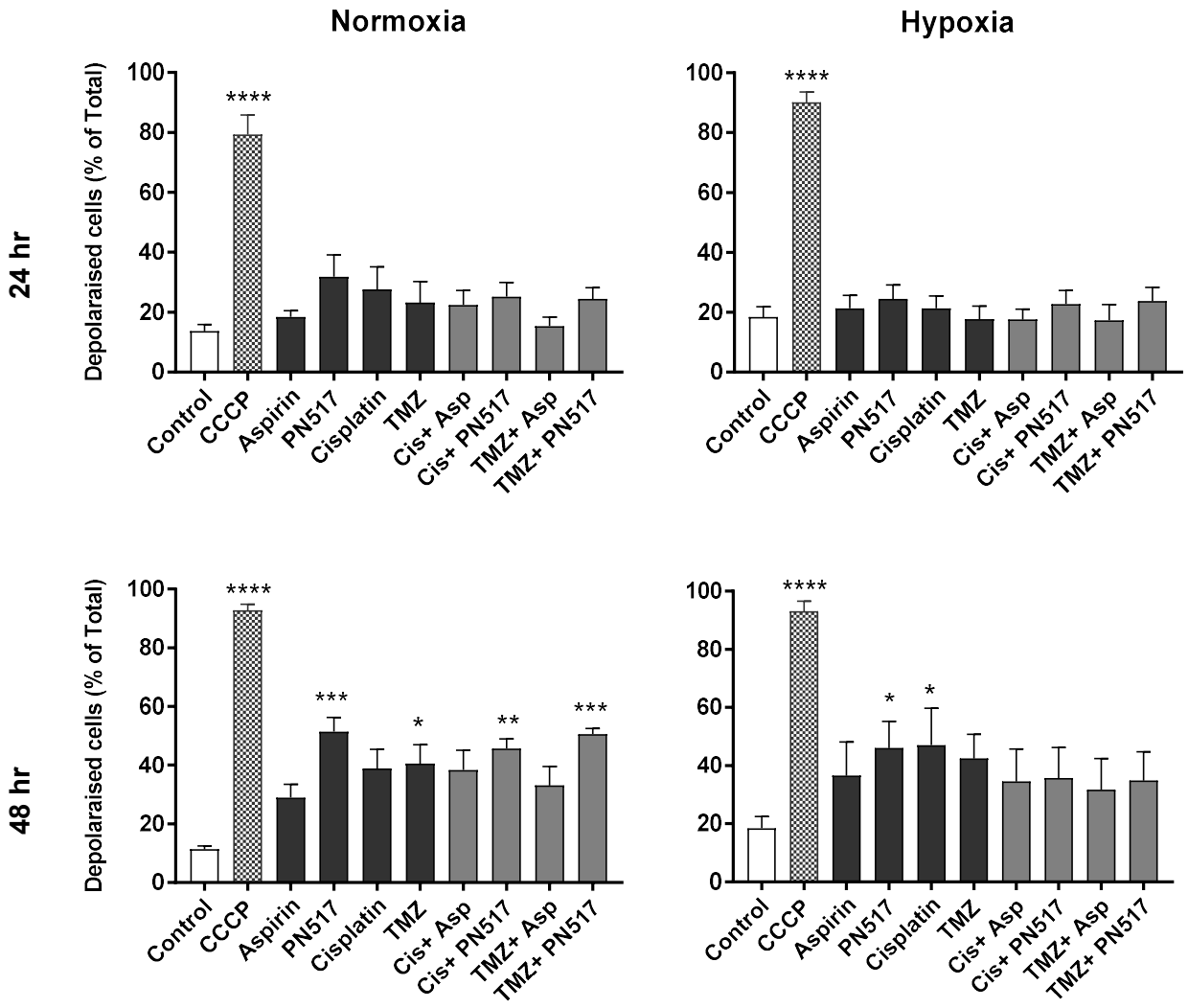

Figure 4. 11. The effect of drug treatment on the mitochondrial membrane potential in the U87-MG cell line under normoxia and hypoxia. Data shows the relative proportions of depolarised cells following 24 and 48 hr of drug treatment using JC-1 staining indicated by shifting from red to green fluorescence. Values represent mean ±SEM of four independent experiments. A two-way ANOVA was used to identify significant effects, with Tukey's multiple comparison test, *P < 0.05; **P < 0.01; ***P < 0.001; ****P < 0.0001. The experimental procedure was performed as described in Materials and Methods section 2.2.11.

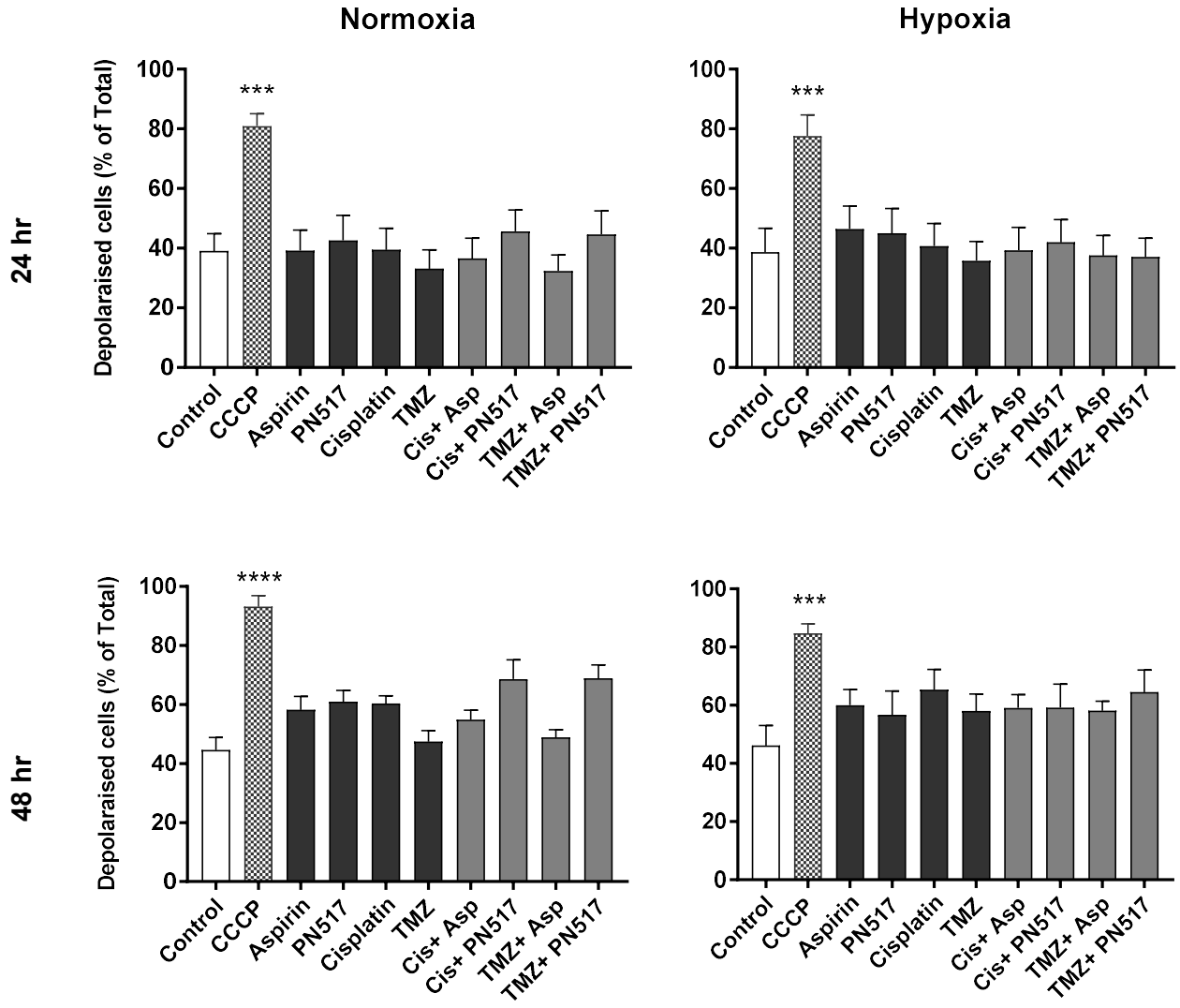

Figure 4. 12. The effect of drug treatment on the mitochondrial membrane potential in the SVG-p12 cell line under normoxia or hypoxia. Data shows the relative proportions of depolarised cells following 24 and 48 hr of drug treatment using JC-1 staining indicated by shifting from red to green fluorescence. Values represent mean ±SEM of four independent experiments. A two-way ANOVA was used to identify significant effects, with Tukey's multiple comparison test, *P < 0.05; **P < 0.01; ***P < 0.001; ****P < 0.0001. The experimental procedure was performed as described in Materials and Methods section 2.2.11.

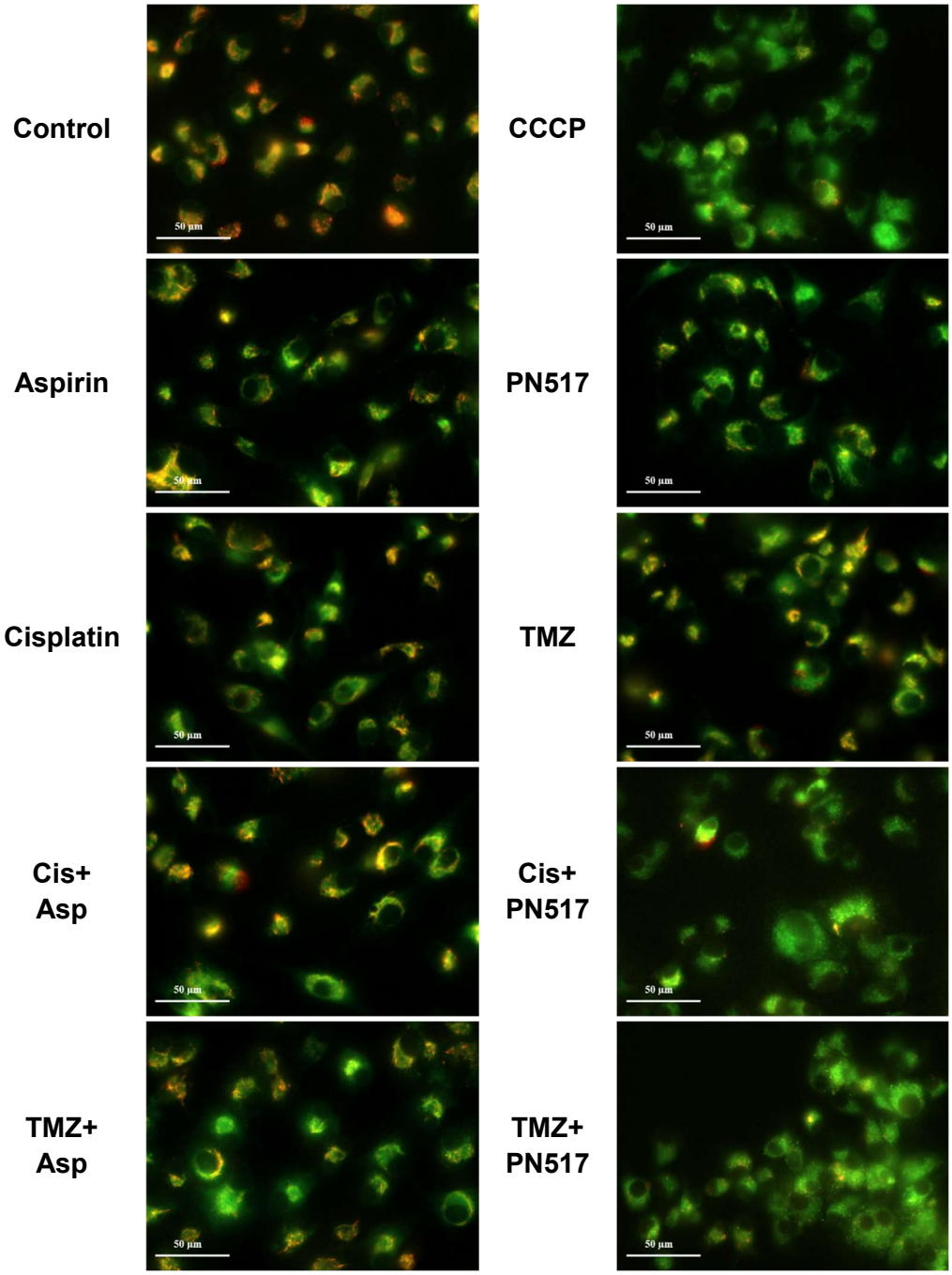

Figure 4. 13. Representative fluorescence microscopy images illustrating the effect of drug treatment on mitochondrial membrane potential in U87-MG cells under normoxia. Cells were stained with JC-1 and 7-AAD dyes after 48 hr of drug treatment. An intact mitochondrial membrane potential resulted in JC-1 aggregation in the mitochondria as illustrated by the red/orange fluorescent signal, while a depolarised membrane potential leads to JC-1 monomer release into the cytosol illustrated by green fluorescent signal (Scale bar: 50 µm). The experimental procedure was performed as described in Materials and Methods section 2.2.11.

Stress and apoptosis proteins levels assessment:

Following the effects observed in apoptosis, autophagy and mitopotential assays, and the effect of drug treatment on the activation of proteins playing essential roles in cellular response to stress and in cell death pathways was investigated. Hsp27 and c-Jun proteins play an important role in stress-induced apoptosis and autophagy processes, hence, the effect drug treatment on Hsp27 and c-Jun activation was examined after 24 hour of drug treatment in the U87-MG cell line at the same drug concentrations used for cell proliferation and cell cycle analysis (IC_{25}) under normoxia and hypoxia. Effects on proteins phosphorylation were determined using specific antibodies for Phospho-Hsp27 (Ser82) and Phospho-c-Jun(Ser73) using immunoblotting and quantified as a fold change of the untreated cells by densitometry. The housekeeping β-actin protein was used for normalisation of all samples to correct any loading differences between lanes. The experimental conditions applied can be found in the appendix (Table 9.2).

All treatments appeared to increase Hsp27 phosphorylation, particularly under hypoxia (Fig 4.14). The effect of PN517 treatment appeared to increase Hsp27 phosphorylation more than aspirin, with the largest effect in Hsp27 activation among monotherapies being by cisplatin. However, there were no significant differences compared to control for all treatments ($p>0.05$).

With respect to c-Jun phosphorylation levels, only cisplatin and TMZ showed a trend toward an increase in the phosphorylation of c-Jun under normoxia. PN517 treatment appeared to result in greater levels of phosphorylated protein than aspirin. Overall lower levels of phosphorylated protein were observed under hypoxia compared to normoxia. However, no significant effect was observed following any of the drug treatments under both conditions ($p<0.05$) (Fig 4.15).

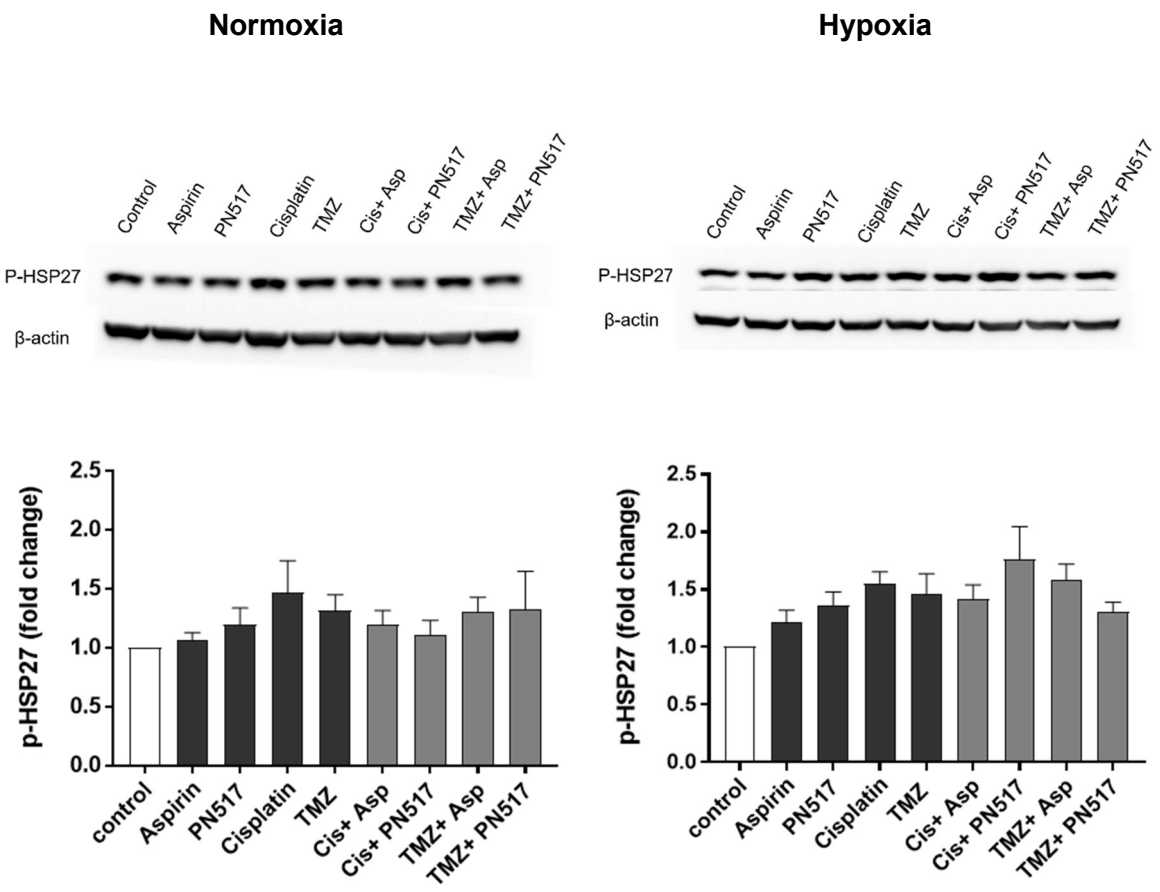

Figure 4. 14. Representative immunoblots and densitometric analysis of phosphorylation levels of Hsp27 protein in the U87-MG cell line under normoxia and hypoxia. Data indicate the fold change in phospho-Hsp27 levels following 24 hr of drug treatment compared to control as determined by densitometry. Values represent mean ±SEM of six independent experiments. A two-way ANOVA was used to identify significant effects, with Tukey's multiple comparison test, *P < 0.05; **P < 0.01; ***P < 0.001; ****P < 0.0001. The experimental procedure was performed as described in Materials and Methods section 2.2.16.

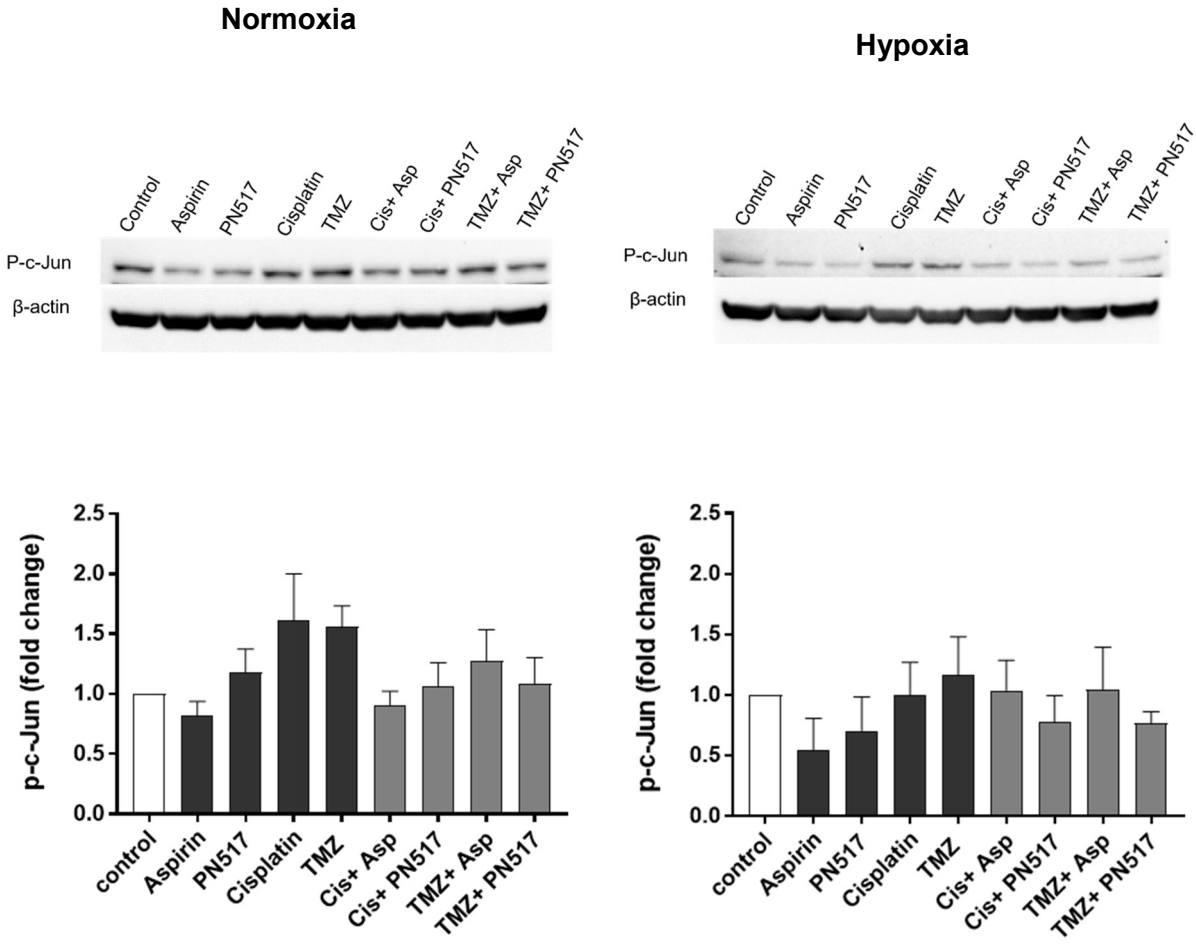

Figure 4. 15. Representative immunoblots and densitometric analysis of phosphorylation levels of c-Jun protein in the U87-MG cell line under normoxia and hypoxia. Data indicate the fold change in phospho-c-Jun levels following 24 hr of drug treatment compared to control as determined by densitometry. Values represent mean ±SEM of six independent experiments. A two-way ANOVA was used to identify significant effects, with Tukey's multiple comparison test, *P < 0.05; **P < 0.01; ***P < 0.001; ****P < 0.0001. The experimental procedure was performed as described in Materials and Methods section 2.2.16.

4.3. Discussion

Aspirin and its analogue PN517 have been found to reduce cell viability and proliferation in both cell lines tested, however the pattern of results from these assays and cell cycle analysis did not correlate directly suggesting a role for other mechanisms in the cytotoxic effect. Another factor can affect cell viability in addition to cell proliferation is cell death that can occur through different mechanisms. There are conflicting results in the literature as to which pathway is most important for induction of cell death by NSAIDs in glioma (Thoms *et al.*, 2007). Thus, the ability of the drug treatment to induce cell death was evaluated and the mode of cell death was investigated to include apoptosis, autophagy and necrosis.

4.3.1. Apoptosis

Apoptosis occurs via different pathways, often with more than one triggered simultaneously (Leist and Jäättelä, 2001; Nikoletopoulou *et al.*, 2013). As mentioned in Chapter 1, multiple alterations in gene expression, including amplification or deletion, take place in GBM. These alteration in genes such as *EGFR*, *MTOR* and *VEGF* result in changes in cell growth and cell death enabling glioma cells to evade apoptotic signals induced by the cytotoxic drugs and confer chemoresistance (Normanno *et al.*, 2006; Kanu *et al.*, 2009; Minniti *et al.*, 2009). Therefore, it has been well recognised that apoptosis resistance is a major regulator of glioblastoma survival and progression, and targeting apoptosis resistance would lead to better treatment efficacy and increase patients' survival (Krakstad and Chekenya, 2010). Accordingly, the failure of many chemotherapeutic drugs has been attributed to the inability of these drugs to induce apoptosis (Kerr *et al.*, 1972; Shah and Schwartz, 2001; Elmore, 2007; Vanlangenakker *et al.*, 2008; Fulda *et al.*, 2010). Hence, it was vital to assess the effects of drug treatment on apoptosis induction in U87-MG cells.

A vital reported mechanism for the anti-tumour activity of aspirin and other NSAIDs is the induction of apoptosis. Aspirin has been shown to induce apoptosis in several cancer cell lines such as colorectal adenoma and carcinoma cells (Elder *et al.*, 1996), mouse Neuro 2a cells (Dikshit *et al.*, 2006), oesophageal

squamous carcinoma cells (Li *et al.*, 2009), human hepatoma cells (Raza *et al.*, 2011) and myeloma cell lines (Ding *et al.*, 2014). COX-2 selective inhibitors have also been shown to have similar activity, such as NS-398 (Liu *et al.*, 1999; Elder *et al.*, 2000), ninesulide (Li *et al.*, 2009) and SC326 (Doherty *et al.*, 2009). More importantly, in glioblastoma cells, an enhancement of apoptosis has been demonstrated following exposure to aspirin, indomethacin and ibuprofen in T98G cells (Amin *et al.*, 2003; Gomes and Colquhoun, 2012) and with using COX-2 selective inhibitors in U87-MG cells (Kang *et al.*, 2009).

The results examining the induction of apoptosis in this chapter demonstrate that short-term treatment with aspirin can enhance apoptosis in a glioblastoma cell line with the analogue PN517 being more efficacious than aspirin (Fig 4.3). These findings confirm results found in other studies where it was demonstrated that diaspirins (including PN517) induce apoptosis in colorectal cancer cells to a greater extent than aspirin and that apoptotic effects appear at a lower concentration than for aspirin (Deb *et al.*, 2011; Claudius *et al.*, 2014). Remarkably, the current apoptosis data at early timepoints (24 and 48 hr) showed that PN517 was the most efficacious treatment particularly in U87-MG cells, while that was not the case in SVG-p12 cells suggesting some level of selectivity for the glioblastoma cell line over the non-cancerous cell line (Fig 4.4).

This study found that aspirin and PN517 resulted in larger percentages of early and late apoptotic cells following drug treatment in both cell lines with only a small necrotic cell population, which would suggest that these drugs reduce cell viability via induction of cell death occurred mainly by apoptosis induction (Fig 4.3). Using an *in vitro* luciferase assay, a previous study in the lab found that both aspirin and PN517 activated caspase 8 and caspase 9 in a time and concentration dependent manner in the U87-MG cells, suggesting the involvement of both extrinsic and intrinsic apoptosis pathways (unpublished data). It was observed also that both PN517 and aspirin showed a similar efficacy in the activation of caspase 9, but aspirin produced a greater activation of caspase 8, with the lowest activation in both enzymes observed following cisplatin treatment at early timepoints. These findings were supported by western blotting (unpublished data).

These findings are consistent with the literature where aspirin induction of apoptosis has been described to be mediated by several mechanisms. As stated earlier, the increased PG levels caused by COX-2 have been linked to increased proliferation, and decreased apoptosis (Kökoğlu *et al.*, 1998; Zimmermann *et al.*, 1999). Hence, aspirin and other NSAIDs can enhance apoptosis by COX-dependent mechanisms. This was supported by several studies where the concentration of aspirin and nimesulide required to inhibit PGE2 production correlated with the inhibition of proliferation and induction of apoptosis (Li *et al.,* 2009). Therefore, one possible explanation for inducing apoptosis by aspirin and its analogue can be due to their anti-inflammatory mechanism by inhibiting COX-2 expression thus reducing PG levels.

However, other reports failed to find a correlation between COX-2 expression and NSAID-induced apoptosis (Molina *et al.*, 1999; Elder *et al.*, 2000). Concerning aspirin, a significant decrease in cell growth and induction of apoptosis by COX-independent mechanisms was found in HCT116 and SW480 human colon cancer cell lines after aspirin treatment (Goel *et al.*, 2003). In line with that, different studies showed that aspirin can induce apoptosis by affecting several pathways including through downregulation of the anti-apoptotic protein Bcl-2, upregulation of the pro-apoptotic protein Bax, activation of caspase 8, caspase 9 and caspase 3, release of cytochrome c, inhibition of ATP synthesis and downregulation of VEGF (Dikshit *et al.*, 2006; Raza *et al.*, 2011; Gomes and Colquhoun, 2012; Ding *et al.*, 2014). Thus, it would be interesting to investigate these effectors to confirm their involvement in aspirin/PN517-induced apoptosis.

Another important pathway that has been emerged as a significant cause of glioma initiation and progression is the canonical Wnt/β-catenin signalling pathway. In addition, studies have linked PGE2 to tumour growth by activating β-catenin (Castellone *et al.*, 2005). Aspirin has been shown to exert antineoplastic action by inhibition of the β catenin/TCF signalling pathway and enhancing apoptosis in glioma cells (Lan *et al.*, 2011) and colorectal cancer (Hawcroft *et al.*, 2002; Dihlmann *et al.*, 2003). Studies also have indicated that aspirin may induce apoptosis in GBM cell lines by down-regulating STAT3 signalling and reduce the expression of different target genes contributing in glioblastoma survival (Kim *et*

al., 2009). It was found that aspirin inhibits the phosphorylation and activation of STAT3 by reducing the expression and secretion of interleukin-6. These findings were of high importance in glioblastoma since interleukins such as IL-6 are frequently expressed in human glioma cells (Sasaki *et al.*, 2001). That would also suggest another possible explanation for aspirin/PN517-induced apoptosis in U87-MG cells but needs further investigation.

Additionally, the upregulation of NF-κB pathway has been implicated in apoptosis reduction in many cancer types including brain tumours (Nogueira *et al.*, 2011). NF-κB activity is higher with increasing grade of astrocytic tumours, hence GBM shows particularly high activity for this pathway (Angileri *et al.*, 2008; Korkolopoulou *et al.*, 2008). Inhibition of NF-κB activation has been demonstrated to reduce brain tumour growth, invasion and angiogenesis (Xie *et al.*, 2008). Aspirin is known to inhibit the NF-κB pathway by inhibiting IκB-kinase β activity (IKKβ) (Yin *et al.*, 1998). Treating the SW480 colorectal cancer cell line with aspirin and diaspirins results in stimulation of the NF-κB pathway associated with a significant reduction in basal levels of NF-κB transcriptional activity (Claudius *et al.*, 2014). However, it was reported that the diaspirin analogues (including PN517) did not induce nucleolar translocation of RelA in contrast to aspirin, suggesting different mechanisms underlying the repression of NF-κB transcription, hence, the authors suggested structure-activity relationships important for the pro-apoptotic response to aspirin (Claudius *et al.*, 2014). These findings would also support the current findings of this study where differences in the efficacy between aspirin and PN517 were observed. More recent review article has indicated that although there is a consensus in the literature that NSAIDs induce repression of NF-κB -driven transcription, the pathway to this repression appears to be cell type and context dependent (Chen and Stark, 2017). Therefore, the induction of apoptosis by aspirin and PN517 observed in this study needs to be further investigated in order to examine the contribution of NF-κB pathway and confirm any difference in the effect between the two compounds.

Regarding cisplatin, results obtained from apoptosis assay showed that prolonged exposure of cells to cisplatin leads mainly to apoptotic cell death,

however a small proportion of cells may undergo necrosis (Fig 4.3). Although cisplatin can induce structural changes in cells, it primarily works *via* DNA intercalation causing anomalies in cell replication and transient cell cycle arrest in the early S phase leading to a final G2/M phase arrest and eventually to apoptosis (Qin and Ng, 2002; Wang and Lippard, 2005; Florea and Busselberg, 2011). Previously, studies showed that apoptosis induced by cisplatin is triggered by JNK/c-Jun mediated induction of FasL, dose-dependently, which also associated with activation of caspase-8 along with caspase-9 and -3 in sensitive cells (Brozovic *et al.*, 2004; Christmann *et al.*, 2007). These results can explain a trend towards increasing phospho-c-Jun levels observed by western blotting following treatment with cisplatin (Fig 4.15).

Both extrinsic and intrinsic pathways of apoptosis were reported to be involved in cisplatin-induced cell death. However, the predominant apoptosis occurs via the mitochondrial signalling pathway through activated caspase-3. Cisplatin has been shown to induce mitochondrial membrane permeabilization and the release of the mitochondrial inter-membrane proapoptotic molecules (Cummings and Schnellmann, 2002; Jiang *et al.*, 2004; Florea and Busselberg, 2011). That was supported by the results obtained from the mitopotential assay where an increase in the depolarisation of the mitochondrial membrane was observed and can serve as an indicator for early stage of apoptosis (Fig 4.11).

Due to the mechanism of action of cisplatin and in accordance to previous studies, the number of apoptotic cells increased in a time dependent manner (Fig 4.3). Additionally, cisplatin's effect was also suggested to be concentration dependent where it seemed to show an early effect on cell death only at higher concentrations, such as 100μM. Moreover, the mode of cell death has been related to drug concentration, with necrosis occurring with high concentrations and apoptosis with lower concentrations (Sancho-Martínez *et al.*, 2011).

Since cisplatin selectively affects cells which turn over rapidly, cell death will occur at a faster rate in those cell populations than in other cells with a slower proliferation rate. That was supported with previous findings in the lab where fast growing glioma cell lines (like 1321N1 and GOS-3) showed reduced viability and

higher cell death in the first 24 hours following treatment with cisplatin compared to the slower proliferating cell lines SVG-p12 and U87-MG which responded more slowly to cisplatin treatment (unpublished data). That could provide an explanation for the increased but insignificant apoptosis induction observed in this study with cisplatin treatment. Moreover, it can be noted that cisplatin is not selective for U87-MG cells and exerts its effects on non-cancerous SVG-p12 cells too where higher proportions of apoptotic and necrotic cells were found compared to U87-MG cell line, which encourages the need for the investigation of drugs that are selective to cancerous cells (Fig 4.4).

With respect to TMZ, apoptosis was induced after 72 hours, however, it was not found to be significant as monotherapy in U87-MG cells (Fig 4.3). This is linked to its mechanism of action which is dependent on its ability to add methyl groups to the purine bases of DNA in malignant cells. This methylation causes lesions at the N^7 or O^6 position of guanine residues, damaging the DNA and triggering a cascade of processes resulting in apoptosis of the GBM cell. Hence, as the cells proliferate, an additive cytotoxic effect is seen (Patel *et al.*, 2014). Studies have verified that TMZ-triggered apoptosis in gliomas is a late response (occurring after at least 120 hr of drug treatment) which requires extensive cell proliferation (Tomicic *et al.*, 2015). Additionally, the repair of O^6-methylguanine lesion by MGMT prevents apoptosis (Roos *et al.*, 2007), as described previously in section 1.5.2. These results support the timescale of efficacy observed by the results of this study where TMZ showed a trend towards inducing apoptosis that increased with longer incubation but was not significant over 72 hr of drug treatment (Fig 4.3).

Apoptosis triggered following TMZ methylation is demonstrated to be greatly stimulated by p53, with an observation that p53 wild-type expressing glioma cell lines (e.g. U87-MG) are more sensitive than p53 mutant cell lines (e.g. U138-MG). However, both p53 wild-type and mutant glioma cells were able to undergo apoptosis in response to the O^6-methylguanine lesion concluding that p53 is not thoroughly required to induce cell death (Roos *et al.*, 2007). In p53 wild-type glioma cells, apoptosis is induced by Fas/CD95/Apo-1 receptor over expression and activation of Fas-dependent apoptotic pathway including caspase-8. This

upregulation of Fas was explained by the fact of p53 being a transcriptional activator of Fas (Pohl *et al.*, 1999). On the other hand, in p53 mutated glioma cells, the same DNA lesion did not induce Fas and caspase-8 activation whereas it triggered the intrinsic mitochondrial apoptotic pathway less effectively. This pathway occurs by Bcl-2 degradation and caspase-9 and -3 activations, but the potency of TMZ to trigger the mitopotential pathway was clearly lower than the death receptor pathway (Roos *et al.*, 2007). Nevertheless, there are also opposite reports showing a protective function of p53 in glioma cells exposed to TMZ indicating cell type-specific effects (Hirose *et al.*, 2001; Xu *et al.*, 2005). Another report identified JNK/c-Jun activation as a late pro-apoptotic response of U87-MG cells treated with TMZ as a result of AP-1 triggering induction of the proapoptotic protein BIM. BIM induces apoptosis by causing mitochondrial permeabilization and the release of apoptogenic factors activating caspases including caspase-9. These findings may explain the increases in depolarised cells observed in the mitopotential assay and the higher levels of activated c-Jun observed in this study (Fig 4.15).

Interestingly though, a contradictory report has shown that inhibition of JNK enhances the TMZ-induced cytotoxicity in U87-MG cells and this increased sensitivity associated with enhanced senescence (Ohba *et al.*, 2009), concluding that JNK produces different events depending on the time scale of drug exposure (Tomicic *et al.*, 2015). Furthermore, it was proposed that O^6-methylguanine-induced apoptosis in glioma cells was preceded by secondary lesions that cause replication interference in the subsequent DNA replication cycle leading ultimately to the formation of DNA double-strand breaks (DSBs) (Ochs and Kaina, 2000). Taken together, it was demonstrated that cell death induced by TMZ in gliomas is due to apoptosis with several factors determining the sensitivity of gliomas to TMZ including MGMT, p53, proliferation rate and DSB repair (Roos *et al.*, 2007).

While examining the effect of drug combinations on the induction of apoptosis, it was observed that aspirin combinations did not significantly increase apoptosis compared to the respective monotherapy. In contrast, PN517 combinations, particularly the combination of PN517 with TMZ, produced a significant

enhancement in apoptosis levels when compared to TMZ or PN517 alone, an effect maintained over 72 hours although less obvious under hypoxia (Fig 4.3). This supports the synergistic effect observed for this combination in the viability assay and could suggest that while a mono-therapy would require daily dosing to maintain efficacy, a combination treatment might have a greater treatment interval. Combined with lower doses of each individual drug in combination, this decreased treatment frequency might improve the side effect profile of the chemotherapy and may also reduce the rate at which resistance to TMZ develops.

A hypoxic environment is well known to inhibit apoptosis caused by drug treatments leading to chemotherapy resistance through the effect on non-apoptotic pathways and to protect the cells from the drug-induced senescence through a mechanism mediated, mainly by HIF-1α dependent up-regulation of hypoxia response element – containing genes (Sullivan *et al.*, 2008). For example, a reduction in the activity of p53 under hypoxia causes inhibition of cell apoptosis, and cells are more likely to undergo DNA repair following DNA injuries in hypoxia whereas these injuries were shown to be greater and longer lasting in cells under normoxia environment (Brown and William, 2004). Hypoxia also reduces cell-senescence following treatment with chemotherapeutic drugs (Sullivan *et al.*, 2008). These observations correlate well with the western blotting results showing lower levels of p-c-Jun and higher levels of p-Hsp27 meaning less apoptosis is induced by drug treatment under hypoxia. As already mentioned, as most anticancer drugs are more effective against rapidly proliferating cells, their cytotoxic effect may be reduced under hypoxia due to the slower growth of cells. This effect was observed with TMZ treatment where a smaller apoptotic population was found under hypoxia even after prolonged treatment with TMZ compared to the control, an effect that was also replicated in its combination treatments. Additionally, HIF-1α expression reduces the mitochondrial activity of the cell, initiates mitophagy and supresses mitochondrial biogenesis. This leads to reduced cell death and increased drug resistance under hypoxia (Kim *et al.*, 2006; Zhang *et al.*, 2007), providing a potential explanation for the reduced effect of TMZ under hypoxia.

There are few caveats concerning the validity of the apoptosis quantification results using flow cytometry. Firstly, it has been reported that some cell types may be damaged due to trypsinisation to suspend adherent cells prior to analysis using a flow cytometer. As a result, cells would be take up PI resulting in false PI staining results for necrotic/dead cells (Van Engeland *et al.*, 1996). Nearly all manufacturers of apoptosis kits have made use of cells in suspension as sample cells for quantitative analysis of their products. Although they suggested different methods for trypsinising and harvesting cell monolayers, all these methods result in damage of the cell membrane (Van Engeland *et al.*, 1996). This finding might provide an explanation for the overall higher levels of apoptosis found in the SVG-p12 cells as they needed a longer period of trypsinisation to detach them from the surface of the culturing plates compared to U87-MG cells.

Secondly, apoptotic cells can also display plasma membrane rupture consistent with necrosis via a process called apoptotic necrosis (Fink and Cookson, 2005). This secondary necrosis occurs when apoptotic bodies have been formed in the absence of phagocytosis, which can lead to the bodies breaking. It is therefore difficult to determine how a necrotic cell truly died. Additionally, an issue has been raised about the cell population appearing in the upper-right quadrant positive for PI staining, either as late apoptotic, necrotic or dead cells. This means the technique is unable to define the mechanism of cell death once the cells reach the upper right quadrant and data analysis is unable to differentiate accurately between the various cell populations since that cell membrane has similar permeability. This is particularly challenging as different analysis methods are followed in the literature by individual studies (Rieger *et al.*, 2010). This can suggest that the late apoptotic cell population acquired during this study could include necrotic or apoptotic cells. If that was the case, the data obtained from SVG-p12 cells could suggest that the larger effect by the drug treatment was due to necrosis or necroptosis (Fig 4.4).

4.3.2. Autophagy

The autophagy process plays a variety of roles in cells, including removal of damaged organelles, regulation of metabolism, cellular survival and as a method of programmed cell death, and can be triggered in response to cellular stress and

rises in cellular metabolic demands (Parzych and Klionsky, 2014). Therefore, triggering autophagy, as an alternative method of cell destruction, is a possible mechanism by which anticancer therapies can induce cell death and has been identified as a potential therapeutic target in GBM (Palumbo *et al.*, 2012). For example, malignant glioma cells can be radiosensitised by inducing autophagy (Daido *et al.*, 2005). In line with this, it was found that curcumin suppresses the growth of malignant gliomas *in vitro* and *in vivo* through induction of autophagy (Aoki *et al.*, 2007). Also, metformin can induce autophagy in different cancer cells such as colon cancer, hepatocellular carcinoma, and lymphoma, leading to a reduction in cell growth (Buzzai *et al.*, 2007; Lindqvist *et al.*, 2018). In contrast, autophagy has been described as a cytoprotective process in established tumours. It has been found to be upregulated in human gliomas as compared to normal brain, and many studies have suggested that glioma cells are relatively susceptible to autophagy induction, whereas they appear resistant to apoptosis (Jennewein *et al.*, 2016). *Ex vivo* analyses of human GBM tissue specimens revealed that survival was significantly higher in patients with low levels of autophagy than in those with high levels of autophagy. This could confirm the hypothesized role for the cytoprotection mechanism exerted by the autophagic flux which can represent an important survival strategy of GBM cancer cells (Yang *et al.*, 2011).

Autophagy is enhanced in GBM after treatment with standard cancer therapeutics as an effective pathway to eliminate the presence of damaged DNA, cellular proteins, and organelles, thus enhancing cell survival and resistance to therapy (Jawhari *et al.*, 2016). Recent literature shows extensive investigation of autophagy inhibition in combination with glioblastoma standard and novel therapies (Ma *et al.*, 2017; Buccarelli *et al.*, 2018; Lohitesh *et al.*, 2018). For example, autophagy inhibition was shown to sensitise malignant glioma cells to radiation (Ito *et al.*, 2005).

Autophagy inhibition has also been shown to sensitise GBM cells to novel compounds under investigation in GBM treatment. For example, the EGFR inhibitor Erlotinib, in combination with autophagy inhibition increased cellular death compared to either agent alone in GBM (Eimer *et al.*, 2011). In addition,

the cytotoxicity of imatinib, another tyrosine kinase inhibitor, was enhanced against human GBM cells combined with late stage (maturation) autophagy inhibition (Shingu *et al.*, 2009). Accordingly, PI3K/mTOR inhibition with NVP-BEZ235 combined with autophagy maturation inhibition induced greater GBM cell death than either agent alone *in vitro* and *in vivo*. This evidence suggests, within GBM, late stage (maturation) autophagy inhibition may prove to be a promising therapeutic approach (Fan *et al.*, 2010).

However, autophagy cytoprotection is pharmacologic/stress specific and excessive autophagy has been implicated in autophagic cell death. This highlights the importance of autophagy investigation in different tumours and with different therapies, as they do not all produce the same autophagic effects (Nikoletopoulou *et al.*, 2013). In the current study, the effects of drug treatment on autophagy regulation was investigated by flowcytometry in addition to looking at different autophagic proteins. PI3K Class III forms different protein complexes, which are organized in a different and multi-layered manner to initiate autophagy. PIK3R4 regulates the kinase activity of PI3K class III and the PIK3R4/PI3K class III complex interacts with beclin-1 to play a role during several stages of autophagy (Zhong *et al.*, 2009). Atg14 is combined with PIK3R4, PI3K class III, and beclin-1 (ATG14-containing PI3K complex) inducing autophagy by stimulating autophagosome formation. Likewise, the UVRAG (ultraviolet radiation resistance-associated gene) protein competes with Atg14 for beclin-1 binding, forming a mutually exclusive complex with PIK3R4, PI3K class III, and beclin-1 that regulates autophagosome maturation (UVRAG-containing PI3K complex) (Sun *et al.*, 2008). Aspirin was found to increase the autophagic activity in U87-MG cells and more significantly, also the combinations of aspirin with cisplatin or TMZ (Fig 4.5). Interestingly, aspirin was more effective at inducing autophagy than its analogue PN517, an observation supported by western blotting analysis for autophagic regulatory proteins (PI3K Class III, PIK3R4 and Atg14) (Fig 4.8-4.10). These findings suggest the presence of different mechanisms of action for aspirin and PN517 in agreement with previous observations (Claudius et al., 2014; Bashir et al., 2019).

Different NSAIDs have been found to induce autophagy via different signalling pathways and the anti-tumour effects of NSAIDs can be considered to be related to their autophagy-modulating effects: either activation or inhibition of autophagy (Yu *et al.*, 2018). Aspirin has been shown to inhibit mTOR signalling, activate AMP-activated protein kinase, and induce protective autophagy in colorectal cancer cells (Din *et al.*, 2012). Recently, another study has demonstrated that salicylate induces autophagy via the inhibition of the acetyltransferase EP300 rather than AMPK activation and that aspirin may mediate antiaging, antineoplastic and pro-health effects or anticancer and anti-cardiovascular disease effects via the induction of autophagy (Castoldi *et al.*, 2018). Another recent report showed that aspirin induces autophagy in human hepatocellular carcinoma cells (HCC) dependent on Beclin-1 expression, suggesting a chemoprotective and inhibitory effect of aspirin on HCC development (Huang *et al.*, 2018). However, aspirin combined with ABT-737 (a small-molecule Bcl-2/Bcl-xL antagonist) induced protective autophagy at early timepoints (12 hr) in different human cancer cell lines, which changed into apoptosis at later timepoints (48 hr). It was demonstrated that p38 acted as a switch from a cytoprotective signal to a death-promoting signal (Zhang *et al.*, 2015). Consequently, it is important to determine the fate of tumour cells treated with NSAIDs. The indistinct effect of autophagy in cancer may depend on the type of tumour, stage of tumorigenesis, tumour microenvironment, as well as genetic and epigenetic factors. Furthermore, the dose and duration of administration can be additional factors that alter the sensitisation effects of NSAIDs (Chen and Stark, 2017). Hence, the results obtained in this study with aspirin and PN517 in terms of cell death and survival have been interpreted with caution until tested *in vivo*.

Consistent with previous reports, TMZ was found to up-regulate autophagy in GBM (Kanzawa *et al.*, 2004; Ohba *et al.*, 2009; Knizhnik *et al.*, 2013) (Fig 4.5). This was again supported by western blotting where a trend towards activation of the PI3K Class III, PIK3R4 and especially Atg14 was observed (Fig 4.8-4.10). Kanzawa and colleagues demonstrated that TMZ induces autophagy, but not apoptosis, at early stages in different malignant glioma cell lines and that TMZ-induced autophagy might provide a mechanism of self-defence for cancer cells (Kanzawa *et al.*, 2004). The authors found that autophagy inhibition at different

stages has different outcomes on TMZ-induced autophagy. Autophagy inhibition at the initiation stage with a PI3K class III inhibitor, which inhibits microtubule-associated protein light chain 3 (LC3) localisation, suppresses the anti-tumour effect of TMZ. Yet, autophagy inhibition at the maturation stage using with an inhibitor of vacuole type H^+-ATPase, where LC3 localisation is not suppressed, sensitized cells to TMZ and stimulated apoptosis via activation of caspase -3 (Kanzawa *et al.*, 2004). It has been suggested that glioma cells undergo autophagy, senescence and apoptosis in a specific time-dependent manner after TMZ treatment (Knizhnik *et al.*, 2013). In this case, autophagy, which is the earliest event upon TMZ treatment, stimulates cells to undergo senescence rather than apoptosis. Furthermore, inhibition of autophagy and thereby senescence leads to an increase in apoptosis upon TMZ treatment, explaining why inhibition of JNK at the same time can enhance senescence and reduce apoptosis (Ohba *et al.*, 2009).

JNKs have been shown to play a role in apoptosis as well as non-apoptotic programmed cell death mechanisms including those of necroptosis, ferroptosis, pyroptosis, and autophagy. It works by stimulating or inhibiting cell death in a context-dependent manner by altering the expression of specific genes and modulating the activities of pro- and anti-apoptotic proteins through distinct phosphorylation events (Dhanasekaran and Reddy, 2017). A very recent report confirmed that JNK signalling can trigger both autophagy and apoptosis in glioma cells and demonstrated that autophagy and apoptosis may inhibit each other (Liu *et al.*, 2019). Additionally, c-Jun, a member of the Jun family, can be upregulated in response to stress. The transcriptional activity of c-Jun is regulated by phosphorylation at Ser63 and Ser73 through SAPK/JNK (Stress-activated protein kinase/c-Jun NH2-terminal kinase) (Davis, 2000). SAPK/JNK pathway have been considered to involve in many cellular processes including proliferation, apoptosis, motility, metabolism and DNA repair (Johnson and Nakamura, 2007). That finding supports the results of this study where markedly higher autophagy and less apoptosis was observed after TMZ treatment at 24 hr, with a parallel increase in p-c-Jun levels found by western blotting that could be related to either stimulating autophagy or inducing apoptosis (Fig 4.15). It could be more likely inducing autophagy and inhibiting apoptosis since that PN517 reduced the p-c-

Jun levels but increased the efficacy for TMZ when combined together in cell viability assay.

On the other hand, Shen and colleagues showed that TMZ can induce cell autophagy, thereby suppressing the development of glioblastomas (Shen *et al.*, 2016). Therefore, it was also suggested that amplifying autophagy can sensitise the cells to TMZ and induce cell death. For example, rapamycin, an mTORC1 inhibitor, and therefore an autophagy inducer, has also been shown to sensitise GBM cells to TMZ (Palumbo *et al.*, 2012). In addition, exposure of human U87-MG glioma cells to honokiol caused cell death and significantly enhanced TMZ-induced insults by inducing autophagy and consequent apoptosis. Pre-treatment with 3-methyladenine (3-MA) and CLQ caused significant attenuations in the combination- induced cell autophagy and apoptosis in human glioma cells. Honokiol may boost the TMZ-induced autophagy of malignant glioma (Chio *et al.*, 2018). These finding can provide an explanation for the enhanced efficacy of TMZ when combined with aspirin. As aspirin produced an induction of autophagy this may boost the TMZ-induced apoptosis in U87-MG cells (Fig 4.5).

In contrast to TMZ, cisplatin results from the autophagy assay indicated autophagy induction following drug treatment but to lesser extent than TMZ (Fig 4.5). This effect was generally consistent with the immunoblotting analysis for regulatory proteins constituting the PI3K complex, responsible for initiation of the autophagic process. Similarly, it was previously reported that the endoplasmic reticulum (ER) stress produced by cisplatin may induce cell autophagy, cell apoptosis and the complicated regulatory network between them. Also, the inhibition of autophagy was shown to increase cisplatin-induced apoptosis by increasing endoplasmic reticulum stress in U251 human glioma cells (Zhang *et al.*, 2015). Inhibition of cisplatin-induced autophagy was found to block the formation of autophagosomes and enhanced cisplatin-induced caspase-3, -6 and -7 activation, nuclear fragmentation and apoptosis. This provides a potential mechanism by which autophagy induction in response to cisplatin mounts an adaptive response that promotes cellular survival and suppresses and delays the onset of an apoptosis (Kaushal *et al.*, 2008). Similarly, novel therapeutic strategy like Long non-coding RNAs (lncRNAs) has been shown to decrease autophagy

induced by cisplatin and improve the chemosensitivity of U87 cells to cisplatin by enhancing apoptosis (Ma *et al.*, 2017). These findings may provide an explanation for the autophagy pattern observed following cisplatin treatment which could be induced as protective mechanism by the cells.

Another report showed that upregulation of beclin-1 (*BECN1*) was detected in cisplatin-treated cells, and knockdown of BECN1 reduced cisplatin-induced autophagy and subsequently improved cisplatin-induced apoptosis in human bladder cancer cells (Lin et al., 2017). Also, inhibition of cisplatin-induced autophagy using bafilomycin A1, CLQ, or ATG7/ATG12 shRNAs significantly enhanced cytotoxicity of cisplatin toward human bladder cancer cells. These results further indicated that cisplatin induced protective autophagy which may contribute to the development of cisplatin resistance and result in treatment failure (Lin *et al.*, 2017). Supportive results were observed in breast cancer where cisplatin-induced autophagy protects breast cancer cells from apoptosis (Jiang *et al.*, 2017) and in human lung cancer cells where inhibition of autophagy promotes cisplatin-induced apoptotic cell death through the inhibition of Atg5 and Beclin-1 (Chen *et al.*, 2018). However, a contradictory study showed that scutellarin, an active flavone, promotes cisplatin-induced cytotoxic autophagy via c-MET/AKT signalling pathway sensitizing cells to cisplatin in non-small cell lung cancer (Sun *et al.*, 2018). These findings indicate the important role which autophagy might play in the cells treated with cisplatin and how autophagy modulation can alter the overall response of the cells.

Cisplatin activates several signal transduction pathways mediated by ROS, DNA damage, p53, TNFα, mitogen-activated protein kinases (ERK, JNK, p38) and cell cycle inhibitors. It has been demonstrated that one or more of these pathways may participate in the induction of autophagy as well as in apoptosis, such as JNK/c-Jun pathway (Kaushal *et al.*, 2008). Accordingly, c-Jun level increases observed in the current study by western blotting analysis following the treatment with cisplatin could also be playing different roles either in apoptosis or autophagy processes (Fig 4.15).

Hsp27 is a stress-activated multifunctional chaperone. Hsp27 expression increases several-fold in response to stress in order to confer cellular resistance to the adverse environmental change. Hsp27 is phosphorylated at Ser15, Ser78, and Ser82 by MAPKAPK 2 (MAP Kinase Activated Protein Kinase 2) because of the activation of the p38 MAP kinase pathway and Hsp27 has been shown to decrease apoptotic cell death in multiple pathways (Landry *et al.*, 1992). It is highly expressed in glioblastoma and other cancers where it inhibits treatment-induced apoptosis and causes treatment resistance (Nomura *et al.*, 2007; Chen *et al.*, 2011). Hsp27 is a substrate of MAPK and PI3 K-Akt, both of which are overactive in many cancers, including GBM. The p38MAPK/Hsp27 pathway has also been suggested as an important regulator of GBM cell migration and potential target to inhibit brain invasion (Nomura *et al.*, 2007).

Hsp27 regulates components of both stress- and receptor-induced apoptotic pathways and is known to be critical for dynamic intracellular trafficking during autophagy (Kang *et al.*, 2011). The pro-autophagic role of Hsp27 might involve the ability of small heat shock proteins to deliver protein aggregates toward the autophagosome (Vos *et al.*, 2011). When considering cytoprotective autophagy, a large number of studies have demonstrated that Hsp27 possesses cytoprotective effects by inducing autophagy in different types of cancer cells (Kim *et al.*, 2005; Wong and Cuervo, 2010; Rodríguez *et al.*, 2019). Autophagy and HSPs regulate protein homeostasis and maintain important physiological functions (Wong and Cuervo, 2010). It has been suggested that the autophagic process can sequester mitochondria before cytochrome c release, in this way inhibiting apoptosis (Ashrafi and Schwarz, 2013). Accordingly, current data showed that all treatments appear to increase Hsp27 phosphorylation by western blotting analysis which is in not unexpected result (Fig 4.14). This could be associated with inducing autophagy or attempting to inhibit apoptosis.

Several chemical compounds that inhibit Hsp27 significantly reduce drug resistance, while promoting Hsp27 expression triggered autophagic cell survival as well as inhibited apoptosis in colon cancer cells for example (Rodriguez *et al.*, 2019). In addition, it was shown that the inhibition of Hsp27 in prostate cancer cells promoted apoptosis by inhibiting autophagy, reducing proteasome activity

and amplifying ER stress (Kumano *et al.*, 2012). Similarly, Hsp27 inhibited cisplatin-induced cell death by activation of autophagy in human hepatocellular carcinoma cells (Chen *et al.*, 2011). However, these observations highlight the need to clarify the molecular interplay between Hsp27 and autophagy. In line with this, the current changes observed by western blotting following cisplatin treatment may play a role in autophagy or apoptosis pathways. However, these changes were not significant within the experiential conditions tested warranting further investigation to examine its exact contribution in the stress response following drug treatments.

As discussed above, a large number of studies have revealed that the standard strategies for glioblastoma treatment induce autophagy, which contributes to therapy resistance. In this regard, as autophagy could promote cell survival or autophagic cell death, modulating autophagy using pharmacological inhibitors or inducers has received considerably more attention in an attempt to sensitise standard treatment for glioma treatment (Daido *et al.*, 2005; Yan *et al.*, 2016). However, the fundamental question that constantly arises after any applied treatment is whether autophagic activity in dying cells is the cause of cell death or is an attempt to prevent it. Usually to know if autophagy plays a pro-survival or a pro-death role, an autophagy inhibitor is added along with drug treatment causing cell death, hence if cell death increased that can indicate autophagy playing a survival role, and vice versa. There are contradictory studies about autophagy induced signalling following cisplatin and TMZ treatment (pro-survival or pro-death). Consequently, the results obtained in this study regarding the combinations may have two possible explanations (Fig 4.5). On one hand, assuming that cisplatin or TMZ-induced autophagy is a self-defence mechanism in response to drug treatment and serves as a cytoprotective process, PN517 would be more efficacious than aspirin because it did not increase (even inhibited at some times) the autophagy induced by cisplatin and TMZ as appeared through the autophagy levels by the flow cytometry results. Hence, PN517 could be sensitising the cells to the standard drug treatment whereas aspirin does not have this advantage. On the other hand, assuming autophagy induced following drug treatment is a cell death mechanism, aspirin would be more effective by

amplifying this pathway and providing additive effect in the combinations, while PN517 does not exhibit this activity.

However, another possible scenario is that both drugs have efficacy but through different mechanisms. Aspirin was a more potent autophagy inducer (which was evidenced by the results) that could cause excessive autophagy in the cells and induce autophagic cell death in the combination treatments. Whereas, PN517 did not seem to increase autophagy, yet caused more stress to the cells and switched autophagy to apoptosis. Both mechanisms are consistent with other studies and well established in the literature as already described.

4.3.3. Mitochondrial Membrane Potential

The mitochondrial membrane potential (ΔΨm) forms the transmembrane potential of hydrogen ions which is employed to make ATP (Mitchell, 1978). ΔΨm plays a vital role in mitochondrial homeostasis through selective elimination of dysfunctional mitochondria and transporting ions and proteins which are necessary for healthy mitochondrial functioning (Zamzami *et al.*, 1995). The levels of ΔΨm and ATP in the cell are kept relatively stable, however, sustained changes in ΔΨm normal levels may be toxic and induce loss of cell viability (Izyumov *et al.*, 2004). Different drug treatments can affect the mitochondrial membrane potential leading the cells to enter the depolarisation state. However, one critical factor is the time the mitochondrion stays in a state of depolarisation (Yaniv *et al.*, 2010). Short-term depolarization may not lead to significant changes in mitochondrial functioning but can result in the activation of mitophagy processes where mitochondria are recycled without inducing cell death (Jin *et al.*, 2010), while prolonged depolarization (the exact time is difficult to establish) leads to cell death associated with release of cytochrome C, AIF and other factors (Zorov *et al.*, 1992). Depending on the severity of the mitochondrial damage, it can induce cell death by apoptosis or, if the damage is extensive, by necrosis (Zamzami *et al.*, 2005).

The current study has performed the mitopotential assay aiming to monitor the changes in the mitochondrial membrane potential following drug treatment. As expected, all drug treatments showed depolarisation of the mitochondrial

membrane started at 24 hr and increased after 48 hours of the treatment (Fig 4.11). The mitopotential assay results could be related to either apoptosis, autophagy or autophagic necrosis. However, the effect patterns were more consistent and correlates well with the apoptosis results by Annexin V/PI staining (e.g. PN517 was markedly more efficacious in disrupting the mitochondrial membrane potential than aspirin), suggesting that the loss of the mitochondrial membrane potential following the drug treatment is leading ultimately to apoptosis.

These current findings are with agreement in previous results where accumulating evidence has shown that two common targets of NSAIDs are the mitochondria and calcium signalling pathways (Suzuki *et al.*, 2010; Ralph *et al.*, 2015). Multiple studies demonstrated that apoptosis induced by aspirin and other NSAIDs is mediated by oxidative stress and excessive ROS generation which is potentially toxic to mitochondrial and cellular functions and might result in opening of mitochondrial PTPCs. In addition, ROS generation results in oxidation of cardiolipin which decreases its contact with cytochrome c, thereby facilitating cytochrome c release and opening of L-type calcium channels (LTCCs), activating the mitochondrial death pathway. Therefore, it was suggested that a better understanding of the molecular mechanisms underlying the aspirin-mediated modification of PTPCs and LTCCs may help in the development of cancer selective therapies, since cancer cells appeared to be more sensitive to the modulation of these two types of channels than normal cells (Suzuki *et al.*, 2010).

A recent report has demonstrated that indomethacin impairs the physiological balance of mitochondrial dynamics by promoting mitochondrial dysfunction designated by compromised fatty acid oxidation, reduced complex I activity, and ATP depletion leading ultimately to apoptosis (Mazumder *et al.*, 2019). Another study reported the same mechanism of action, where aspirin was found to induce oxidative stress and mitochondrial dysfunction in HepG2 hepatoma cancer cells by mitochondrial apoptosis (Raza and John, 2012). The authors reported that mitochondrial respiratory functions were affected. While only a marginal inhibition of Complex I activity was observed, a significant inhibition in Complex IV

(cytochrome c oxidase) activity was seen. Also, aspirin produced a substantial decrease in cellular ATP level with increasing concentration. Interestingly, it was noted that altered glutathione (GSH)-redox metabolism in HepG2 cells play a critical role in aspirin-induced cytotoxicity, where GSH depletion enlarged the effects of aspirin on mitochondrial functions and apoptosis. Hence, it was proposed that manipulation of GSH homeostasis is potentially significant in increasing the efficacy of anti-inflammatory chemotherapeutic drugs by inducing targeted apoptosis (Raza and John, 2012). Accordingly, the effects seen in this study with the mitopotential assays with aspirin and PN517 might be associated with their ability to induce apoptosis (Fig 4.11).

In summary, this chapter investigated the effects of drug treatments on cell death and survival. The data showed that both aspirin and PN517 induce apoptosis with reduction in mitochondrial membrane potential whereas only aspirin induce autophagy, suggesting a difference in the underlying mechanism of action for the two drugs. TMZ induced autophagy at early timepoint and seemed to induce apoptosis with longer incubation. Cisplatin induced autophagy at early timepoint but significantly induced loss in mitochondrial membrane potential with a pattern towards inducing apoptosis with longer incubation. Previous studies indicated mutual regulation between autophagy and apoptosis in tumour cell survival following chemotherapy. While the role of autophagy in cancer onset and progression appears still controversial, regulation of autophagy may contribute to an improved response to therapy, hence warranting further studies. More investigations into the effects of the drug treatment on mitochondrial heath and the metabolic activity are continued in the next chapter.

CHAPTER 5: EFFECT OF DRUG TREATMENT ON CELLULAR METABOLIC ACTIVITY

5.1. Introduction

Cancer cells are highly dependent on metabolic pathways to generate the necessary energy for several oncogenic processes such as rapid proliferation, survival, invasion, and metastasis. Several lines of evidence showed that cancer cells exhibit profound metabolic alterations to support these processes, and demonstrated three major components contributing to the metabolic transformation of cancer cells including aerobic glycolysis, mitochondrial reprogramming, and deregulated lipid metabolism (Gottlieb and Tomlinson, 2005; Hanahan and Weinberg, 2011). Accordingly, cancer cells may alter glucose, lipid or amino acid metabolism, and shift the balance between anabolic and catabolic processes to adapt to the nutritional conditions of the tumour microenvironment (Newsholme *et al.*, 1985; Fadaka *et al.*, 2017). To this end, metabolic reprogramming has been emerged as a critical target in therapeutic intervention where these processes may be analysed directly via metabolic measurements. Hence, understanding the metabolic reprogramming of GBM cells is essential to clarify the fundamental mechanisms of GBM progression as well as to reveal metabolic liabilities of GBM cells which can be exploited for therapeutic targeting.

Adenosine triphosphate (ATP) is the main source of cellular energy, and the two major energy-producing pathways in the cell are glycolysis or oxidative phosphorylation (mitochondrial respiration). However, most cells can switch between these two pathways altering their bioenergetic profiles, thereby adapting to changes in their environment (Dang and Semenza, 1999; Jacobs *et al.*, 2008). There are many different methods available for examining the cellular bioenergetics and metabolic phenotyping for different cell types as well as monitoring shifts between mitochondrial respiration and glycolysis which can occur due to genetic, pharmacological, or environmental manipulation.

Mitochondrial respiration assays have provided insight into the contribution of mitochondrial function in cancer pathogenesis that may have clinical implications. In these assays, the rate of oxygen consumed by cells (oxygen consumption rate; OCR) can be used as an indicator of mitochondrial respiration and constitutes an efficient way to follow metabolic activity of cells. Furthermore, oxygen

consumption is also used to analyse cytotoxicity in drug screening development as an early marker of cell death (Simonnet *et al.*, 2014). Three methods are commonly used to measure OCR of cells or tissues including electron paramagnetic resonance oximetry (EPR), Clark oxygen electrode, and quenched-fluorescence oxygen-sensing assay (Diepart *et al.*, 2010). Although the EPR technique is relatively easy, it is expensive and does not allow the measurement of multiple samples simultaneously (James *et al.*, 1995). The Clark oxygen electrode is reliable method and still used in many laboratories, however, it requires large amount of materials and is more suitable for isolated mitochondria and permeabilized cells (Li and Graham, 2012). In contrast, quenched-fluorescence oxygen-sensing methods are usually preferred for evaluating mitochondrial respiration in intact cells. They are based on the ability of oxygen to quench the excited state of probes, hence, the depletion of oxygen by the cells increases the probe signal, reflecting changes in mitochondrial activity (Hynes *et al.*, 2006). This technique allows for the measurement of small changes in cellular respiration and minor differences in respiratory effects of different reagents (Heerlein *et al.*, 2005).

Monitoring of glycolytic activity is essential while identifying the metabolic phenotype of a specific cell type or studying the effects of metabolic modulators, particularly in cancer cells. The glycolytic pathway results in the production and extrusion of protons into the extracellular medium which is predominately from the excretion of lactic acid per unit time after its conversion from pyruvate, leading to the acidification of the medium surrounding the cell. Therefore, extracellular acidification rate (ECAR) can be used an indicator of lactic acid production or glycolysis (Wu *et al.*, 2007). Multiple studies use external pH meters to quantify glycolytic activity, however, other metabolic processes in cells, such as CO_2 production by the tricarboxylic acid (TCA) cycle, can change the pH of the media complicating this analysis (Mookerjee *et al.*, 2015).

Investigating the contribution of both mitochondrial respiration and glycolytic activity to cellular bioenergetics is not possible in most assay formats. However, the XF Extracellular Flux Analyzer can simultaneously determine both the aerobic and glycolytic components of cellular bioenergetics in living cells in real time by

dual-fluorescent biosensors, one measures oxygen consumption rate and the other measures extracellular acidification rate, where OCR is reported in pmol/min and ECAR in mpH/min (Bulua *et al.*, 2011; Chacko *et al.*, 2013). Therefore, this technology allows to attain more comprehensive assessment of cellular bioenergetics and analyse the dynamic interplay between the two major energy-producing pathways in cancer cells. Importantly, the phenotypic evaluation of cancer cells in response to different metabolic substrates or inhibitors can be evaluated (Nicholls *et al.*, 2010; Dranka *et al.*, 2011).

One important test that can be performed using Seahorse XFp Extracellular Flux Analyzer is the Cell Mito Stress Test which is a standard assay to evaluate mitochondrial respiration by directly measuring the oxygen consumption rate (OCR) of the cells using the. This test uses modulators of respiration that target components of the electron transport chain (ETC) in the mitochondria to determine key parameters of metabolic function (Fig 5.1).

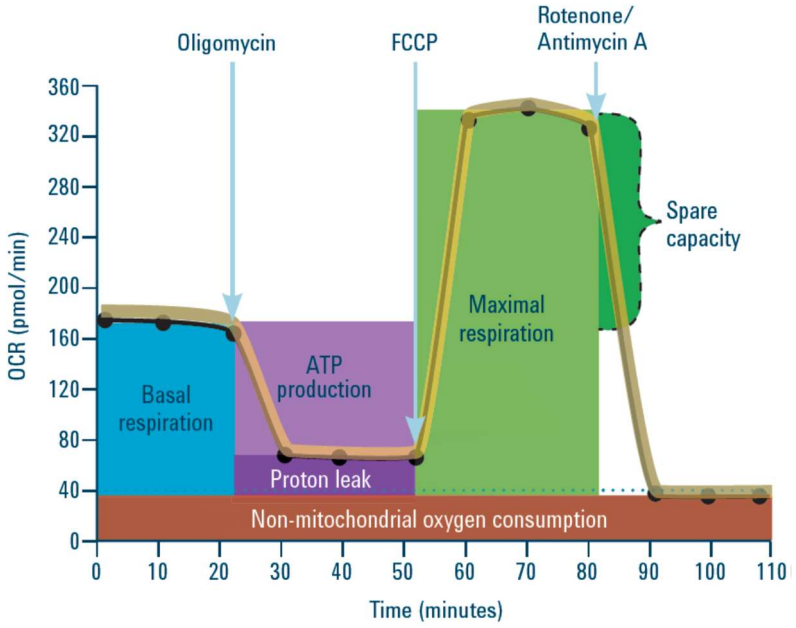

Figure 5. 1. Seahorse XFp Cell Mito Stress Test profile of the key parameters of mitochondrial respiration. Sequential compound injections measure basal respiration, ATP production, proton leak, maximal respiration, spare respiratory capacity, and non-mitochondrial respiration (Source; Seahorse Bioscience).

The initial OCR values of the cells represent the oxygen consumed through mitochondrial and non-mitochondrial pathways. Basal mitochondrial respiration rate can be calculated. Three compounds (oligomycin, FCCP, and a mix of

rotenone and antimycin A) are serially injected to reveals three key parameters of cellular respiration: ATP–linked respiration, maximal respiration, and non-mitochondrial respiration, respectively. The difference between the maximal and the basal respirations constitutes the spare respiratory capacity which measures the ability of the cell to generate ATP via oxidative phosphorylation in response to increased energy demand. Additionally, some internally normalised parameters like the coupling efficiency and the relative spare respiratory capacity can be analysed. Equations used for calculating the different key parameters can be found in the appendix (Fig 9.17).

To monitor glycolysis, the Seahorse XF Glycolysis Stress Test is used. This test assesses glycolytic function in cells by directly measuring the extracellular acidification rate (ECAR) using the Seahorse XFp Analyzer. Through the additions of glucose, oligomycin, and 2-deoxyglucose (2-DG), this test provides a comprehensive method to measure the key parameters of glycolytic flux: glycolysis, glycolytic capacity, glycolytic reserve, as well as non-glycolytic acidification (Fig 5.2).

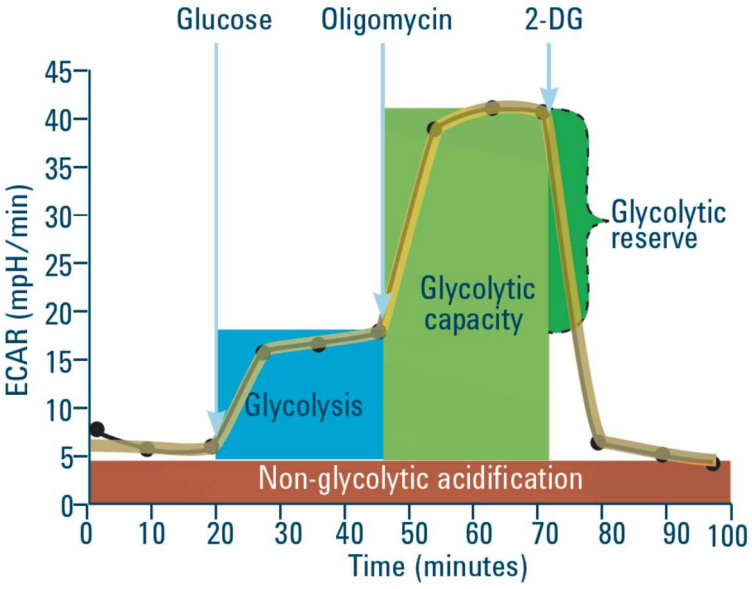

Figure 5. 2. Seahorse XFp Glycolysis Stress Test profile of the key parameters of glycolytic function. Sequential compound injections measure glycolysis, glycolytic capacity, and allow calculation of glycolytic reserve and non-glycolytic acidification (Source; Seahorse Bioscience).

The difference between glycolytic capacity and glycolysis rate defines glycolytic reserve which is indicative of the cellular ability to increase the glycolytic rate upon increased energy demand. Equations used for calculating the different key parameters can be found in the appendix (Fig 9.18).

In this context, other procedures can be used to reveal and quantify the metabolic alterations that underlie malignant cell proliferation. For example, the measurement of glucose uptake and lactate excretion by malignant cells can detect shifts in glucose catabolism. In addition, determining the activity of rate-limiting glycolytic enzymes may provide insights into points of metabolic regulation (Teslaa and Teitell, 2014). Glycolytic flux can be quantified by measuring glucose uptake and lactate excretion with several colorimetric and fluorometric assays. Although these assays for the measurements of extracellular fluid concentrations of glucose and lactate are relatively inexpensive and straightforward, they do not provide information on other possible fates for glucose-derived carbons. For example, other metabolic processes that consume or add metabolic intermediates to the glycolytic pathway remain undefined, which may impact glycolytic flux measurements and complicate data interpretations (Teslaa and Teitell, 2014).

There are many commercially available kits to detect lactate concentration, the end product of glycolysis, produced and secreted by cultured cells (Teslaa and Teitell, 2014; Rogatzki *et al.*, 2015). In these assays, lactate dehydrogenase catalyses oxidation of lactate, yielding pyruvate and NADH which can directly reduce different reagents. The intensity of fluorescence or absorbance of a reduced product is proportional to the lactate concentration in the media, and is thus an indirect measurement of glycolysis (Teslaa and Teitell, 2014). In line with this, the activity of different glycolytic enzymes may limit the rate of glycolysis, and therefore, control the maximum possible flux (Teslaa and Teitell, 2014). glyceraldehyde-3-phosphate dehydrogenase (GAPDH) a key enzyme that catalyses the redox reaction in the glycolytic pathway by converting glyceraldehyde-3-phosphate (GAP) to 1, 3-bisphosphate glycerate (BPG) with a reduction of NAD+ to NADH. Although GAPDH has long been used as a house-keeping enzyme in western blotting and the reverse transcription polymerase

chain reaction (RT-PCR) analyses (Mori *et al.*, 2008), accumulating evidence suggests that GAPDH also has additional non-enzymatic functions with distinct subcellular distributions including cytoplasm, cell membranes and nucleus (Tisdale, 2001; Zheng *et al.*, 2003; Harada *et al.*, 2007; Sirover, 2011). In addition to glycolytic function, this enzyme has been implicated in numerous cellular processes such as membrane trafficking, iron metabolism, nuclear translocation, RNA transport, DNA replication and apoptosis (Colell *et al.*, 2009; Sheokand *et al.*, 2014). Deregulation of GAPDH activity correlates with abnormal cell proliferation and carcinogenesis, and increased GAPDH levels were observed in different human cancer types and often associated with reduced survival (Altenberg and Greulich, 2004; Guo *et al.*, 2013). Therefore, accurate quantitation of GAPDH activity is important for studying cellular physiology and may be a critical marker of cancer cell progression and prognosis (Zhang *et al.*, 2015). Different commercially available kits provide simple and sensitive method for monitoring GAPDH activity in the cells. In these assays, GAPDH catalyses the conversion of GAP into BPG and an intermediate, which reacts with a developer to form a coloured product and the absorbance is measured in kinetic mode.

In summary, drug treatment can influence GBM cell viability by impairing metabolic activity and altering different bioenergetics of the cells. The current study has established the effect of aspirin and PN517 on cell viability at early timepoints by PrestoBlue assay which rely on the metabolic activity of the cells, with identified effects on mitochondrial health observed by the mitopotential assay. Therefore, this chapter aimed to investigate the effect of the drug treatment on cell metabolism at an early timepoint (24 hr) and to monitor any changes in the various bioenergetic profiles of U87-MG and SVG-p12 cell lines under both normoxia and hypoxia. For that purpose, the Seahorse XFp Extracellular Flux Analyser (Seahorse Bioscience) was employed to monitor the changes in the mitochondrial respiration and glycolytic functions following mono and combined therapy. Additionally, lactate production and GAPDH enzymatic activity were investigated in response to drug treatment in U87-MG cells using fluorometric and colorimetric assays.

5.2. Results

5.2.1. Studying bioenergetic profiles of U87-MG and SVG-p12 cells.

In order to examine the bioenergetic profile of both U87-MG and SVG-p12 cell lines, optimization assays were firstly performed including cell seeding density titration and the compound injection titration to determine optimal nontoxic experimental conditions for accurate analysis. Mitochondrial and glycolytic profiles of both cell lines were studied under normoxia to compare contributing metabolic pathways and bioenergetics parameters between both cell lines. Mitochondrial stress test and glycolytic stress test assays were performed by measuring oxygen consumption and extracellular acidification rates, respectively, in real time using XFp Extracellular Flux Analyser. Additionally, the mitochondrial and glycolytic functions parameters were calculated by the Seahorse Report Generator software.

The U87-MG cell line showed a significantly lower overall mitochondrial activity (oxidative phosphorylation) represented by lower oxygen consumption rates compared to the non-cancerous cell line SVG-p12 (Fig 5.3.A). As a result, there were significant decreases observed in the respiration bioenergetic parameters of U87-MG cells compared to SVG-p12 cells including the basal respiration rate (15 ±1.9 vs. 42 ±4.1 pmol/min, $p<0.0001$), ATP- linked respiration (11.5 ±1.6 vs. 35.8 ±3.7 pmol/min, $p<0.0001$), and the maximal respiration (29.5 ±2.3 vs. 69 ±6.4 pmol/min, $p<0.0001$) (Fig 5.3.B). However, there was no significant difference between the two cell lines in respect to proton leak, non-mitochondrial respiration, or coupling efficiency ($p>0.05$). It is worth noting that the spare respiratory capacity was significantly higher in U87-MG cells (218 ±15.3% vs. 166.7 ±3.4%, $p<0.0001$) (Fig. 5.3.C).

In contrast, the U87-MG cell line showed a significant increase in glycolytic activity with a significant increase in the extracellular acidification rate observed following glucose addition compared to the con-cancerous cell line SVG-p12 (Fig 5.4.A). Accordingly, glycolytic parameter analysis indicated significantly higher rate of glycolysis in the U87-MG cell line compared to SVG-p12 cells (45.1 ±2.3 vs. 65.7 ±2.8 mpH/min, $p<0.001$) (Fig 5.4.B). There was no significant difference

between the two cell lines with respect to the glycolytic capacity and non-glycolytic acidification (p>0.05). However, the glycolytic reserve for U87-MG cells was lower than for SVG-p12 (190.2 ±9.7% vs. 117.7 ±3.3%, p<0.0001) (Fig. 5.4.C).

When comparing the metabolic phenotyping for both cell lines, OCR/ECAR ratio, representing the relative contribution of basal respiration versus glycolysis, was significantly lower for U87-MG compared to SVG-p12 cells (1.06 ±0.1 vs. 0.24 ±0.03%, p<0.0001) (Fig 5.5.A) which was consistent with a significant increase in the Warburg effect estimated by dividing ECAR after glucose injection by OCR values at baseline (p<0.0001) (Fig 5.5.B). Also, these data were presented by percentages of the two different pathways used for generating energy, oxidative phosphorylation and glycolysis, for each cell line. Data showed that while SVG-p12 cells equivalently rely on both pathways for generating energy, U87-MG cells showed a significantly higher percentage of glycolysis and lower percentage of oxidative phosphorylation (p<0.0001) (Fig 5.5.C).

Additionally, when U87-MG cells were exposed to hypoxia, they showed generally less metabolic activity with lower OCR and ECAR values (p<0.05). However, the metabolic phenotyping remained similar to that seen under normoxia with no significant difference in the OCR/ECAR ratio or Warburg effect (p>0.05) (Fig 5.6).

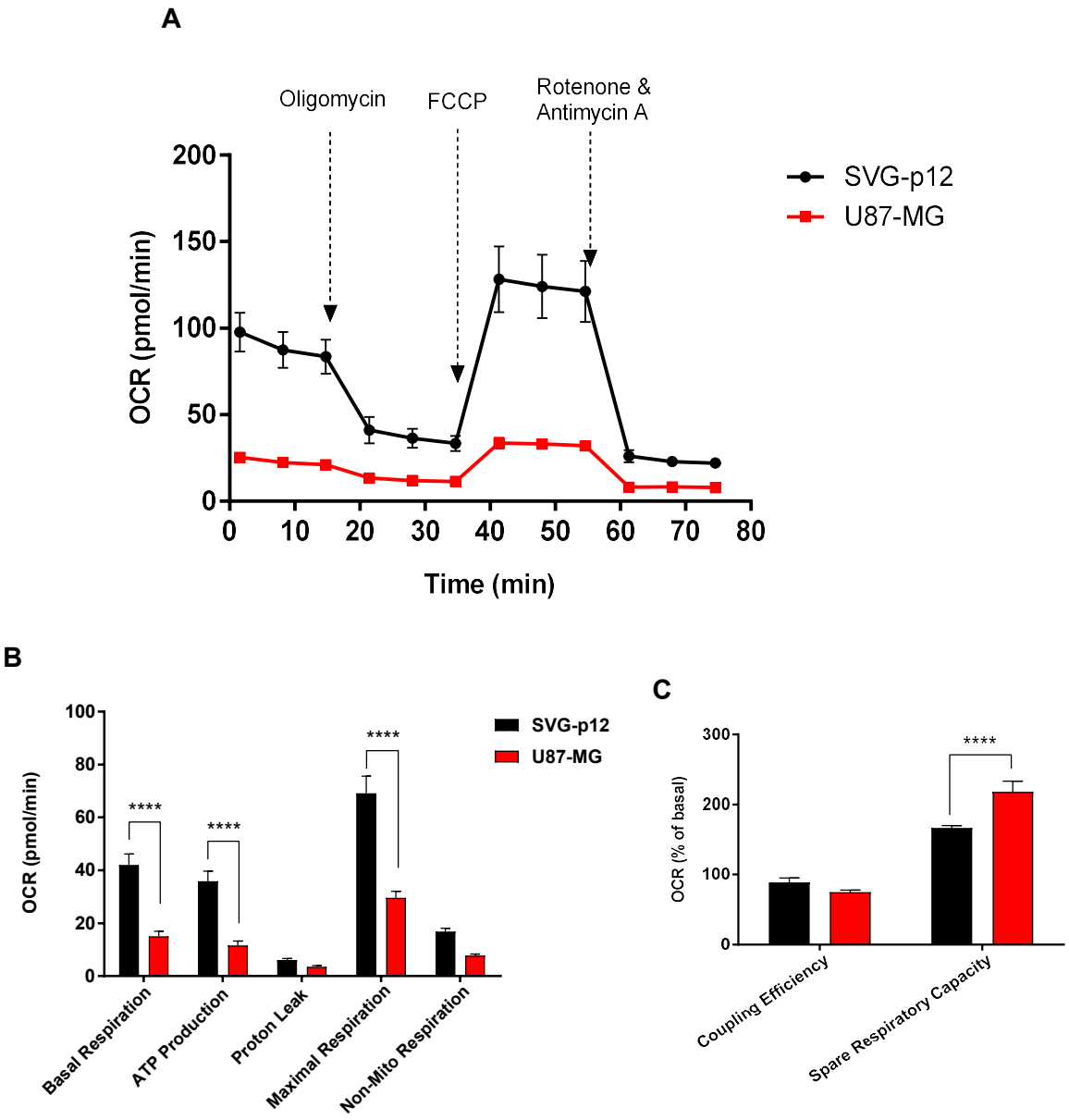

Figure 5. 3. The mitochondrial respiration profile of U87-MG cell line compared to the non-cancerous SVG-p12 cell line. Cells were incubated for 48 hr with culture media at 37C° with CO_2 under normoxia then incubated for 45 min 37C° without CO_2. A mitochondrial stress test was performed using XFp Extracellular Flux Analyser. A) Oxygen consumption rates were measured using sequential addition of oligomycin (1µM final), FCCP (0.5µM final), and rotenone+ antimycin A (0.5µM final). Arrows indicate the points at which the indicated compounds were added. B and C) Bioenergetic parameters of mitochondrial and non-mitochondrial respiration. Values represents mean ± SEM generated from five independent experiments. A two-way ANOVA was used to identify significant effects, with Bonferroni's multiple comparison test, *P < 0.05; **P < 0.01; ***P < 0.001; ****P < 0.0001. The experimental procedure was performed as described in Materials and Methods section 2.2.12.

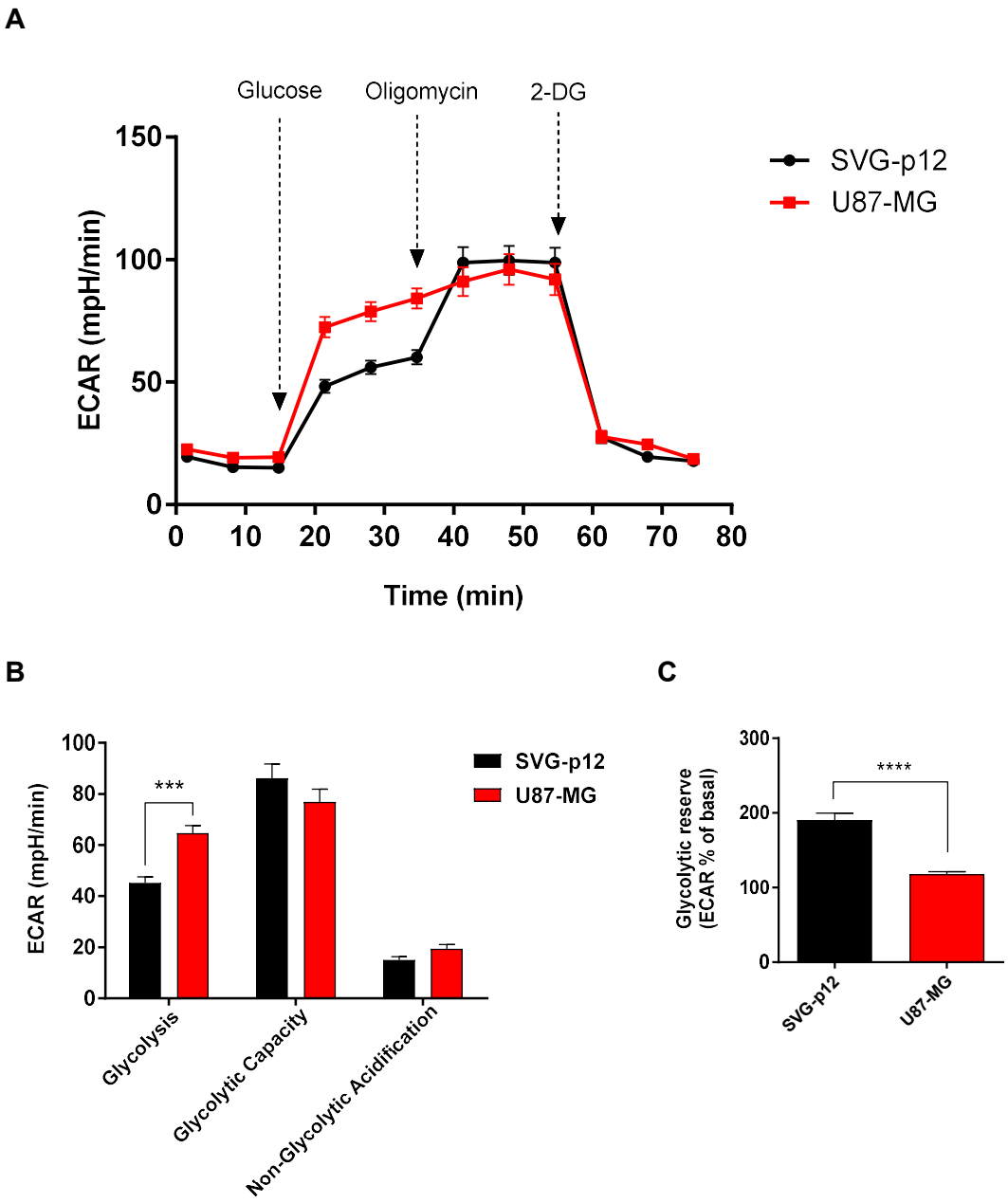

Figure 5. 4. The glycolytic activity profile of U87-MG cell line compared to the non-cancerous SVG-p12 cell line. Cells were incubated for 48 hr with culture media at 37C° with CO_2 under normoxia then incubated for 45 min 37C° without CO_2. A glycolytic stress test was performed using XFp Extracellular Flux Analyser. A) Extracellular acidification rates were measured using sequential addition of glucose (10mM final), oligomycin (1µM final), and 2-deoxyglucose (2-DG; 50mM final). Arrows indicate the points at which the indicated compounds were added. B and C) Bioenergetic parameters of glycolytic function. Values represents mean ± SEM generated from five independent experiments. A two-way ANOVA was used to identify significant effects, with Bonferroni's multiple comparison test, *P < 0.05; **P < 0.01; ***P < 0.001; ****P < 0.0001. The experimental procedure was performed as described in Materials and Methods section 2.2.12.

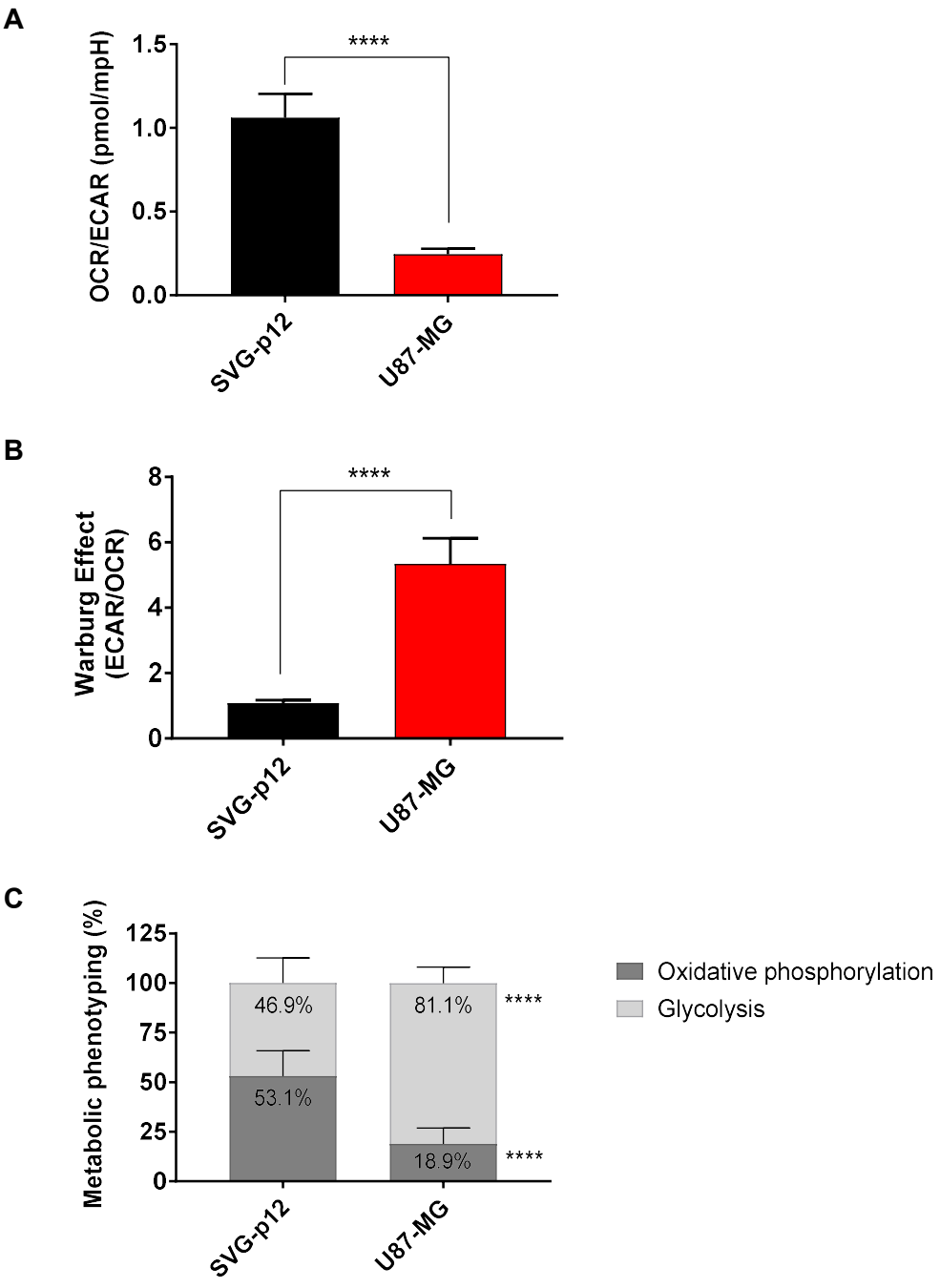

Figure 5. 5. The changes in metabolic phenotyping of U87-MG cells compared to SVG-p12 cell line under normoxia. A) OCR/ECAR ratio representing the relative contribution of basal respiration versus glycolysis as acquired by XFp Extracellular Flux Analyser for U87-MG and SVG-p12 cell lines. B) Warburg effect estimated by dividing ECAR after glucose injection by OCR values at baseline. C) Metabolic phenotyping for U87-MG and SVG-p12 cell lines represented by contribution percentages of oxidative phosphorylation and glycolysis in generating energy. Values represents mean ± SEM generated from five independent experiments. A two-way ANOVA was used to identify significant effects, with Bonferroni's multiple comparison test, *P < 0.05; **P < 0.01; ***P < 0.001; ****P < 0.0001. The experimental procedure was performed as described in Materials and Methods section 2.2.12.

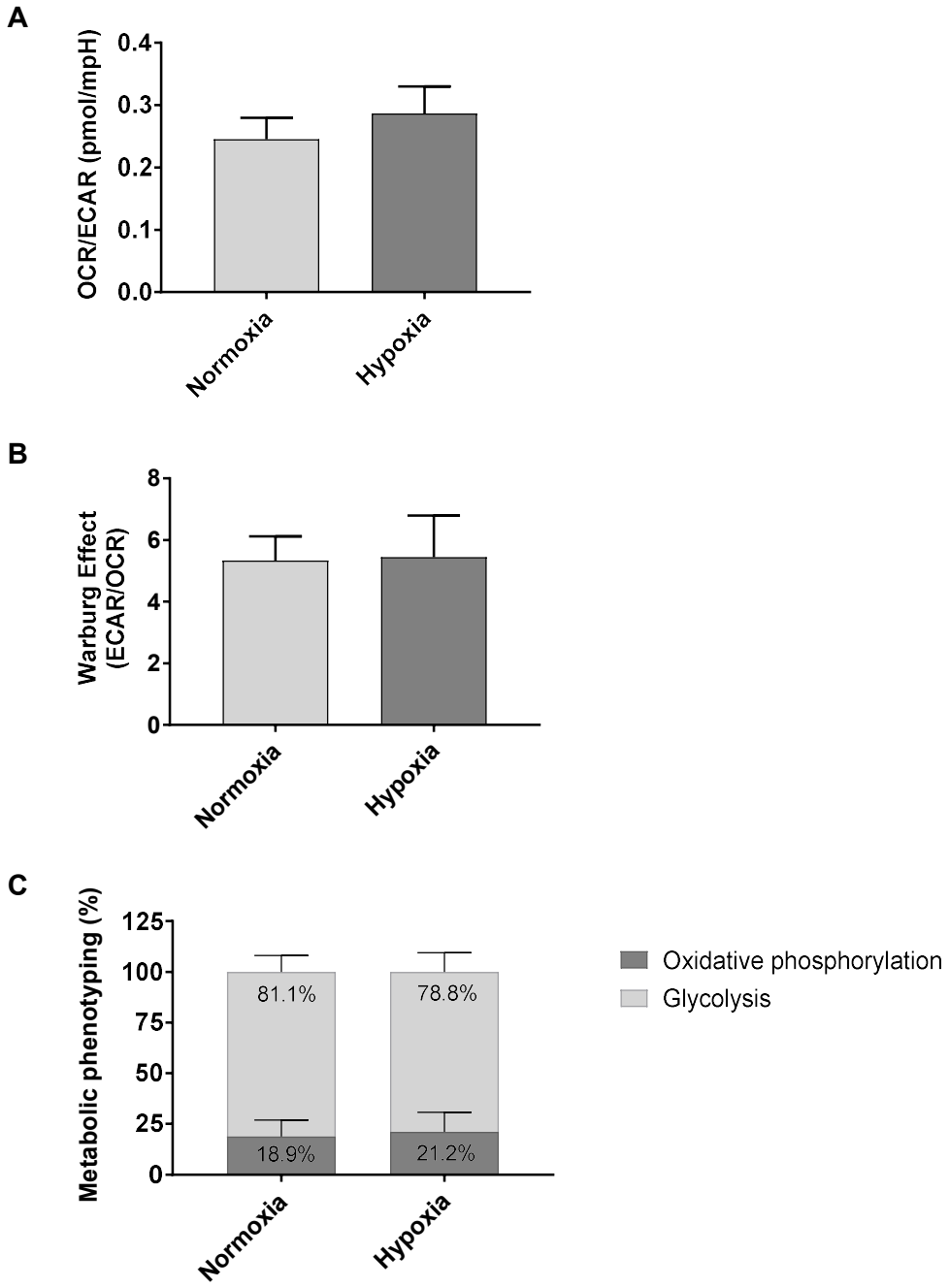

Figure 5. 6. The changes in metabolic phenotyping of U87-MG cell line under hypoxia. A) OCR/ECAR ratio representing the relative contribution of basal respiration versus glycolysis as acquired by XFp Extracellular Flux Analyser for U87-MG cell lines under normoxia and hypoxia. B) Warburg effect estimated by dividing ECAR after glucose injection by OCR values at baseline. C) Metabolic phenotyping for U87-MG cell line under normoxia and hypoxia represented by contribution percentages of oxidative phosphorylation and glycolysis in generating energy. Values represents mean ± SEM generated from five independent experiments. A two-way ANOVA was used to identify significant effects, with Bonferroni's multiple comparison test, *P < 0.05; **P < 0.01; ***P < 0.001; ****P < 0.0001. The experimental procedure was performed as described in Materials and Methods section 2.2.12.

5.2.2. Effects of drug treatment on cell mitochondrial activity

In order to investigate whether the drug treatments can affect the mitochondrial respiration activity and the oxidative phosphorylation of the cells, the Mito stress test was performed for U87-MG using Seahorse XFp Extracellular Flux Analyser, under normoxia and hypoxia. The drug treatments were added at IC_{50}, as determined by the cell viability concentration-response curves after 48 hr. Mitochondrial profiles and respiration bioenergetics parameters were studied in U87-MG cell line following 24 hr of drug treatment, separately or in combination. In addition, the test was performed for the control SVG-p12 cell lines under normoxia.

In the U87-MG cell, it can be seen from the mitochondrial respiration profiles acquired by Seahorse analyser (Fig 5.7) that PN517 and its combinations showed the greatest effect on the oxygen consumption rates with a reduction in both basal and maximal respiration rates, while other drug treatments did not show overt effects. Also, no change was observed in the rates of non-mitochondrial respiration.

Under normoxia, neither aspirin, cisplatin nor TMZ showed an effect on any of the basal respiration, ATP production or proton leak rates ($p>0.05$) (Fig 5.8). In contrast, PN517 and its combinations significantly reduced the basal respiration and ATP production rates. While the basal respiration of the control was 14.6 ±1.7 pmol/min, it was reduced to 9.5 ±1.7 pmol/min with PN517 ($p<0.05$), to 7.8 ±1.1 pmol/min with cisplatin and PN517 combination ($p<0.05$), and to 5.7 ±1 pmol/min with TMZ and PN517 combination ($p<0.05$). Similarly, ATP production rates for these treatments were significantly lower than the control. While the ATP production rate of the control was 11.2 ±1.3 pmol/min, it was reduced to 4.2 ±2.2 pmol/min with PN517 ($p<0.05$), to 3.5 ±0.6 pmol/min with cisplatin and PN517 combination ($p<0.05$), and to 3.3 ±0.6 pmol/min with TMZ and PN517 combination ($p<0.05$). Under hypoxia, all treatments appeared to reduce basal respiration approximately equally but there was no significant difference compared to the control ($p>0.05$). PN517 and its combinations showed the biggest effect on ATP production under hypoxia but again that was not significant ($p>0.05$) (Fig 5.8).

Regarding the respiration rates linked to proton leak, both aspirin and PN517 seem to lead to the biggest increase in proton leak under normoxia, however, there was no significant difference in the proton leak rates with any of the drug treatments (p>0.05). In general, proton leak was noted to be lower under hypoxia, again with no significant difference with any of the drug treatments (p>0.05) (Fig 5.8).

When comparing maximal respiration rates under normoxia, a similar pattern to the basal respiration rates was observed. PN517 had the greatest effect either alone or in combination on maximal respiration reduction (Fig 5.9). While the maximal respiration of the control was 29.1 ±2.1 pmol/min, it was reduced to 13.9 ±2.6 pmol/min with PN517 (p<0.01), to 12.1 ±1.4 pmol/min with cisplatin and PN517 combination (p<0.001), and to 10.9 ±1.9 pmol/min with TMZ and PN517 combination (p<0.001). Additionally, PN517 significantly enhanced the effect of cisplatin monotherapy on the maximal respiration rate (p<0.01), and to a greater extent with TMZ monotherapy (p<0.001).

Aspirin showed a similar effect to PN517 in reducing the maximal respiration rates, however there were no significant differences for aspirin monotherapy or combined therapy compared to the control (p>0.05). Furthermore, the maximal respiration reduction following treatment with the combination of TMZ and PN517 was significantly higher than the combination of TMZ and aspirin (p<0.05). With regards the non-mitochondrial respiration rates, no significant effect was observed for the drug treatments (p>0.05). Similar patterns of drug treatment effects on maximal and non-mitochondrial respiration were observed under hypoxia but were not significantly different to control (p>0.05) (Fig 5.9).

When studying the internally normalised parameters of the mitochondrial function, PN517 and its combinations showed a trend towards reducing the mitochondrial coupling efficiency, however, no significant differences were observed (p>0.05). Both aspirin and PN517 produced a significant reduction in the spare respiratory capacity (159.2 ±8.7%, p<0.05 and 147.5 ±7.1%, p<0.01, respectively) compared to the control (218 ±15.3%) (Fig 5.10). Additionally, the PN517 combinations with cisplatin or TMZ showed a significant reduction in the

spare respiratory capacity (151.7 ±16.5%, $p<0.05$ and 167.5 ±6.3%, $p<0.01$, respectively). Similar patterns of the drug treatment effects on coupling efficiency and spare respiratory capacity were observed under hypoxia but were not significantly different to control ($p>0.05$) (Fig 5.10).

Regarding the effect of drug treatment on the mitochondrial respiratory activity of SVG-p12 cells (Fig 5.11), all drug treatments seemed to reduce the mitochondrial activity with a distinct effect for TMZ which was different in U87-MG cells. When studying the different mitochondrial key parameters, PN517 showed similar effects to those seen in the U87-MG cells in reducing basal respiration and ATP production rates (Fig 5.12). However, only the decrease in the basal respiration was significantly different from the control (29.1 ±2.3 pmol/min vs. 48.5 ±6.8 pmol/min, $p<0.05$). Interestingly, TMZ also produced a significant reduction in the basal respiration and ATP production rates of SVG-p12 cells with a significant difference for basal respiration rate compared to the control (29.4 ±3.7 pmol/min vs. 48.5 ±6.8 pmol/min, $p<0.05$). Additionally, the PN517 combination with cisplatin produced a significant reduction in both basal respiration and ATP production rates ($p<0.01$). Similarly, PN517 combination with TMZ resulted in a significant reduction in both basal respiration and ATP production rates ($p<0.001$). Also, no significant effect was observed for the drug treatment on proton leak ($p>0.05$) (Fig 5.12).

The maximal respiration rates were consistent with the basal rates (Fig 5.13), where PN517 and TMZ produced significant reductions in the maximal respiration rates (41 ±4 pmol/min, $p<0.01$ and 46.6 ±6 pmol/min, $p<0.05$, respectively) compared to the control (80.3 ±11.2 pmol/min). Also, PN517 treatment resulted in a significant reduction in the maximal respiration when combined with cisplatin ($p<0.01$) or TMZ ($p<0.001$). Interestingly, both PN517 and TMZ showed a trend towards reducing the non-mitochondrial respiration rates of SVG-p12 cells, however, no significant effect was observed ($p>0.05$). Additionally, none of the drug treatments either as monotherapy or combinations showed significant effects on coupling efficiency or spare respiratory capacity ($p>0.05$) (Fig 5.13).

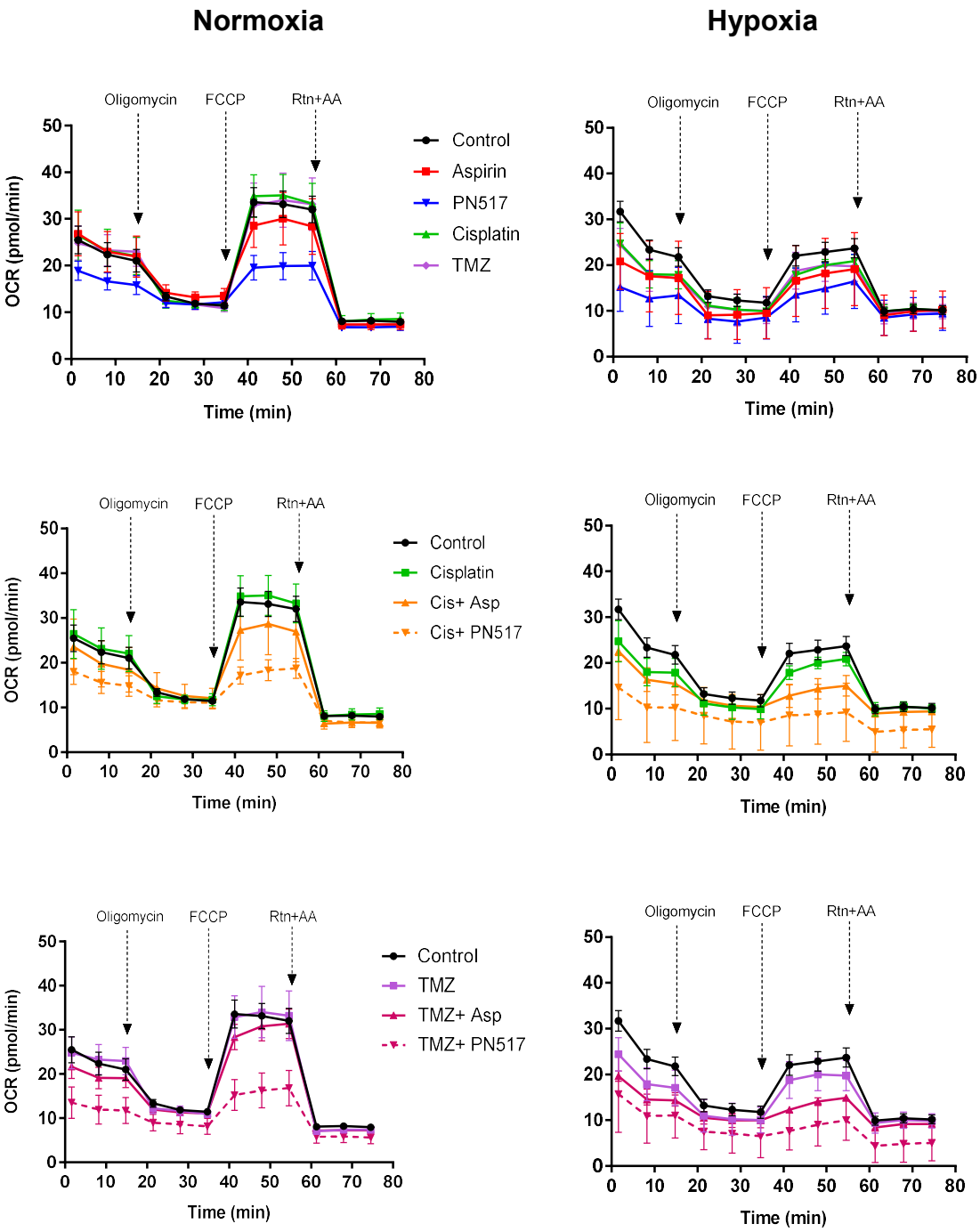

Figure 5. 7. The effect of drug treatment on mitochondrial activity in U87-MG cell line under normoxia and hypoxia. A mitochondrial stress test was performed using XFp Extracellular Flux Analyser following drug treatment for 24 hr and oxygen consumption rates were measured using sequential addition of oligomycin (1μM final), FCCP (0.5μM final), and rotenone+ antimycin A (0.5μM final). Arrows indicate the approximate points at which the indicated compounds were added. Values represents mean ± SEM generated from five independent experiments under normoxia and three independent experiments under hypoxia. A two-way ANOVA was used to identify significant effects, with Tukey's multiple comparison test. The experimental procedure was performed as described in Materials and Methods section 2.2.12.

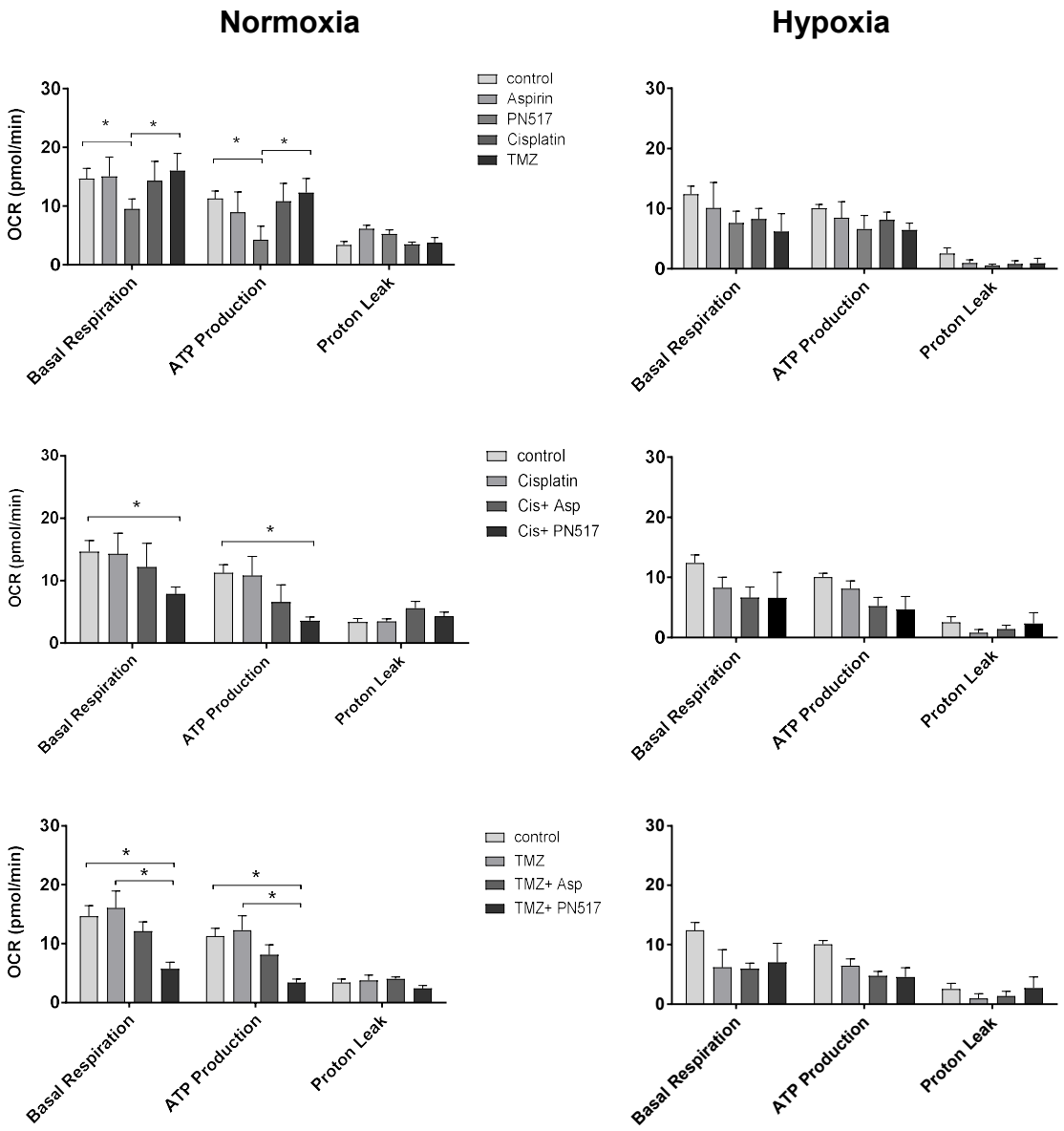

Figure 5. 8. The effect of drug treatment on basal respiration, ATP production and proton leak rates in the U87-MG cell line under normoxia and hypoxia. Data shows basal respiration, ATP-linked respiration, and proton leak-linked respiration generated by Seahorse Report Generator and plotted using GraphPad Prism. Values represent mean ± SEM generated from five independent experiments under normoxia and three independent experiments under hypoxia. A two-way ANOVA was used to identify significant effects, with Tukey's multiple comparison test, *P < 0.05; **P < 0.01; ***P < 0.001; ****P < 0.0001. The experimental procedure was performed as described in Materials and Methods section 2.2.12.

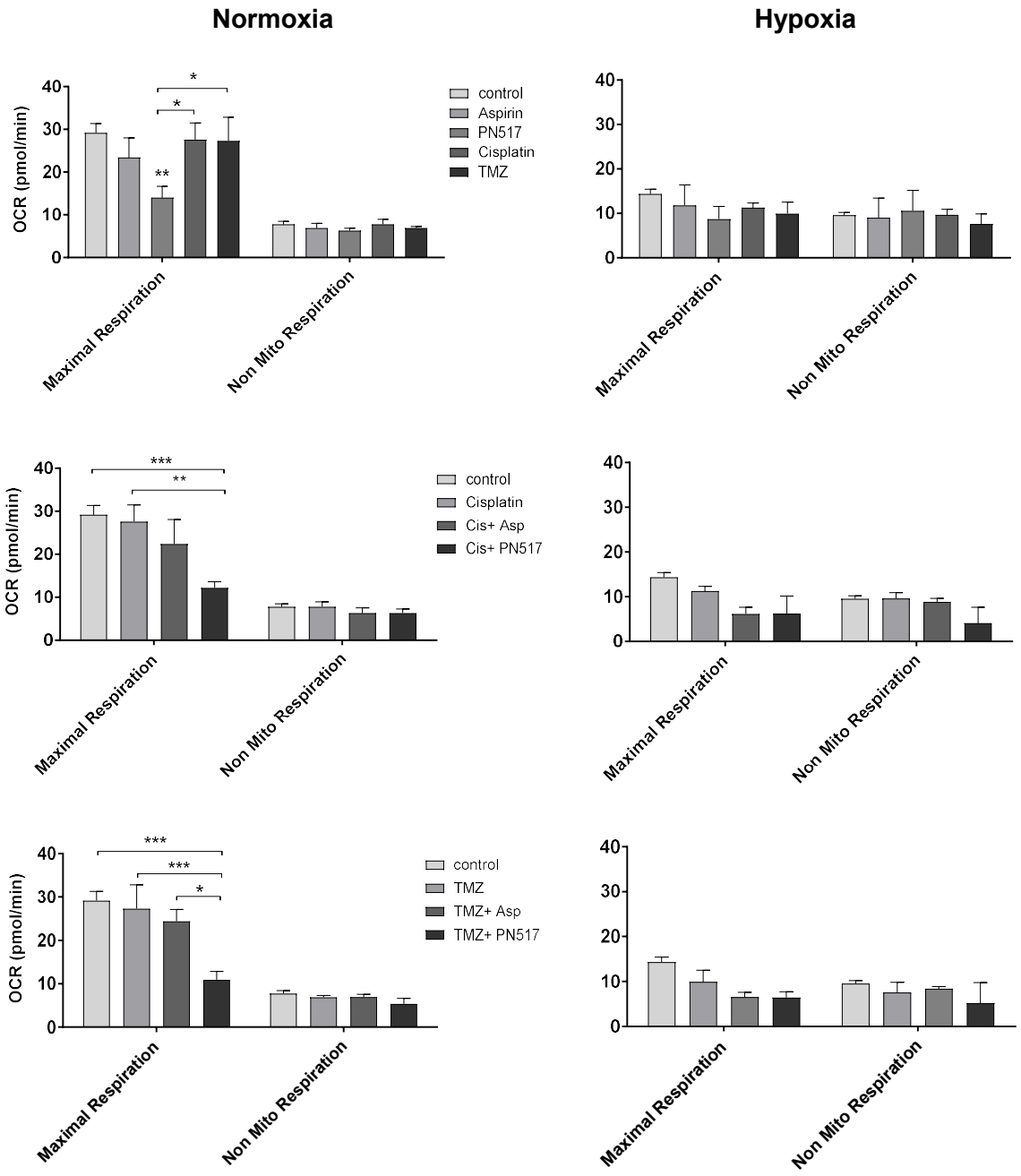

Figure 5. 9. The effect of drug treatment on maximal respiration and non-Mito respiration rates in the U87-MG cell line under normoxia and hypoxia. Data shows maximal respiration and non-mitochondrial respiration generated by Seahorse Report Generator and plotted using GraphPad Prism. Values represent mean ± SEM generated from five independent experiments under normoxia and three independent experiments under hypoxia. A two-way ANOVA was used to identify significant effects, with Tukey's multiple comparison test, *P < 0.05; **P < 0.01; ***P < 0.001; ****P < 0.0001. The experimental procedure was performed as described in Materials and Methods section 2.2.12.

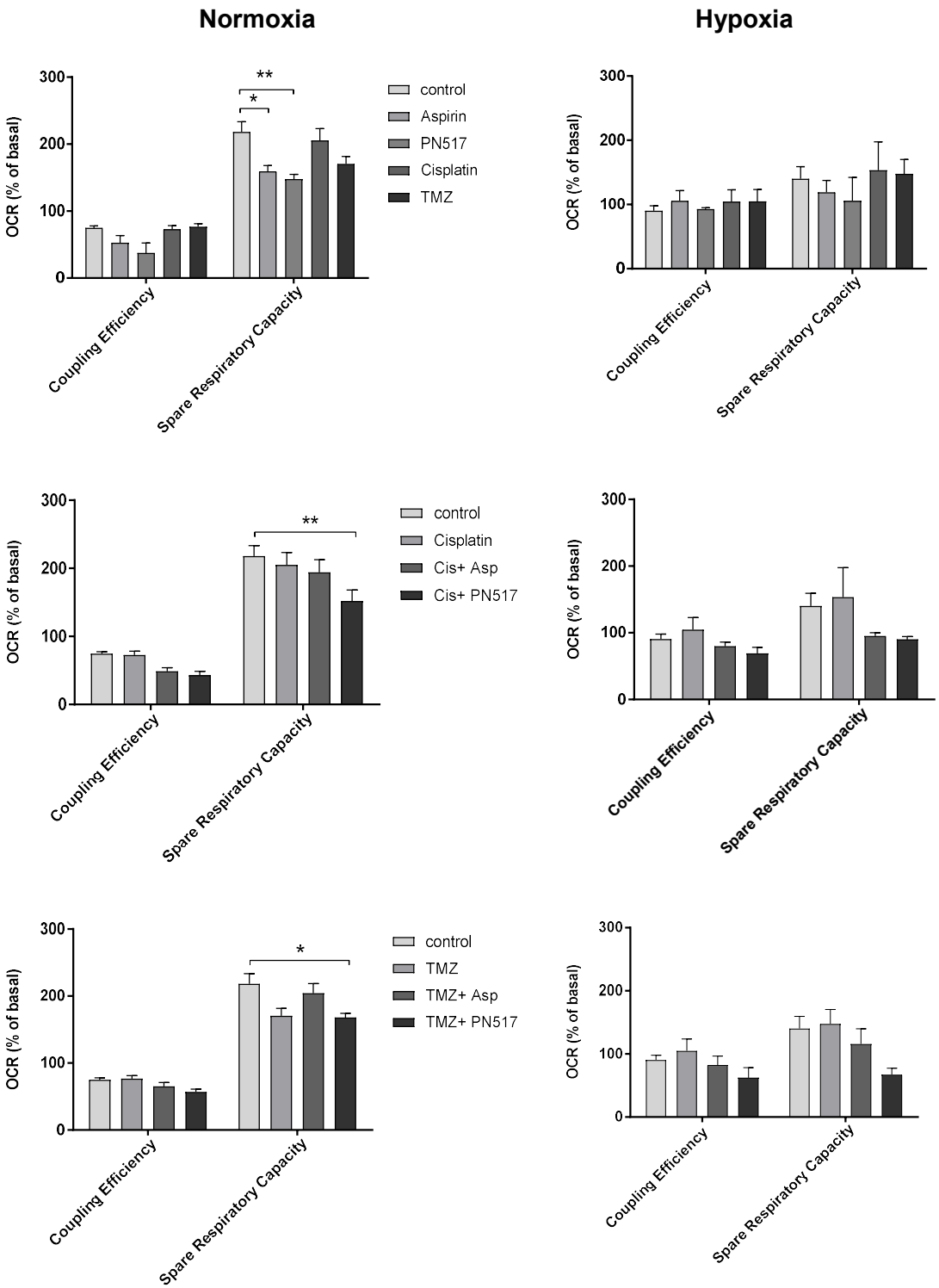

Figure 5. 10. The effect of drug treatment on the coupling efficiency and spare respiratory capacity in the U87-MG cell line under normoxia and hypoxia. Data shows coupling efficiency spare respiratory capacity generated by Seahorse Report Generator and plotted using GraphPad Prism. Values represent mean ± SEM generated from five independent experiments under normoxia and three independent experiments under hypoxia. A two-way ANOVA was used to identify significant effects, with Tukey's multiple comparison test, *P < 0.05; **P < 0.01; ***P < 0.001; ****P < 0.0001. The experimental procedure was performed as described in Materials and Methods section 2.2.12.

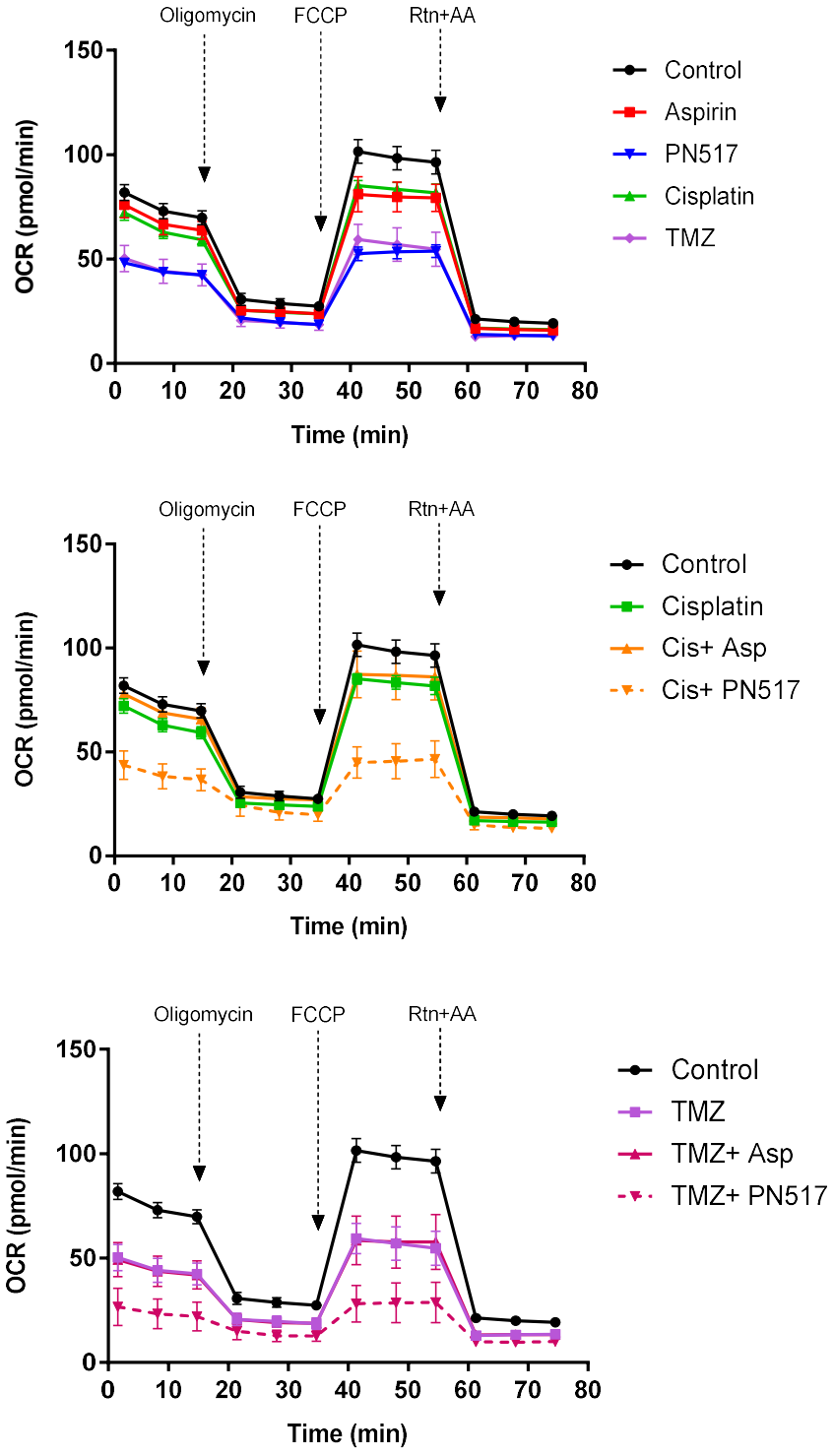

Figure 5. 11. The effect of drug treatment on the mitochondrial activity in the SVG-p12 cell line under normoxia. A mitochondrial stress test was performed using XFp Extracellular Flux Analyser following drug treatment for 24 hr and oxygen consumption rates were measured using sequential addition of oligomycin (1μM final), FCCP (0.5μM final), and rotenone+ antimycin A (0.5μM final). Values represent mean ± SEM generated from four independent experiments under normoxia. Arrows indicate the approximate points at which the indicated compounds were added. A two-way ANOVA was used to identify significant effects, with Tukey's multiple comparison test. The experimental procedure was performed as described in Materials and Methods section 2.2.12.

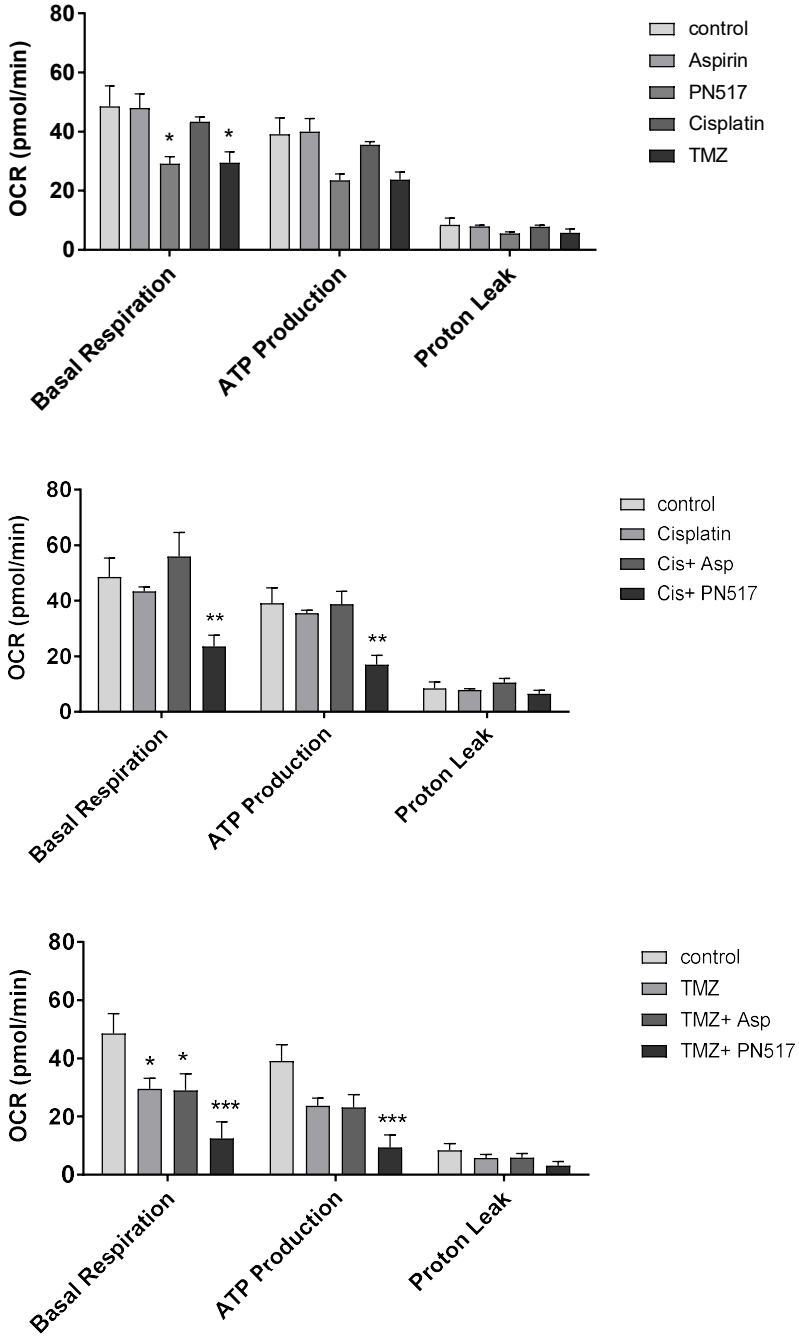

Figure 5. 12. The effect of drug treatment on basal respiration, ATP production and proton leak rates in the SVG-p12 cell line under normoxia. Data shows coupling efficiency spare respiratory capacity generated by Seahorse Report Generator and plotted using GraphPad Prism. Values represent mean ± SEM generated from four independent experiments under normoxia. A two-way ANOVA was used to identify significant effects, with Tukey's multiple comparison test, *P < 0.05; **P < 0.01; ***P < 0.001; ****P < 0.0001. The experimental procedure was performed as described in Materials and Methods section 2.2.12.

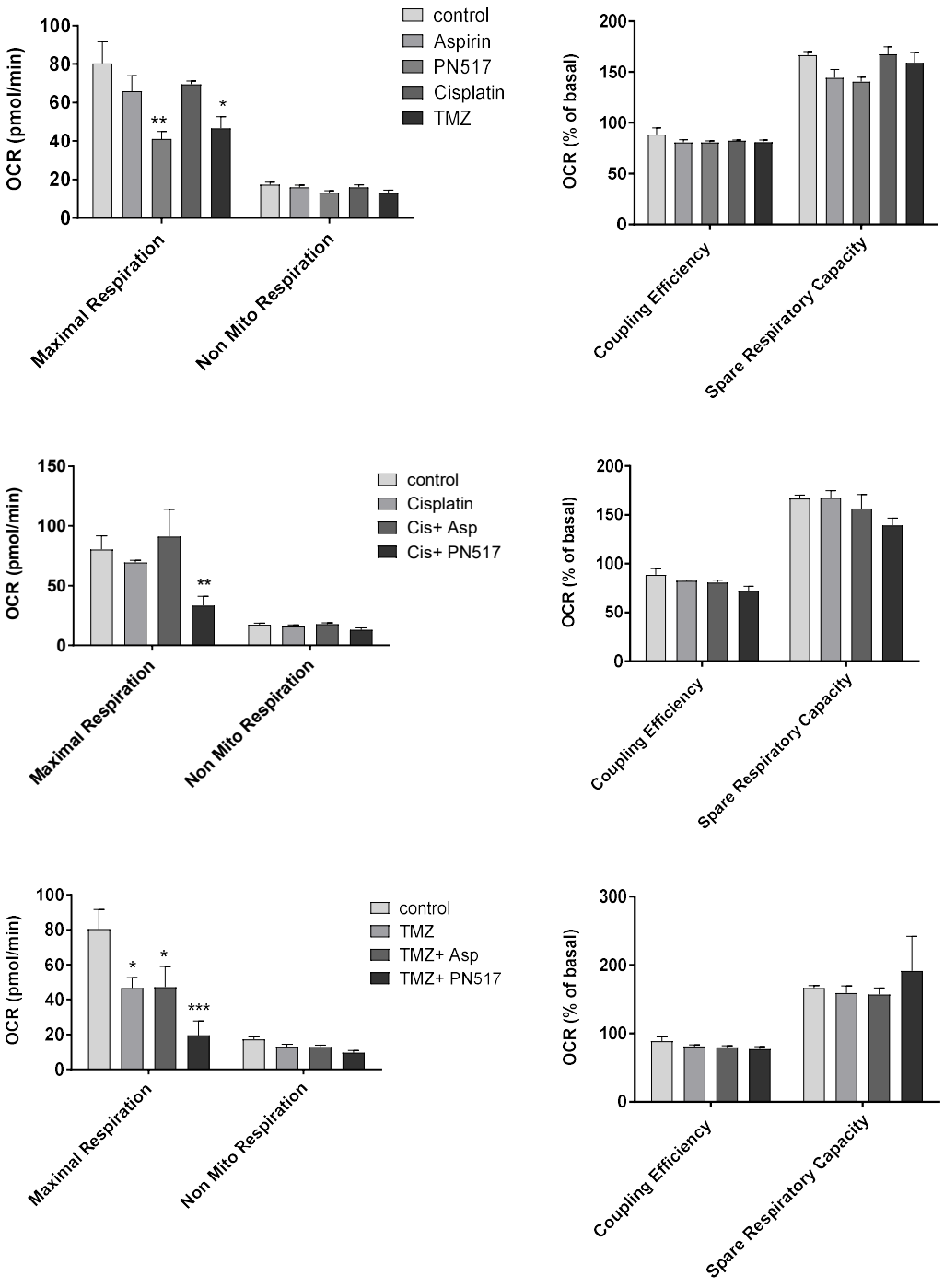

Figure 5. 13. The effect of drug treatment on the maximal respiration, spare respiration and coupling efficiency in the SVG-p12 cell line under normoxia. Data shows coupling efficiency spare respiratory capacity generated by Seahorse Report Generator and plotted using GraphPad Prism. Values represent mean ± SEM generated from four independent experiments under normoxia. A two-way ANOVA was used to identify significant effects, with Tukey's multiple comparison test, *P < 0.05; **P < 0.01; ***P < 0.001; ****P < 0.0001. The experimental procedure was performed as described in Materials and Methods section 2.2.12.

5.2.3. Effects of drug treatment on glycolytic activity

In order to investigate the effects of the drug treatment on the glycolytic activity of the tested cells, the Glycolysis Stress test was performed for U87-MG using Seahorse XFp Extracellular Flux Analyser, under normoxia and hypoxia. The drug treatment was added at IC_{50}, as determined by the cell viability concentration-response curves after 48 hr. Glycolytic profiles and glycolytic bioenergetic parameters were studied in the U87-MG cell line following 24 hr of drug treatment, separately or in combination. In addition, the test was performed for the control SVG-p12 cell line under normoxia.

Generally, the glycolytic function profiles of the U87-MG cell line showed obvious effects for PN517 and TMZ on the extracellular acidification rates, as well as an enhanced effect being observed in the combination of PN517 with cisplatin or TMZ compared to the respective monotherapy (Fig 5.14). Under normoxia, drug treatment with PN517 or TMZ monotherapy significantly reduced the glycolysis rate (47.9 ±3.6 mpH/min, $p<0.05$ and 44.3 ±5.3 mpH/min, $p<0.01$) compared to the control (64.4 ±2.3 mpH/min). Accordingly, these monotherapies produced a significant reduction in the glycolytic capacity (47.2 ±5.6 mpH/min, $p<0.0001$ and 50.7 ±3.3 mpH/min, $p<0.0001$) compared to the control (76.4 ±3.7 mpH/min). Although aspirin also showed a trend towards reducing glycolytic capacity, PN517 was significantly more efficacious than aspirin ($p<0.01$) (Fig 5.15).

PN517 combined with cisplatin significantly enhanced the effect of cisplatin alone in reducing glycolysis rate ($p<0.001$) and glycolytic capacity ($p<0.0001$). Also, PN517 combined with TMZ significantly enhanced the effect of TMZ alone in reducing glycolysis rate ($p<0.05$) and glycolytic capacity ($p<0.001$). Aspirin monotherapy did not produce a significant effect on glycolysis or glycolytic capacity on its own under normoxia ($p>0.05$), but in combination it enhanced the effect of cisplatin ($p>0.001$) and TMZ ($p>0.05$) (Fig 5.15).

A similar pattern of effect was observed under hypoxia. Both PN517 and TMZ significantly reduced glycolytic capacity compared to the control ($p<0.05$ and $p<0.01$, respectively). Cisplatin combined with PN517 significantly reduced glycolysis rate ($p<0.01$) and glycolytic capacity ($p<0.0001$). Also, cisplatin

combined with aspirin significantly reduced glycolytic capacity (p<0.01). TMZ combined with PN517 significantly reduced glycolysis rate (p<0.05) and glycolytic capacity (p<0.01). Finally, TMZ combined with aspirin significantly reduced glycolysis rate (p<0.0001) and glycolytic capacity (p<0.0001) (Fig 5.15).

With regards to non-glycolytic acidification rates, PN517 and TMZ appeared to reduce ECAR rates, however only the combinations of TMZ with aspirin or PN517 showed significant differences compared to the control (p<0.05 and p<0.01) (Fig. 5.16). No significant effect was observed for the drug treatments on the glycolytic reserve (p>0.05) (Fig 5.17).

Regarding the SVG-p12 cell line, a similar pattern of effect of drug treatments was observed in general under normoxia to the U87-MG cell line, with PN517 and TMZ producing the greatest effect on glycolytic activity (Fig 5.18). Similar to U87-MG cell, PN517 and TMZ seemed to reduce glycolysis rate but no significant differences were observed (p>0.05). However, the combinations of PN517 with cisplatin or TMZ significantly reduced the glycolysis rate in SVG-p12 cells (p<0.05 and p<0.01, respectively) (Fig 5.19).

Glycolytic capacity rates of SVG-p12 cells exhibited a similar pattern of effect to U87-MG following drug treatment. Only PN517 and TMZ significantly reduced glycolytic capacity (p<0.05). Additionally, PN517 combined with cisplatin significantly enhanced the effect of cisplatin (p<0.001) and TMZ (p<0.01) (Fig 5.19). Although PN517, TMZ and PN517 combinations appeared to reduce the non-glycolytic acidification rates, there were no significant differences (p>0.05) (Fig 5.20). Moreover, there was no significant effect for any of the drug treatments on the glycolytic reserve (p>0.05) (Fig 5.20).

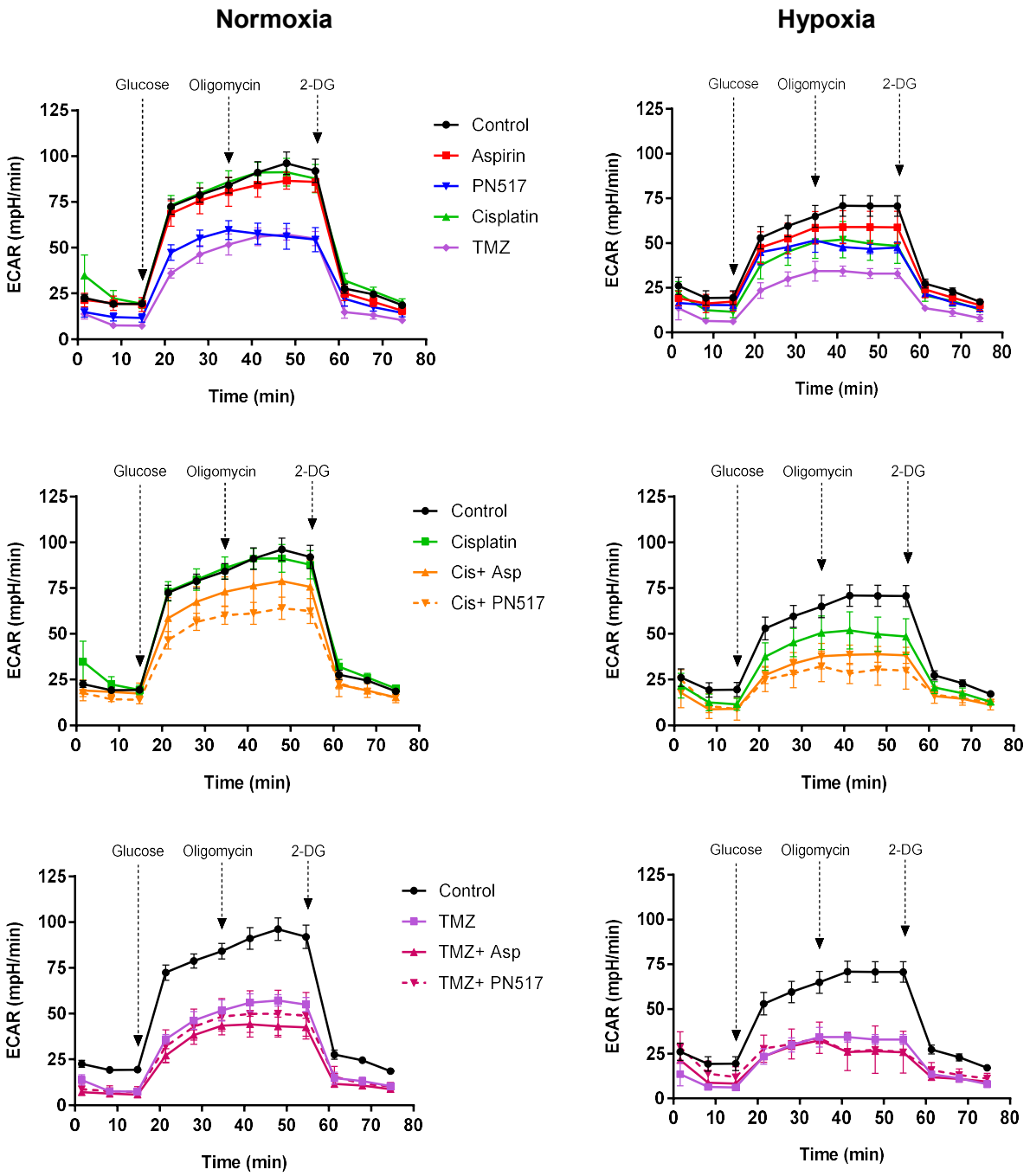

Figure 5. 14. The effect of drug treatment on glycolytic activity in the U87-MG cell line under normoxia and hypoxia. A glycolysis stress test was performed using XFp Extracellular Flux Analyser following drug treatment for 24 hr and extracellular acidification rates were measured using sequential addition of glucose (10mM final), oligomycin (1µM final), and 2-deoxyglucose (2-DG; 50mM final). Arrows indicate the points at which the indicated compounds were added. Values represent mean ± SEM generated from five independent experiments under normoxia and three independent experiments under hypoxia. A two-way ANOVA was used to identify significant effects, with Tukey's multiple comparison test. The experimental procedure was performed as described in Materials and Methods section 2.2.12.

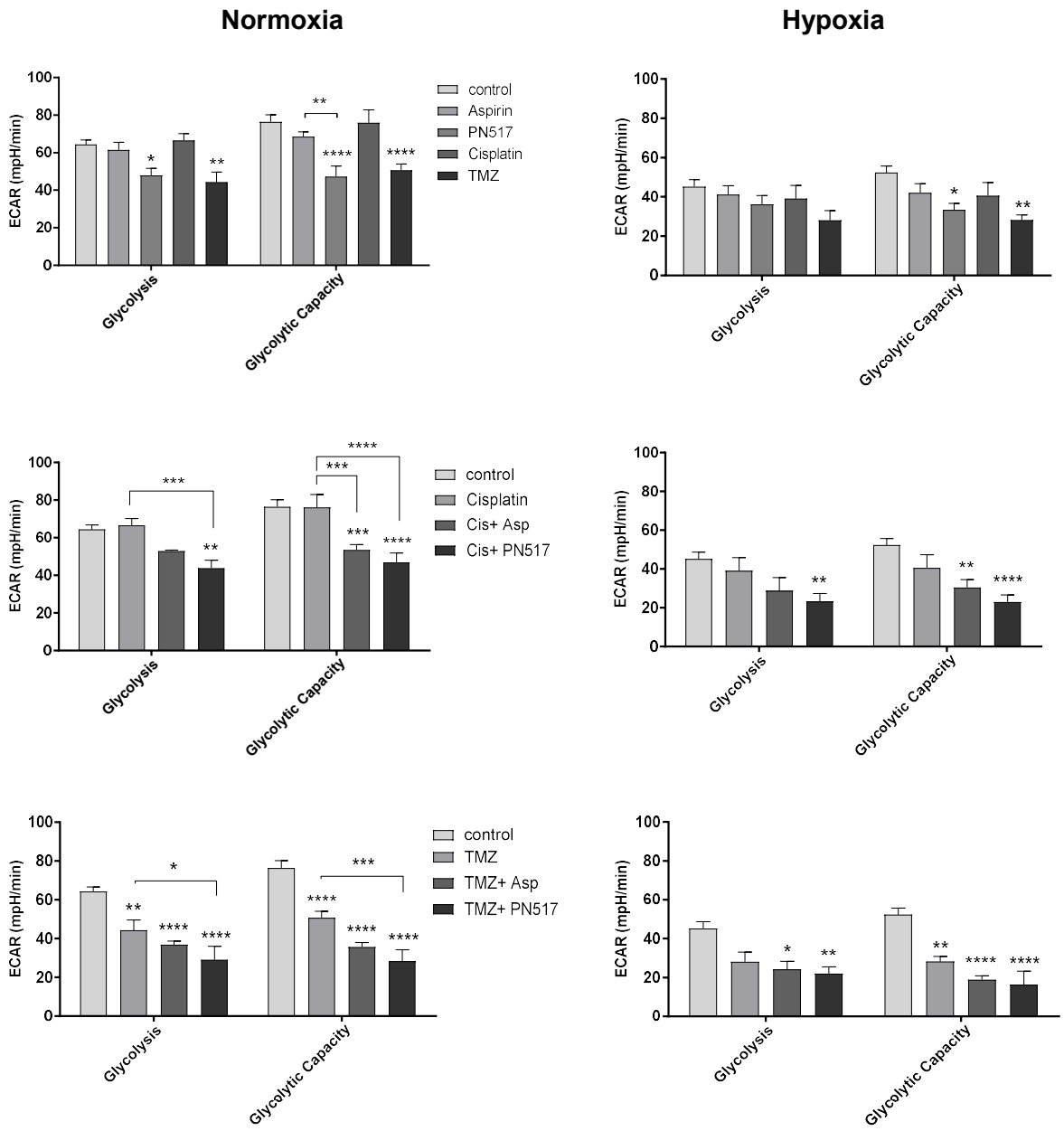

Figure 5. 15. The effect of drug treatment on glycolysis, and glycolytic capacity rates in the U87-MG cell line under normoxia and hypoxia. Data shows glycolysis and glycolytic capacity rates generated by Seahorse Report Generator and plotted using GraphPad Prism. Values represent mean ± SEM generated from five independent experiments under normoxia and three independent experiments under hypoxia. A two-way ANOVA was used to identify significant effects, with Tukey's multiple comparison test, *P < 0.05; **P < 0.01; ***P < 0.001; ****P < 0.0001. The experimental procedure was performed as described in Materials and Methods section 2.2.12.

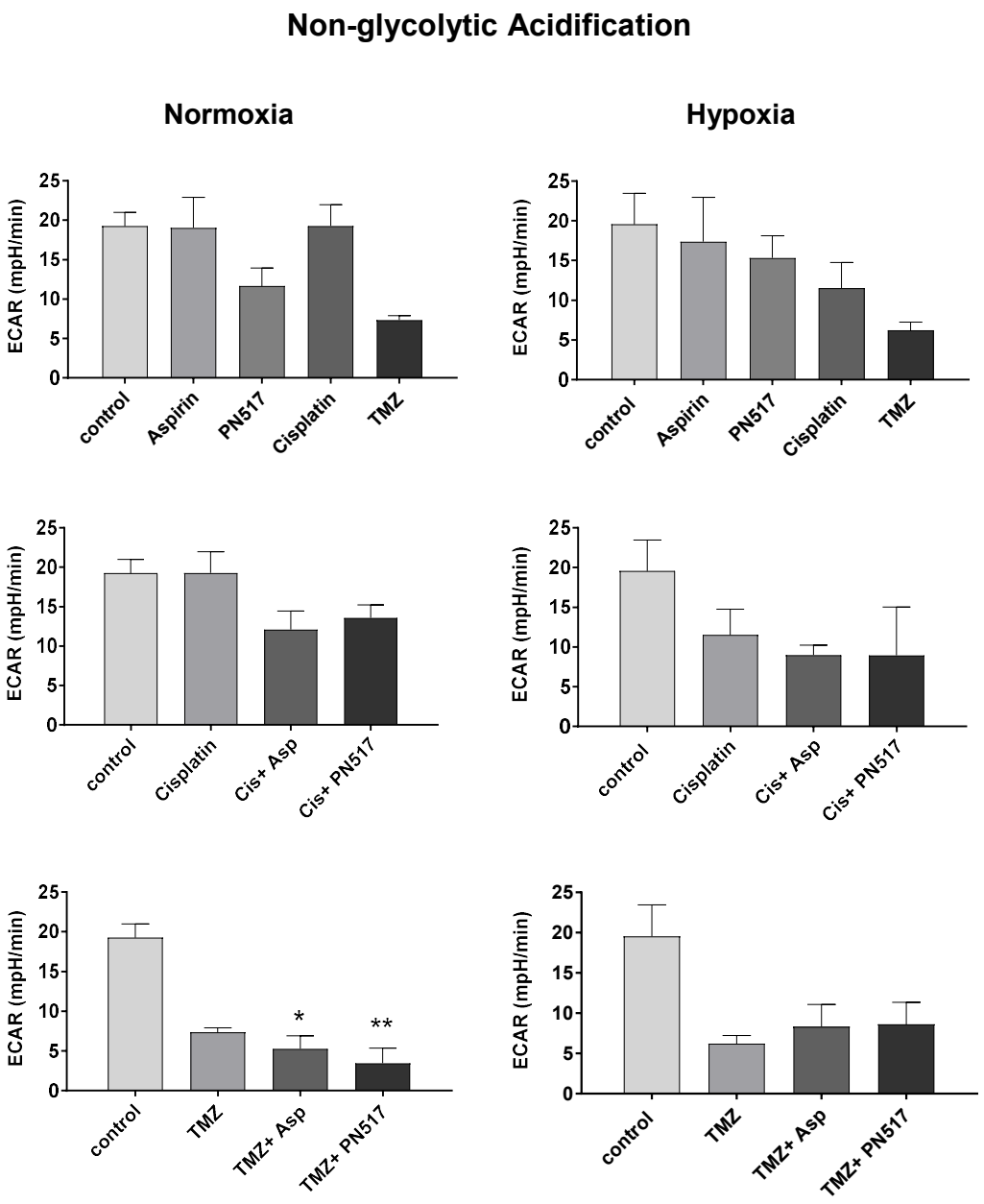

Figure 5. 16. The effect of drug treatment on the non-glycolytic acidification rate in the U87-MG cell line under normoxia and hypoxia. Data shows glycolysis and glycolytic capacity rates generated by Seahorse Report Generator and plotted using GraphPad Prism. Values represent mean ± SEM generated from five independent experiments under normoxia and three independent experiments under hypoxia. A two-way ANOVA was used to identify significant effects, with Bonferroni's multiple comparison test, *P < 0.05; **P < 0.01; ***P < 0.001; ****P < 0.0001. The experimental procedure was performed as described in Materials and Methods section 2.2.12.

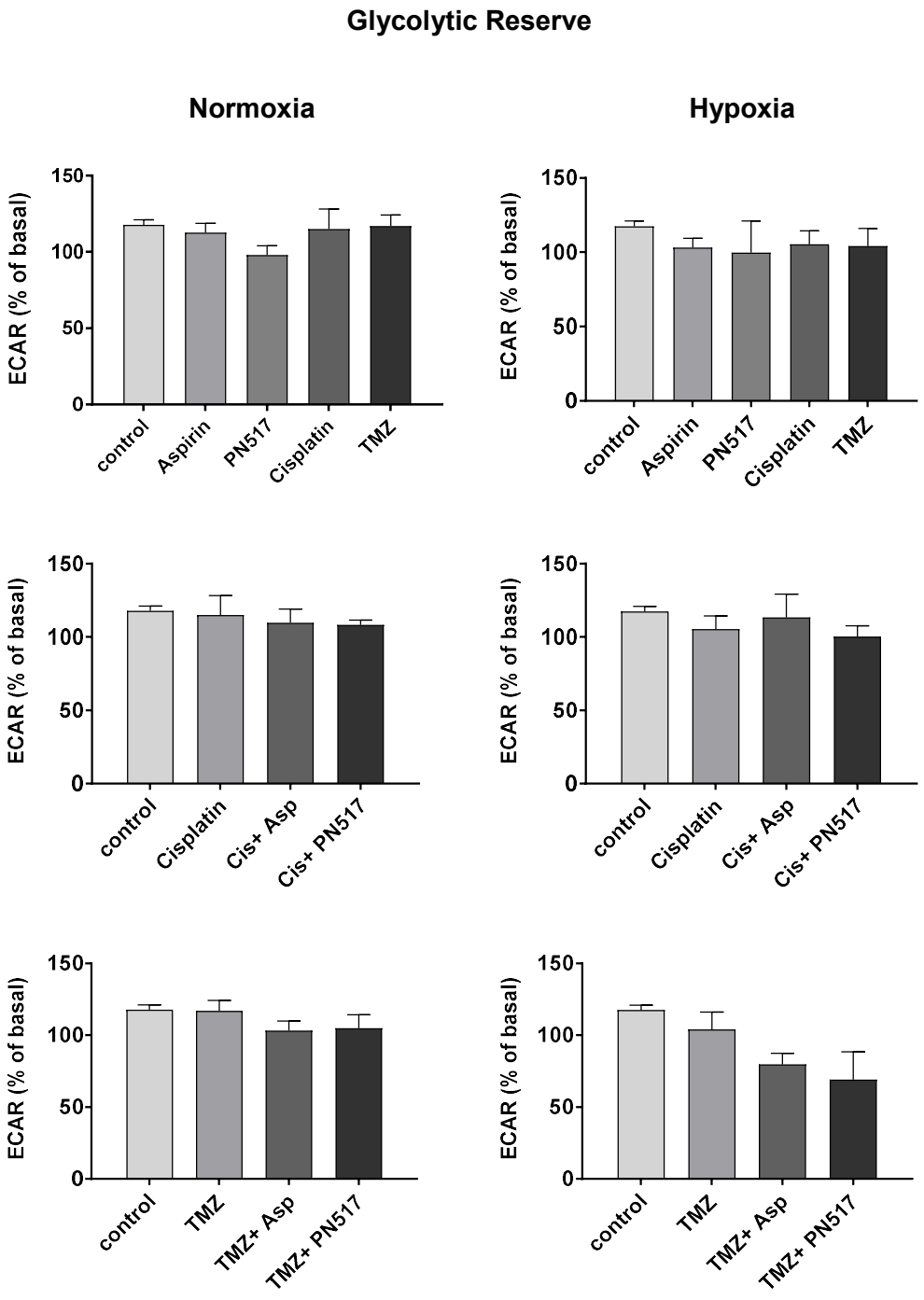

Figure 5. 17. The effect of drug treatment on the glycolytic reserve rate in the U87-MG cell line under normoxia or hypoxia. Data shows glycolysis and glycolytic capacity rates generated by Seahorse Report Generator and plotted using GraphPad Prism. Values represent mean ± SEM generated from five independent experiments under normoxia and three independent experiments under hypoxia. A two-way ANOVA was used to identify significant effects, with Bonferroni's multiple comparison test, *P < 0.05; **P < 0.01; ***P < 0.001; ****P < 0.0001. The experimental procedure was performed as described in Materials and Methods section 2.2.12.

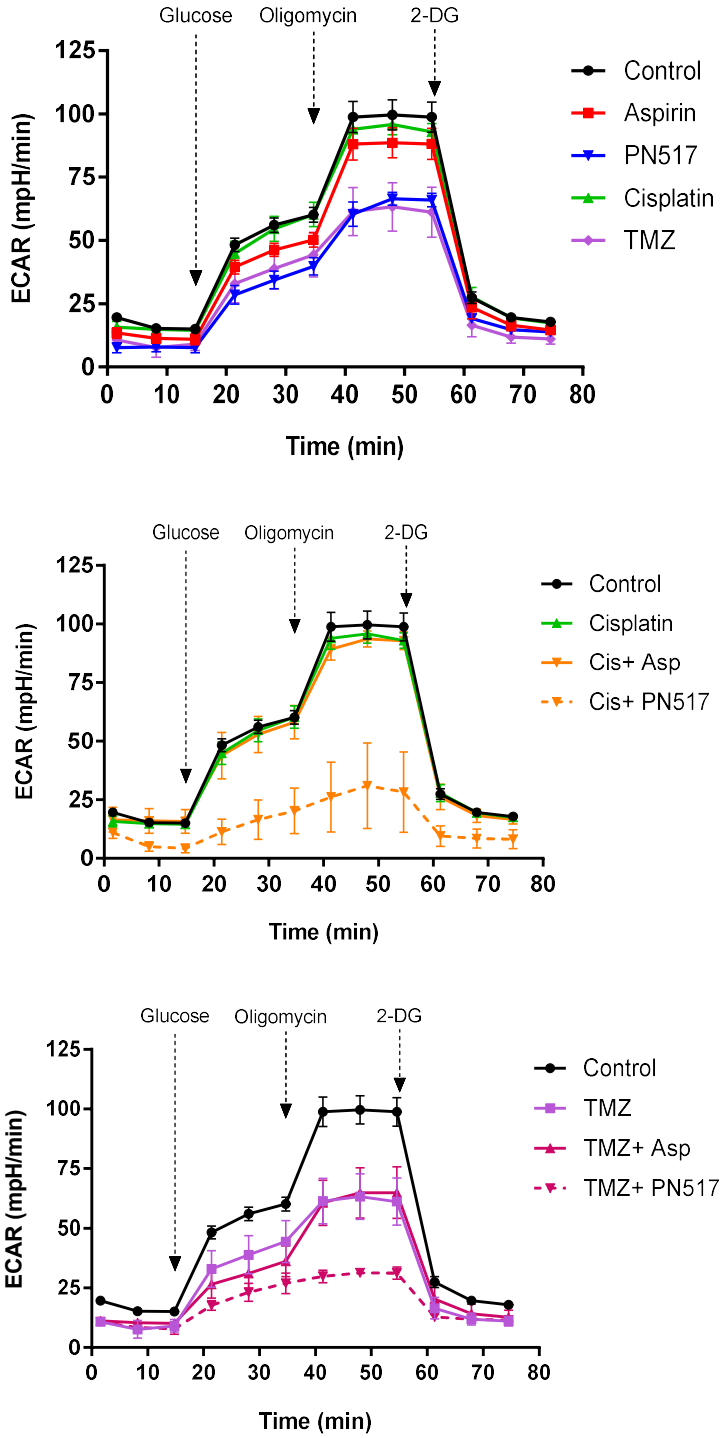

Figure 5. 18. The effect pf drug treatment on glycolytic activity in SVG-p12 cell line under normoxia. A glycolysis stress test was performed using XFp Extracellular Flux Analyser following drug treatment for 24 hr and extracellular acidification rates were measured using sequential addition of glucose (10mM final), oligomycin (1µM final), and 2-deoxyglucose (2-DG; 50mM final). Arrows indicate the points at which the indicated compounds were added. Values represents mean ± SEM generated from four independent experiments under normoxia. A two-way ANOVA was used to identify significant effects, with Tukey's multiple comparison test. The experimental procedure was performed as described in Materials and Methods section 2.2.12.

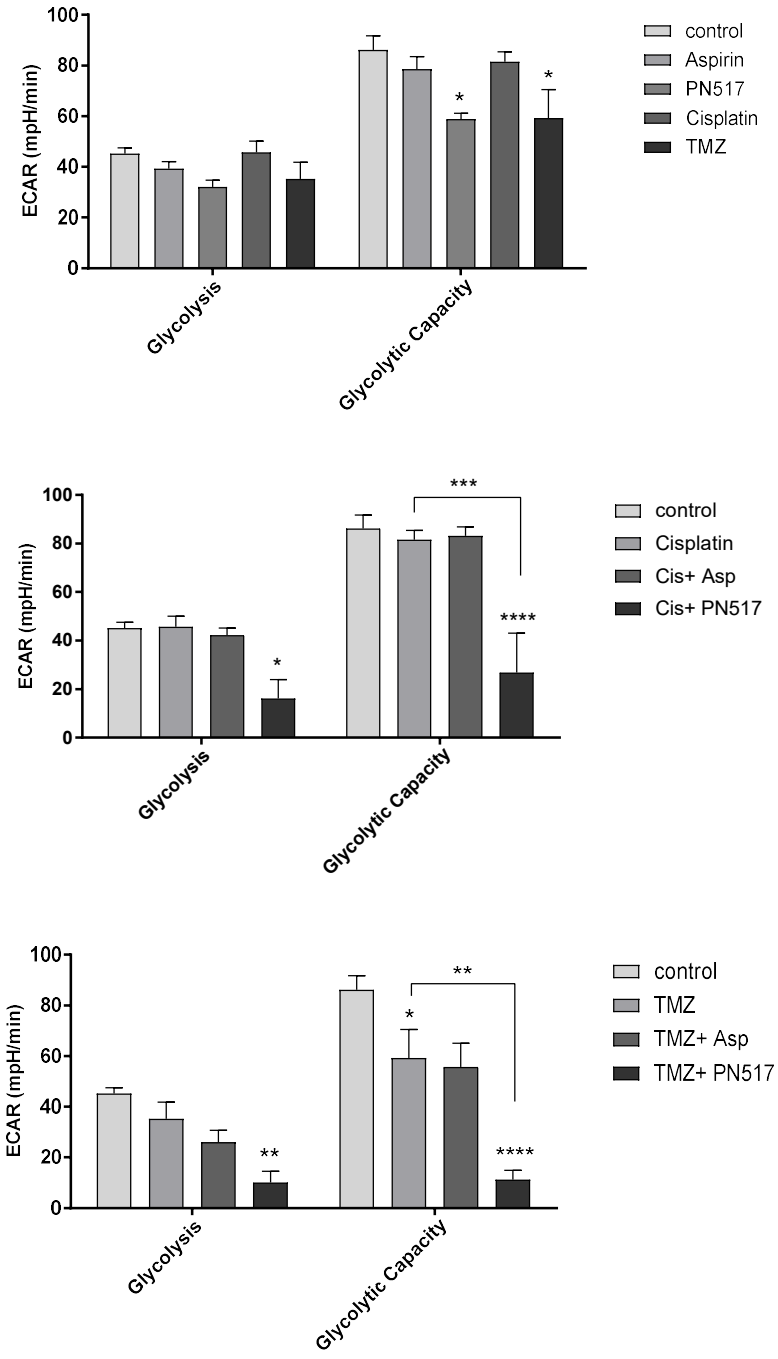

Figure 5. 19. The effect of drug treatment on glycolysis and glycolytic capacity rates in the SVG-p12 cell line under normoxia. Data shows glycolysis and glycolytic capacity rates generated by Seahorse Report Generator and plotted using GraphPad Prism. Values represent mean ± SEM generated from four independent experiments under normoxia. A two-way ANOVA was used to identify significant effects, with Tukey's multiple comparison test, *P < 0.05; **P < 0.01; ***P < 0.001; ****P < 0.0001. The experimental procedure was performed as described in Materials and Methods section 2.2.12.

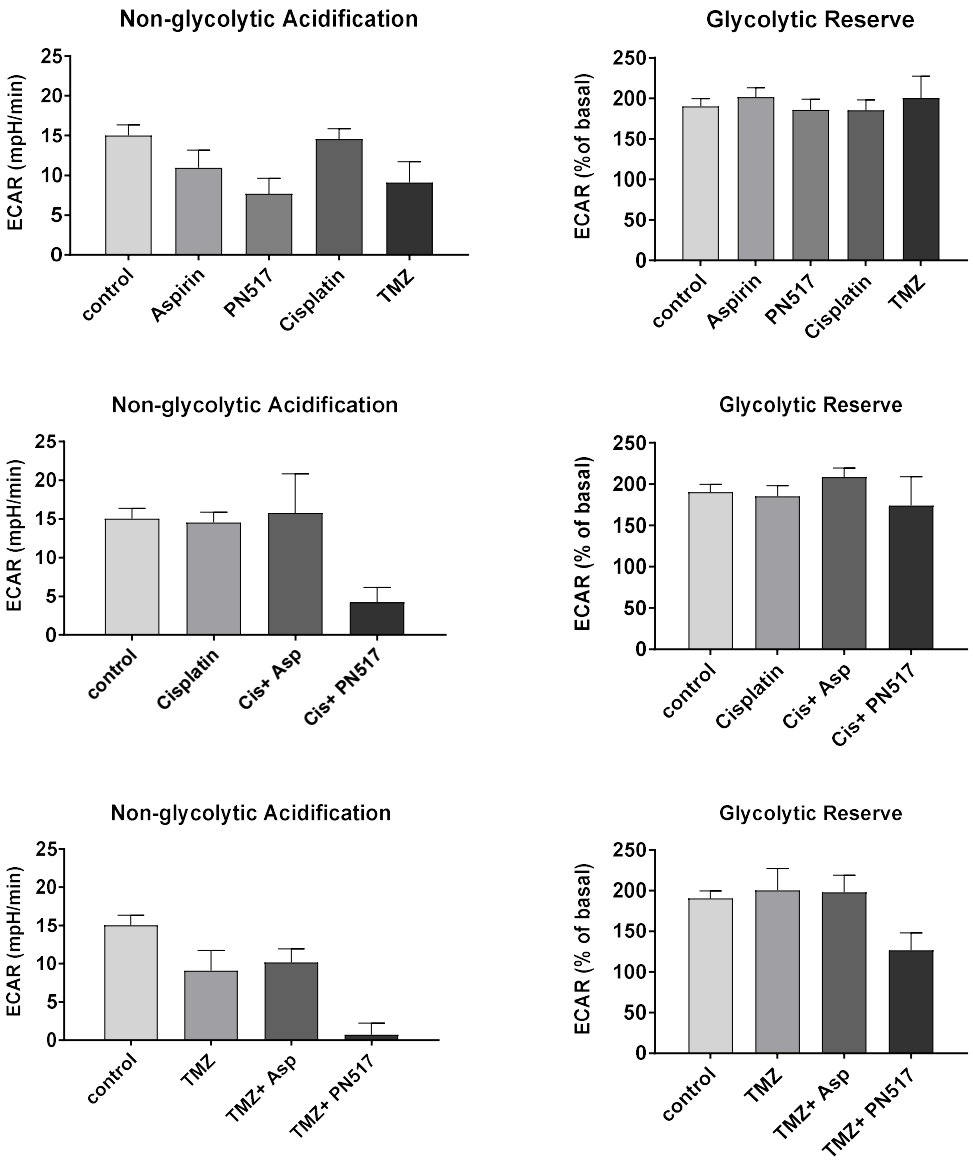

Figure 5. 20. The effect of drug treatment on non-glycolytic acidification and glycolytic reserve rates in the SVG-p12 cell line under normoxia. Data shows glycolysis and glycolytic capacity rates generated by Seahorse Report Generator and plotted using GraphPad Prism. Values represent mean ± SEM generated from four independent experiments under normoxia. A two-way ANOVA was used to identify significant effects, with Bonferroni's multiple comparison test, *P < 0.05; **P < 0.01; ***P < 0.001; ****P < 0.0001. The experimental procedure was performed as described in Materials and Methods section 2.2.12.

5.2.4. Effects of drug treatment on lactate production

Another method to examine the effect of drug treatment on glycolysis activity is by measuring the lactate excretion by cells. Drug treatments were added, separately or in combination, to the U87-MG cell line under normoxia and hypoxia at IC_{50} as determined by the cell viability concentration-response curves after 48 hr. Following 24 hr of drug treatment the culture media was replaced with assay media and incubated for 3.5 hr then samples were collected and frozen. After collecting the samples for five independent experiments, the change in the lactate concentration in the extracellular assay media was measured using EnzyFluo™ L-lactate fluorometric assay.

Data showed that all drug treatments appeared to reduce lactate production under both conditions with PN517 and TMZ showing the greatest effect of the monotherapy (Fig 5.21). However, TMZ was the sole monotherapy to produce a significant reduction in lactate concentration under normoxia compared to the control (28.8 ±3.2 μM vs. 47.9 ±4.1 μM, $p<0.05$). With regards the combined therapy, a significant reduction in lactate concentration was observed with the combination of PN517 and cisplatin (30.1 ±4.5 μM vs. 47.9 ±4.1 μM, $p<0.05$). A similar result was produced by the combination of aspirin and TMZ (30.8 ±3.2 μM vs. 47.9 ±4.1 μM, $p<0.05$), and the greatest reduction in the lactate concentration was observed with the combination of PN517 and TMZ (24 ±2.8 μM vs. 47.9 ±4.1 μM, $p<0.001$). Under hypoxia, a similar pattern of effect was observed following drug treatment. However, only TMZ and its combinations produced a significant decrease in lactate production. The lactate concentration was reduced to 32.1 ±3.7 μM compared to 49.2 ±4.1 μM in the control ($p<0.05$). Although the combination effect of TMZ and aspirin was significant ($p<0.05$), it did not seem to enhance the efficacy of TMZ monotherapy. In contrast the combination with PN517 enhanced the efficacy of TMZ and produced the greatest reduction in lactate production ($p<0.01$) (Fig 5.21).

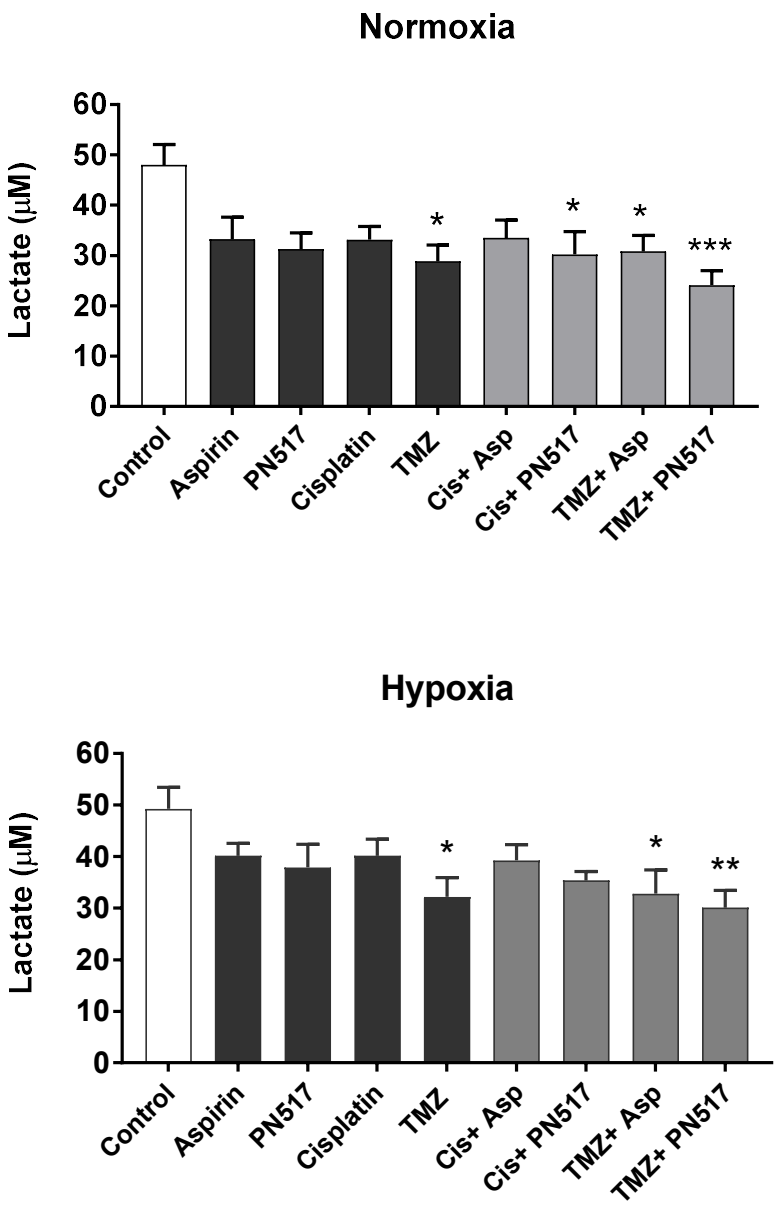

Figure 5. 21. The effect of drug treatment on lactate production in the U87-MG cell line under normoxia and hypoxia. Data represent lactate concentration (μM) after treating cells for 24 hr and incubating with assay media to excrete lactate for 3.5 hr. Values represent mean ± SEM generated from five independent experiments under normoxia and hypoxia. A two-way ANOVA was used to identify significant effects, with Bonferroni's multiple comparison test, *P < 0.05; **P < 0.01; ***P < 0.001; ****P < 0.0001. The experimental procedure was performed as described in Materials and Methods section 2.2.13.

5.2.5. Effects of drug treatment on GAPDH enzymatic activity

To further characterise the effect of the drug treatment on the glycolytic activity, the enzymatic activity of GAPDH was investigated following 24 hr of drug treatment in U87-MG cell line under, normoxia and hypoxia. The drug treatment was added, separately or in combination, to the U87-MG cell line at IC_{50} as determined by the cell viability concentration-response curves after 48 hr. GAPDH activity was monitored following drug treatment using GAPDH activity colorimetric assay kit in kinetic mode.

The results showed that under normoxia GAPDH activity was marginally reduced with aspirin treatment but was reduced to a much greater extent by PN517 (Fig 5.22). Cisplatin also induced a small reduction in enzyme activity and the effect was greater with TMZ. PN517 showed the greatest effect among all monotherapies and it was the single treatment which produced statistically significant changes compared to the control (58.5 ±6.5% vs. 100%, $p>0.05$). Generally, the drug combinations showed lower levels of GAPDH enzymatic activity compared to the monotherapy and both aspirin and PN517 appeared to enhance the effect of cisplatin and TMZ, however, only PN517 combinations with either cisplatin or TMZ produced a significant reduction in the enzyme activity compared to control. The combination of PN517 with cisplatin or TMZ reduced the percentage of GAPDH activity to 52.9 ±5.7% and 51.5 ±3.2% respectively ($p<0.05$).

Under hypoxia, the overall levels of GAPDH activity following drug treatment were higher compared to normoxia, but a similar pattern of treatment effect was observed (Fig 5.22). PN517 appeared to have the greatest efficacy among monotherapies (63 ±7.3%), however, no significant differences were found with any of the monotherapies compared to the control ($p>0.05$). Regarding drug combinations, both aspirin and PN517 enhanced the efficacy of cisplatin and TMZ but only PN517 combinations produced significant differences compared to the control. The combination of PN517 with cisplatin or TMZ reduced the percentage of GAPDH activity to 58.1 ±5.4% and 61.8 ±4.8% respectively ($p<0.05$).

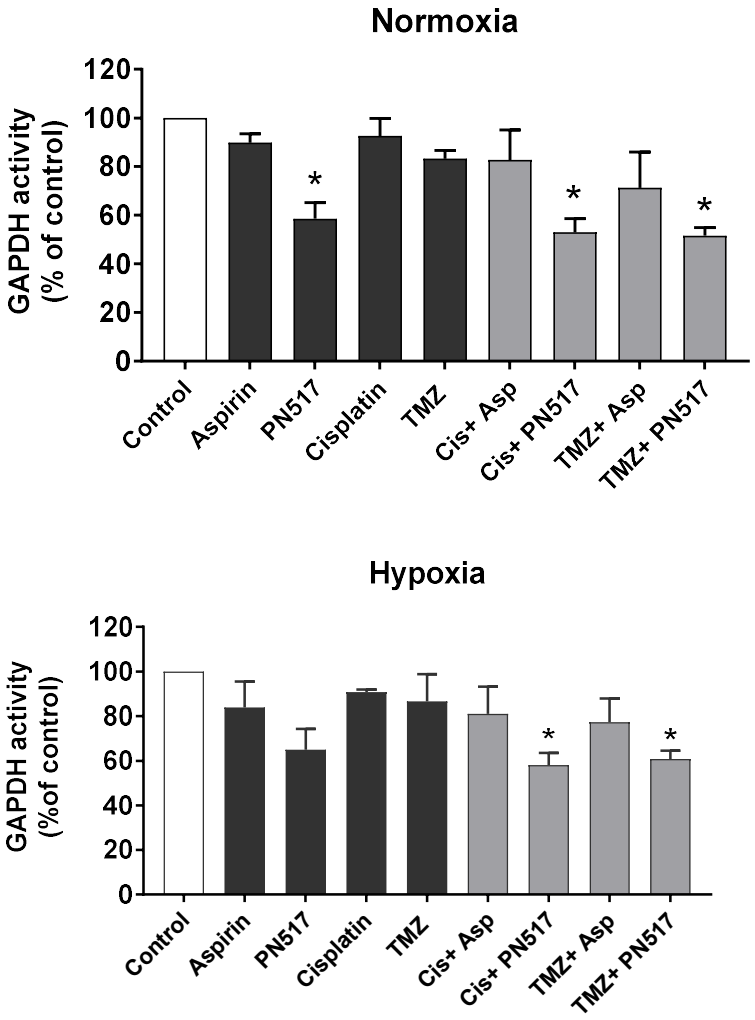

Figure 5. 22. The effect of drug treatment on GAPDH enzymatic activity in the U87-MG cell line under normoxia and hypoxia. Data represent GAPDH enzymatic activity as percentage of control after drug treatment for 24 hr and measuring enzymatic activity in kinetic mode. Values represent mean ± SEM generated from two independent experiments under normoxia and hypoxia. A two-way ANOVA was used to identify significant effects, with Bonferroni's multiple comparison test, *P < 0.05; **P < 0.01; ***P < 0.001; ****P < 0.0001. The experimental procedure was performed as described in Materials and Methods section 2.2.14.

5.3. Discussion

5.3.1. Metabolic characterisation of the cell lines

Normal cells generate ATP and biosynthetic precursors through a combination of multiple metabolic pathways; mainly by oxidative phosphorylation and glycolysis. Cancer cells, on the other hand, dramatically reprogram their metabolism to support rapid and invasive growth (Barger and Plas, 2010). Collective evidence confirm that cancer cells undergo a complex metabolic reprogramming to meet the increased demands for macromolecules and energy for proliferation. This altered metabolism links with oncogene activation or loss of tumour suppressor genes in various signalling pathways resulting in competitive advantages for transformed cells (Hanahan and Weinberg, 2011).

Understanding cancer cellular metabolism and its regulatory pathways has now become a major area of cancer research, and usage of an extracellular flux analyser has provided a powerful tool for investigating the cellular bioenergetics and reduced the need for using other more difficult techniques. Through extracellular flux analysis metabolic programming of individual cancer cell types can be characterised and used to identify metabolic liabilities driving cancer cell progression and proliferation. In the current study, the Seahorse XFp Extracellular Flux Analyser was employed for monitoring shifts in substrate utilization and metabolism of GBM cells through measurement of OCR, as an indicator of mitochondrial respiration, and ECAR, as an indicator of glycolysis. Moreover, measuring the metabolic pathways in GBM cells and their compensatory interplay is important for understanding cellular drug resistance and discovering potential drugs relatively specific for cancer cells.

A comparison of the cellular bioenergetics and metabolic pathways between the glioblastoma cell line (U87-MG) and the non-cancerous control cell line (SVG-p12) was performed with results showing a significant change in the metabolism phenotyping between the two cell lines (Fig 5.3 &5.4). As anticipated, a significant metabolic alteration consistent with Warburg effect was observed in U87-MG cells with large shift towards glycolysis compared to SVG-p12 cells (Fig 5.4 &5.6). U87-MG cells exhibited significantly higher rates of proton production (ECAR)

following glucose injection compared to SVG-p12 cells. Bioenergetic profiles showed that SVG-p12 cells efficiently use both oxidative phosphorylation and glycolysis pathways. These cells displayed high basal respiration that increased even more in the presence of FCCP (Fig 5.3). It was noted that SVG-p12 glycolysis increased in the presence of glucose and that almost doubled in the presence of oligomycin, indicating that these cells possess both an important respiratory reserve and glycolytic reserve. U87-MG cells, in contrast, were highly glycolytic with higher glucose-stimulated proton production compared to SVG-p12, which is near maximal, given the minimal increase in lactate production when oligomycin was added (Fig 5.4). U87-MG basal respiration was significantly lower than SVG-p12 indicating that U87-MG cells rely almost exclusively on glycolysis, usually due to low mitochondrial content or dysfunction. However, it is worth noting that U87-MG maximal respiration doubles in the presence of FCCP, and the spare respiratory capacity was significantly higher than SVG-p12 with similar coupling efficiency, all suggesting that mitochondrial respiratory function is still intact.

Despite the initial hypothesis of Warburg that aerobic glycolysis in cancer cells is caused by inherent mitochondrial dysfunction, several lines of evidence indicate that the oxidative capacity of mitochondria is intact in cancer cells with no overt defects on oxidative metabolism (Zu and Guppy, 2004). Many reports have supported this theory and established that cancer cells exhibit a glycolytic phenotype despite functionally active mitochondria (Fantin *et al.*, 2006). It has been clarified that cancer cells tend towards aerobic glycolysis despite the mitochondrial capacity indicating that the glycolytic phenotype is sufficient to satisfy the fundamental requirements for cell proliferation and progression (Vander Heiden *et al.*, 2009). Previous study showed that the mitochondria in human astrocytoma cells taken from different patient biopsies display heterogeneous pathological transformations which were attributable to cellular variability and diversity of microenvironment conditions of these tumours (Arismendi-Morillo and Castellano-Ramirez, 2008). Although that study suggested that most of astrocytoma cells are inable to produce satisfactory amount of energy via oxidative phosphorylation, the ultrastructural mitochondrial pathology indicated that possibly both glycolytic inhibition and mitochondrial

respiration inhibition or down-regulation would be potential target for therapeutic strategies of astrocytoma tumours (Arismendi-Morillo and Castellano-Ramirez, 2008).

Based on the findings of this study, it can be hypothesized that the U87-MG metabolic phenotype reflects altered bioenergetic requirements to support proliferation and that the glycolytic pathway seems to be the main source of energy in U87-MG cells. This assumption is supported by the observation that exposure to oligomycin did not significantly increase ECAR and the cells showed very little glycolytic reserve (Fig 5.4). As they do not consume much oxygen to generate ATP by oxidative phosphorylation, they are relying nearly on their maximum glycolytic capacity to compensate ATP production. Increased glycolysis flux supports the proliferation of cancer cells by generating additional energy in the form of ATP and providing glucose-derived metabolic intermediates for nucleotide, lipid, and protein biosynthesis (Locasale, 2013).

A large number of studies have reported metabolic alterations and a switch to glycolytic activity exhibiting the Warburg effect in different cancer cells, indicating that targeting the resulting metabolic phenotypes may be a productive therapeutic strategy (Hardie *et al.*, 2017). For example, phenotypic analysis of pancreatic cancer cells showed metabolic changes consistent with mitochondrial dysfunction, including reduced oxygen consumption and increased glycolysis (Hardie *et al.*, 2017). Another study profiled the metabolic phenotype of two human non-small cell carcinoma cell lines, H460 and A549. Both cell lines displayed a dependency on glycolysis, however, H460 cells were shown to be more glycolytic than A549 cells having a greater impairment of mitochondrial respiration (Wu *et al.*, 2007). The relationship between metabolism and malignant transformation was analysed at different stages of oncogenic progression. Transformation of fibroblasts by H-RasV12/E1A oncogenes increased oxidative phosphorylation activity, accompanied by cell death at low passage number whereas in high passage number cells, OCR declined while ECAR increased consistent with the Warburg effect, leading to increased growth rates and tumour forming potential (De Groof *et al.*, 2009). The cells in this study were used over a range of relatively low passage number and displayed consistent results. That

would indicate that passage number has not played a role in the current results and the observed metabolic phenotyping of U87-MG cells is due to its characteristics.

GBM, like most cancers, presents the fundamental metabolic phenomenon, the Warburg effect, where cancer cells utilize aerobic glycolysis as the primary source of ATP (Deberardinis *et al.*, 2008; Jones and Thompson, 2009). Furthermore, studies showed that reversal of the Warburg effect could inhibit U87-MG cell proliferation indicating that the modulation of GBM cell bioenergetics and reversal of Warburg effect might provide a novel therapy for GBM. A higher extracellular acidification rate and maximal mitochondrial respiration rate has been observed in U87-MG cells compared to neuroblastoma SH-SY5Y cells (Poteet *et al.*, 2013). It was demonstrated that lactate dehydrogenase expression levels were higher in U87-MG cells and primary cultured astrocytes than in SH-SY5Y cells and neurons. In addition, it was found that mRNA levels of succinate dehydrogenase and peroxisome proliferator-activated receptor-γ were high in U87-MG cells, suggesting high capacity for mitochondrial metabolism and uptake of fatty acids related to synthesis of the cell membrane, respectively (Kim *et al.*, 2015).

In a recent study by Hujber and colleagues, significant differences in the metabolic phenotype was found between different glioma cell lines (Hujber *et al.*, 2018). The lowest respiration rate was produced by U87-MG cell line, while the highest basal rate was observed in U373 MG cell line. Furthermore, the highest lactate production rate following glucose addition, regardless of the presence of a mitochondrial respiratory inhibitor or not, was observed in U87-MG cell line. The authors also reported that the glutaminolysis-driven respiratory capacity was significantly higher in U251 cell line than in U87 MG or U373 MG. In contrast, U373 MG cells, which have both high glucose utilisation and high respiratory capacity, exhibited the fastest proliferation rate. Their data also revealed that IDH1 mutation and related 2-hydroxyglutarate (2-HG) accumulation led to increase in the basal respiration and decrease in the glycolytic capacity (Hujber *et al.*, 2018). Other studies also have asserted that α-ketoglutarate (α-KG), an intermediate metabolite in the Krebs cycle, and the associated amino acid

glutamate play central role in the metabolic alterations of glioma cells (Maus and Peters, 2017). These findings support the current obtained data where U87-MG cells exhibited clear glycolytic activity with low mitochondrial respiratory activity, and may suggest that other metabolic pathways like glutamate metabolism can play an important role in the cells survival (Fig 5.5 &5.6).

Interestingly, recent studies have indicated that there is very wide variation in cancer cell metabolic phenotypes within different tumours of the same cancer type, meaning one cell line could show different responsiveness to chemotherapy drugs to other cell lines of the same cancer (Dar *et al.*, 2017). Cellular bioenergetic profiling of numerous ovarian cancer cell lines revealed significant bioenergetics diversity and showed heterogeneity in using glycolysis or oxidative phosphorylation as energy sources. For instance, chemosensitive ovarian cancer cell lines (A2780 and PEO1) exhibited a glycolytic phenotype, whereas the chemoresistant cell lines (C200 and PEO4) revealed a high metabolically active phenotype with a metabolic flexibility in using different energy pathways and ability to switch between oxidative phosphorylation or glycolysis (Dar *et al.*, 2017). Therefore, it can be concluded from the previous studies that the results obtained in this study using U87-MG cell line might be different when using other GBM cell line with different metabolic phenotyping, which would also have an impact on the drug treatments efficacy. Accordingly, it can be suggested that glioma biopsy would need to be metabolically profiled before a treatment option for a patient was selected.

Several oncogenes and tumour suppressors have been shown to play a role in metabolic regulation of cancer cells. Different oncogenic proteins like PI3 kinase, AKT, and RAS as well as tumour suppressors such as PTEN, retinoblastoma, and p53 have been reported to play a role in directing the metabolic transformation of cancer cells (Levine and Puzio-Kuter, 2010; Iurlaro *et al.*, 2014). Additionally, other factors associated with the proliferation or survival of cancer cells, such as NF-κB, have also been shown to regulate cancer cellular metabolism (Hayden and Ghosh, 2004; Levine and Puzio-Kuter, 2010). Accordingly, different bioenergetic pathways within glioma cells have been reported to critically contribute to tumour biology and connect to pro-oncogenic

signalling such as AMPK, mTOR and HIF signalling (Strickland and Stoll, 2017). For example, one study demonstrated that microRNA-451 regulates LKB1/AMPK signalling and allows adaptation to metabolic stress in glioma cells (Godlewski *et al.*, 2010). Furthermore, mutations in p53 and isocitrate dehydrogenase IDH1 and IDH2 have been implicated in oncogenic signalling and establishing metabolic phenotypes in genetically-defined subsets of malignant glioma (Godlewski *et al.*, 2010). Specific mutations in IDH were shown to be linked to tumorigenesis particularly in GBM and acute myeloid leukaemia (Yan *et al.*, 2009) but not other tumours (Bleeker *et al.*, 2009). Therefore, multiple signalling pathways might be involved in the metabolic phenotyping observed with U87-MG cells in the current study which would be interesting to identify and target these metabolic liabilities.

In WHO grade II/III gliomas, mutations in IDH are the most prevalent genetic abnormalities and IDH-mutated tumours comprises approximately 80% of all clinical cases (Zhong *et al.*, 2009; Suzuki *et al.*, 2015). Emerging studies have demonstrated greater sensitivity to chemotherapy in low-grade gliomas and secondary GBMs, and the occurrence of IDH mutations predicts longer survival clinically (Suzuki *et al.*, 2015). Neomorphic changes in IDH enzyme redirect carbon-based metabolites into unusable 2-HG leading to reprogramming of the Krebs cycle by altering glutamine utilization and pyruvate metabolism. The metabolic reprogramming and compromised oxidative metabolism may restrict physiologically important metabolic routes, such as ATP generation and macromolecule synthetic pathways resulting in the increased vulnerability of IDH1 mutant cells to cancer treatment (Dang *et al.*, 2009; Izquierdo-Garcia *et al.*, 2015). These observations were reported by different studies. For example, IDH1 mutation was shown to increase U87-MG glioma cell sensitivity to radiation therapy in mild hypoxic conditions (Wang *et al.*, 2014). Also, the defects found in oxidative metabolism and 2-HG production have been shown to confer sensitivity to chemotherapy in IDH1-mutated glioma cells. For instance, IDH1 mutation sensitized glioma cells to therapies such as TMZ by inducing greater DNA damage and apoptotic changes in mutant glioma cells (Lu *et al.*, 2017). In that study, U87 and U251 stable cell lines ectopically expressing wild-type IDH1, and established IDH1 mutant U87 MG or U251 MG cell lines were used. It was found that IDH1 mutant cells were more vulnerable to TMZ treatment *in vitro* suggesting

that the metabolic defects in IDH-mutated cells confer cytotoxicity by production of 2-HG. It was also demonstrated that compromised oxidative metabolism and decreased NAD^+ pool in IDH1-mutated cells can impair the PARP-dependent DNA repair mechanism leading to significantly elevated DNA damage and cell death (Lu *et al.*, 2017). Accordingly, the emergence of metabolic enzymes such as IDH1 and many others (e.g. PKM2 (pyruvate kinase muscle isozyme M2), SDH (succinate dehydrogenase), FH (fumarate hydratase) and PDK1(pyruvate dehydrogenase kinase 1)) as important regulators of cancer cell growth (Jones and Thompson, 2009). Also, the genome analysis data of GBM tumours revealed that AMPK isoforms are highly expressed within the cells (Chhipa *et al.*, 2018). It was demonstrated that oncogenic stress chronically activates AMPK in GBM stem cells and regulates GBM bioenergetics through the transcription factors HIF-1α and GABPA (GA binding protein alpha chain). Taken together, all previous studies suggest that metabolic regulation is a key factor of tumour progression and that understanding metabolic rewiring in cancer cell has the potential to open a new area of metabolic therapy for cancer treatment. Accordingly, current data of the combined therapy obtained in this study has also supported these findings where the metabolic modulation by PN517 in the combined therapy significantly enhanced the effect of both cisplatin and TMZ. However, the exact underlying mechanism for the effects on the metabolic pathways still need further investigation.

Effect of hypoxia on cellular metabolism

Cancer cells exhibit alterations to essential chemical processes of macromolecules (carbohydrates, proteins, lipids, and nucleic acids) within the microenvironment of the tumour where the availability of basic nutrients such as glucose, glutamine, and oxygen is limited (Newsholme *et al.*, 1985; Vander Heiden *et al.*, 2009). Such alteration can occur because of increased hypoxia, which leads the cells to rely on reductive carboxylation of glutamine-derived α-ketoglutarate almost exclusively for lipid synthesis (Metallo *et al.*, 2012). Moreover, glutamine-dependent reductive carboxylation has been recognised as the major source of acetyl CoA in ETC-deficient cancer cells (Mullen *et al.*, 2012).

Additionally, transformed and hypoxic cells scavenge unsaturated fatty acids from lysophospholipids to support their growth (Kamphorst *et al.*, 2013). Importantly, it was noted in some cases that cancer cells display other metabolic profiles such as the reverse Warburg effect, in which the cancerous cells use oxidative stress to extract nutrients from surrounding cells (Martinez-Outschoorn *et al.*, 2011), or metabolic symbiosis, where malignant cells within the same tumour may simultaneously use glycolysis and oxidative phosphorylation through using the lactate produced by glycolysis to fuel ATP production via oxidative phosphorylation in other cells (Ho *et al.*, 2012). The effects of hypoxia on cellular biology and metabolism will be studied further in chapter 6.

Regarding hypoxia experiments of this study, U87-MG untreated control cells continued to rely on their maximum glycolytic capacity and did not show a significant shift in the metabolic phenotyping compared to normoxia. Nevertheless, the spare mitochondrial capacity was remarkably lower under hypoxia meaning they also rely on their maximum respiration. Many reports have demonstrated that cancer cells rapidly exploit metabolism to adapt and survive through metabolic plasticity, however, cancer cell adaptation strategies go beyond glycolysis and the metabolic phenotype and vulnerabilities of cancer cells were shown to be highly variable between different cell lines (Dar *et al.*, 2017; Hardie *et al.*, 2017). Accordingly, the changes observed in U87-MG metabolic activity under hypoxia may be due to the cells adapting to the different environmental conditions, with other pathways like glutaminolysis might be involved (Fig 5.6).

5.3.2. Effect of drug treatment on cell metabolism

In addition to obtaining the mitochondrial and glycolytic profiles for U87-MG and SVG-p12 cell lines, the current study determined any changes in the bioenergetic profiles in response to drug treatment with aspirin and its analogue PN517, as monotherapy or in combination with the standard chemotherapy drugs. The effects of drug treatment on mitochondrial function (measured by OCR) and glycolytic functions (measured by ECAR) were assessed using Mito Stress and Glycolysis Stress tests, respectively.

Cisplatin

The results showed that cisplatin did not affect U87-MG metabolic activity as no significant effect was observed on either mitochondrial respiration or glycolysis. Also, none of the mitochondrial or glycolytic key parameters were changed following the drug treatment (Fig 5.8-5.10 &5.15-5.17). However, cisplatin seemed to be more efficacious in SVG-p12 cells in which a trend towards reducing each of basal respiration, maximal respiration, ATP production, coupling efficiency as well as glycolytic capacity was observed (Fig 5.12-5.13 &5.19).

There is controversy relating to metabolic alteration by cisplatin in the literature, where studies have reported an inconsistent response to cisplatin treatment in different cancer cell lines. For example, one study showed a reduction in glucose uptake after cisplatin treatment in ovarian cancer (Liang et al., 2008). It was demonstrated that glucose transporter GLUT1 protein levels did not change after cisplatin treatment, however, the membrane localization of GLUT1 was lost. Additionally, it was reported that cisplatin-resistant cancer cells generally grow slower and display less uptake of various compounds, including nutrients. In other study using HeLa cells, cisplatin had anti-metabolic activities resulting in reduced oxidative phosphorylation, glycolysis and glycolytic reserve, while enhancing the Warburg effect (Heymann *et al.*, 2018). This finding is in contrast to the results reported here, but may be explained by differences in treatment concentrations or cell type, as the study by Heymann and colleagues used higher cisplatin concentrations and/or longer incubation periods. That was supported by different studies where different effects of cisplatin might occur due to different concentrations and time of exposure (Desoize, 2002; Florea and Busselberg, 2011). Similar results were found for the human uterine cervical cancer cell line SiHa where cisplatin reduced glycolysis and suppressed glycolysis-related protein expression including GLUT1 and GLUT4 (Wang *et al.*, 2016). Furthermore, mitochondrial accumulation of cisplatin was reported to damage mitochondrial structure and function (Dzamitika *et al.*, 2006) and it was thought to be a possible explanation for the impaired cellular respiration observed in HeLa cells. However, significantly higher concentrations (100-500 μM) were used which might explain not seeing the same effect in the current study (Fig 5.8-5.10).

In cisplatin -resistant lung cancer cells, it was noted that these cells have high levels of reactive oxygen species and undergo metabolic reprogramming (Wangpaichitr *et al.*, 2017). The cells were shown to be no longer dependent on the glycolytic pathway, but reliant on amino acids for energy production and biosynthesis. They were found to take up greater amounts of glutamine and secreted higher levels of glutamate. The key glycolytic enzymes hexokinase-2 (HK2) and lactate dehydrogenase A (LDHA), in addition to lactate production were also decreased in all examined cisplatin -resistant cell lines. Further recent studies supported similar findings and demonstrated that cisplatin resistant cells show specific metabolic alterations where a decrease in oxidative phosphorylation and increase in glutamine dependency were observed, suggesting that targeting these metabolic vulnerabilities by combination therapies might offer a unique method to treat cancer cells (Geoghegan *et al.*, 2017; Castedo *et al.*, 2018). Accordingly, another explanation for not seeing an effect in cisplatin treated cells is due to cells being resistant to metabolic changes by cisplatin and not due to low concentrations used. Hence, impairing the metabolic flexibility might be useful method to sensitise cells to cisplatin as observed in the combination with PN517 (Fig 5.8-5.10 &5.15-5.17).

In contrast, another study reported that glucose metabolism is upregulated in cisplatin-resistant chondrosarcoma cells and the underlying mechanism was suggested to be related to the EGFR signalling pathway which was reported to be highly activated in human chondrosarcoma cell lines (Song *et al.*, 2014). EGFR was shown to be involved in the regulation of glucose metabolism by stabilizing the sodium/glucose cotransporter (SGLT1) and facilitating glucose transport into cells (Weihua *et al.*, 2008). Cisplatin treatment, in turn, was shown to activate EGFR in multiple cancer cell lines (Benhar *et al.*, 2002) and this overexpression of EGFR contributed to cisplatin resistance through the upregulation of glycolysis key enzymes. Accordingly, the combination of an EGFR inhibitor or anaerobic glycolysis inhibitor with cisplatin displayed synergistic inhibition effects on cisplatin-resistant chondrosarcoma cells (Song *et al.*, 2014). These findings suggest a possible mechanism for the combinations of aspirin and PN517 with the standard chemotherapy drugs and will be discussed further in the final discussion.

Therefore, it can be noted that several cell lines respond differently to cisplatin which could be related to their initial metabolic phenotyping and their metabolic plasticity (Alborzinia *et al.*, 2011). It was revealed that the cisplatin-induced cytotoxicity and the contribution of mitochondrial dysfunction varies among cells and depend on cell proliferation, mitochondrial redox status, mitochondrial DNA integrity and bioenergetic function (Marullo *et al.*, 2013). For instance, cisplatin induced elevations in ROS, DNA damage and cell death in IDH1-mutant HCT116 colorectal cancer cells and U251 glioma cells compared with IDH1 wild-type cells due to heightened vulnerability of oxidative phosphorylation metabolism. Hence, it was concluded that altered oxidative stress responses and impaired mitochondrial activity underlie the sensitivity of IDH1-mutant cancer cells to cisplatin (Khurshed *et al.*, 2018). Taken together, the effects of cisplatin on the metabolic regulation appear to be depend on different tumour types and the mechanisms are still under investigation (Song *et al.*, 2014). Therefore, although cisplatin did not produce remarked effect on cell metabolism using U87-MG cells in this study, that might be different in other GBM cells displaying different metabolic phenotyping.

TMZ

Regarding TMZ effects on the cellular metabolic activity in the current study, no significant effects were observed on U87-MG mitochondrial respiration while significant effects on the glycolytic activity was observed with lower extracellular acidification rates associated with reduction in both glycolysis rate and glycolytic capacity (Fig 5.8-5.10 &5.15). In contrast, in the SVG-p12 non-cancerous cell line, TMZ was more efficacious in impairing metabolic activity of the cells where it produced a decrease in glycolytic capacity as well as reducing the overall oxygen consumption rate, with a significant reduction in the basal and maximal respiration rates that could be in part due to the fact that they have higher functional mitochondria (Fig 5.12-5.13 &5.19-5.20).

It has been reported that TMZ-induced DNA damage leads to PARP activation resulting in cytoplasmic NAD^+ depletion, which inhibits glycolysis (Oliva *et al.*, 2010; Su *et al.*, 2018). However, the oxygen consumption rate and ATP

production were found to be increased by TMZ in other studies suggesting an adaptive response to DNA damage and high energy demand. Consistent results were found in U251 glioblastoma cells where TMZ-induced DNA damage significantly reduced the level of NAD^+ via PARP activity, therefore, suppressed glycolysis led to reduce energy production in the cells. Both basal glycolysis and glycolytic capacity were reduced by TMZ, however, no decrease the intracellular ATP levels was observed. Additionally, it was reported that TMZ suppressed protein expression of glycolytic enzymes (PKM2 and LDHA) in GSC923 GBM cells but not GSC827 GBM cells. Although some reports suggested that TMZ induces mitochondrial dysfunction, no significant apoptosis was detected at the timepoint tested (48 hr) in all investigated GBM cell lines (Su *et al.*, 2018). However, another study reported that no cellular metabolic changes were observed in the GBM8401 glioblastoma cell line following TMZ treatment with no overt decrease in OCR or ECAR (Hsu *et al.*, 2018). A recent study in 2019 investigating metabolic activity of different GBM cell lines reported that TMZ did not affect mitochondrial respiration activity in U87-MG cells while little decrease in T98G mitochondrial respiration was observed with significant reduction in ATP-linked respiration (Desai *et al.*, 2019). Accordingly, the previous results are supporting current findings where TMZ produced significant inhibition in glycolytic activity but with no significant effect on mitochondrial respiration in U87-MG cells (Fig 5.8-5.10 &5.15).

Aspirin and PN517

Previous reports showed that some NSAIDs act as mitochondrial uncouplers and inhibit oxidative phosphorylation even at low millimolar range. However, the potency of the NSAID effects on mitochondrial function and killing cancer cells does not seem to correlate with their uncoupling activity or effects on oxidative phosphorylation, suggesting that modifying mitochondrial function is not the direct cause of the high dose NSAID toxicity on normal cells (Ralph *et al.*, 2015). Regarding aspirin, current findings of the metabolic activity analysis showed a trend towards reducing both mitochondrial and glycolytic functions in U87-MG cells allowing drug treatment, however, aspirin only produced a significant reduction in the mitochondrial spare respiratory capacity (Fig 5.10). Concerning the SVG-p12 cell line, aspirin produced a similar pattern of results, with no

significant effect for any of the bioenergetic parameters. However, when aspirin was combined with cisplatin or TMZ, it appeared to enhance the effects of the monotherapy of cisplatin or TMZ in U87-MG cells but not in SVG-p12 cells (Fig 5.12-5.13). A high spare respiratory capacity permits rapid adaptation to metabolic changes, and growing evidence has shown that the spare respiratory capacity provides additional metabolic choice for energy compensation, potentially offering new therapeutic target (Keuper *et al.*, 2014). As aspirin showed significant reduction in the mitochondrial respiratory capacity, it might suggest a therapeutic potential for aspirin in the treatment of GBM when combined with other therapies (Fig 5.10).

Aspirin treatment directly reduced glycolysis and cell viability in human breast cancer cells by inhibiting the key regulatory enzyme, phosphofructokinase (Spitz et al., 2009). Similar results were also observed in pancreatic cancer cells (Jiang et al., 2016). However, the relative anticancer activities of different NSAIDs varied considerably among cancer cell lines analysed *in vitro* (Ralph *et al.*, 2015). Despite the availability of substantial epidemiological data for aspirin effects, the studies have displayed the need for further investigation of aspirin-dependent metabolic alterations in cancer cells to confirm any beneficial consequences of aspirin in cancer treatment (Bilani *et al.*, 2017). The current study also supports this need for further investigation regarding aspirin effects on metabolism pathways in GBM cells since it showed slight but not significant effect on glycolytic and mitochondrial activity, an effect was not totally consistent with the previous findings and could be due to different experimental conditions or different cell type used (Fig 5.15-5.17).

The aspirin analogue PN517 showed a similar pattern or effect to aspirin, yet it was markedly more efficacious in impairing both mitochondrial respiratory activity and glycolytic activity (Fig 5.7 &5.14). The mitochondrial bioenergetics analysis indicated that PN517 significantly reduced basal, maximal, and spare respiration associated with significant decrease in ATP production in U87-MG cells. Both aspirin and PN517 seemed also to increase respiration linked to proton leak. Hence, all OCR measurements suggest that PN517 and its combinations have a rapid impact on mitochondrial function which was greater than the other

monotherapies, and correlates well with the cell viability and apoptosis assay results where PN517 showed a significant cell viability reduction and apoptosis induction at this timepoint (24 hr). These findings are supported by the fact that OCR measurements are mainly used for high-throughput cytotoxicity assessment since oxygen consumption is one of the most sensitive parameters for cytotoxicity (Simonnet *et al.*, 2014).

In addition, PN517 significantly reduced glycolysis rate and glycolytic capacity in U87-MG cells and clearly enhanced the effect of cisplatin and TMZ. SVG-p12 cells exhibited a similar pattern of response to PN517 treatment with some differences. Although PN517 reduced both basal and maximal respiration rates, it did not show a significant effect on the ATP production or spare respiratory capacity of SVG-p12 cells. Furthermore, PN517 did not significantly reduced the glycolysis rate of SVG-p12 cells though it did significantly decrease the glycolytic capacity. As already mentioned, different cell lines might exhibit diverse metabolic phenotypes with varying flexibility in using energy pathways which can be associated with survival adaptation and chemoresistance (Simões *et al.*, 2015; Dar *et al.*, 2017). Additionally, previous findings suggested that the effectiveness of antiglycolytic approach may depend on the degree of glycolytic phenotype in cancer cells, and that the selectivity of cancer-expressed transporters can be exploited for targeting tumour cells (Birsoy *et al.*, 2013).

Importantly, while monotherapy with the current standard chemotherapy drugs, cisplatin and TMZ, produced effects on the metabolic activity of SVG-p12 control cell line, both aspirin and PN517 showed higher efficacy in U87-MG cell line, suggesting that aspirin and its analogue are more selective for GBM cells than the current treatments. Suppressed glycolytic function following PN517 treatment is unlikely to be related to mitochondrial dysfunction since that compensation of energy production would lead to glycolytic upregulation rather than downregulation. In the context of robust inhibition of both energy producing pathways by PN517, GBM cells are expected to undergo cell death with a lower chance of developing resistant mechanisms (Su *et al.*, 2018).

Generally, the Seahorse analysis of drug treatments showed similar patterns of efficacy under hypoxia. Interestingly, all drug treatments appeared to impair both mitochondrial respiration and glycolytic function of U87-MG cells with PN517 being the most efficacious drug treatment. However, effects under hypoxia did not reach the statistical significance for any of the drug treatments. It is worth noting that one limitation for hypoxic experiment that following treating cells under hypoxia assays had to be performed in the instrument under normoxic conditions, hence, reoxygenation after hypoxia can be a quite disturbing factor leading to unexpected results (Liu *et al.*, 2009).

As discussed earlier, metabolic remodelling from oxidative phosphorylation to aerobic glycolysis, is associated with glucose being converted into lactate and released extracellularly. Net conversion of glucose to lactate at neutral pH releases protons and acidifies the medium, hence extracellular acidification rate is commonly used as a direct and quantitative measure of glycolytic rate (Wu *et al.*, 2007). To test experimentally the assumption that ECAR reflects lactate excretion, lactate production rates are usually measured. Measurement of glycolytic rate using extracellular acidification requires differentiation between respiratory and glycolytic acid production, therefore the low pH results from lactic acid accumulation by glycolysis can be assessed by measuring lactate concentration in the culture media (Mookerjee *et al.*, 2015). Recent studies demonstrated that the use of extracellular lactate measurements can be a sensitive, safe, stable, and easy-to-implement technique for measuring cellular metabolic changes *in vitro* and showed that extracellular lactate levels strongly correlated with T cell proliferation and metabolic rewiring to aerobic glycolysis (Grist *et al.*, 2018).

Similarly, various reports measured L-lactate production rate under different conditions or reagents as an indicator for glycolytic activity in the cells (Konrad *et al.*, 2017; Wu *et al.*, 2018). In the current study, all drug treatments produced a trend towards reduced lactate production, which was not completely consistent with the results from the glycolysis stress test (Fig 5.21). This difference may be partially explained by the different experimental conditions applied where the media constituents and incubation times varied, and this may have influenced the

results. However, only the TMZ and PN517 combination produced a significant reduction in lactate concentration in the media compared to the control under both normoxia and hypoxia. These results correlate well with the findings of the Seahorse analysis and confirm that U87-MG cells decrease glycolysis rate in response to TMZ and PN517 (Fig 5.21).

To further investigate the anti-glycolytic effect of the drug treatment, GAPDH enzymatic activity was tested. Remarkably, PN517, as single treatment or combined with the standard chemotherapy drugs, inhibited GAPDH activity in U87-MG glioblastoma cell line. GAPDH is a key glycolytic enzyme and has been found to be highly expressed in cancer cells (Tokunaga *et al.*, 1987). Metabolic Flux Control Analysis for several glycolytic enzymes revealed GAPDH as rate limiting during the Warburg effect in cancer cells. Therefore, inhibiting GAPDH activity exerts larger reduction in glycolytic flux in cells undergoing more Warburg effect than in cells with lower glycolytic activity. The authors showed that the effect of changed GAPDH activity is amplified under Warburg effect and that partial GAPDH inhibition is tolerable in normal cells while being selective for highly glycolytic tumour cells (Liberti *et al.*, 2017). Accordingly, these findings support the current results obtained in this study where the significant inhibition in glycolytic activity observed with PN517 treatment might be attributed to decrease in GAPDH activity hence impairing the glycolytic pathway and reducing the lactate production (Fig 5.22).

Although the anticancer effect of targeting GAPDH has been known for a few decades, previous reports discouraged GAPDH therapeutic potential due to toxicity concerns because of its cellular abundance and ubiquitous nature as well as lack of substantial preclinical data (Ganapathy-Kanniappan, 2018). However, recent advances in understanding the cancer-related roles of GAPDH (Fig 5.23), along with the significant progress in drug delivery methods have lessened these concerns and led to a renewed interest in targeting GAPDH for cancer therapy.

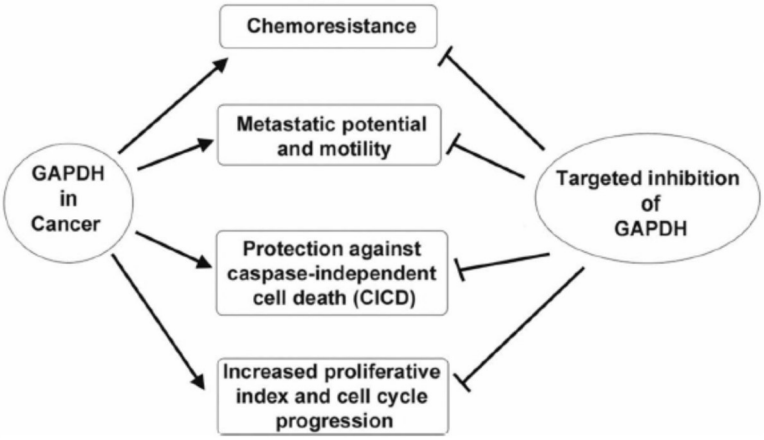

Figure 5. 23. Schematic diagram showing the anticancer advantages of targeting GAPDH (Ganapathy-Kanniappan *et al.*, 2012).

Jung and colleagues demonstrated that targeting GAPDH activity with the triazine-based small molecule, GAPDS, showed greater toxicity against cancer cells and selectively inhibited cell migration and invasion in different human cancer cell lines (Jung *et al.*, 2014). The authors showed that GAPDS treatment reduced GAPDH levels in the cytoplasm, which would modulate the secondary additional functions of this enzyme. They also found that GAPDH regulates tubulin expression in cancer cells which may explain the anti-invasive properties of GAPDS. By inhibiting GAPDH, GAPDS was shown to induce the expression of apoptosis markers and reduces tubulin expression in cancer cells (Jung *et al.*, 2014). Accordingly, since PN517 also reduced GAPDH activity, it can be speculated that it would also have anti-invasive properties and have a potential therapeutic role in GBM.

GAPDH is known as virulence factor that can colocalize with microtubules in cancer cells and contributes to cell invasion into host tissues (Andrade *et al.*, 2004). GAPDH can also bind plasminogen on the cell surface and regulate the cleavage of plasminogen into plasmin, which initiates cell invasion. Hence, these findings have indicated that strategies to target the secondary functions of GAPDH may yield potent therapeutics for cancer cells. Authors also observed that GAPDH expression is less affected by GAPDS treatment under hypoxia attributing this to the increased expression of GAPDH, which is known to occur in the hypoxic environment (Xu *et al.*, 2005). Many other studies showed that GAPDH gene expression is increased under hypoxia stress via HIF-1 signalling

(Graven *et al.*, 1994; Graven *et al.*, 1999). However, opposing results were reported in other studies where no hypoxia-induced regulatory effect on GAPDH expression was observed in glioma cancer (Said *et al.*, 2007) or in other cell lines like human hepatocellular carcinoma, mouse hepatoma, human colon cancer, and human lung adenocarcinoma (Said *et al.*, 2009). Importantly, PN517 produced its effects under normoxia as well as hypoxia, unlike GAPDS (Fig 5.22).

Another example of GAPDH inhibition was reported using ascorbate (Ma *et al.*, 2017). Ascorbate was cytotoxic to human neuroblastoma cells through the production of H_2O_2, which led to ATP depletion and inhibited GAPDH leading to cell death. It was indicated that by formation of H_2O_2, ascorbate reduces cellular NAD^+, hence inhibits GAPDH leading to glycolysis inhibition which in turn causes ATP crisis in neuroblastoma cells that results in cell death. These findings suggested that targeting the activity GAPDH, as a critical enzyme in the glycolysis pathway, may have potential therapeutic value in cancer treatment and again support the potential of PN517 as effective antiglycolytic therapy in GBM.

Furthermore, as described earlier, GAPDH is a multifunctional protein that is involved in several cellular processes are associated with cancer progression besides glycolysis. Hence, disruption of glycolysis by GAPDH inhibition could have multiple secondary effects in cancer cells (Ganapathy-Kanniappan *et al.*, 2012). GAPDH was shown to be associated with aggressive malignant behaviour of cancer cells and poor prognosis of lung cancer patients (Tokunaga *et al.*, 1987; Revillion *et al.*, 2000; Puzone *et al.*, 2013). In addition, GAPDH expression was noted to be elevated in colon cancer and further increased in metastasis liver metastatic tissue suggesting an important role of GAPDH in promoting tumour growth and metastasis. However, the underlying mechanism by which GAPDH promotes cancer growth and metastasis remains unclear (Tang *et al.*, 2012).

Similar results were found in another study which showed that silencing GAPDH resulted in a significant reduction of glycolysis accompanied by a decrease in cell proliferation in colon cancer cell lines (Liu *et al.*, 2017). In addition, the authors revealed that GAPDH suppression significantly abrogated EMT phenotype, which is tightly associated with key steps during cancer metastasis involving cell

migration and invasion (Thiery and Sleeman, 2006) and caused a downregulation of gene expression involved in cancer stem-like cells and EMT of colon cancer cells. At the molecular level, the study suggested that GAPDH could physically interact with the transcriptional factor Sp1 (specificity protein 1) and promote the expression of SNAIL (Zinc finger protein SNAI1), leading to EMT and an increased cell mobility and cancer metastasis. In addition, suppression of GAPDH expression resulted in a significant decrease in SNAIL expression, leading to inhibition of EMT and attenuation of colon cancer cell migration *in vitro* and reduced metastasis *in vivo* (Liu *et al.*, 2017). Similar results were found in breast cancer cells where GAPDH activity was upregulated upon induction of an EMT-like programming of heightened malignancy, whereas GAPDH inactivation impaired glycolytic metabolism, ATP generation, nucleotide and fatty acid metabolism, and oncogenic signalling pathways (Louie *et al.*, 2016). Taken together, these findings provide potential explanation for the different effects on cell proliferation and migration observed after PN517 treatment in the current study which might be related to the reduction in GAPDH activity and its secondary functions, hence reducing tumour invasion and metastasis. Also, it could also be argued that PN517 can be used as a preventative treatment due to the fact that EMT is a characteristic of cancer stem cells (Mani *et al.*, 2008), so by preventing it, PN517 might stop GBM arising in the first place.

Another study has demonstrated the efficacy of a natural compound, koningic acid, in altering the Warburg effect by targeting the glycolytic enzyme GAPDH, identified it as a potential novel therapeutic to target cancer's altered energy metabolism (Liberti *et al.*, 2017). Accordingly, it was suggested that due to the metabolic adaptation to glycolysis, cancer cells may be more sensitive to antiglycolytic, anti-GAPDH approach than their healthy counterparts or non-glycolytic cells (Shestov *et al.*, 2014). Consequently, PN517 is not alone in having therapeutic potential though targeting GAPDH and these compounds might represent an emerging therapeutic class. Taken together, despite few previous reports showing contradictory results for GAPDH targeting potential, emerging accumulating evidence established the role of GAPDH in promoting cancer growth and metastasis. The recent expert's opinion has revived hope and enthusiasm to consider a safe and efficacious glycolytic/ GAPDH inhibitors as a

molecular target for cancer therapy (Ganapathy-Kanniappan, 2018). Therefore, current results obtained with PN517 support its potential therapeutic value through targeting GAPDH glycolytic and secondary activities warranting further investigations.

In summary, the metabolic activity investigations revealed new possible underlying mechanism for PN517 which was significantly different from the parent drug aspirin. Aspirin did not produce significant effects on the metabolic activity of the treated cells apart from reducing the mitochondrial respiration capacity, whereas PN517 effectively inhibited both mitochondrial and glycolytic activities with significant reduction in GAPDH enzymatic activity. Regarding the standard chemotherapies, TMZ inhibited the glycolytic activity without affecting the mitochondrial respiration function, whereas cisplatin did not produce any significant effect in the metabolic activity of GBM cells.

CHAPTER 6: HYPOXIA-ADAPTED CELL CULTURES AND 3D SPHEROID CULTULRES

6.1. Introduction

Mammalian cells can tolerate a wide range of oxygen tension, and this tolerance depends on the type, function and location of the cells (Liu and Simon, 2004; Walmsley *et al.*, 2005). Oxygen pressures and gradients play vital roles in modulating biological processes in both physiologic and pathologic events (Allen and Bhatia, 2003). A hypoxic microenvironment is a fundamentally important hallmark of solid tumours and has been recognized as a cause of malignancy and poor patient prognosis across a broad range of tumour types, however, the microenvironment within solid tumours can be highly heterogeneous (Meyer *et al.*, 2015). Like many solid tumours, GBM tumours are characterised by a heterogeneous pattern of oxygenation and the larger the volume of the hypoxic area, the poorer the prognosis (Spence *et al.*, 2008). Studies using oxygen-sensitive electrodes have shown that normal level of oxygen in human brain tissue can range from 5 to 8% O_2. In contrast, mean oxygen levels in high-grade gliomas range from 0.75% to 2.76% O_2 (Kayama *et al.*, 1991; Rampling *et al.*, 1994; Collingridge *et al.*, 1999; Beppu *et al.*, 2002; Whittle *et al.*, 2010).

Tumour cells in a hypoxic region show reduced proliferation and resistance to chemo- or radiotherapy (Saggar *et al.*, 2013). The differing oxygen levels experienced by tumour cells are varied with respect to localisation within the solid tumour and duration of the hypoxic episodes (Vaupel, 2013). Tumour cells grown under different oxygen conditions display complex changes in gene expression mainly mediated by HIF signalling (Maxwell *et al.*, 2001; Koch *et al.*, 2003; Liu and Simon, 2004) and depending on the microenvironment of specific population of tumour cells, they can show different characteristics of cell activity including proliferation, oncogenic pathway activation, and metabolism (Okuyama *et al.*, 2010), which in turn can affect the mechanism of action of many drugs (Maxwell *et al.*, 2001; Koch *et al.*, 2003). Therefore, investigations of the tumour cells biology in various hypoxic conditions might be critical for improving cancer therapeutic efficacy, and many studies have emphasised the necessity to investigate both acute and chronic hypoxia exposure times to ensure suitable observation of any potential hypoxia induced resistance in cancer models (Cowman *et al.*, 2019).

Recent progress has been made in understanding the responses of cancer cells to acute hypoxia, and following the discovery of hypoxia-inducible factor-1α (HIF-1α), transcriptional regulation in response to acute hypoxia has been largely characterised (Semenza, 2012). In contrast, tumour cells characteristics in chronic hypoxia and how cancer cells respond to the different condition of chronic hypoxia remains unclear (Petrova *et al.*, 2018; Al Tameemi *et al.*, 2019; Mylonis *et al.*, 2019). One factor hindering improved understanding of the cancer cells response to chronic hypoxia is the lack of established *in vitro* models to investigate the drug treatment efficacy in the prolonged hypoxic conditions. Most cancer studies under hypoxia have been carried out within 24 h or up to a few days because most cancer cell lines cannot survive the severe depletion of oxygen or nutrients for a longer period (Endo *et al.*, 2014). Accordingly, some researchers have investigated the effects of prolonged incubation under hypoxic conditions up to several weeks on the growth of different cancer cells *in vitro* and indicated that although chronic hypoxia-adapted cells might not directly contribute to tumour growth, they can be a reservoir of tumorigenic cells and important cause for tumour recurrence and chemoresistance (Endo *et al.*, 2014; Cowman *et al.*, 2019).

Several technologies have been developed for controlling oxygen levels in both macro and micro environments. Current techniques for controlling oxygen of macro-environments include using hypoxic workstations, perfusion chambers or oxygen scavenging agents. However, one challenge has been associated with these approaches is providing only a single condition of a hypoxic level at a time (Allen *et al.*, 2001) and being not able to provide physiological oxygen gradients found *in vivo* or control at the microscale. Furthermore, oxygen scavenging agents can alter the cell growth environment and may affect cellular responses (Adler *et al.*, 2010).

In line with this, and as controlling oxygen tensions is critical for mimicking physiologically relevant *in vivo* environments for cells, multicellular tumour spheroids grown in three-dimensional (3D) cell culture are increasingly being used in cancer research. The GBM microenvironment is complex and although two-dimensional (2D) cell monolayers are simple to culture and provide

convenient testing platforms for screening anti-cancer drugs, they are not accurately representative of the tumour microenvironment, morphologically or functionally (Tung *et al.*, 2011).

On the other hand, animal models for GBM cancer recapitulate the tumour microenvironment to some extent, however, these models are difficult to develop, time consuming, expensive and frequently fail to reflect human tumour biology (Aggarwal *et al.*, 2009). Strikingly, *in vitro* multicellular tumour spheroids have been shown to bridge the complexity gap between flat monolayer cell culture and *in vivo* animal models and have become valuable models for studying drug resistance. Therefore, efforts have shifted focus onto 3D spheroids where tumour cells typically exhibit several features of GBM cancer microenvironment such as relevant morphology, cell-cell interaction, increased cell survival, and a hypoxic core in comparison to traditional monolayer cultures (Godugu *et al.*, 2013; Lee *et al.*, 2013).

Different methods have been used to create multicellular tumour spheroid models, each with their different advantages and disadvantages, such as liquid overlay on agar, hanging drops, gel/matrix-based culture, polymeric scaffolds and microfluidic devices (Lv *et al.*, 2017). However, no standardised and rapid protocols are currently available, and variability in cancer spheroid formation has been a persistent problem for researchers in this field. The reproducibility of spheroid formation appears to be linked to medium composition and volume, cell density, duration in cell culture, and most importantly, the interactions of cells with the culturing plate itself (Costa *et al.*, 2018).

The formation and characterization of uniform and reproducible 3D tumour spheroids *in vitro* was shown to be achieved using ultralow attachment plates such as Thermo Scientific™ Nunclon™ Sphera™ plates. These plates have a polymer-coated culture surface that inhibits the binding of extracellular matrix (ECM) proteins, which typically mediate cell adhesion. The consistent formation of cancer spheroids in these ultralow attachment plate makes it an ideal platform for modelling 3D tumour growth for cell-based drug discovery procedures, co-culture studies, and high-throughput screening. Additionally, drug treatment can

also be administered directly to spheroids growing in ultralow attachment plates and cell viability and cell functions can be conveniently evaluated using fluorescence- based and colorimetric assays.

Viability assays can be performed using different cell viability reagents like PrestoBlue and MTT. Importantly, 3D spheroids can be visualised using different LIVE/DEAD Viability/Cytotoxicity assays which provide sensitive, safe, and efficient discrimination between viable and non-viable cells. The LIVE/DEAD Viability/Cytotoxicity assays are relatively quick and easy two-color assays to determine viability of cells in a population based on plasma membrane integrity and esterase activity that are distinguishing characteristics of live cells. For example, it is possible to discriminate live from dead cells by simultaneously staining with green-fluorescent CFDA-SE to indicate intracellular esterase activity and red-fluorescent propidium iodide to indicate loss of plasma membrane integrity.

Having established the effects of the drug treatment on glioblastoma monolayers under normoxia (ambient air ~21% O_2) and acute hypoxia (direct exposure to 1% O_2), it was intended in this chapter to generate a chronic hypoxia-adapted glioblastoma cell line to simulate real hypoxic conditions as much as possible with the aim of characterizing the metabolic changes that occur in U87-MG cells under chronic hypoxia and to find out whether prolonged duration of hypoxic exposures leads to different responses to drug treatment than those reported in most available studies which generally expose cells to a maximum of 72 h of hypoxia. Additionally, this chapter aimed to employ a 3D spheroid model of glioblastoma in order to investigate the effect of the drug treatment in an environment that better simulates the various characterises of the real tumour *in vivo*.

6.2. Results

6.2.1. Hypoxia-adapted Cell Culture

In the current study, hypoxia-adapted U87-MG and SVG-p12 cell lines were generated by exposing the cells to decreasing levels of oxygen. At 5% O_2 both U87-MG and SVG-p12 cells were able to grow and proliferate under these conditions which resemble the physiological conditions of the brain tissue and both cell lines were harvested for liquid nitrogen storage. After reducing the oxygen level further to 1% O_2, U87-MG cells were still able to proliferate although at slower rate compared to the previous stage whereas SVG-p12 cells did not proliferate at this low concentration of oxygen and harvesting of cells was a challenge. Following exposure of the adapted U87-MG cells to more severe hypoxic conditions by reducing the oxygen concentration to 0.1% O_2, it was noted that cells did not proliferate and could not adapted to this severe hypoxia for more than few days.

While generating the hypoxia-adapted cell lines, it was intended to perform a viability assay for aspirin at the end of each stage of oxygen adaption in order to compare treatment efficacy in different conditions throughout adaptation. Both U87-MG and SVG-p12 cells were treated with same range of aspirin concentrations used previously for normoxia and acute hypoxia experiments, and the PrestoBlue viability assay was performed following 48 hr of drug treatment. Thereafter, concentration response curves and IC_{50} values were established using GraphPad Prism software.

The obtained data revealed that aspirin reduced cell viability in a concentration-dependent manner in both U87-MG and SVG-p12 hypoxia-adapted cell lines (Fig 6.1). When comparing the different culturing conditions, cells in acute hypoxia appeared to be more sensitive to aspirin treatment in both cell lines. Aspirin cytotoxicity was significantly lower under normoxia compared to acute hypoxia ($p<0.05$ in U87-MG and $p<0.01$ in SVG-p12). Additionally, both hypoxia-adapted cell lines appeared to be less sensitive to aspirin compared with the acute hypoxic cells.

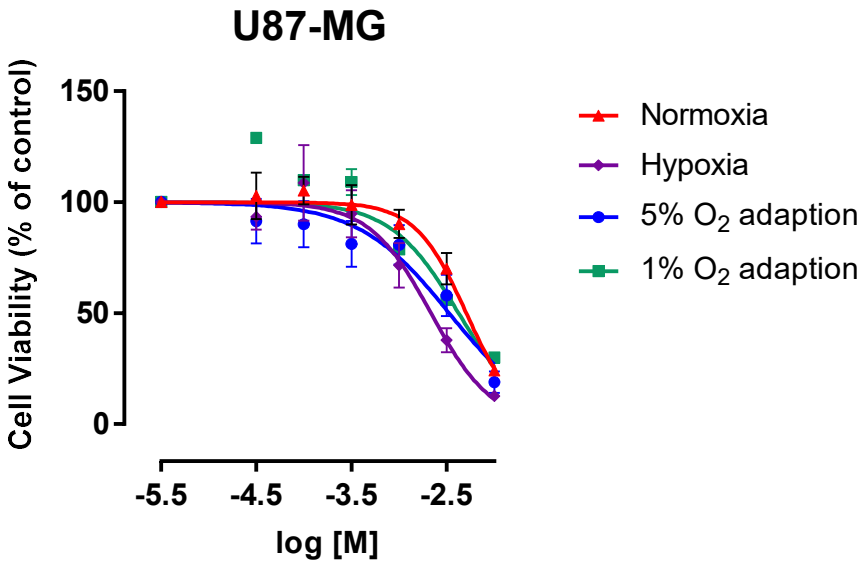

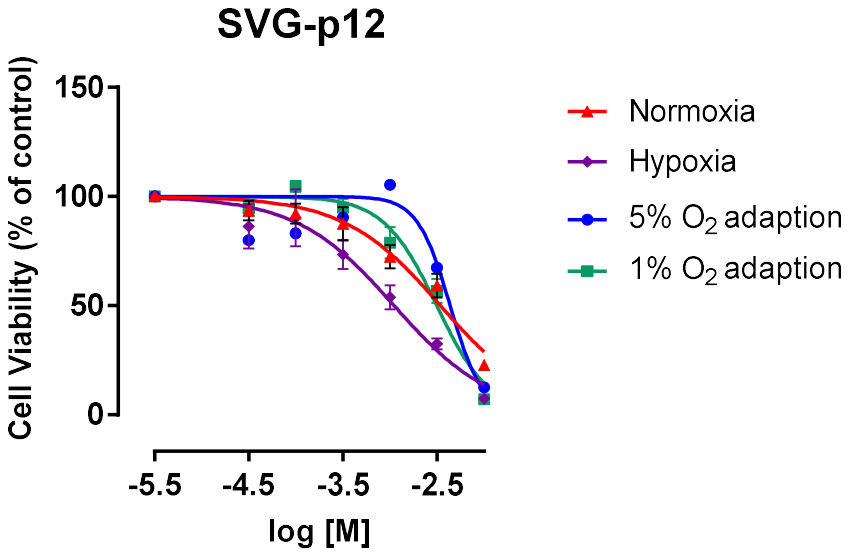

IC_{50} (mM)	Normoxia	Hypoxia	5% O_2 adapted	1% O_2 adapted
U87-MG	5.096	2.164	3.362	4.227
SVG-p12	3.436	1.105	4.352	3.138

Figure 6. 1. Concentration- response curve of aspirin under different conditions of hypoxia in U87-MG and SVG-p12 cells lines. The concentration-response curve of the drug treatment and IC_{50} values were established using the PrestoBlue® reagent after 48 hours of treatment. Values represent mean ± SEM of six independent experiments for cells under normoxia or acute hypoxia and two independent experiments for hypoxia adapted cells. A two-way ANOVA was used to identify significant effects, with Tukey's multiple comparison test, *P < 0.05; **P < 0.01; ***P < 0.001; ****P < 0.0001. The experimental procedure was performed as described in Materials and Methods section 2.2.5.

6.2.1.1. Effects of drug treatment on viability of 1% O_2 hypoxia-adapted cells

Following generation of the hypoxia adapted cell lines, it was planned initially to investigate the effects of the drug treatment on the adapted cells at 1% O_2 concentration in order to monitor any variance in the cellular responsiveness to drug treatment compared to the cells exposed directly to the same level of oxygen without adaptation (acute hypoxia). Both U87-MG and SVG-p12 1% O_2 adapted cells were drug treated, separately or in combination, at IC_{50} concentrations obtained from concentration-response curves at 48 hr under acute hypoxia. Cells were incubated for 24, 48, and 72 hours prior to determining cell viability using the PrestoBlue assay.

In U87-MG adapted cells all drug treatments appeared to decrease cell viability in a time dependent manner, however only cisplatin showed significant difference in cell viability between the 24 hr timepoint and the subsequent timepoints (p<0.05). Looking at the overall pattern of effect over three days (Fig 6.2), cisplatin seemed to be most effective monotherapy in the hypoxia adapted cells, and PN517 was slightly more effective than aspirin with similar efficacy to TMZ. However, the drug combinations were more effective than monotherapies, particularly those with TMZ. At 24 hr after drug treatment, only the combined therapy showed a significant effect in reducing cell viability compared to the control (p<0.01 for the combination of cisplatin and aspirin whereas p<0.0001 for the other combinations) (Fig 6.3). At 48 and 72 hr of drug treatment, the pattern was very similar where cisplatin produced significant decrease in cell viability compared to the control (p<0.0001). Additionally, cell viability was reduced with PN517 and TMZ treatment (p<0.05) but not with aspirin (p>0.05). All drug combinations also significantly reduced cell viability at 48 and 72 hr of drug treatment (p<0.0001) (Fig 6.3).

When examining drug treatment effects on the U87-MG hypoxia-adapted cells compared to acute hypoxic cells, the relative cell viability values were always higher in the adapted cells, hence treatments were less effective compared to the acute hypoxic cells (Fig 6.4). However, there was no significant difference between the acute and chronic hypoxia-adapted U87-MG cells except for the combination of cisplatin and aspirin at 72 hr of drug treatment (p<0.05). The

pattern was similar for both cell types where PN517 was the most effective monotherapy at 24 hr of drug treatment while cisplatin was the most effective monotherapy at later timepoints. Also, in both cell types the combined therapy produced a greater reduction in cell viability compared to monotherapy where the combinations of PN517 produced the largest effects.

Regarding SVG-p12 cells, most treatments produced a clear time dependent effect on cell viability where effects increased at 48 and 72 hours (Fig 6.5). A significant decrease in cell viability at 72 hr of treatment was observed with TMZ and its combination with aspirin compared to 24 hr ($p<0.05$ and $p<0.01$, respectively). In addition, cisplatin combination with either aspirin or PN517 showed a significant decrease in cell viability over time where cell viability values at 48 and 72 hr values were lower than 24 hr ($p<0.05$ and $p<0.01$, respectively) (Fig 6.6).

Generally, SVG-p12 cells after hypoxia adaption seemed to be more sensitive to drug treatment compared to U87-MG cells. Following 24 hr of drug treatment, a significant reduction in cell viability was observed with PN517 treatment compared to the control ($p<0.05$) as well as PN517 combinations ($p<0.0001$). Similarly, aspirin combinations with cisplatin or TMZ showed a significant difference in cell viability compare to control ($p<0.05$ and $p<0.001$, respectively) (Fig 6.). At 48 hr of drug treatment, a significant reduction in cell viability was observed with PN517, cisplatin and TMZ treatment compared to the control ($p<0.01$, $p<0.01$ and $p<0.0001$, respectively) as well as all drug combinations ($p<0.0001$), but no significant effect was observed with aspirin ($p>0.05$). However, all monotherapies and combined therapies showed a significant reduction in cell viability at 72 hr (Fig 6.6). Cell viability was significantly reduced with aspirin, PN517, cisplatin and TMZ treatment compared to the control ($p<0.05$, $p<0.0001$, $p<0.001$ and $p<0.0001$, respectively) as well as all drug combinations ($p<0.0001$).

When comparing drug treatment effects on the SVG-p12 hypoxia-adapted cells to acute hypoxic ones, the drug treatments did not show a pattern towards less efficacy in the adapted cells as seen in U87-MG cells. The drug effects were very

similar in both conditions and no significant difference was observed expect for cisplatin which was more effective in the acute hypoxic cells (p<0.01) (Fig 6.7).

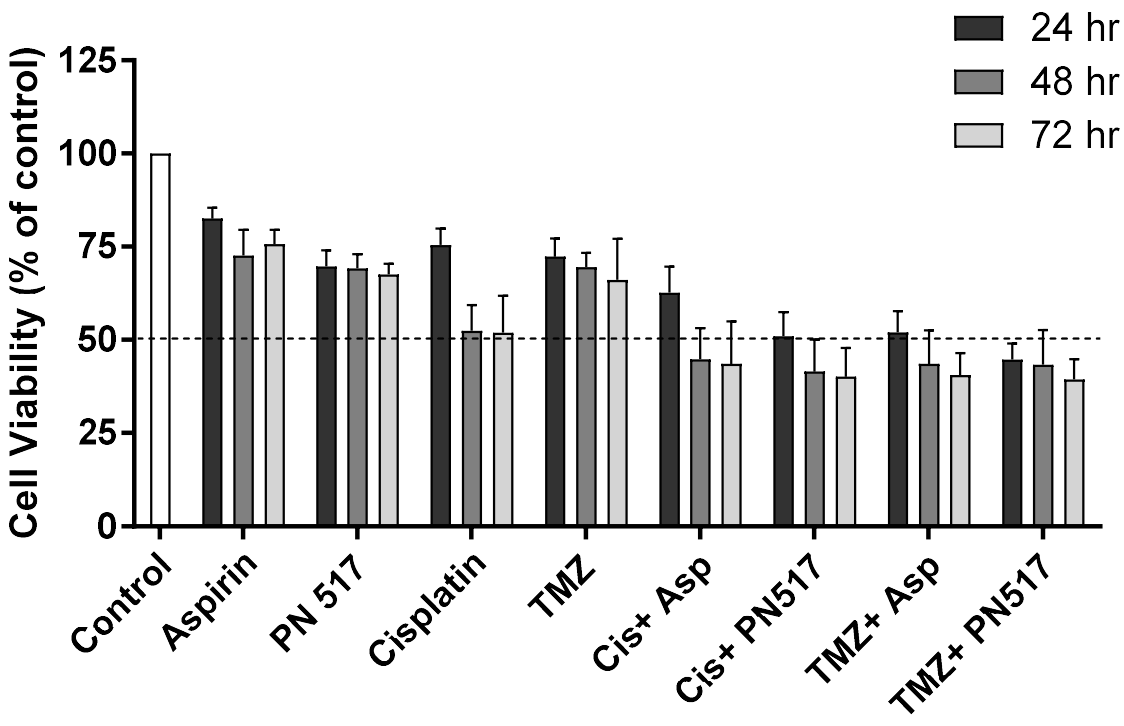

Figure 6. 2. The effect of drug treatment on cell viability of U87-MG hypoxia-adapted cells. Cell viability assay was performed under 1% O_2 hypoxia using the PrestoBlue reagent over 24, 48 and 72 hours of drug treatment at IC_{50} as determined by concentration-response curves at 48 hr at 1% O_2. Values represent mean ± SEM of six independent experiments. A two-way ANOVA was used to identify significant effects, with Tukey's multiple comparison test, *P < 0.05; **P < 0.01; ***P < 0.001; ****P < 0.0001. The experimental procedure was performed as described in Materials and Methods section 2.2.6.

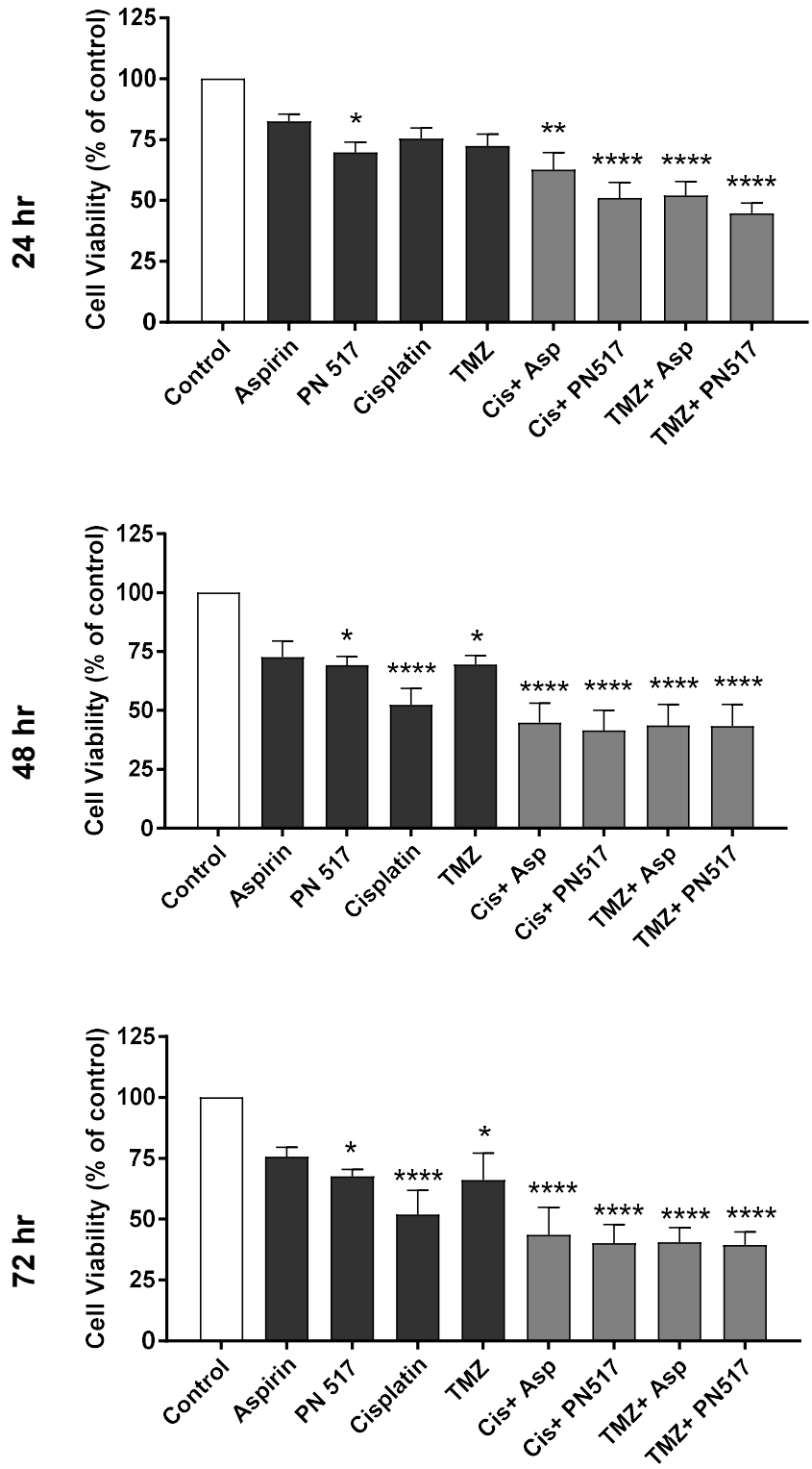

Figure 6. 3. The effect of combined therapy on cell viability of U87-MG hypoxia-adapted cells. Cell viability assay was performed under 1% O_2 hypoxia using the PrestoBlue reagent over 24, 48 and 72 hours of drug treatment at IC_{50} as determined by concentration-response curves at 48 hr at 1% O_2. Values represent mean ± SEM of six independent experiments. A two-way ANOVA was used to identify significant effects, with Tukey's multiple comparison test, *P < 0.05; **P < 0.01; ***P < 0.001; ****P < 0.0001. The experimental procedure was performed as described in Materials and Methods section 2.2.6.

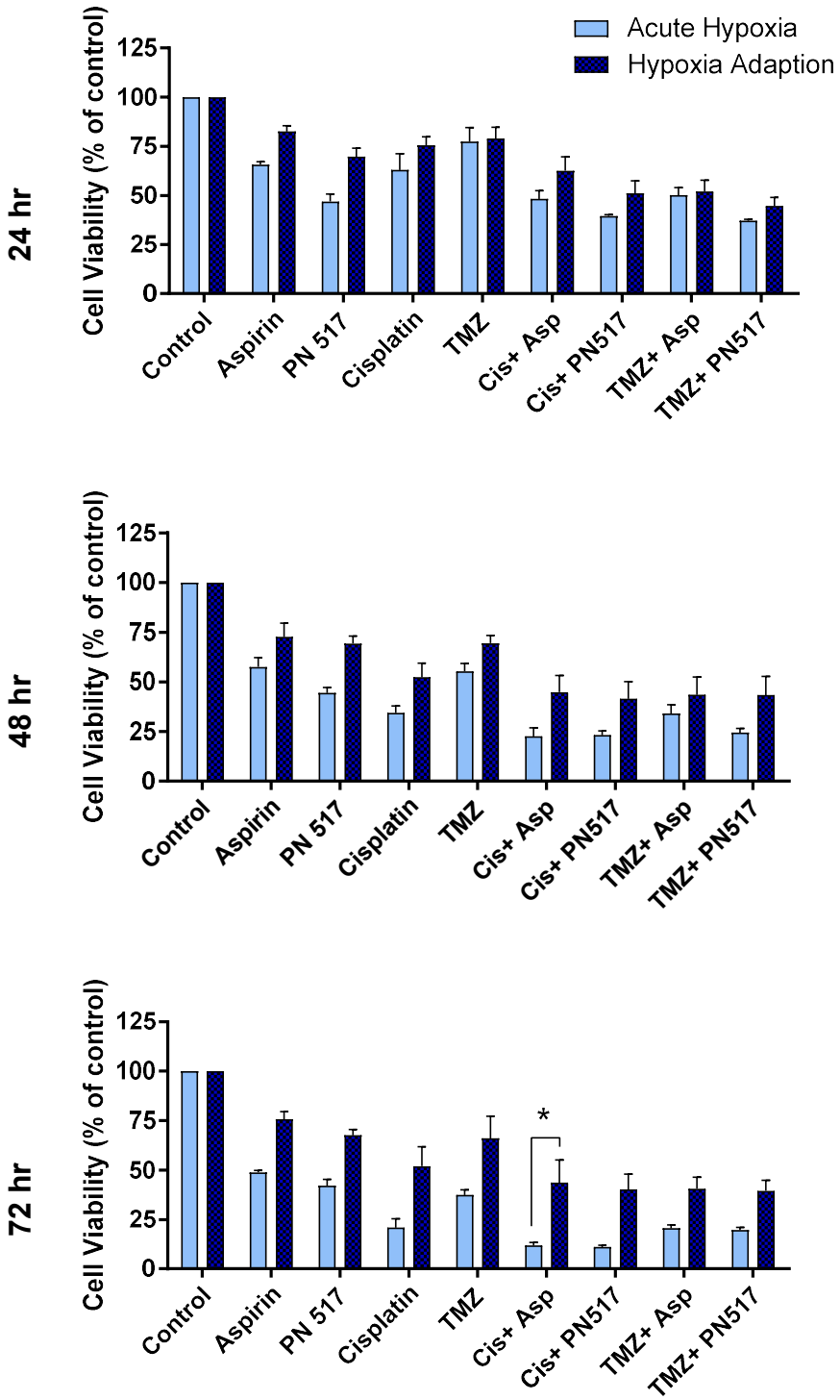

Figure 6. 4. The effect of drug treatment on cell viability of U87-MG cells under both acute hypoxia and hypoxia adaption conditions. Cell viability assay was performed under 1% O_2 hypoxia using the PrestoBlue reagent over 24, 48 and 72 hours of drug treatment at IC_{50} as determined by concentration-response curves at 48 hr at 1% O_2. Values represent mean ± SEM of three independent experiments for acute hypoxia and six independent experiments for hypoxia adaption. A two-way ANOVA was used to identify significant effects, with Tukey's multiple comparison test, *P < 0.05; **P < 0.01; ***P < 0.001; ****P < 0.0001. The experimental procedure was performed as described in Materials and Methods section 2.2.6. The experimental procedure was performed as described in Materials and Methods section 2.2.6.

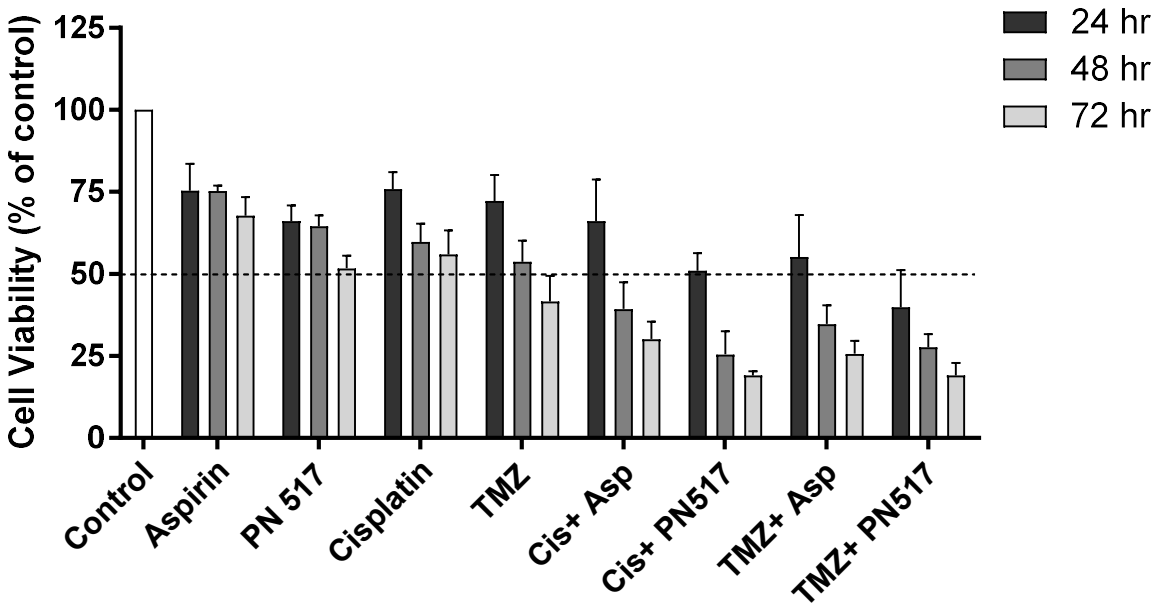

Figure 6. 5. The effect of drug treatment on cell viability of SVG-p12 hypoxia-adapted cells. Cell viability assay was performed under 1% O_2 hypoxia using the PrestoBlue reagent over 24, 48 and 72 hours of drug treatment at IC_{50} as determined by concentration-response curves at 48 hr at 1% O_2. Values represent mean ± SEM of three independent experiments. A two-way ANOVA was used to identify significant effects, with Tukey's multiple comparison test, *P < 0.05; **P < 0.01; ***P < 0.001; ****P < 0.0001. The experimental procedure was performed as described in Materials and Methods section 2.2.6.

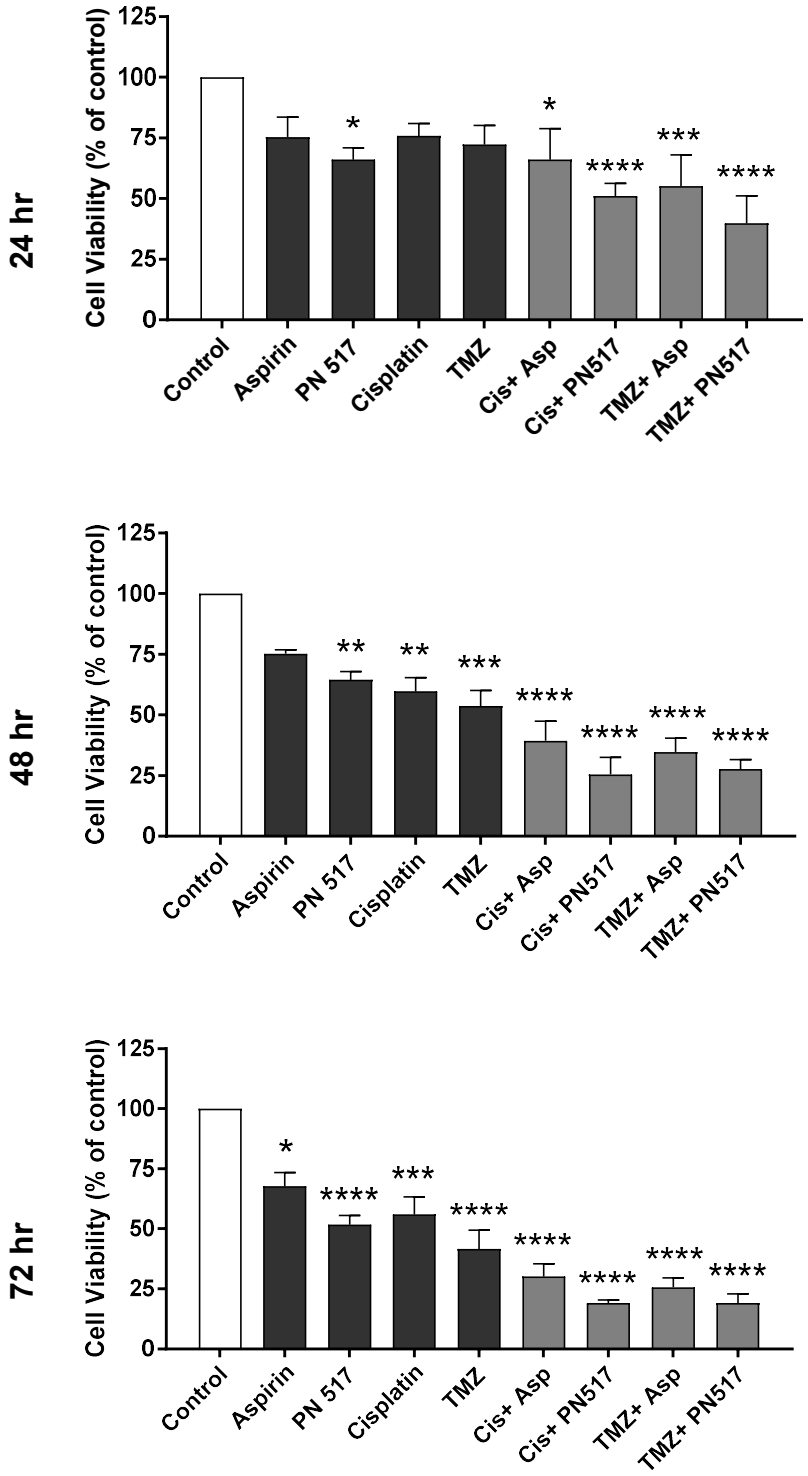

Figure 6. 6. The effect of combined therapy on cell viability of SVG-p12 hypoxia-adapted cells. Cell viability assay was performed under 1% O_2 hypoxia using the PrestoBlue reagent over 24, 48 and 72 hours of drug treatment at IC_{50} as determined by concentration-response curves at 48 hr at 1% O_2. Values represent mean ± SEM of three independent experiments. A two-way ANOVA was used to identify significant effects, with Tukey's multiple comparison test, *P < 0.05; **P < 0.01; ***P < 0.001; ****P < 0.0001. The experimental procedure was performed as described in Materials and Methods section 2.2.6.

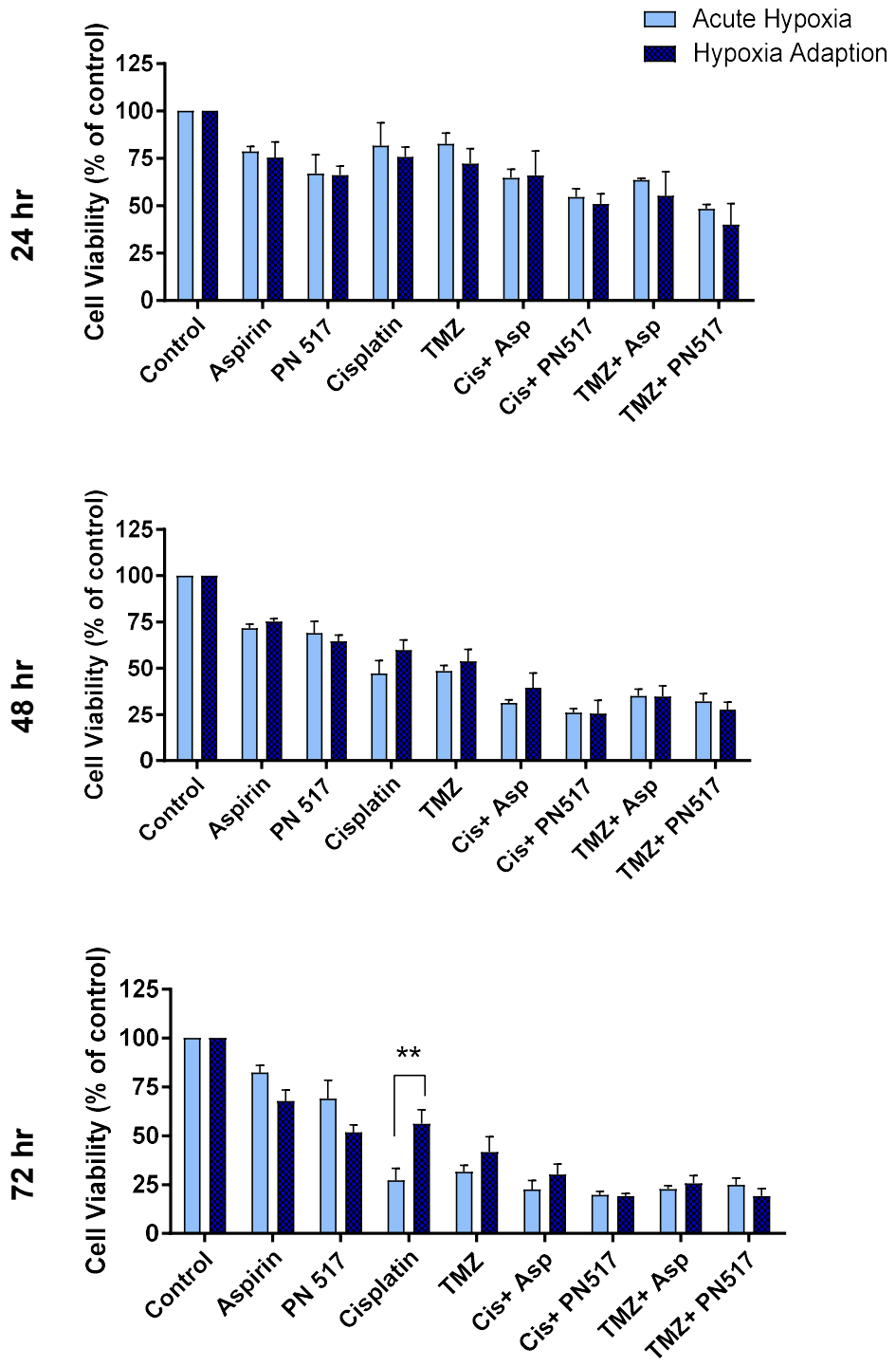

Figure 6. 7. The effect of drug treatment on cell viability of SVG-p12 under both acute hypoxia and hypoxia adaption conditions. Cell viability assay was performed under 1% O_2 hypoxia using the PrestoBlue reagent over 24, 48 and 72 hours of drug treatment at IC_{50} as determined by concentration-response curves at 48 hr at 1% O_2. Values represent mean ± SEM of three independent experiments for both conditions. A two-way ANOVA was used to identify significant effects, with Tukey's multiple comparison test, *P < 0.05; **P < 0.01; ***P < 0.001; ****P < 0.0001. The experimental procedure was performed as described in Materials and Methods section 2.2.6.

6.2.1.2. Effects of drug treatment on autophagy of 1% O_2 hypoxia-adapted cells

Autophagy induction was monitored in U87-MG and SVG-p12 hypoxia-adapted cells at 1% O_2 following 24 hr of drug treatment using Cyto-ID staining and flow cytometry. IC_{50} values determined from mono-treatment cell viability for 48 hr under hypoxia were used for all drugs either separately or in combination. Rapamycin and Chloroquine were included as a positive control (Rap+CLQ).

In U87-MG hypoxia-adapted cells, a clear induction of autophagy was observed by the positive control (p<0.0001) while little induction was observed by any treatment (Fig 6.8). Only TMZ among the drug treatments significantly induced autophagy compared to the control (p<0.05). Aspirin and its combinations appeared to induce more autophagy than PN517. Additionally, all drug treatments produced a trend towards less induction of autophagy in the hypoxia-adapted cells compared to the acute hypoxic condition. However, only the combination of cisplatin and aspirin induced a significantly lower level of autophagy in the hypoxia-adapted cells.

Regarding SVG-p12 hypoxia-adapted cells, the positive control also produced a significant induction of autophagy (p<0.01) but the effect was greater in acute hypoxia (p<0.0001). There was no significant difference observed for any of the drug treatments, either mono or combined therapy (p>0.05). Monotherapies produced a trend towards less efficacy in inducing autophagy in the adapted cells compared to the acute hypoxic cells, but the effects were very similar with the combinations. However, only TMZ induced a significantly lower level of autophagy in the hypoxia-adapted cells (Fig 6.8).

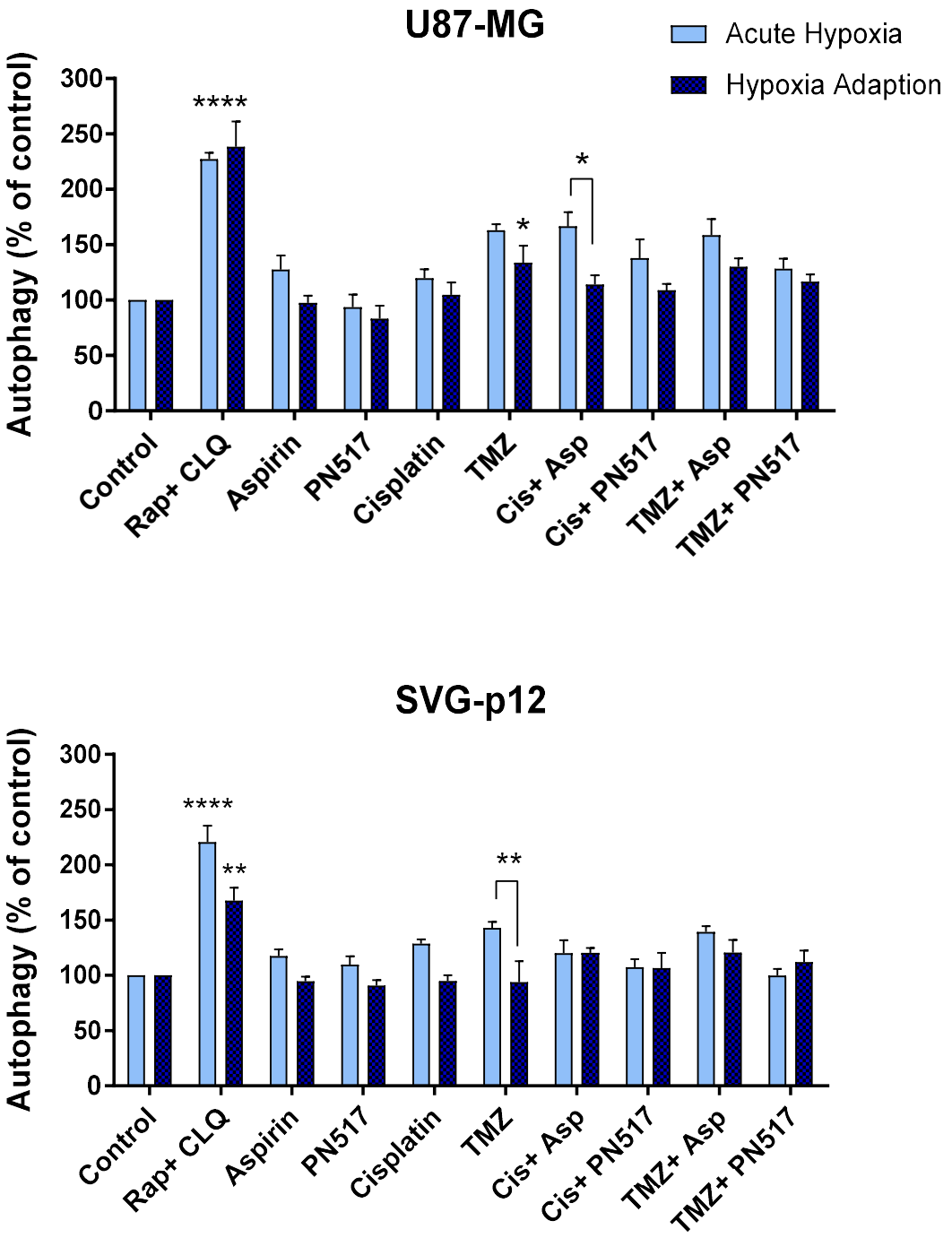

Figure 6. 8. The effect of drug treatment on inducing autophagy in U87-MG and SVG-p12 hypoxia-adapted cells. Data illustrates autophagy levels observed using Cyto-ID staining after 24 hours of drug treatment as a percentage of control. Values represent mean ±SEM of six independent experiment. A two-way ANOVA was used to identify significant effects, with Tukey's multiple comparison test, *P < 0.05; **P < 0.01; ***P < 0.001; ****P < 0.0001. The experimental procedure was performed as described in Materials and Methods section 2.2.10.

6.2.1.3. Effects of drug treatment on metabolic activity of 1% O_2 hypoxia-adapted U87-MG cells

In order to examine the bioenergetic profiles of both U87-MG hypoxia-adapted cell lines for control and treated cells, the Seahorse Extracellular Flux Analyser was used. Both mitochondrial stress tests and glycolytic stress tests were performed by measuring oxygen consumption and extracellular acidification rates, respectively, in real time. Additionally, the mitochondrial and glycolytic functions parameters were calculated by the Seahorse Report Generator software. The effect of the drug treatment was investigated following 24 hr of drug treatment, separately or in combination at IC_{50} as determined by the concentration-response cell viability curves after 48 hr under hypoxia. Hypoxia-adapted cells were cultured, incubated and treated under 1% O_2, however, the assays were performed under normoxia.

When comparing the untreated control of U87-MG hypoxia-adapted cells with the previous results obtained in normoxia and acute hypoxia, no significant difference observed in the basal respiration rate ($p>0.05$) (Fig 6.9). ATP production appears less effected by oligomycin addition in the adapted cells, but no significant difference observed in the respiration rates linked to ATP production or proton leak between the various conditions ($p>0.05$). Additionally, both the acute and adapted cells seemed to increase the non-mitochondrial respiration rate but that was not significantly different ($p>0.05$).

However, maximal respiration was significantly lower in the both acute hypoxic and adapted cells versus normoxia with the results of the adapted cells lying somewhere in between ($p<0.01$ and $p<0.05$, respectively) (Fig 6.9). Accordingly, acute cells had less spare respiratory capacity for mitochondrial ATP production compared to normoxia ($p<0.05$) and respiratory capacity was higher than in the acute hypoxic cells but not significantly different ($p>0.05$). It was noted that coupling efficiency was greater in the hypoxia-adapted cells but again with no significant difference ($p>0.05$).

In contrast, the adapted cells showed lower level of glycolysis compared to normoxia but not significantly different (p>0.05), as opposed to the acute cells where they showed significantly lower glycolytic activity compared to normoxic cells (p<0.0001) (Fig 6.10). There was marginal increase in the glycolysis capacity and decrease in the glycolytic reserve in the adapted cells compared to the cells under acute hypoxia (p>0.05). Also, hypoxia-adapted cells showed a trend towards reducing the non-glycolytic acidification rates, but no significant difference observed (p>0.05). Moreover, the hypoxia-adapted cells showed a trend towards lower OCR/ECAR ratio and higher Warburg effect compared to the cells under normoxia or acute hypoxia (Fig 6.10).

The effect of the drug treatment on the hypoxia-adapted U87-MG cells was examined. In general, data showed that PN517 and its combinations had the greatest efficacy on the mitochondrial respiration activity followed by aspirin (Fig 6.11). However, when comparing the bioenergetic parameters PN517 showed the lowest basal respiration and ATP production rate among monotherapies. Also, PN517 combination appeared to enhance the effect of cisplatin or TMZ, however, no significant difference was found for any of the treatments compared to the control (p>0.05) (Fig 6.12). Similarly, the lowest rate of maximal respiration was noted with PN517 and its combinations with no significant difference observed (p>0.05) (Fig 6.13). Additionally, the coupling efficiency seemed to be reduced with all drug treatments particularly with cisplatin treatments. Interestingly, aspirin was the only monotherapy that appeared to reduce the spare respiratory capacity, but no significant difference was observed (p>0.05) (Fig 6.14). When glycolysis was examined, all monotherapies showed inhibited glycolytic activity in general with PN517 and its combination producing the most antiglycolytic activity (Fig 6.15). Accordingly, the bioenergetic analysis showed that both PN517 and TMZ reduced glycolysis and glycolytic capacity. Also, the combinations of aspirin or PN517 appeared to enhance the effect of cisplatin and TMZ monotherapy but no significant differences were observed (p>0.05) (Fig 6.16). Interestingly, all drug treatments produced less non-glycolytic acidification especially with cisplatin but again with no significant differences observed (p>0.05) (Fig 6.17).

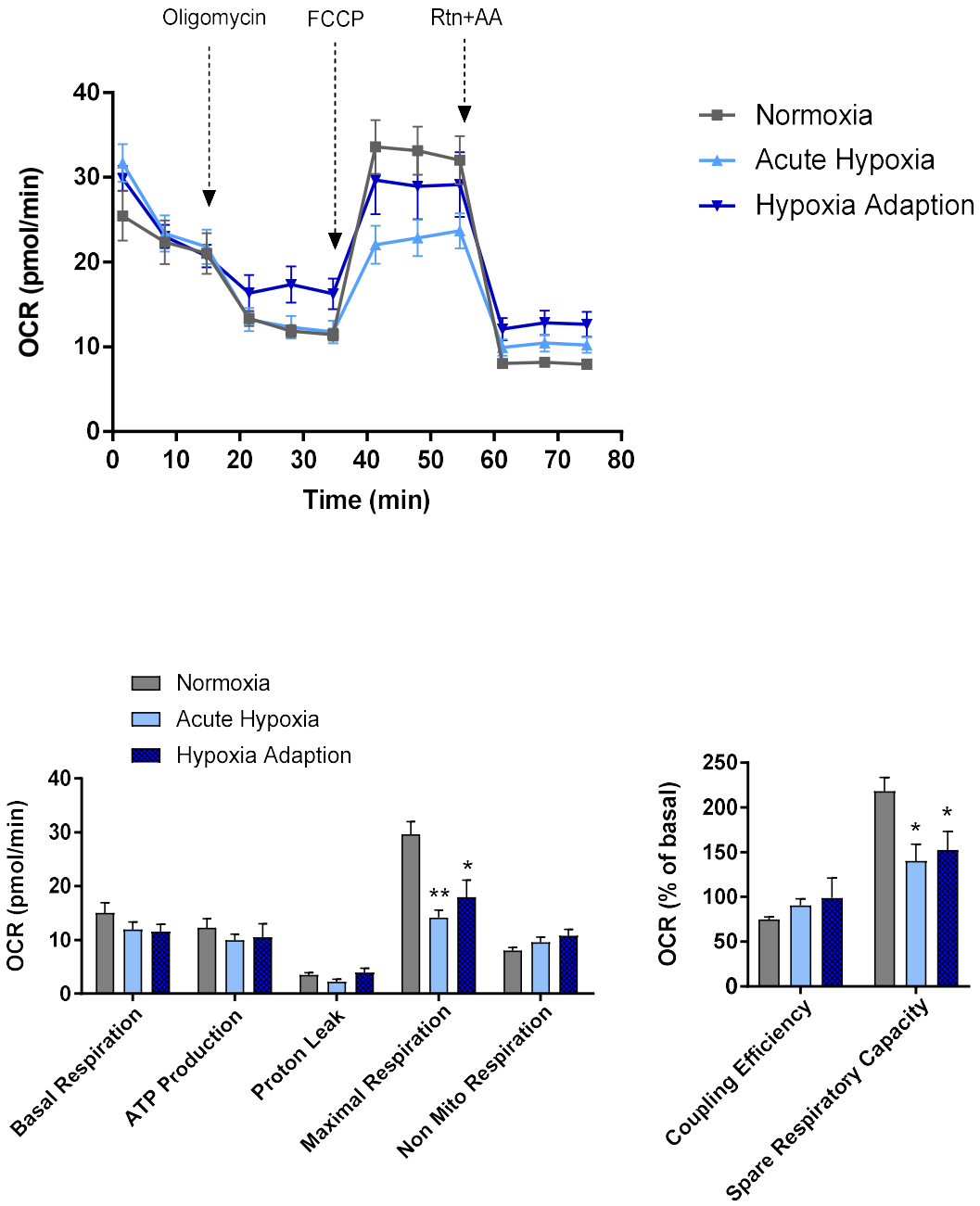

Figure 6. 9. Comparison of the mitochondrial respiration activity in both acute hypoxic and adapted U87-MG cell lines. Cells were incubated for 48 hr with culture media at 37°C with CO_2 under normoxia or 1% O_2 hypoxia then incubated for 45 min at 37°C without CO_2. A mitochondrial stress test was performed using XFp Extracellular Flux Analyser under normoxia and bioenergetic parameters were calculated. Values represent mean ± SEM generated from five independent experiments for normoxia, three independent experiments for acute hypoxia and four independent experiments for hypoxia adapted cells. A two-way ANOVA was used to identify significant effects, with Bonferroni's multiple comparison test, *P < 0.05; **P < 0.01; ***P < 0.001; ****P < 0.0001. The experimental procedure was performed as described in Materials and Methods section 2.2.12.

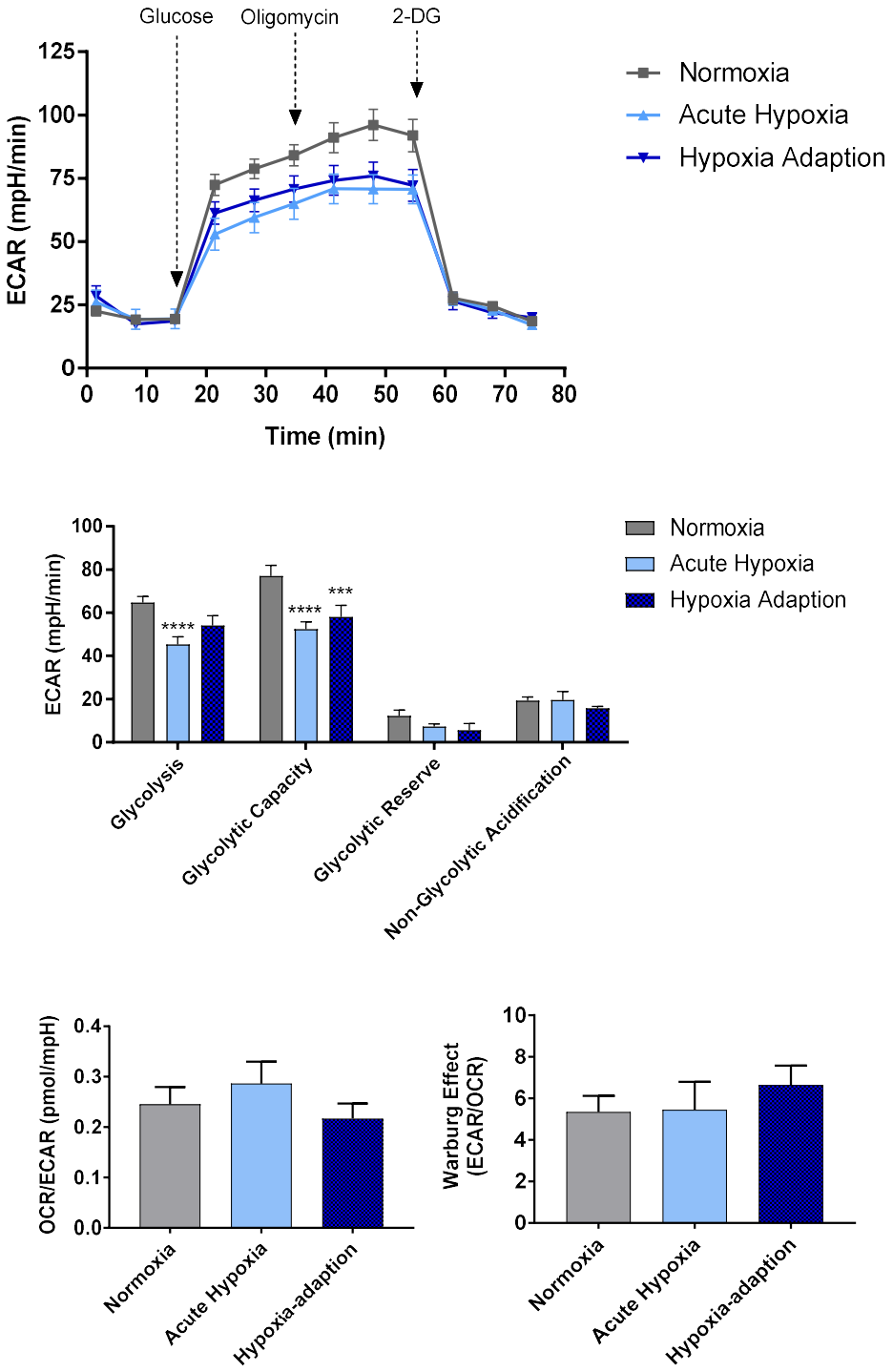

Figure 6. 10. Comparison of the glycolytic activity in both acute hypoxic and adapted U87-MG cell lines. Cells were incubated for 48 hr with culture media at 37°C with CO_2 under normoxia or 1% O_2 hypoxia then incubated for 45 min at 37°C without CO_2. A glycolysis stress test was performed using XFp Extracellular Flux Analyser under normoxia and bioenergetic parameters were calculated. Values represent mean ± SEM generated from five independent experiments for normoxia, three independent experiments for acute hypoxia and four independent experiments for hypoxia adapted cells. A two-way ANOVA was used to identify significant effects, with Bonferroni's multiple comparison test, *P < 0.05; **P < 0.01; ***P < 0.001; ****P < 0.0001. The experimental procedure was performed as described in Materials and Methods section 2.2.12.

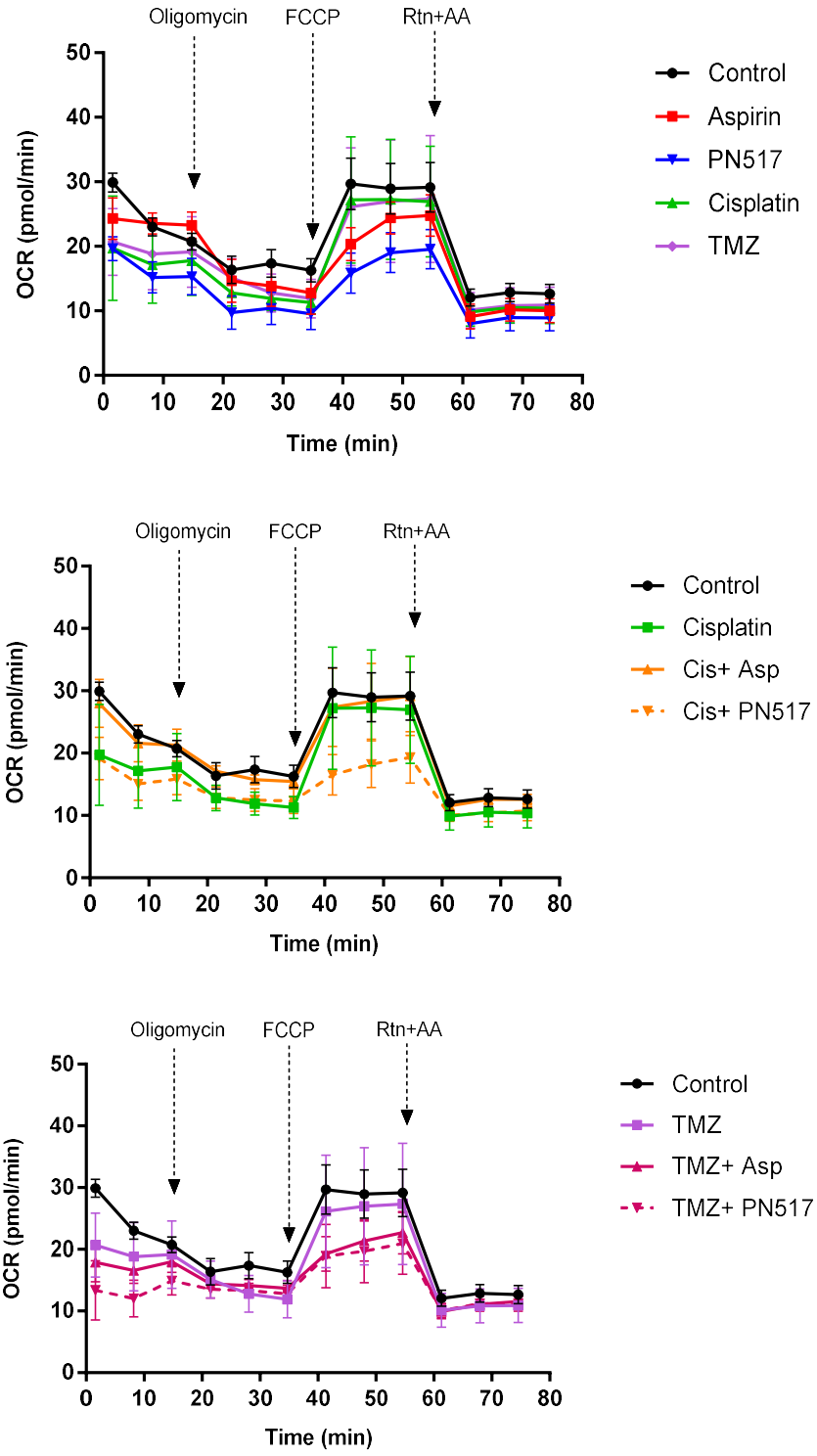

Figure 6. 11. The effect of drug treatment on mitochondrial activity in U87-MG hypoxia-adapted cells. A mitochondrial stress test was performed using XFp Extracellular Flux Analyser following drug treatment for 24 hr and oxygen consumption rates were measured using sequential addition of oligomycin (1μM final), FCCP (0.5μM final), and rotenone+ antimycin A (0.5μM final). Arrows indicate the points at which the indicated compounds were added. Values represents mean ± SEM generated from four independent experiments. A two-way ANOVA was used to identify significant effects, with Tukey's multiple comparison test. The experimental procedure was performed as described in Materials and Methods section 2.2.12.

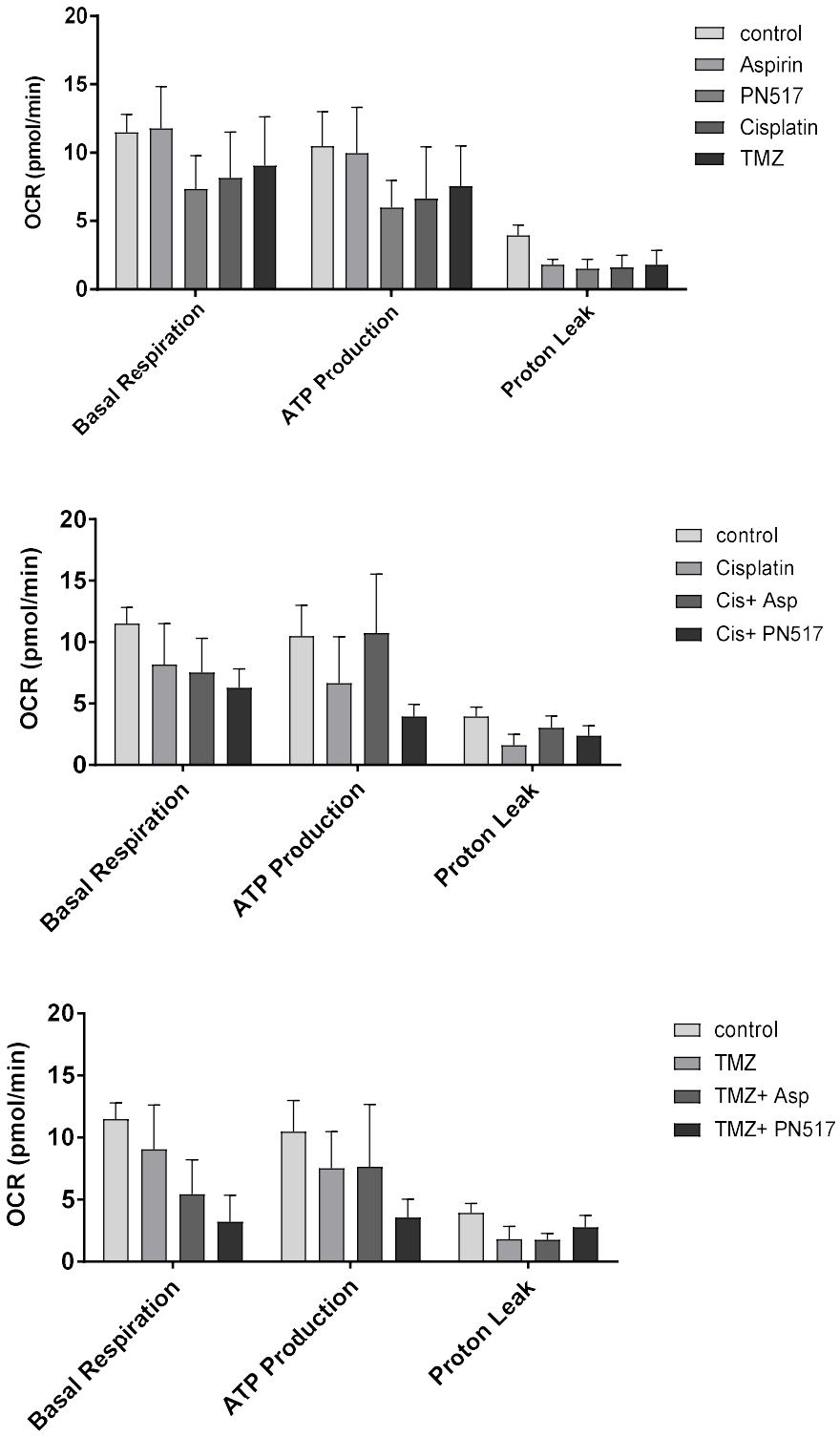

Figure 6. 12. The effect of drug treatment on basal respiration, ATP production and proton leak rates in U87-MG hypoxia-adapted cells. Data shows basal respiration, ATP-linked respiration, and proton leak-linked respiration generated by Seahorse Report Generator and plotted using GraphPad Prism. Values represent mean ± SEM generated from four independent experiments. A two-way ANOVA was used to identify significant effects, with Tukey's multiple comparison test, *P < 0.05; **P < 0.01; ***P < 0.001; ****P < 0.0001. The experimental procedure was performed as described in Materials and Methods section 2.2.12.

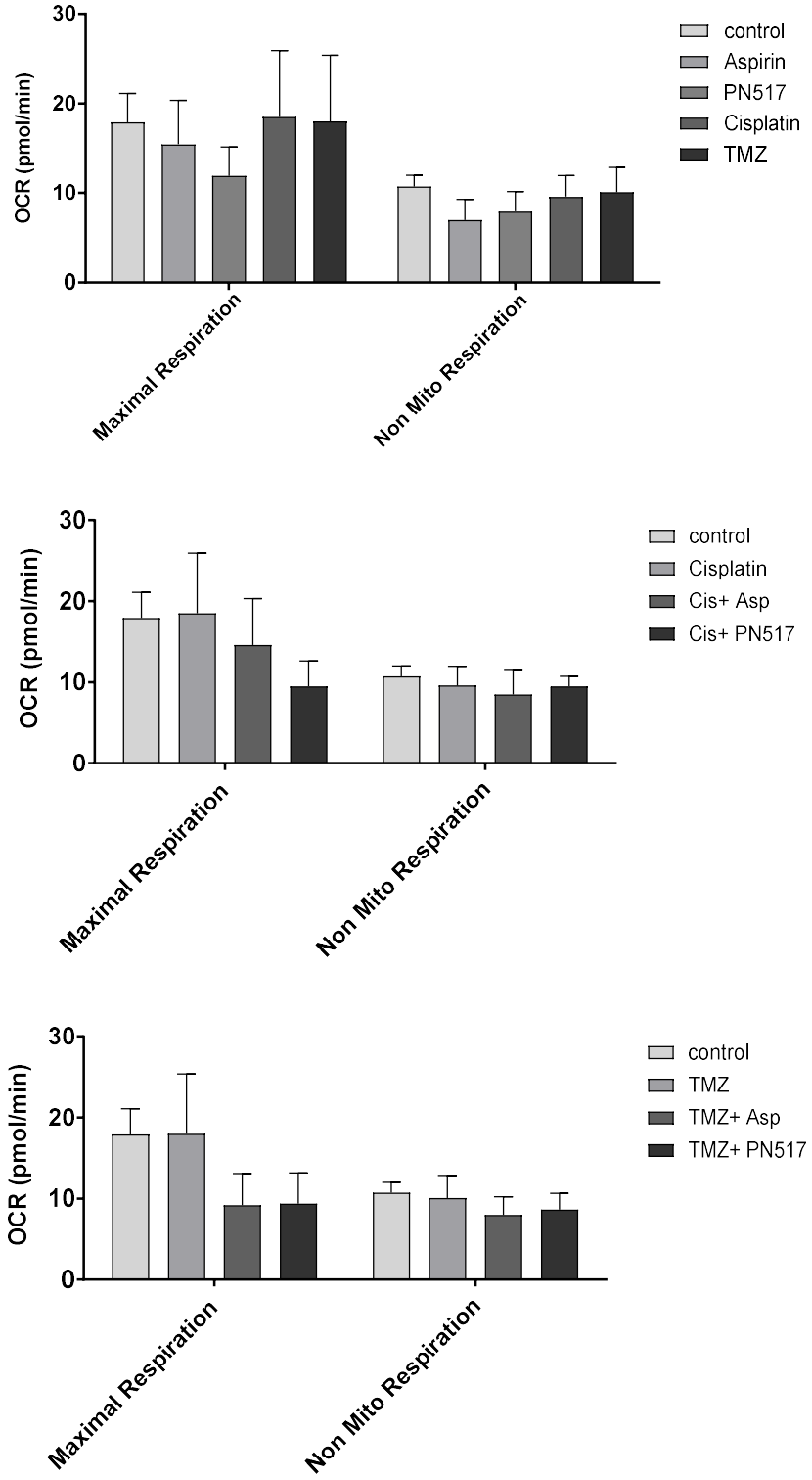

Figure 6. 13. The effect of drug treatment on maximal respiration and non-mito respiration rates in U87-MG hypoxia-adapted cells. Data shows maximal respiration and non-mitochondrial respiration generated by Seahorse Report Generator and plotted using GraphPad Prism. Values represent mean ± SEM generated from four independent experiments. A two-way ANOVA was used to identify significant effects, with Bonferroni's multiple comparison test, *P < 0.05; **P < 0.01; ***P < 0.001; ****P < 0.0001. The experimental procedure was performed as described in Materials and Methods section 2.2.12.

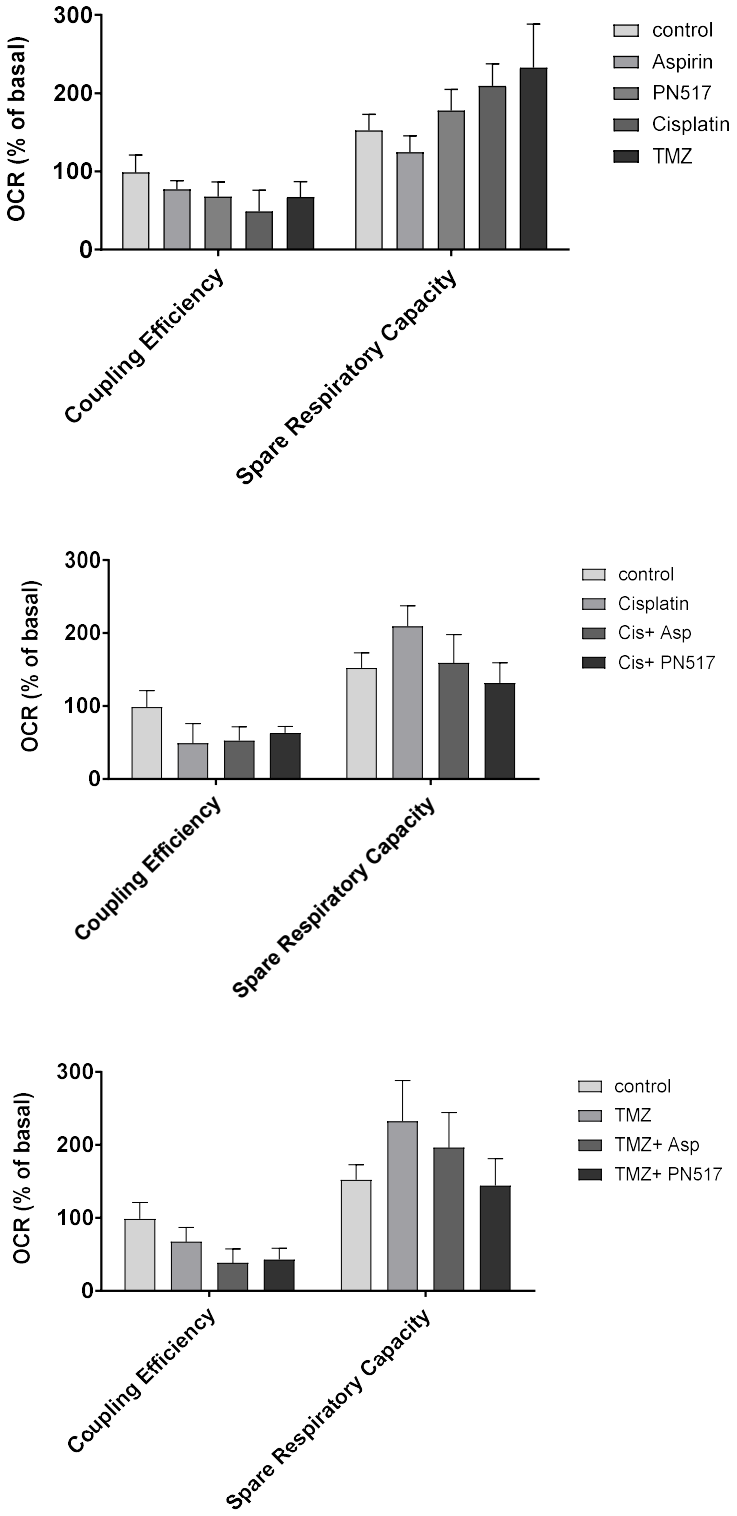

Figure 6. 14. The effect of drug treatment on coupling efficiency and spare respiratory capacity in U87-MG hypoxia-adapted cells. Data shows coupling efficiency spare respiratory capacity generated by Seahorse Report Generator and plotted using GraphPad Prism. Values represent mean ± SEM generated from for independent experiments. A two-way ANOVA was used to identify significant effects, with Bonferroni's multiple comparison test, *P < 0.05; **P < 0.01; ***P < 0.001; ****P < 0.0001. The experimental procedure was performed as described in Materials and Methods section 2.2.12.

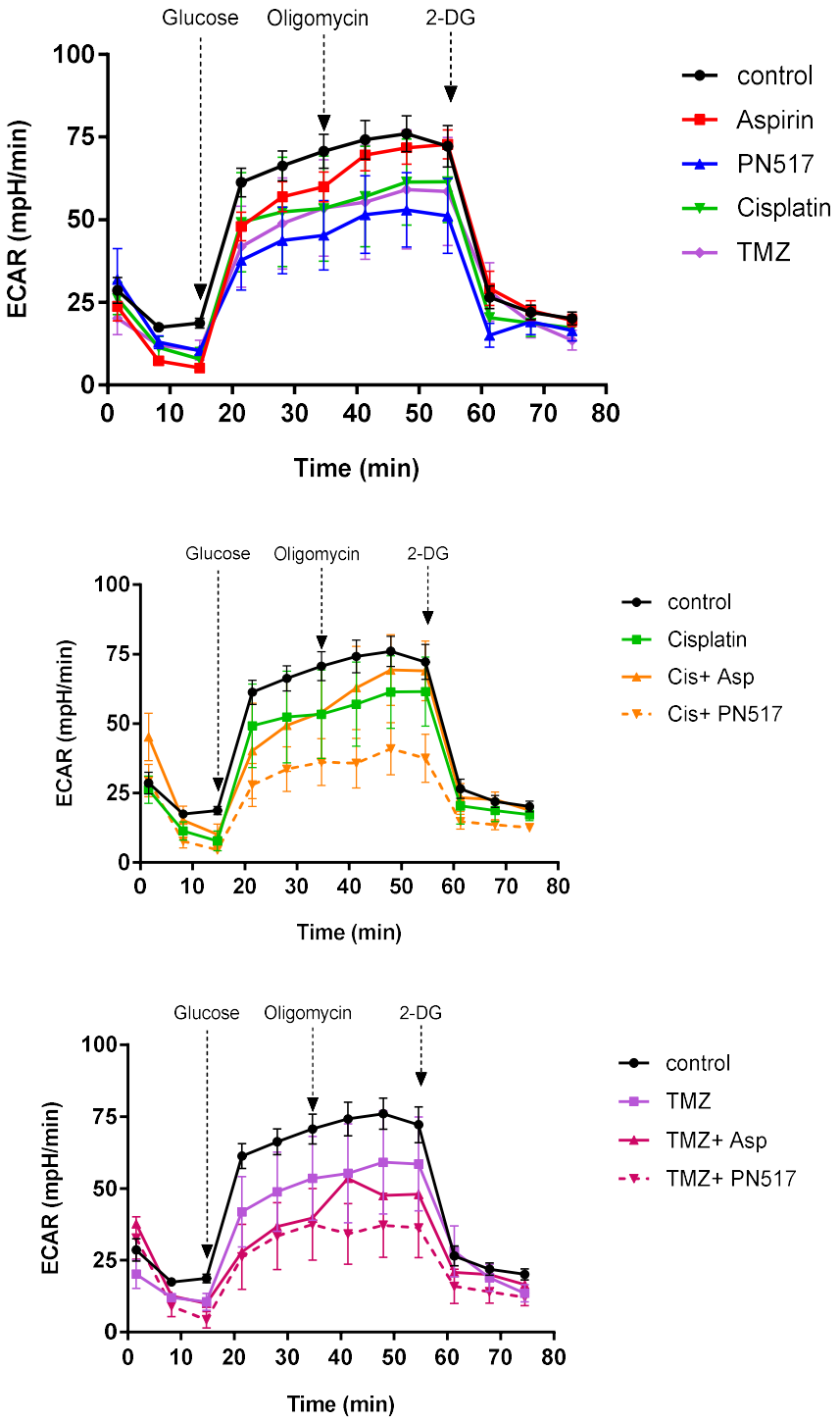

Figure 6. 15. The effect of drug treatment on glycolytic activity in U87-MG hypoxia-adapted cells. A glycolysis stress test was performed using XFp Extracellular Flux Analyser following drug treatment for 24 hr and extracellular acidification rates were measured using sequential addition of glucose (10mM final), oligomycin (1µM final), and 2-deoxyglucose (2-DG; 50mM final). Arrows indicate the points at which the indicated compounds were added. Values represent mean ± SEM generated from four independent experiments. A two-way ANOVA was used to identify significant effects, with Tukey's multiple comparison test. The experimental procedure was performed as described in Materials and Methods section 2.2.12.

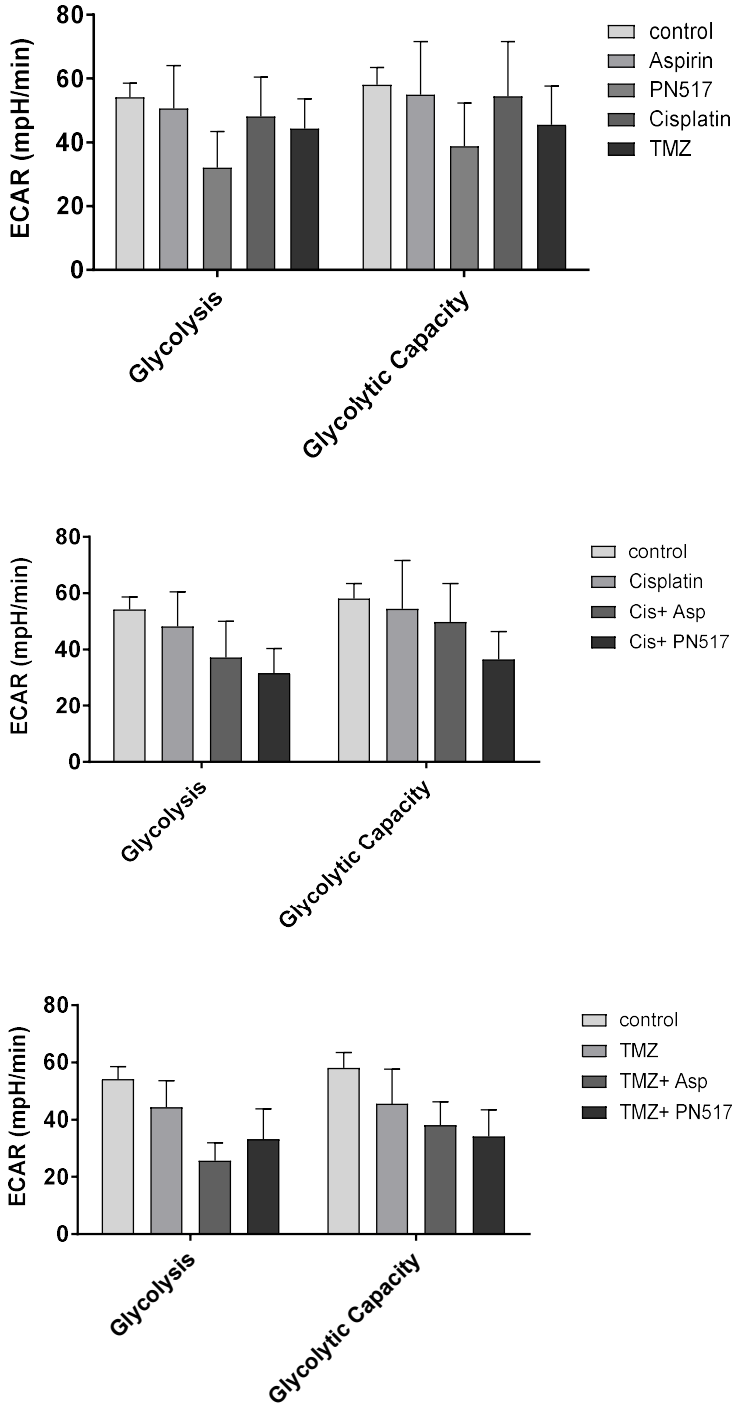

Figure 6. 16. The effect of drug treatment on glycolysis and glycolytic capacity in U87-MG hypoxia-adapted cells. Data shows glycolysis and glycolytic capacity rates generated by Seahorse Report Generator and plotted using GraphPad Prism. Values represent mean ± SEM generated from four independent experiments under. A two-way ANOVA was used to identify significant effects, with Bonferroni's multiple comparison test, *P < 0.05; **P < 0.01; ***P < 0.001; ****P < 0.0001. The experimental procedure was performed as described in Materials and Methods section 2.2.12.

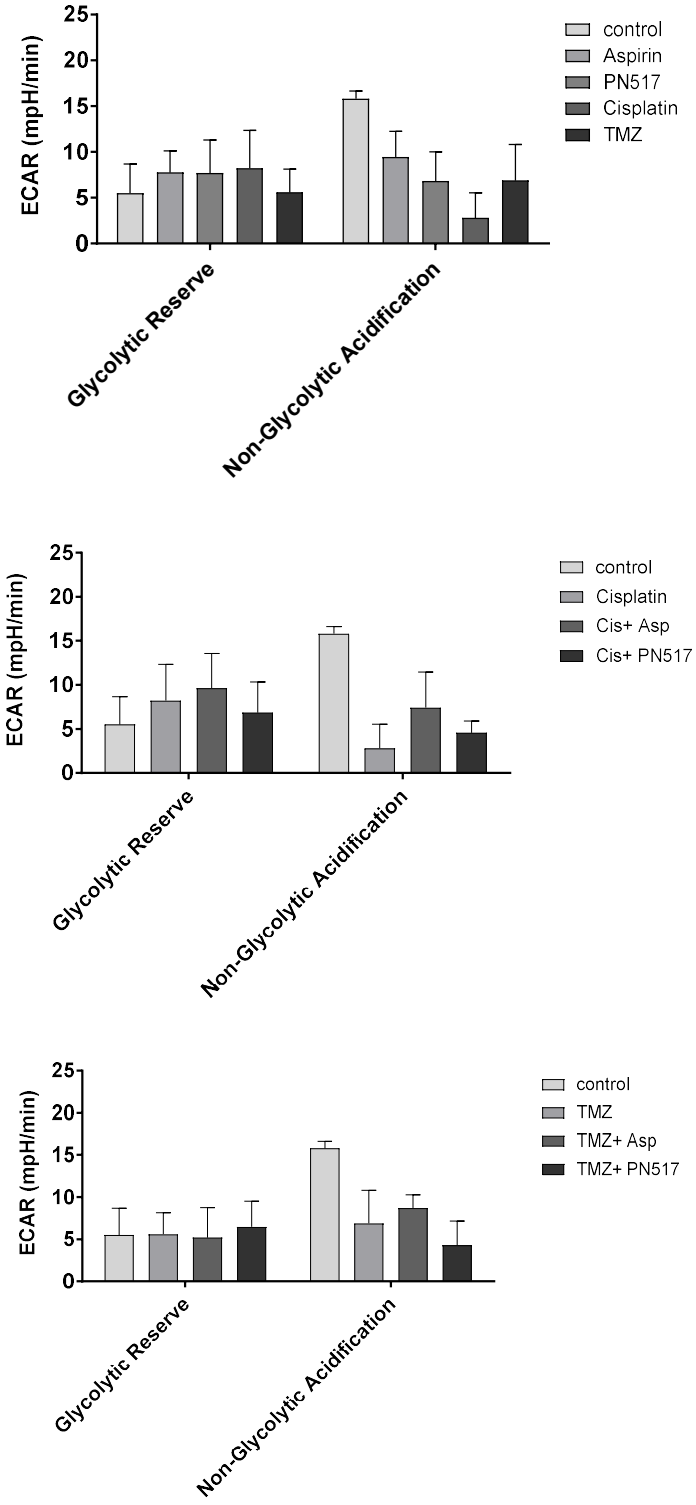

Figure 6. 17. The effect of drug treatment on glycolytic reserve and non-glycolytic acidification in U87-MG hypoxia-adapted cells. Data shows glycolytic reserve and non-glycolytic acidification rates generated by Seahorse Report Generator and plotted using GraphPad Prism. Values represent mean ± SEM generated from four independent experiments. A two-way ANOVA was used to identify significant effects, with Bonferroni's multiple comparison test, *P < 0.05; **P < 0.01; ***P < 0.001; ****P < 0.0001. The experimental procedure was performed as described in Materials and Methods section 2.2.12.

6.2.1.4. Effects of hypoxia exposure on HIF-1 proteins

In order to investigate changes in the regulation of HIF-1 proteins among the different culturing conditions, western blotting analysis was performed to detect any alterations in HIF-1α and HIF-1β expression levels. In addition, changes in the regulation of HIF-1α and HIF-1β were examined after 24 hour of drug treatment with aspirin or PN517. U87-MG cells were incubated in the corresponding oxygen concentration for three days and treated with aspirin or PN517 for 24 hr at same concentrations used for cell proliferation and cell cycle analysis (IC_{25}). Effects on protein expression and regulation were determined by specific antibodies using immunoblotting and quantified as a fold change of the untreated cells by densitometry. The housekeeping β-actin protein was used for normalisation of all samples to correct any loading differences between lanes. The experimental conditions applied can be found in the appendix (Table 9.2)

Data showed that there was a large fold increase in HIF-1α expression under hypoxia conditions compared to normoxia (Fig 6.18). The control U87-MG cells showed 40.2 ±11.8 fold increase in HIF-1α levels when incubated under acute hypoxia ($p<0.05$) (Fig 6.18). HIF-1α expression was even more increased when U87-MG cells were adapted to 5% O_2 and showed 64.4 ±22 fold change compared to normoxic cells ($p<0.01$) (Fig 6.18). Similarly, HIF-1α expression was increased when U87-MG cells were adapted to 1% O_2 and showed 43.3 ±15.4 fold change compared to normoxic cells ($p<0.05$). Interestingly, both aspirin, and PN517 to a greater extent, showed a trend towards decreasing HIF-1α expression under all studied conditions, however, no significant differences were observed when compared to the control of the same condition (Fig 6.18).

With regards HIF-1β expression, hypoxic conditions seemed to increase the level of HIF-1β protein. However, only in the hypoxia adaption at 5% O_2 there was significant increase over normoxia to 8.1 ±3.4 fold ($p<0.05$). Also, the drug treatment with aspirin or PN517 did not significantly change the HIF-1β level ($p>0.05$) (Fig 6.19).

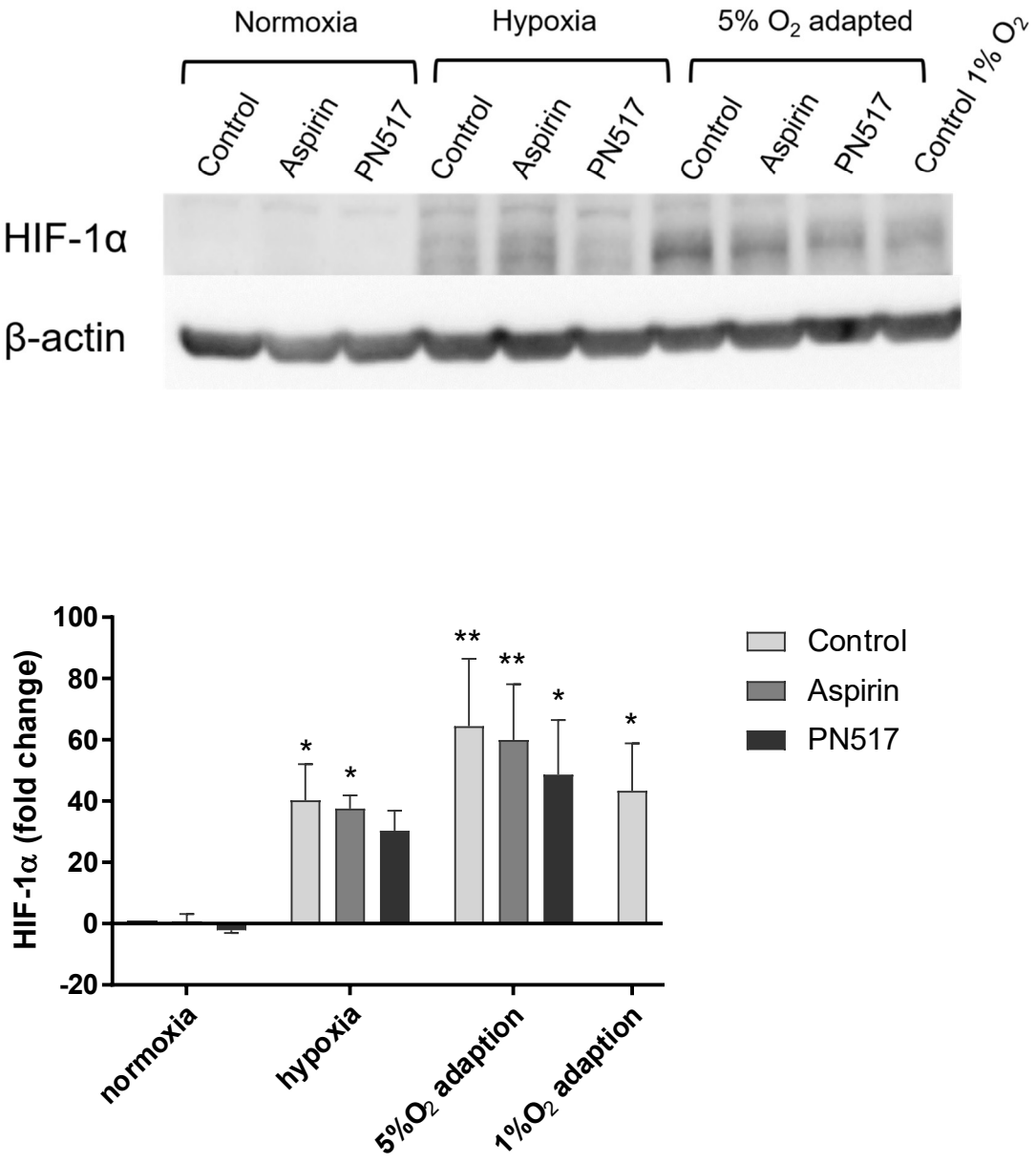

Figure 6. 18. Representative immunoblot and densitometric analysis of HIF-1α levels in U87-MG cell line under normoxia, acute hypoxia, 5% O_2 hypoxia adaption and 1% O_2 hypoxia adaption. Data indicate the fold change of HIF-1α levels following 24 hr of drug treatment as determined by densitometry. Values represent mean ±SEM of four independent experiment. A two-way ANOVA was used to identify significant effects, with Tukey's multiple comparison test, *P < 0.05; **P < 0.01; ***P < 0.001; ****P < 0.0001. The experimental procedure was performed as described in Materials and Methods section 2.2.16.

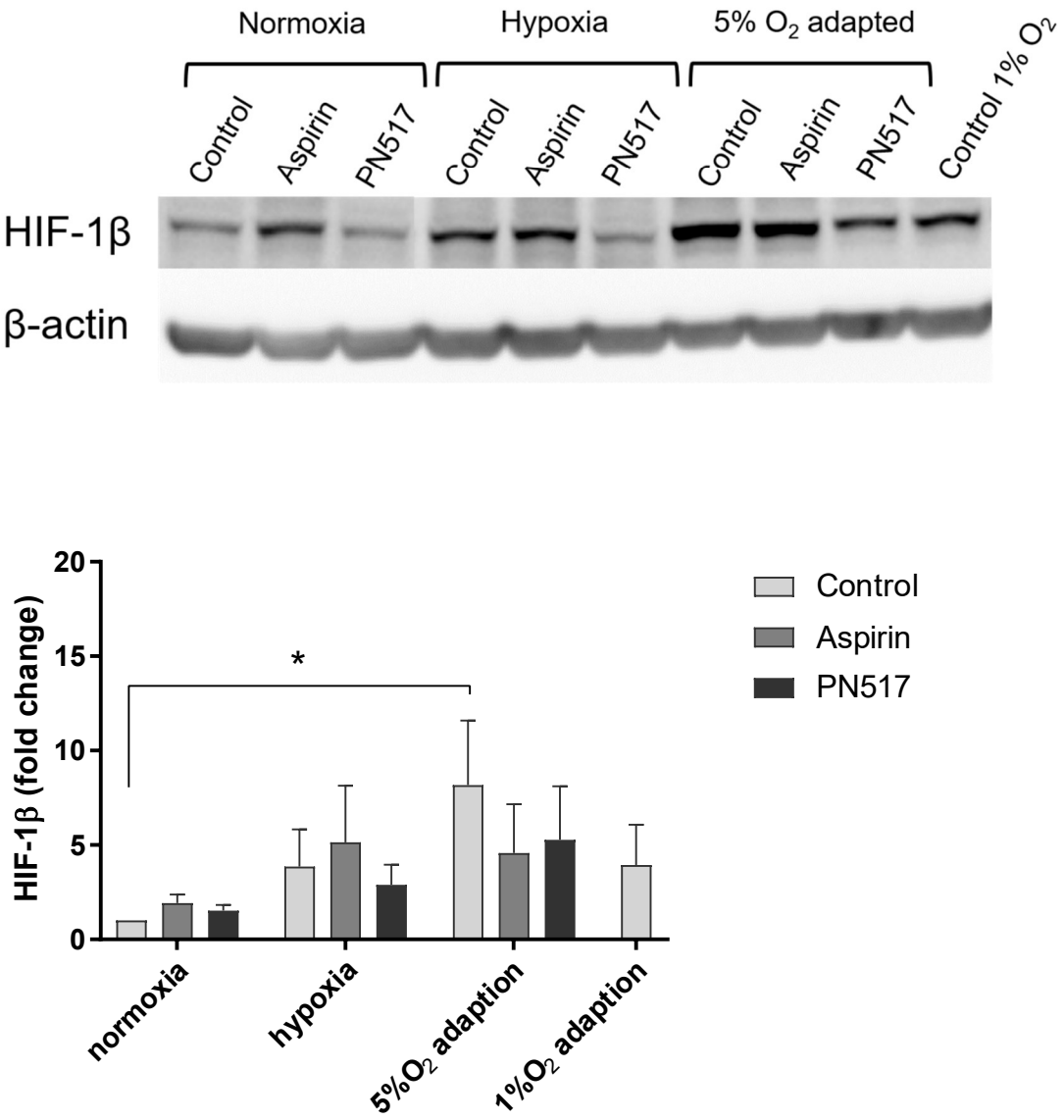

Figure 6. 19. Representative immunoblot and densitometric analysis of HIF-1β levels in U87-MG cell line under normoxia, acute hypoxia, 5% O_2 hypoxia adaption and 1% O_2 hypoxia adaption. Data indicate the fold change of HIF-1β levels following 24 hr of drug treatment as determined by densitometry. Values represent mean ±SEM of four independent experiment. A two-way ANOVA was used to identify significant effects, with Tukey's multiple comparison test, *P < 0.05; **P < 0.01; ***P < 0.001; ****P < 0.0001. The experimental procedure was performed as described in Materials and Methods section 2.2.16.

6.2.2. 3D Spheroids Cell Culture

6.2.2.1. Spheroids characterisation

To monitor the formation of 3D U87-MG spheroids in Nunclon Sphera plates, cells were seeded into Nunclon Sphera 96-well L-bottom plates in complete media under normoxia or hypoxia and images were taken every day after seeding over five days. U87-MG spheroids formed after only 24 hours of incubation even at the lowest seeding density of 250 cells/well, and spheroids formation exhibited highly uniform shape with well-defined edges and clean backgrounds, as well as very few “satellite colonies” at all seeding densities (Fig 6.20).

Spheroid size was estimated by measuring the diameters of the spheroids to monitor growth over the culture period. Data showed that U87-MG displayed reproducible spheroid growth as demonstrated by size measurements where diameter increased over time as well as with higher seeding cell number under both normoxia and hypoxia (Fig 6.21). However, spheroids appeared to reach a plateau at day 5 after seeding. Also, starting diameter was not different between conditions, however, potentially due to lower proliferation rates, the maximum diameter was lower under hypoxia.

Additionally, U87-MG spheroid cell health assessments were performed using the PrestoBlue cell viability reagent which detects the reducing power of live cells. After seven days of seeding, PrestoBlue reagent was added to each well and incubated at 37ºC and 5% CO2 under normoxia or hypoxia for an additional 1-5 hr and fluorescence was measured every hour on the microplate reader. The fluorescence signals were normalized by spheroid size where a higher ratio indicates healthier spheroids. Data showed the ability to detect the difference in cell viability after 4 hours of incaution with PrestoBlue reagent (Fig 6.22) and there was a clear correlation between seeding density and PrestoBlue fluorescence.

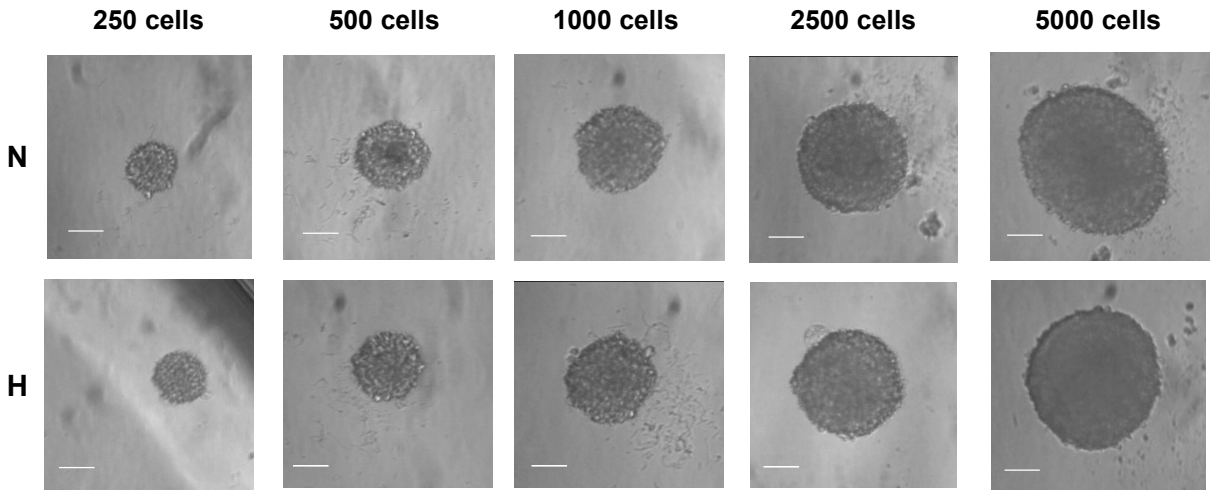

Figure 6. 20. Formation of U87-MG spheroids after 24 hr of seeding at different cell densities. U87-MG cells were seeded in Thermo Scientific™ Nunclon™ Sphera™ 96-well L-bottom plates at densities of 250–5000 cells/well in 200 µl/well complete growth media. Plates were briefly centrifuged at 250 xg for 5 min and incubated at 37°C with 5% CO_2 under normoxia (N) or hypoxia (H). Media was changed after 72 hr by carefully removing 100 µl of medium from each well and replenishing with 100 µl of fresh growth medium. Formation and growth of spheroids were imaged using inverted light microscope with 10X magnification (scale bar; 100 µm). The experimental procedure was performed as described in Materials and Methods section 2.2.1.

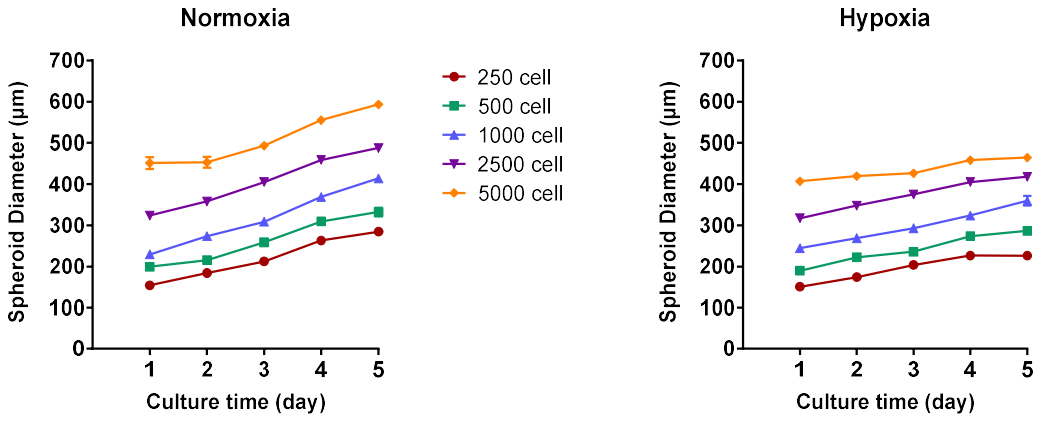

Figure 6. 21. Assessment of U87-MG spheroid growth under normoxia and hypoxia. Growth kinetics of U87-MG spheroids grown in Nunclon™ Sphera plates at increasing seeding densities were evaluated by measuring spheroid diameter (µm) over a period of five days after seeding. Values represent the mean ± SEM of four replicates for each cell number. A two-way ANOVA was used to identify significant effects, with Tukey's multiple comparison test. The experimental procedure was performed as described in Materials and Methods section 2.2.1.

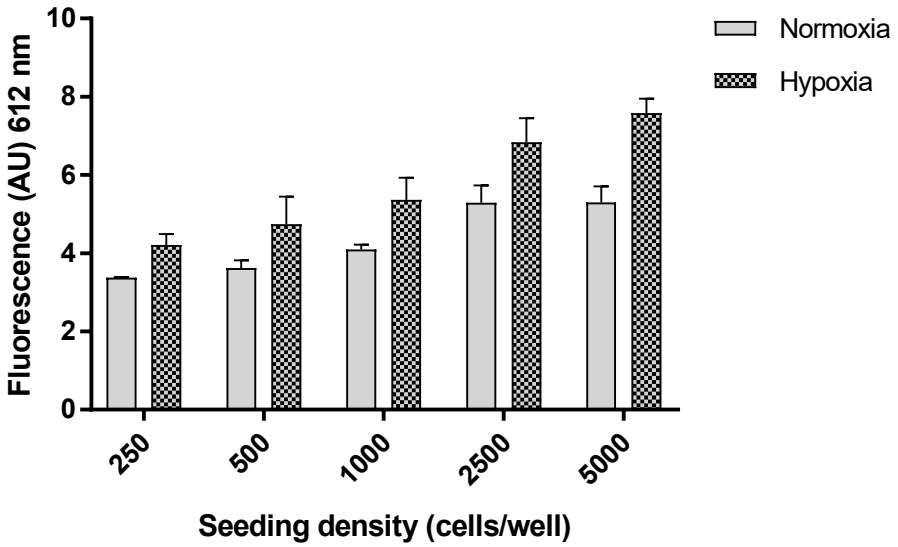

Figure 6. 22. Assessment of U87-MG spheroid cell health and viability under normoxia and hypoxia. Spheroid cell health was assessed using PrestoBlue cell viability reagent. After 7 days of spheroid culture, 20 µl of 10X PrestoBlue reagent was added to each well of the Nunclon Sphera plates, which were then incubated at 37ºC and 5% CO_2 under normoxia or hypoxia for an additional 4 hr before reading fluorescence on the microplate reader. The fluorescence signals were normalized by spheroid size. Values represent the mean ± SEM of four replicates for each cell number. The experimental procedure was performed as described in Materials and Methods section 2.2.1.

6.2.1.2. Effects of drug treatment on 3D culture viability

Following optimization of the process of spheroid formation, the effect of drug treatment on cell viability of U87-MG spheroids was investigated. U87-MG spheroids of 300-350μm diameter were formed after 24 hr of seeding 2500 cell/well in Nunclon Sphera plates under normoxia and hypoxia. Drug treatment was added, separately or in combination, at IC_{50} concentrations obtained from concentration-response cell viability curves at 48 hr. Cells were incubated for 48 and 72 hours prior to determining viability using the PrestoBlue assay.

In general, all drug treatments produced a time dependent effect on the cell viability of U87-MG spheroids where drugs showed obvious higher efficacy at 72 hours than at 48 hours in both normoxia and hypoxia (Fig 6.23). Interestingly, both aspirin and PN517 were more effective than cisplatin or TMZ. Combinations of either aspirin or PN517 with cisplatin and TMZ are typically more efficacious than the monotherapies, but most obviously with TMZ. Remarkably, there were fewer effects observed under hypoxia, although a time dependent effect was detected with overall similar pattern of drug treatment to normoxia (Fig 6.23).

At 48 hr of drug treatment under normoxia, cisplatin did not seem to reduce cell viability, whereas TMZ showed a small effect. Aspirin also reduced cell viability, but the change was not significant ($p>0.05$). Only PN517 among monotherapies produced a significant reduction in cell viability to 71.1 ±4.5% of control ($p<0.05$) (Fig 6.24). Importantly, PN517 effect was also significantly different from cisplatin ($p<0.05$). The drug combinations of cisplatin with aspirin showed enhanced effect over cisplatin, however, this combined effect was still not significant compared to the control ($p>0.05$). When cisplatin was combined with PN517, the combination effect significantly reduced cell viability to 64.6 ±5.6% of control ($p<0.001$). Additionally, the combinations of TMZ with either aspirin or PN517 produced significant decreases in cell viability compared to the control (52.5 ±5.6%, $p<0.0001$ and 50.1 ±5.9%, $p<0.0001$, respectively). Importantly, cisplatin and PN517 combination significantly enhanced the effect of cisplatin monotherapy ($p<0.01$). Likewise, TMZ effect was significantly enhanced when combined with aspirin ($p<0.001$) or PN517 ($p<0.0001$).

Following 72 hr of drug treatment under normoxia, cisplatin reduced cell viability but did not produce a significant difference compared to the control (p>0.05). Both TMZ and aspirin produced significant decreases in cell viability, to 64.7 ±6.6% (p<0.01) and 61.7 ±3.3% (p<0.01), respectively (Fig 6.24). PN517 produced the greatest efficacy among the monotherapies with a significant reduction in cell viability to 38.6 ±3.7% of control (p<0.0001), and PN517 effect was also significantly different from cisplatin (p<0.001). All drug combinations produced a significant decrease in cell viability compared to the control (p>0.0001) with the combination of TMZ and PN517 being the most effective treatment (27.2 ±3.9% of control). Aspirin enhanced the effect of cisplatin and TMZ monotherapies when in combination (p<0.05), while PN517 enhanced cisplatin (p<0.0001) and TMZ (p<0.01) effects to a greater extent (Fig 6.24).

In contrast, drug treatments did not result in any significant decrease in cell viability under hypoxia at 48 hr, although the combined therapy appeared to enhance the efficacy of individual treatments. However, at 72 hr of drug treatment, the combination of cisplatin with aspirin significantly reduced cell viability to 76.3 ±4.1% of control (p<0.05). Also, the combinations of TMZ with either aspirin or PN517 produced a significant decrease in cell viability compared to the control (62.7 ±9.3%, p<0.0001 and 60.2 ±5.4%, p<0.0001, respectively). In addition, these combinations significantly enhanced the efficacy of TMZ alone (p<0.05) (Fig 6.24).

To further demonstrate the viability of the U87-MG spheroids following drug treatment, the LIVE/DEAD viability/cytotoxicity assay was performed, which detects plasma membrane integrity and intracellular esterase activity. U87-MG spheroids of 300-350μm diameter were formed after 24 hr of seeding 2500 cell/well in Nunclon Sphera plates under normoxia and hypoxia. Drug treatment was added, separately or in combination, at IC_{50} concentrations obtained from concentration-response cell viability curves at 48 hr. Cells were incubated for 72 hours prior to staining with CFDA-SE and PI to detect live and dead cells, respectively. Under normoxia, it could be clearly seen form the spheroid images that PN517 and its combinations as well as TMZ, especially in combination, resulted in a higher proportion of dead cells in the spheroids associated with

higher red fluorescence signal compared to the control (Fig 6.25). Additionally, it was observed that spheroids of these combinations were notably smaller in size and distorted. However, a similar pattern yet less obvious effect was observed for the drug treatments under hypoxia (Fig 6.26).

Finally, a comparison of drug treatment effects on U87-MG cell viability was made between the previous results obtained from the 2D monolayers and the 3D spheroids models. It can be clearly seen that drug treatments were always more effective in the 2D monolayers (Fig 6.27). However, the same patterns of efficacy were observed, particularly under normoxia, so aspirin and PN517 being more effective than cisplatin or TMZ, and combinations with TMZ being the most effective. At 48 hr of drug treatment under normoxia, there was no significant difference in aspirin effect on cell viability between 2D and 3D models. In contrast, PN517, cisplatin and TMZ were significantly less effective in the 3D spheroids ($p<0.001$, $p<0.0001$ and $p<0.0001$, respectively) (Fig 6.27). Also, cisplatin and TMZ combinations were less effective in the 3D spheroids ($p<0.001$ and $p<0.05$). However, at 72 hr of drug treatment, a greater decrease in cell viability was observed in the 3D spheroids and the values were only significantly different from the 2D cultures with the treatment of cisplatin ($p<0.0001$) TMZ ($p<0.0001$) or the combination of cisplatin and aspirin ($p<0.05$) (Fig 6.27). Interestingly, under hypoxia, all drug treatments were significantly less effective in the 3D spheroid cultures compared to the 2D monolayers at both timepoints ($p<0.0001$), with drug combinations of PN517 still showing the highest efficacy (Fig 6.28).

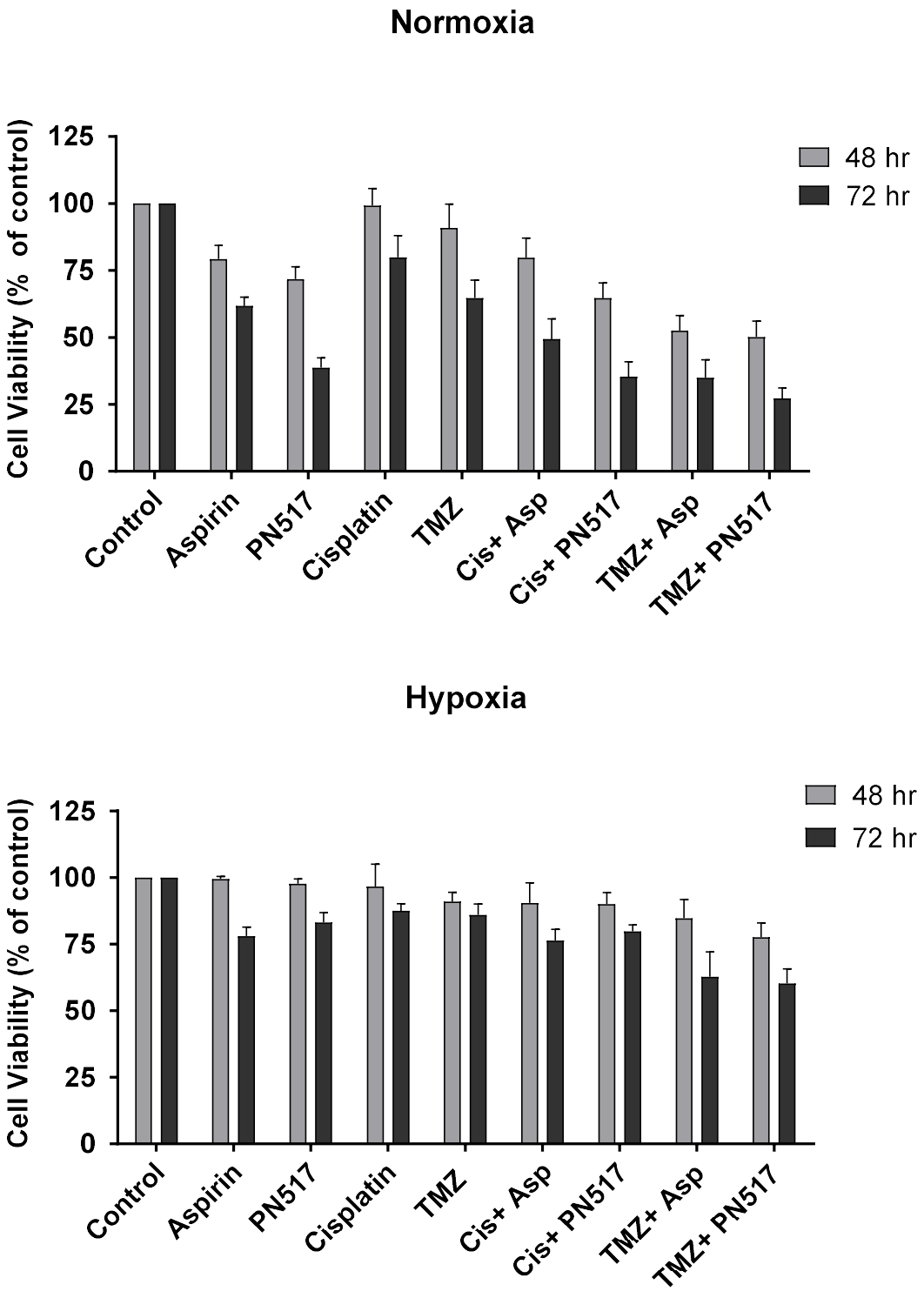

Figure 6. 23. The effect of drug treatment on cell viability of U87-MG spheroids under normoxia and hypoxia. A cell viability assay was performed under normoxia and hypoxia using the PrestoBlue reagent over 48 and 72 hours of drug treatment at IC_{50} as determined by concentration-response curves at 48 hr. Values represent mean ± SEM of five independent experiments. A two-way ANOVA was used to identify significant effects, with Tukey's multiple comparison test, *P < 0.05; **P < 0.01; ***P < 0.001; ****P < 0.0001. The experimental procedure was performed as described in Materials and Methods section 2.2.6.

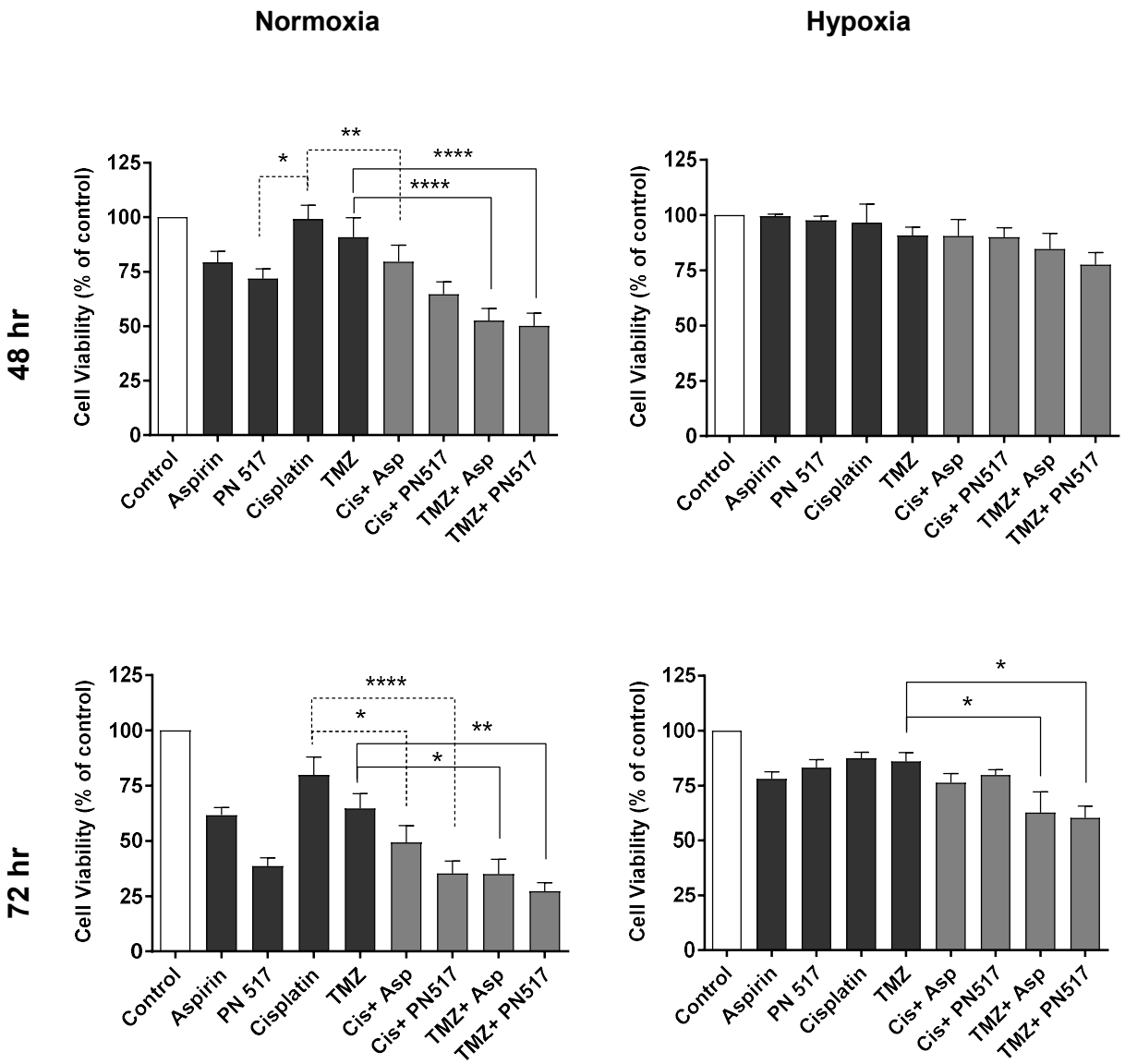

Figure 6. 24. The effect of combined therapy on cell viability of U87-MG spheroids under normoxia and hypoxia. A cell viability assay was performed under normoxia and hypoxia using the PrestoBlue reagent over 48 and 72 hours of drug treatment at IC_{50} as determined by concentration-response curves at 48 hr. Values represent mean ± SEM of five independent experiments. A two-way ANOVA was used to identify significant effects, with Tukey's multiple comparison test, *P < 0.05; **P < 0.01; ***P < 0.001; ****P < 0.0001. The experimental procedure was performed as described in Materials and Methods section 2.2.6.

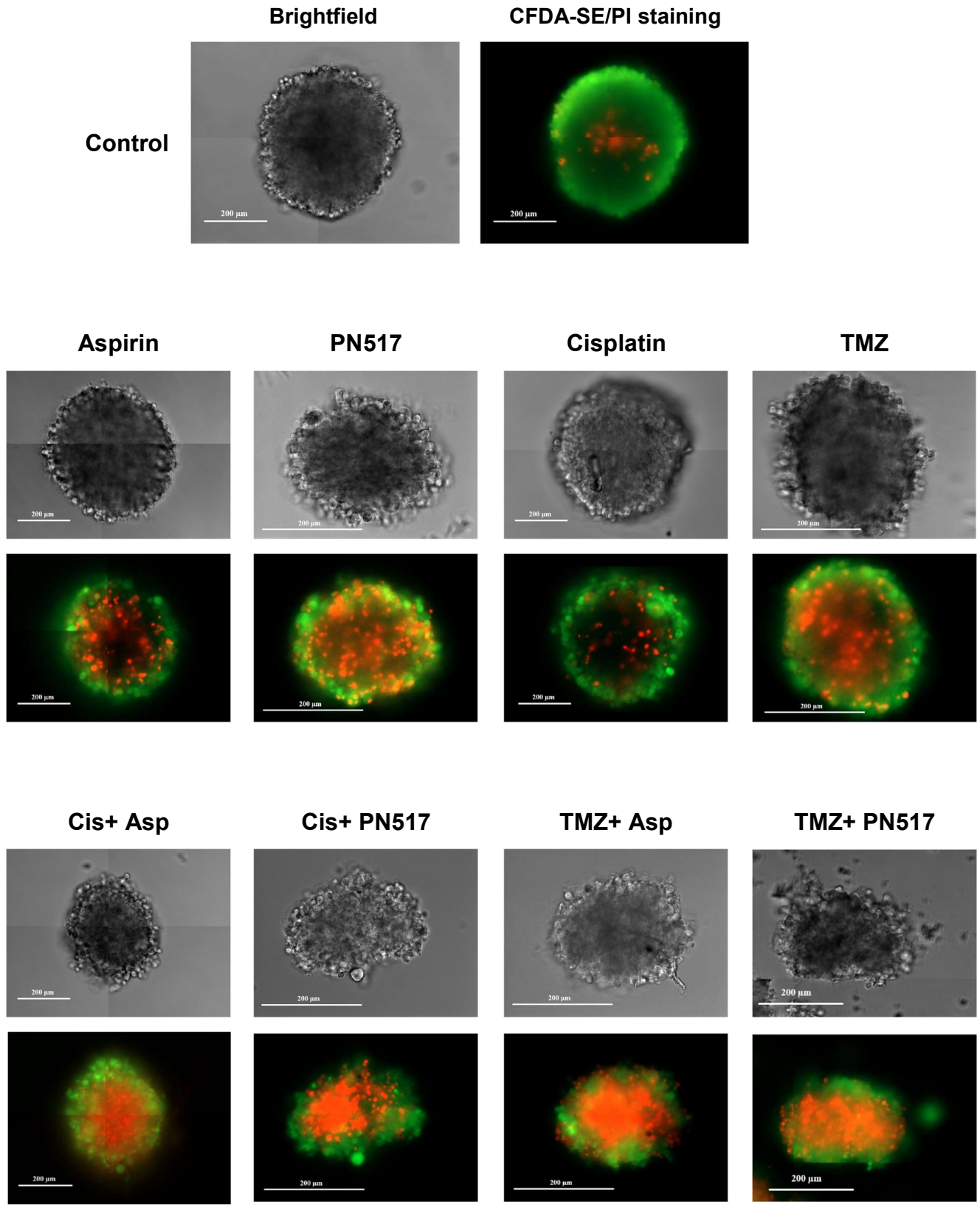

Figure 6. 25. Representative microscopic images of Live/Dead cell viability assay in U87-MG spheroids under normoxia. Live/dead imaging of U87-MG spheroids with initial seeding of 2500 cells/well was performed following 72 hr of drug treatment. Figure shows Brightfield images and CFDA-SE/PI staining where live cells stained with CFDA-SE (green) and dead cells with PI (red). The experimental procedure was performed as described in Materials and Methods section 2.2.7.

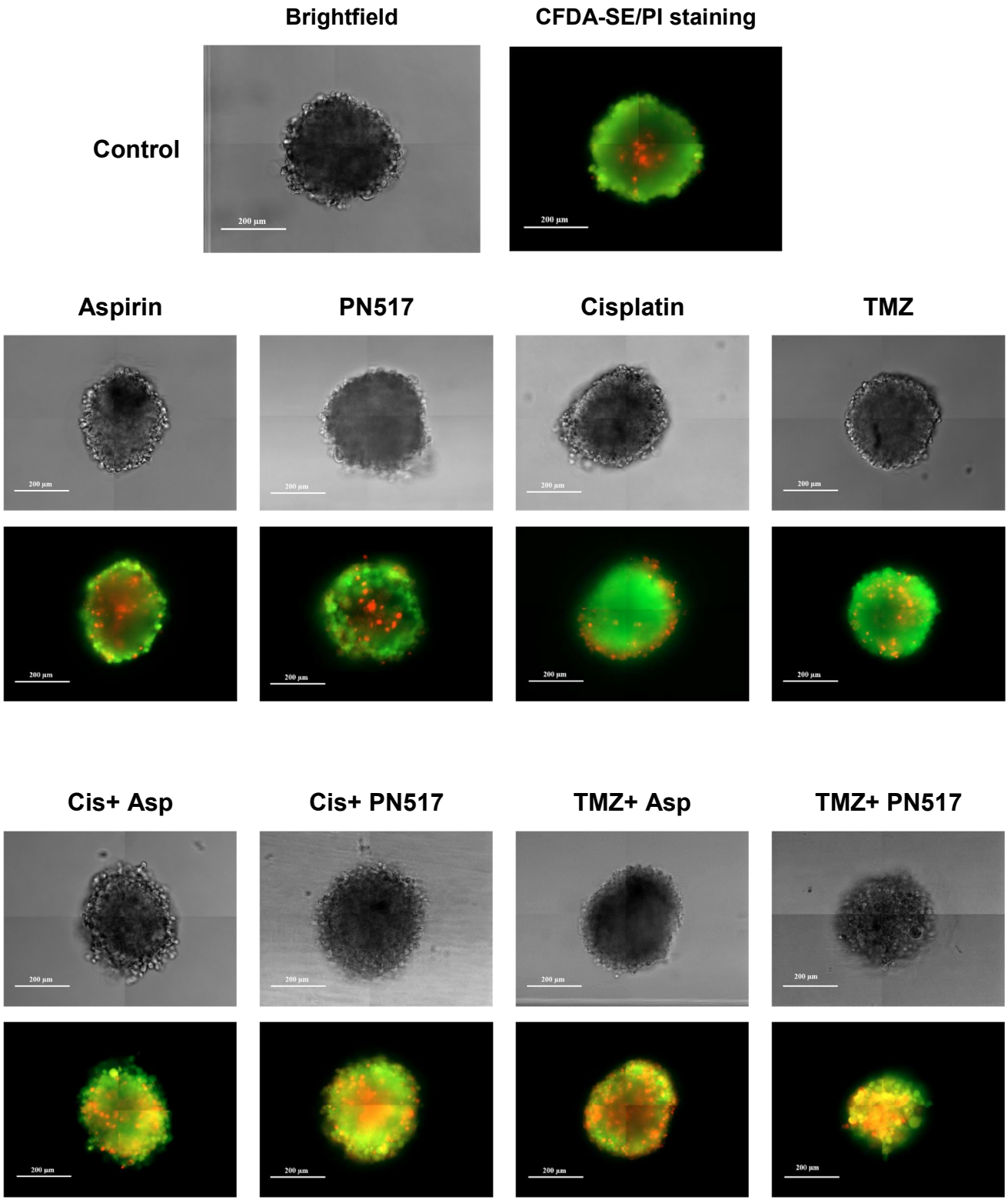

Figure 6. 26. Representative microscopic images of Live/Dead cell viability assay in U87-MG spheroids under hypoxia. Live/dead imaging of U87-MG spheroids with initial seeding of 2500 cells/well was performed following 72 hr of drug treatment. Figure shows Brightfield images and CFDA-SE/PI staining where live cells stained with CFDA-SE (green) and dead cells with PI (red). The experimental procedure was performed as described in Materials and Methods section 2.2.7.

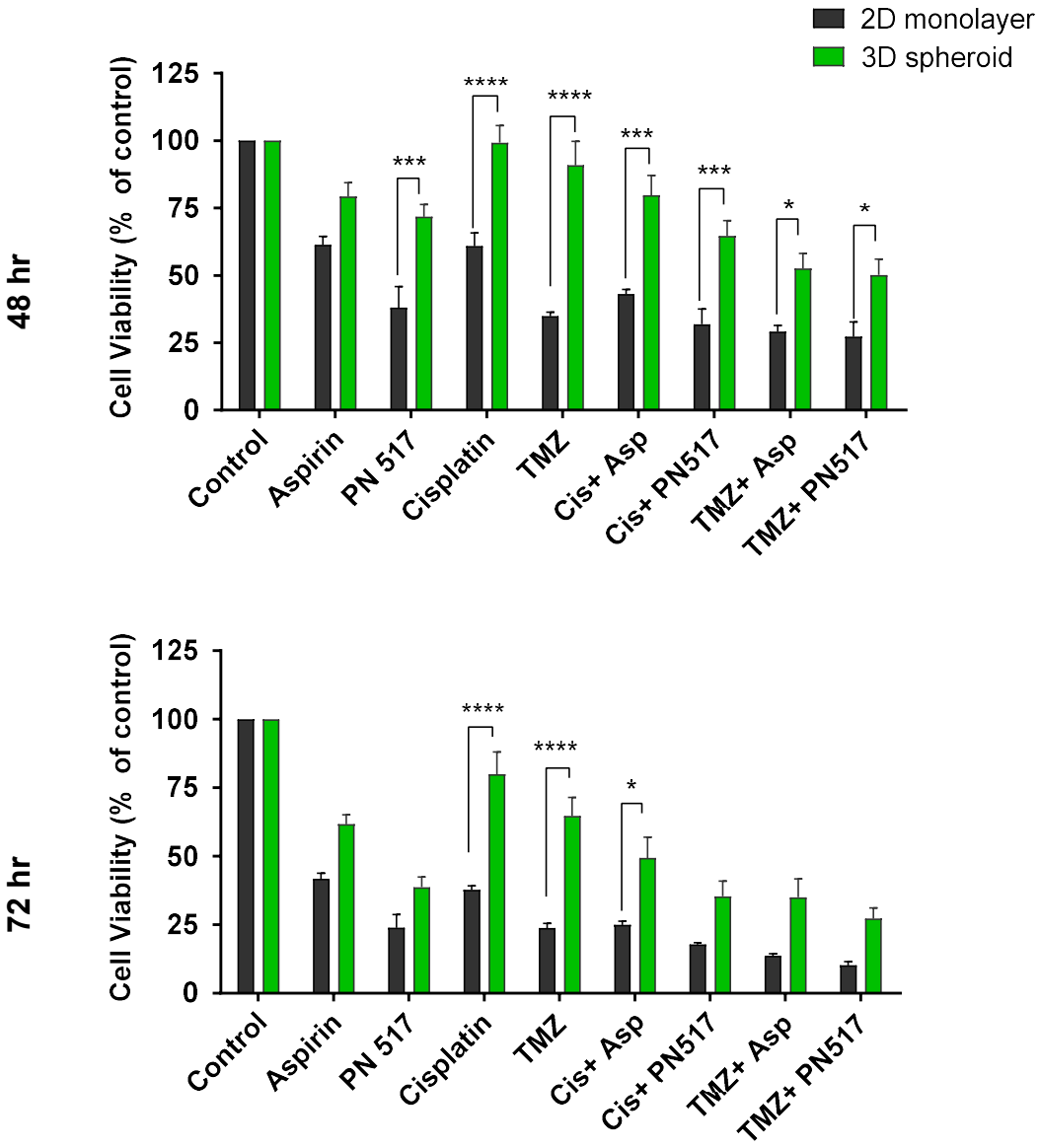

Figure 6. 27. Comparison of the effect of the drug treatment in U87-MG 3D spheroids and 2D monolayers under normoxia. A cell viability assay was performed using the PrestoBlue reagent over 48 and 72 hours of drug treatment at IC_{50} as determined by concentration-response curves at 48 hr. Values represent mean ± SEM of three independent experiments in 2D cultures and five independent experiments in 3D cultures. A two-way ANOVA was used to identify significant effects, with Tukey's multiple comparison test, *P < 0.05; **P < 0.01; ***P < 0.001; ****P < 0.0001. The experimental procedure was performed as described in Materials and Methods section 2.2.6.

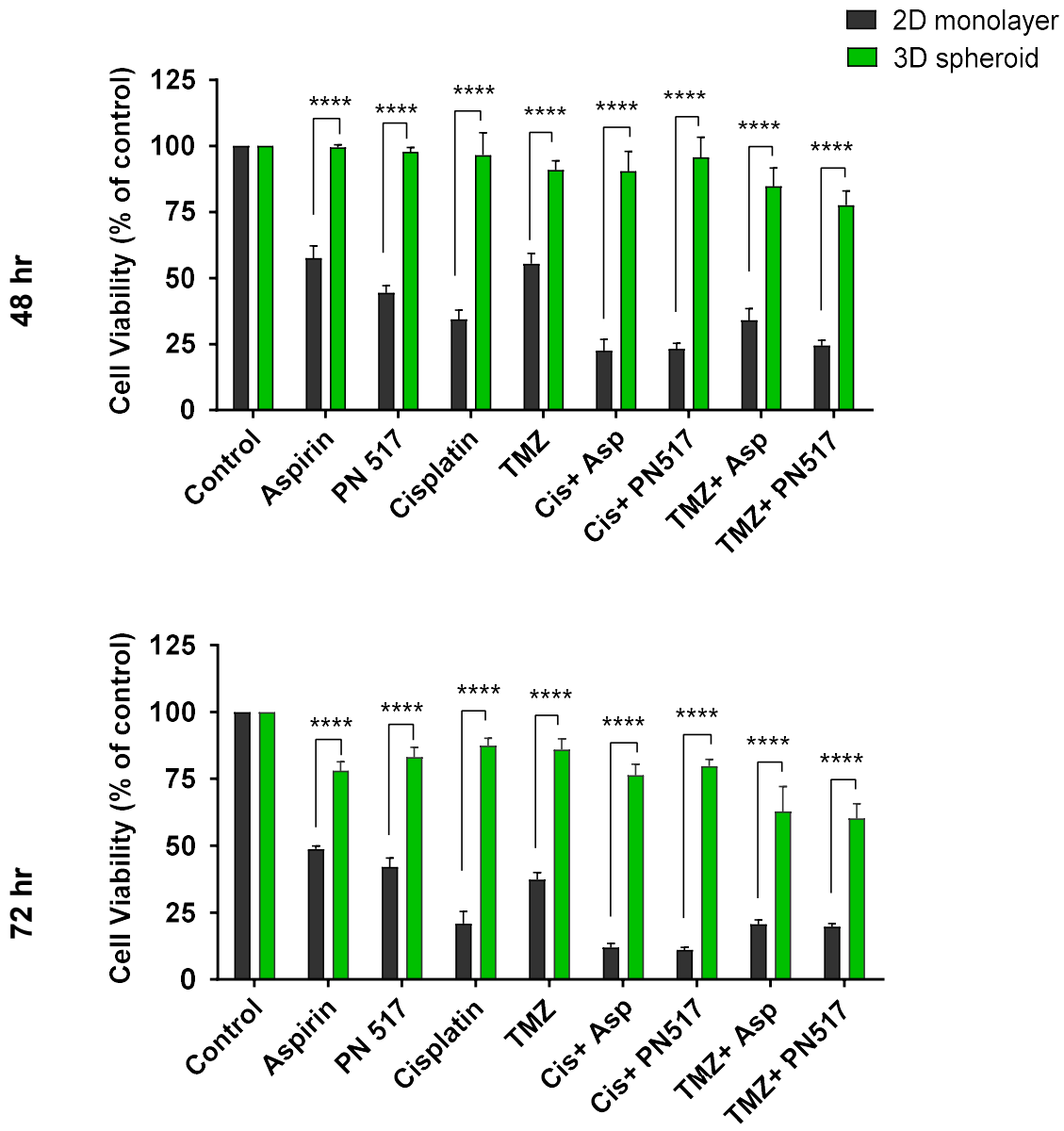

Figure 6. 28. Comparison of the effect of the drug treatment in U87-MG 3D spheroids and 2D monolayers under hypoxia. A cell viability assay was performed using the PrestoBlue reagent over 48 and 72 hours of drug treatment at IC_{50} as determined by concentration-response curves at 48 hr. Values represent mean ± SEM of three independent experiments in 2D cultures and five independent experiments in 3D cultures. A two-way ANOVA was used to identify significant effects, with Tukey's multiple comparison test, *P < 0.05; **P < 0.01; ***P < 0.001; ****P < 0.0001. The experimental procedure was performed as described in Materials and Methods section 2.2.6.

6.2.1.3. Effects of drug treatment on Lactate production

To investigate the effect of drug treatment on glycolytic activity of U87-MG spheroids, a lactate production assay was performed. U87-MG spheroids of 400-450μm diameter were formed after 24 hr of seeding 2500 cell/well in Nunclon Sphera plates under normoxia and hypoxia. Drug treatment was added, separately or in combination, at IC_{50} concentrations obtained from concentration-response cell viability curves at 48 hr. Following 24 hr of drug treatment the culture media was replaced with assay media and incubated for 3.5 hr then samples were collected and frozen. After collecting the samples for three independent experiments, the change in the lactate concentration in the extracellular assay media was measured using EnzyFluo^{TM} L-lactate fluorometric assay.

Data showed a similar pattern of results to the 2D cultures where all treatments appeared to reduce lactate production. PN517 was more effective than aspirin in reducing lactate production, and PN517 combinations appeared to be the most efficacious treatment under both normoxia and hypoxia (Fig 6.29). However, there were no significant differences observed for any or the monotherapies or combined therapies (p>0.05).

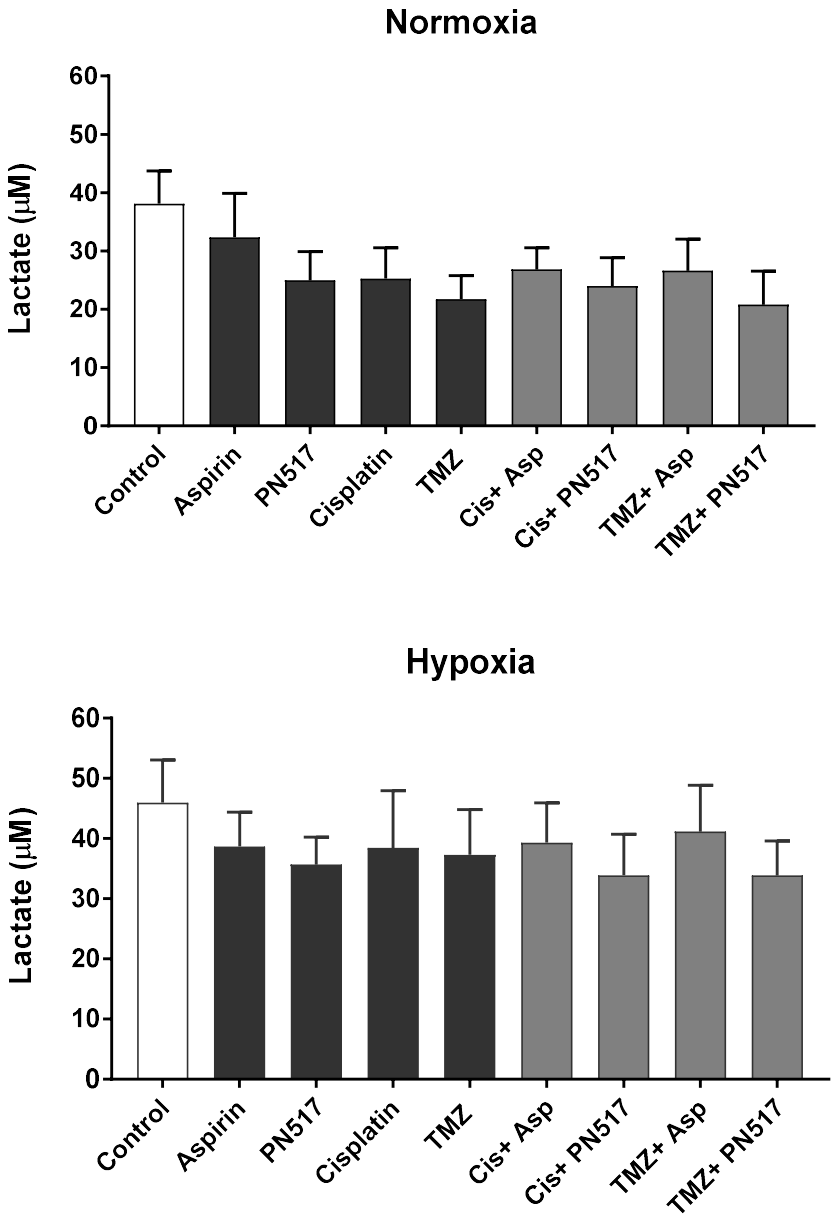

Figure 6. 29. The effect of drug treatment on lactate production in U87-MG spheroids under normoxia and hypoxia. Data represent lactate concentration (μM) after treating cells for 24 hr and incubating with assay media to excrete lactate for 3.5 hr. Values represent mean ± SEM generated from three independent experiments under normoxia and hypoxia. A two-way ANOVA was used to identify significant effects, with Bonferroni's multiple comparison test, *P < 0.05; **P < 0.01; ***P < 0.001; ****P < 0.0001. The experimental procedure was performed as described in Materials and Methods section 2.2.13.

6.3. Discussion

6.3.1. Chronic hypoxia-adapted cells

In contrast to other features of GBM tumour malignancy, the effects of hypoxia on GBM survival and response to drug treatment are poorly characterised. The aim of this chapter was to generate chronic hypoxia-adapted cell lines and investigate the effect of drug treatment on the adapted cells comparing the results with the acute hypoxic cells.

Experiments have shown that both U87-MG and SVG-p12 cells were able to grow and proliferate effectively at 5% O_2, which resembles the physiological conditions found in the brain. Some studies have indicated also that astrocytes are able to withstand extended periods of hypoxia (Swanson, 1992; Véga *et al.*, 2006). However, at 1% O_2 hypoxia, U87-MG cells were only able to continue proliferating yet at slower rate, while SVG-p12 cells exhibited substantially slower proliferation rate, an effect that may be because they are more sensitive to the acidosis often occurs during hypoxia (Norenberg *et al.*, 1987; Giffard *et al.*, 1990).

Additionally, it was observed that 1% O_2 adapted U87-MG cells could not sustain proliferation under severe hypoxia of 0.1% O_2 and died after a few days. Similar results were found in many studies where cell cycle arrest was induced in severe hypoxia or anoxia (Åmellem and Pettersen, 1991; Graeber *et al.*, 1994; Beppu *et al.*, 2002) and that long-term exposure to severe hypoxia results in cell death in different glioblastoma cell lines due to necrosis or cell cycle arrest (Richards *et al.*, 2016). However, investigations in brain tumours have shown that the proportion of severely hypoxic cells is low while the majority of tumour cells are exposed to moderate hypoxia (>0.5% O_2) (Evans *et al.*, 2004). The most severe regions of hypoxia in GBM are present adjacent to regions of necrosis, forming one of the defining characteristics of GBM called pseudopalisading necrosis. These cells were found to express high levels of HIF-1α and matrix metalloproteinases and are thought to have high migration capacity in a drive to move towards more favourable environment (Zagzag *et al.*, 2000; Søndergaard *et al.*, 2002). For that reason, areas of necrosis are associated with higher grade tumours and poorer prognosis (Hammoud *et al.*, 1996).

Hypoxia adaptation mechanism

At a cellular level, the chief regulator of oxygen homeostasis is the HIF signalling pathway. Under hypoxic conditions, HIF-1α is no longer degraded, and translocated to the nucleus activating the transcription of hundreds of genes for regulating cellular processes such as angiogenesis, glycolysis and invasion leading to tumour progression (Dengler *et al.*, 2014; Masoud and Li, 2015). HIF-1α expression is positively associated with tumour grade in gliomas, with the highest expression observed in high-grade gliomas (Zagzag *et al.*, 2000; Søndergaard *et al.*, 2002). Although HIF-1α is only present in small amounts above 1% O_2, cumulative evidence suggests a pro-proliferative role for HIF-1α in physiological oxygen conditions. For example, neural progenitor cells display an increased proliferation at 10% O_2 mediated by HIF-1α. In addition, the moderate induction of HIF-1α at 5% O_2 has been shown to encourage proliferation of both cancer and noncancerous cell lines, suggesting an important role for HIF-1α in normal cell physiology (Zhao *et al.*, 2008; Carrera *et al.*, 2014).

As anticipated, current data showed that HIF-1α levels are significantly increased several fold following hypoxia exposure (Fig 6.18). Numerous studies have confirmed the ability of GBM cells to respond to hypoxia by increasing HIF-1α stabilisation using western blot in different cell lines (Richards *et al.*, 2016; Eales *et al.*, 2018). On the other hand, results of HIF-1β protein expression also showed a trend toward increasing HIF-1β levels under hypoxia (Fig 6.19). These findings are also consistent with a previous study where HIF-1β was significantly upregulated in the nucleus under hypoxia which caused a small increase in the total protein levels (Li *et al.*, 2016). HIF-1β is necessary for the assembly and functionality of an active HIF complex (Dengler *et al.*, 2014) suggesting that both proteins are essential for the activation of the HIF pathway in U87-MG cells.

The U87-MG cell line exhibited the ability to tolerate prolonged exposure to hypoxia and enabled the generation of the chronic hypoxia-adapted U87-MG cells. In fact, decrease in oxygen supply to the cells leads to biochemical changes that can either result in cells adaptation to hypoxia or cause cell death. Accordingly, research has shown that many cancer cell lines were not able to survive the chronic hypoxic conditions while other cell lines did by using different

mechanisms of adaptation (Endo *et al.*, 2014). An initial moderate increase in HIF-1α is important for cell adaptation to hypoxia, consequently, cancer cells respond to hypoxia via stimulation of angiogenesis by VEGF, apoptosis inhibition by Bcl-2, modification of cellular metabolism, acclimatising to extracellular acidic pH and upregulation of metastasis proteins (Graeber *et al.*, 1996; Zhou *et al.*, 2006; Vander Heiden *et al.*, 2009).

While some cell lines have not shown any changes to cell cycle distribution under hypoxia, other cell lines were found to exhibit slower progression through each phase of the cell cycle following long-term exposure to hypoxia (Richards *et al.*, 2016). Severe hypoxia, on the other hand, can induces transient G1 arrest in cells as a possible mechanism to protect the cells from proceeding into the S phase, where they are more sensitive to hypoxia-related DNA injuries (Graeber *et al.*, 1994). These findings may also correlate well with the current results where U87-MG cells showed slower proliferation rate under chronic hypoxia while could not survive upon sever hypoxia exposure. Some reports indicated that HIF-1α mediated induction of p21 and p27 expression for hypoxia-induced G1 cell cycle arrest (Gardner *et al.*, 2001), while others found no involvement of HIF-1α in hypoxia-induced G1 arrest (Goda *et al.*, 2003). The reason for these inconsistencies is unclear but may be due to differences in cell lines and methods (Richards *et al.*, 2016).

Modulation of cellular metabolism is known as a fundamental mechanism whereby cancer cells adapt to hypoxic environment. As previously described, hypoxia is a driving force to switch cellular metabolism from mitochondrial oxidative phosphorylation to glycolysis. Many important metabolic responses to hypoxia are controlled by HIF-1, which stimulates the transcription of genes encoding for metabolic reprogramming (Semenza, 2011). Cancer cells under hypoxia induce the expression of glycolytic enzymes to elevate the glycolytic metabolic flux for ATP generation and inactivate the enzyme responsible for the entry of glucose-derived carbons in the mitochondria pyruvate dehydrogenase (PDH) (Sutendra and Michelakis, 2013). However, mitochondria can overcome PDH inhibition in different ways to maintain their function. For example, one mechanism involves a diversion of glucose-derived pyruvate to oxaloacetate

through the mitochondrial enzyme pyruvate carboxylase (PC) which has been shown to play an important role in the growth of cancer cells, especially in glutamine-deprived conditions (Cheng *et al.*, 2011). Another mechanism is exploiting glutamine as an alternative carbon source. Glutamine oxidation in the mitochondria (namely glutaminolysis) is predominantly important for cancer cells such as human glioma, which require glutamine for survival and proliferation (Deberardinis *et al.*, 2007). The glutaminolysis process has been thought to occur only under specific circumstances, such as hypoxia and overt mitochondrial dysfunction as major means of ATP production and contributes to the synthesis of anabolic precursors, such as oxaloacetate and aspartate (Gameiro *et al.*, 2013). Recent reports have demonstrated also that glutaminolysis is a hallmark of GBM metabolism to produce ATP and that both glucose and glutamine are the primary fuels causing the rapid growth of GBM (Chinopoulos and Seyfried, 2018). Another study using GBM cell line in hypoxia concluded that glutamate is the major source for carbon under hypoxic conditions (Wise *et al.*, 2011). These results have contributed to a growing literature on the importance of glutamine in metabolism, especially in cells grown in a hypoxic environment (Frezza *et al.*, 2011) suggesting that simultaneous restriction of these two substrates as effective way to reduce cancer viability and invasion. Another recent study has demonstrated that same tumour cells can exhibit different metabolic phenotypes depending on their microenvironment including the Warburg effect, the reverse Warburg effect and glutamine addiction (Shan *et al.*, 2018).

These findings might correlate with the metabolic analysis for the adapted U87-MG cells to some extent where cells showed a pattern towards reducing oxygen consumption rate with no significant increase in glycolytic capacity (Fig 6.9 &6.10). Additionally, the conventional notion that a reduction in oxygen consumption rate will be only caused by oxygen limitation at mitochondria has been challenged by a phenomenon known as oxygen conformance, by which oxygen consumption under hypoxia decreases to maintain cellular survival without either compensatory increase in anaerobic energy production or a loss of cellular viability (Gnaiger, 2003). A study by Li and colleagues demonstrated that it is the gradual reduction of oxygen levels and not the acute change that triggers oxygen conformance where cellular metabolism is downregulate (Li *et al.*, 2013).

They also suggested that metabolic responses to hypoxia are significantly affected by glucose availability rather than oxygen levels. Metabolic activity was inhibited when cells experienced hypoxia with medium or low glucose media but not decreased in the presence of high glucose media. Furthermore, it was demonstrated that although oligomycin can induce an increase in glycolysis to meet the ATP demand, it may produce a minimal effect if glycolysis function is working closely to its maximal capacity or if the basal glycolytic rate is limited by a low resting demand for ATP (Mookerjee *et al.*, 2016). These findings might provide an explanation of why there was no significant increase in the glycolytic activity of U87-MG adapted cells to greater extent since it was already showing high glycolytic activity near to its maximum capacity. Furthermore, it can be suggested that in order to adapt to hypoxia, the cells might have undergone oxygen conformance because oxygen consumption decreased without either compensatory increase in glycolysis production or sings of cell death (Fig 6.9 &6.10).

As a result of low oxygen availability, high glycolysis and production of metabolic acids, tumour cells often undergo extracellular acidic stress (Lindner and Raghavan, 2009). Investigations have confirmed the capacity of tumour cells to acidify the extracellular environment while maintaining intracellular neutral/alkaline pH by several mechanisms (Gillies *et al.*, 1981). Under hypoxia, tumour cells develop additional important pH regulating systems such as MCT4 and the membrane-associated carbonic anhydrases CAIX and CAXII which contributes to the acidification of the extracellular tumour environment and restores a permissive intracellular pH allowing acclimatisation of cells under hypoxia and a blockade or slow release cell death (Pantuck *et al.*, 2003; Korkolopoulou *et al.*, 2007). Hypoxia also selects cells with low p53 expression, thus reducing or inhibiting p53-induced apoptosis in hypoxic cells. Upon exposure to hypoxia, a post-translational modification of the p53 gene occurs, thus making it active and in turn promoting transcription of cell cycle regulating or apoptotic genes (Graeber *et al.*, 1996; Zhou *et al.*, 2006). Additionally, studies found that p53 plays an important role in negative regulation of hypoxia-stimulated glycolysis in cancer cells through RRAD (Ras-related associated with diabetes) a recently identified p53 target (Zhang *et al.*, 2014). Also, p53 induced RRAD

expression under hypoxia inhibits glycolysis mainly through inhibition of GLUT1 translocation to the plasma membrane of cells. These results revealed an important role of p53 in antagonizing the stimulating effect of hypoxia on glycolysis and maintaining homeostasis of glucose metabolism under hypoxic conditions, thus contributing greatly to p53's function in tumour suppression. Accordingly, these findings also may provide possible mechanism by which the U87-MG cells have adapted the long exposure of hypoxia by upregulating pH systems to tolerate acidosis and by selecting low-p53 expressing cells, which needs to be confirmed.

It has been demonstrated that cancer cell responses under hypoxia are a product of the interplay between many factors including the dominant oxygen tension, hypoxia-induced signalling, interacting genetic defects, and cellular damage by ROS (Eales *et al.*, 2016). An interplay was reported between HIF, p53 and myc in hypoxia for altering cell metabolism. The relationship between p53 and HIF is not fully understood: hypoxia has been shown to induce p53 stability in some cases, whereas not in others, and the mechanism by which this occurs is unclear (Schmid *et al.*, 2004). It was suggested that severity and duration of the hypoxia can have a role, with more severe oxygen tensions provoking a strong stabilization, perhaps through DNA damage–response mechanisms (Hammond *et al.*, 2002). These findings might explain some of the difference in responses to hypoxia exposure where at 1% hypoxia the cells were able to adapt and survive, probably by interplay between HIF, p53, and myc, whereas under sever hypoxia this interplay switch to more stabilisation of p53 to induce cell death.

Additionally, it is well known that hypoxia adaptation mediated by HIF-1α suppresses mitochondrial activity and mitochondrial biogenesis leading to reduced cell death and increased drug resistance (Kim *et al.*, 2006; Papandreou *et al.*, 2006; Zhang *et al.*, 2007). The efficiency of the electron transport chain under hypoxic conditions is reduced leading to increased mitochondrial ROS production (Guzy and Schumacker, 2006). Increased ROS levels play a major role in HIF-1 nuclear translocation and stabilization, whereas excessive ROS production can result in cellular damage and ultimately cell death. Therefore, one global strategy to hinder oxidative metabolism is to reduce mitochondrial mass

through the process of mitophagy. Lowering mitochondrial mass not only protects against excessive ROS but also degrades and recycles unusable organelles providing building blocks for other cellular processes (Daskalaki *et al.*, 2018). However, hypoxia induces a selective form of autophagy in which mitochondria, but not other cellular organelles are degraded (namely mitophagy). In hypoxic cells, HIF-1 activates transcription of the BNIP3 (BCL2 interacting protein 3) and BNIP3L (BCL2 interacting protein 3 Like) genes, which encode mitochondrial proteins that activate mitochondria-selective autophagy in hypoxic cells (Bellot *et al.*, 2009). Failure to induce BNIP3 expression in HIF-1-deficient or BNIP3-deficient cells leads to higher ROS production under conditions of chronic hypoxia and thus ROS-induced cell death (Zhang *et al.*, 2008).

Current data from the autophagy assay showed a similar pattern of response to drug treatment for both hypoxia conditions with no increase observed in the induction of autophagy under chronic hypoxia (Fig 6.8). This may be attributed to the lower overall metabolic activity in the hypoxia-adapted cells since autophagy is an energy demanded processes and requires mitochondrial activity for maximal autophagic response, and forced induction of autophagy may lead to autophagic cell death (Thomas *et al.*, 2018). However, the current data analysed the non-selective macroautophagy and not the mitochondrial-selective autophagy that is activated under hypoxia. To distinguish between these processes other methods can be used (Section 7.3).

Hypoxia-induced cell death

In some conditions of acute hypoxia or chronic hypoxia, as well as severe hypoxia, tumour cells cannot adapt because of the hypoxic-stress induced cell death. Hypoxia produces an environment of stress leading to DNA damage, cell cycle arrest and ultimately cell death during the acclimatisation period. Otherwise, as discussed previously, hypoxia selects cells with decreased p53 activity, thus reducing their apoptosis and allowing them to proliferate and adapt. It was reported that if HIF-1α and p53 were stabilized concurrently, direct interaction between them can affect transcription of p53 target genes. This observation was challenged by showing that HIF-1α was not required for p53 activation under hypoxia (Wenger *et al.*, 1998). Another conflicting report showed that HIF-1 is

stabilized at relatively modest hypoxia levels whereas p53 is only accumulated under severe hypoxia limiting possible interactions of these two proteins (Suzuki *et al.*, 2001).

Importantly, the resultant genetic instability under hypoxia can either amplify an already existing proapoptotic signal or independently induce apoptosis. These responses were shown to be likely dependent on the severity of oxygen deficiency and on the specific cellular context. Some signalling pathways were only triggered by severe hypoxia or anoxia (0.2% O_2) as shown for p53 stimulation, suggesting that mild and severe oxygen levels can trigger different signalling pathways with different apoptotic outcomes (Hammond *et al.*, 2002; Achison and Hupp, 2003). Therefore, severe reductions in oxygen tension can activate several upstream components of the intrinsic apoptosis pathway. Furthermore, episodes of reoxygenation upon hypoxia exposure can induce additional DNA damage. These effects will lead to stimulation of apoptotic signalling which eventually result in apoptotic cell death if not opposed (Sendoel and Hengartner, 2014).

It has been widely accepted that ROS play critical roles in cell signalling and homeostasis (Schieber and Chandel, 2014). Higher basal level of ROS are present in cancer cells than in normal cells and believed to be involved in tumour occurrence and development, tumour metastasis and gene regulation for many signalling pathways, like the activation of HIF, in different cell types (Ma *et al.*, 2009; Kolamunne *et al.*, 2013). However, some studies have observed an increase in ROS production under hypoxia, while others have found a decrease in ROS under hypoxia (Huang *et al.*, 2008). While undergoing various environmental stresses, ROS levels can increase intensely leading to oxidative damage to the cells (Cheresh *et al.*, 2013). For example, treatment with cobalt chloride ($CoCl_2$), a hypoxia-mimicking reagent, in TE-1 oesophageal squamous carcinoma cells, it led to a significant decrease in mitochondrial respiratory chain complex subunit expression and an increase in intracellular ROS production resulting in a dramatic reduction in the oxygen consumption rates and increase in the extracellular acidification rates, indicating that hypoxia could cause mitochondrial dysfunction by ROS upregulation, thus affecting the cellular

bioenergy metabolism and survival of tumour cells. Therefore, it was suggested that tumour cells may exhibit distinct changes in bioenergy metabolism in response to different oxidative stress (Zhang *et al.*, 2017). Many reports showed that the status of glucose metabolism changes prior to cell death when cells are stressed (Byfield *et al.*, 2005). Previous findings have supported the concept that glucose metabolism regulates cell death pathways. It was shown that energy depletion results in cell death by different forms (necrosis, apoptosis or autophagy) where all of them can be affected by glucose metabolism status and ATP levels (Luca *et al.*, 2005).

For many cancer lines, prolonged hypoxic exposure can result in cell death which is not a direct effect of hypoxia but is secondary to acidosis. In one study during hypoxia in A549 adenocarcinoma cells, HIF-1α was shown to induce activity of the glycolysis pathway and decreases the pH of the growth medium leading to increased hypoxia-induced apoptosis. It was found that apoptosis induced by HIF-1α overexpression was partially inhibited by increasing the buffering capacity of the growth medium (Luo *et al.*, 2006). Taken together, these different previous findings can provide several explanations of why SVG-p12 cells showed a significant reduction in cell proliferation and number after long exposure to 1% hypoxia. Similarly, U87-MG could not survive under 0.1% severe hypoxic conditions, an observation may also be attributed to ROS upregulation and inducing hypoxia- cell death.

Hypoxia and treatment resistance

GBM cells in a hypoxic regions of the tumours have shown reduced proliferation, resistance to chemo- or radiotherapy and poor prognosis (Saggar *et al.*, 2013). Nevertheless, cancer research trying to recreate more physiologically relevant oxygen tensions are lacking, with massive discrepancies found in literature investigating the effects of chronic hypoxia *in vitro* rendering studies hard to compare (Bayer and Vaupel, 2012). For example, one study examined gene expression profile for three human cancer cell lines exposed to experimental chronic or transient hypoxia conditions. It was found that gene expression of 240 probe sets was altered in all tested cell lines. However, the cell-type specific

variability in response to both types of hypoxia was significant (Olbryt *et al.*, 2014).

On the other hand, another study investigated the changes in gene expression accompanying chronic hypoxia in MCF7 breast cancer cell line. It was observed that exposing cells to long-term hypoxia (weeks) results in different gene expression alterations than those induced by short-term hypoxia (less than 72 hours). The underlying mechanism was suggested to link to modifications on the proteomic level rather than the genomic level which was consistent with other studies where protein levels of hypoxia responsive genes where shown to be upregulated instead of their messenger RNAs under chronic hypoxia (Feda'h and Zihlif, 2014). In colon cancer cell lines, sensitivity to cisplatin *in vitro* was also significantly different for the hypoxia-adapted cells compared with the paternal cells, suggesting a modification in pathways leading to apoptosis upon DNA damage, particularly p53. It was thought that the generation of the hypoxia-adapted cell lines provides a model for events within hypoxic areas of colon cancers, and for the acquisition of resistance and sensitivity properties that may have therapeutic implications (Yao *et al.*, 2005).

Azad and colleagues have examined two glioma and breast cancer cell lines for cell death response in hypoxia (<1% O_2). They found that cells growing under hypoxia will initially employ adaptive strategies, but if hypoxia was sustained, cell death will ultimately occur. However, they demonstrated that accurate mechanisms of hypoxia-induced cell death remain uncertain as all apoptosis, necrosis and autophagy were reported in response to hypoxic stress (Azad *et al.*, 2008). The authors suggested that chronic hypoxia is a typical environment of tumour progression as rapid cellular proliferation will lead the tumour to outgrow its available oxygen supply. Furthermore, it was reported that the extent of tumour hypoxia associates with neoplastic aggression, increased resistance to therapy-induced apoptosis and reduced overall patient survival (Azad *et al.*, 2008). Thus, treatment resistance under hypoxia is a known issue, and the current data showed that hypoxia-adapted U87-MG cells are more resistant to drug treatment compared to their acute hypoxic counterparts. This observation is in line with the previous studies reported that hypoxia increases chemo-resistance (Koch *et al.*,

2003; Rohwer *et al.*, 2010). The reason for this resistance can include various mechanisms. One mechanism by which hypoxia is believed to increase resistance to chemotherapy is the initiation of cell cycle arrest and reducing cell proliferation. The suppressed proliferation rate of the cells under hypoxia by inducing cyclin-dependent kinase inhibitor $p27^{Kip1}$ which inhibits the activation of cyclin E-Cdk2 or cyclin D-Cdk4 complexes thus controlling cell cycle progression at G1 phase (Wartenberg *et al.*, 2003). As classical chemotherapeutic drugs target rapidly diving cells, the reduced proliferation rate is thought to allow hypoxic cells to escape cell death (Harrison and Blackwell, 2004). Accordingly, the slower proliferation rate of hypoxic adapted cells can be one explanation for the reduced efficiency of cisplatin and TMZ due to their mechanism of action. Other studies have confirmed the findings where a reduced efficacy of cisplatin and other cell-cycle dependent drugs was observed under hypoxia (Koch *et al.*, 2003; Rohwer *et al.*, 2010). However, other research suggested that only a small proportion of cells will be exposed to hypoxia severe enough to cause cell cycle arrest, and of these cells a proportion will undergo cell death. It is therefore likely that other mechanisms play a more important role in hypoxia-mediated chemoresistance.

One such mechanism for reduced drug cytotoxicity under hypoxia is through the *MDR* (multi-drug resistance) gene and over expression of the gene product P-glycoprotein (P-gp), which has been identified to increase chemo-resistance towards a variety of drugs by acting as an efflux pump in various types of cancer including glioma (Liu *et al.*, 2000; Comerford *et al.*, 2002; Gottesman, 2002; Wartenberg *et al.*, 2003). For example, the increased expression of the ABCB1 and p-glycoprotein drug transporters was reported to induce chemoresistance in GBM (Chou *et al.*, 2012). Furthermore, DNA injuries caused to the cells under normoxia are believed to be greater and more permanent than under hypoxia, where a reduction in the activity of p53 causes inhibition of cell apoptosis, and cells are more likely to undergo restoration following DNA injuries (Zhou *et al.*, 2006). The hypoxic environment has been also been associated with increased expression of MGMT, a DNA repair protein highly involved in cellular resistance to temozolomide (Pistollato *et al.*, 2010). These findings are in agreement with the current results where TMZ was less efficient in acute hypoxia compared to normoxia and to a greater extent under chronic hypoxia (Fig 6.4).

In one report investigating some GBM cell lines including U87-MG, it was shown that chronic hypoxia, but not acute hypoxia induced resistance to chemotherapy and X-ray irradiation (Cowman *et al.*, 2019). This acquired resistance after chronic hypoxia was present but less obvious in other GBM cell lines, suggesting that this heterogeneity of the cellular response to hypoxia might be due to the differences in the molecular signature of different cell lines beyond HIF activation. The authors observed remarked effects of hypoxia adaptations in U87-MG cells in agreement with previous reports (Hsieh *et al.*, 2010; Cho *et al.*, 2011). They found wide transcriptional changes after prolonged hypoxia, particularly in the expression of genes involved in repairing double strand breaks (DSB). However, it was demonstrated that timing and severity of hypoxic exposure has a large impact on cell adaptation and sensitivity to DNA damaging agents where short time exposure (minutes-hours) is thought to regulate repair proteins through post-translational modifications and alterations to translation proficiency, whereas long exposure (days-weeks) causes changes to transcription and epigenetic alterations (Scanlon and Glazer, 2015). Although long-term hypoxia exposure stimulates different adaptive mechanisms among cell lines, they were thought to ultimately meet on the inability to activate p53, thus mediating resistance to cell death (Cowman *et al.*, 2019). That might provide possible explanation of why U87-MG adapted cells showed greater resistance to drug treatments (Fig 6.4).

A further mechanism for increasing drug resistance under hypoxia is mediated by HIF-1α which modulates the metabolic activity and suppresses mitochondrial biogenesis leading to reduced cell death and increased drug resistance (Kim *et al.*, 2006; Papandreou *et al.*, 2006; Zhang *et al.*, 2007). It was previously described how cancer cells undergo metabolic transformation including the switch to aerobic glycolysis, profound mitochondrial reprogramming as well as the deregulation of lipid metabolism, which altogether cooperate to sustain cell proliferation. However, metabolic phenotypes are considerably variable, and can serve as a critical predictor of cancer proliferation, vulnerabilities, and resistance to therapies (Dar *et al.*, 2017; Hardie *et al.*, 2017). Therefore, the unique metabolic programming and plasticity in glioblastoma cells may influence cell fate like other types of cancer (Simões *et al.*, 2015; Tavares-Valente *et al.*, 2018).

Additionally, it has been shown that the ability to reduce the basal metabolic rate and undergo a hypometabolic state has been recognised as life-saver mechanism for many organisms when the energy source such as oxygen and nutrition are restricted (Storey, 2001). Accordingly, downregulation of mTORC1 activity has been widely reported as important mechanism for tumour cells to survive under acute hypoxia and stressful conditions (Brugarolas *et al.*, 2004; Okuyama *et al.*, 2010). However, the response of cancer cells to chronic hypoxia is less well understood. Endo and colleagues have examined several pancreatic and colorectal cancer cell lines for weeks under 1% oxygen conditions and identified a pancreatic cancer cell line (AsPC-1) able to survive under these conditions most other tested cell lines died within 7 days (Endo *et al.*, 2014). The authors indicated that AsPC-1 cells entered a state of dormancy where they alter proliferation and metabolic status. After 7 days of hypoxia, both oxygen consumption rate and glycolysis were attenuated. ATP turnover, as well, was markedly decreased under chronic hypoxia. After exposure to acute hypoxia, the gene expression levels of glycolytic enzymes and transporters such as GLUT1, HK2, and PDK1 increased. In contrast, the expression levels of these genes decreased in the cancer cells in dormancy (Endo *et al.*, 2014). Accordingly, the metabolic changes observed in the metabolic activity for the U87-MG hypoxia-adapted cells might have played a significant role in acclimatisation to hypoxia and rendering the cells more resistance to drug treatments (Fig 6.12-6.14 &6.16-6.17).

It was also found also that HIF-1α protein levels were increased after exposure to hypoxia and maintained until day 7, suggesting that HIF-1α partially contributes to the induction of dormant status. Their results were accompanied by decreased AKT phosphorylation. However, it was indicated that HIF-1α and AKT independently regulate cell adaption in chronic hypoxia. Conserving the energy source by decreasing energy demand might be a strategy of cancer cells to survive in a chronically deteriorated microenvironment. These chronic hypoxia-adapted cells showed remarkable chemoresistant characteristics (Endo *et al.*, 2014).

HIF-1 as a target for GBM treatment

Because of the master role for the HIF pathway in cell survival under hypoxia, many studies suggested targeting HIF as potential therapy for several cancers. For example, blocking HIF1 response reduced lactate levels and enhanced response to radiotherapy with improved killing of hypoxic radioresistant (Leung *et al.*, 2017). Studies have shown that cell viability of U87-MG cells can be compromised to facilitate apoptosis in a caspase-dependent/p53 independent mechanism by the inhibition of HIF-1α transactivation (Dai *et al.*, 2003). Additionally, it has been shown that HIF-1α activity is associated with GBM responsiveness to TMZ, hence, its downregulation improves the response of TMZ-resistant cells (Lo Dico *et al.*, 2018).

Interestingly, aspirin and PN517 appeared to reduce HIF-1α levels although the effect was not significant under the experimental conditions used (Fig 6.18). Previous studies in hepatoma cells reported that GLUT1 and HIF-1α could be reduced by aspirin suggesting that aspirin downregulated GLUT1 through targeting NF-κB or NF-κB/HIF-1α signalling leading to the inhibition of cell proliferation *in vitro* and *in vivo* (Liu *et al.*, 2019). Similarly, GLUT-1 was suggested to have a significant role in glioma tumour biology through HIF-1 regulation (Jensen and Chkheidze, 2011). These findings may explain why aspirin showed higher efficacy in reducing glycolysis activity under hypoxia which could be related to reducing HIF-1α (Fig 6.18).

Maturu and colleagues demonstrated the role of the COX-2 pathway in creating an immunosuppressive microenvironment within the tumour, reporting HIF-1α as a target for COX-2. They showed that COX-2 pathway components such as COX-2, HIF-1α, p-ERK1/2, and p-STAT3 were upregulated in mouse and human tumour tissues confirming the efficacy of COX-2 inhibitors in decreasing tumour cell growth *in vivo* (Maturu *et al.*, 2017). Cross talk between HIF-1 and COX-2 signalling was reported and shown to contribute to the mechanisms that promote hypoxia adaptation and tumour progression. In the hypoxic conditions, HIF-1α acts as a positive inducer for COX-2 expression which in turn enhance HIF-1 transcriptional activity via β-catenin (Greenhough *et al.*, 2009). Furthermore, it was demonstrated that the COX-2 pathway effectively upregulates HIF-2α activity

under hypoxia by reducing VHL levels and stimulating HIF-2α nuclear translocation by MAPK pathway in hepatocellular carcinoma. More importantly, COX-2/HIF-2α was associated with cancer cell resistance to chemotherapeutic drugs in hypoxic conditions while COX-2 inhibitors synergistically enhanced the antitumour activity of the drugs (Dong *et al.*, 2018). All these results suggested the usage of NSAIDs as adjuvants to current chemotherapy/radiation regimens.

6.3.2. 3D cell culture

As cancer cell lines are selected cells with ability to grow under culturing conditions enriched with oxygen, nutrition and growth factors, these cells might have lost the ability to repress proliferation under hypoxia and stressed conditions. Thus, 3D spheroids could provide a better platform to investigate the effects of hypoxia by providing oxygen gradient that is more representative of the real tumour microenvironment. In the current study, formation and characterization of uniform and reproducible 3D U87-MG spheroids *in vitro* was established using the ultralow attachment Nunclon™ Sphera™ plates (Fig 6.20 &6.21). This method allowed the consistent formation of viable and healthy U87-MG spheroids representing the distinct characteristics of GBM tumours enabled to use high-quality spheroids model for subsequent analysis. After model developing, the impact of all drug treatments, separately or in combination, was studied on 3D cell cultures in comparison to 2D cell cultures sensitivity.

Although monolayer cell cultures represent a gold standard high throughput screen for effectiveness of chemotherapeutic agents, this model of culture does not reproduce the 3D structural properties of actual tumours. In fact, the physiological features of a monolayer culture of cells growing on a flat 2D tissue culture can vary greatly from those of cells in 3D cultures. Therefore, there has been increasing interest recently in using 3D cancer spheroids before proceeding to clinical trials due to the fact that 3D spheroids have several physiological characteristics better mimic the architecture and microenvironment of living tissue.

First, culturing cells on the traditional tissue cultureware surface results in compatibly flat cells with simple geometry. This method forces the cells to adhere

by one side to the surface with no opportunity for cellular contact on the opposite side leading to changes in cell shape which ultimately can modify cellular function (Baker and Chen, 2012). In contrast, culturing tumour cell lines in 3D structure allows for cell-cell interactions and promotes histological morphology related to the tumour type they were derived from (Lee *et al.*, 2013). Second, while cells growing in 2D monolayers are exposed to the same oxygen concentration and pH level, 3D cultures allow for multiple hypoxic conditions and the generation of oxygen gradient with a hypoxic regions and necrotic core. Accordingly, a gradient of protons extending from peripheral zone to the necrotic core of the spheroid is established and creates a pH gradient which is the inverse of the oxygen gradient. The lower the oxygen level, the more protons accumulate, thus, reflecting the tumour microenvironment (Lin and Chang, 2008) (Fig 6.30). Higher lactate production in hypoxic cells can kill the cell in 2D cultures, especially if the media not buffered, while in 3D cultures cells can exhibit ‘‘metabolic symbiont’’ model where lactate produced by hypoxic cells is used by aerobic cells (Kennedy *et al.*, 2013). However, it is widely thought that CO_2 production from oxidative mitochondrial metabolism is a great contributor to solid tumour acidity rather than glycolytic activity. Accordingly, it was also suggested that CO_2 is a primary contributor of extracellular acidification in 3D cancer models (Swietach *et al.*, 2009). Thus, establishing 2D monolayers from the tumour may select for rare cells which can grow in a highly uncommon environment, and these cells could not offer the best culture for modelling tumours. In line with this, the U87-MG spheroids generated in this study might have undergone to morphological changes with different oxygen and pH levels which can have a great impact on drug efficacy. Current results showed a difference in response between 2D and 3D cell culture models for U87-MG cell line where a significantly lower sensitivity was detected for 3D cell culture compared to monolayer cell culture (Fig 6.27 &6.28).

Third, when tumour cells are cultured in a flat monolayer, they proliferate relatively at the same rate across the surface. Nevertheless, growing the same cells in 3D cultures creates zones of variant proliferation with cell proliferating more rapidly in the outside zone of the spheroid (Fig 6.30) (Lin and Chang, 2008). This difference in the proliferation rate was suggested to be related to many

factors such as the oxygen and nutrient gradients across the spheroid (Lin and Chang, 2008) and the ECM-dependent changes in intracellular signalling (Kim *et al.*, 2011). Accordingly, U87-MG spheroids might have different cells populations with varying rates of cell proliferation. That feature would mostly affect TMZ and cisplatin due to their mechanism of action, and consistently, they were significantly lower efficacious in 3D cell culture compared to monolayer cell culture.

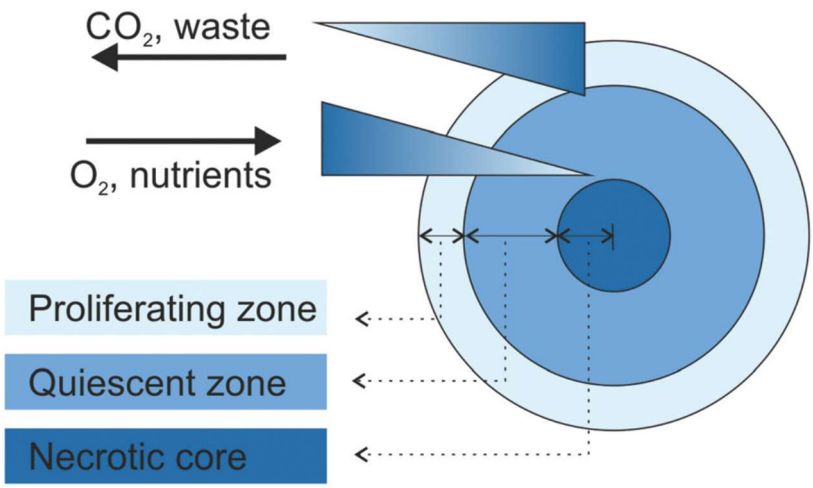

Figure 6. 30. Different cellular proliferation zones in 3D spheroid culture. A typical spheroid has an outer layer of proliferative cells, an internal layer of quiescent hypoxic cells and necrotic cells in the core (Lin and Chang, 2008)

Fourth, culturing cells in 2D monolayers may lack the cellular heterogeneity occurs across a population of cells within the same tumour as noted by variations in proliferation rate, gene expression, and differentiation leading to morphological and functional changes (Marjanovic *et al.*, 2013). On the other hand, cells in 3D cultures were thought to exhibit phenotypic heterogeneity of tumour cells which might be caused by clonal selection pressure and gene expression alteration due to the oxygen, growth factor and nutrient gradients (Lawrenson *et al.*, 2011), or by increased expression of "stemness-related genes" (Busse *et al.*, 2013). These genetic changes can alter cellular behaviour such as cell migration and differentiation which are inevitably associated with the severity of tumour progression. Additionally, the phenotypic heterogeneity makes developing drugs to kill the entire tumour challenging due to the fact that cell physiologies can be widely different (Fessart *et al.*, 2013). Fifth, unlike classical monolayer-based models, cells cultured in 3D spheroids deposit ECM constituents that regulates

the cell dynamic behaviour and enable the cells to move within their spheroid in similar way they would move in living tissue (Pampaloni *et al.*, 2007). Mainly, ECM-cell interactions may be responsible for the expression of proteinases such as MMPs which can modify ECM structure and promote cancer cell migration (Lu *et al.*, 2012). Therefore, 3D spheroids are accurate representative models for cell migration, survival, and growth. Accordingly, U87-MG spheroids might also display ECM-cell interactions, cellular heterogeneity and different genetic expression, which in turn may lead to different cell physiologies and behaviours and increased drug resistance that was observed compared to the monolayers (Fig 6.27 &6.28).

Sixth, culturing cells in 3D spheroids reveals a more realistic drug response. Several mechanisms were proved for enhanced resistance to chemotherapy when compared to the same cells grown in monolayers. While tumour cells in monolayers are exposed to same concentration of drug, in 3D spheroids the tumour cells inside the spheroid are protected from drug penetration by the cells on the outside of the spheroid (Perche and Torchilin, 2012). Declined diffusion of drugs to hypoxic areas due to increased distance from blood vessels is also likely to play a major role in drug resistance (Trédan *et al.*, 2007). However, 3D spheroids showed chemoprotection from some drugs compared to the 2D culture despite complete penetration of the drug (Aljitawi *et al.*, 2014) suggesting that mechanisms of drug resistance are more complicated than just failure to entirely penetrate the tumour *in vivo* or 3D culture *in vitro*. Another mechanism has been suggested linked to the different proliferation rates within the spheroid (Chitcholtan *et al.*, 2013). In addition, tumour cells can increase expression of several drug resistance genes and microRNAs leading to enhanced drug resistance in 3D culture compared to 2D culture (Longati *et al.*, 2013). For example, hypoxia was found to increase the expression of MDR-associated P-gp in Hepa1 tumour spheroids after incubation under hypoxic conditions (1% O_2) for 72 hours, and that depends on a functionally active HIF-1/ARNT heterodimer (Wartenberg *et al.*, 2003). Consequently, 3D cultures provide several mechanisms of drug resistance found in tumours, offering the opportunity to either eliminate poor drug candidates before proceeding to *in vivo* animal models and clinical trials, or to identify promising drugs that would fail in classical 2D

monolayers-based assays (Hirschhaeuser *et al.*, 2010). All current results showed a difference in response between 2D and 3D cell culture models for U87-MG cell line where a significant lowered sensitivity was detected for 3D cell culture compared to monolayer cell culture probably due to 3D cellular heterogeneity, drug penetration and/or resistance phenotypes that reproduces partly tumour response *in vivo* as described above (Fig 6.27 &6.28).

U87-MG spheroids showed a lower rate of proliferation under hypoxia which was not unexpected due to the fact that U87-MG cells display less proliferation as observed from the growth curves under hypoxia. In 3D culture models, previous studies showed that cells forming spheroids may or may not proliferate according to cell type and the extracellular matrix environment (Benton *et al.*, 2014; Edmondson *et al.*, 2016) and spheroid diameters might stop to increase if spheroids reached their growth plateau (Dubois *et al.*, 2017).

Hypoxic spheroids showed significantly lower sensitivity than normoxic spheroids, probably correlated to their respective non-proliferative/proliferative profiles. In tumour tissue, hypoxic gradients develop by cellular respiration of prevailing cells and promote the development of hypoxic regions in cells distal from oxygen-supplying blood vessels, hence, hypoxic cells are usually not adequately exposed to anti-cancer drugs (Brown and Giaccia, 1998). This distance from blood vessels also causes a reduction in the rate of cell proliferation (Brown and Wilson, 2004). Accordingly, U87-MG spheroids incubated in normoxia resemble the tumour regions near the blood vessels whereas U87-MG spheroids incubated in hypoxia mimic hypoxic tumour regions distal from blood vessels. Additionally, other studies supported the use of spheroids cultured under hypoxia as model system for hypoxic tumour regions showing that HIF-1α strongly accumulated in tumour spheroids cultured under hypoxia while it was only weakly detected in normoxic conditions (Klutzny *et al.*, 2017).

Additionally, while there is no definitive proof of the presence of stem cells, accumulating evidence illustrated the tendency for the 3D spheroid microenvironment to create a “stem cell-like” population comparable to the *in vivo* population that is thought to be responsible for tumour drug resistance. Therefore,

characterizing and reproducing the microenvironment responsible for initiation and survival of cancer stem cells *in vitro* can be the quickest pathway to potential treatment, particularly for deadly cancers like glioblastoma (Filatova *et al.*, 2013). Numerous studies have employed 3D culture models for testing different therapies. Not surprisingly, most of the studies showed 3D cultures to be intrinsically much more resistant to drug treatment and radiotherapy as compared to the same cells grown as monolayer cell cultures (Inoue *et al.*, 1996). These findings were consistent with the current results where all drug treatments showed less efficacy in 3D U87-MG cultures compared to the 2D monolayers.

For instance, one study performed a comparison of 2D *vs.* 3D cell culture viability of triple-negative basal-like breast cancer cell lines in the presence of three conventional chemotherapeutic drugs cisplatin, docetaxel and epirubicin after 5 days of treatment and the results showed that spheroids were clearly less sensitive than monolayer cell cultures, but the effect seemed to be cell line- and drug-dependent. It was demonstrated that metabolic activity of cells cultured in 3D was lower than cells cultured in monolayer, probably due to cellular heterogeneity as well described necrotic or quiescent areas in spheroids (Dubois *et al.*, 2017). The quiescent cell population sequestered inside the spheroid will be protected from drugs like cisplatin and docetaxel which rely on cell division to induce their cytotoxic effects, but once the outer cells are dead these cells are free to re-enter the cell cycle again. Importantly, if therapy is stopped too early, the protected quiescent cells may be able to recapitulate a tumour that was shrunk but not completely killed. These data suggest that 3D models may be adapted to the evaluation of conventional cytotoxic drugs (Dubois *et al.*, 2017). That also can provide important explanation for the significantly reduced effect of cisplatin in U87-MG spheroids as compared to the monolayers.

These results were consistent with many others in the literature. For example, Li and colleagues compared the effects of cisplatin and other drugs on cell viability using 2D and 3D cell cultures of HepG2 cells and showed that the multicellular morphology of the 3D cultures caused a differentiated phenotype leading to increased cell-cell adhesion and G1 phase cell cycle arrest which increased cellular resistance to apoptosis induced by cisplatin (Lin and Chang, 2008) .

Another study using mesothelioma spheroid found that the 3D spheroids developed resistance to a variety of apoptotic stimuli, including combinations of TRAIL, ribotoxic stressors, histone deacetylase, and proteasome inhibitors which were highly effective against mesothelioma cells when grown in 2D monolayers (Barbone *et al.*, 2008). Similar results were obtained with other previous experiments which confirmed that several tumour spheroids were more resistant to anti-cancer drugs like doxorubicin compared with the corresponding 2D cell cultures. This increased resistance in the spheroid cells was thought to be due to cell–cell contact response, internal protective mechanisms, and/or mass transfer limitations (Yu *et al.*, 2010; Neto *et al.*, 2015). These findings again suggest that 3D cultures of U87-MG might display multiple features which were not found in the U87-MG monolayers and caused the increase in the drug resistance.

Another study used the human colorectal cancer 3D spheroids model to evaluate the impact on drug response to clinically relevant drug treatments. The authors of the paper demonstrated concentration-response effects for different anti-cancer drugs and showed that IC_{50} values were significantly higher in the 3D spheroids compared to the conventional 2D culture system, confirming that 3D spheroids cultures are much more resistant to treatment than the same cells in monolayer (Galateanu *et al.*, 2016). Their results were similarly explained by the fact that the spheroids mirror tumour behaviour as they contain each of surface-exposed and deeply hidden cells, well-oxygenated and hypoxic cells as well as proliferating and non-proliferating cells. It was also demonstrated that spheroids dimension may play a role alongside with the cell-cell and cell-matrix contact, which enhance the viability of the cells. Furthermore, they reported that the 3D model blocks the diffusion of the drug to all the cells since the cells on the outer layers of the spheroid provide a natural barrier, suggesting that the heterogeneity of some drug uptake might be responsible for the noticed resistance of spheroids to diverse treatment methods. Therefore, they reported a potential enhancement of the effects of the drugs following their encapsulation into liposomes (Galateanu *et al.*, 2016). Accordingly, the current observations regarding greater resistance to drug treatment in U87-MG spheroids might be investigated after encapsulation into liposomes and examine any enhancement in drug efficacy.

Regarding the effect of the endogenous ECM expression, other reports comparing 3D to 2D pancreatic carcinoma cell culture showed that extracellular matrix proteins were significantly increased in 3D spheroids such as lumican, SNED1, DARP32, and miR-146a, indicating a role for these ECM proteins in protecting cells which provide mechanical properties that act as a barrier to drug diffusion. Interestingly, SNED1 (sushi, nidogen and EGF-like domains 1) was strongly up-regulated at early timepoints (2–4 days) and thought to convey cellular resistance against platinum compounds. SNED1 has been identified as a cisplatin-resistance related gene in head and neck squamous carcinoma (Yamano *et al.*, 2010). These findings confirmed the presence of a more matrix-rich phenotype in 3D culture that may be advantageous for drug screening as it simulates more closely the *in vivo* situation (Longati *et al.*, 2013). However, drug penetration through the spheroids was demonstrated to be impaired by many structural features of the 3D culture including the size of the spheroids and specific interactions between tumour cells and their microenvironment, both cell-cell and cell-matrix adhesion which are likely to vary from one cell type to another (Grantab *et al.*, 2006).

Importantly, it is well known that the extracellular matrix contributes to epithelial to mesenchymal transition EMT which is induced by hypoxia in 3D spheroid models (Lee *et al.*, 2016). Growing cells in 3D cultures resulted in acquisition of mesenchymal traits and lowered expression of epithelial marker compared with that in traditional 2D cultures, which is indicative of epithelial–mesenchymal transition in the spheroids (Kuo *et al.*, 2012). The stimulation of EMT has also been linked to therapy resistance in carcinomas, with similar findings reported for the resistance of GBM to standard chemotherapeutics. All three main families of EMT transcription factors have been revealed to be involved in the activation of EMT phenotype and the aggressive properties of glioma cells (Joseph *et al.*, 2015; Liao *et al.*, 2015). Therefore, it would be interesting to investigate the effect of the drug treatments on ECM and EMT proteins in U87-MG 3D cultures.

Similarly for TMZ, multiple studies have demonstrated reduced efficacy in 3D cultures compared to 2D models (Kessel *et al.*, 2017; Nunes *et al.*, 2019) and that was explained by different mechanisms found in 3D cultures described

above. Human GBM spheroids in turn were shown to be more resistant to alkylating agent-based chemotherapies where the estimated IC_{50} for TMZ of cells cultured in 3D was three times higher than cells cultured in 2D monolayers (Wang *et al.*, 2016). A recent study by Musah-Eroje and Watson in 2019 Compared GBM cells cultured in the 2D and 3D models. As anticipated, when GBM cells were cultured in the 3D model were significantly more resistant to temozolomide in the 3D cultures and this resistance was enhanced by hypoxia. The authors found that GBM cells cultured in the 3D structure behaved in a different way to their 2D counterparts, both morphologically and in response to chemotherapy. They demonstrated that the microenvironmental factors within GBM spheroids influence cells sensitivity to TMZ where they tended towards a stem-like phenotype, suggesting that 3D cultures of GBM could be a highly-predictive replacement model for *in vitro* drug testing in order to understand and overcome temozolomide resistance in GBM (Musah-Eroje and Watson, 2019). The current results in this study were highly comparable with the previous studies as described above where authors demonstrated a higher resistance in 3D spheroids toward different therapeutic drugs (e.g. camptothecin, fluorouracil, carmustine, cisplatin, gemcitabine, lomustine, paclitaxel, temozolomide, and trastuzumab) than 2D cell cultures (Kessel *et al.*, 2017; Nunes *et al.*, 2019).

However, this observation cannot be generalized since some drugs like the proteasome inhibitor PS-341 exhibited similar or higher activity in spheroids than in the 2D monolayer cultures in different cancer cell types. Likewise, the COX-2 selective inhibitor NS-398 was found to reduce proliferation rate equally in both 2D and 3D cell cultures (Mehta *et al.*, 2012). As previously described, different resistance mechanisms can evolve in 3D cultures which can vary depending on the cell type and drug in use, its mechanism of action and ability to penetrate deeply in the 3D spheroids. It has been revealed that some drugs can penetrate only to a depth of a few cells despite prolonged exposure whereas others can easily diffuse through spheroids. Lack of drug penetration can be due to different factors including binding to surface cells, pH gradients, barriers to drug transport because of extracellular matrix and cell-cell interactions. Moreover, drug penetration within a spheroid is suggested to be affected by the drug molecule structure and its charge (Mehta *et al.*, 2012).

Interestingly, the current findings showed that after 3 days of drug treatment of the U87-MG spheroids under normoxia, aspirin and PN517 showed no significant difference in their effectiveness compared to 2D monolayers as opposed to cisplatin and TMZ where 3D spheroids were significantly more resistant. Furthermore, the combined therapy effectively enhanced the cell sensitivity to cisplatin and TMZ. Although in spheroids under hypoxia, which mimics the far regions of the tumours, were significantly more resistant to all monotherapies, but the combinations again showed enhanced efficacy for cisplatin and TMZ. These findings may suggest better penetration and/or responsiveness for aspirin and PN517 to U87-MG spheroids and confirm the synergistic effect with the standard chemotherapeutic drugs. Having established these results in the 3D model of GBM cells which mirror the *in vivo* microenvironment of the real tumour, it can be further concluded that aspirin and PN517 may have potential therapeutic value in glioblastoma treatment.

CHAPTER 7: FINAL DISCUSSION AND FUTURE WORK

7.1. Final discussion

Glioblastoma multiforme (GBM), now simply called glioblastoma, is the most aggressive form among infiltrative gliomas and represents up to 54% of all gliomas and 16% of all primary brain tumours (Ostrom *et al.*, 2017). Patients with this glioma type face high morbidity and mortality and most do not survive more than 2 years even after optimal treatment (Brem *et al.*, 1972; Preusser *et al.*, 2011; Joseph *et al.*, 2015). Although standard therapeutic approaches could extend survival of patients, most cases eventually display resistance to drug treatment with recurrence always observed (Hombach-Klonisch *et al.*, 2018). As patient outcomes in glioblastoma remain poor with the standard care being mostly palliative and rarely curative, continued research into promising therapeutics are necessary to enhance the treatment of GBM. New approaches are being developed for GBM treatment with a variety of strategies such as TTFs, immunotherapy, monoclonal antibodies, PARP inhibitors with more focus recently on repurposing existing drugs. Several candidates for potential repurposing in GBM treatment have been investigated such as disulfiram, metformin and aspirin (Brenneman *et al.*, 2016; Chae *et al.*, 2016; Navone *et al.*, 2018).

Research has shown that GBM may be caused by many genetic and epigenetic alterations in glial cells (Kanu *et al.*, 2009). Different genetic alterations have been identified, including p53 mutation, loss of heterozygosity LOH#10, PTEN mutation, MGMT methylation, HIF upregulation and EGFR amplification (Kleihues and Ohgaki, 1999; Hegi *et al.*, 2005; Hervey-Jumper and Berger, 2014). Most researchers and clinicians believe that targeting multiple pathways concurrently in GBM will have a better chance of improving patient survival. Various potential targets have been identified including EGFR and PI3K/Akt pathways, NF-κB and Wnt/β-catenin pathways, p53/Rb pathway, as well as STAT3 and interleukins. All these pathways contribute to several biological processes of GBM such as cell survival, proliferation, apoptosis, angiogenesis, migration and invasion, thus are vital for tumourigenesis and metastasis. Notably, COX enzymes have been revealed to be involved in most of these pathways in different tumour models and critically overexpressed in glioma associating with tumour grade, chronic inflammation and poor clinical outcome, hence suggesting

COX pathway regulation as attractive target in gliomas (Shono *et al.*, 2001). Accordingly, anti-inflammatory agents (e.g. NSAIDs) in combination with cytotoxic agents were suggested to provide an improved approach for GBM therapy. Furthermore, the blood brain barrier is a major challenge to the delivery of chemotherapeutic drugs into the brain, which many NSAIDs have successfully overcome (Novakova *et al.*, 2014).

The universal pharmacology of aspirin and other NSAIDs is recognised to be the inhibition of COX-1 and COX-2 enzymes, hence preventing the generation of prostanoids from arachidonic acid. These prostanoids influence many health conditions such as inflammation, asthma, platelet function, cardiovascular homeostasis and cancer (Smyth *et al.*, 2009). Chemopreventitive and chemotherapeutic effects of aspirin have been widely studied in different types of cancer (Bruno *et al.*, 2012; Yue *et al.*, 2014). The first proof in man was obtained from three large UK trials based on daily use of aspirin versus non-aspirin for about four years duration of treatment where aspirin reduced mortality from several cancers (Rothwell *et al.*, 2011). Cumulative evidence has shown the benefits of aspirin in the prevention of colorectal cancer which have made it currently one of the most attractive candidates for the chemoprevention of colorectal cancer (Johnson *et al.*, 2010; Benamouzig *et al.*, 2012; Bosetti *et al.*, 2012), and also led to the recommendation of low dose aspirin for the prevention of colorectal cancer by the United States Preventative Services Task Force (Chan and Ladabaum, 2016).

Several potential therapeutic mechanisms of action have been suggested for aspirin as an antiproliferative and chemopreventative agent which include; (i) the common pathway by which aspirin works as an anti-inflammatory drug via irreversible COX suppression through non-enzymatic acetylation of a single serine residue leading ultimately to the inhibition of prostaglandin biosynthesis (Patrono *et al.*, 2008; Schrör, 2011; Patrignani *et al.*, 2017) ; (ii) inhibition of NF-κB activity (Stark *et al.*, 2001; Gurpinar *et al.*, 2013); (iii) inhibition of the JNK pathway (Schwenger *et al.*, 1997); (iv) activation of AMP kinase (Hawley *et al.*, 2012); (v) induction of apoptosis via the Wnt-β-catenin pathway (Deng *et al.*, 2009); (vi) normalising EGFR expression (Li *et al.*, 2015); (vii) increasing the

expression of DNA repair proteins (Goel *et al.*, 2003); (viii) and inhibition of VEGF leading to suppression of angiogenesis (Borthwick *et al.*, 2006; Ouyang *et al.*, 2008).

However, even with low doses, aspirin has been found to correlate with some health risks such as gastrointestinal (GI) toxicity, particularly GI bleeding and peptic ulcer, which have been shown to be age-dependent (Lowe, 2001; Li *et al.*, 2017). Several randomised trials have reported an approximate twofold increase in GI effects either with enteric-coated or a buffered aspirin formulation (Roderick *et al.*, 1993; Rodrı´ Guez *et al.*, 2001). However, there are opposing data regarding the effect of dose and period of aspirin treatment on the risk of GI bleeding (Huang *et al.*, 2010). Some studies suggested that higher risk of GI bleeding presents with short period of aspirin treatment whereas GI mucosa adapts to the side effect when used for a longer period (Griffin *et al.*, 1991; Langman *et al.*, 1994) . Other studies showed that increased risk in GI bleeding with aspirin usage is cumulative overtime (Nelson *et al.*, 1994). These inconsistencies in the data were attributed possibly to diverse conditions of the individual studies (Huang *et al.*, 2010). Nevertheless, the administration of proton-pump inhibitors in combination with aspirin significantly reduced the risk of GI complications (Rodríguez *et al.*, 2016). On the other hand, the symptoms of GI side effects were shown to be worse in the presence of *H. pylori* infection, although it did not initiate NSAID gastropathy. Hence, it has been recommended for patients to undergo *H. pylori* screening before starting aspirin therapy to reduce the possibility of GI complications (Goggin *et al.*, 1993). Consequently, most reports have reinforced that the use of aspirin needs to be balanced against an increased risk of bleeding in some individuals (Fig 7.1).

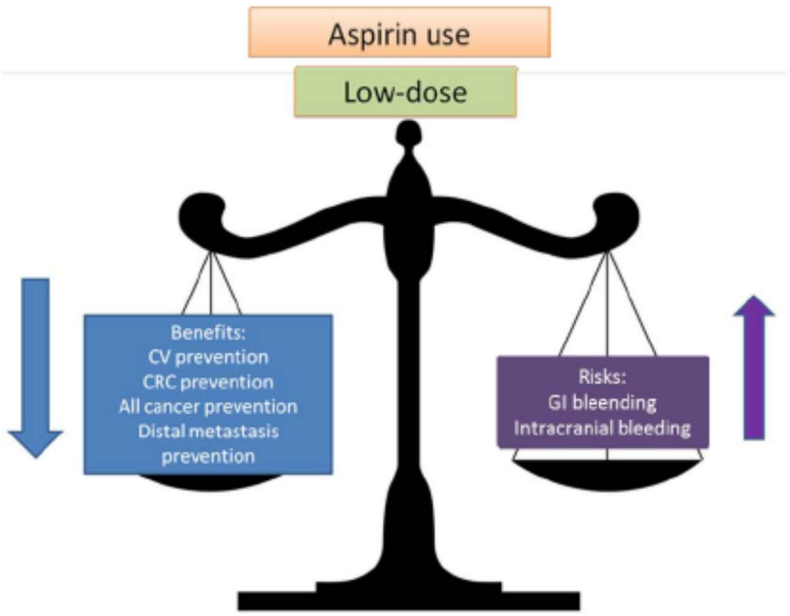

Figure 7. 1. Balancing risks and benefits of aspirin use as chemopreventive agent (Dovizio *et al.*, 2012).

In line with this, different aspirin analogues have been developed and tested aiming to reduce the side effects of aspirin while maintaining or increasing its anti-cancer effects. Many of these analogues have shown promise in colorectal and oesophageal cancers (Deb *et al.*, 2011; Claudius *et al.*, 2014; Kilari *et al.*, 2018), however, there have been no published studies on the efficacy of these analogues for GBM tumours. Therefore, investigations were established to evaluate the effect of different analogues using several gliomas cell lines, identifying fumaroyldiaspirin (PN517) as the compound with highest efficacy.

This project has characterised the effect of aspirin and its novel analogue PN517 as well as the standard chemotherapeutic agents (temozolomide and cisplatin) using a range of assays in U87-MG glioblastoma cell line. The primary aim examined cell viability to reveal any possible synergistic effect for aspirin or PN517 when combined with the standard treatment of GBM, with the remaining aims focusing on characterising the mechanisms of action of all drug treatments, either individually or in combination, including the investigation of cell proliferation, cell cycle, cell migration, different forms of cell death (apoptosis, necrosis, autophagy), mitochondrial membrane potential and metabolic activity. An important additional aim of this project was to examine the effect of the drug

treatment under varying conditions of hypoxia either in 2D or 3D culture environment that more closely recapitulates the *in vivo* tumour microenvironment, allowing for better translation of the data to the clinic. Having established the potent efficacy of PN517 and the enhanced effectiveness of the standard chemotherapy drugs in PN517 combinations, these initial aims have been met while generating many intriguing results, hence, the final discussion aims to incorporate the results from each chapter and present an overall interpretation of the findings.

7.1.1. Aspirin and PN517

To summarise aspirin findings, viability assay has shown that aspirin reduced U87-MG viability under normoxia in a concentration and time dependent manner (Fig 3.7). Although aspirin produced a reduction in cell proliferation comparable to TMZ, it did not produce any significant effects on cell cycle distribution consistent with no change in cyclin D1 or p-cyclin D1 levels (Fig 3.27 &3.28). Additionally, wound healing assay was also performed to investigate the effects on collective cell migration but that was not affected by aspirin treatment (Fig 3.35). Thus, it was suggested that aspirin does not induce cell cycle arrest due to DNA damage and other mechanisms may be involved, and needed further investigation.

Subsequently, this study examined the different types of cell death that may be induced following drug treatment and showed that aspirin induced both apoptosis and autophagy, an effect that was significant at early time points (Fig 4.3 &4.5). These effects correlated with a slight decrease in mitochondrial membrane potential, no significant change in stress proteins, however, aspirin remarkably showed a trend towards inducing autophagy and increasing autophagic protein expression (Fig 4.8-4.10). Therefore, although aspirin can mediate cell apoptosis through a mitochondrial pathway as can be suggested by the results, this may not necessarily be the major contributor towards cell death and other mechanisms such as autophagic cell death may be involved.

As previously described, metabolism reprogramming is a hallmark for many cancers including GBM where glucose metabolism increases significantly in

cancer cells and glycolysis becomes the main source for ATP generation, a phenotype has been valued for decades as the Warburg effect (Gatenby and Gillies, 2004). In line with this, current study showed that U87-MG cells exhibited Warburg effect when compared to the control non-cancerous SVG-p12 cell line (Fig 5.3 &5.4). Recently, the use of the extracellular flux analyser has become a predominant tool for studying the biology and bioenergetics of cancer cells. Therefore, this study investigated the effect of drug treatment on cellular metabolism activity. The combination of the mitochondrial and glycolytic stress tests revealed the effects of drug treatment on both aerobic glycolysis and oxidative phosphorylation pathways. Regarding aspirin treatment, it did not alter basal respiration but reduced the maximal respiration with a decrease in respiratory capacity (Fig 5.9). It also produced a marginal reduction in the glycolytic activity with a reduction in the lactate production (Fig 5.21). This trend was more obvious under hypoxia. In fact, aspirin was first shown to reduce glycolysis a long time ago, where incubation of human platelets with aspirin inhibited glycolysis and ATP levels (Doery *et al.*, 1969). Current investigations also did not show significant decrease in GAPDH enzymatic activity following aspirin treatment (Fig 5.22).

As discussed in earlier chapters, aspirin may have induced glioblastoma cell death through different mechanisms leading ultimately to apoptosis. The anti-cancer effects of aspirin have been mostly linked to its ability to inhibit the COX enzymes resulting in a reduction in prostaglandin production. COX-2 has been associated with tumourigenesis in many cancers with remarkable upregulation in high-grade glioma leading to elevated prostaglandin levels associated with an increase in proliferation and angiogenesis, and inhibition of apoptosis and immune surveillance (Kökoğlu *et al.*, 1998; Joki *et al.*, 2000; Shono *et al.*, 2001). However, while numerous studies have suggested the involvement of COX enzymes in the mechanism of apoptosis induction, it has been reported that different doses of aspirin influence different pathways (Arrieta *et al.*, 2001), with low aspirin concentrations inhibiting COX enzymes and prostaglandins production, whereas high concentrations affecting COX independent mechanisms such as β-catenin/wnt signalling pathway (Lan *et al.*, 2011). Aspirin concentration used in this study (1-3 mM) were lower than those used by Lan

where 10-20 mM of aspirin produced modulation of β-catenin/wnt pathway, suggesting involvement of COX inhibiting or other pathways in the effects seen with aspirin in this study.

Although COX-2 is associated with growth factors, oncogenes and carcinogens, COX-1 was suggested to be the reason that aspirin reduces the risk of colorectal cancer at very low doses that could not maintain COX-2 inhibition (Thun *et al.*, 1991; Giovannucci *et al.*, 1995). However, COX-2 expression can differ between cell lines and is likely to be associated with the cell characteristics and not directly with malignancy (Sheng *et al.*, 1998; Elder *et al.*, 2000). Aspirin was also reported to inhibit EGFR activation in COX-1 expressing ovarian cancer cells demonstrating an interaction between EGFR-activated and COX signalling pathways (Cho *et al.*, 2013). Additionally, a recent study showed that aspirin rapidly perturb EGFR internalisation with proposing activation of p38 MAPK as a potential rapid target implicated as regulator of EGFR internalisation (Bashir *et al.*, 2019). Since aspirin can affect both COX-1 and COX-2, a correlation between both could be the key to activation of different pathways. A previous study in this lab found that aspirin activated both intrinsic and extrinsic pathways of apoptosis as well as inhibited EGFR activation in U87-MG cells, in agreement with the literature suggesting that STAT3 and NF-κB signalling are involved, however further work is required to confirm this hypothesis.

Failure to achieve meaningful improvements with many proposed therapeutic strategies for cancer treatment can be attributed to not using conditions modeling the tumour environment during characterisation (Metzcar *et al.*, 2019). Hypoxia is one of the most important features of the GBM microenvironment, exerting an adverse effect on tumour aggressiveness and patient prognosis (Joseph *et al.*, 2015). GBM tumours are present with areas of mild hypoxia leading to severe hypoxia and necrosis in addition to areas of acute hypoxia and reoxygenation. A reduction in the partial pressure of oxygen leads to the activation of the hypoxia inducible factor HIF pathway which is an important regulator of transcription under hypoxia. The protein level of HIF-1α is undetectable when the oxygen tension is high (21%). Upon hypoxia exposure, stabilisation and increase in the HIF- 1α level occurs leading ultimate to the transcription of a wide array of genes involved

in the cellular adaptation to hypoxia (Strese *et al.*, 2013). Alterations to several cellular processes occurs in order to adapt to hypoxia such as proliferation, angiogenesis, apoptosis, mitochondrial function and glucose metabolism (Koong *et al.*, 1994; Seta *et al.*, 2002; Courtnay *et al.*, 2015), all of which could lead to chemo- and radio-resistance. Furthermore, resistance to therapy triggered by a chronic hypoxic exposure was also explained by a broad gene expression remodelling of components of the DNA DSB sensing machinery, subsequently affecting the activation of DNA repair mechanisms (Scanlon and Glazer, 2015). This diversity of hypoxic conditions within tumours makes it hard to generalize the hypoxia effect on tumour biology, therefore, investigations using different conditions will be of high importance to evaluate the efficacy of drug treatment (Eales *et al.*, 2016). However, studies are rarely undertaken in hypoxic conditions.

The current study showed that aspirin, in most assays, produced very similar effects under acute hypoxia compared to normoxia, and even greater effects in some cases at early timepoints like cell viability, apoptosis and metabolism. However, that was not the case in the hypoxia adapted cells where it showed lower efficacy compared to acute hypoxic cells, but the difference was not significant (Fig 6.4).

Another model employed in the project was U87-MG 3D spheroid cultures, simulating the growth and microenvironment of GBM that cannot be replicated by 2D monolayer cultures. 3D cultures, first described over thirty years ago, are used to assess cellular responses to novel compounds with the aim that *in vitro* results more closely translate to the *in vivo* situation (Sutherland *et al.*, 1981; Lee *et al.*, 2008). 3D spheroids are more resistant to drug treatment than their corresponding 2D monolayers in most cases, particularly when limited drug penetration is expected (Nederman *et al.*, 1981). For instance, cell-cell contacts promote cell survival through activation of signalling pathways such as PI3K/Akt, NF-κB and Stat3. Additionally, the decrease in cell division rate within the spheroid impairs the effects of numerous anti-cancer drugs which most of them exert selective toxicity on dividing cells. Moreover, drug binding to ECM slows down drugs movement towards target cells and changes the number of available drug molecules. Hence. there has been more focus in recent years on the

spheroid model as a better representative of the *in vivo* environment than monolayer cultures (Mehta *et al.*, 2012).

Similar to the chronic hypoxic cells, aspirin was not any less effective in 3D U87-MG cultures under normoxia but was less effective in the hypoxic 3D cultures (Fig 6.23). To date, most literature examining a role for aspirin or prostaglandin signalling has used established cell lines with few publications using primary or 3D cultures (Kökoğlu *et al.*, 1998; Joki *et al.*, 2000; Shono *et al.*, 2001). However, the COX-2 inhibitor, NS-398, was tested using both 2D monolayer and 3D glioma spheroids using U87-MG and U-251MG human glioblastoma cell lines. It was reported that proliferation rate was reduced in both 2D and 3D cultures by aspirin treatment, however, there was only a moderate increase in apoptosis and less inhibition of tumour invasion in the spheroid cultures. These results might be in consistence with the current results where aspirin also produced less efficacy in the 3D cultures. Another study investigated aspirin in the human hepatoma cell line HepG2 and it was shown to be was similarly not toxic in 2D and 3D HepG2 cell cultures and slightly increased with repeated exposure. In contrast, sensitivity to other hepatotoxic compounds was noticeably increased with repeated exposures in 3D spheroids (Ramaiahgari *et al.*, 2014). These differences can be explained by different spheroids formation method in that study where spheroids only about 100μm size were used which was sufficient for oxygen diffusion and allowed for more penetration of the compounds.

Regarding the novel aspirin analogue PN517, current data showed that PN517 reduced U87-MG cell viability under normoxia in a concentration and time dependent manner (Fig 3.7). Like aspirin, PN517 produced a reduction in cell proliferation comparable to TMZ without any significant effect on cell cycle distribution in agreement with no change in cyclin D1 or p-cyclin D1 levels (Fig 3.27 &3.28). Remarkably, the cell viability efficacy of PN517 was not replicated in the proliferation assay, where cisplatin decreased proliferation to a much greater extent, suggesting a difference in the signalling pathways altered by PN517 in cell viability and proliferation (Fig 3.13). This may be related to metabolic alteration or apoptosis by PN517 possibly being the main cause for reducing cell viability. However, cell migration was significantly reduced after

PN517 treatment as observed by the clear inhibition of wound healing (Fig 3.35). While monitoring different forms of cell death, PN517 also induced apoptosis which started significantly at early time points in conjunction with a reduction in the mitochondrial membrane potential (Fig 4.3 &4.11). However, no significant change in stress proteins was observed (Fig 4.14 &4.15).

These results mostly supported the previous papers that investigated PN517 in colorectal cancer cell lines (Deb *et al*., 2011; Claudius *at al*., 2014). They reported that PN517 decreased cell viability, repressed NF-κB signalling, decreased cyclin D1 expression, but did not affect cell cycle. Whereas, the current study found no effect on either cell cycle or cyclin D1 expression indicating that tumour specific differences may influence efficacy. Similarly, results from a separate study from this lab found that PN517 produced different effects on cell cycle in different glioma cell lines, which was explained by the link between p53 and COX-2 expression, as wild type p53 has been shown to inhibit COX-2 expression *in vitro* (Subbaramaiah *et al.*, 1999). In fact, COX-dependent activation of p53 is not unique to glioma and similar findings were reported in colon and oral cancer (Swamy *et al.*, 2003; Gu *et al.*, 2005). It was demonstrated that loss of p53 causes a disruption in cell cycle regulation and can also lead to increased COX-2 expression in glioma. This elevated COX expression and the resultant production of PGE2 may provide a further potential mechanism for changes in proliferation. These expression differences may explain why PN517 changed the cell cycle distribution and proliferation of the lower grade glioma cell lines (1321N1 and GOS-3) at an earlier time point and lower drug concentration than in the high grade U87-MG cell line. Furthermore, it was previously thought that sensitivity to aspirin analogues clearly differed from cell type to cell type due to differences in specific targets for different compounds (Din *et al.*, 2004). Also, differences in cytotoxicity between studies may be due to several reasons such as dissolution solvents used, buffering solutions used and duration of treatment.

Like aspirin, PN517 also has been shown to activate both intrinsic and extrinsic pathways of apoptosis in U87-MG cells and inhibit EGFR activation (data not shown). More recently, Bashir and colleagues found that PN517 perturbed EGF

internalization observed in colorectal and oesophageal cancer cell lines (Bashir *et al.*, 2019). This effect will result in a decrease in proliferation by preventing translocation of the EGFR into the nucleus where it acts as a transcription factor (Lin *et al.*, 2001). The EGFR also phosphorylates the proliferating cell nuclear antigen (PCNA) while in the nucleus thus disrupting interaction with mismatch-recognition proteins MutSα and MutSβ. This subsequently will lead to interruption of DNA MMR and proliferation of cells with damaged DNA, which potentially cause genetic instability (Ortega *et al.*, 2015). It has been found that aspirin and PN517 prevent the translocation of EGF from the surface of the cell membrane towards the nucleus, suggesting that these drugs may have the ability to promote genetic stability in cancer cells as they prevent inaccuracy in DNA replication, hence preventing tumour progression (Claudius *et al.*, 2014). These findings correlated well with observed increase in the expression of DNA MMR proteins (hMLH1, hPMS2, hMSH2 and hMSH6) in many colorectal cell lines after treatment with aspirin (Goel *et al.*, 2003). In addition, these findings might provide a mechanism for the reduced proliferation and induction of apoptosis observed with PN517 in this study (Fig 4.3).

In fact, EGFR and NF-κB signalling are closely linked (Shostak and Chariot, 2015) and the interplay reported between EGFR and NF-κB is as a result of the overactivation of NF-κB in cells that overexpress EGFR (Lehman *et al.*, 2017) which is found in most glioblastoma cell lines (Xu *et al.*, 2017). Also, it has been reported that PN517 can perturb NF-κB activity in colorectal cells and that salicylates can potentially antagonise wound healing (Claudius et al., 2014). The effect of PN517 on EGFR is therefore beneficial in cancer therapy, nevertheless, the mechanism of action for PN517 cannot be determined until further studies are performed on the effects to the downstream EGFR signalling pathway.

This study aimed to further characterise the effects of PN517 using assays not investigated thus far with PN517. Autophagy induction was tested and, unlike aspirin, PN517 did not show any increase in the autophagic activity with no significant increase in the levels of the autophagic proteins, suggesting that cells exposed to PN517 are unable to induce autophagy either as survival or death mechanisms (Fig 4.5). Hence, this study has discovered a major difference

between aspirin and PN517 which support the concept that they are not just the same compound.

Additionally, this study investigated for the first time the effect of PN517 on cellular metabolism and key bioenergetics. Data showed that PN517 significantly impaired the glycolytic activity with reducing glycolysis rate and glycolytic capacity in addition to reducing lactate production (Fig 5.14 &5.21)). Furthermore, PN517 significantly affected mitochondrial activity by reducing each of basal respiration, ATP production and the maximal respiration (Fig 5.7). These effects can provide one explanation for the lack of autophagy induction following treatment with PN517. It has been reported that defects in glycolysis and oxidative phosphorylation have opposing effects on autophagy, where a shift toward aerobic glycolysis can decrease autophagy, and a shift toward oxidative phosphorylation can enhance autophagy, suggesting that targeting mitochondrial oxidative phosphorylation for cancer therapy will inhibit both mitochondrial metabolism and autophagy (Weinberg and Chandel, 2015; Thomas *et al.*, 2018). Similarly, it was observed that cell autophagy induction may occur through triggering expression of autophagic proteins in function mitochondria, as was found in TMZ (Chio *et al.*, 2018). Importantly, these adverse metabolic changes produced by PN517 could be proposed as novel mechanisms of action for this analogue which might eventually lead to cell death. In fact, numerous mechanisms of cell death are known to be controlled by metabolic signals, therefore there has been an increasing interest in studying the interaction between cell death pathways and metabolic events (Fulda, 2014). The findings of these studies have shown that different forms of cell death and multiple intracellular signal transduction pathways are tightly regulated by the availability of cellular metabolites and the general bioenergetic status of the cells. For example, ATP is a fundamental molecule that plays a key role in metabolism regulation as well as the decision between inducing apoptosis or necrosis cell death which has been shown to be dependent in part on the intracellular content of ATP (Leist *et al.*, 1997). Additionally, the mitochondrial PTPCs and cytoplasmic multiprotein complexes have been shown to be involved in the bioenergetic regulation of cell death (Schulze-Osthoff *et al.*, 1992; Kroemer *et al.*, 2007).

Furthermore, a direct link between glucose metabolism and apoptosis has been found in cancer cells (Gatenby and Gillies, 2004) where glycolysis activity is elevated to produce energy and cell death programs are suppressed to ensure cell survival. The most studied conjunction between metabolism and cell death is the effect of glucose metabolism on the intrinsic pathway of apoptosis. It was observed that glucose loss results in reduced level of Mcl-1 (Alves *et al.*, 2006; Zhao *et al.*, 2007) stimulating BH3-only proteins Noxa and Bim (Yang *et al.*, 1997), and Bax activation (Chi *et al.*, 2000; Vander Heiden *et al.*, 2001). These observations highly suggest that Bcl-2 family members are regulated by glucose metabolism. Therefore, it would be important to investigate the effect of PN517 on Bcl-2 proteins in GBM cells and it association with the antiglycolytic effects.

Current investigations have additionally shown that PN517 significantly reduced GAPDH enzymatic activity in U87-MG cells which can be one explanation for the decreased glycolysis rate (Fig 5.22). GAPDH has been considered as a crucial enzyme for glucose metabolism and is noticeably upregulated in glycolytic cancer cells. The prediction of glycolytic phenotype in cancer cells and its sensitivity to glycolytic/GAPDH inhibitor have been an important step toward the development of an effective strategy for cancer treatment. Consequently, several studies have considered GAPDH inhibition as anti-cancer potential therapeutic target (Ganapathy-Kanniappan *et al.*, 2012; Yun *et al.*, 2015). However, GAPDH has pleiotropic functions independent of its recognised role in glycolysis and the ability of the drugs to modulate GAPDH secondary functions has been considered significant because mitochondrial respiration remains intact in cancer cells although glycolysis is elevated, suggesting that inhibiting only the enzyme function of GAPDH may be inefficient for producing anticancer activity (Koppenol *et al.*, 2011). For example, it has been shown that GAPDH can bind active Akt which induces overexpression of the anti-apoptotic Bcl-xL and escape from caspase-independent cell death (Jacquin *et al.*, 2013). Hence, it would be interesting to examine if PN517 can perturb this binding to Akt and the possible outcomes on cell survival.

Additionally, there has been a reported link between autophagy and GAPDH in cancer. GAPDH stimulates autophagy acting as a pro-survival mechanism in

cancer cells to support the energy consumption due to rapid cell proliferation even in stressing conditions. These findings have also reinforced GAPDH as a therapeutic target for autophagy regulation in cancer therapy (Soltany-Rezaee-Rad *et al.*, 2014; Butera *et al.*, 2019).

On the other hand, it was reported that metabolic changes due to GAPDH inhibition may play an important role in affecting migration and invasion, suggesting that GAPDH might affect cell mobility and metastasis indirectly by affecting energy production via its function in glycolysis (Liu *et al.*, 2017). Another study suggested that GAPDH may promote EMT and affect cell migration and metastasis through its nonmetabolic function in the nucleus where GAPDH could interact with Sp1 (specificity protein 1) under oxidative stress conditions, and activate *SNAIL* transcription (Sirover, 2011). Accordingly, cell migration inhibition by PN517, as observed by the wound healing assay, may be due to reducing GAPDH enzymatic activity, hence decreasing energy production. However, further investigation is needed to assess the effect of PN517 treatment on changes in either GAPDH enzyme activity or transcriptional activity.

However, it is worth noting that inhibition of GAPDH activity occurred at 24 hr of drug treatment which at the same timepoint PN517 significantly induced apoptosis and it was previously argued that the nuclear localization of GAPDH and reduced GAPDH activity occurs during apoptosis (Ishitani *et al.*, 1998; Fuchs *et al.*, 2003). That also could suggest that the reduced activity of GAPDH might be a result of apoptosis and not the cause, which needs further investigations to confirm at earlier timescale.

In summary, the current metabolic study provides new insights into the mechanism by which PN517 may inhibit the progression of GBM. PN517 has been found to dramatically suppress mitochondrial respiration and ATP production and simultaneously inhibited the cellular glycolytic rate consistent with targeting of GAPDH activity. Hence, it can be proposed that the apoptosis induced by PN517 may be due to severe impairment in the energy metabolism.

Most importantly, PN517 produced similar efficacy under acute hypoxia or even greater efficacy at early timepoints such as effects on cell viability, apoptosis, and metabolism.

Tumour acidosis accompanied with hypoxia promotes tumour cell migration and invasion by the degradation of the extracellular matrix, exerts immunosuppressive effects which enhance tumour progression, and associates with multi-drug resistance (MDR) due to the neutralization of weak base drugs rendering them less efficient (Sauvant *et al.*, 2008). All of which has contributed to consider tumour acidosis as an indicator of bad prognosis. Therefore, new potential anticancer approach targeted the addiction of cells to glycolysis and the regulation of pH homeostasis. Therefore, another advantage for the PN517 could be reducing acidosis by decreasing glycolytic function and lactate production, which in turn may reduce metastasis and immunosuppression *in vivo*. Although PN517 showed less efficacy in the hypoxia adapted cells and in 3D cultures, the difference was not significant compared to acute hypoxia except for hypoxic 3D cultures. That would mean that PN517 may also be efficient treatment in the hypoxic regions of GBM but needs further investigations *in vivo* to confirm.

Comparison between aspirin and PN517 compounds

When comparing PN517 to the parent compound aspirin, PN517 always showed greater efficacy than aspirin and greater efficacy than cisplatin in many assays including cell viability, migration, apoptosis, mitopotential and metabolic assays. These findings are an important indicator of the therapeutic potential of this novel analogue.

The differences between aspirin and its analogue PN517 could be due to differences in inhibition of COX enzymes. COX inhibition by different aspirin analogues was tested previously in the lab and showed that COX-1 activity was reduced most by aspirin while PN517 showed greater inhibition of COX-2 activity (data not shown). Although other analogues produced even greater inhibition of COX-2 activity but PN517 was the most efficacious suggesting the involvement of COX-independent mechanisms. It was similarly shown that PN517 was more efficacious in reducing cell viability and inducing apoptosis in the colorectal

cancer cells (Deb et al., 2011). Thereafter, Claudius found that both aspirin and PN517 repressed NF-κB-driven transcription. However, the mechanism underlying this inhibition differs between the two compounds where PN517 activity was not associated with nucleolar accumulation of RelA in contrast to aspirin, and PN517 had a more rapid and significant effect than aspirin for all assays performed (Claudius et al., 2014). Kilari also confirmed the differences in the efficiency between aspirin and its analogues in many oesophageal cancer cell lines where PN517 always showed greater efficacy than aspirin in cell viability and apoptosis assays (Kilari et al., 2018). More recently, Bashir has found that PN517 decreases EGFR expression and inhibits EGFR phosphorylation more than aspirin (Bashir et al., 2019). These findings are in consistent with the current findings where PN517 was more efficacious than aspirin in inducing apoptosis and inhibiting wound healing.

The authors suggested that increased activity is at least, in part, due to structural differences. Initially, it was supposed that effects of these compounds could be due to the salicylate moiety of the chemical structure. For example, diflunisal is an NSAID containing salicylate as part of its substructure (Fig 7.2), and works similarly to salicylic acid as an anti-inflammatory and has been found to inhibit the growth of cancer cells *in vitro* and *in vivo* (Shirakawa *et al.*, 2016). However, studies comparing aspirin with salicylic acid have shown that IC_{50} of salicylic acid is higher than that of aspirin with observing greater efficacy for aspirin in many assays including cell viability and apoptosis which suggests that the cytotoxic effect of aspirin does not solely depend on its salicylate moiety but on the parent compound (Deb et al., 2011, Claudius et al., 2014, Kilari et al., 2018, Bashir et al., 2019). The authors also proposed structure-activity relationships important for the pro-apoptotic response to aspirin.

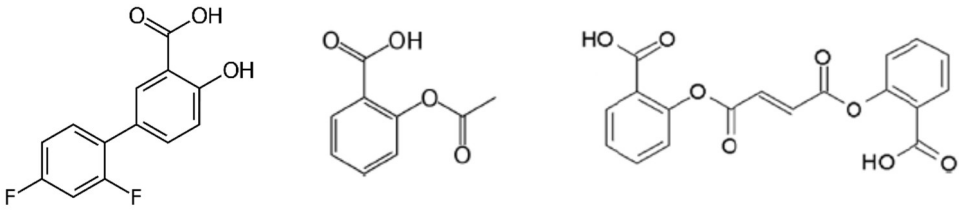

Figure 7. 2. Chemical structure of Diflunisal, Aspirin and PN517.

The differences between aspirin and PN517 concerning NF-κB pathway and cell cycle arrest observed by Claudius could be explained by the aspirin analogues retaining the salicylate part of the aspirin molecule, but losing the acetyl constituent. This might imply that NF-κB regulation is directly linked with the salicylate component, while the nucleolar translocation of RelA and cell cycle arrest with the acetylating potential (Claudius et al., 2014). Furthermore, the additional analogues reported by Kilari and Bashir has also confirmed a relationship between compounds effeicacy and their structure. The compounds with single benzene ring, such as aspirin and its isomers, displayed their effects in a similar manner. Likewise, the thioaspirin analogues had similar effects different from diaspirin compounds that compose of two benzene rings. Hence, similarities in the effects displayed by these compounds may be attributed to their chemical structures (Kilari et al., 2018, Bashir et al., 2019).

As earlier stated, diaspirins have been always more efficacious than aspirin itself. It has been suggested that the enhanced efficacy of diaspirins could be due to their structures that closely resemble two aspirin molecules bound together, which might be hydrolysed yielding two aspirin molecules, and any increased efficacy of these compounds would be replicated by adding a double dose of aspirin. Therefore, a treatment equivalent to a double dose of aspirin was tested previously in this lab and also as part of this current study (data not shown). However, this treatment did not replicate the efficacy of PN517 in the PrestoBlue cell viability assay suggesting that its efficacy is due to some other structural characteristic and not simply because it resembles two aspirin molecules. These findings support the development of PN517 as a unique chemical entity and not merely as an increased dose of aspirin.

Additionally, when examining multiple aspirin analogues, it was reported that increased activity can be partially associated with the presence of two or more suitably spaced aromatic rings. In this regard, it was indicated to the significance of two salicylate moieties separated by ~8-10Å in the analogue molecule. Consequently, it has been speculated that PN517 may exhibit greater toxicity as a result of its increased symmetry and reduced number of conformers (Claudius et al., 2014). On the other hand, the chemical stability of the drugs is of high

importance since it becomes less efficacious when undergoes degradation. It is well known that aspirin is rapidly deacetylated to salicylic acid, which is further metabolized by glucuronidation, hydroxylation, and glycine conjugation (Hutt *et al.*, 1986; Takanashi *et al.*, 2000). As mentioned earlier, the major enzyme involved in aspirin metabolism is the polymorphic enzyme CYP2C9 which can present as fast and slow metabolising forms (Miners and Birkett, 1998; Takanashi *et al.*, 2000). It was reported that CYP2C9 is expressed in glioma with greater expression in higher grades, however, it not well known if there is any heterogeneity in the expression of the polymorphic forms between different gliomas (Knüpfer *et al.*, 2006). In this study the U87-MG cell line was used and would be expected to have a high level of CYP2C9 expression, providing a potential explanation as to why the IC_{50} values for aspirin and PN517 did not decrease further with longer incubations. The simplest explanation for this outcome is that the drugs are rapidly undergoing metabolism to form inactive metabolites. However, the structure of PN517 may undergo less or slower metabolism than aspirin which may explain greater efficacy although this suggestion needs further investigation.

It is noteworthy that both aspirin and PN517 exhibited some variation in responses between different cell lines (Claudius et al., 2014). In fact, three factors at least may explain these differences. The first might simply be related to COX expression and prostaglandin production. Regarding gliomas, COX-2 expression has been shown to be found in both normal brain and glioma specimens, but its expression is significantly higher in high-grade glioma than low- grade glioma and normal brain tissue. Furthermore, it was noted that its expression is higher in slow growing cells than fast growing (Joki *et al.*, 2000). A second factor is CYP2C9 expression which might differ largely between different cell types as described above, and a third factor is EGFR expression, a recognised target for aspirin related compounds *in vitro*, where studies have revealed the highest EGFR expression in high-grade gliomas (Andersson *et al.*, 2004). Consequently, different characterises of the cell line would imply the diversity in the resultant effects of aspirin and PN517. Accordingly, the U87-MG cell line used in this study would be expected to exhibit characteristics of high COX-2 expression, high EGFR expression as well as high CYP2C9 expression which would affect the

overall efficacy of aspirin and its analogues. The degree of involvement for each factor would also depend on the mechanism of action for each drug and the signalling pathways affected. Numerous pathways have been linked with aspirin and glioma either COX-dependent or independent pathways such as NF-κB, EGFR, Wnt/β-catenin, PI3K/Akt and STAT3. However, many of the pathways are interlinked and regulated by COX enzymes or prostaglandins either directly or indirectly, thus, they are not completely COX independent pathways (Hashemi Goradel *et al.*, 2019). The crosstalk between these pathways proves the complexity of intracellular signalling making it difficult to characterise the mechanism of action of novel drugs or identify the particular protein/proteins being critical for efficacy.

7.1.2. Temozolomide

In summary, this project has established that effects of the current standard chemotherapy of GBM, temozolomide (TMZ), on U87-MG cell line. However, it was difficult to establish the concentration-response curves due to its prodrug nature, and its IC_{50} was estimated about 1mM after 48 hr of drug treatment (Table 3.1). Current results showed that TMZ under normoxia reduced U87-MG cell viability in a time-dependent manner, caused a cell cycle arrest in G2/M phase and reduced cell proliferation with a trend towards reducing total cyclin D1 protein levels (Fig 3.7, 3.13, 3.21, 3.27 &3.28). However, in the wound healing assay, TMZ did not significantly inhibit wound healing in U87-MG cell monolayer (Fig 3.35). TMZ showed a trend towards inducing apoptosis which was consistent with an increase in the depolarisation of the mitochondrial membrane potential, with a small fraction of cells undergoing necrosis, but these effects did not increase over time (Fig 4.3). However, the induction of apoptosis was not significant within the duration of time tested, which was also correlated with an increase, but not significant, in the activation of Hsp27 and c-Jun stress proteins (Fig 4.14 &4.15). However, these increases may also be associated with autophagy where TMZ was shown to induce autophagy in U87-MG cells at an early timepoint (24hr) that was more significant under hypoxia with a pattern towards increasing the level of the autophagic protein Atg14 (Fig 4.5).

These findings were consistent with previous studies where TMZ methylation caused lesions at the N^7 or O^6 position of guanine residues, damaging the DNA and triggering a cascade of processes resulting in apoptosis of the GBM cells. Hence, as the cells proliferate, an additive cytotoxic effect is seen (Patel *et al.*, 2014). Studies also have verified that TMZ-triggered apoptosis in gliomas is a late response (occurring after at least 120 hr of drug treatment) which requires extensive cell proliferation (Tomicic *et al.*, 2015). Furthermore, studies showed similar results in terms of upregulating autophagy following TMZ treatment that was interpreted as a response to adverse cellular conditions (Kanzawa *et al.*, 2004), and represents another underlying mechanism to circumvent TMZ-induced damage, aside from MGMT (Würstle *et al.*, 2017).

As already mentioned, autophagy can be initiated by cells to cope with many stresses to cellular health and does not directly result in cell death, unlike apoptosis and necrosis. In fact, apoptosis and autophagy have been shown to interact via crosstalk and each may occur simultaneously or sequentially. Although the cross-talk between apoptosis and autophagy might be complex and sometimes contradictory, it is certainly critical to the deciding the fate of the tumour cells (Nikoletopoulou *et al.*, 2013). In this regard, many proteins originally thought to be involved in autophagy processes are now found to play a role in apoptosis. Likewise, anti-apoptotic proteins also showed a role in blocking autophagic cell death. The complex Bcl-2: Beclin-1, for example can play a role in the switch between autophagy and apoptosis processes (Marquez and Xu, 2012). This may correlate well with the current observation where autophagy happens within 24 hr of TMZ treatment, potentially as protective mechanism, but with longer treatment incubation, it switches to apoptosis.

On the other hand, each form of cell death has different energy requirements that can influence the cell death processes, hence, changes in metabolic status can alter cell death pathways. For example, decreased glucose availability can switch apoptosis to necrosis when energy becomes depleted (Leist *et al.*, 1997; Lieberthal *et al.*, 1998) . In fact, the three major forms of cell death may be influenced by glucose metabolism (Edinger and Thompson, 2004). Necrosis can occur when ATP levels decrease dramatically, and with an inability of the cells to

maintain intracellular homeostasis, therefore, cells simply break down without requiring any ATP for death. In contrast, apoptosis is an energy dependent system that requires ATP For caspase activation (Budihardjo *et al.*, 1999). Autophagy also is an energy dependent process can be induced when the uptake of extracellular nutrient sources decreases, thus, cells switch to use intracellular components to support mitochondrial oxidation and energy production. Nutrient generation by autophagy is mostly beneficial for the cells as more ATP could be produced from mitochondria. However, autophagy can become lethal when digestion occur excessively and most of the cytoplasm becomes consumed (Shintani and Klionsky, 2004). Similarly, autophagy induced by TMZ might be initially induced to protect the cells whereas when combined with aspirin excessive autophagy might cause cell death.

TMZ monotherapy, at early timepoint, produced a decrease in glycolysis activity and lactate production of cells while not affecting mitochondrial activity (Fig 5.7, 5.14 &5.21). However, TMZ did not significantly reduce GAPDH enzymatic activity suggesting affecting different glycolytic enzymes or proteins in the glycolytic pathway (Fig 5.22). One reported observation is that TMZ-induced DNA damage leads to PARP activation resulting in cytoplasmic NADþ depletion, which inhibits glycolysis (Oliva *et al.*, 2010; Su *et al.*, 2018). This reduction in glycolytic activity may be the reason for autophagy induction as there is a known link between metabolism and autophagy processes. Growing research into the mechanisms regulating autophagy has revealed that autophagy activity is enhanced in response to glucose starvation or impaired glycolysis to maintain energy homeostasis and support metabolism and growth (Kim *et al.*, 2011). By reducing glycolysis and maintaining the mitochondrial activity, TMZ might have caused an induction of autophagy at early time points in agreement with the reported findings that inducing autophagy requires functional mitochondria and oxidative phosphorylation functions (Thomas *et al.*, 2018).

While comparing the different culturing conditions, TMZ was significantly less effective under hypoxia which was clear in many assays like cell viability, proliferation and apoptosis. However, this was not a consistent finding where in assays such as cell cycle analysis or autophagy, where TMZ showed equal or higher efficacy. Therefore, a chronic hypoxia-adapted U87-MG cell line was

generated, and interestingly, TMZ showed less efficacy in the hypoxia adapted cells compared to the acute hypoxic conditions. These observations were not surprising and can be explained simply by the slower rate of proliferation under hypoxia. This slower proliferation was already demonstrated by the results obtained from the growth curves and wound healing assay where a reduction in the rate of cell growth and proliferation was observed for control samples under hypoxia as opposed to normoxia. It is known that hypoxia results in a slower cell cycle progression whereas extreme hypoxia induces a pre S-phase arrest in cells (Åmellem *et al.*, 1994). In addition, other mechanisms have already been described for the enhanced resistance under hypoxia, like the tendency to select cells with a low p53 expression reducing cell apoptosis, reducing mitochondrial activity, cellular restoration following DNA injuries and increase in the expression of MDR1 gene.

Importantly, another factor related to hypoxia is lower pH levels occurring by acidosis which could restrict the conversion of TMZ to its active metabolite. In fact, acidosis is one factor can lead to the discrepancy of *in vitro* and *in vivo* results obtained with TMZ or other drugs. It was demonstrated that acidic pH of the cell medium (pH 6.5) found *in vitro* experiments significantly decreased the cytotoxic effect of TMZ (Buccarelli *et al.*, 2018). Hence, the pH variation which may occur *in vitro* can provide an explanation for TMZ low efficacy in many assays in this study and the results inconsistency. Accordingly, approaches to buffer tumour microenvironment pH before standard chemotherapy administration have been proposed by both preclinical and clinical studies (Robey *et al.*, 2009; Pötzl *et al.*, 2017). These findings reinforce the importance of using physiologically relevant oxygen tensions when investigating treatments for GBM. In addition, the development of drugs capable of exerting effects in acidic microenvironment often characterizes tumours is needed (Buccarelli *et al.*, 2018).

Apart from hypoxia, tumour cells cultured in 2D monolayers *in vitro* may lack other features of the real tumour microenvironment, therefore, there is an increasing interest in using 3D spheroids cultures for modelling tumours (Tung *et al.*, 2011). It has been widely accepted that spheroid cultures exhibit enhanced resistance to the many drugs over 2D standard monolayer cultures. Reasons for this

difference between 2D and 3D cultures involve several factors including drug penetration, cell–cell interaction, varying cell proliferation and microenvironment (such as O_2, pH, extracellular matrix) within spheroids (Mehta *et al.*, 2012). Consequently, 3D cultures represent the ideal conditions for tumour cells mimicking their natural behaviour *in vivo*, hence providing better models for drug screening tests. Interestingly, a previous study that generated 3D spheroids from different GBM cell lines found that U87-MG cells formed proliferative spheroids *in vitro*, whereas U251 cells formed non- proliferative spheroids (Kolchinsky and Roninson, 1997). The distribution of a fluorescent vinblastine derivative in the 3D GBM spheroids was more heterogeneous than in 2D monolayers. Furthermore, they found that U87-MG cells increased their resistance about 40-fold in spheroids compared to monolayers and that MDR1 expression decreased the accumulation of 3H-vinblastine and fluorescent vinblastine derivative in the spheroids indicating that MDR1 is more efficient in conferring drug resistance in spheroids than in monolayers. Accordingly, these results can provide an impotent explanation of the significantly reduced efficacy for TMZ and other drug treatments in U87-MG spheroids compared to the monolayers (Fig 6.27 &6.28). Therefore, it can be suggested that the 3D structure of the U87-MG spheroids formed in this study might have affected the distribution and the accumulation of the tested drugs and increased MDR1 expression. This resistance was observed to a greater extent in the hypoxic 3D culture which represent non-proliferative spheroids stimulating the distal part of the tumour from blood vessels, emphasising the need to use 3D cultures in assessing novel compounds for the treatment of GBM.

7.1.3. Cisplatin

Due to the prodrug nature of TMZ, it often does not generate reproducible effects *in vitro*, therefore, it is commonly replaced in research by other standard chemotherapeutic drugs such as cisplatin, hence it was also utilised in this study. Current data showed that cisplatin produced potent cytotoxic effects under normoxia and reduced U87-MG cell viability in a concentration and time dependent manner (Fig 3.7). It inhibited mitosis by causing a cell cycle arrest in G2/M phase and significantly reduced cell proliferation with no obvious effect on the expression or phosphorylation level of cyclin D1 (Fig 3.7, 3.13 &3.21). These

findings were in consistent with some previous reports where cisplatin did not show a significant change in cyclin D1 expression (Zhang *et al.*, 2015), or produced a transient increase in the level of cyclin D1 and eventually decreases cyclin D1 as part of its killing mechanism (El-Kady *et al.*, 2011). Additionally, it was indicated that cisplatin treatment leads to the lethal-7 (Let-7b) miRNAs suppression, which in turn up-regulates cyclin D1 expression (Guo *et al.*, 2013). Therefore, the effect seen in cell cycle arrest following cisplatin treatment might be caused by interfering with different cell cycle proteins and checkpoints. That was also observed with different cell lines where cisplatin treatment produced blockade of CDKs 1, 2, 3, and 4 and transcriptional CDKs 7 and 9, ultimately resulting in arrest at G1/S and G2/M, downregulation of the transcriptional apparatus, and repression of anti-apoptotic proteins (Syn *et al.*, 2018).

Also, cisplatin in this study showed a trend towards inhibiting wound healing although the effect was not significant, an effect was in agreement with previous data where most of the studies have seen an enhanced effect of cisplatin on cell migration and invasion when in combination with other chemotherapy (Karam *et al.*, 2010). In contrast, one study showed that cisplatin can induce EGFR phosphorylation could result in its nuclear translocation and lead to interaction with DNA protein kinase, mediating DNA repair (Benhar *et al.*, 2002). Thus, cisplatin mediated EGFR activation is a survival mechanism by the cell, that in turn, reduces the efficacy of cisplatin (Ahsan *et al.*, 2010). That might support the current findings where the combination of cisplatin with PN517 has significantly enhanced the anti-migration effect of cisplatin, possibly due to reducing EGFR.

When investigating cell death, cisplatin treatment induced apoptosis which increased over time, a finding confirmed by an increase in the depolarisation of the mitochondrial membrane potential, and increases in the levels of the phosphorylated stress proteins p-Hsp27 and p-c-Jun (Fig 4.3, 4.14 &4.15). These findings were in agreement with previous studies which reported that cisplatin causes cell death mainly *via* the mitochondrial signalling pathway associated to activated caspase-3 (Cummings and Schnellmann, 2002; Jiang *et al.*, 2004; Florea and Büsselberg, 2006). It has been suggested that cisplatin activates pro-apoptotic pathways through mitochondrial and Fas-associated mechanisms

(Friesen *et al.*, 1999; Cullen *et al.*, 2007). However, the oxidative stress was considered one of the most important mechanisms involved in cisplatin toxicity, resulting in loss of mitochondrial protein sulfhydryl group, calcium uptake inhibition and decrease of mitochondrial membrane potential (Saad *et al.*, 2004). The current findings of the mitopotential assay can correlate well with the previous findings where significant increase in the mitochondrial depolarisation was observed (Fig 4.11).

Cisplatin treatment of U87-MG cells initiate autophagy and increased the expression of autophagic proteins (PI3K in Class III, PIK3R4 and Atg14) which may be as a cytoprotective mechanism (Fig 4.5). However, the effects were not significant. When monitoring the metabolic activity with seahorse analyser, cisplatin did not seem to affect neither mitochondrial phosphorylation nor glycolytic activity at early time point and although it showed a trend towards reducing lactate production, but it did not produce any significant effects on the bioenergetics parameters. Also, no effect on GAPDH enzymatic activity was observed after cisplatin treatment (Fig 5.22). These results supported previous findings were also cisplatin showed to induce autophagy and delay the onset of apoptosis (Kaushal *et al.*, 2008; Ma *et al.*, 2017). It was also previously reported that the endoplasmic reticulum (ER) stress produced by cisplatin may induce cell autophagy, cell apoptosis and the complicated regulatory network between them. Also, the inhibition of autophagy was shown to increase cisplatin-induced apoptosis by increasing endoplasmic reticulum stress in U251 human glioma cells (Zhang *et al.*, 2015). However, current data of cisplatin may contradict metabolic findings for other studies at times where cisplatin showed to induce or reduce glycolysis in different studies and theses discrepancy might occur due to different concentrations and time of exposure or cell type used (Desoize, 2002; Florea and Busselberg, 2011).

Furthermore, cisplatin cytotoxicity was found to be significantly reduced under hypoxia compared to normoxia where it showed higher IC_{50} and less effect on proliferation and cell cycle. Cell sensitivity was further reduced in the hypoxia-adapted U87-MG cells and more significantly in the 3D cultures, as a decrease in cell proliferation was observed under hypoxia, cisplatin cytotoxicity reduced.

Not only low proliferation rate can induce cisplatin resistance in U87-MG spheroids, but other factors such as reduced accumulation and increased MDR1 expression may imply the reduced efficacy of cisplatin. These findings supported many previous findings where cisplatin was shown to be less effective in 3D cultures indicating the need for higher doses that may not be tolerated by the patients (Dubois *et al.*, 2017)

7.1.4. Combined therapy

In general, combination therapies have been reported to exploit the chances for improved efficacy, reduced toxicity, and decrease development of drug resistance, hence, combined therapy strategies have become a standard for the treatment in several areas such as cancer (W. Humphrey *et al.*, 2011). The combined effects of the drugs on cancer cells are complex, however, combination therapies are increasingly investigated in refractory and heterogenous tumours such as GBM due to the fact that monotherapies have been proven ineffective. Accordingly, because of the failure of conventional chemotherapies in treating GBM, more efforts focusing on therapeutic combinations have been spent to target multiple components of cancer cell survival and proliferation which may enhance the cytotoxic effect and overcome drug resistance (Tan *et al.*, 2018; Vengoji *et al.*, 2018; Cardoso *et al.*, 2019). The current study investigated the efficacy of the combined therapy of aspirin or PN517 with the standard chemotherapeutic drugs cisplatin and TMZ and aimed to compare their effectiveness with the monotherapy in order to discover any synergism.

Generally, all drug combinations showed improved efficacy in reducing U87-MG cell viability when compared to the monotherapies (Table 7.1). PN517 combinations enhanced efficacy of TMZ and cisplatin to a greater degree than aspirin combinations, where the combination of PN517 with TMZ was always the most efficacious treatment in most assays. Importantly, PN517 combinations significantly enhanced the effects of both cisplatin and TMZ on cell viability at earlier timepoint of incubation than aspirin.

Table 7. 1. Effects of combined therapy on the established assays. (↑) enhancement in drug effect compared to monotherapy, (-) no enhancement in the drug effect compared to monotherapy, (~) showing a trend towards enhancing the effect of the monotherapy

Assay	Asp+ Cis	Asp+ TMZ	PN517+ Cis	PN517+ TMZ
Viability	↑	↑	↑	↑
Proliferation	-	↑	~	↑
Cell cycle	-	-	~	↑
Migration	~	~	↑	↑
Apoptosis	-	-	↑	↑
Mitopotential	-	-	↑	↑
Autophagy	↑	↑	-	-
Mito stress	~	~	↑	↑
Glyco stress	↑	-	↑	↑
GAPDH	~	~	↑	↑

Importantly, the enhanced effect seen with the combined therapies was also replicated under acute hypoxia. Although the combinations showed less efficacy when tested in the chronic hypoxia-adapted cells and 3D spheroid cultures, they exhibited the same pattern of efficacy. PN517 combinations were the most efficacious, in particular the combination of PN517 and TMZ which always showed the greatest effectiveness even in the most resistant model, the hypoxic 3D spheroids, and still both aspirin and PN517 significantly enhancing the effect of the standard TMZ monotherapy. It was reported that the influence of epigenetic alterations in response to hypoxia may be amplified by increased cytokine production where an interaction between COX and HIF pathways has been described (Greenhough *et al.*, 2009; Watson *et al.*, 2009; Dong *et al.*, 2018). Therefore, it can be proposed that aspirin and PN517, by affecting COX activity and reducing cytokine production, are producing enhanced efficacy for the combination therapy under hypoxia as well.

Different potential underlying mechanisms can be suggested to explain the enhanced cytotoxic effects of the combined therapy. They include:

a) Inhibition of COX-2 pathway

COX-2 has been shown to play an important role in supporting cancer recurrence and resistance to chemo- and radiotherapy reducing patient's survival in many types of cancers (Li *et al.*, 2017). COX-2 levels are elevated within the tumour microenvironment and it induces inflammation, promotes angiogenesis, metastasis and cancer stem-like activity as well as apoptotic resistance (Greenhough *et al.*, 2009; Todoric *et al.*, 2016). Furthermore, COX-2 mediated hypoxic response within the tumour microenvironment and its connections with antiapoptotic mediators promotes cancer cell resistance to chemotherapeutic drugs (Dong *et al.*, 2018). Therefore, COX-2 inhibition has been suggested to provide beneficial therapeutic outcomes in cancer patients by reducing the risk of metastasis and sensitizing cancer cells to standard treatments like radio- and chemotherapy (Das *et al.*, 2017; Xu *et al.*, 2017). For example, the combination of temozolomide and celecoxib was proposed to inhibit glioma progression through anti-angiogenic mechanisms, reducing tumour oedema (Kerschbaumer *et al.*, 2015). Such combinations have been reported to synergistically increase the antitumoral effect for chemotherapeutic agents and improve the overall response when administered before radiotherapy. Another study has demonstrated that aspirin combined with cisplatin can significantly reduce the drug resistance of cisplatin in tumour therapy (Cheng *et al.*, 2014). Additionally, due to the fact that several signalling pathways contribute to the regulation of COX-2, chemotherapeutic agents can adversely induce COX-2 activity due to effects on upstream modulators of COX-2 (Hashemi Goradel *et al.*, 2019). Taken together, it has been proposed that selecting suitable chemotherapy drugs alongside modification of the type and dose for a COX-2 inhibitor, depending on the cancer type, would act as an effective adjuvant strategy for targeting cancer (Hashemi Goradel *et al.*, 2019).

Regarding the novel diaspirin compounds, enhanced efficacy of platinum compounds was observed when applied in combination as demonstrated by a reduction in the ID_{50} of cisplatin (Kilari et al., 2018). This effect relates to one of

the main aims of combined therapy, which is to achieve a decrease in effective dose in order to alleviate side effects and this decrease in doses needed for platinum compounds has been widely considered of utmost importance because of their narrow therapeutic index (Alcindor and Beauger, 2011).Interestingly, PN517 showed strong synergistic effect with different platinum compounds which increased at higher doses, indicating an advantageous chemotherapy strategy since maximum cytotoxicity against cancer cells is key factor for effective therapy (Chou, 2010), suggesting this as a promising combination for the treatment of cancer. Taken together, one possibility for the enhanced effects of the combined therapy seen in the current study can be due to the ability of both aspirin and PN517 to inhibit COX-2 enzyme activity in U87-MG cell line.

b) Inhibition of EGFR pathway

Several EGFR inhibitors have been found to inhibit tumour growth including erlotinib, gefitinib, and cetuximab (Herbst, 2004). As already mentioned, EGFR is responsible for growth progression in many cancers, particularly in primary GBM (Mendelsohn and Baselga, 2000). The EGFR signalling pathway is complicated and results in reduced apoptosis, increased cell proliferation, angiogenesis and metastasis (Mitsudomi and Yatabe, 2010). Unfortunately, standard chemotherapeutic drugs, in turn, have been shown to activate EGFR. For example, cisplatin-induced DNA damage was reported to activate EGFR in multiple cancer cell lines (Benhar *et al.*, 2002). This EGFR activation has been shown to occur *via* p38 MAPK activating DNA protein kinase to mediate DNA repair and works as a survival mechanism in response to cisplatin (Ahsan *et al.*, 2010). However, cisplatin mediated EGFR activation was slow and only occurring when DNA adducts start forming (Benhar *et al.*, 2002). Additionally, it was suggested that this overexpression of EGFR contributed to cisplatin resistance through the upregulation of key glycolysis enzymes. Current results also support these findings where U87-MG cells showed high glycolytic activity and moderate sensitivity to cisplatin under the experimental conditions tested. Accordingly, the combination of an EGFR inhibitor or anaerobic glycolysis inhibitor with cisplatin displayed synergistic inhibition effects on cisplatin-resistant chondrosarcoma cells (Song *et al.*, 2014). TMZ also has been reported to induce the production of EGFR to regulate the expression of the multi-drug resistance gene MDR1 in GBM

cells, and that giving an inhibitor of EGFR kinase such as erlotinib to nude mice with GBM prevented temozolomide induced resistance (Munoz *et al.*, 2014). Furthermore, hypoxia environment, which is a hallmark of GBM induces amplification of gene transcription and translation of EGFR (Wang *et al.*, 2012). Altogether, these findings suggest that inhibiting EGFR would be beneficial for enhancing the current treatment of GBM.

Importantly, both aspirin and PN517 disturb EGFR internalisation and regulate EGF-induced Ras/MAPK activation and the signalling pathway altogether in colorectal cancer cell lines (Bashir et al., 2019), in agreement with earlier findings which showed that also regulation of EGFR activation correlated with synergistic effects when oxaliplatin and gefitinib were used in combination in same colorectal cell lines (Van Schaeybroeck et al., 2005). Hence, it has been suggested that inhibiting EGFR pathway by aspirins and PN517 supported synergistic effects when combined with oxaliplatin for colorectal cancer, and also emphasised the potential of these compounds where EGFR amplification, overexpression and constitutive activation is notable in cancers such as GBM (Bashir et al., 2019). Consequently, another possibility for the enhanced effects of the combined therapy seen in the current study could be due to the ability of both aspirin and PN517 to inhibit EGFR internalisation and expression in U87-MG cell line. Nevertheless, further studies will be needed to identify the particular effects these compounds have on what particular protein in the EGFR downstream signalling pathway.

c) Autophagy modulation

The role of autophagy in the occurrence and progression of cancer is still controversial. On one hand, autophagy allows tumour cell to survive under adverse environmental conditions, but on the other, when internal energy resources are exhausted, it results in cell death (Parzych and Klionsky, 2014). Therefore, modulating autophagy using pharmacological inhibitors or inducers has received considerable attention in an attempt to sensitise standard treatment for glioma treatment (Daido *et al.*, 2005; Yan *et al.*, 2016).

Aspirin combinations were found to significantly increase the autophagic activity in U87-MG cells, suggesting a mechanism for the enhanced efficacy of cisplatin and TMZ when combined with aspirin through amplification of autophagy leading ultimately to autophagic cell death. Similarly, previous studies have shown that salicylate can suppress tumour development by switching the cell death pathway from tumour-promoting necrotic cell death to tumour-suppressive autophagic cell death (Lim *et al.*, 2008). In contrast, autophagy is enhanced in GBM after treatment with standard cancer therapeutics to enhance cell survival and resistance to therapy (Jawhari *et al.*, 2016). Autophagy inhibition has been revealed to encourage genomic instability, disturb cellular metabolism and prevent resistance to chemotherapy or radiotherapy (Michaud *et al.*, 2011). Accordingly, current findings for the combination of PN517 with TMZ may suggest a mechanism for the enhanced efficacy of this combination due a trend towered reducing autophagy induced by TMZ, however, further investigations are needed to confirm that.

d) Apoptosis amplification

Although aspirin itself induces apoptosis in U87-MG cell line, in combinations it did not increase apoptosis induction over the monotherapy of cisplatin or TMZ. In contrast, PN517 significantly enhanced apoptosis, both early and late, to a greater extent than cisplatin or TMZ. In neuroblastoma, NSAIDs enhanced chemotherapy induced apoptosis by augmentation of p53, deregulation of Bcl-2 family proteins and increase ROS (Lau *et al.*, 2007; Hiľovská *et al.*, 2015). More importantly, while the standard drugs were noted to induce apoptosis at late time points (>72 hr), which is related to the mechanism of action requiring cell proliferation, PN517 combinations significantly induced apoptosis at early time points (24 and 48 hr). Thus, it might be possible that PN517, by activating apoptosic pathways is sensitising the tumour cells to cisplatin and TMZ effects, amplifying apoptosis, and decreasing the chance of cells becoming resistant to chemotherapy.

e) Modulating cellular metabolism

As described earlier, cancer cells display an altered metabolism that may rely on one or both of the key metabolic pathways, oxidative phosphorylation or

glycolysis. The ability of cancer cells to switch between pathways is a crucial strategy causing cancer cell adaptation. Several lines of evidence indicated that rapid changes in cancer cell metabolism are a critical strategy in cellular resistance (Dar *et al.*, 2017). Accumulating evidence has suggested that energy metabolism is vital for the maintenance of chronic inflammation by providing energy and controlling the immune response by metabolic signals (Inoki *et al.*, 2012; Powell *et al.*, 2012). Therefore, targeting cancer metabolism vulnerabilities has been widely investigated and already produced multiple new potential therapeutic agents (Koukourakis *et al.*, 2017; Shi *et al.*, 2019). GBM, in turn, is characterized by mitochondrial hyperpolarization associated with the metabolic remodelling (Warburg effect) and apoptosis resistance (Michelakis *et al.*, 2010). Many studies, including in GBM, suggest that reversing the Warburg effect would enhance the efficiency of standard cancer treatments as well as sensitising resistant cells through targeting and exploiting the metabolic adaptations of the cancer cells (Wangpaichitr *et al.*, 2017). For example, 2-DG combined with cisplatin has enhanced cytotoxicity to human head and neck cancer cells via metabolic oxidative stress suggesting that inhibition of glycolysis sensitizes cancer cells to cisplatin treatment (Van Oosterwijk *et al.*, 2011). Koukourakis and colleagues also showed sensitization of GBM cells to radiotherapy and TMZ, by inhibiting glycolysis using 2-DG (Koukourakis *et al.*, 2017). Similarly, the combination of WZB117, a Glut1 inhibitor, and cisplatin displayed synergistic anticancer effects in non-small cell lung carcinoma cell (Liu *et al.*, 2012).

Dichloroacetate (DCA) is normally used to treat lactic acidosis and has been used as a metabolic modulator in cancer cells. DCA inhibits PDK1 and can alter tumour metabolism by stimulating mitochondrial activity to force glycolytic cells into oxidative phosphorylation, hence reversing the Warburg effect (Stacpoole, 1989). DCA alone has been demonstrated to possess modest anti-cancer activity in both *in vitro* and *in vivo* models of glioblastoma. Importantly, it has high efficacy for GBM stem cells, that may undergo the same metabolic and mitochondrial remodelling of GBM cells but to a greater extent, by reversing this mitochondrial remodelling and inducing apoptosis in GBM stem cells both *in vitro* and *in vivo* (Michelakis *et al.*, 2010). Importantly, DCA has been able to potentiate the effects of GBM standard therapies *in vitro* and *in vivo* by controlling the metabolic state

of cancer cells, binding to EGFR and reversing Warburg effect (Michelakis *et al.*, 2010; Shen *et al.*, 2015; Velpula *et al.*, 2017). Therefore, current cytotoxic effects shown by PN517 treatment, either alone or in combinations with cisplatin and TMZ, might be due to similar effects as noted by the significant reduction in glycolytic function of U87-MG cells, hence, reversing the intense Warburg effect seen in these cells.

Methylene blue (MB) is another proof of the concept compound that suggests reversal of the Warburg effect might be a novel therapy for GBM. MB reversed Warburg effect evidenced by the increase in oxygen consumption and reduction in lactate production leading to cell proliferation inhibition in both temozolomide sensitive and resistant GBM cell lines (Poteet *et al.*, 2013). Similarly, TG02, a pyrimidine-based multi-kinase inhibitor, synergistically decreased energy production with TMZ. The combination induced mitochondrial dysfunction but did not fully explain the synergistic cytotoxic effects. On the other hand, glycolytic capacity and protein expression of key glycolytic enzymes (HK2, PKM2, and LDHA) were decreased in the combination of TG02 and TMZ. The reduction in energy production by glycolysis increases cellular reliance on alternative energy sources, particularly oxidative phosphorylation. Consequently, synergistic effects of TG02 and TMZ was suggested to be relate in part to impairment of both glycolysis and mitochondrial function, which further elevated the energy requirements for DNA repair by TMZ treatment (Su *et al.*, 2018). Therefore, this might represent a possible mechanism for the efficacy of PN517 treatment found in the current study as it was found to inhibit both pathways of energy production. It may be that U87-MG cells were unable to reprogram metabolism when they were exposed to PN517, and this ultimately led to cell death due to energy deficiency. This may provide a novel strategy for treatment of GBM and also help to solve the problems of drug resistance of GBM by combination with a current treatment.

In line with this, recent papers published in 2019 identified another metabolic modulator in the combination treatment for glioblastoma. Sun and colleagues identified R406, the active metabolite of Syk inhibitor, with remarkable cytotoxicity against GBM stem cells but not normal neural stem cells. R406 induced a

metabolic shift from glycolysis to oxidative phosphorylation with subsequent production of excess ROS, therefore, R406 reduced tumour growth and sensitized GBM cells to TMZ in GBM xenograft mouse models (Sun *et al.*, 2019). Also recently, Gboxin (complex V inhibitor), was described as a small molecule that specifically inhibits the growth of primary glioblastoma cells but not that of mouse embryonic fibroblasts or neonatal astrocytes (Shi *et al.*, 2019). Gboxin rapidly and irreversibly compromises oxygen consumption and inhibits the activity of F0F1 ATP synthase in GBM cells. The authors suggested that the increased proton gradient and pH in cancer cell mitochondria is a mode of action that can be targeted in the development of antitumour reagents (Shi *et al.*, 2019). Another recent study reported on the anticancer potential of the combination of biochanin A, isoflavone, with TMZ against U87-MG and T98 G glioblastoma cell lines. A shift in the metabolic phenotype of cells from glycolytic to oxidative phosphorylation was observed with the combination treatment and the cells showed a significant impairment in complex IV activity (Desai *et al.*, 2019). All these recent studies have confirmed that metabolism remodelling in GBM is a significant new approach to enhance the efficacy of current treatments, a finding consistent with the observations with PN517 combination treatments in this study.

As described above, tumour acidosis can induce cell migration and metastasis and increase drug resistance due to the neutralization of weak base drugs rendering them less efficient in addition to increased chromosomal instability (Morita, 1995; Sauvant *et al.*, 2008). Hence, it has been suggested that reducing tumour acidosis would decrease metastatic formation and sensitise cells to chemotherapeutic agents. This approach has been considered to be mostly relevant to hypoxic tumour cells or glycolysis addicted cells that may be highly sensitive to inhibition of pH regulation (Chiche *et al.*, 2010), and these two factors are hallmarks of GBM (Michelakis *et al.*, 2010). Accordingly, it was reported in GBM cell lines that bioenergetic modulators decreased cell viability and migratory/invasion abilities as well as amplified the cytotoxicity of TMZ *in vitro* and *in vivo* (Tavares-Valente *et al.*, 2018). The authors confirmed that metabolic modulation has the potential to be used as a therapy to decrease the aggressiveness of tumours or to be combined with conventional drugs used in glioma treatment and reported that metabolic disruption by glycolytic inhibitors

induced an increase in extracellular pH compared to untreated cells. It was previously shown that blockage of lactate efflux, through MCT inhibition, decreased the migration and invasion abilities in different cancer models (Miranda-Goncalves *et al.*, 2012; Santos *et al.*, 2014), and hence, the authors hypothesized that the metabolic inhibition reduced lactate production and accordingly decreased lactate and proton efflux, increasing extracellular pH, and cell motility was compromised. These findings would suggest a possible mechanism for PN517 reducing wound healing, since PN517 effectively decreased glycolytic activity and lactate production, hence reducing the extracellular acidification and increasing the pH of the media, inhibiting cell migration.

In line with this, it has been already mentioned that the activity of TMZ or the derived metabolite MTIC appears to be pH dependent (pH > 7). Additionally, there is some debate about their mechanism of action as well as a lack of specificity about where activation occurs, inside or outside of tumour cells (Denny *et al.*, 1994; Shen *et al.*, 1995). Therefore, the activity of TMZ could be altered with the pH gradient, and that can explain the chemosensitization of cells when pre-treated with the bioenergetic modulators or in a combined way with conventional drugs. Similarly, it can be concluded from the current findings that PN517 may enhance the efficacy of TMZ monotherapy when in combination by inhibiting glycolysis and increasing extracellular pH levels leading to activation of TMZ and sensitising U87-MG cells to the active metabolite MITC. This can be supported by the observations of the combination of PN517 and TMZ where it always exerts the highest effectiveness among drug treatment.

f) Reversing MDR phenotype

On the other hand, efficacy of the current therapies for GBM is poor due to the development of the multidrug resistance (MDR) phenotype with tumour recurrence (Lee, 2016). Reducing tumour energy via bioenergetic modulators may potentiate conventional chemotherapeutic agents, as many of the proteins associated with the MDR phenotype are energy dependent (Bredel and Zentner, 2002). Studies have shown that overexpression of these resistance proteins either in the blood brain barrier or in GBM cells, prevents TMZ cytotoxicity (Spiegl-

Kreinecker *et al.*, 2002; Veringa *et al.*, 2013; Munoz *et al.*, 2015). Therefore, it has been suggested that metabolic inhibition could be one of the strategies used for targeting the MDR phenotype in order to overcome the low efficacy of current treatment regimens. As PN517 showed this metabolic inhibition in the current study, it can also be suggested that this novel analogue may reduce cellular resistance to cisplatin and TMZ by affecting the MDR phenotype of the treated cells which need further investigation. Taken together, it can be suggested that PN517 may act as a bioenergetic modulator in GBM and sensitise tumour cells to current therapeutic drugs, especially when combined with TMZ. These results provide strong support for the therapeutic potential of this novel compound PN517 for the treatment of GBM in combination with the standard chemotherapy drug, TMZ. Although multiple mechanisms have been suggested, the precise mechanism for the synergy between PN517 and TMZ remains to be completely determined.

Last, but not least, another possibility for the remarkable efficacy of PN517 combinations is the ability of PN517 to reduce GAPDH enzymatic activity. As already described, this can be attributed to the important role of GAPDH in the glycolytic activity or other cellular events associated with tumour progression such as proliferation, metastasis, survival and chemoresistance (Ganapathy-Kanniappan *et al.*, 2012). However, the current study has yielded preliminary results which need further investigation.

7.1.5. Effect on the control cell line SVG-p12

Many of the cancer research publications do not include normal control cell line while screening novel compounds which is important to test drug toxicity on the normal non-cancerous cells. For example, the project of the National Cancer Institute (NCI)60 at the late 1980s included several human tumour cell lines from different cancer types for anticancer drug screening but did not include non-cancerous cell lines as controls. The reason behind that has been reported to be the normal cell lines available at that time which were observed to be either very resistant or very sensitive to the cytotoxic effects of the examined anticancer agents (Shoemaker, 2006). It was believed that the resistant or sensitive normal

cells may underestimate or overestimate the anticancer potential of the tested drugs, respectively (López-Lázaro, 2015).

In this study the SV40-immortalized glial cell line SVG-p12 was used as control model and to test for treatment selectivity. Many advantages have been reported for using immortalized cell lines, such as being well characterized and homogeneous populations making them standard cell lines used by different labs. However, one main disadvantage to using immortalized cells is that they cannot considered totally normal cells since they divide indeterminately and may show unique gene expression patterns that are not found in any cell type *in vivo* (Carter and Shieh, 2015).

It can be noted from the current results that TMZ, the standard chemotherapy drug for GBM, exerts its effects on SVG-p12 cells to approximately same level as U87-MG cancer cells, was even more potent in some cases such as in cell viability and metabolic activity assays, and as such did not show any real selectivity towards glioblastoma cells. Likewise, cisplatin affected the control SVG-p12 cells in a similar way and its effects on apoptosis, necrosis and mitochondrial activity were more in fact greater. These findings support the necessity for the development of drugs that are selective to cancerous cells.

Although aspirin did not show consistent selectivity towards U87-MG cells, it produced less potent effects towards the non-cancerous cells SVG-p12 in cell viability and apoptosis assays. Regarding PN517, it produced similar efficacy on SVG-p12 cell viability and induced a clear reduction in wound healing, yet it did not reach statistical significance. Similarly, apoptosis, depolarisation, and metabolic changes increased in SVG-p12 cells after PN517 treatment, but effects were not significant compared to the control. Most importantly, different aspirin analogues were tested in an *in vivo* tumour mouse model of colorectal cancer where low dose (1mg/kg) was administered every day for 10 days by intravenous injection. The results showed that diaspirins significantly inhibited tumour growth with almost complete suppression by PN517, however, it had no side effects observed following drug treatment compared to the control group animals (Claudius et al., 2014). This is in contrast to chemotherapeutic drugs like cisplatin

whose toxicity limits their use. However, the combinations of aspirin and PN517 also produced enhanced efficacy over the standard chemotherapeutics in the SVG-p12 cell line, suggesting further work is required. In summary, these important findings emphasise the therapeutic potential for PN517 in the treatment of glioma.

7.2. Conclusion

It is well established that the development of new antineoplastic drugs is associated with a number of problems, such as the clinical translation of drugs in development and economic pressures on health systems especially with increasing cancer incidence. Consequently, repurposing of existing non-oncological drugs, mainly the low-cost, widely available drugs with known toxicity profiles, has been proposed as a valuable strategy to address these issues (Pantziarka *et al.*, 2014). Based on encouraging findings in the literature regarding the chemopreventive and chemoprotective activity of aspirin and its ability to enhance the efficacy of multiple classical anti-cancer drugs in GBM treatment (Navone *et al.*, 2018), this *in vitro* project investigated the anticancer effects of aspirin and characterised the novel aspirin analogue PN517 in different GBM models.

Current findings have shown that aspirin has cytotoxic activity in the glioblastoma cell line U87-MG reducing cell viability, inhibiting proliferation, inducing apoptosis and promoting autophagy. Also, aspirin combinations significantly enhanced the efficacy of cisplatin or TMZ monotherapy confirming the potential of aspirin treatment as adjuvant therapy in GBM patients with considering the possible side effects. In addition, PN517, which has been shown to have no overt side effects *in vivo* (Claudius et al., 2014), was more efficacious than aspirin, and in many assays had greater efficacy than cisplatin, and has been suggested to have a different mechanism of action than aspirin. PN517 reduced cell viability, inhibited proliferation, suppressed wound healing, inhibited GAPDH enzymatic activity, produced simultaneously glycolytic and mitochondrial dysfunction resulting in cellular energy metabolism disorder, and produced a loss of mitochondrial membrane potential leading ultimately to apoptosis. Furthermore, the

combinations of PN517 with cisplatin or TMZ significantly enhanced the efficacy of the single drug treatment where the combination of PN517 and TMZ was always the most effective drug treatment.

In addition, this study characterized the changes in cellular sensitivity under various culturing conditions, using a novel system of chronic hypoxia-adapted GBM cell lines and 3D cultures, offering a high degree of clinical and biological relevance to *in vivo* models. This study provides evidence that chronic hypoxia and the complex microenvironment of 3D cultures induce chemo-resistance toward temozolomide and cisplatin. However, despite the more challenging environment, drug treatments showed similar patterns of efficacy with the combinations of PN517 being the most efficacious.

Taken together, PN517 represents a novel aspirin analogue with significant therapeutic potential for the treatment of GBM showing promising results when combined with the standard chemotherapy drug, temozolomide, and should be investigated further *in vivo*.

7.3. Future work

Throughout the thesis, different signalling pathways have been described that may be involved in the mechanism of action of PN517 and its combinations with the standard chemotherapy drugs generating intriguing results. These results may provide a better assessment of therapeutic potential because they contain various tumour models. However, further assays could help to establish these proposed mechanisms and several investigations can be recommended in the future work.

Hypoxia studies

To study the effects of hypoxia on cellular response to drug treatments, it is important to acclimatise cells to hypoxia in order to adjust energy metabolism and protein expression, and reduce oxidative stress (Watson *et al.*, 2009). However, most studies of cell culture are performed under normoxia which is not representative of the oxygen levels found within tumours with some studies including hypoxia conditions for short duration of time (hours-days), whereas in

this study notable changes and differences were found among different models which justify the need for experiments involving short and prolonged duration of exposure to hypoxia. These findings illustrate the importance of using physiologically relevant oxygen concentrations in future studies before drawing conclusions about the effects of drug treatment on cell fate.

However, some technical limitations challenged this study regarding hypoxia studies, such as not always being able to perform hypoxia experiment in continuous hypoxic conditions with Seahorse analyser. Therefore, it was planned to obtain some preliminary data only for U87-MG cell line with culturing the cells under hypoxia while performing the assays by Seahorse analyser under normoxia.

Additionally, it has been reported that a range from 12-43% of tumour areas are exposed to cycling hypoxia which can have direct consequences on tumour cells behaviour, induces metastasis and increases chemo- and radio-resistance (Cairns *et al.*, 2001; Rofstad *et al.*, 2007; Olbryt *et al.*, 2014). Therefore, it would be beneficial to expose cells to cycling hypoxia and measure the levels of different proteins that are affected by hypoxia as well as testing the effects of the drug treatments on tumour cell exposed to the cycling hypoxia. This would expand the knowledge towards understanding the behaviour of cells under hypoxia and help in designing strategies to overcome this.

Monitoring effects on autophagy

Having obtained multiple results concerning the effects of the drug treatments on autophagy process, there are some concerns about autophagy quantification using the commercially available kits with flow cytometry that should be taken into consideration. These assays are advised to be used in conjunction with other methods of monitoring autophagy rather than being used alone. In addition, it is recommended to measure autophagy flux as a demonstration of a complete autophagic pathway. These autophagic assays could be validated using genetic or pharmacological inhibitors of autophagy to monitor whether autophagic activity in dying cells is the cause of cell death or is an attempt to prevent it (Singh and Bhaskar, 2018). In addition, it would be useful to investigate the effect of the drug

treatment on mitophagy as it is considered the most type of autophagy induced under hypoxia. Mitophagy can be monitored by fluorescence microscopy for co-localization of mitochondria with autophagosomes or lysosomes or by Western blotting to measure mitochondrial protein degradation and citrate synthase activity (Ding and Yin, 2012). Recently several assays have been developed for monitoring mitophagy including MitoTimer, mt-Keima, and mito-QC that may be more reliable than previous methods and allow to quantify mitophagy *in vivo* (Williams *et al.*, 2017).

Mechanisms underlying apoptosis

Although high efficacy of the aspirin analogue PN517 and its combinations was observed in apoptosis and mitopotential assays, it is still essential to further characterise the mechanisms involved in these effects. As mentioned earlier, there have been some concern about the validity of the apoptosis quantification results using flow cytometry with Annexin-V and PI kits. In addition, A recent overview and assessment of the fluorescent probes used for ΔΨm measurements have pointed out limited applicability for some probes because of the frequent events of consistently uninterpretable experimental data (Zorova *et al.*, 2018). First, these probes cannot respond quickly to fast changes in the membrane potential which could be important for some investigations. Also, non-specific binding and changes in fluorescence independent of ΔΨm such as interaction with intra-mitochondrial components or other cellular components can occur. In addition, they suffer from being unwanted photosensitizers leading to results that are not straightforwardly interpretable because of the induced photodamage (Zorova *et al.*, 2018). Nevertheless, despite these considerations it is felt that these probes are sufficiently reliable and can provide a valid estimation of ΔΨm under carefully controlled conditions.

Further characterisation of the mechanisms involved in apoptosis induction should be conducted in future studies. For example, apoptosis due to calcium release can be examined using calcium channel blockers such as TMB-8, dantrolene, Fura-2 and EGTA. TMB-8, Fura-2 and dantrolene are intracellular calcium channel blockers, whereas EGTA is an extracellular calcium channel blocker. Hence, the usage of specific blockers would reveal if apoptosis due to

PN517 is *via* intracellular or extracellular calcium release or neither (Wertz and Dixit, 2000). Additionally, caspase activation can be investigated by flow cytometric analysis using anti-CD95 (Bantel *et al.*, 2001), or by measurement of caspase cleavage of synthetic substrates upon their incubation with lysates of apoptotic cells or using caspase inhibitors that work by reversible or irreversible binding to caspases forming adducts in the cysteine residues of the caspases.

Western blotting

Although levels of different proteins were assessed in this study by immunoblotting, numerous proteins of different intracellular signalling pathways may be involved in the mechanism of action of PN517 and can be detected in the future work. For example, the expression and activity of both COX-1 and COX-2 enzymes in GBM cell lines and 3D cultures should be established. Also, caspase activation can be examined, and relative levels quantified. Due to the controversy of the cell cycle and cyclin D1 results between studies, the effects on cell cycle progression could be confirmed by using other cyclin-specific antibodies for immunoblotting with different concentration and timepoints. Measurements of cyclin A, B and E, p21/WAF1, p38 kinase, MAPK, p53, Cdc2 and Cdc25c could provide a further insight into the cell cycle arrest mechanisms. Furthermore, since elevated Akt and STATs signalling are found in cell lines with mutated EGFR (Sordella *et al.*, 2004), western blot analysis could be used to establish if PN517 interferes with Akt expression and phosphorylation which could conclude if this compound has a downstream effect on the EGFR signalling pathway. Another indication of PN517 having a downstream effect on the EGFR signalling pathway would be by assessing the effect on STAT3 and p-STAT3; STAT5 and p-STAT5 (Schindler and Darnell, 1995). From a clinical perspective, the development of HIF inhibitors that target either HIF mRNA transcription, translation, or HIF stabilisation might help resensitising hypoxic tumours and reducing treatment resistance (Masoud and Li, 2015). Importantly, the current study has shown a pattern of reduce levels of HIF-1 proteins in response to PN517 treatment, a finding that needs to be confirmed.

Combination index calculation

Although this study has proved the enhanced effect of the combined therapy of two drugs compared to the monotherapy, the degree of the combination effect between the drugs cannot be exactly identified. This can be achieved in future studies using software like CompuSyn Inc. software which produces several drug concentration-effect calculations using the Median Effect methods described by Chou and Tatalay to calculate the Combination Index (CI) and the Dose Reduction Index (DRI) (Chou and Talalay, 1984). The CI is the quantitative measure of the degree of drug interaction in terms of synergism (CI < 1), additive effect (CI = 1), or antagonism (CI > 1) while the DRI is the measure of favourable dose reduction when two drugs are used in combination.

Investigation ability to cross the blood brain barrier (BBB)

As mentioned earlier, the poor prognosis for GBM is at least partly due to the lack of successful drug delivery across the BBB. Hence, drug delivery in glioblastoma deserves explicit attention as otherwise new experimental therapies will continue to fail. The transport of PN517 across BBB in a flow-based 3D cell culture apparatus can be studied using the Flocel Dynamic *in vitro* Blood Brain Barrier (DIV-BBB) model (FlocelInc, Ohio, USA). The advantage of using this model over any other BBB *in vitro* model is replicating the physiological levels of shear stress experienced by *in situ* endothelial cells. In addition, it allows the formation of physiological trans-endothelial resistance and gap junctions. Consequently, this model closely mimics the *in vivo* BBB, both functionally and anatomically (Naik and Cucullo, 2012). The current study has already started using Flocel DIV-BBB model with both sheer and cyclic stress to assess the ability of treatments to cross the BBB. Keeping in mind the time scale of this project and limited budget, there was no opportunity to continue with the BBB studies and it is recommended to continue this study in the future.

Finally, while this study has used normal and hypoxia-adapted monolayers in addition to spheroid cultures which accelerate the translation of research into clinical practice, the gold standard model would be using a nude mouse model to determine the efficacy of PN517. The efficacy of peripheral delivery of PN517 in either the prevention of GBM development or in the treatment of established tumours can be examined.

CHAPTER 8: REFERENCES

Aapro, M. & Alberts, D. S. 1981. Dexamethasone as an antiemetic in patients treated with cisplatin. *New England Journal of Medicine,* 305**,** 520.

Aas, A. T., Tønnessen, T. I., Brun, A. & Salford, L. G. 1995. Growth inhibition of rat glioma cells in vitro and in vivo by aspirin. *Journal of Neuro-Oncology,* 24**,** 171-180.

Abbruzzese, C., Matteoni, S., Signore, M., Cardone, L., Nath, K., Glickson, J. D. & Paggi, M. G. 2017. Drug repurposing for the treatment of glioblastoma multiforme. *Journal of Experimental & Clinical Cancer Research,* 36**,** 169.

Achison, M. & Hupp, T. R. 2003. Hypoxia attenuates the p53 response to cellular damage. *Oncogene,* 22**,** 3431-3440.

Adler, M., Polinkovsky, M., Gutierrez, E. & Groisman, A. 2010. Generation of oxygen gradients with arbitrary shapes in a microfluidic device. *Lab on a Chip,* 10**,** 388-391.

Agarwala, S. S. & Kirkwood, J. M. 2000. Temozolomide, a novel alkylating agent with activity in the central nervous system, may improve the treatment of advanced metastatic melanoma. *Oncologist,* 5**,** 144-151.

Agarwalla, P., Barnard, Z., Fecci, P., Dranoff, G. & Curry Jr, W. T. 2012. Sequential immunotherapy by vaccination with GM-CSF expressing glioma cells and CTLA-4 blockade effectively treats established murine intracranial tumors. *Journal of Immunotherapy,* 35**,** 385-389.

Aggarwal, B. B., Danda, D., Gupta, S. & Gehlot, P. 2009. Models for prevention and treatment of cancer: problems vs promises. *Biochemical Pharmacology,* 78**,** 1083-1094.

Ahsan, A., Hiniker, S. M., Ramanand, S. G., Nyati, S., Hegde, A., Helman, A., Menawat, R., Bhojani, M. S., Lawrence, T. S. & Nyati, M. K. 2010. Role of epidermal growth factor receptor degradation in cisplatin-induced cytotoxicity in head and neck cancer. *Cancer Research,* 70**,** 2862-2869.

Al Hassan, M., Fakhoury, I., El Masri, Z., Ghazale, N., Dennaoui, R., El Atat, O., Kanaan, A. & El-Sibai, M. 2018. Metformin Treatment Inhibits Motility and Invasion of Glioblastoma Cancer Cells. *Analytical Cellular Pathology,* 2018**,** 5917470.

Al Tameemi, W., Dale, T. P., Al-Jumaily, R. M. K. & Forsyth, N. R. 2019. Hypoxia-modified cancer cell metabolism. *Frontiers in Cell and Developmental Biology,* 7**,** 4.

Alborzinia, H., Can, S., Holenya, P., Scholl, C., Lederer, E., Kitanovic, I. & Wölfl, S. 2011. Real-time monitoring of cisplatin-induced cell death. *PloS One,* 6**,** e19714.

Alcindor, T. & Beauger, N. 2011. Oxaliplatin: a review in the era of molecularly targeted therapy. *Current Oncology,* 18**,** 18-25.

Algra, A. M. & Rothwell, P. M. 2012. Effects of regular aspirin on long-term cancer incidence and metastasis: a systematic comparison of evidence from observational studies versus randomised trials. *The lancet oncology,* 13**,** 518-527.

Alifieris, C. & Trafalis, D. T. 2015. Glioblastoma multiforme: Pathogenesis and treatment. *Pharmacology & Therapeutics,* 152**,** 63-82.

Aljitawi, O. S., Li, D., Xiao, Y., Zhang, D., Ramachandran, K., Stehno-Bittel, L., Van Veldhuizen, P., Lin, T. L., Kambhampati, S. & Garimella, R. 2014. A novel three-dimensional stromal-based model for in vitro chemotherapy sensitivity testing of leukemia cells. *Leukemia & Lymphoma,* 55**,** 378-391.

Allen, C. B., Schneider, B. K. & White, C. W. 2001. Limitations to oxygen diffusion and equilibration in in vitro cell exposure systems in hyperoxia and hypoxia. *American Journal of Physiology-Lung Cellular and Molecular Physiology,* 281**,** L1021-L1027.

Allen, J. W. & Bhatia, S. N. 2003. Formation of steady-state oxygen gradients in vitro: Application to liver zonation. *Biotechnology and Bioengineering,* 82**,** 253-262.

Altaner, C. 2008. Glioblastoma and stem cells - Minireview. *Neoplasma,* 55**,** 369-374.

Altenberg, B. A. & Greulich, K. 2004. Genes of glycolysis are ubiquitously overexpressed in 24 cancer classes. *Genomics,* 84**,** 1014-1020.

Alves, N. L., Derks, I. A., Berk, E., Spijker, R., Van Lier, R. A. & Eldering, E. 2006. The Noxa/Mcl-1 axis regulates susceptibility to apoptosis under glucose limitation in dividing T cells. *Immunity,* 24**,** 703-716.

Amaravadi, R. K., Lippincott-Schwartz, J., Yin, X.-M., Weiss, W. A., Takebe, N., Timmer, W., Dipaola, R. S., Lotze, M. T. & White, E. 2011. Principles and current strategies for targeting autophagy for cancer treatment. *Clinical Cancer Research,* 17**,** 654-666.

Åmellem, Ø., Löffler, M. & Pettersen, E. 1994. Regulation of cell proliferation under extreme and moderate hypoxia: the role of pyrimidine (deoxy) nucleotides. *British Journal of Cancer,* 70**,** 857-866.

Åmellem, Ø. & Pettersen, E. 1991. Cell inactivation and cell cycle inhibition as induced by extreme hypoxia: the possible role of cell cycle arrest as a protection against hypoxia-induced lethal damage. *Cell Proliferation,* 24**,** 127-141.

Amin, R., Kamitani, H., Sultana, H., Taniura, S., Islam, A., Sho, A., Ishibashi, M., Eling, T. E. & Watanabe, T. 2003. Aspirin and indomethacin exhibit antiproliferative effects and induce apoptosis in T98G human glioblastoma cells. *Neurological Research,* 25**,** 370-376.

Andersson, U., Guo, D., Malmer, B., Bergenheim, A. T., Brännström, T., Hedman, H. & Henriksson, R. 2004. Epidermal growth factor receptor family (EGFR, ErbB2–4) in gliomas and meningiomas. *Acta Neuropathologica,* 108**,** 135-142.

Andoniou, C. E., Sutton, V. R., Wikstrom, M. E., Fleming, P., Thia, K. Y., Matthews, A. Y., Kaiserman, D., Schuster, I. S., Coudert, J. D. & Eldi, P. 2014. A natural genetic variant of granzyme B confers lethality to a common viral infection. *PLoS Pathogens,* 10**,** e1004526.

Andrade, J., Pearce, S. T., Hu, Z. & Barroso, M. 2004. Interactions among p22, glyceraldehyde-3-phosphate dehydrogenase and microtubules. *Biochemical Journal,* 384**,** 327-336.

Angileri, F. F., Aguennouz, M., Conti, A., La Torre, D., Cardali, S., Crupi, R., Tomasello, C., Germano, A., Vita, G. & Tomasello, F. 2008. Nuclear factor-kappa B activation and differential expression of survivin and Bcl-2 in human grade 2-4 astrocytomas. *Cancer,* 112**,** 2258-2266.

Annabi, B., Laflamme, C., Sina, A., Lachambre, M.-P. & Béliveau, R. 2009. A MT1-MMP/NF-κB signaling axis as a checkpoint controller of COX-2 expression in CD133 (+) U87 glioblastoma cells. *Journal of Neuroinflammation,* 6**,** 8-11.

Aoki, H., Takada, Y., Kondo, S., Sawaya, R., Aggarwal, B. B. & Kondo, Y. 2007. Evidence that curcumin suppresses the growth of malignant gliomas *in vitro* and *in vivo* through induction of autophagy: role of Akt and extracellular signal-regulated kinase signaling pathways. *Molecular Pharmacology,* 72**,** 29-39.

Apel, A., Herr, I., Schwarz, H., Rodemann, H. P. & Mayer, A. 2008. Blocked autophagy sensitizes resistant carcinoma cells to radiation therapy. *Cancer Research,* 68**,** 1485-1494.

Arismendi-Morillo, G. J. & Castellano-Ramirez, A. V. 2008. Ultrastructural mitochondrial pathology in human astrocytic tumors: potentials implications pro-therapeutics strategies. *Journal of Electron Microscopy,* 57**,** 33-39.

Arrieta, O., Guevara, P., Reyes, S., Palencia, G., Rivera, E. & Sotelo, J. 2001. Paradoxical effect of aspirin on the growth of C6 rat glioma and on time of development of ENU-induced tumors of the nervous system. *Journal of Cancer Research and Clinical Oncology,* 127**,** 681-686.

Ashkenazi, A. & Dixit, V. M. 1998. Death receptors: signaling and modulation. *Science,* 281**,** 1305-1308.

Ashrafi, G. & Schwarz, T. L. 2013. The pathways of mitophagy for quality control and clearance of mitochondria. *Cell Death and Differentiation,* 20**,** 31-42.

Aslantürk, Ö. S. 2018. In vitro cytotoxicity and cell viability assays: principles, advantages, and disadvantages, *InTech*.2.

Azad, M. B., Chen, Y. & Gibson, S. B. 2009. Regulation of autophagy by reactive oxygen species (ROS): implications for cancer progression and treatment. *Antioxidants & Redox Signaling,* 11**,** 777-790.

Azad, M. B., Chen, Y., Henson, E. S., Cizeau, J., Mcmillan-Ward, E., Israels, S. J. & Gibson, S. B. 2008. Hypoxia induces autophagic cell death in apoptosis-competent cells through a mechanism involving BNIP3. *Autophagy,* 4**,** 195-204.

Baker, B. M. & Chen, C. S. 2012. Deconstructing the third dimension–how 3D culture microenvironments alter cellular cues. *Journal of Cell Science,* 125**,** 3015-3024.

Balkwill, F. & Mantovani, A. 2001. Inflammation and cancer: back to Virchow? *The Lancet,* 357**,** 539-545.

Bantel, H., Lugering, A., Poremba, C., Lugering, N., Held, J., Domschke, W. & Schulze-Osthoff, K. 2001. Caspase activation correlates with the degree of inflammatory liver injury in chronic hepatitis C virus infection. *Hepatology,* 34**,** 758-767.

Barbone, D., Yang, T.-M., Morgan, J. R., Gaudino, G. & Broaddus, V. C. 2008. Mammalian target of rapamycin contributes to the acquired apoptotic resistance of human mesothelioma multicellular spheroids. *Journal of Biological Chemistry,* 283**,** 13021-13030.

Barger, J. F. & Plas, D. R. 2010. Balancing biosynthesis and bioenergetics: metabolic programs in oncogenesis. *Endocrine-related Cancer,* 17**,** R287-304.

Barker, F. G., Davis, R. L., Chang, S. M. & Prados, M. D. 1996. Necrosis as a prognostic factor in glioblastoma multiforme. *Cancer: Interdisciplinary International Journal of the American Cancer Society,* 77**,** 1161-1166.

Barker Ii, F. G., Simmons, M. L., Chang, S. M., Prados, M. D., Larson, D. A., Sneed, P. K., Wara, W. M., Berger, M. S., Chen, P. & Israel, M. A. 2001. EGFR overexpression and radiation response in glioblastoma multiforme. *International Journal of Radiation Oncology* Biology* Physics,* 51**,** 410-418.

Barry, M. & Bleackley, R. C. 2002. Cytotoxic T lymphocytes: all roads lead to death. *Nature Reviews Immunology,* 2**,** 401-409.

Bashir, A. I. J., Kankipati, C. S., Jones, S., Newman, R. M., Safrany, S. T., Perry, C. J. & Nicholl, I. D. 2019. A novel mechanism for the anticancer activity of aspirin and salicylates. *International Journal of Oncology,* 54**,** 1256-1270.

Basso, J., Miranda, A., Sousa, J., Pais, A. & Vitorino, C. 2018. Repurposing drugs for glioblastoma: From bench to bedside. *Cancer Letters,* 428**,** 173-183.

Basudhar, D., Bharadwaj, G., Cheng, R. Y., Jain, S., Shi, S., Heinecke, J. L., Holland, R. J., Ridnour, L. A., Caceres, V. M., Spadari-Bratfisch, R. C., Paolocci, N., Velazquez-

Martinez, C. A., Wink, D. A. & Miranda, K. M. 2013. Synthesis and chemical and biological comparison of nitroxyl- and nitric oxide-releasing diazeniumdiolate-based aspirin derivatives. *Journal of Medicinal Chemistry,* 56**,** 7804-7820.

Batchelor, T. T., Mulholland, P., Neyns, B., Nabors, L. B., Campone, M., Wick, A., Mason, W., Mikkelsen, T., Phuphanich, S. & Ashby, L. S. 2013. Phase III randomized trial comparing the efficacy of cediranib as monotherapy, and in combination with lomustine, versus lomustine alone in patients with recurrent glioblastoma. *Journal of Clinical Oncology,* 31**,** 3212-3218.

Bayer, C. & Vaupel, P. 2012. Acute versus chronic hypoxia in tumors. *Strahlentherapie und Onkologie,* 188**,** 616-627.

Bellail, A. C., Hunter, S. B., Brat, D. J., Tan, C. & Van Meir, E. G. 2004. Microregional extracellular matrix heterogeneity in brain modulates glioma cell invasion. *The International Journal of Biochemistry & Cell Biology,* 36**,** 1046-1069.

Bellot, G., Garcia-Medina, R., Gounon, P., Chiche, J., Roux, D., Pouysségur, J. & Mazure, N. M. 2009. Hypoxia-induced autophagy is mediated through hypoxia-inducible factor induction of BNIP3 and BNIP3L via their BH3 domains. *Molecular and Cellular Biology,* 29**,** 2570-2581.

Benamouzig, R., Uzzan, B., Deyra, J., Martin, A., Girard, B., Little, J. & Chaussade, S. 2012. Prevention by daily soluble aspirin of colorectal adenoma recurrence: 4-year results of the APACC randomised trial. *Gut,* 61**,** 255-261.

Benhar, M., Engelberg, D. & Levitzki, A. 2002. Cisplatin-induced activation of the EGF receptor. *Oncogene,* 21**,** 8723-8731.

Benton, G., Arnaoutova, I., George, J., Kleinman, H. K. & Koblinski, J. 2014. Matrigel: from discovery and ECM mimicry to assays and models for cancer research. *Advanced Drug Delivery Reviews,* 79**,** 3-18.

Beppu, T., Kamada, K., Yoshida, Y., Arai, H., Ogasawara, K. & Ogawa, A. 2002. Change of oxygen pressure in glioblastoma tissue under various conditions. *Journal of Neuro-Oncology,* 58**,** 47-52.

Berendsen, S., Broekman, M., Seute, T., Snijders, T., Van Es, C., De Vos, F., Regli, L. & Robe, P. 2012. Valproic acid for the treatment of malignant gliomas: review of the preclinical rationale and published clinical results. *Expert Opinion on Investigational Drugs,* 21**,** 1391-1415.

Bielecka, A. M. & Obuchowicz, E. 2017. Antidepressant drugs can modify cytotoxic action of temozolomide. *European Journal of Cancer Care,* 26**,** e12551.

Bien-Moller, S., Lange, S., Holm, T., Bohm, A., Paland, H., Kupper, J., Herzog, S., Weitmann, K., Havemann, C., Vogelgesang, S., Marx, S., Hoffmann, W., Schroeder, H. W. & Rauch, B. H. 2016. Expression of S1P metabolizing enzymes and receptors correlate with survival time and regulate cell migration in glioblastoma multiforme. *Oncotarget,* 7**,** 13031-13046.

Bilani, N., Bahmad, H. & Abou-Kheir, W. 2017. Prostate cancer and aspirin use: Synopsis of the proposed molecular mechanisms. *Frontiers in Pharmacology,* 8**,** 145.

Binello, E. & Germano, I. M. 2011. Stem cells as therapeutic vehicles for the treatment of high-grade gliomas. *Journal of Neuro-Oncology,* 14**,** 256-265.

Binello, E. & Germano, I. M. 2011. Targeting glioma stem cells: a novel framework for brain tumors. *Cancer Science,* 102**,** 1958-1966.

Birsoy, K., Wang, T., Possemato, R., Yilmaz, O. H., Koch, C. E., Chen, W. W., Hutchins, A. W., Gultekin, Y., Peterson, T. R. & Carette, J. E. 2013. MCT1-mediated transport

of a toxic molecule is an effective strategy for targeting glycolytic tumors. *Nature Genetics,* 45**,** 104-149.

Blair, D. & Dauner, A. 1992. Extrapyramidal symptoms are serious side-effects of antipsychotic and other drugs. *The Nurse Practitioner,* 17**,** 56-67.

Bleeker, F. E., Lamba, S., Leenstra, S., Troost, D., Hulsebos, T., Vandertop, W. P., Frattini, M., Molinari, F., Knowles, M. & Cerrato, A. 2009. IDH1 mutations at residue p. R132 (IDH1R132) occur frequently in high-grade gliomas but not in other solid tumors. *Human Mutation,* 30**,** 7-11.

Boele, F. W., Klein, M., Reijneveld, J. C., Verdonck-De Leeuw, I. M. & Heimans, J. J. 2014. Symptom management and quality of life in glioma patients. *CNS Oncology,* 3**,** 37-47.

Borthwick, G. M., Johnson, A. S., Partington, M., Burn, J., Wilson, R. & Arthur, H. M. 2006. Therapeutic levels of aspirin and salicylate directly inhibit a model of angiogenesis through a Cox-independent mechanism. *The FASEB Journal,* 20**,** 2009-2016.

Bosetti, C., Rosato, V., Gallus, S., Cuzick, J. & La Vecchia, C. 2012. Aspirin and cancer risk: a quantitative review to 2011. *Annals of Oncology,* 23**,** 1403-1415.

Boueroy, P., Aukkanimart, R., Boonmars, T., Sriraj, P., Ratanasuwan, P., Juasook, A., Wonkchalee, N., Vaeteewoottacharn, K. & Wongkham, S. 2017. Inhibitory effect of aspirin on cholangiocarcinoma cells. *Asian Pacific Journal of Cancer Prevention,* 18**,** 3091-3096.

Braganhol, E., Zamin, L. L., Canedo, A. D., Horn, F., Tamajusuku, A. S., Wink, M. R., Salbego, C. & Battastini, A. M. 2006. Antiproliferative effect of quercetin in the human U138MG glioma cell line. *Anti-Cancer Drugs,* 17**,** 663-671.

Brandes, A. A., Tosoni, A., Basso, U., Reni, M., Valduga, F., Monfardini, S., Amistà, P., Nicolardi, L., Sotti, G. & Ermani, M. 2004. Second-line chemotherapy with irinotecan plus carmustine in glioblastoma recurrent or progressive after first-line temozolomide chemotherapy: a phase II study of the Gruppo Italiano Cooperativo di Neuro-Oncologia (GICNO). *Journal of Clinical Oncology,* 22**,** 4779-4786.

Brat, D. J., Castellano-Sanchez, A. A., Hunter, S. B., Pecot, M., Cohen, C., Hammond, E. H., Devi, S. N., Kaur, B. & Van Meir, E. G. 2004. Pseudopalisades in glioblastoma are hypoxic, express extracellular matrix proteases, and are formed by an actively migrating cell population. *Cancer Research,* 64**,** 920-927.

Brat, D. J. & Van Meir, E. G. 2004. Vaso-occlusive and prothrombotic mechanisms associated with tumor hypoxia, necrosis, and accelerated growth in glioblastoma. *Laboratory Investigation,* 84**,** 397-405.

Bray, F. & Møller, B. 2006. Predicting the future burden of cancer. *Nature Reviews Cancer,* 6**,** 63-74.

Bredel, M. & Zentner, J. 2002. Brain-tumour drug resistance: the bare essentials. *The Lancet Oncology,* 3**,** 397-406.

Brem, S., Cotran, R. & Folkman, J. 1972. Tumor angiogenesis: a quantitative method for histologic grading. *Journal of the National Cancer Institute,* 48**,** 347-356.

Brenneman, B. R., Floyd, D. H., Harris, T. & Purow, B. 2016. Assessing and augmenting the immune response to glioblastoma using repurposed pharmaceuticals. AACR.

Brisman, R., Housepian, E. M., Chang, C., Duffy, P. & Balis, E. 1976. Adjuvant nitrosourea therapy for glioblastoma. *Archives of Neurology,* 33**,** 745-750.

Bromage, D. I. & Yellon, D. M. 2015. The pleiotropic effects of metformin: time for prospective studies. *Cardiovascular Diabetology,* 14**,** 109.

Brown, J. M. & Giaccia, A. J. 1998. The unique physiology of solid tumors: Opportunities (and problems) for cancer therapy. *Cancer Research,* 58**,** 1408-1416.

Brown, J. M. & William, W. R. 2004. Exploiting tumour hypoxia in cancer treatment. *Nature Reviews Cancer,* 4**,** 437-447.

Browning, R. J., Reardon, P. J. T., Parhizkar, M., Pedley, R. B., Edirisinghe, M., Knowles, J. C. & Stride, E. 2017. Drug delivery strategies for platinum-based chemotherapy. *American Chemical Society Nano,* 11**,** 8560-8578.

Brozovic, A., Fritz, G., Christmann, M., Zisowsky, J., Jaehde, U., Osmak, M. & Kaina, B. 2004. Long-term activation of SAPK/JNK, p38 kinase and fas-L expression by cisplatin is attenuated in human carcinoma cells that acquired drug resistance. *International Journal of Cancer,* 112**,** 974-985.

Brugarolas, J., Lei, K., Hurley, R. L., Manning, B. D., Reiling, J. H., Hafen, E., Witters, L. A., Ellisen, L. W. & Kaelin, W. G. 2004. Regulation of mTOR function in response to hypoxia by REDD1 and the TSC1/TSC2 tumor suppressor complex. *Genes & Development,* 18**,** 2893-2904.

Bruick, R. K. & Mcknight, S. L. 2001. A conserved family of prolyl-4-hydroxylases that modify HIF. *Science,* 294**,** 1337-1340.

Brunner, T., Wasem, C., Torgler, R., Cima, I., Jakob, S. & Corazza, N. Fas (CD95/Apo-1) ligand regulation in T cell homeostasis, cell-mediated cytotoxicity and immune pathology. Seminars in Immunology, 2003. 167-176.

Bruno, A., Dovizio, M., Tacconelli, S. & Patrignani, P. 2012. Mechanisms of the antitumoural effects of aspirin in the gastrointestinal tract. *Best Practice & Research Clinical Gastroenterology,* 26**,** e1-e13.

Buccarelli, M., Marconi, M., Pacioni, S., De Pasqualis, I., D'alessandris, Q. G., Martini, M., Ascione, B., Malorni, W., Larocca, L. M. & Pallini, R. 2018. Inhibition of autophagy increases susceptibility of glioblastoma stem cells to temozolomide by igniting ferroptosis. *Cell Death & Disease,* 9**,** 841.

Budihardjo, I., Oliver, H., Lutter, M., Luo, X. & Wang, X. 1999. Biochemical pathways of caspase activation during apoptosis. *Annual Review of Cell and Developmental Biology,* 15**,** 269-290.

Bulua, A. C., Simon, A., Maddipati, R., Pelletier, M., Park, H., Kim, K.-Y., Sack, M. N., Kastner, D. L. & Siegel, R. M. 2011. Mitochondrial reactive oxygen species promote production of proinflammatory cytokines and are elevated in TNFR1-associated periodic syndrome (TRAPS). *Journal of Experimental Medicine,* 208**,** 519-533.

Burger, P. C. & Kleihues, P. 1989. Cytologic composition of the untreated glioblastoma with implications for evaluation of needle biopsies. *Cancer,* 63**,** 2014-2023.

Burn, J., Gerdes, A.-M., Macrae, F., Mecklin, J.-P., Moeslein, G., Olschwang, S., Eccles, D., Evans, D. G., Maher, E. R. & Bertario, L. 2011. Long-term effect of aspirin on cancer risk in carriers of hereditary colorectal cancer: an analysis from the CAPP2 randomised controlled trial. *The Lancet,* 378**,** 2081-2087.

Burnet, N., Jefferies, S., Benson, R., Hunt, D. & Treasure, F. 2005. Years of life lost (YLL) from cancer is an important measure of population burden—and should be considered when allocating research funds. *British Journal of Cancer,* 92**,** 241-301.

Burnet, N., Jena, R., Burton, K., Tudor, G., Scaife, J., Harris, F. & Jefferies, S. 2014. Clinical and practical considerations for the use of intensity-modulated radiotherapy and image guidance in neuro-oncology. *Clinical Oncology,* 26**,** 395-406.

Burri, S. H., Gondi, V., Brown, P. D. & Mehta, M. P. 2018. The evolving role of tumor treating fields in managing glioblastoma: Guide for oncologists. *American Journal of Clinical Oncology,* 41**,** 191-196.

Busse, A., Letsch, A., Fusi, A., Nonnenmacher, A., Stather, D., Ochsenreither, S., Regenbrecht, C. R. & Keilholz, U. 2013. Characterization of small spheres derived from various solid tumor cell lines: are they suitable targets for T cells? *Clinical & Experimental Metastasis,* 30**,** 781-791.

Butera, G., Mullappilly, N., Masetto, F., Palmieri, M., Scupoli, M. T., Pacchiana, R. & Donadelli, M. 2019. Regulation of Autophagy by Nuclear GAPDH and Its Aggregates in Cancer and Neurodegenerative Disorders. *International Journal of Molecular Sciences,* 20**,** 2062-2074.

Buzzai, M., Jones, R. G., Amaravadi, R. K., Lum, J. J., Deberardinis, R. J., Zhao, F., Viollet, B. & Thompson, C. B. 2007. Systemic treatment with the antidiabetic drug metformin selectively impairs p53-deficient tumor cell growth. *Cancer Research,* 67**,** 6745-6752.

Byfield, M. P., Murray, J. T. & Backer, J. M. 2005. hVps34 is a nutrient-regulated lipid kinase required for activation of p70 S6 kinase. *Journal of Biological Chemistry,* 280**,** 33076-33082.

Cadigan, K. M. & Peifer, M. 2009. Wnt Signaling from Development to Disease: Insights from Model Systems. *Cold Spring Harbor Perspectives in Biology,* 1**,** a002881.

Cairns, R. A., Harris, I. S. & Mak, T. W. 2011. Regulation of cancer cell metabolism. *Nature Reviews Cancer,* 11**,** 85-95.

Cairns, R. A., Kalliomaki, T. & Hill, R. P. 2001. Acute (cyclic) hypoxia enhances spontaneous metastasis of KHT murine tumors. *Cancer Research,* 61**,** 8903-8908.

Calogero, A., Porcellini, A., Lombari, V., Fabbiano, C., Arcella, A., Miscusi, M., Ponti, D. & Ragona, G. 2011. Sensitivity to cisplatin in primary cell lines derived from human glioma correlates with levels of EGR-1 expression. *Cancer Cell International,* 11**,** 5.

Campregher, C., Honeder, C., Chung, H., Carethers, J. M. & Gasche, C. 2010. Mesalazine reduces mutations in transforming growth factor β receptor II and activin type II receptor by improvement of replication fidelity in mononucleotide repeats. *Clinical Cancer Research,* 16**,** 1950-1956.

Cantor, J. R. & Sabatini, D. M. 2012. Cancer cell metabolism: one hallmark, many faces. *Cancer Discovery,* 2**,** 881-898.

Capdevila, L., Cros, S., Ramirez, J.-L., Sanz, C., Carrato, C., Romeo, M., Etxaniz, O., Hostalot, C., Massuet, A. & Cuadra, J. L. 2014. Neoadjuvant cisplatin plus temozolomide versus standard treatment in patients with unresectable glioblastoma or anaplastic astrocytoma: a differential effect of MGMT methylation. *Journal of Neuro-Oncology,* 117**,** 77-84.

Cardoso, A., Sousa, M., Morais, C. M., Oancea-Castillo, L. R., Régnier-Vigouroux, A., Rebelo, O., Tão, H., Barbosa, M., Pedroso De Lima, M. C. & Jurado, A. S. 2019. MiR-144 overexpression as a promising therapeutic strategy to overcome glioblastoma cell invasiveness and resistance to chemotherapy. *Human Molecular Genetics,* 28**,** 2738-2751.

Carlsson, S. K., Brothers, S. P. & Wahlestedt, C. 2014. Emerging treatment strategies for glioblastoma multiforme. *EMBO Molecular Medicine,* 6**,** 1359-1370.

Carpenter, A. B. 2019. Recombinant Oncolytic Poliovirus for Glioblastoma: A Current Review of PVS (RIPO). *Georgetown Medical Review,* 3**,** 7789-7794.

Carrera, S., Senra, J., Acosta, M. I., Althubiti, M., Hammond, E. M., De Verdier, P. J. & Macip, S. 2014. The role of the HIF-1α transcription factor in increased cell division at physiological oxygen tensions. *PloS One,* 9**,** e97938.

Carter, M. & Shieh, J. C. 2015. Guide to research techniques in neuroscience, *Academic Press*.

Casper, D., Lekhraj, R., Yaparpalvi, U. S., Pidel, A., Jaggernauth, W. A., Werner, P., Tribius, S., Rowe, J. D. & Lasala, P. A. 2000. Acetaminophen selectively reduces glioma cell growth and increases radiosensitivity in culture. *Journal of Neuro-Oncology,* 46**,** 215-229.

Castedo, M., Obrist, F. & Kroemer, G. 2018. Cisplatin resistance coupled to enhanced sensitivity to metabolic interventions. *Molecular & Cellular Oncology,* 5**,** e1526004.

Castellone, M. D., Teramoto, H., Williams, B. O., Druey, K. M. & Gutkind, J. S. 2005. Prostaglandin E2 promotes colon cancer cell growth through a Gs-axin-ß-catenin signaling axis. *Science,* 310**,** 1504-1510.

Castoldi, F., Pietrocola, F., Maiuri, M. C. & Kroemer, G. 2018. Aspirin induces autophagy via inhibition of the acetyltransferase EP300. *Oncotarget,* 9**,** 24574-24575.

Cecchini, M. J., Amiri, M. & Dick, F. A. 2012. Analysis of cell cycle position in mammalian cells. *Journal of Visualized Experiments***,** e3491.

Chaabane, W., User, S. D., El-Gazzah, M., Jaksik, R., Sajjadi, E., Rzeszowska-Wolny, J. & Łos, M. J. 2013. Autophagy, apoptosis, mitoptosis and necrosis: interdependence between those pathways and effects on cancer. *Archivum Immunologiae et Therapiae Experimentalis,* 61**,** 43-58.

Chacko, B. K., Kramer, P. A., Ravi, S., Johnson, M. S., Hardy, R. W., Ballinger, S. W. & Darley-Usmar, V. M. 2013. Methods for defining distinct bioenergetic profiles in platelets, lymphocytes, monocytes, and neutrophils, and the oxidative burst from human blood. *Laboratory Investigation,* 93**,** 690-700.

Chae, Y. K., Arya, A., Malecek, M.-K., Shin, D. S., Carneiro, B., Chandra, S., Kaplan, J., Kalyan, A., Altman, J. K. & Platanias, L. 2016. Repurposing metformin for cancer treatment: current clinical studies. *Oncotarget,* 7**,** 40767-40780.

Chan, A. T. & Ladabaum, U. 2016. Where do we stand with aspirin for the prevention of colorectal cancer? The USPSTF recommendations. *Gastroenterology,* 150**,** 14-18.

Chan, A. T., Ogino, S. & Fuchs, C. S. 2009. Aspirin use and survival after diagnosis of colorectal cancer. *Jama,* 302**,** 649-658.

Chandel, N. S., Mcclintock, D. S., Feliciano, C. E., Wood, T. M., Melendez, J. A., Rodriguez, A. M. & Schumacker, P. T. 2000. Reactive oxygen species generated at mitochondrial Complex III stabilize HIF-1-alpha during hypoxia: a mechanism of O2 sensing. *Journal of Biological Chemistry,* 275**,** 25130-25138.

Charest, G., Sanche, L., Fortin, D., Mathieu, D. & Paquette, B. 2012. Glioblastoma Treatment: Bypassing the Toxicity of Platinum Compounds by Using Liposomal Formulation and Increasing Treatment Efficiency With Concomitant Radiotherapy. *International Journal of Radiation Oncology* Biology* Physics,* 84**,** 244-249.

Charles, N. A., Holland, E. C., Gilbertson, R., Glass, R. & Kettenmann, H. 2012. The brain tumor microenvironment. *Glia,* 60**,** 502-514.

Chaudhry, A., Benson, L., Varshaver, M., Farber, O., Weinberg, U., Kirson, E. & Palti, Y. 2015. NovoTTF™-100A System (Tumor Treating Fields) transducer array layout planning for glioblastoma: a NovoTAL™ system user study. *World Journal of Surgical Oncology,* 13**,** 316.

Chen, J. & Stark, L. A. 2017. Aspirin Prevention of Colorectal Cancer: Focus on NF-kappaB Signalling and the Nucleolus. *Biomedicines,* 5**,** 43.

Chen, J. C., Chang, M. L. & Muench, M. O. 2003. A kinetic study of the murine mixed lymphocyte reaction by 5,6-carboxyfluorescein diacetate succinimidyl ester labeling. *Journal of Immunological Methods,* 279**,** 123-133.

Chen, J. H., Zhang, L. M., Zhou, H., Wang, W., Luo, Y. Z., Yang, H. & Yi, H. H. 2018. Inhibition of autophagy promotes cisplatin-induced apoptotic cell death through Atg5 and Beclin 1 in A549 human lung cancer cells. *Molecular Medicine Reports,* 17**,** 6859-6865.

Chen, R., Dai, R. Y., Duan, C. Y., Liu, Y. P., Chen, S. K., Yan, D. M., Chen, C. N., Wei, M. & Li, H. 2011. Unfolded protein response suppresses cisplatin-induced apoptosis via autophagy regulation in human hepatocellular carcinoma cells. *Folia Biologica,* 57**,** 87-95.

Chen, S., Bubeck, D., Macdonald, B. T., Liang, W. X., Mao, J. H., Malinauskas, T., Llorca, O., Aricescu, A. R., Siebold, C., He, X. & Jones, E. Y. 2011. Structural and Functional Studies of LRP6 Ectodomain Reveal a Platform for Wnt Signaling. *Developmental Cell,* 21**,** 848-861.

Chen, S., Li, X., Lu, D., Xu, Y., Mou, W., Wang, L., Chen, Y., Liu, Y., Li, X. & Li, L.-Y. 2013. SOX2 regulates apoptosis through MAP4K4-survivin signaling pathway in human lung cancer cells. *Carcinogenesis,* 35**,** 613-623.

Cheng, Q., Shi, H., Wang, H., Min, Y., Wang, J. & Liu, Y. 2014. The ligation of aspirin to cisplatin demonstrates significant synergistic effects on tumor cells. *Chemical Communications,* 50**,** 7427-7430.

Cheng, T., Sudderth, J., Yang, C., Mullen, A. R., Jin, E. S., Matés, J. M. & Deberardinis, R. J. 2011. Pyruvate carboxylase is required for glutamine-independent growth of tumor cells. *Proceedings of the National Academy of Sciences,* 108**,** 8674-8679.

Cheresh, P., Kim, S.-J., Tulasiram, S. & Kamp, D. W. 2013. Oxidative stress and pulmonary fibrosis. *Biochimica et Biophysica Acta (BBA)-Molecular Basis of Disease,* 1832**,** 1028-1040.

Cheung, H.-H., Liu, X. & Rennert, O. M. 2012. Apoptosis: Reprogramming and the fate of mature cells. *ISRN Cell Biology,* 2012**,** 685852.

Chhipa, R. R., Fan, Q., Anderson, J., Muraleedharan, R., Huang, Y., Ciraolo, G., Chen, X., Waclaw, R., Chow, L. M. & Khuchua, Z. 2018. AMP kinase promotes glioblastoma bioenergetics and tumour growth. *Nature Cell Biology,* 20**,** 823-835.

Chi, M. M., Pingsterhaus, J., Carayannopoulos, M. & Moley, K. H. 2000. Decreased glucose transporter expression triggers BAX-dependent apoptosis in the murine blastocyst. *Journal of Biological Chemistry,* 275**,** 40252-40257.

Chiche, J., Brahimi-Horn, M. C. & Pouyssegur, J. 2010. Tumour hypoxia induces a metabolic shift causing acidosis: a common feature in cancer. *Journal of Cellular and Molecular Medicine,* 14**,** 771-794.

Chiche, J., Ilc, K., Durivault, J., Brahimi-Horn, M. C. & Pouysségur, J. 2009. Abstract# 234: The HIF-induced carbonic anhydrases CAIX and XII regulate intracellular pH. Validation of CAIX and XII as anticancer targets. *AACR*, 234.

Chinopoulos, C. & Seyfried, T. N. 2018. Mitochondrial substrate-level phosphorylation as energy source for glioblastoma: review and hypothesis. *ASN Neuro,* 10.

Chio, C. C., Chen, K. Y., Chang, C. K., Chuang, J. Y., Liu, C. C., Liu, S. H. & Chen, R. M. 2018. Improved effects of honokiol on temozolomide-induced autophagy and apoptosis of drug-sensitive and -tolerant glioma cells. *BMC Cancer,* 18**,** 379-394.

Chitcholtan, K., Asselin, E., Parent, S., Sykes, P. H. & Evans, J. J. 2013. Differences in growth properties of endometrial cancer in three dimensional (3D) culture and 2D cell monolayer. *Experimental Cell Research,* 319**,** 75-87.

Cho, M., Kabir, S. M., Dong, Y., Lee, E., Rice, V. M., Khabele, D. & Son, D.-S. 2013. Aspirin blocks EGF-stimulated cell viability in a COX-1 dependent manner in ovarian cancer cells. *Journal of Cancer,* 4**,** 671-678.

Cho, Y.-J., Tsherniak, A., Tamayo, P., Santagata, S., Ligon, A., Greulich, H., Berhoukim, R., Amani, V., Goumnerova, L. & Eberhart, C. G. 2011. Integrative genomic analysis of medulloblastoma identifies a molecular subgroup that drives poor clinical outcome. *Journal of Clinical Oncology,* 29**,** 1424-1430.

Choi, Y. W. & Lim, I. K. 2014. Sensitization of metformin-cytotoxicity by dichloroacetate via reprogramming glucose metabolism in cancer cells. *Cancer Letters,* 346**,** 300-308.

Chou, C.-W., Wang, C.-C., Wu, C.-P., Lin, Y.-J., Lee, Y.-C., Cheng, Y.-W. & Hsieh, C.-H. 2012. Tumor cycling hypoxia induces chemoresistance in glioblastoma multiforme by upregulating the expression and function of ABCB1. *Neuro-oncology,* 14**,** 1227-1238.

Chou, T. C. 2010. Drug Combination Studies and Their Synergy Quantification Using the Chou-Talalay Method. *Cancer Research,* 70**,** 440-446.

Chou, T. C. & Talalay, P. 1984. Quantitative analysis of dose-effect relationships: the combined effects of multiple drugs or enzyme inhibitors. *Advances in Enzyme Regulation,* 22**,** 27-55.

Chou, W. Y., Marky, L. A., Zaunczkowski, D. & Breslauer, K. J. 1987. The thermodynamics of drug-DNA interactions: ethidium bromide and propidium iodide. *Journal of Biomolecular Structure and Dynamics,* 5**,** 345-359.

Chou, Y. C., Chang, M. Y., Wang, M. J., Harnod, T., Hung, C. H., Lee, H. T., Shen, C. C. & Chung, J. G. 2015. PEITC induces apoptosis of Human Brain Glioblastoma GBM8401 Cells through the extrinsic- and intrinsic -signaling pathways. *Neurochemistry International,* 81**,** 32-40.

Christmann, M., Tomicic, M. T., Aasland, D. & Kaina, B. 2007. A role for UV-light-induced c-Fos: stimulation of nucleotide excision repair and protection against sustained JNK activation and apoptosis. *Carcinogenesis,* 28**,** 183-190.

Chuang, D. F. & Lin, X. 2019. Targeted Therapies for the Treatment of Glioblastoma in Adults. *Current Oncology Reports,* 21**,** 61.

Ciotti, M., Marrone, A., Potter, C. & Owens, I. S. 1997. Genetic polymorphism in the human UGT1A6 (planar phenol) UDP-glucuronosyltransferase: pharmacological implications. *Pharmacogenetics,* 7**,** 485-495.

Clark, M. J., Homer, N., O'connor, B. D., Chen, Z., Eskin, A., Lee, H., Merriman, B. & Nelson, S. F. 2010. U87MG decoded: the genomic sequence of a cytogenetically aberrant human cancer cell line. *PLoS Genetics,* 6**,** e1000832.

Claudius, A.-K., Kankipati, C. S., Kilari, R. S., Hassan, S., Guest, K., Russell, S. T., Perry, C. J., Stark, L. A. & Nicholl, I. D. 2014. Identification of aspirin analogues that repress NF-κB signalling and demonstrate anti-proliferative activity towards colorectal cancer in vitro and in vivo. *Oncology Reports,* 32**,** 1670-1680.

Cohn, L. & Delamarre, L. 2014. Dendritic cell-targeted vaccines. *Frontiers in Immunology,* 5**,** 255.

Colell, A., Green, D. & Ricci, J. 2009. Novel roles for GAPDH in cell death and carcinogenesis. *Cell Death and Differentiation,* 16**,** 1573-1581.

Collingridge, D. R., Piepmeier, J. M., Rockwell, S. & Knisely, J. P. 1999. Polarographic measurements of oxygen tension in human glioma and surrounding peritumoural brain tissue. *Radiotherapy and Oncology,* 53**,** 127-131.

Colotta, F., Allavena, P., Sica, A., Garlanda, C. & Mantovani, A. 2009. Cancer-related inflammation, the seventh hallmark of cancer: links to genetic instability. *Carcinogenesis,* 30**,** 1073-1081.

Combs, S. E., Wagner, J., Bischof, M., Welzel, T., Wagner, F., Debus, J. & Schulz-Ertner, D. 2008. Postoperative treatment of primary glioblastoma multiforme with radiation and concomitant temozolomide in elderly patients. *International Journal of Radiation Oncology* Biology* Physics,* 70**,** 987-992.

Comerford, K. M., Wallace, T. J., Karhausen, J., Louis, N. A., Montalto, M. C. & Colgan, S. P. 2002. Hypoxia-inducible factor-1-dependent regulation of the multidrug resistance (MDR1) gene. *Cancer Research,* 62**,** 3387-3394.

Cossarizza, A., Baccaranicontri, M., Kalashnikova, G. & Franceschi, C. 1993. A new method for the cytofluorometric analysis of mitochondrial membrane potential using the J-aggregate forming lipophilic cation 5, 5′, 6, 6′-tetrachloro-1, 1′, 3, 3′-tetraethylbenzimidazolcarbocyanine iodide (JC-1). *Biochemical and Biophysical Research Communications,* 197**,** 40-45.

Costa, E. C., De Melo-Diogo, D., Moreira, A. F., Carvalho, M. P. & Correia, I. J. 2018. Spheroids formation on non-adhesive surfaces by liquid overlay technique: Considerations and practical approaches. *Biotechnology Journal,* 13**,** 1700417.

Courtnay, R., Ngo, D. C., Malik, N., Ververis, K., Tortorella, S. M. & Karagiannis, T. C. 2015. Cancer metabolism and the Warburg effect: the role of HIF-1 and PI3K. *Molecular Biology Reports,* 42**,** 841-851.

Cowman, S., Fan, Y. N., Pizer, B. & Sée, V. 2019. Decrease of Nibrin expression in chronic hypoxia is associated with hypoxia-induced chemoresistance in some brain tumour cells. *BMC Cancer,* 19**,** 300.

Crosio, C., Fimia, G. M., Loury, R., Kimura, M., Okano, Y., Zhou, H., Sen, S., Allis, C. D. & Sassone-Corsi, P. 2002. Mitotic phosphorylation of histone H3: spatio-temporal regulation by mammalian Aurora kinases. *Molecular and Cellular Biology,* 22**,** 874-885.

Crunkhorn, S. 2019. Targeting cancer cell metabolism in glioblastoma. *Nature Reviews Cancer,* 19**,** 250.

Cuddapah, V. A., Robel, S., Watkins, S. & Sontheimer, H. 2014. A neurocentric perspective on glioma invasion. *Nature Reviews Neuroscience,* 15**,** 455-465.

Cullen, K. J., Yang, Z. J., Schumaker, L. & Guo, Z. M. 2007. Mitochondria as a critical target of the chemotheraputic agent cisplatin in head and neck cancer. *Journal of Bioenergetics and Biomembranes,* 39**,** 43-50.

Cummings, B. S. & Schnellmann, R. G. 2002. Cisplatin-induced renal cell apoptosis: caspase 3-dependent and-independent pathways. *Journal of Pharmacology and Experimental Therapeutics,* 302**,** 8-17.

Dai, S., Huang, M. L., Hsu, C. Y. & Chao, K. C. 2003. Inhibition of hypoxia inducible factor 1α causes oxygen-independent cytotoxicity and induces p53 independent apoptosis in glioblastoma cells. *International Journal of Radiation Oncology* Biology* Physics,* 55**,** 1027-1036.

Daido, S., Yamamoto, A., Fujiwara, K., Sawaya, R., Kondo, S. & Kondo, Y. 2005. Inhibition of the DNA-dependent protein kinase catalytic subunit radiosensitizes malignant glioma cells by inducing autophagy. *Cancer Research,* 65**,** 4368-4375.

Dang, C. V. & Semenza, G. L. 1999. Oncogenic alterations of metabolism. *Trends in Biochemical Sciences,* 24**,** 68-72.

Dang, L., White, D. W., Gross, S., Bennett, B. D., Bittinger, M. A., Driggers, E. M., Fantin, V. R., Jang, H. G., Jin, S. & Keenan, M. C. 2009. Cancer-associated IDH1 mutations produce 2-hydroxyglutarate. *Nature,* 462**,** 739-744.

Dar, S., Chhina, J., Mert, I., Chitale, D., Buekers, T., Kaur, H., Giri, S., Munkarah, A. & Rattan, R. 2017. Bioenergetic adaptations in chemoresistant ovarian cancer cells. *Scientific Reports,* 7**,** 8760.

Das, U., Biswas, S., Chattopadhyay, S., Chakraborty, A., Sharma, R. D., Banerji, A. & Dey, S. 2017. Radiosensitizing effect of ellagic acid on growth of Hepatocellular carcinoma cells: An *in vitro* study. *Scientific Reports,* 7**,** 14043.

Dasari, S. & Tchounwou, P. B. 2014. Cisplatin in cancer therapy: Molecular mechanisms of action. *European Journal of Pharmacology,* 740**,** 364-378.

Daskalaki, I., Gkikas, I. & Tavernarakis, N. 2018. Hypoxia and selective autophagy in cancer development and therapy. *Frontiers in Cell and Developmental Biology,* 6**,** 104.

Davis, R. J. 2000. Signal transduction by the JNK group of MAP kinases. *Inflammatory Processes:. Springer.*103**,** 239-252.

De Groof, A. J., Te Lindert, M. M., Van Dommelen, M. M., Wu, M., Willemse, M., Smift, A. L., Winer, M., Oerlemans, F., Pluk, H. & Fransen, J. A. 2009. Increased OXPHOS activity precedes rise in glycolytic rate in H-RasV12/E1A transformed fibroblasts that develop a Warburg phenotype. *Molecular Cancer,* 8**,** 54.

De Groot, J. F., Fuller, G., Kumar, A. J., Piao, Y., Eterovic, K., Ji, Y. & Conrad, C. A. 2010. Tumor invasion after treatment of glioblastoma with bevacizumab: radiographic and pathologic correlation in humans and mice. *Neuro-oncology,* 12**,** 233-242.

Deb, J., Dibra, H., Shan, S., Rajan, S., Manneh, J., Kankipati, C. S., Perry, C. J. & Nicholl, I. D. 2011. Activity of aspirin analogues and vanillin in a human colorectal cancer cell line. *Oncology Reports,* 26**,** 557-565.

Deberardinis, R. J. & Chandel, N. S. 2016. Fundamentals of cancer metabolism. *Science Advances,* 2**,** e1600200.

Deberardinis, R. J., Lum, J. J., Hatzivassiliou, G. & Thompson, C. B. 2008. The biology of cancer: metabolic reprogramming fuels cell growth and proliferation. *Cell Metabolism,* 7**,** 11-20.

Deberardinis, R. J., Mancuso, A., Daikhin, E., Nissim, I., Yudkoff, M., Wehrli, S. & Thompson, C. B. 2007. Beyond aerobic glycolysis: transformed cells can engage in glutamine metabolism that exceeds the requirement for protein and nucleotide synthesis. *Proceedings of the National Academy of Sciences,* 104**,** 19345-19350.

Denecker, G., Vercammen, D., Declercq, W. & Vandenabeele, P. 2001. Apoptotic and necrotic cell death induced by death domain receptors. *Cellular and Molecular Life Sciences,* 58**,** 356-370.

Deng, L., Hu, S., Baydoun, A., Chen, J., Chen, X. & Cong, X. 2009. Aspirin induces apoptosis in mesenchymal stem cells requiring Wnt/β-catenin pathway. *Cell Proliferation,* 42**,** 721-730.

Dengler, V. L., Galbraith, M. D. & Espinosa, J. M. 2014. Transcriptional regulation by hypoxia inducible factors. *Critical Reviews in Biochemistry and Molecular Biology,* 49**,** 1-15.

Denny, B. J., Wheelhouse, R. T., Stevens, M. F., Tsang, L. L. & Slack, J. A. 1994. NMR and molecular modeling investigation of the mechanism of activation of the antitumor drug temozolomide and its interaction with DNA. *Biochemistry,* 33**,** 9045-9051.

Desai, V., Jain, A., Shaghaghi, H., Summer, R., Lai, J. C. & Bhushan, A. 2019. Combination of Biochanin A and Temozolomide Impairs Tumor Growth by Modulating Cell Metabolism in Glioblastoma Multiforme. *Anticancer Research,* 39**,** 57-66.

Desoize, B. 2002. Cancer and metals and metal compounds: part I--carcinogenesis. *Critical Reviews in Oncology/Hematology,* 42**,** 1.

Devita, V. T., Jr., Young, R. C. & Canellos, G. P. 1975. Combination versus single agent chemotherapy: a review of the basis for selection of drug treatment of cancer. *Cancer,* 35**,** 98-110.

Dhanasekaran, D. N. & Reddy, E. P. 2017. JNK-signaling: A multiplexing hub in programmed cell death. *Genes Cancer,* 8**,** 682-694.

Diaz, R. J., Ali, S., Qadir, M. G., Macarena, I., Ivan, M. E. & Komotar, R. J. 2017. The role of bevacizumab in the treatment of glioblastoma. *Journal of Neuro-Oncology,* 133**,** 455-467.

Dibra, H. K., Brown, J. E., Hooley, P. & Nicholl, I. D. 2010. Aspirin and alterations in DNA repair proteins in the SW480 colorectal cancer cell line. *Oncology Reports,* 24**,** 37-46.

Didonato, J. A., Mercurio, F. & Karin, M. 2012. NF-κB and the link between inflammation and cancer. *Immunological Reviews,* 246**,** 379-400.

Diepart, C., Verrax, J., Calderon, P. B., Feron, O., Jordan, B. F. & Gallez, B. 2010. Comparison of methods for measuring oxygen consumption in tumor cells in vitro. *Analytical Biochemistry,* 396**,** 250-256.

Dihlmann, S., Klein, S. & Von Knebel Doeberitz, M. 2003. Reduction of β-catenin/T-cell transcription factor signaling by aspirin and indomethacin is caused by an increased stabilization of phosphorylated β-catenin. *Molecular Cancer Therapeutics,* 2**,** 509-516.

Dikshit, P., Chatterjee, M., Goswami, A., Mishra, A. & Jana, N. R. 2006. Aspirin induces apoptosis through the inhibition of proteasome function. *Journal of Biological Chemistry,* 281**,** 29228-29235.

Din, F. V., Valanciute, A., Houde, V. P., Zibrova, D., Green, K. A., Sakamoto, K., Alessi, D. R. & Dunlop, M. G. 2012. Aspirin inhibits mTOR signaling, activates AMP-activated protein kinase, and induces autophagy in colorectal cancer cells. *Gastroenterology,* 142**,** 1504-15 e3.

Din, F. V. N., Dunlop, M. G. & Stark, L. A. 2004. Evidence for colorectal cancer cell specificity of aspirin effects on NF kappa B signalling and apoptosis. *British Journal of Cancer,* 91**,** 381-388.

Ding, J. H., Yuan, L. Y., Huang, R. B. & Chen, G. A. 2014. Aspirin inhibits proliferation and induces apoptosis of multiple myeloma cells through regulation of Bcl-2 and Bax and suppression of VEGF. *European Journal of Haematology,* 93**,** 329-339.

Ding, L. J., Yuan, C. J., Wei, F., Wang, G. Y., Zhang, J., Bellail, A. C., Zhang, Z. B., Olson, J. J. & Hao, C. H. 2011. Cisplatin Restores TRAIL Apoptotic Pathway in Glioblastoma-Derived Stem Cells through Up-regulation of DR5 and Down-regulation of c-FLIP. *Cancer Investigation,* 29**,** 511-520.

Ding, W.-X. & Yin, X.-M. 2012. Mitophagy: mechanisms, pathophysiological roles, and analysis. *Journal of Biological Chemistry,* 393**,** 547-64.

Doery, J., Hirsh, J. & De Gruchy, G. 1969. Aspirin: its effect on platelet glycolysis and release of adenosine diphosphate. *Science,* 165**,** 65-67.

Doherty, G. A., Byrne, S. M., Molloy, E. S., Malhotra, V., Austin, S. C., Kay, E. W., Murray, F. E. & Fitzgerald, D. J. 2009. Proneoplastic effects of PGE 2 mediated by EP4 receptor in colorectal cancer. *BMC Cancer,* 9**,** 207.

Dong, H., Liu, G., Jiang, B., Guo, J., Tao, G., Yiu, W., Zhou, J. & Li, G. 2014. The effects of aspirin plus cisplatin on SGC7901/CDDP cells in vitro. *Biomedical Reports,* 2**,** 344-348.

Dong, X.-F., Liu, T.-Q., Zhi, X.-T., Zou, J., Zhong, J.-T., Li, T., Mo, X.-L., Zhou, W., Guo, W.-W. & Liu, X. 2018. COX-2/PGE2 Axis Regulates HIF2α Activity to Promote Hepatocellular Carcinoma Hypoxic Response and Reduce the Sensitivity of Sorafenib Treatment. *Clinical Cancer Research,* 24**,** 3204-3216.

Dovizio, M., Tacconelli, S., Sostres, C., Ricciotti, E. & Patrignani, P. 2012. Mechanistic and pharmacological issues of aspirin as an anticancer agent. *Pharmaceuticals,* 5**,** 1346-1371.

Dranka, B. P., Benavides, G. A., Diers, A. R., Giordano, S., Zelickson, B. R., Reily, C., Zou, L., Chatham, J. C., Hill, B. G. & Zhang, J. 2011. Assessing bioenergetic function in response to oxidative stress by metabolic profiling. *Free Radical Biology and Medicine,* 51**,** 1621-1635.

Drew, D. A., Cao, Y. & Chan, A. T. 2016. Aspirin and colorectal cancer: the promise of precision chemoprevention. *Nature Reviews Cancer,* 16**,** 173-186.

Driever, P., Knüpfer, M., Cinatl, J. & Wolff, J. 1999. Valproic acid for the treatment of pediatric malignant glioma. *Klinische Pädiatrie,* 211**,** 323-328.

Du, C., Fang, M., Li, Y., Li, L. & Wang, X. 2000. Smac, a mitochondrial protein that promotes cytochrome c–dependent caspase activation by eliminating IAP inhibition. *Cell,* 102**,** 33-42.

Dubois, C., Dufour, R., Daumar, P., Aubel, C., Szczepaniak, C., Blavignac, C., Mounetou, E., Penault-Llorca, F. & Bamdad, M. 2017. Development and cytotoxic response of two proliferative MDA-MB-231 and non-proliferative SUM1315 three-dimensional cell culture models of triple-negative basal-like breast cancer cell lines. *Oncotarget,* 8**,** 95316.

Duyndam, M. C. A., Van Berkel, M. P. A., Dorsman, J. C., Rockx, D. a. P., Pinedo, H. M. & Boven, E. 2007. Cisplatin and doxorubicin repress Vascular Endothelial Growth Factor expression and differentially down-regulate Hypoxia-inducible Factor I activity in human ovarian cancer cells. *Biochemical Pharmacology,* 74**,** 191-201.

Dzamitika, S., Salerno, M., Pereira-Maia, E., Le Moyec, L. & Garnier-Suillerot, A. 2006. Preferential energy-and potential-dependent accumulation of cisplatin–gutathione complexes in human cancer cell lines (GLC4 and K562): A likely role of mitochondria. *Journal of Bioenergetics and Biomembranes,* 38**,** 11-21.

Eales, K., Hollinshead, K. & Tennant, D. 2016. Hypoxia and metabolic adaptation of cancer cells. *Oncogenesis,* 5**,** e190.

Eales, K. L., Wilkinson, E. A., Cruickshank, G., Tucker, J. H. & Tennant, D. A. 2018. Verteporfin selectively kills hypoxic glioma cells through iron-binding and increased production of reactive oxygen species. *Scientific Reports,* 8**,** 14358.

Eastman, A. 1987. The formation, isolation and characterization of DNA adducts produced by anticancer platinum complexes. *Pharmacology & Therapeutics,* 34**,** 155-166.

Edinger, A. L. & Thompson, C. B. 2004. Death by design: apoptosis, necrosis and autophagy. *Current Opinion in Cell Biology,* 16**,** 663-669.

Edland, R. W., Javid, M. & Ansfield, F. J. 1971. Glioblastoma multiforme: an analysis of the results of postoperative radiotherapy alone versus radiotherapy and concomitant 5-fluorouracil (a prospective randomized study of 32 cases). *American Journal of Roentgenology,* 111**,** 337-342.

Edmondson, R., Adcock, A. F. & Yang, L. 2016. Influence of matrices on 3D-cultured prostate cancer cells' drug response and expression of drug-action associated proteins. *PloS One,* 11**,** e0158116.

Eimer, S., Belaud-Rotureau, M. A., Airiau, K., Jeanneteau, M., Laharanne, E., Veron, N., Vital, A., Loiseau, H., Merlio, J. P. & Belloc, F. 2011. Autophagy inhibition cooperates with erlotinib to induce glioblastoma cell death. *Cancer Biology & Therapy,* 11**,** 1017-1027.

El-Kady, A., Sun, Y., Li, Y. X. & Liao, D. J. 2011. Cyclin D1 inhibits whereas c-Myc enhances the cytotoxicity of cisplatin in mouse pancreatic cancer cells via regulation of several members of the NF-kappaB and Bcl-2 families. *Journal of Carcinogenesis,* 10**,** 24.

Elder, D. J., Hague, A., Hicks, D. J. & Paraskeva, C. 1996. Differential growth inhibition by the aspirin metabolite salicylate in human colorectal tumor cell lines: enhanced apoptosis in carcinoma and in vitro-transformed adenoma relative to adenoma relative to adenoma cell lines. *Cancer Research,* 56**,** 2273-2276.

Elder, D. J., Halton, D. E., Crew, T. E. & Paraskeva, C. 2000. Apoptosis induction and cyclooxygenase-2 regulation in human colorectal adenoma and carcinoma cell lines by the cyclooxygenase-2-selective non-steroidal anti-inflammatory drug NS-398. *International Journal of Cancer,* 86**,** 553-560.

Elder, D. J. E., Hague, A., Hicks, D. J. & Paraskeva, C. 1996. Differential growth inhibition by the aspirin metabolite salicylate in human colorectal tumor cell lines: Enhanced apoptosis in carcinoma and in vitro-transformed adenoma relative to adenoma cell lines. *Cancer Research,* 56**,** 2273-2276.

Elmore, S. 2007. Apoptosis: a review of programmed cell death. *Toxicologic Pathology,* 35**,** 495-516.

Endo, H., Okuyama, H., Ohue, M. & Inoue, M. 2014. Dormancy of cancer cells with suppression of AKT activity contributes to survival in chronic hypoxia. *PloS One,* 9**,** e98858.

England, B., Huang, T. & Karsy, M. 2013. Current understanding of the role and targeting of tumor suppressor p53 in glioblastoma multiforme. *Tumor Biology,* 34**,** 2063-2074.

Evans, S. M., Judy, K. D., Dunphy, I., Jenkins, W. T., Hwang, W. T., Nelson, P. T., Lustig, R. A., Jenkins, K., Magarelli, D. P., Hahn, S. M., Collins, R. A., Grady, M. S. & Koch, C.

J. 2004. Hypoxia is important in the biology and aggression of human glial brain tumors. *Clinical Cancer Research,* 10**,** 8177-8184.

Evans, S. M., Judy, K. D., Dunphy, I., Jenkins, W. T., Nelson, P. T., Collins, R., Wileyto, E. P., Jenkins, K., Hahn, S. M. & Stevens, C. W. 2004. Comparative measurements of hypoxia in human brain tumors using needle electrodes and EF5 binding. *Cancer Research,* 64**,** 1886-1892.

Fadaka, A., Ajiboye, B., Ojo, O., Adewale, O., Olayide, I. & Emuowhochere, R. 2017. Biology of glucose metabolization in cancer cells. *Journal of Oncological Sciences,* 3**,** 45-51.

Fan, J., Kamphorst, J. J., Mathew, R., Chung, M. K., White, E., Shlomi, T. & Rabinowitz, J. D. 2013. Glutamine-driven oxidative phosphorylation is a major ATP source in transformed mammalian cells in both normoxia and hypoxia. *Molecular Systems Biology,* 9**,** 712.

Fan, Q. W., Cheng, C., Hackett, C., Feldman, M., Houseman, B. T., Nicolaides, T., Haas-Kogan, D., James, C. D., Oakes, S. A., Debnath, J., Shokat, K. M. & Weiss, W. A. 2010. Akt and autophagy cooperate to promote survival of drug-resistant glioma. *Science Signaling,* 3**,** ra81.

Fan, Z., Beresford, P. J., Oh, D. Y., Zhang, D. & Lieberman, J. 2003. Tumor suppressor NM23-H1 is a granzyme A-activated DNase during CTL-mediated apoptosis, and the nucleosome assembly protein SET is its inhibitor. *Cell,* 112**,** 659-672.

Fantin, V. R., St-Pierre, J. & Leder, P. 2006. Attenuation of LDH-A expression uncovers a link between glycolysis, mitochondrial physiology, and tumor maintenance. *Cancer Cell,* 9**,** 425-434.

Feda'h, H. & Zihlif, M. A. 2014. Gene expression alterations in chronic hypoxic MCF7 breast cancer cell line. *Genomics,* 104**,** 477-481.

Ferris, J. S., Mccoy, L., Neugut, A. I., Wrensch, M. & Lai, R. 2012. HMG CoA reductase inhibitors, NSAIDs and risk of glioma. *International Journal of Cancer,* 131**,** E1031-E1037.

Fessart, D., Begueret, H. & Delom, F. 2013. Three-dimensional culture model to distinguish normal from malignant human bronchial epithelial cells. *European Respiratory Journal,* 42**,** 1345-1356.

Fietkau, R., Putz, F., Lahmer, G., Semrau, S. & Buslei, R. 2013. Can MGMT promoter methylation status be used as a prognostic and predictive marker for glioblastoma multiforme at the present time? : Springer.

Filatova, A., Acker, T. & Garvalov, B. K. 2013. The cancer stem cell niche (s): the crosstalk between glioma stem cells and their microenvironment. *Biochimica et Biophysica Acta,* 1830**,** 2496-2508.

Filippi-Chiela, E. C., Thome, M. P., Bueno E Silva, M. M., Pelegrini, A. L., Ledur, P. F., Garicochea, B., Zamin, L. L. & Lenz, G. 2013. Resveratrol abrogates the temozolomide-induced G2 arrest leading to mitotic catastrophe and reinforces the temozolomide-induced senescence in glioma cells. *BMC Cancer,* 13**,** 147.

Fink, S. L. & Cookson, B. T. 2005. Apoptosis, pyroptosis, and necrosis: mechanistic description of dead and dying eukaryotic cells. *Infection and Immunity,* 73**,** 1907-1916.

Florea, A.-M. & Büsselberg, D. 2006. Occurrence, use and potential toxic effects of metals and metal compounds. *Biometals,* 19**,** 419-427.

Florea, A. M. & Busselberg, D. 2011. Cisplatin as an anti-tumor drug: cellular mechanisms of activity, drug resistance and induced side effects. *Cancers,* 3**,** 1351-1371.

Florea, A. M. & Busselberg, D. 2011. Cisplatin as an anti-tumor drug: cellular mechanisms of activity, drug resistance and induced side effects. *Cancers (Basel),* 3**,** 1351-71.
Foster, A. C. & Kemp, J. A. 2006. Glutamate-and GABA-based CNS therapeutics. *Current Opinion in Pharmacology,* 6**,** 7-17.
Franovic, A., Gunaratnam, L., Smith, K., Robert, I., Patten, D. & Lee, S. 2007. Translational up-regulation of the EGFR by tumor hypoxia provides a nonmutational explanation for its overexpression in human cancer. *Proceedings of the National Academy of Sciences of the United States of America,* 104**,** 13092-13097.
Frezza, C., Zheng, L., Tennant, D. A., Papkovsky, D. B., Hedley, B. A., Kalna, G., Watson, D. G. & Gottlieb, E. 2011. Metabolic profiling of hypoxic cells revealed a catabolic signature required for cell survival. *PloS One,* 6**,** e24411.
Frezza, M., Hindo, S., Chen, D., Davenport, A., Schmitt, S., Tomco, D. & Ping Dou, Q. 2010. Novel metals and metal complexes as platforms for cancer therapy. *Current Pharmaceutical Design,* 16**,** 1813-1825.
Friedman, H. S., Kerby, T. & Calvert, H. 2000. Temozolomide and treatment of malignant glioma. *Clinical Cancer Research,* 6**,** 2585-2597.
Friedman, H. S., Prados, M. D., Wen, P. Y., Mikkelsen, T., Schiff, D., Abrey, L. E., Yung, W., Paleologos, N., Nicholas, M. K. & Jensen, R. 2009. Bevacizumab alone and in combination with irinotecan in recurrent glioblastoma. *Journal of Clinical Oncology,* 27**,** 4733-4740.
Friesen, C., Fulda, S. & Debatin, K. M. 1999. Cytotoxic drugs and the CD95 pathway. *Leukemia,* 13**,** 1854-1858.
Fuchs, J., Podda, M. & Packer, L. 2003. Redox-genome interactions in health and disease, *CRC Press*.
Fulda, S. 2014. Cross talk between cell death regulation and metabolism. *Methods in Enzymology. Elsevier*.542**,** 81-90.
Fulda, S., Gorman, A. M., Hori, O. & Samali, A. 2010. Cellular stress responses: cell survival and cell death. *International Journal of Cell Biology,* 2010**,** 214074.
Furnari, F. B., Fenton, T., Bachoo, R. M., Mukasa, A., Stommel, J. M., Stegh, A., Hahn, W. C., Ligon, K. L., Louis, D. N. & Brennan, C. 2007. Malignant astrocytic glioma: genetics, biology, and paths to treatment. *Genes & Development,* 21**,** 2683-2710.
Galateanu, B., Hudita, A., Negrei, C., Ion, R. M., Costache, M., Stan, M., Nikitovic, D., Hayes, A. W., Spandidos, D. A. & Tsatsakis, A. M. 2016. Impact of multicellular tumor spheroids as an in vivo-like tumor model on anticancer drug response. *International Journal of Oncology,* 48**,** 2295-2302.
Galia, A., Calogero, A., Condorelli, R., Fraggetta, F., La Corte, C., Ridolfo, F., Bosco, P., Castiglione, R. & Salemi, M. 2012. PARP-1 protein expression in glioblastoma multiforme. *European Journal of Histochemistry,* 56**,** e9.
Gameiro, P. A., Laviolette, L. A., Kelleher, J. K., Iliopoulos, O. & Stephanopoulos, G. 2013. Cofactor balance by nicotinamide nucleotide transhydrogenase (NNT) coordinates reductive carboxylation and glucose catabolism in the tricarboxylic acid (TCA) cycle. *Journal of Biological Chemistry,* 288**,** 12967-12977.
Ganapathy-Kanniappan, S. 2018. Evolution of GAPDH as a druggable target of tumor glycolysis? : Taylor & Francis.
Ganapathy-Kanniappan, S., Kunjithapatham, R. & Geschwind, J.-F. 2012. Glyceraldehyde-3-phosphate dehydrogenase: a promising target for molecular therapy in hepatocellular carcinoma. *Oncotarget,* 3**,** 940-953.

Gao, L. & Williams, J. L. 2012. Nitric oxide-donating aspirin induces G2/M phase cell cycle arrest in human cancer cells by regulating phase transition proteins. *International Journal of Oncology,* 41**,** 325-330.

Gardner, L. B., Li, Q., Park, M. S., Flanagan, W. M., Semenza, G. L. & Dang, C. V. 2001. Hypoxia inhibits G1/S transition through regulation of p27 expression. *Journal of Biological Chemistry,* 276**,** 7919-7926.

Garraway, L. A. & Lander, E. S. 2013. Lessons from the cancer genome. *Cell,* 153**,** 17-37.

Garrido, C., Galluzzi, L., Brunet, M., Puig, P., Didelot, C. & Kroemer, G. 2006. Mechanisms of cytochrome c release from mitochondria. *Cell Death and Differentiation,* 13**,** 1423-1433.

Gasche, C., Goel, A., Natarajan, L. & Boland, C. R. 2005. Mesalazine improves replication fidelity in cultured colorectal cells. *Cancer Research,* 65**,** 3993-3997.

Gatenby, R. A. & Gillies, R. J. 2004. Why do cancers have high aerobic glycolysis? *Nature Reviews Cancer,* 4**,** 891.

Geoghegan, F., Buckland, R. J., Rogers, E. T., Khalifa, K., O'connor, E. B., Rooney, M. F., Behnam-Motlagh, P., Nilsson, T. K., Grankvist, K. & Porter, R. K. 2017. Bioenergetics of acquired cisplatin resistant H1299 non-small cell lung cancer and P31 mesothelioma cells. *Oncotarget,* 8**,** 94711-94725.

Gerthofer, V., Kreutz, M., Renner, K., Jachnik, B., Dettmer, K., Oefner, P., Riemenschneider, M., Proescholdt, M., Vollmann-Zwerenz, A. & Hau, P. 2018. Combined Modulation of Tumor Metabolism by Metformin and Diclofenac in Glioma. *International Journal of Molecular Sciences,* 19**,** 2586.

Ghobrial, I. M., Witzig, T. E. & Adjei, A. A. 2005. Targeting apoptosis pathways in cancer therapy. *Cancer Journal for Clinicians,* 55**,** 178-194.

Ghosh, R. D., Ghuwalewala, S., Das, P., Mandloi, S., Alam, S. K., Chakraborty, J., Sarkar, S., Chakrabarti, S., Panda, C. K. & Roychoudhury, S. 2016. MicroRNA profiling of cisplatin-resistant oral squamous cell carcinoma cell lines enriched with cancer-stem-cell-like and epithelial-mesenchymal transition-type features. *Scientific Reports,* 6**,** 23932.

Giaccia, A., Siim, B. G. & Johnson, R. S. 2003. HIF-1 as a target for drug development. *Nature Reviews Drug discovery,* 2**,** 803-811.

Giffard, R. G., Monyer, H. & Choi, D. W. 1990. Selective vulnerability of cultured cortical glia to injury by extracellular acidosis. *Brain Research,* 530**,** 138-141.

Gil-Ad, I., Shtaif, B., Levkovitz, Y., Dayag, M., Zeldich, E. & Weizman, A. 2004. Characterization of phenothiazine-induced apoptosis in neuroblastoma and glioma cell lines. *Journal of Molecular Neuroscience,* 22**,** 189-198.

Giladi, M., Schneiderman, R. S., Voloshin, T., Porat, Y., Munster, M., Blat, R., Sherbo, S., Bomzon, Z., Urman, N. & Itzhaki, A. 2015. Mitotic spindle disruption by alternating electric fields leads to improper chromosome segregation and mitotic catastrophe in cancer cells. *Scientific Reports,* 5**,** 18046.

Gillies, R., Alger, J. & Shulman, R. 1981. Intracellular pH measured by NMR: methods and results. *Kroc Foundation Series,* 15**,** 79-104.

Giovannucci, E., Egan, K. M., Hunter, D. J., Stampfer, M. J., Colditz, G. A., Willett, W. C. & Speizer, F. E. 1995. Aspirin and the risk of colorectal cancer in women. *New England Journal of Medicine,* 333**,** 609-614.

Gnaiger, E. 2003. Oxygen conformance of cellular respiration. *Hypoxia. Springer***,** 39-55.

Goda, N., Ryan, H. E., Khadivi, B., Mcnulty, W., Rickert, R. C. & Johnson, R. S. 2003. Hypoxia-inducible factor 1α is essential for cell cycle arrest during hypoxia. *Molecular and Cellular Biology,* 23**,** 359-369.

Godlewski, J., Nowicki, M. O., Bronisz, A., Nuovo, G., Palatini, J., De Lay, M., Van Brocklyn, J., Ostrowski, M. C., Chiocca, E. A. & Lawler, S. E. 2010. MicroRNA-451 regulates LKB1/AMPK signaling and allows adaptation to metabolic stress in glioma cells. *Molecular Cell,* 37**,** 620-632.

Godugu, C., Patel, A. R., Desai, U., Andey, T., Sams, A. & Singh, M. 2013. AlgiMatrix™ based 3D cell culture system as an in-vitro tumor model for anticancer studies. *PloS One,* 8**,** e53708.

Goel, A., Chang, D. K., Ricciardiello, L., Gasche, C. & Boland, C. R. 2003. A novel mechanism for aspirin-mediated growth inhibition of human colon cancer cells. *Clinical Cancer Research,* 9**,** 383-390.

Goggin, P., Collins, D., Jazrawi, R., Jackson, P., Corbishley, C., Bourke, B. & Northfield, T. 1993. Prevalence of Helicobacter pylori infection and its effect on symptoms and non-steroidal anti-inflammatory drug induced gastrointestinal damage in patients with rheumatoid arthritis. *Gut,* 34**,** 1677-1680.

Goldberg, R. M., Sargent, D. J., Morton, R. F., Fuchs, C. S., Ramanathan, R. K., Williamson, S. K., Findlay, B. P., Pitot, H. C. & Alberts, S. R. 2004. A randomized controlled trial of fluorouracil plus leucovorin, irinotecan, and oxaliplatin combinations in patients with previously untreated metastatic colorectal cancer. *Journal of Clinical Oncology,* 22**,** 23-30.

Gomes, R. N. & Colquhoun, A. 2012. E series prostaglandins alter the proliferative, apoptotic and migratory properties of T98G human glioma cells in vitro. *Lipids in Health and Disease,* 11**,** 171.

Goping, S., Barry, M., Liston, P., Sawchuk, T., Constantinescu, G., Michalak, K. M., Shostak, I., Roberts, D. L., Hunter, A. M. & Korneluk, R. 2003. Granzyme B-induced apoptosis requires both direct caspase activation and relief of caspase inhibition. *Immunity,* 18**,** 355-365.

Gordan, J. D., Bertout, J. A., Hu, C.-J., Diehl, J. A. & Simon, M. C. 2007. HIF-2α promotes hypoxic cell proliferation by enhancing c-myc transcriptional activity. *Cancer cell,* 11**,** 335-347.

Gottesman, M. M. 2002. Mechanisms of cancer drug resistance. *Annual Review of Medicine,* 53**,** 615-627.

Gottfried, E., Lang, S. A., Renner, K., Bosserhoff, A., Gronwald, W., Rehli, M., Einhell, S., Gedig, I., Singer, K. & Seilbeck, A. 2013. New aspects of an old drug–diclofenac targets MYC and glucose metabolism in tumor cells. *PloS One,* 8**,** e66987.

Gottlieb, E. & Tomlinson, I. P. 2005. Mitochondrial tumour suppressors: a genetic and biochemical update. *Nature Reviews Cancer,* 5**,** 857-866.

Gough, W., Hulkower, K. I., Lynch, R., Mcglynn, P., Uhlik, M., Yan, L. & Lee, J. A. 2011. A Quantitative, Facile, and High-Throughput Image-Based Cell Migration Method Is a Robust Alternative to the Scratch Assay. *Journal of Biomolecular Screening,* 16**,** 155-163.

Gozuacik, D. & Kimchi, A. 2004. Autophagy as a cell death and tumor suppressor mechanism. *Oncogene,* 23**,** 2891-2906.

Grada, A., Otero-Vinas, M., Prieto-Castrillo, F., Obagi, Z. & Falanga, V. 2017. Research Techniques Made Simple: Analysis of Collective Cell Migration Using the Wound Healing Assay. *Journal of Investigative Dermatology,* 137**,** E11-E16.

Graeber, T. G., Osmanian, C., Jacks, T., Housman, D. E., Koch, C. J., Lowe, S. W. & Giaccia, A. J. 1996. Hypoxia-mediated selection of cells with diminished apoptotic potential in solid tumours. *Nature,* 379**,** 88-91.

Graeber, T. G., Peterson, J. F., Tsai, M., Monica, K., Fornace, A. & Giaccia, A. J. 1994. Hypoxia induces accumulation of p53 protein, but activation of a G1-phase checkpoint by low-oxygen conditions is independent of p53 status. *Molecular and Cellular Biology,* 14**,** 6264-6277.

Grantab, R., Sivananthan, S. & Tannock, I. F. 2006. The penetration of anticancer drugs through tumor tissue as a function of cellular adhesion and packing density of tumor cells. *Cancer Research,* 66**,** 1033-1039.

Graven, K. K., Troxler, R. F., Kornfeld, H., Panchenko, M. V. & Farber, H. W. 1994. Regulation of endothelial cell glyceraldehyde-3-phosphate dehydrogenase expression by hypoxia. *Journal of Biological Chemistry,* 269**,** 24446-24453.

Graven, K. K., Yu, Q., Pan, D., Roncarati, J. S. & Farber, H. W. 1999. Identification of an oxygen responsive enhancer element in the glyceraldehyde-3-phosphate dehydrogenase gene. *Biochimica et Biophysica Acta (BBA)-Gene Structure and Expression,* 1447**,** 208-218.

Grayson, W. L., Zhao, F., Izadpanah, R., Bunnell, B. & Ma, T. 2006. Effects of hypoxia on human mesenchymal stem cell expansion and plasticity in 3D constructs. *Journal of Cellular Physiology,* 207**,** 331-339.

Green, D. R. & Reed, J. C. 1998. Mitochondria and apoptosis. *Science,* 281**,** 1309-1312.

Greenhough, A., Smartt, H. J., Moore, A. E., Roberts, H. R., Williams, A. C., Paraskeva, C. & Kaidi, A. 2009. The COX-2/PGE 2 pathway: key roles in the hallmarks of cancer and adaptation to the tumour microenvironment. *Carcinogenesis,* 30**,** 377-386.

Griffin, M. R., Piper, J. M., Daugherty, J. R., Snowden, M. & Ray, W. A. 1991. Nonsteroidal anti-inflammatory drug use and increased risk for peptic ulcer disease in elderly persons. *Annals of Internal Medicine,* 114**,** 257-263.

Grist, J. T., Jarvis, L. B., Georgieva, Z., Thompson, S., Sandhu, H. K., Burling, K., Clarke, A., Jackson, S., Wills, M. & Gallagher, F. A. 2018. Extracellular lactate: a novel measure of t cell proliferation. *The Journal of Immunology,* 200**,** 1220-1226.

Gritti, M., Würth, R., Angelini, M., Barbieri, F., Peretti, M., Pizzi, E., Pattarozzi, A., Carra, E., Sirito, R. & Daga, A. 2014. Metformin repositioning as antitumoral agent: selective antiproliferative effects in human glioblastoma stem cells, via inhibition of CLIC1-mediated ion current. *Oncotarget,* 5**,** 11252-11268.

Grosch, S., Maier, T. J., Schiffmann, S. & Geisslinger, G. 2006. Cyclooxygenase-2 (COX-2)-independent anticarcinogenic effects of selective COX-2 inhibitors. *Journal of the National Cancer Institute,* 98**,** 736-747.

Grossman, S. A. & Batara, J. F. Current management of glioblastoma multiforme. Seminars in oncology, 2004. Elsevier, 635-644.

Grossman, S. A., Ye, X., Lesser, G., Sloan, A., Carraway, H., Desideri, S. & Piantadosi, S. 2011. Immunosuppression in patients with high-grade gliomas treated with radiation and temozolomide. *Clinical Cancer Research,* 17**,** 5473-5480.

Gu, Q., Wang, J. D., Xia, H. H., Lin, M. C., He, H., Zou, B., Tu, S. P., Yang, Y., Liu, X. G. & Lam, S. K. 2005. Activation of the caspase-8/Bid and Bax pathways in aspirin-induced apoptosis in gastric cancer. *Carcinogenesis,* 26**,** 541-546.

Guo, C., Liu, S. & Sun, M.-Z. 2013. Novel insight into the role of GAPDH playing in tumor. *Clinical and Translational Oncology,* 15**,** 167-172.

Guo, J. Y., Xia, B. & White, E. 2013. Autophagy-mediated tumor promotion. *Cell,* 155**,** 1216-1219.

Guo, Y., Yan, K., Fang, J., Qu, Q., Zhou, M. & Chen, F. 2013. Let-7b expression determines response to chemotherapy through the regulation of cyclin D1 in glioblastoma. *Journal of Experimental & Clinical Cancer Research,* 32**,** 41.

Gupta, S. K., Smith, E. J., Mladek, A. C., Tian, S., Decker, P. A., Kizilbash, S. H., Kitange, G. J. & Sarkaria, J. N. 2018. PARP Inhibitors for Sensitization of Alkylation Chemotherapy in Glioblastoma: Impact of Blood-Brain Barrier and Molecular Heterogeneity. *Frontiers in Oncology,* 8**,** 670.

Gurpinar, E., Grizzle, W. E. & Piazza, G. A. 2013. COX-independent mechanisms of cancer chemoprevention by anti-inflammatory drugs. *Frontiers in Oncology,* 3**,** 181.

Guzy, R. D. & Schumacker, P. T. 2006. Oxygen sensing by mitochondria at complex III: the paradox of increased reactive oxygen species during hypoxia. *Experimental Physiology,* 91**,** 807-819.

Ha, E. T., Antonios, J. P., Soto, H., Prins, R. M., Yang, I., Kasahara, N., Liau, L. M. & Kruse, C. A. 2014. Chronic inflammation drives glioma growth: cellular and molecular factors responsible for an immunosuppressive microenvironment. *Neuroimmunol Neuroinflammation,* 1**,** 66-76.

Hall, M. D., Telma, K. A., Chang, K. E., Lee, T. D., Madigan, J. P., Lloyd, J. R., Goldlust, I. S., Hoeschele, J. D. & Gottesman, M. M. 2014. Say No to DMSO: Dimethylsulfoxide Inactivates Cisplatin, Carboplatin, and Other Platinum Complexes. *Cancer Research,* 74**,** 3913-3922.

Halperin, E. C., Bentel, G., Heinz, E. R. & Burger, P. C. 1989. Radiation therapy treatment planning in supratentorial glioblastoma multiforme: an analysis based on post mortem topographic anatomy with CT correlations. *International Journal of Radiation Oncology* Biology* Physics,* 17**,** 1347-1350.

Hambardzumyan, D., Becher, O. J., Rosenblum, M. K., Pandolfi, P. P., Manova-Todorova, K. & Holland, E. C. 2008. PI3K pathway regulates survival of cancer stem cells residing in the perivascular niche following radiation in medulloblastoma *in vivo*. *Genes & development,* 22**,** 436-448.

Hambardzumyan, D. & Bergers, G. 2015. Glioblastoma: Defining Tumor Niches. *Trends Cancer,* 1**,** 252-265.

Hammond, E. M., Denko, N. C., Dorie, M. J., Abraham, R. T. & Giaccia, A. J. 2002. Hypoxia links ATR and p53 through replication arrest. *Molecular and Cellular Biology,* 22**,** 1834-1843.

Hammoud, M. A., Sawaya, R., Shi, W., Thall, P. F. & Leeds, N. E. 1996. Prognostic significance of preoperative MRI scans in glioblastoma multiforme. *Journal of Neuro-Oncology,* 27**,** 65-73.

Hanahan, D. & Weinberg, R. A. 2000. The hallmarks of cancer. *Cell,* 100**,** 57-70.

Hanahan, D. & Weinberg, R. A. 2011. Hallmarks of Cancer: The Next Generation. *Cell,* 144**,** 646-674.

Hara, T., Nakamura, K., Matsui, M., Yamamoto, A., Nakahara, Y., Suzuki-Migishima, R., Yokoyama, M., Mishima, K., Saito, I. & Okano, H. 2006. Suppression of basal autophagy in neural cells causes neurodegenerative disease in mice. *Nature,* 441**,** 885-889.

Harada, N., Yasunaga, R., Higashimura, Y., Yamaji, R., Fujimoto, K., Moss, J., Inui, H. & Nakano, Y. 2007. Glyceraldehyde-3-phosphate dehydrogenase enhances

transcriptional activity of androgen receptor in prostate cancer cells. *Journal of Biological Chemistry,* 282**,** 22651-22661.

Hardie, R.-A., Van Dam, E., Cowley, M., Han, T.-L., Balaban, S., Pajic, M., Pinese, M., Iconomou, M., Shearer, R. F. & Mckenna, J. 2017. Mitochondrial mutations and metabolic adaptation in pancreatic cancer. *Cancer & Metabolism,* 5**,** 2.

Harrison, L. & Blackwell, K. 2004. Hypoxia and anemia: factors in decreased sensitivity to radiation therapy and chemotherapy? *The Oncologist,* 9**,** 31-40.

Hashemi Goradel, N., Najafi, M., Salehi, E., Farhood, B. & Mortezaee, K. 2019. Cyclooxygenase-2 in cancer: A review. *Journal of Cellular Physiology,* 234**,** 5683-5699.

Hastak, K., Alli, E. & Ford, J. M. 2010. Synergistic chemosensitivity of triple-negative breast cancer cell lines to poly (ADP-Ribose) polymerase inhibition, gemcitabine, and cisplatin. *Cancer Research,* 70**,** 7970-7980.

Hatanpaa, K. J., Burma, S., Zhao, D. & Habib, A. A. 2010. Epidermal growth factor receptor in glioma: signal transduction, neuropathology, imaging, and radioresistance. *Neoplasia,* 12**,** 675-684.

Hawcroft, G., D'amico, M., Albanese, C., Markham, A. F., Pestell, R. G. & Hull, M. A. 2002. Indomethacin induces differential expression of β-catenin, γ-catenin and T-cell factor target genes in human colorectal cancer cells. *Carcinogenesis,* 23**,** 107-114.

Hawley, S. A., Fullerton, M. D., Ross, F. A., Schertzer, J. D., Chevtzoff, C., Walker, K. J., Peggie, M. W., Zibrova, D., Green, K. A., Mustard, K. J., Kemp, B. E., Sakamoto, K., Steinberg, G. R. & Hardie, D. G. 2012. The ancient drug salicylate directly activates AMP-activated protein kinase. *Science,* 336**,** 918-922.

Hayden, M. S. & Ghosh, S. 2004. Signaling to NF-κB. *Genes & Development,* 18**,** 2195-2224.

Heerlein, K., Schulze, A., Hotz, L., Bartsch, P. & Mairbaurl, H. 2005. Hypoxia decreases cellular ATP demand and inhibits mitochondrial respiration of a549 cells. *American Journal of Respiratory Cell and Molecular Biology,* 32**,** 44-51.

Hegi, M. E., Diserens, A.-C., Gorlia, T., Hamou, M.-F., De Tribolet, N., Weller, M., Kros, J. M., Hainfellner, J. A., Mason, W. & Mariani, L. 2005. MGMT gene silencing and benefit from temozolomide in glioblastoma. *New England Journal of Medicine,* 352**,** 997-1003.

Hegi, M. E., Diserens, A. C., Godard, S., Dietrich, P. Y., Regli, L., Ostermann, S., Otten, P., Van Melle, G., De Tribolet, N. & Stupp, R. 2004. Clinical trial substantiates the predictive value of O-6-methylguanine-DNA methyltransferase promoter methylation in glioblastoma patients treated with temozolomide. *Clinical Cancer Research,* 10**,** 1871-1874.

Helmlinger, G., Yuan, F., Dellian, M. & Jain, R. K. 1997. Interstitial pH and pO(2) gradients in solid tumors in vivo: High-resolution measurements reveal a lack of correlation. *Nature Medicine,* 3**,** 177-182.

Henriksen, S., Tylden, G. D., Dumoulin, A., Sharma, B. N., Hirsch, H. H. & Rinaldo, C. H. 2014. The human fetal glial cell line SVG p12 contains infectious BK polyomavirus. *Journal of Virology,* 88**,** 7556-7568.

Henry, W. S., Laszewski, T., Tsang, T., Beca, F., Beck, A. H., Mcallister, S. S. & Toker, A. 2017. Aspirin suppresses growth in PI3K-mutant breast cancer by activating AMPK and inhibiting mTORC1 signaling. *Cancer Research,* 77**,** 790-801.

Herbst, R. S. 2004. Review of epidermal growth factor receptor biology. *International Journal of Radiation Oncology* Biology* Physics,* 59**,** S21-S26.

Hervey-Jumper, S. L. & Berger, M. S. 2014. Role of surgical resection in low-and high-grade gliomas. *Current Treatment Options in Neurology,* 16**,** 284.

Hesketh, P. J. 2008. Chemotherapy-induced nausea and vomiting. *New England Journal of Medicine,* 358**,** 2482-2494.

Heymann, P. G. B., Henkenius, K. S. E., Ziebart, T., Braun, A., Hirthammer, K., Halling, F., Neff, A. & Mandic, R. 2018. Modulation of Tumor Cell Metabolism by Laser Photochemotherapy with Cisplatin or Zoledronic Acid *In Vitro*. *Anticancer Research,* 38**,** 1291-1301.

Hiľovská, L., Jendželovský, R. & Fedoročko, P. 2015. Potency of non-steroidal anti-inflammatory drugs in chemotherapy. *Molecular and Clinical Oncology,* 3**,** 3-12.

Hirose, Y., Berger, M. S. & Pieper, R. O. 2001. p53 effects both the duration of G(2)/M arrest and the fate of temozolomide-treated human glioblastoma cells. *Cancer Research,* 61**,** 1957-1963.

Hirschhaeuser, F., Menne, H., Dittfeld, C., West, J., Mueller-Klieser, W. & Kunz-Schughart, L. A. 2010. Multicellular tumor spheroids: an underestimated tool is catching up again. *Journal of Biotechnology,* 148**,** 3-15.

Hirst, J. J., Teixeira, F. J., Zakar, T. & Olson, D. M. 1995. Prostaglandin endoperoxide-H synthase-1 and-2 messenger ribonucleic acid levels in human amnion with spontaneous labor onset. *The Journal of Clinical Endocrinology & Metabolism,* 80**,** 517-523.

Ho, I. A. & Shim, W. S. 2017. Contribution of the microenvironmental niche to glioblastoma heterogeneity. *BioMed Research International,* 2017**,** 9634172.

Ho, J., De Moura, M. B., Lin, Y., Vincent, G., Thorne, S., Duncan, L. M., Hui-Min, L., Kirkwood, J. M., Becker, D. & Van Houten, B. 2012. Importance of glycolysis and oxidative phosphorylation in advanced melanoma. *Molecular Cancer,* 11**,** 76.

Hodi, F. S., O'day, S. J., Mcdermott, D. F., Weber, R. W., Sosman, J. A., Haanen, J. B., Gonzalez, R., Robert, C., Schadendorf, D. & Hassel, J. C. 2010. Improved survival with ipilimumab in patients with metastatic melanoma. *New England Journal of Medicine,* 363**,** 711-723.

Höing, B., Kanaan, O., Altenhoff, P., Petri, R., Thangavelu, K., Schlüter, A., Lang, S., Bankfalvi, A. & Brandau, S. 2018. Stromal versus tumoral inflammation differentially contribute to metastasis and poor survival in laryngeal squamous cell carcinoma. *Oncotarget,* 9**,** 8415.

Holmquist-Mengelbier, L., Fredlund, E., Löfstedt, T., Noguera, R., Navarro, S., Nilsson, H., Pietras, A., Vallon-Christersson, J., Borg, Å. & Gradin, K. 2006. Recruitment of HIF-1α and HIF-2α to common target genes is differentially regulated in neuroblastoma: HIF-2α promotes an aggressive phenotype. *Cancer Cell,* 10**,** 413-423.

Holzer, A. K., Manorek, G. H. & Howell, S. B. 2006. Contribution of the major copper influx transporter CTR1 to the cellular accumulation of cisplatin, carboplatin, and oxaliplatin. *Molecular Pharmacology,* 70**,** 1390-1394.

Hombach-Klonisch, S., Mehrpour, M., Shojaei, S., Harlos, C., Pitz, M., Hamai, A., Siemianowicz, K., Likus, W., Wiechec, E. & Toyota, B. D. 2018. Glioblastoma and chemoresistance to alkylating agents: involvement of apoptosis, autophagy, and unfolded protein response. *Pharmacology & Therapeutics,* 184**,** 13-41.

Hong, I. S., Ipema, H. J., Gabay, M. P. & Lodolce, A. E. 2011. Medication repurposing: new uses for old drugs. *Journal of Pharmacy Technology,* 27**,** 132-140.

Hong, S.-S., Lee, H. & Kim, K.-W. 2004. HIF-1α: a valid therapeutic target for tumor therapy. *Cancer Research and Treatment: Official Journal of Korean Cancer Association,* 36**,** 343.

Hsieh, C.-H., Lee, C.-H., Liang, J.-A., Yu, C.-Y. & Shyu, W.-C. 2010. Cycling hypoxia increases U87 glioma cell radioresistance via ROS induced higher and long-term HIF-1 signal transduction activity. *Oncology Reports,* 24**,** 1629-1636.

Hsieh, C. H., Lin, Y. J., Wu, C. P., Lee, H. T., Shyu, W. C. & Wang, C. C. 2015. Livin Contributes to Tumor Hypoxia-Induced Resistance to Cytotoxic Therapies in Glioblastoma Multiforme. *Clinical Cancer Research,* 21**,** 460-470.

Hsu, H., Xiong, J. & Goeddel, D. V. 1995. The TNF receptor 1-associated protein TRADD signals cell death and NF-κB activation. *Cell,* 81**,** 495-504.

Hsu, S. P., Kuo, J. S., Chiang, H.-C., Wang, H.-E., Wang, Y.-S., Huang, C.-C., Huang, Y.-C., Chi, M.-S., Mehta, M. P. & Chi, K.-H. 2018. Temozolomide, sirolimus and chloroquine is a new therapeutic combination that synergizes to disrupt lysosomal function and cholesterol homeostasis in GBM cells. *Oncotarget,* 9**,** 6883.

Huang, E. S., Strate, L. L., Ho, W. W., Lee, S. S. & Chan, A. T. 2010. A prospective study of aspirin use and the risk of gastrointestinal bleeding in men. *PLoS One,* 5**,** e15721.

Huang, L. E., Arany, Z., Livingston, D. M. & Bunn, H. F. 1996. Activation of hypoxia-inducible transcription factor depends primarily upon redox-sensitive stabilization of its α subunit. *Journal of Biological Chemistry,* 271**,** 32253-32259.

Huang, S. M. A., Mishina, Y. M., Liu, S. M., Cheung, A., Stegmeier, F., Michaud, G. A., Charlat, O., Wiellette, E., Zhang, Y., Wiessner, S., Hild, M., Shi, X. Y., Wilson, C. J., Mickanin, C., Myer, V., Fazal, A., Tomlinson, R., Serluca, F., Shao, W. L., Cheng, H., Shultz, M., Rau, C., Schirle, M., Schlegl, J., Ghidelli, S., Fawell, S., Lu, C., Curtis, D., Kirschner, M. W., Lengauer, C., Finan, P. M., Tallarico, J. A., Bouwmeester, T., Porter, J. A., Bauer, A. & Cong, F. 2009. Tankyrase inhibition stabilizes axin and antagonizes Wnt signalling. *Nature,* 461**,** 614-620.

Huang, X.-Z., Wang, J., Huang, C., Chen, Y.-Y., Shi, G.-Y., Hu, Q.-S. & Yi, J. 2008. Emodin enhances cytotoxicity of chemotherapeutic drugs in prostate cancer cells: the mechanisms involve ROS-mediated suppression of multidrug resistance and hypoxia inducible factor-1. *Cancer Biology & Therapy,* 7**,** 468-475.

Huang, Z. J., Fang, W. L., Liu, W. H., Wang, L., Liu, B., Liu, S. M. & Liu, S. J. 2018. Aspirin induces Beclin-1-dependent autophagy of human hepatocellular carcinoma cell. *European Journal of Pharmacology,* 823**,** 58-64.

Hujber, Z., Horváth, G., Petővári, G., Krencz, I., Dankó, T., Mészáros, K., Rajnai, H., Szoboszlai, N., Leenders, W. P. & Jeney, A. 2018. GABA, glutamine, glutamate oxidation and succinic semialdehyde dehydrogenase expression in human gliomas. *Journal of Experimental & Clinical Cancer Research,* 37**,** 271.

Hutt, A., Caldwell, J. & Smith, R. 1986. The metabolism of aspirin in man: a population study. *Xenobiotica,* 16**,** 239-249.

Hwang, S. H., Han, B. I. & Lee, M. 2018. Knockout of ATG5 leads to malignant cell transformation and resistance to Src family kinase inhibitor PP2. *Journal of Cellular Physiology,* 233**,** 506-515.

Hwang, S. L., Lee, K. S., Lin, C. L., Lieu, A. S., Cheng, C. Y., Loh, J. K., Hwang, Y. F., Su, Y. F. & Howng, S. L. 2004. Effect of aspirin and indomethacin on prostaglandin E2 synthesis in C6 glioma cells. *Kaohsiung Journal of Medical Sciences,* 20**,** 1-5.

Hynes, J., Marroquin, L. D., Ogurtsov, V. I., Christiansen, K. N., Stevens, G. J., Papkovsky, D. B. & Will, Y. 2006. Investigation of drug-induced mitochondrial toxicity using fluorescence-based oxygen-sensitive probes. *Toxicological Sciences,* 92**,** 186-200.

Ilina, O. & Friedl, P. 2009. Mechanisms of collective cell migration at a glance. *Journal of Cell Science,* 122**,** 3203-3208.

Inoki, K., Kim, J. & Guan, K.-L. 2012. AMPK and mTOR in cellular energy homeostasis and drug targets. *Annual Review of Pharmacology and Toxicology,* 52**,** 381-400.

Inoue, T., Inoue, T., Teshima, T., Murayama, S., Shimizutani, K., Fuchiata, H. & Furukawa, S. 1996. Phase III trial of high and low dose rate interstitial radiotherapy for early oral tongue cancer. *International Journal of Radiation Oncology* Biology* Physics,* 36**,** 1201-1204.

Ishitani, R., Tanaka, M., Sunaga, K., Katsube, N. & Chuang, D.-M. 1998. Nuclear localization of overexpressed glyceraldehyde-3-phosphate dehydrogenase in cultured cerebellar neurons undergoing apoptosis. *Molecular Pharmacology,* 53**,** 701-707.

Ito, H., Daido, S., Kanzawa, T., Kondo, S. & Kondo, Y. 2005. Radiation-induced autophagy is associated with LC3 and its inhibition sensitizes malignant glioma cells. *International Journal of Oncology,* 26**,** 1401-1410.

Iurlaro, R., León-Annicchiarico, C. L. & Muñoz-Pinedo, C. 2014. Regulation of cancer metabolism by oncogenes and tumor suppressors. *Methods in Enzymology. Elsevier*.542**,** 59-80.

Izquierdo-Garcia, J. L., Viswanath, P., Eriksson, P., Cai, L., Radoul, M., Chaumeil, M. M., Blough, M., Luchman, H. A., Weiss, S. & Cairncross, J. G. 2015. IDH1 mutation induces reprogramming of pyruvate metabolism. *Cancer Research,* 75**,** 2999-3009.

Izyumov, D. S., Avetisyan, A. V., Pletjushkina, O. Y., Sakharov, D. V., Wirtz, K. W., Chernyak, B. V. & Skulachev, V. P. 2004. "Wages of fear": transient threefold decrease in intracellular ATP level imposes apoptosis. *Biochimica et Biophysica Acta,* 1658**,** 141-147.

Jacobs, E. J., Thun, M. J., Bain, E. B., Rodriguez, C., Henley, S. J. & Calle, E. E. 2007. A large cohort study of long-term daily use of adult-strength aspirin and cancer incidence. *Journal of the National Cancer Institute,* 99**,** 608-615.

Jacobs, S. R., Herman, C. E., Maciver, N. J., Wofford, J. A., Wieman, H. L., Hammen, J. J. & Rathmell, J. C. 2008. Glucose uptake is limiting in T cell activation and requires CD28-mediated Akt-dependent and independent pathways. *The Journal of Immunology,* 180**,** 4476-4486.

Jacquin, M., Chiche, J., Zunino, B., Beneteau, M., Meynet, O., Pradelli, L., Marchetti, S., Cornille, A., Carles, M. & Ricci, J. 2013. GAPDH binds to active Akt, leading to Bcl-xL increase and escape from caspase-independent cell death. *Cell Death and Differentiation,* 20**,** 1043-1054.

Jain, K. K. 2018. A Critical Overview of Targeted Therapies for Glioblastoma. *Frontiers in Oncology,* 8**,** 419.

Jain, R. K., Di Tomaso, E., Duda, D. G., Loeffler, J. S., Sorensen, A. G. & Batchelor, T. T. 2007. Angiogenesis in brain tumours. *Nature Reviews Neuroscience,* 8**,** 610-622.

James, P. E., Jackson, S. K., Grinberg, O. Y. & Swartz, H. M. 1995. The effects of endotoxin on oxygen consumption of various cell types in vitro: an EPR oximetry study. *Free Radical Biology and Medicine,* 18**,** 641-647.

Jawhari, S., Ratinaud, M. H. & Verdier, M. 2016. Glioblastoma, hypoxia and autophagy: a survival-prone 'menage-a-trois'. *Cell death and disease,* 7**,** e2434.

Jennewein, L., Ronellenfitsch, M. W., Antonietti, P., Ilina, E. I., Jung, J., Stadel, D., Flohr, L.-M., Zinke, J., Von Renesse, J. & Drott, U. 2016. Diagnostic and clinical relevance of the autophago-lysosomal network in human gliomas. *Oncotarget,* 7**,** 20016-20032.

Jensen, R. L. 2009. Brain tumor hypoxia: tumorigenesis, angiogenesis, imaging, pseudoprogression, and as a therapeutic target. *Journal of Neuro-Oncology,* 92**,** 317-335.

Jensen, R. L. & Chkheidze, R. 2011. The Role of Glucose Transporter-1 (GLUT-1) in Malignant Gliomas. *Tumors of the Central Nervous System. Springer*.1**,** 99-108.

Jiang, M.-J., Dai, J.-J., Gu, D.-N., Huang, Q. & Tian, L. 2016. Aspirin in pancreatic cancer: chemopreventive effects and therapeutic potentials. *Biochimica et Biophysica Acta (BBA)-Reviews on Cancer,* 1866**,** 163-176.

Jiang, M., Yi, X. L., Hsu, S., Wang, C. Y. & Dong, Z. 2004. Role of p53 in cisplatin-induced tubular cell apoptosis: dependence on p53 transcriptional activity. *American Journal of Physiology-Renal Physiology,* 287**,** F1140-F1147.

Jiang, Y. L., Ji, F. H., Liu, Y. F., He, M. J., Zhang, Z. Q., Yang, J. H., Wang, N., Zhong, C. L., Jin, Q. N., Ye, X. S. & Chen, T. M. 2017. Cisplatin-induced autophagy protects breast cancer cells from apoptosis by regulating yes-associated protein. *Oncology Reports,* 38**,** 3668-3676.

Jin, S. M., Lazarou, M., Wang, C., Kane, L. A., Narendra, D. P. & Youle, R. J. 2010. Mitochondrial membrane potential regulates PINK1 import and proteolytic destabilization by PARL. *Journal of Cell Biology,* 191**,** 933-942.

Johanns, T. M., Miller, C. A., Liu, C. J., Perrin, R. J., Bender, D., Kobayashi, D. K., Campian, J. L., Chicoine, M. R., Dacey, R. G. & Huang, J. 2019. Detection of neoantigen-specific T cells following a personalized vaccine in a patient with glioblastoma. *Oncoimmunology,* 8**,** e1561106.

Johnson, C. C., Hayes, R. B., Schoen, R. E., Gunter, M. J. & Huang, W.-Y. 2010. Non-steroidal anti-inflammatory drug use and colorectal polyps in the Prostate, Lung, Colorectal, And Ovarian Cancer Screening Trial. *The American Journal of Gastroenterology,* 105**,** 2646-2655.

Johnson, G. L. & Nakamura, K. 2007. The c-jun kinase/stress-activated pathway: regulation, function and role in human disease. *Biochimica et Biophysica Acta (BBA)-Molecular Cell Research,* 1773**,** 1341-1348.

Joki, T., Heese, O., Nikas, D. C., Bello, L., Zhang, J. P., Kraeft, S. K., Seyfried, N. T., Abe, T., Chen, L. B., Carroll, R. S. & Black, P. M. 2000. Expression of cyclooxygenase 2 (COX-2) in human glioma and in Vitro inhibition by a specific COX-2 inhibitor, NS-398. *Cancer Research,* 60**,** 4926-4931.

Jones, R. G. & Thompson, C. B. 2009. Tumor suppressors and cell metabolism: a recipe for cancer growth. *Genes & Development,* 23**,** 537-548.

Joseph, J. V., Conroy, S., Pavlov, K., Sontakke, P., Tomar, T., Eggens-Meijer, E., Balasubramaniyan, V., Wagemakers, M., Den Dunnen, W. F. & Kruyt, F. A. 2015. Hypoxia enhances migration and invasion in glioblastoma by promoting a

mesenchymal shift mediated by the HIF1α–ZEB1 axis. *Cancer letters,* 359**,** 107-116.

Joza, N., Susin, S. A., Daugas, E., Stanford, W. L., Cho, S. K., Li, C. Y., Sasaki, T., Elia, A. J., Cheng, H.-Y. M. & Ravagnan, L. 2001. Essential role of the mitochondrial apoptosis-inducing factor in programmed cell death. *Nature,* 410**,** 549-554.

Jung, D.-W., Kim, W.-H., Seo, S., Oh, E., Yim, S.-H., Ha, H.-H., Chang, Y.-T. & Williams, D. R. 2014. Chemical targeting of GAPDH moonlighting function in cancer cells reveals its role in tubulin regulation. *Chemistry & Biology,* 21**,** 1533-1545.

Kambe, A., Yoshioka, H., Kamitani, H., Watanabe, T., Baek, S. J. & Eling, T. E. 2009. The cyclooxygenase inhibitor sulindac sulfide inhibits EP4 expression and suppresses the growth of glioblastoma cells. *Cancer Prevention Research,* 2**,** 1088-1099.

Kamphorst, J. J., Cross, J. R., Fan, J., De Stanchina, E., Mathew, R., White, E. P., Thompson, C. B. & Rabinowitz, J. D. 2013. Hypoxic and Ras-transformed cells support growth by scavenging unsaturated fatty acids from lysophospholipids. *Proceedings of the National Academy of Sciences,* 110**,** 8882-8887.

Kamura, T., Sato, S., Iwai, K., Czyzyk-Krzeska, M., Conaway, R. C. & Conaway, J. W. 2000. Activation of HIF1α ubiquitination by a reconstituted von Hippel-Lindau (VHL) tumor suppressor complex. *Proceedings of the National Academy of Sciences,* 97**,** 10430-10435.

Kandoth, C., Mclellan, M. D., Vandin, F., Ye, K., Niu, B., Lu, C., Xie, M., Zhang, Q., Mcmichael, J. F. & Wyczalkowski, M. A. 2013. Mutational landscape and significance across 12 major cancer types. *Nature,* 502**,** 333-339.

Kang, K. B., Zhu, C., Yong, S. K., Gao, Q. & Wong, M. C. 2009. Enhanced sensitivity of celecoxib in human glioblastoma cells: induction of DNA damage leading to p53-dependent G 1 cell cycle arrest and autophagy. *Molecular Cancer,* 8**,** 66.

Kang, R., Livesey, K. M., Zeh, H. J., 3rd, Lotze, M. T. & Tang, D. 2011. Metabolic regulation by HMGB1-mediated autophagy and mitophagy. *Autophagy,* 7**,** 1256-1258.

Kanu, O. O., Hughes, B., Di, C., Lin, N., Fu, J., Bigner, D. D., Yan, H. & Adamson, C. 2009. Glioblastoma multiforme oncogenomics and signaling pathways. *Clinical Medicine Insights: Oncology,* 3**,** 39-52.

Kanzawa, T., Germano, I. M., Komata, T., Ito, H., Kondo, Y. & Kondo, S. 2004. Role of autophagy in temozolomide-induced cytotoxicity for malignant glioma cells. *Cell Death and Differentiation,* 11**,** 448-457.

Karam, A. K., Santiskulvong, C., Fekete, M., Zabih, S., Eng, C. & Dorigo, O. 2010. Cisplatin and PI3kinase inhibition decrease invasion and migration of human ovarian carcinoma cells and regulate matrix-metalloproteinase expression. *Cytoskeleton (Hoboken),* 67**,** 535-544.

Kardosh, A., Blumenthal, M., Wang, W. J., Chen, T. C. & Schonthal, A. H. 2004. Differential effects of selective COX-2 inhibitors on cell cycle regulation and proliferation of glioblastoma cell lines. *Cancer Biology & Therapy,* 3**,** 55-62.

Kargman, S., Charleson, S., Cartwright, M., Frank, J., Riendeau, D., Mancini, J., Evans, J. & O'neill, G. 1996. Characterization of prostaglandin G/H synthase 1 and 2 in rat, dog, monkey, and human gastrointestinal tracts. *Gastroenterology,* 111**,** 445-454.

Karpel-Massler, G., Pareja, F., Aimé, P., Shu, C., Chau, L., Westhoff, M.-A., Halatsch, M.-E., Crary, J. F., Canoll, P. & Siegelin, M. D. 2014. PARP inhibition restores extrinsic apoptotic sensitivity in glioblastoma. *PloS One,* 9**,** e114583.

Karran, P., Macpherson, P., Ceccotti, S., Dogliotti, E., Griffin, S. & Bignami, M. 1993. O6-methylguanine residues elicit DNA repair synthesis by human cell extracts. *The Journal of Biological Chemistry,* 268**,** 15878-15886.

Kast, R. 2010. Glioblastoma chemotherapy adjunct via potent serotonin receptor-7 inhibition using currently marketed high-affinity antipsychotic medicines. *British Journal of Pharmacology,* 161**,** 481-487.

Kaur, G. & Dufour, J. M. 2012. Cell lines: Valuable tools or useless artifacts. Taylor & Francis.

Kaushal, G. P., Kaushal, V., Herzog, C. & Yang, C. 2008. Autophagy delays apoptosis in renal tubular epithelial cells in cisplatin cytotoxicity. *Autophagy,* 4**,** 710-712.

Kawasaki, Y., Saito, T., Shirota-Someya, Y., Ikegami, Y., Komano, H., Lee, M.-H., Froelich, C. J., Shinohara, N. & Takayama, H. 2000. Cell death-associated translocation of plasma membrane components induced by CTL. *The Journal of Immunology,* 164**,** 4641-4648.

Kayama, T., Yoshimoto, T., Fujimoto, S. & Sakurai, Y. 1991. Intratumoral oxygen pressure in malignant brain tumor. *Journal of Neurosurgery,* 74**,** 55-59.

Kennedy, K. M., Scarbrough, P. M., Ribeiro, A., Richardson, R., Yuan, H., Sonveaux, P., Landon, C. D., Chi, J.-T., Pizzo, S. & Schroeder, T. 2013. Catabolism of exogenous lactate reveals it as a legitimate metabolic substrate in breast cancer. *PloS One,* 8**,** e75154.

Kerr, J. F., Wyllie, A. H. & Currie, A. R. 1972. Apoptosis: a basic biological phenomenon with wideranging implications in tissue kinetics. *British Journal of Cancer,* 26**,** 239.

Kerschbaumer, J., Schmidt, F. A., Grams, A. E., Nowosielski, M., Pinggera, D., Brawanski, K. R., Petr, O., Thome, C., Tuettenberg, J. & Seiz, M. 2015. Dual anti-angiogenic chemotherapy with temozolomide and celecoxib in selected patients with malignant glioma not eligible for standard treatment. *Anticancer Research,* 35**,** 4955-4960.

Kessel, S., Cribbes, S., Déry, O., Kuksin, D., Sincoff, E., Qiu, J. & Chan, L. L.-Y. 2017. High-Throughput 3D tumor spheroid screening method for cancer drug discovery using Celigo image cytometry. *SLAS TECHNOLOGY: Translating Life Sciences Innovation,* 22**,** 454-465.

Keuper, M., Jastroch, M., Yi, C.-X., Fischer-Posovszky, P., Wabitsch, M., Tschöp, M. H. & Hofmann, S. M. 2014. Spare mitochondrial respiratory capacity permits human adipocytes to maintain ATP homeostasis under hypoglycemic conditions. *The FASEB Journal,* 28**,** 761-770.

Khurshed, M., Aarnoudse, N., Hulsbos, R., Hira, V. V., Van Laarhoven, H. W., Wilmink, J. W., Molenaar, R. J. & Van Noorden, C. J. 2018. IDH1-mutant cancer cells are sensitive to cisplatin and an IDH1-mutant inhibitor counteracts this sensitivity. *The FASEB Journal,* 32**,** 6344-6352.

Kilari, R., Bashir, A., Devitt, A., Perry, C., Safrany, S. & Nicholl, I. D. 2018. The cytotoxicity and synergistic potential of aspirin and aspirin analogues towards oesophageal and colorectal cancer. *Current Clinical Pharmacology,* 14**,** 141 - 151.

Kilic-Eren, M., Boylu, T. & Tabor, V. 2013. Targeting PI3K/Akt represses Hypoxia inducible factor-1α activation and sensitizes Rhabdomyosarcoma and Ewing's sarcoma cells for apoptosis. *Cancer Cell International,* 13**,** 36.

Kim, H. P., Wang, X., Zhang, J., Suh, G. Y., Benjamin, I. J., Ryter, S. W. & Choi, A. M. 2005. Heat shock protein-70 mediates the cytoprotective effect of carbon monoxide:

involvement of p38β MAPK and heat shock factor-1. *The Journal of Immunology,* 175**,** 2622-2629.

Kim, J., Han, J., Jang, Y., Kim, S. J., Lee, M. J., Ryu, M. J., Kweon, G. R. & Heo, J. Y. 2015. High-capacity glycolytic and mitochondrial oxidative metabolisms mediate the growth ability of glioblastoma. *International Journal of Oncology,* 47**,** 1009-1016.

Kim, J. W., Tchernyshyov, I., Semenza, G. L. & Dang, C. V. 2006. HIF-1-mediated expression of pyruvate dehydrogenase kinase: a metabolic switch required for cellular adaptation to hypoxia. *Cell Metabolism,* 3**,** 177-185.

Kim, S.-H., Turnbull, J. & Guimond, S. 2011. Extracellular matrix and cell signalling: the dynamic cooperation of integrin, proteoglycan and growth factor receptor. *The Journal of Endocrinology,* 209**,** 139-151.

Kim, S. R., Bae, M. K., Kim, J. Y., Wee, H. J., Yoo, M. A. & Bae, S. K. 2009. Aspirin induces apoptosis through the blockade of IL-6-STAT3 signaling pathway in human glioblastoma A172 cells. *Biochemical and Biophysical Research Communications,* 387**,** 342-347.

Kirson, E. D., Dbalý, V., Tovaryš, F., Vymazal, J., Soustiel, J. F., Itzhaki, A., Mordechovich, D., Steinberg-Shapira, S., Gurvich, Z. & Schneiderman, R. 2007. Alternating electric fields arrest cell proliferation in animal tumor models and human brain tumors. *Proceedings of the National Academy of Sciences,* 104**,** 10152-10157.

Kirson, E. D., Gurvich, Z., Schneiderman, R., Dekel, E., Itzhaki, A., Wasserman, Y., Schatzberger, R. & Palti, Y. 2004. Disruption of cancer cell replication by alternating electric fields. *Cancer Research,* 64**,** 3288-3295.

Kischkel, F., Hellbardt, S., Behrmann, I., Germer, M., Pawlita, M., Krammer, P. & Peter, M. 1995. Cytotoxicity-dependent APO-1 (Fas/CD95)-associated proteins form a death-inducing signaling complex (DISC) with the receptor. *The EMBO Journal,* 14**,** 5579-5588.

Kleihues, P. & Ohgaki, H. 1999. Primary and secondary glioblastomas: from concept to clinical diagnosis. *Journal of Neuro-Oncology,* 1**,** 44-51.

Kleihues, P., Soylemezoglu, F., Schäuble, B., Scheithauer, B. W. & Burger, P. C. 1995. Histopathology, classification, and grading of gliomas. *Glia,* 15**,** 211-221.

Kleinstein, S. E., Heath, L., Makar, K. W., Poole, E. M., Seufert, B. L., Slattery, M. L., Xiao, L., Duggan, D. J., Hsu, L. & Curtin, K. 2013. Genetic variation in the lipoxygenase pathway and risk of colorectal neoplasia. *Genes, Chromosomes and Cancer,* 52**,** 437-449.

Klionsky, D. J., Abdelmohsen, K., Abe, A., Abedin, M. J., Abeliovich, H., Acevedo Arozena, A., Adachi, H., Adams, C. M., Adams, P. D. & Adeli, K. 2016. Guidelines for the use and interpretation of assays for monitoring autophagy. *Autophagy,* 12**,** 1-222.

Klutzny, S., Lesche, R., Keck, M., Kaulfuss, S., Schlicker, A., Christian, S., Sperl, C., Neuhaus, R., Mowat, J. & Steckel, M. 2017. Functional inhibition of acid sphingomyelinase by Fluphenazine triggers hypoxia-specific tumor cell death. *Cell Death & Disease,* 8**,** e2709.

Knights, K. M., Mangoni, A. A. & Miners, J. O. 2010. Defining the COX inhibitor selectivity of NSAIDs: implications for understanding toxicity. *Expert Review of Clinical Pharmacology,* 3**,** 769-776.

Knizhnik, A. V., Roos, W. P., Nikolova, T., Quiros, S., Tomaszowski, K. H., Christmann, M. & Kaina, B. 2013. Survival and Death Strategies in Glioma Cells: Autophagy, Senescence and Apoptosis Triggered by a Single Type of Temozolomide-Induced DNA Damage. *Plos One,* 8**,** e55665.

Knupfer, H., Stanitz, D. & Preiss, R. 2006. CYP2C9 polymorphisms in human tumors. *Anticancer Research,* 26**,** 299-305.

Koch, S., Mayer, F., Honecker, F., Schittenhelm, M. & Bokemeyer, C. 2003. Efficacy of cytotoxic agents used in the treatment of testicular germ cell tumours under normoxic and hypoxic conditions in vitro. *British Journal of Cancer,* 89**,** 2133-2139.

Kodela, R., Chattopadhyay, M., Goswami, S., Gan, Z. Y., Rao, P. P., Nia, K. V., Velázquez-Martínez, C. A. & Kashfi, K. 2013. Positional isomers of aspirin are equally potent in inhibiting colon cancer cell growth: Differences in mode of cyclooxygenase inhibition. *Journal of Pharmacology and Experimental Therapeutics,* 345**,** 85-94.

Kökoğlu, E., Tüter, Y., Sandıkçı, K., Yazıcı, Z., Ulakoğlu, E., Sönmez, H. & Özyurt, E. 1998. Prostaglandin E2 levels in human brain tumor tissues and arachidonic acid levels in the plasma membrane of human brain tumors. *Cancer Letters,* 132**,** 17-21.

Kolamunne, R. T., Dias, I. H., Vernallis, A. B., Grant, M. M. & Griffiths, H. R. 2013. Nrf2 activation supports cell survival during hypoxia and hypoxia/reoxygenation in cardiomyoblasts; the roles of reactive oxygen and nitrogen species. *Redox Biology,* 1**,** 418-426.

Kolchinsky, A. & Roninson, I. 1997. Drug resistance conferred by MDR1 expression in spheroids formed by glioblastoma cell lines. *Anticancer Research,* 17**,** 3321-3327.

Konrad, C., Kawamata, H., Bredvik, K. G., Arreguin, A. J., Cajamarca, S. A., Hupf, J. C., Ravits, J. M., Miller, T. M., Maragakis, N. J. & Hales, C. M. 2017. Fibroblast bioenergetics to classify amyotrophic lateral sclerosis patients. *Molecular Neurodegeneration,* 12**,** 76.

Koong, A. C., Chen, E. Y. & Giaccia, A. J. 1994. Hypoxia causes the activation of nuclear factor κB through the phosphorylation of IκBα on tyrosine residues. *Cancer Research,* 54**,** 1425-1430.

Koontongkaew, S., Monthanapisut, P. & Saensuk, T. 2010. Inhibition of arachidonic acid metabolism decreases tumor cell invasion and matrix metalloproteinase expression. *Prostaglandins & Other Lipid Mediators,* 93**,** 100-108.

Kopp, E. & Ghosh, S. 1994. Inhibition of NF-kappa B by sodium salicylate and aspirin. *Science,* 265**,** 956-959.

Koppenol, W. H., Bounds, P. L. & Dang, C. V. 2011. Otto Warburg's contributions to current concepts of cancer metabolism. *Nature Reviews Cancer,* 11**,** 325-337.

Korkolopoulou, P., Levidou, G., Saetta, A. A., El-Habr, E., Eftichiadis, C., Demenagas, P., Thymara, I., Xiromeritis, K., Boviatsis, E., Thomas-Tsagli, E., Panayotidis, I. & Patsouris, E. 2008. Expression of nuclear factor-kappaB in human astrocytomas: relation to pI kappa Ba, vascular endothelial growth factor, Cox-2, microvascular characteristics, and survival. *Human Pathology,* 39**,** 1143-1152.

Korkolopoulou, P., Perdiki, M., Thymara, I., Boviatsis, E., Agrogiannis, G., Kotsiakis, X., Angelidakis, D., Rologis, D., Diamantopoulou, K. & Thomas-Tsagli, E. 2007. Expression of hypoxia-related tissue factors in astrocytic gliomas. A multivariate survival study with emphasis upon carbonic anhydrase IX. *Human Pathology,* 38**,** 629-638.

Koukourakis, M., Tsolou, A., Pouliliou, S., Lamprou, I., Papadopoulou, M., Ilemosoglou, M., Kostoglou, G., Ananiadou, D., Sivridis, E. & Giatromanolaki, A. 2017. Blocking LDHA glycolytic pathway sensitizes glioblastoma cells to radiation and temozolomide. *Biochemical and Biophysical Research Communications,* 491**,** 932-938.

Krakstad, C. & Chekenya, M. 2010. Survival signalling and apoptosis resistance in glioblastomas: opportunities for targeted therapeutics. *Molecular cancer,* 9**,** 135.

Kroemer, G., Galluzzi, L. & Brenner, C. 2007. Mitochondrial membrane permeabilization in cell death. *Physiological Reviews,* 87**,** 99-163.

Kumano, M., Furukawa, J., Shiota, M., Zardan, A., Zhang, F., Beraldi, E., Wiedmann, R. M., Fazli, L., Zoubeidi, A. & Gleave, M. E. 2012. Cotargeting Stress-Activated Hsp27 and Autophagy as a Combinatorial Strategy to Amplify Endoplasmic Reticular Stress in Prostate Cancer. *Molecular Cancer Therapeutics,* 11**,** 1661-1671.

Kumar, A. & Singh, S. M. 2012. Priming effect of aspirin for tumor cells to augment cytotoxic action of cisplatin against tumor cells: implication of altered constitution of tumor microenvironment, expression of cell cycle, apoptosis, and survival regulatory molecules. *Molecular and Cellular Biochemistry,* 371**,** 43-54.

Kumar, P., Nagarajan, A. & Uchil, P. D. 2018. Analysis of Cell Viability by the MTT Assay. *Cold Spring Harb Protoc,* 2018.

Kuo, C.-T., Chiang, C.-L., Huang, R. Y.-J., Lee, H. & Wo, A. M. 2012. Configurable 2D and 3D spheroid tissue cultures on bioengineered surfaces with acquisition of epithelial–mesenchymal transition characteristics. *NPG Asia Materials,* 4**,** e27.

Lacasse, E., Mahoney, D., Cheung, H., Plenchette, S., Baird, S. & Korneluk, R. 2008. IAP-targeted therapies for cancer. *Oncogene,* 27**,** 6252-6275.

Lai, A., Tran, A., Nghiemphu, P. L., Pope, W. B., Solis, O. E., Selch, M., Filka, E., Yong, W. H., Mischel, P. S. & Liau, L. M. 2011. Phase II study of bevacizumab plus temozolomide during and after radiation therapy for patients with newly diagnosed glioblastoma multiforme. *Journal of Clinical Oncology,* 29**,** 142-148.

Laine, L. 2002. The gastrointestinal effects of nonselective NSAIDs and COX-2-selective inhibitors. *Seminars in Arthritis and Rheumatism,* 32**,** 25-32.

Lalloo, A., Chao, P., Hu, P., Stein, S. & Sinko, P. J. 2006. Pharmacokinetic and pharmacodynamic evaluation of a novel in situ forming poly(ethylene glycol)-based hydrogel for the controlled delivery of the camptothecins. *The Journal of Controlled Release,* 112**,** 333-342.

Lan, F., Yue, X., Han, L., Yuan, X., Shi, Z., Huang, K., Yang, Y., Zou, J., Zhang, J. & Jiang, T. 2011. Antitumor effect of aspirin in glioblastoma cells by modulation of beta-catenin/T-cell factor-mediated transcriptional activity. *Journal of Neurosurgery,* 115**,** 780-788.

Lan, J., Xue, Y., Chen, H., Zhao, S., Wu, Z., Fang, J., Han, C. & Lou, M. 2014. Hypoxia-induced miR-497 decreases glioma cell sensitivity to TMZ by inhibiting apoptosis. *FEBS Letters,* 588**,** 3333-3339.

Lan, X., Jörg, D. J., Cavalli, F. M., Richards, L. M., Nguyen, L. V., Vanner, R. J., Guilhamon, P., Lee, L., Kushida, M. M. & Pellacani, D. 2017. Fate mapping of human glioblastoma reveals an invariant stem cell hierarchy. *Nature,* 549**,** 227-232.

Landry, J., Lambert, H., Zhou, M., Lavoie, J., Hickey, E., Weber, L. & Anderson, C. 1992. Human HSP27 is phosphorylated at serines 78 and 82 by heat shock and mitogen-activated kinases that recognize the same amino acid motif as S6 kinase II. *Journal of Biological Chemistry,* 267**,** 794-803.

Langman, M., Weil, J., Wainwright, P., Lawson, D., Rawlins, M., Logan, R., Murphy, M., Vessey, M. & Colin-Jones, D. 1994. Risks of bleeding peptic ulcer associated with individual non-steroidal anti-inflammatory drugs. *The Lancet,* 343**,** 1075-1078.

Lapidus, K. A., Soleimani, L. & Murrough, J. W. 2013. Novel glutamatergic drugs for the treatment of mood disorders. *Neuropsychiatric Disease and Treatment,* 9**,** 1101-1112.

Lara-Velazquez, M., Al-Kharboosh, R., Jeanneret, S., Vazquez-Ramos, C., Mahato, D., Tavanaiepour, D., Rahmathulla, G. & Quinones-Hinojosa, A. 2017. Advances in brain tumor surgery for glioblastoma in adults. *Brain Sciences,* 7**,** 166.

Lau, L., Hansford, L., Cheng, L., Hang, M., Baruchel, S., Kaplan, D. & Irwin, M. 2007. Cyclooxygenase inhibitors modulate the p53/HDM2 pathway and enhance chemotherapy-induced apoptosis in neuroblastoma. *Oncogene,* 26**,** 1920-1931.

Lawrenson, K., Sproul, D., Grun, B., Notaridou, M., Benjamin, E., Jacobs, I. J., Dafou, D., Sims, A. H. & Gayther, S. A. 2011. Modelling genetic and clinical heterogeneity in epithelial ovarian cancers. *Carcinogenesis,* 32**,** 1540-1549.

Laws, E. R., Parney, I. F., Huang, W., Anderson, F., Morris, A. M., Asher, A., Lillehei, K. O., Bernstein, M., Brem, H. & Sloan, A. 2003. Survival following surgery and prognostic factors for recently diagnosed malignant glioma: data from the Glioma Outcomes Project. *Journal of Neurosurgery,* 99**,** 467-473.

Lawson, H. C., Sampath, P., Bohan, E., Park, M. C., Hussain, N., Olivi, A., Weingart, J., Kleinberg, L. & Brem, H. 2007. Interstitial chemotherapy for malignant gliomas: the Johns Hopkins experience. *Journal of Neuro-Oncology,* 83**,** 61-70.

Lee, C., Siu, A. & Ramos, D. M. 2016. Multicellular Spheroids as a Model for Hypoxia-induced EMT. *Anticancer Research,* 36**,** 6259-6263.

Lee, H. C., Park, I. C., Park, M. J., An, S., Woo, S. H., Jin, H. O., Chung, H. Y., Lee, S. J., Gwak, H. S. & Hong, Y. J. 2005. Sulindac and its metabolites inhibit invasion of glioblastoma cells via down-regulation of Akt/PKB and MMP-2. *Journal of Cellular Biochemistry,* 94**,** 597-610.

Lee, J., Giordano, S. & Zhang, J. 2012. Autophagy, mitochondria and oxidative stress: cross-talk and redox signalling. *Biochemical Journal,* 441**,** 523-540.

Lee, J. E., Lim, J. H., Hong, Y. K. & Yang, S. H. 2018. High-dose metformin plus temozolomide shows increased anti-tumor effects in glioblastoma in vitro and in vivo compared with monotherapy. *Cancer Research and Treatment: Official Journal of Korean Cancer Association,* 50**,** 1331-1342.

Lee, J. M., Mhawech-Fauceglia, P., Lee, N., Parsanian, L. C., Lin, Y. G., Gayther, S. A. & Lawrenson, K. 2013. A three-dimensional microenvironment alters protein expression and chemosensitivity of epithelial ovarian cancer cells in vitro. *Laboratory Investigation,* 93**,** 528-542.

Lee, S. Y. 2016. Temozolomide resistance in glioblastoma multiforme. *Genes & Diseases,* 3**,** 198-210.

Lee, W., Belkhiri, A., Lockhart, A. C., Merchant, N., Glaeser, H., Harris, E. I., Washington, M. K., Brunt, E. M., Zaika, A. & Kim, R. B. 2008. Overexpression of OATP1B3 confers apoptotic resistance in colon cancer. *Cancer Research,* 68**,** 10315-10323.

Lehman, H. L., Welsh, P. A., Kidacki, M., Warrick, J. I. & Stairs, D. B. 2017. The Interplay Between p120ctn and EGFR Causes Esophageal Squamous Cell Carcinoma Invasion Through NFkB. *The FASEB Journal,* 31**,** 178.11-178.11.

Leidgens, V., Seliger, C., Jachnik, B., Welz, T., Leukel, P., Vollmann-Zwerenz, A., Bogdahn, U., Kreutz, M., Grauer, O. M. & Hau, P. 2015. Ibuprofen and diclofenac restrict migration and proliferation of human glioma cells by distinct molecular mechanisms. *PloS One,* 10**,** e0140613.

Leist, M. & Jäättelä, M. 2001. Four deaths and a funeral: from caspases to alternative mechanisms. *Nature Reviews Molecular cell biology,* 2**,** 589-598.

Leist, M., Single, B., Castoldi, A. F., Kühnle, S. & Nicotera, P. 1997. Intracellular adenosine triphosphate (ATP) concentration: a switch in the decision between apoptosis and necrosis. *Journal of Experimental Medicine,* 185**,** 1481-1486.

Lemasters, J. J. & Ramshesh, V. K. 2007. Imaging of mitochondrial polarization and depolarization with cationic fluorophores. *Methods in Cell Biology,* 80**,** 283-295.

Leucht, S., Cipriani, A., Spineli, L., Mavridis, D., Örey, D., Richter, F., Samara, M., Barbui, C., Engel, R. R. & Geddes, J. R. 2013. Comparative efficacy and tolerability of 15 antipsychotic drugs in schizophrenia: a multiple-treatments meta-analysis. *The Lancet,* 382**,** 951-962.

Leung, E., Cairns, R. A., Chaudary, N., Vellanki, R. N., Kalliomaki, T., Moriyama, E. H., Mujcic, H., Wilson, B. C., Wouters, B. G. & Hill, R. 2017. Metabolic targeting of HIF-dependent glycolysis reduces lactate, increases oxygen consumption and enhances response to high-dose single-fraction radiotherapy in hypoxic solid tumors. *BMC Cancer,* 17**,** 418.

Levin, S., Bucci, T. J., Cohen, S. M., Fix, A. S., Hardisty, J. F., Legrand, E. K., Maronpot, R. R. & Trump, B. F. 1999. The nomenclature of cell death: recommendations of an ad hoc Committee of the Society of Toxicologic Pathologists. *Toxicologic Pathology,* 27**,** 484-490.

Levine, A. J. & Puzio-Kuter, A. M. 2010. The control of the metabolic switch in cancers by oncogenes and tumor suppressor genes. *Science,* 330**,** 1340-1344.

Levine, B. & Kroemer, G. 2008. Autophagy in the pathogenesis of disease. *Cell,* 132**,** 27-42.

Li, E.-Y., Huang, W.-Y., Chang, Y.-C., Tsai, M.-H., Chuang, E. Y., Kuok, Q.-Y., Bai, S.-T., Chao, L.-Y., Sher, Y.-P. & Lai, L.-C. 2016. Aryl hydrocarbon receptor activates NDRG1 transcription under hypoxia in breast cancer cells. *Scientific Reports,* 6**,** 20808.

Li, H., Zhu, F., Boardman, L. A., Wang, L., Oi, N., Liu, K., Li, X., Fu, Y., Limburg, P. J. & Bode, A. M. 2015. Aspirin prevents colorectal cancer by normalizing EGFR expression. *EBioMedicine,* 2**,** 447-455.

Li, J., Zhang, X. L., Sejas, D. P., Bagby, G. C. & Pang, Q. S. 2004. Hypoxia-induced nucleophosmin protects cell death through inhibition of p53. *Journal of Biological Chemistry,* 279**,** 41275-41279.

Li, J., Zhou, Y., Wang, H., Gao, Y., Li, L., Hwang, S. H., Ji, X. & Hammock, B. D. 2017. COX-2/sEH dual inhibitor PTUPB suppresses glioblastoma growth by targeting epidermal growth factor receptor and hyaluronan mediated motility receptor. *Oncotarget,* 8**,** 87353-87363.

Li, L., Geraghty, O. C., Mehta, Z., Rothwell, P. M. & Study, O. V. 2017. Age-specific risks, severity, time course, and outcome of bleeding on long-term antiplatelet treatment after vascular events: a population-based cohort study. *The Lancet,* 390**,** 490-499.

Li, P., Zhang, S., Yu, Z., Wu, Y., Liu, X., Xu, C. & Cho, C. 2009. Effects of cyclooxygenase-2 non-selective and selective inhibitors on proliferation inhibition and apoptosis induction of esophageal squamous carcinoma cells. *Diseases of the Esophagus,* 22**,** 21-31.

Li, W., Hu, Z.-F., Chen, B. & Ni, G.-X. 2013. Response of C2C12 myoblasts to hypoxia: the relative roles of glucose and oxygen in adaptive cellular metabolism. *BioMed Research International,* 2013**,** 326346.

Li, Z. & Graham, B. H. 2012. Measurement of mitochondrial oxygen consumption using a Clark electrode. *Mitochondrial Disorders. Springer*, 63-72.

Liang, C. C., Park, A. Y. & Guan, J. L. 2007. In vitro scratch assay: a convenient and inexpensive method for analysis of cell migration in vitro. *Nature Protocols,* 2, 329-33.

Liang, X.-J., Finkel, T., Shen, D.-W., Yin, J.-J., Aszalos, A. & Gottesman, M. M. 2008. SIRT1 contributes in part to cisplatin resistance in cancer cells by altering mitochondrial metabolism. *Molecular Cancer Research,* 6, 1499-1506.

Liao, H., Bai, Y., Qiu, S., Zheng, L., Huang, L., Liu, T., Wang, X., Liu, Y., Xu, N. & Yan, X. 2015. MiR-203 downregulation is responsible for chemoresistance in human glioblastoma by promoting epithelial-mesenchymal transition via SNAI2. *Oncotarget,* 6, 8914-8928.

Liau, L. M., Ashkan, K., Tran, D. D., Campian, J. L., Trusheim, J. E., Cobbs, C. S., Heth, J. A., Salacz, M., Taylor, S. & D'andre, S. D. 2018. First results on survival from a large Phase 3 clinical trial of an autologous dendritic cell vaccine in newly diagnosed glioblastoma. *Journal of Translational Medicine,* 16, 142.

Liberti, M. V., Dai, Z., Wardell, S. E., Baccile, J. A., Liu, X., Gao, X., Baldi, R., Mehrmohamadi, M., Johnson, M. O. & Madhukar, N. S. 2017. A predictive model for selective targeting of the Warburg effect through GAPDH inhibition with a natural product. *Cell Metabolism,* 26, 648-659.

Lieberthal, W., Menza, S. A. & Levine, J. S. 1998. Graded ATP depletion can cause necrosis or apoptosis of cultured mouse proximal tubular cells. *American Journal of Physiology-Renal Physiology,* 274, F315-F327.

Lim, S.-C., Kim, S. M., Choi, J. E., Kim, C. H., Duong, H.-Q., Han, S. I. & Kang, H. S. 2008. Sodium salicylate switches glucose depletion-induced necrosis to autophagy and inhibits high mobility group box protein 1 release in A549 lung adenocarcinoma cells. *Oncology Reports,* 19, 1165-1171.

Lin, J. F., Lin, Y. C., Tsai, T. F., Chen, H. E., Chou, K. Y. & Hwang, T. I. S. 2017. Cisplatin induces protective autophagy through activation of BECNI in human bladder cancer cells. *Drug Design Development and Therapy,* 11, 1517-1533.

Lin, R. Z. & Chang, H. Y. 2008. Recent advances in three-dimensional multicellular spheroid culture for biomedical research. *Biotechnology Journal: Healthcare Nutrition Technology,* 3, 1172-1184.

Lin, S.-Y., Makino, K., Xia, W., Matin, A., Wen, Y., Kwong, K. Y., Bourguignon, L. & Hung, M.-C. 2001. Nuclear localization of EGF receptor and its potential new role as a transcription factor. *Nature Cell Biology,* 3, 802-808.

Lindner, D. & Raghavan, D. 2009. Intra-tumoural extra-cellular pH: a useful parameter of response to chemotherapy in syngeneic tumour lines. *British Journal of Cancer,* 100, 1287-1291.

Lindqvist, L. M., Tandoc, K., Topisirovic, I. & Furic, L. 2018. Cross-talk between protein synthesis, energy metabolism and autophagy in cancer. *Current Opinion in Genetics & Development,* 48, 104-111.

Linos, E., Raine, T., Alonso, A. & Michaud, D. 2007. Atopy and risk of brain tumors: a meta-analysis. *Journal of the National Cancer Institute,* 99, 1544-1550.

Liu, G., Yuan, X., Zeng, Z., Tunici, P., Ng, H., Abdulkadir, I. R., Lu, L., Irvin, D., Black, K. L. & John, S. Y. 2006. Analysis of gene expression and chemoresistance of CD133+ cancer stem cells in glioblastoma. *Molecular Cancer,* 5, 67.

Liu, K., Tang, Z., Huang, A., Chen, P., Liu, P., Yang, J., Lu, W., Liao, J., Sun, Y. & Wen, S. 2017. Glyceraldehyde-3-phosphate dehydrogenase promotes cancer growth and metastasis through upregulation of SNAIL expression. *International Journal of Oncology,* 50**,** 252-262.

Liu, L. & Simon, M. C. 2004. Regulation of transcription and translation by hypoxia. *Cancer Biology & Therapy,* 3**,** 492-497.

Liu, P., Brown, S., Goktug, T., Channathodiyil, P., Kannappan, V., Hugnot, J., Guichet, P., Bian, X., Armesilla, A. & Darling, J. 2012. Cytotoxic effect of disulfiram/copper on human glioblastoma cell lines and ALDH-positive cancer-stem-like cells. *British Journal of Cancer,* 107**,** 1488-1497.

Liu, R. H., Siemiarczuk, A. & Sharom, F. J. 2000. Intrinsic fluorescence of the P-glycoprotein multidrug transporter: Sensitivity of tryptophan residues to binding of drugs and nucleotides. *Biochemistry,* 39**,** 14927-14938.

Liu, T. F., Cai, J., Gibo, D. M. & Debinski, W. 2009. Reoxygenation of hypoxic glioblastoma multiforme cells potentiates the killing effect of an interleukin-13-based cytotoxin. *Clinical Cancer Research,* 15**,** 160-168.

Liu, X.-H., Kirschenbaum, A., Yao, S., Stearns, M. E., Holland, J. F., Claffey, K. & Levine, A. C. 1999. Upregulation of vascular endothelial growth factor by cobalt chloride-simulated hypoxia is mediated by persistent induction of cyclooxygenase-2 in a metastatic human prostate cancer cell line. *Clinical & Experimental Metastasis,* 17**,** 687-694.

Liu, X., Zhao, P., Wang, X., Wang, L., Zhu, Y., Song, Y. & Gao, W. 2019. Celastrol mediates autophagy and apoptosis via the ROS/JNK and Akt/mTOR signaling pathways in glioma cells. *The Journal of Experimental & Clinical Cancer Research,* 38**,** 184.

Liu, Y., Cao, Y., Zhang, W., Bergmeier, S., Qian, Y., Akbar, H., Colvin, R., Ding, J., Tong, L. & Wu, S. 2012. A small-molecule inhibitor of glucose transporter 1 downregulates glycolysis, induces cell-cycle arrest, and inhibits cancer cell growth in vitro and in vivo. *Molecular Cancer Therapeutics,* 11**,** 1672-1682.

Liu, Y., Feng, J., Sun, M., Liu, B., Yang, G., Bu, Y., Zhao, M., Wang, T.-J., Zhang, W.-Y. & Yuan, H.-F. 2019. Aspirin inhibits the proliferation of hepatoma cells through controlling GLUT1-mediated glucose metabolism. *Acta Pharmaceutica Sinica B,* 40**,** 122-132.

Liu, Y., Li, Q., Zhou, L., Xie, N., Nice, E. C., Zhang, H., Huang, C. & Lei, Y. 2016. Cancer drug resistance: redox resetting renders a way. *Oncotarget,* 7**,** 42740-42761.

Lo Dico, A., Martelli, C., Diceglie, C., Lucignani, G. & Ottobrini, L. 2018. Hypoxia-Inducible Factor-1alpha Activity as a Switch for Glioblastoma Responsiveness to Temozolomide. *Frontiers in Oncology,* 8**,** 249.

Lo, H.-W., Cao, X., Zhu, H. & Ali-Osman, F. 2010. Cyclooxygenase-2 is a novel transcriptional target of the nuclear EGFR-STAT3 and EGFRvIII-STAT3 signaling axes. *Molecular Cancer Research,* 8**,** 232-245.

Lo, H. W. & Hung, M. C. 2006. Nuclear EGFR signalling network in cancers: linking EGFR pathway to cell cycle progression, nitric oxide pathway and patient survival. *British Journal of Cancer,* 94**,** 184-188.

Loboda, A., Jozkowicz, A. & Dulak, J. 2010. HIF-1 and HIF-2 transcription factors—similar but not identical. *Molecules and Cells,* 29**,** 435-442.

Locasale, J. W. 2013. Serine, glycine and one-carbon units: cancer metabolism in full circle. *Nature Reviews Cancer,* 13**,** 572-583.

Locksley, R. M., Killeen, N. & Lenardo, M. J. 2001. The TNF and TNF receptor superfamilies: integrating mammalian biology. *Cell,* 104**,** 487-501.

Logan, C. Y. & Nusse, R. 2004. The Wnt signaling pathway in development and disease. *Annual Review of Cell and Developmental Biology,* 20**,** 781-810.

Lohitesh, K., Saini, H., Srivastava, A., Mukherjee, S., Roy, A. & Chowdhury, R. 2018. Autophagy inhibition potentiates SAHA-mediated apoptosis in glioblastoma cells by accumulation of damaged mitochondria. *Oncology Reports,* 39**,** 2787-2796.

Lonardi, S., Tosoni, A. & Brandes, A. A. 2005. Adjuvant chemotherapy in the treatment of high grade gliomas. *Cancer Treatment Reviews,* 31**,** 79-89.

Longati, P., Jia, X., Eimer, J., Wagman, A., Witt, M.-R., Rehnmark, S., Verbeke, C., Toftgård, R., Löhr, M. & Heuchel, R. L. 2013. 3D pancreatic carcinoma spheroids induce a matrix-rich, chemoresistant phenotype offering a better model for drug testing. *BMC cancer,* 13**,** 95.

Longo, D. L. & Baden, L. R. 2018. Exploiting viruses to treat diseases. *The New England Journal of Medicine,* 379**,** 194-196.

López-Lázaro, M. 2015. Two preclinical tests to evaluate anticancer activity and to help validate drug candidates for clinical trials. *Oncoscience,* 2**,** 91.

Lord, S., Liu, D., Haider, S., Gaude, E., Teoh, E., Neel, P., Zhang, Q., Gleeson, F., Wakelam, M. & Frezza, C. 2016. Integrating dynamic 18F-FDG PET-CT, tumor metabolomics and functional genomics to understand metformin's pharmacodynamic effects in breast cancer: results of a phase 0 clinical trial. AACR.

Lou, Y.-W., Wang, P.-Y., Yeh, S.-C., Chuang, P.-K., Li, S.-T., Wu, C.-Y., Khoo, K.-H., Hsiao, M., Hsu, T.-L. & Wong, C.-H. 2014. Stage-specific embryonic antigen-4 as a potential therapeutic target in glioblastoma multiforme and other cancers. *Proceedings of the National Academy of Sciences,* 111**,** 2482-2487.

Louie, S. M., Grossman, E. A., Crawford, L. A., Ding, L., Camarda, R., Huffman, T. R., Miyamoto, D. K., Goga, A., Weerapana, E. & Nomura, D. K. 2016. GSTP1 is a driver of triple-negative breast cancer cell metabolism and pathogenicity. *Cell Chemical biology,* 23**,** 567-578.

Louis, D. N., Ohgaki, H., Wiestler, O. D., Cavenee, W. K., Burger, P. C., Jouvet, A., Scheithauer, B. W. & Kleihues, P. 2007. The 2007 WHO classification of tumours of the central nervous system. *Acta Neuropathologica,* 114**,** 97-109.

Louis, D. N., Perry, A., Reifenberger, G., Von Deimling, A., Figarella-Branger, D., Cavenee, W. K., Ohgaki, H., Wiestler, O. D., Kleihues, P. & Ellison, D. W. 2016. The 2016 World Health Organization classification of tumors of the central nervous system: a summary. *Acta Neuropathologica,* 131**,** 803-820.

Lowe, G. D. 2001. Who should take aspirin for primary prophylaxis of coronary heart disease? : BMJ Journal Heart.

Lowe, S. W. & Lin, A. W. 2000. Apoptosis in cancer. *Carcinogenesis,* 21**,** 485-495.

Lu, K., Chakroborty, D., Sarkar, C., Lu, T., Xie, Z., Liu, Z. & Basu, S. 2012. Triphala and its active constituent chebulinic acid are natural inhibitors of vascular endothelial growth factor-a mediated angiogenesis. *PLoS One,* 7**,** e43934.

Lu, K. V. & Bergers, G. 2013. Mechanisms of evasive resistance to anti-VEGF therapy in glioblastoma. *CNS Oncology,* 2**,** 49-65.

Lu, P., Weaver, V. M. & Werb, Z. 2012. The extracellular matrix: a dynamic niche in cancer progression. *Journal of Cell Biology,* 196**,** 395-406.

Lu, Y., Kwintkiewicz, J., Liu, Y., Tech, K., Frady, L. N., Su, Y.-T., Bautista, W., Moon, S. I., Macdonald, J. & Ewend, M. G. 2017. Chemosensitivity of IDH1-mutated gliomas

due to an impairment in PARP1-mediated DNA repair. *Cancer Research,* 77**,** 1709-1718.

Luca, T. D., Morré, D. M., Zhao, H. & James Morré, D. 2005. NAD+/NADH and/or CoQ/CoQH2 ratios from plasma membrane electron transport may determine ceramide and sphingosine-1-phosphate levels accompanying G1 arrest and apoptosis. *Biofactors,* 25**,** 43-60.

Luciani, M. G., Campregher, C. & Gasche, C. 2007. Aspirin blocks proliferation in colon cells by inducing a G1 arrest and apoptosis through activation of the checkpoint kinase ATM. *Carcinogenesis,* 28**,** 2207-2217.

Luo, F., Liu, X., Yan, N., Li, S., Cao, G., Cheng, Q., Xia, Q. & Wang, H. 2006. Hypoxia-inducible transcription factor-1α promotes hypoxia-induced A549 apoptosis via a mechanism that involves the glycolysis pathway. *BMC Cancer,* 6**,** 26.

Lv, D., Hu, Z., Lu, L., Lu, H. & Xu, X. 2017. Three-dimensional cell culture: A powerful tool in tumor research and drug discovery. *Oncology Letters,* 14**,** 6999-7010.

Ly, J. D., Grubb, D. & Lawen, A. 2003. The mitochondrial membrane potential (Δψ m) in apoptosis; an update. *Apoptosis,* 8**,** 115-128.

Ma, B., Gao, Z., Lou, J., Zhang, H., Yuan, Z., Wu, Q., Li, X. & Zhang, B. 2017. Long noncoding RNA MEG3 contributes to cisplatininduced apoptosis via inhibition of autophagy in human glioma cells. *Molecular Medicine Reports,* 16**,** 2946-2952.

Ma, E., Chen, P., Wilkins, H. M., Wang, T., Swerdlow, R. H. & Chen, Q. 2017. Pharmacologic ascorbate induces neuroblastoma cell death by hydrogen peroxide mediated DNA damage and reduction in cancer cell glycolysis. *Free Radical Biology and Medicine,* 113**,** 36-47.

Ma, K., Zhang, Y., Zhu, D. & Lou, Y. 2009. Protective effects of asiatic acid against D-galactosamine/lipopolysaccharide-induced hepatotoxicity in hepatocytes and kupffer cells co-cultured system via redox-regulated leukotriene C4 synthase expression pathway. *European Journal of Pharmacology,* 603**,** 98-107.

Ma, Y., Galluzzi, L., Zitvogel, L. & Kroemer, G. 2013. Autophagy and cellular immune responses. *Immunity,* 39**,** 211-227.

Macheret, M. & Halazonetis, T. D. 2015. DNA Replication Stress as a Hallmark of Cancer. *Annual Review of Pathology: Mechanisms of Disease,* 10**,** 425-448.

Maddocks, O. D., Berkers, C. R., Mason, S. M., Zheng, L., Blyth, K., Gottlieb, E. & Vousden, K. H. 2013. Serine starvation induces stress and p53-dependent metabolic remodelling in cancer cells. *Nature,* 493**,** 542-546.

Maiuri, M. C., Zalckvar, E., Kimchi, A. & Kroemer, G. 2007. Self-eating and self-killing: crosstalk between autophagy and apoptosis. *Nature Reviews Molecular Cell Biology,* 8**,** 741-752.

Majno, G. & Joris, I. 1995. Apoptosis, oncosis, and necrosis. An overview of cell death. *The American Journal of Pathology,* 146**,** 3-15.

Mamenta, E. L., Poma, E. E., Kaufmann, W. K., Delmastro, D. A., Grady, H. L. & Chaney, S. G. 1994. Enhanced replicative bypass of platinum-DNA adducts in cisplatin-resistant human ovarian carcinoma cell lines. *Cancer Research,* 54**,** 3500-3505.

Mani, S. A., Guo, W., Liao, M.-J., Eaton, E. N., Ayyanan, A., Zhou, A. Y., Brooks, M., Reinhard, F., Zhang, C. C. & Shipitsin, M. 2008. The epithelial-mesenchymal transition generates cells with properties of stem cells. *Cell,* 133**,** 704-715.

Manini, I., Caponnetto, F., Bartolini, A., Ius, T., Mariuzzi, L., Di Loreto, C., Beltrami, A. & Cesselli, D. 2018. Role of microenvironment in glioma invasion: what we learned from in vitro models. *International Journal of Molecular Sciences,* 19**,** 147.

Mantovani, A., Allavena, P., Sica, A. & Balkwill, F. 2008. Cancer-related inflammation. *Nature,* 454**,** 436-444.

Marjanovic, N. D., Weinberg, R. A. & Chaffer, C. L. 2013. Cell plasticity and heterogeneity in cancer. *Clinical Chemistry,* 59**,** 168-179.

Marquez, R. T. & Xu, L. 2012. Bcl-2: Beclin 1 complex: multiple, mechanisms regulating autophagy/apoptosis toggle switch. *American Journal of Cancer Research,* 2**,** 214-221.

Martinez-Outschoorn, U. E., Pavlides, S., Howell, A., Pestell, R. G., Tanowitz, H. B., Sotgia, F. & Lisanti, M. P. 2011. Stromal–epithelial metabolic coupling in cancer: integrating autophagy and metabolism in the tumor microenvironment. *The International Journal of Biochemistry & Cell Biology,* 43**,** 1045-1051.

Martinvalet, D., Zhu, P. & Lieberman, J. 2005. Granzyme A induces caspase-independent mitochondrial damage, a required first step for apoptosis. *Immunity,* 22**,** 355-370.

Marullo, R., Werner, E., Degtyareva, N., Moore, B., Altavilla, G., Ramalingam, S. S. & Doetsch, P. W. 2013. Cisplatin induces a mitochondrial-ROS response that contributes to cytotoxicity depending on mitochondrial redox status and bioenergetic functions. *PloS One,* 8**,** e81162.

Masoud, G. N. & Li, W. 2015. HIF-1 alpha pathway: role, regulation and intervention for cancer therapy. *Acta Pharmaceutica Sinica B,* 5**,** 378-389.

Massey, T. & Robertson, N. 2018. Repurposing drugs to treat neurological diseases. *Journal of Neurology,* 265**,** 446-448.

Mather, J. P. & Roberts, P. E. 1998. Introduction to cell and tissue culture: theory and technique, *Springer Science & Business Media*.1.

Maturu, P., Jones, D., Ruteshouser, E. C., Hu, Q., Reynolds, J. M., Hicks, J., Putluri, N., Ekmekcioglu, S., Grimm, E. A. & Dong, C. 2017. Role of cyclooxygenase-2 pathway in creating an immunosuppressive microenvironment and in initiation and progression of Wilms' tumor. *Neoplasia,* 19**,** 237-249.

Maus, A. & Peters, G. J. 2017. Glutamate and α-ketoglutarate: key players in glioma metabolism. *Amino Acids,* 49**,** 21-32.

Maxwell, P. H., Pugh, C. W. & Ratcliffe, P. J. 2001. Activation of the HIF pathway in cancer. *Current Opinion in Genetics & Development,* 11**,** 293-299.

Mazumder, S., De, R., Debsharma, S., Bindu, S., Maity, P., Sarkar, S., Saha, S. J., Siddiqui, A. A., Banerjee, C. & Nag, S. 2019. Indomethacin impairs mitochondrial dynamics by activating the PKCζ–p38–DRP1 pathway and inducing apoptosis in gastric cancer and normal mucosal cells. *Journal of Biological Chemistry,* 294**,** 8238-8258.

Mcgirt, M. J., Chaichana, K. L., Gathinji, M., Attenello, F. J., Than, K., Olivi, A., Weingart, J. D., Brem, H. & Redo Quiñones-Hinojosa, A. 2009. Independent association of extent of resection with survival in patients with malignant brain astrocytoma. *Journal of Neurosurgery,* 110**,** 156-162.

Mcgranahan, T., Therkelsen, K. E., Ahmad, S. & Nagpal, S. 2019. Current State of Immunotherapy for Treatment of Glioblastoma. *Current Treatment Options in Oncology,* 20**,** 24.

Mckeown, S. 2014. Defining normoxia, physoxia and hypoxia in tumours—implications for treatment response. *The British Journal of Radiology,* 87**,** 12.

Mehta, G., Hsiao, A. Y., Ingram, M., Luker, G. D. & Takayama, S. 2012. Opportunities and challenges for use of tumor spheroids as models to test drug delivery and efficacy. *Journal of Controlled Release,* 164**,** 192-204.

Melguizo, C., Prados, J., González, B., Ortiz, R., Concha, A., Alvarez, P. J., Madeddu, R., Perazzoli, G., Oliver, J. A. & López, R. 2012. MGMT promoter methylation status and MGMT and CD133 immunohistochemical expression as prognostic markers in glioblastoma patients treated with temozolomide plus radiotherapy. *Journal of Translational Medicine,* 10**,** 250.

Melillo, G. 2004. HIF-1: a target for cancer, ischemia and inflammation—too good to be true? : Taylor & Francis.

Melstrom, K. & Sentovich, S. M. 2017. Colon and Rectal Surgical Emergencies. *Surgical Emergencies in the Cancer Patient. Springer***,** 177-187.

Mendelsohn, J. & Baselga, J. 2000. The EGF receptor family as targets for cancer therapy. *Oncogene,* 19**,** 6550-6565.

Merchant, T. E., Pollack, I. F. & Loeffler, J. S. Brain tumors across the age spectrum: biology, therapy, and late effects. Seminars in Radiation Oncology, 2010. Elsevier, 58-66.

Mestre, J. R., Subbaramaiah, K., Sacks, P. G., Schantz, S. P., Tanabe, T., Inoue, H. & Dannenberg, A. J. 1997. Retinoids suppress epidermal growth factor-induced transcription of cyclooxygenase-2 in human oral squamous carcinoma cells. *Cancer Research,* 57**,** 2890-2895.

Metallo, C. M., Gameiro, P. A., Bell, E. L., Mattaini, K. R., Yang, J., Hiller, K., Jewell, C. M., Johnson, Z. R., Irvine, D. J. & Guarente, L. 2012. Reductive glutamine metabolism by IDH1 mediates lipogenesis under hypoxia. *Nature,* 481**,** 380-U166.

Metzcar, J., Wang, Y., Heiland, R. & Macklin, P. 2019. A review of cell-based computational modeling in cancer biology. *JCO Clinical Cancer Informatics,* 2**,** 1-13.

Meyer, M., Reimand, J., Lan, X., Head, R., Zhu, X., Kushida, M., Bayani, J., Pressey, J. C., Lionel, A. C. & Clarke, I. D. 2015. Single cell-derived clonal analysis of human glioblastoma links functional and genomic heterogeneity. *Proceedings of the National Academy of Sciences,* 112**,** 851-856.

Michaud, M., Martins, I., Sukkurwala, A. Q., Adjemian, S., Ma, Y., Pellegatti, P., Shen, S., Kepp, O., Scoazec, M. & Mignot, G. 2011. Autophagy-dependent anticancer immune responses induced by chemotherapeutic agents in mice. *Science,* 334**,** 1573-1577.

Michelakis, E., Sutendra, G., Dromparis, P., Webster, L., Haromy, A., Niven, E., Maguire, C., Gammer, T.-L., Mackey, J. & Fulton, D. 2010. Metabolic modulation of glioblastoma with dichloroacetate. *Science Translational Medicine,* 2**,** 31ra34.

Milano, M. T., Okunieff, P., Donatello, R. S., Mohile, N. A., Sul, J., Walter, K. A. & Korones, D. N. 2010. Patterns and timing of recurrence after temozolomide-based chemoradiation for glioblastoma. *International Journal of Radiation Oncology* Biology* Physics,* 78**,** 1147-1155.

Miller, C. R. & Perry, A. 2007. Glioblastoma: morphologic and molecular genetic diversity. *Archives of Pathology & Laboratory Medicine,* 131**,** 397-406.

Miners, J. O. & Birkett, D. J. 1998. Cytochrome P4502C9: an enzyme of major importance in human drug metabolism. *British journal of clinical pharmacology,* 45**,** 525-538.

Minniti, G., Muni, R., Lanzetta, G., Marchetti, P. & Enrici, R. M. 2009. Chemotherapy for glioblastoma: current treatment and future perspectives for cytotoxic and targeted agents. *Anticancer research,* 29**,** 5171-5184.

Miranda-Goncalves, V., Honavar, M., Pinheiro, C., Martinho, O., Pires, M. M., Pinheiro, C., Cordeiro, M., Bebiano, G., Costa, P. & Palmeirim, I. 2012. Monocarboxylate transporters (MCTs) in gliomas: expression and exploitation as therapeutic targets. *Journal of Neuro-Oncology,* 15**,** 172-188.

Mitchell, P. 1978. Citation Classics - Chemiosmotic Coupling in Oxidative and Photosynthetic Phosphorylation. *Current Contents***,** 14-14.

Mitsudomi, T. & Yatabe, Y. 2010. Epidermal growth factor receptor in relation to tumor development: EGFR gene and cancer. *FEBS Journal,* 277**,** 301-308.

Mittal, S., Klinger, N. V., Michelhaugh, S. K., Barger, G. R., Pannullo, S. C. & Juhász, C. 2018. Alternating electric tumor treating fields for treatment of glioblastoma: rationale, preclinical, and clinical studies. *Journal of Neurosurgery,* 128**,** 414-421.

Miyashita, H., Nitta, Y., Mori, S., Kanzaki, A., Nakayama, K., Terada, K., Sugiyama, T., Kawamura, H., Sato, A. & Morikawa, H. 2003. Expression of copper-transporting P-type adenosine triphosphatase (ATP7B) as a chemoresistance marker in human oral squamous cell carcinoma treated with cisplatin. *Oral Oncology,* 39**,** 157-162.

Mizushima, N., Levine, B., Cuervo, A. M. & Klionsky, D. J. 2008. Autophagy fights disease through cellular self-digestion. *Nature,* 451**,** 1069-1075.

Mizushima, N., Yoshimori, T. & Levine, B. 2010. Methods in mammalian autophagy research. *Cell,* 140**,** 313-326.

Molenaar, R. J., Verbaan, D., Lamba, S., Zanon, C., Jeuken, J. W., Boots-Sprenger, S. H., Wesseling, P., Hulsebos, T. J., Troost, D. & Van Tilborg, A. A. 2014. The combination of IDH1 mutations and MGMT methylation status predicts survival in glioblastoma better than either IDH1 or MGMT alone. *Journal of Neuro-Oncology,* 16**,** 1263-1273.

Molina, M. A., Sitja-Arnau, M., Lemoine, M. G., Frazier, M. L. & Sinicrope, F. A. 1999. Increased cyclooxygenase-2 expression in human pancreatic carcinomas and cell lines: growth inhibition by nonsteroidal anti-inflammatory drugs. *Cancer research,* 59**,** 4356-4362.

Momekov, G., Bakalova, A. & Karaivanova, M. 2005. Novel approaches towards development of non-classical platinum-based antineoplastic agents: design of platinum complexes characterized by an alternative DNA-binding pattern and/or tumor-targeted cytotoxicity. *Current Medicinal Chemistry,* 12**,** 2177-2191.

Momekov, G., Ferdinandov, D., Bakalova, A., Zaharieva, M., Konstantinov, S. & Karaivanova, M. 2006. In vitro toxicological evaluation of a dinuclear platinum (II) complex with acetate ligands. *Archives of Toxicology,* 80**,** 555-560.

Montezuma, M. a. P., Fonseca, F. P., Benites, B. M., Soares, C. D., Do Amaral-Silva, G. K., De Almeida, O. P., Soares, F. A., Pagano, R. L. & Fregnani, E. R. 2018. COX-2 as a determinant of lower disease-free survival for patients affected by ameloblastoma. *Pathology-Research and Practice,* 214**,** 907-913.

Mookerjee, S. A., Goncalves, R. L., Gerencser, A. A., Nicholls, D. G. & Brand, M. D. 2015. The contributions of respiration and glycolysis to extracellular acid production. *Biochimica Et Biophysica Acta (BBA)-Bioenergetics,* 1847**,** 171-181.

Mookerjee, S. A., Nicholls, D. G. & Brand, M. D. 2016. Determining maximum glycolytic capacity using extracellular flux measurements. *PLoS One,* 11**,** e0152016.

Mori, R., Wang, Q., Danenberg, K. D., Pinski, J. K. & Danenberg, P. V. 2008. Both β-actin and GAPDH are useful reference genes for normalization of quantitative RT-PCR in human FFPE tissue samples of prostate cancer. *The Prostate,* 68**,** 1555-1560.

Mori, T., Fujiwara, Y., Yano, M., Tamura, S., Yasuda, T., Takiguchi, S. & Monden, M. 2003. Prevention of peritoneal metastasis of human gastric cancer cells in nude mice by S-1, a novel oral derivative of 5-fluorouracil. *Oncology,* 64**,** 176-182.

Morita, T. 1995. Low pH leads to sister-chromatid exchanges and chromosomal aberrations, and its clastogenicity is S-dependent. *Mutation Research/Environmental Mutagenesis and Related Subjects,* 334**,** 301-308.

Morselli, E., Galluzzi, L., Kepp, O., Marino, G., Michaud, M., Vitale, I., Maiuri, M. C. & Kroemer, G. 2011. Oncosuppressive functions of autophagy. *Antioxidants & Redox Signaling,* 14**,** 2251-2269.

Mosmann, T. 1983. Rapid colorimetric assay for cellular growth and survival: application to proliferation and cytotoxicity assays. *Journal of Immunological Methods,* 65**,** 55-63.

Mostofa, A., Punganuru, S. R., Madala, H. R., Al-Obaide, M. & Srivenugopal, K. S. 2017. The process and regulatory components of inflammation in brain oncogenesis. *Biomolecules,* 7**,** 34.

Movafagh, S., Crook, S. & Vo, K. 2015. Regulation of hypoxia-inducible factor-1a by reactive oxygen species: new developments in an old debate. *Journal of Cellular Biochemistry,* 116**,** 696-703.

Mullen, A. R., Wheaton, W. W., Jin, E. S., Chen, P.-H., Sullivan, L. B., Cheng, T., Yang, Y., Linehan, W. M., Chandel, N. S. & Deberardinis, R. J. 2012. Reductive carboxylation supports growth in tumour cells with defective mitochondria. *Nature,* 481**,** 385-U171.

Munn, L. L. 2017. Cancer and inflammation. *Wiley Interdisciplinary Reviews: Systems Biology and Medicine,* 9**,** e1370.

Munoz, J. L., Rodriguez-Cruz, V., Greco, S. J., Nagula, V., Scotto, K. W. & Rameshwar, P. 2014. Temozolomide induces the production of epidermal growth factor to regulate MDR1 expression in glioblastoma cells. *Molecular Cancer Therapeutics,* 13**,** 2399-2411.

Munoz, J. L., Walker, N. D., Scotto, K. W. & Rameshwar, P. 2015. Temozolomide competes for P-glycoprotein and contributes to chemoresistance in glioblastoma cells. *Cancer Letters,* 367**,** 69-75.

Murai, J., Zhang, Y., Morris, J., Ji, J., Takeda, S., Doroshow, J. H. & Pommier, Y. 2014. Rationale for poly (ADP-ribose) polymerase (PARP) inhibitors in combination therapy with camptothecins or temozolomide based on PARP trapping versus catalytic inhibition. *Journal of Pharmacology and Experimental Therapeutics,* 349**,** 408-416.

Murat, A., Migliavacca, E., Hussain, S. F., Heimberger, A. B., Desbaillets, I., Hamou, M.-F., Rüegg, C., Stupp, R., Delorenzi, M. & Hegi, M. E. 2009. Modulation of angiogenic and inflammatory response in glioblastoma by hypoxia. *PloS One,* 4**,** e5947.

Murteira, S., Millier, A. & Toumi, M. 2014. Drug repurposing in pharmaceutical industry and its impact on market access: market access implications. *Journal of Market Access & Health Policy,* 2**,** 22814.

Musah-Eroje, A. & Watson, S. 2019. A novel 3D in vitro model of glioblastoma reveals resistance to temozolomide which was potentiated by hypoxia. *Journal of Neuro-Oncology*, 1-10.

Muz, B., De La Puente, P., Azab, F. & Azab, A. K. 2015. The role of hypoxia in cancer progression, angiogenesis, metastasis, and resistance to therapy. *Hypoxia,* 3, 83-92.

Mylonis, I., Simos, G. & Paraskeva, E. 2019. Hypoxia-Inducible Factors and the Regulation of Lipid Metabolism. *Cells,* 8, E214.

Nabors, L. B., Portnow, J., Ammirati, M., Baehring, J., Brem, H., Butowski, N., Fenstermaker, R. A., Forsyth, P., Hattangadi-Gluth, J. & Holdhoff, M. 2017. NCCN guidelines insights: central nervous system cancers, version 1.2017. *Journal of the National Comprehensive Cancer Network,* 15, 1331-1345.

Naik, P. & Cucullo, L. 2012. In vitro blood-brain barrier models: Current and perspective technologies. *Journal of Pharmaceutical Sciences,* 101, 1337-1354.

Nan, H., Hutter, C. M., Lin, Y., Jacobs, E. J., Ulrich, C. M., White, E., Baron, J. A., Berndt, S. I., Brenner, H. & Butterbach, K. 2015. Association of aspirin and NSAID use with risk of colorectal cancer according to genetic variants. *Jama,* 313, 1133-1142.

Narita, Y. 2015. Bevacizumab for glioblastoma. *Therapeutics and Clinical Risk Management,* 11, 1759-1765.

Natarajan, M., Stewart, J. E., Golemis, E. A., Pugacheva, E. N., Alexandropoulos, K., Cox, B. D., Wang, W., Grammer, J. R. & Gladson, C. L. 2006. HEF1 is a necessary and specific downstream effector of FAK that promotes the migration of glioblastoma cells. *Oncogene,* 25, 1721-1732.

Navone, S. E., Guarnaccia, L., Cordiglieri, C., Crisà, F. M., Caroli, M., Locatelli, M., Schisano, L., Rampini, P., Miozzo, M. & La Verde, N. 2018. Aspirin affects tumor angiogenesis and sensitizes human glioblastoma endothelial cells to temozolomide, bevacizumab, and sunitinib, impairing vascular endothelial growth factor-related signaling. *World Neurosurgery,* 120, e380-e391.

Nederman, T., Carlsson, J. & Malmqvist, M. 1981. Penetration of substances into tumor tissue—a methodological study on cellular spheroids. *In Vitro,* 17, 290-298.

Nelson, R. L., Davis, F. G., Sutter, E., Sobin, L. H., Kikendall, J. W. & Bowen, P. 1994. Body iron stores and risk of colonic neoplasia. *JNCI: Journal of the National Cancer Institute,* 86, 455-460.

Neto, A., Correia, C., Oliveira, M., Rial-Hermida, M., Alvarez-Lorenzo, C., Reis, R. & Mano, J. 2015. A novel hanging spherical drop system for the generation of cellular spheroids and high throughput combinatorial drug screening. *Biomaterials Science,* 3, 581-585.

Network, C. G. a. R. 2008. Comprehensive genomic characterization defines human glioblastoma genes and core pathways. *Nature,* 455, 1061.

Neuwelt, E. A., Frenkel, E. P., Diehl, J., Vu, L., Rapoport, S. & Hill, S. 1980. Reversible osmotic blood-brain barrier disruption in humans: implications for the chemotherapy of malignant brain tumors. *Neurosurgery,* 7, 44-52.

Newsholme, E., Crabtree, B. & Ardawi, M. 1985. The role of high rates of glycolysis and glutamine utilization in rapidly dividing cells. *Bioscience Reports,* 5, 393-400.

Nicholls, D. G., Darley-Usmar, V. M., Wu, M., Jensen, P. B., Rogers, G. W. & Ferrick, D. A. 2010. Bioenergetic profile experiment using C2C12 myoblast cells. *JoVE (Journal of Visualized Experiments)*, e2511.

Nikoletopoulou, V., Markaki, M., Palikaras, K. & Tavernarakis, N. 2013. Crosstalk between apoptosis, necrosis and autophagy. *Biochimica et Biophysica Acta (BBA)-Molecular Cell Research,* 1833**,** 3448-3459.

Noda, K., Nishiwaki, Y., Kawahara, M., Negoro, S., Sugiura, T., Yokoyama, A., Fukuoka, M., Mori, K., Watanabe, K. & Tamura, T. 2002. Irinotecan plus cisplatin compared with etoposide plus cisplatin for extensive small-cell lung cancer. *New England Journal of Medicine,* 346**,** 85-91.

Nogueira, L., Ruiz-Ontanon, P., Vazquez-Barquero, A., Moris, F. & Fernandez-Luna, J. L. 2011. The NFkappaB pathway: a therapeutic target in glioblastoma. *Oncotarget,* 2**,** 646-53.

Nojima, H. 1997. Cell cycle checkpoints, chromosome stability and the progression of cancer. *Human Cell,* 10**,** 221-230.

Nomura, N., Nomura, M., Sugiyama, K. & Hamada, J. I. 2007. Phorbol 12-myristate 13-acetate (PMA)-induced migration of glioblastoma cells is mediated via p38MAPK/Hsp27 pathway. *Biochemical Pharmacology,* 74**,** 690-701.

Norenberg, M. D., Mozes, L. W., Gregorios, J. B. & Norenberg, L.-O. B. 1987. Effects of lactic acid on astrocytes in primary culture. *Journal of Neuropathology & Experimental Neurology,* 46**,** 154-166.

Normanno, N., De Luca, A., Bianco, C., Strizzi, L., Mancino, M., Maiello, M. R., Carotenuto, A., De Feo, G., Caponigro, F. & Salomon, D. S. 2006. Epidermal growth factor receptor (EGFR) signaling in cancer. *Gene,* 366**,** 2-16.

Nørøxe, D. S., Poulsen, H. S. & Lassen, U. 2016. Hallmarks of glioblastoma: a systematic review. *ESMO Open,* 1**,** e000144.

Novakova, I., Subileau, E.-A., Toegel, S., Gruber, D., Lachmann, B., Urban, E., Chesne, C., Noe, C. R. & Neuhaus, W. 2014. Transport rankings of non-steroidal antiinflammatory drugs across blood-brain barrier in vitro models. *PloS One,* 9**,** e86806.

Nunes, A. S., Barros, A. S., Costa, E. C., Moreira, A. F. & Correia, I. J. 2019. 3D tumor spheroids as *in vitro* models to mimic in vivo human solid tumors resistance to therapeutic drugs. *Biotechnology and Bioengineering,* 116**,** 206-226.

O'brien, V. & Brown, R. 2006. Signalling cell cycle arrest and cell death through the MMR System. *Carcinogenesis,* 27**,** 682-692.

Ochs, K. & Kaina, B. 2000. Apoptosis induced by DNA damage O-6-methylguanine is Bcl-2 and caspase-9/3 regulated and Fas/caspase-8 independent. *Cancer Research,* 60**,** 5815-5824.

Ohba, S., Hirose, Y., Kawase, T. & Sano, H. 2009. Inhibition of c-Jun N-terminal kinase enhances temozolomide-induced cytotoxicity in human glioma cells. *Journal of Neuro-Oncology,* 95**,** 307-316.

Ohgaki, H., Dessen, P., Jourde, B., Horstmann, S., Nishikawa, T., Di Patre, P.-L., Burkhard, C., Schüler, D., Probst-Hensch, N. M. & Maiorka, P. C. 2004. Genetic pathways to glioblastoma: a population-based study. *Cancer Research,* 64**,** 6892-6899.

Ohgaki, H. & Kleihues, P. 2007. Genetic pathways to primary and secondary glioblastoma. *The American Journal of Pathology,* 170**,** 1445-1453.

Ohgaki, H. & Kleihues, P. 2013. The definition of primary and secondary glioblastoma. *Clinical Cancer Research,* 19**,** 764-772.

Ohka, F., Natsume, A., Motomura, K., Kishida, Y., Kondo, Y., Abe, T., Nakasu, Y., Namba, H., Wakai, K. & Fukui, T. 2011. The global DNA methylation surrogate LINE-1

methylation is correlated with MGMT promoter methylation and is a better prognostic factor for glioma. *PloS One,* 6**,** e23332.

Okuyama, H., Endo, H., Akashika, T., Kato, K. & Inoue, M. 2010. Downregulation of c-MYC protein levels contributes to cancer cell survival under dual deficiency of oxygen and glucose. *Cancer Research,* 70**,** 10213-10223.

Olbryt, M., Habryka, A., Student, S., Jarząb, M., Tyszkiewicz, T. & Lisowska, K. M. 2014. Global gene expression profiling in three tumor cell lines subjected to experimental cycling and chronic hypoxia. *PLoS One,* 9**,** e105104.

Oliva, C. R., Nozell, S. E., Diers, A., Mcclugage, S. G., Sarkaria, J. N., Markert, J. M., Darley-Usmar, V. M., Bailey, S. M., Gillespie, G. Y. & Landar, A. 2010. Acquisition of temozolomide chemoresistance in gliomas leads to remodeling of mitochondrial electron transport chain. *Journal of Biological Chemistry,* 285**,** 39759-39767.

Omar, A. I. & Mason, W. P. 2009. Temozolomide: The evidence for its therapeutic efficacy in malignant astrocytomas. *Core Evidence,* 4**,** 93-111.

Ortega, J., Li, J. Y., Lee, S., Tong, D., Gu, L. & Li, G.-M. 2015. Phosphorylation of PCNA by EGFR inhibits mismatch repair and promotes misincorporation during DNA synthesis. *Proceedings of the National Academy of Sciences,* 112**,** 5667-5672.

Ostrom, Q. T., Gittleman, H., Liao, P., Rouse, C., Chen, Y., Dowling, J., Wolinsky, Y., Kruchko, C. & Barnholtz-Sloan, J. 2014. CBTRUS statistical report: primary brain and central nervous system tumors diagnosed in the United States in 2007–2011. *Neuro-oncology,* 16**,** iv1-iv63.

Ostrom, Q. T., Gittleman, H., Liao, P., Vecchione-Koval, T., Wolinsky, Y., Kruchko, C. & Barnholtz-Sloan, J. S. 2017. CBTRUS statistical report: primary brain and other central nervous system tumors diagnosed in the United States in 2010–2014. *Neuro-oncology,* 19**,** v1-v88.

Osuka, S., Takano, S., Watanabe, S., Ishikawa, E., Yamamoto, T. & Matsumura, A. 2012. Valproic acid inhibits angiogenesis in vitro and glioma angiogenesis in vivo in the brain. *Neurologia Medico-Chirurgica,* 52**,** 186-193.

Osuka, S. & Van Meir, E. G. 2017. Overcoming therapeutic resistance in glioblastoma: the way forward. *Journal of Clinical Investigation,* 127**,** 415-426.

Ouyang, N., Williams, J. L. & Rigas, B. 2008. NO-donating aspirin inhibits angiogenesis by suppressing VEGF expression in HT-29 human colon cancer mouse xenografts. *Carcinogenesis,* 29**,** 1794-1798.

Palumbo, S., Pirtoli, L., Tini, P., Cevenini, G., Calderaro, F., Toscano, M., Miracco, C. & Comincini, S. 2012. Different involvement of autophagy in human malignant glioma cell lines undergoing irradiation and temozolomide combined treatments. *Journal of Cellular Biochemistry,* 113**,** 2308-2318.

Pampaloni, F., Reynaud, E. G. & Stelzer, E. H. 2007. The third dimension bridges the gap between cell culture and live tissue. *Nature Reviews Molecular Cell Biology,* 8**,** 839-845.

Panet-Raymond, V., Ansbacher, W., Zavgorodni, S., Bendorffe, B., Nichol, A., Truong, P. T., Beckham, W. & Vlachaki, M. 2012. Coplanar versus noncoplanar intensity-modulated radiation therapy (IMRT) and volumetric-modulated arc therapy (VMAT) treatment planning for fronto-temporal high-grade glioma. *Journal of Applied Clinical Medical Physics,* 13**,** 44-53.

Pangburn, H. A., Ahnen, D. J. & Rice, P. L. 2010. Sulindac metabolites induce proteosomal and lysosomal degradation of the epidermal growth factor receptor. *Cancer Prevention Research (Phila),* 3**,** 560-572.

Pangburn, H. A., Kraus, H., Ahnen, D. J. & Rice, P. L. 2005. Sulindac metabolites inhibit epidermal growth factor receptor activation and expression. *Journal of Carcinogenesis,* 4**,** 16.

Pantuck, A. J., Zeng, G., Belldegrun, A. S. & Figlin, R. A. 2003. Pathobiology, prognosis, and targeted therapy for renal cell carcinoma: exploiting the hypoxia-induced pathway. *Clinical Cancer Research,* 9**,** 4641-4652.

Pantziarka, P., Bouche, G., Meheus, L., Sukhatme, V., Sukhatme, V. P. & Vikas, P. 2014. The Repurposing Drugs in Oncology (ReDO) Project. *Ecancermedicalscience,* 8**,** 442.

Paolillo, M., Boselli, C. & Schinelli, S. 2018. Glioblastoma under siege: an overview of current therapeutic strategies. *Brain Sciences,* 8**,** 15.

Papandreou, I., Cairns, R. A., Fontana, L., Lim, A. L. & Denko, N. C. 2006. HIF-1 mediates adaptation to hypoxia by actively downregulating mitochondrial oxygen consumption. *Cell Metabolism,* 3**,** 187-197.

Pardo, J., Bosque, A., Brehm, R., Wallich, R., Naval, J., Müllbacher, A., Anel, A. & Simon, M. M. 2004. Apoptotic pathways are selectively activated by granzyme A and/or granzyme B in CTL-mediated target cell lysis. *Journal of Cell Biology,* 167**,** 457-468.

Park, D. M. & Rich, J. N. 2009. Biology of glioma cancer stem cells. *Molecules and Cells,* 28**,** 7-12.

Park, S.-H., Won, J., Kim, S.-I., Lee, Y., Park, C.-K., Kim, S.-K. & Choi, S.-H. 2017. Molecular testing of brain tumor. *Journal of Pathology and Translational Medicine,* 51**,** 205-223.

Parzych, K. R. & Klionsky, D. J. 2014. An overview of autophagy: morphology, mechanism, and regulation. *Antioxidants & Redox Signaling,* 20**,** 460-473.

Patel, M. A., Kim, J. E., Ruzevick, J., Li, G. & Lim, M. 2014. The future of glioblastoma therapy: synergism of standard of care and immunotherapy. *Cancers (Basel),* 6**,** 1953-1985.

Pathak, R. K., Marrache, S., Choi, J. H., Berding, T. B. & Dhar, S. 2014. The prodrug platin-A: simultaneous release of cisplatin and aspirin. *Angewandte Chemie,* 53**,** 1963-1967.

Pathi, S., Jutooru, I., Chadalapaka, G., Nair, V., Lee, S. O. & Safe, S. 2012. Aspirin inhibits colon cancer cell and tumor growth and downregulates specificity protein (Sp) transcription factors. *PLoS One,* 7**,** e48208.

Patrignani, P., Sacco, A., Sostres, C., Bruno, A., Dovizio, M., Piazuelo, E., Di Francesco, L., Contursi, A., Zucchelli, M. & Schiavone, S. 2017. Low-Dose Aspirin Acetylates Cyclooxygenase-1 in Human Colorectal Mucosa: Implications for the Chemoprevention of Colorectal Cancer. *Clinical Pharmacology & Therapeutics,* 102**,** 52-61.

Patrono, C., Baigent, C., Hirsh, J. & Roth, G. 2008. Antiplatelet drugs: American College of Chest Physicians evidence-based clinical practice guidelines. *Chest,* 133**,** 199S-233S.

Paul, I., Bhattacharya, S., Chatterjee, A. & Ghosh, M. K. 2013. Current Understanding on EGFR and Wnt/beta-Catenin Signaling in Glioma and Their Possible Crosstalk. *Genes Cancer,* 4**,** 427-446.

Perche, F. & Torchilin, V. P. 2012. Cancer cell spheroids as a model to evaluate chemotherapy protocols. *Cancer Biology & Therapy,* 13**,** 1205-1213.

Pérez, J. E., Fritzell, S., Kopecky, J., Visse, E., Darabi, A. & Siesjö, P. 2019. The effect of locally delivered cisplatin is dependent on an intact immune function in an experimental glioma model. *Scientific Reports,* 9**,** 5632.

Perry, J. E., Grossmann, M. E. & Tindall, D. J. 1998. Epidermal growth factor induces cyclin D1 in a human prostate cancer cell line. *The Prostate,* 35**,** 117-124.

Perry, S. W., Norman, J. P., Barbieri, J., Brown, E. B. & Gelbard, H. A. 2011. Mitochondrial membrane potential probes and the proton gradient: a practical usage guide. *Biotechniques,* 50**,** 98-115.

Persano, L., Pistollato, F., Rampazzo, E., Della Puppa, A., Abbadi, S., Frasson, C., Volpin, F., Indraccolo, S., Scienza, R. & Basso, G. 2012. BMP2 sensitizes glioblastoma stem-like cells to Temozolomide by affecting HIF-1 alpha stability and MGMT expression. *Cell Death & Disease,* 3**,** e412.

Persano, L., Rampazzo, E., Della Puppa, A., Pistollato, F. & Basso, G. 2011. The three-layer concentric model of glioblastoma: cancer stem cells, microenvironmental regulation, and therapeutic implications. *The Scientific World Journal,* 11**,** 1829-1841.

Petinou, V., Perry, C. J., Nicholl, I. D., Singh, J., Lea, R. W. & Welsby, P. J. 2014. Characterisation of a Novel Aspirin Analogue in Malignant Glioma. *Journal of Neuro-Oncology,* 16**,** 17-68.

Petrova, V., Annicchiarico-Petruzzelli, M., Melino, G. & Amelio, I. 2018. The hypoxic tumour microenvironment. *Oncogenesis,* 7**,** 10.

Phuphanich, S., Wheeler, C. J., Rudnick, J. D., Mazer, M., Wang, H., Nuno, M. A., Richardson, J. E., Fan, X., Ji, J. & Chu, R. M. 2013. Phase I trial of a multi-epitope-pulsed dendritic cell vaccine for patients with newly diagnosed glioblastoma. *Cancer Immunology, Immunotherapy,* 62**,** 125-135.

Pilkington, G. J. 2001. Brain Tumors in the Elderly. *Pathology of the Aging Human Nervous System,* 2**,** 408-428.

Pistollato, F., Abbadi, S., Rampazzo, E., Persano, L., Della Puppa, A., Frasson, C., Sarto, E., Scienza, R., D'avella, D. & Basso, G. 2010. Intratumoral hypoxic gradient drives stem cells distribution and MGMT expression in glioblastoma. *Stem Cells,* 28**,** 851-862.

Pless, M., Droege, C., Von Moos, R., Salzberg, M. & Betticher, D. 2013. A phase I/II trial of Tumor Treating Fields (TTFields) therapy in combination with pemetrexed for advanced non-small cell lung cancer. *Lung Cancer,* 81**,** 445-450.

Poch, B., Gansauge, F., Schwarz, A., Seufferlein, T., Schnelldorfer, T., Ramadani, M., Beger, H. G. & Gansauge, S. 2001. Epidermal growth factor induces cyclin D1 in human pancreatic carcinoma: evidence for a cyclin D1–dependent cell cycle progression. *Pancreas,* 23**,** 280-287.

Podolsky, S. H. & Greene, J. A. 2011. Combination drugs--hype, harm, and hope. *The New England Journal of Medicine* 365**,** 488-491.

Pohl, U., Wagenknecht, B., Naumann, U. & Weller, M. 1999. p53 enhances BAK and CD95 expression in human malignant glioma cells but does not enhance CD95L-induced apoptosis. *Cell Physiol Biochem,* 9**,** 29-37.

Pore, N., Jiang, Z., Gupta, A., Cerniglia, G., Kao, G. D. & Maity, A. 2006. EGFR tyrosine kinase inhibitors decrease VEGF expression by both hypoxia-inducible factor (HIF)-1-independent and HIF-1-dependent mechanisms. *Cancer Research,* 66**,** 3197-3204.

Poteet, E., Choudhury, G. R., Winters, A., Li, W., Ryou, M.-G., Liu, R., Tang, L., Ghorpade, A., Wen, Y. & Yuan, F. 2013. Reversing the Warburg effect as a treatment for glioblastoma. *Journal of Biological Chemistry,* 288**,** 9153-9164.

Pötzl, J., Roser, D., Bankel, L., Hömberg, N., Geishauser, A., Brenner, C. D., Weigand, M., Röcken, M. & Mocikat, R. 2017. Reversal of tumor acidosis by systemic buffering reactivates NK cells to express IFN-γ and induces NK cell-dependent lymphoma control without other immunotherapies. *International Journal of Cancer,* 140**,** 2125-2133.

Pouysségur, J., Dayan, F. & Mazure, N. M. 2006. Hypoxia signalling in cancer and approaches to enforce tumour regression. *Nature,* 441**,** 437-443.

Powell, J. D., Pollizzi, K. N., Heikamp, E. B. & Horton, M. R. 2012. Regulation of immune responses by mTOR. *Annual Review of Immunology,* 30**,** 39-68.

Preusser, M., De Ribaupierre, S., Wöhrer, A., Erridge, S. C., Hegi, M., Weller, M. & Stupp, R. 2011. Current concepts and management of glioblastoma. *Annals of Neurology,* 70**,** 9-21.

Pu, P., Zhang, Z., Kang, C., Jiang, R., Jia, Z., Wang, G. & Jiang, H. 2009. Downregulation of Wnt2 and beta-catenin by siRNA suppresses malignant glioma cell growth. *Cancer Gene Therapy,* 16**,** 351-361.

Puzone, R., Savarino, G., Salvi, S., Dal Bello, M. G., Barletta, G., Genova, C., Rijavec, E., Sini, C., Esposito, A. I. & Ratto, G. B. 2013. Glyceraldehyde-3-phosphate dehydrogenase gene over expression correlates with poor prognosis in non small cell lung cancer patients. *Molecular Cancer,* 12**,** 97.

Qazi, M. A., Vora, P., Venugopal, C., Sidhu, S. S., Moffat, J., Swanton, C. & Singh, S. K. 2017. Intratumoral heterogeneity: pathways to treatment resistance and relapse in human glioblastoma. *The Annals of Oncology,* 28**,** 1448-1456.

Qin, L. F. & Ng, I. O. L. 2002. Induction of apoptosis by cisplatin and its effect on cell cycle-related proteins and cell cycle changes in hepatoma cells. *Cancer Letters,* 175**,** 27-38.

Qiu, B., Wang, Y., Tao, J. & Wang, Y. 2012. Expression and correlation of Bcl-2 with pathological grades in human glioma stem cells. *Oncology Reports,* 28**,** 155-160.

Quah, B. J. & Parish, C. R. 2010. The use of carboxyfluorescein diacetate succinimidyl ester (CFSE) to monitor lymphocyte proliferation. *Journal of Visualized Experiments,* 2010**,** e2259.

Rahman, R., Smith, S., Rahman, C. & Grundy, R. 2010. Antiangiogenic therapy and mechanisms of tumor resistance in malignant glioma. *Journal of Oncology,* 2010**,** 251231.

Rai, R., Banerjee, M., Wong, D. H., Mccullagh, E., Gupta, A., Tripathi, S., Riquelme, E., Jangir, R., Yadav, S. & Raja, M. 2016. Temozolomide analogs with improved brain/plasma ratios–Exploring the possibility of enhancing the therapeutic index of temozolomide. *Bioorganic & Medicinal Chemistry Letters,* 26**,** 5103-5109.

Ralph, S., Pritchard, R., Rodríguez-Enríquez, S., Moreno-Sánchez, R. & Ralph, R. 2015. Hitting the Bull's-Eye in Metastatic Cancers—NSAIDs Elevate ROS in Mitochondria, Inducing Malignant Cell Death. *Pharmaceuticals,* 8**,** 62-106.

Ramaiahgari, S. C., Den Braver, M. W., Herpers, B., Terpstra, V., Commandeur, J. N., Van De Water, B. & Price, L. S. 2014. A 3D in vitro model of differentiated HepG2 cell spheroids with improved liver-like properties for repeated dose high-throughput toxicity studies. *Archives of Toxicology,* 88**,** 1083-1095.

Ramer, R., Eichele, K. & Hinz, B. 2007. Upregulation of tissue inhibitor of matrix metalloproteinases-1 confers the anti-invasive action of cisplatin on human cancer cells. *Oncogene,* 26**,** 5822-5827.

Rampersad, S. N. 2012. Multiple Applications of Alamar Blue as an Indicator of Metabolic Function and Cellular Health in Cell Viability Bioassays. *Sensors,* 12**,** 12347-12360.

Rampling, R., Cruickshank, G., Lewis, A. D., Fitzsimmons, S. A. & Workman, P. 1994. Direct measurement of pO2 distribution and bioreductive enzymes in human malignant brain tumors. *International Journal of Radiation Oncology* Biology* Physics,* 29**,** 427-431.

Ravikumar, B., Futter, M., Jahreiss, L., Korolchuk, V. I., Lichtenberg, M., Luo, S., Massey, D. C., Menzies, F. M., Narayanan, U. & Renna, M. 2009. Mammalian macroautophagy at a glance. *Journal of Cell Science,* 122**,** 1707-1711.

Raza, H. & John, A. 2012. Implications of altered glutathione metabolism in aspirin-induced oxidative stress and mitochondrial dysfunction in HepG2 cells. *PloS One,* 7**,** e36325.

Raza, H., John, A. & Benedict, S. 2011. Acetylsalicylic acid-induced oxidative stress, cell cycle arrest, apoptosis and mitochondrial dysfunction in human hepatoma HepG2 cells. *European journal of pharmacology,* 668**,** 15-24.

Reardon, D. A., Freeman, G., Wu, C., Chiocca, E. A., Wucherpfennig, K. W., Wen, P. Y., Fritsch, E. F., Curry, W. T., Sampson, J. H. & Dranoff, G. 2014. Immunotherapy advances for glioblastoma. *Journal of Neuro-Oncology,* 16**,** 1441-1458.

Reddy, K., Damek, D., Gaspar, L. E., Ney, D., Waziri, A., Lillehei, K., Stuhr, K., Kavanagh, B. D. & Chen, C. 2012. Phase II trial of hypofractionated IMRT with temozolomide for patients with newly diagnosed glioblastoma multiforme. *International Journal of Radiation Oncology* Biology* Physics,* 84**,** 655-660.

Reifenberger, G., Wirsching, H.-G., Knobbe-Thomsen, C. B. & Weller, M. 2017. Advances in the molecular genetics of gliomas—implications for classification and therapy. *Nature Reviews Clinical Oncology,* 14**,** 434-452.

Retsky, M., Rogers, R., Demicheli, R., Hrushesky, W. J., Gukas, I., Vaidya, J. S., Baum, M., Forget, P., Dekock, M. & Pachmann, K. 2012. NSAID analgesic ketorolac used perioperatively may suppress early breast cancer relapse: particular relevance to triple negative subgroup. *Breast Cancer Research and Treatment,* 134**,** 881-888.

Revillion, F., Pawlowski, V., Hornez, L. & Peyrat, J.-P. 2000. Glyceraldehyde-3-phosphate dehydrogenase gene expression in human breast cancer. *European Journal of Cancer,* 36**,** 1038-1042.

Richards, R., Jenkinson, M. D., Haylock, B. J. & See, V. 2016. Cell cycle progression in glioblastoma cells is unaffected by pathophysiological levels of hypoxia. *PeerJ,* 4**,** e1755.

Rieber, M. & Rieber, M. S. 2006. Cyclin D1 overexpression induces epidermal growth factor-independent resistance to apoptosis linked to BCL-2 in human A431 carcinoma. *Apoptosis,* 11**,** 121-129.

Rieber, M. & Rieber, M. S. 2006. Cyclin D1 overexpression induces epidermal growth factor-independent resistance to apoptosis linked to BCL-2 in human A431 carcinoma. *Apoptosis,* 11**,** 121-9.

Rieder, C. L. 2011. Mitosis in vertebrates: the G2/M and M/A transitions and their associated checkpoints. *Chromosome Research,* 19**,** 291-306.

Rieger, A. M., Hall, B. E., Le, T. L., Schang, L. M. & Barreda, D. R. 2010. Conventional apoptosis assays using propidium iodide generate a significant number of false

positives that prevent accurate assessment of cell death. *Journal of Immunological Methods,* 358**,** 81-92.

Riss, T. L., Moravec, R. A., Niles, A. L., Duellman, S., Benink, H. A., Worzella, T. J. & Minor, L. 2004. Cell Viability Assays. *Assay Guidance Manual.* Bethesda (MD).

Robey, I. F., Baggett, B. K., Kirkpatrick, N. D., Roe, D. J., Dosescu, J., Sloane, B. F., Hashim, A. I., Morse, D. L., Raghunand, N. & Gatenby, R. A. 2009. Bicarbonate increases tumor pH and inhibits spontaneous metastases. *Cancer Research,* 69**,** 2260-2268.

Rocha, C. R. R., Silva, M. M., Quinet, A., Cabral-Neto, J. B. & Menck, C. F. M. 2018. DNA repair pathways and cisplatin resistance: an intimate relationship. *Clinics,* 73**,** e478s.

Roderick, P., Wilkes, H. & Meade, T. 1993. The gastrointestinal toxicity of aspirin: an overview of randomised controlled trials. *British Journal of Clinical Pharmacology,* 35**,** 219-226.

Rodrı´ Guez, L. a. G. A., Az, S. H. D. & De Abajo, F. J. 2001. Association between aspirin and upper gastrointestinal complications: systematic review of epidemiologic studies. *British Journal of Clinical Pharmacology,* 52**,** 563-571.

Rodríguez, L. a. G., Martín-Pérez, M., Hennekens, C. H., Rothwell, P. M. & Lanas, A. 2016. Bleeding risk with long-term low-dose aspirin: a systematic review of observational studies. *PLoS One,* 11**,** e0160046.

Rodríguez, M. E., Arévalo, D. E., Sanabria, L. M., Carrión, F. D. C., Fanelli, M. A. & Rivarola, V. A. 2019. Heat shock protein 27 modulates autophagy and promotes cell survival after photodynamic therapy. *Photochemical & Photobiological Sciences,* 18**,** 546-554.

Rofstad, E. K., Galappathi, K., Mathiesen, B. & Ruud, E.-B. M. 2007. Fluctuating and diffusion-limited hypoxia in hypoxia-induced metastasis. *Clinical Cancer Research,* 13**,** 1971-1978.

Rogatzki, M. J., Ferguson, B. S., Goodwin, M. L. & Gladden, L. B. 2015. Lactate is always the end product of glycolysis. *Frontiers in Neuroscience,* 9**,** 22.

Rohwer, N., Dame, C., Haugstetter, A., Wiedenmann, B., Detjen, K., Schmitt, C. A. & Cramer, T. 2010. Hypoxia-inducible factor 1alpha determines gastric cancer chemosensitivity via modulation of p53 and NF-kappaB. *PLoS One,* 5**,** e12038.

Rong, Y., Durden, D. L., Van Meir, E. G. & Brat, D. J. 2006. 'Pseudopalisading'necrosis in glioblastoma: a familiar morphologic feature that links vascular pathology, hypoxia, and angiogenesis. *Journal of Neuropathology & Experimental Neurology,* 65**,** 529-539.

Roos, W. P., Batista, L. F., Naumann, S. C., Wick, W., Weller, M., Menck, C. F. & Kaina, B. 2007. Apoptosis in malignant glioma cells triggered by the temozolomide-induced DNA lesion O6-methylguanine. *Oncogene,* 26**,** 186-197.

Rosenberg, G. 2007. The mechanisms of action of valproate in neuropsychiatric disorders: can we see the forest for the trees? *Cellular and Molecular Life Sciences,* 64**,** 2090-2103.

Rosenberger, C., Mandriota, S., Jürgensen, J. S., Wiesener, M. S., Hörstrup, J. H., Frei, U., Ratcliffe, P. J., Maxwell, P. H., Bachmann, S. & Eckardt, K.-U. 2002. Expression of hypoxia-inducible factor-1α and-2α in hypoxic and ischemic rat kidneys. *Journal of the American Society of Nephrology,* 13**,** 1721-1732.

Rothwell, P. M., Fowkes, F. G. R., Belch, J. F., Ogawa, H., Warlow, C. P. & Meade, T. W. 2011. Effect of daily aspirin on long-term risk of death due to cancer: analysis of individual patient data from randomised trials. *The Lancet,* 377**,** 31-41.

Rouse, C., Gittleman, H., Ostrom, Q. T., Kruchko, C. & Barnholtz-Sloan, J. S. 2015. Years of potential life lost for brain and CNS tumors relative to other cancers in adults in the United States, 2010. *Journal of Neuro-Oncology,* 18**,** 70-77.

Ruschoff, J., Wallinger, S., Dietmaier, W., Bocker, T., Brockhoff, G., Hofstadter, F. & Fishel, R. 1998. Aspirin suppresses the mutator phenotype associated with hereditary nonpolyposis colorectal cancer by genetic selection. *Proceedings of the National Academy of Sciences of the United States of America,* 95**,** 11301-11306.

Russo, A. L., Kwon, H.-C., Burgan, W. E., Carter, D., Beam, K., Weizheng, X., Zhang, J., Slusher, B. S., Chakravarti, A. & Tofilon, P. J. 2009. *In vitro* and *in vivo* radiosensitization of glioblastoma cells by the poly (ADP-ribose) polymerase inhibitor E7016. *Clinical Cancer Research,* 15**,** 607-612.

Saad, S. Y., Najjar, T. A. & Alashari, M. 2004. Role of non-selective adenosine receptor blockade and phosphodiesterase inhibition in cisplatin-induced nephrogonadal toxicity in rats. *Clinical and Experimental Pharmacology and Physiology,* 31**,** 862-867.

Sachlos, E., Risueño, R. M., Laronde, S., Shapovalova, Z., Lee, J.-H., Russell, J., Malig, M., Mcnicol, J. D., Fiebig-Comyn, A. & Graham, M. 2012. Identification of drugs including a dopamine receptor antagonist that selectively target cancer stem cells. *Cell,* 149**,** 1284-1297.

Saelens, X., Festjens, N., Walle, L. V., Van Gurp, M., Van Loo, G. & Vandenabeele, P. 2004. Toxic proteins released from mitochondria in cell death. *Oncogene,* 23**,** 2861-2874.

Saggar, J. K., Yu, M., Tan, Q. & Tannock, I. F. 2013. The tumor microenvironment and strategies to improve drug distribution. *Frontiers in Oncology,* 3**,** 154.

Said, H. M., Hagemann, C., Stojic, J., Schoemig, B., Vince, G. H., Flentje, M., Roosen, K. & Vordermark, D. 2007. GAPDH is not regulated in human glioblastoma under hypoxic conditions. *BMC Molecular Biology,* 8**,** 55-62.

Said, H. M., Polat, B., Hagemann, C., Anacker, J., Flentje, M. & Vordermark, D. 2009. Absence of GAPDH regulation in tumor-cells of different origin under hypoxic conditions *in–vitro*. *BMC Research Notes,* 2**,** 8.

Sakahira, H., Enari, M. & Nagata, S. 1998. Cleavage of CAD inhibitor in CAD activation and DNA degradation during apoptosis. *Nature,* 391**,** 96-99.

Salmena, L., Carracedo, A. & Pandolfi, P. P. 2008. Tenets of PTEN tumor suppression. *Cell,* 133**,** 403-414.

Salzberg, M., Kirson, E., Palti, Y. & Rochlitz, C. 2008. A pilot study with very low-intensity, intermediate-frequency electric fields in patients with locally advanced and/or metastatic solid tumors. *Oncology Research and Treatment,* 31**,** 362-365.

Sancho-Martínez, S. M., Piedrafita, F. J., Cannata-Andía, J. B., López-Novoa, J. M. & López-Hernández, F. J. 2011. Necrotic concentrations of cisplatin activate the apoptotic machinery but inhibit effector caspases and interfere with the execution of apoptosis. *Toxicological sciences,* 122**,** 73-85.

Santos, F. M., Gonçalves, V. M., Pinheiro, S., Vieira, A. F., Paredes, J., Schmitt, F. C., Baltazar, F. & Pinheiro, C. 2014. Differential sensitivities to lactate transport inhibitors of breast cancer cell lines. *Endocrine-Related Cancer,* 21**,** 1-40.

Sasaki, A., Ishiuchi, S., Kanda, T., Hasegawa, M. & Nakazato, Y. 2001. Analysis of interleukin-6 gene expression in primary human gliomas, glioblastoma xenografts, and glioblastoma cell lines. *Brain Tumor Pathology,* 18**,** 13-21.

Sauvant, C., Nowak, M., Wirth, C., Schneider, B., Riemann, A., Gekle, M. & Thews, O. 2008. Acidosis induces multi-drug resistance in rat prostate cancer cells (AT1) in vitro and in vivo by increasing the activity of the p-glycoprotein via activation of p38. *International Journal of Cancer,* 123**,** 2532-2542.

Scanlon, S. E. & Glazer, P. M. 2015. Multifaceted control of DNA repair pathways by the hypoxic tumor microenvironment. *DNA Repair,* 32**,** 180-189.

Schetter, A. J., Heegaard, N. H. & Harris, C. C. 2009. Inflammation and cancer: interweaving microRNA, free radical, cytokine and p53 pathways. *Carcinogenesis,* 31**,** 37-49.

Scheurer, M. E., Amirian, E. S., Davlin, S. L., Rice, T., Wrensch, M. & Bondy, M. L. 2011. Effects of antihistamine and anti-inflammatory medication use on risk of specific glioma histologies. *International Journal of Cancer,* 129**,** 2290-2296.

Scheurer, M. E., El-Zein, R., Thompson, P. A., Aldape, K. D., Levin, V. A., Gilbert, M. R., Weinberg, J. S. & Bondy, M. L. 2008. Long-term anti-inflammatory and antihistamine medication use and adult glioma risk. *Cancer Epidemiology and Prevention Biomarkers,* 17**,** 1277-1281.

Schieber, M. & Chandel, N. S. 2014. ROS function in redox signaling and oxidative stress. *Current Biology,* 24**,** R453-R462.

Schindler, C. & Darnell, J. E., Jr. 1995. Transcriptional responses to polypeptide ligands: the JAK-STAT pathway. *Annual Review of Biochemistry,* 64**,** 621-651.

Schmid, T., Zhou, J. & Brüne, B. 2004. HIF-1 and p53: communication of transcription factors under hypoxia. *Journal of Cellular and Molecular Medicine,* 8**,** 423-431.

Schrör, K. 2011. Pharmacology and cellular/molecular mechanisms of action of aspirin and non-aspirin NSAIDs in colorectal cancer. *Best Practice & Research Clinical Gastroenterology,* 25**,** 473-484.

Schulze-Osthoff, K., Bakker, A., Vanhaesebroeck, B., Beyaert, R., Jacob, W. A. & Fiers, W. 1992. Cytotoxic activity of tumor necrosis factor is mediated by early damage of mitochondrial functions. Evidence for the involvement of mitochondrial radical generation. *Journal of Biological Chemistry,* 267**,** 5317-5323.

Schwenger, P., Bellosta, P., Vietor, I., Basilico, C., Skolnik, E. Y. & Vilček, J. 1997. Sodium salicylate induces apoptosis via p38 mitogen-activated protein kinase but inhibits tumor necrosis factor-induced c-Jun N-terminal kinase/stress-activated protein kinase activation. *Proceedings of the National Academy of Sciences,* 94**,** 2869-2873.

Schwitalla, S., Fingerle, A. A., Cammareri, P., Nebelsiek, T., Goktuna, S. I., Ziegler, P. K., Canli, O., Heijmans, J., Huels, D. J., Moreaux, G., Rupec, R. A., Gerhard, M., Schmid, R., Barker, N., Clevers, H., Lang, R., Neumann, J., Kirchner, T., Taketo, M. M., Van Den Brink, G. R., Sansom, O. J., Arkan, M. C. & Greten, F. R. 2013. Intestinal tumorigenesis initiated by dedifferentiation and acquisition of stem-cell-like properties. *Cell,* 152**,** 25-38.

Seliger, C., Luber, C., Gerken, M., Schaertl, J., Proescholdt, M., Riemenschneider, M. J., Meier, C. R., Bogdahn, U., Leitzmann, M. F. & Klinkhammer-Schalke, M. 2019. Use of metformin and survival of patients with high-grade glioma. *International Journal of Cancer,* 144**,** 273-280.

Selvendiran, K., Bratasz, A., Tong, L., Ignarro, L. J. & Kuppusamy, P. 2008. NCX-4016, a nitro-derivative of aspirin, inhibits EGFR and STAT3 signaling and mdulates Bcl-2 proteins in cisplatin-resistant human ovarian cancer cells and xenografts. *Cell Cycle,* 7**,** 81-88.

Selznick, L. A., Shamji, M. F., Fecci, P., Gromeier, M., Friedman, A. H. & Sampson, J. 2008. Molecular strategies for the treatment of malignant glioma—genes, viruses, and vaccines. *Neurosurgical Review,* 31**,** 141-155.

Semenza, G. Regulation of metabolism by hypoxia-inducible factor 1. Cold Spring Harbor symposia on quantitative biology, 2011. Cold Spring Harbor Laboratory Press, 347-353.

Semenza, G. L. 2000. HIF-1 and human disease: one highly involved factor. *Genes & Development,* 14**,** 1983-1991.

Semenza, G. L. 2003. The HIF-1 Family of bHLH-PAS Proteins: Master Regulators of Oxygen Homeostasis. *PAS Proteins: Regulators and Sensors of Development and Physiology. Springer***,** 183-204.

Semenza, G. L. 2012. Hypoxia-inducible factors in physiology and medicine. *Cell,* 148**,** 399-408.

Semenza, G. L., Nejfelt, M. K., Chi, S. M. & Antonarakis, S. E. 1991. Hypoxia-inducible nuclear factors bind to an enhancer element located 3'to the human erythropoietin gene. *Proceedings of the National Academy of Sciences,* 88**,** 5680-5684.

Semenza, G. L. & Wang, G. L. 1992. A nuclear factor induced by hypoxia via de novo protein synthesis binds to the human erythropoietin gene enhancer at a site required for transcriptional activation. *Molecular and Cellular Biology,* 12**,** 5447-5454.

Senbabaoglu, F., Cingoz, A., Kaya, E., Kazancioglu, S., Lack, N. A., Acilan, C. & Bagci-Onder, T. 2016. Identification of Mitoxantrone as a TRAIL-sensitizing agent for Glioblastoma Multiforme. *Cancer Biology & Therapy,* 17**,** 546-557.

Sendoel, A. & Hengartner, M. O. 2014. Apoptotic cell death under hypoxia. *Physiology,* 29**,** 168-176.

Seo, K.-W., Choi, U.-S., Jung, Y.-C., Hong, S.-J., Byeun, Y.-E., Kang, M.-S., Pachrin, B., Kim, W.-H., Hwang, C.-Y. & Kim, D.-Y. 2007. Palliative intravenous cisplatin treatment for concurrent peritoneal and pleural mesothelioma in a dog. *Journal of Veterinary Medical Science,* 69**,** 201-204.

Sesen, J., Dahan, P., Scotland, S. J., Saland, E., Dang, V.-T., Lemarié, A., Tyler, B. M., Brem, H., Toulas, C. & Moyal, E. C.-J. 2015. Metformin inhibits growth of human glioblastoma cells and enhances therapeutic response. *PloS One,* 10**,** e0123721.

Seta, K., Spicer, Z., Yuan, Y., Lu, G. & Millhorn, D. 2002. Responding to hypoxia: lessons from a model cell line. *Science Signaling,* 2002**,** re11-re11.

Shackelford, R. E., Kaufmann, W. K. & Paules, R. S. 1999. Cell cycle control, checkpoint mechanisms, and genotoxic stress. *Environmental Health Perspectives,* 107**,** 5-24.

Shah, M. A. & Schwartz, G. K. 2001. Cell cycle-mediated drug resistance: An emerging concept in cancer therapy. *Clinical Cancer Research,* 7**,** 2168-2181.

Shan, M., Dai, D., Vudem, A., Varner, J. D. & Stroock, A. D. 2018. Multi-scale computational study of the Warburg effect, reverse Warburg effect and glutamine addiction in solid tumors. *PLoS Computational Biology,* 14**,** e1006584.

Shang, Y.-Y., Yao, M. & Zhou, Z.-W. 2017. Alisertib promotes apoptosis and autophagy in melanoma through p38 MAPK-mediated aurora a signaling. *Oncotarget,* 8**,** 107076-107088.

Sharma, S., Zhu, L., Yang, S. C., Zhang, L., Lin, J., Hillinger, S., Gardner, B., Reckamp, K., Strieter, R. M. & Huang, M. 2005. Cyclooxygenase 2 inhibition promotes IFN-γ-

dependent enhancement of antitumor responses. *The Journal of Immunology,* 175**,** 813-819.

Shen, F., Decosterd, L., Gander, M., Leyvraz, S., Biollaz, J. & Lejeune, F. 1995. Determination of temozolomide in human plasma and urine by high-performance liquid chromatography after solid-phase extraction. *Journal of Chromatography B: Biomedical Sciences and Applications,* 667**,** 291-300.

Shen, H., Hau, E., Joshi, S., Dilda, P. J. & Mcdonald, K. L. 2015. Sensitization of glioblastoma cells to irradiation by modulating the glucose metabolism. *Molecular Cancer Therapeutics,* 14**,** 1794-1804.

Shen, X., Kan, S., Hu, J., Li, M., Lu, G., Zhang, M., Zhang, S., Hou, Y., Chen, Y. & Bai, Y. 2016. EMC6/TMEM93 suppresses glioblastoma proliferation by modulating autophagy. *Cell Death and Disease,* 7**,** e2043.

Sheng, H., Shao, J., Morrow, J. D., Beauchamp, R. D. & Dubois, R. N. 1998. Modulation of apoptosis and Bcl-2 expression by prostaglandin E2 in human colon cancer cells. *Cancer Research,* 58**,** 362-366.

Sheokand, N., Malhotra, H., Kumar, S., Tillu, V. A., Chauhan, A. S., Raje, C. I. & Raje, M. 2014. Moonlighting cell-surface GAPDH recruits apotransferrin to effect iron egress from mammalian cells. *The Journal of Cell Science,* 127**,** 4279-4291.

Shestov, A. A., Liu, X., Ser, Z., Cluntun, A. A., Hung, Y. P., Huang, L., Kim, D., Le, A., Yellen, G. & Albeck, J. G. 2014. Quantitative determinants of aerobic glycolysis identify flux through the enzyme GAPDH as a limiting step. *Elife,* 3**,** e03342.

Shi, Y., Lim, S. K., Liang, Q., Iyer, S. V., Wang, H.-Y., Wang, Z., Xie, X., Sun, D., Chen, Y.-J. & Tabar, V. 2019. Gboxin is an oxidative phosphorylation inhibitor that targets glioblastoma. *Nature,* 567**,** 341–346.

Shiff, S. J., Qiao, L., Tsai, L. L. & Rigas, B. 1995. Sulindac Sulfide, an Aspirin-Like Compound, Inhibits Proliferation, Causes Cell-Cycle Quiescence, and Induces Apoptosis in Ht-29 Colon Adenocarcinoma Cells. *Journal of Clinical Investigation,* 96**,** 491-503.

Shin, S. Y., Lee, K. S., Choi, Y.-K., Lim, H. J., Lee, H. G., Lim, Y. & Lee, Y. H. 2013. The antipsychotic agent chlorpromazine induces autophagic cell death by inhibiting the Akt/mTOR pathway in human U-87MG glioma cells. *Carcinogenesis,* 34**,** 2080-2089.

Shingu, T., Fujiwara, K., Bogler, O., Akiyama, Y., Moritake, K., Shinojima, N., Tamada, Y., Yokoyama, T. & Kondo, S. 2009. Inhibition of autophagy at a late stage enhances imatinib-induced cytotoxicity in human malignant glioma cells. *International Journal of Cancer,* 124**,** 1060-1071.

Shintani, T. & Klionsky, D. J. 2004. Autophagy in health and disease: a double-edged sword. *Science,* 306**,** 990-995.

Shirakawa, K., Wang, L., Man, N., Maksimoska, J., Sorum, A. W., Lim, H. W., Lee, I. S., Shimazu, T., Newman, J. C. & Schröder, S. 2016. Salicylate, diflunisal and their metabolites inhibit CBP/p300 and exhibit anticancer activity. *Elife,* 5**,** e11156.

Shoemaker, R. H. 2006. The NCI60 human tumour cell line anticancer drug screen. *Nature Reviews Cancer,* 6**,** 813-823.

Shono, T., Tofilon, P. J., Bruner, J. M., Owolabi, O. & Lang, F. F. 2001. Cyclooxygenase-2 expression in human gliomas: prognostic significance and molecular correlations. *Cancer Research,* 61**,** 4375-4381.

Shostak, K. & Chariot, A. 2015. EGFR and NF-κB: partners in cancer. *Trends in Molecular Medicine,* 21**,** 385-393.

Shureiqi, I., Chen, D., Lotan, R., Yang, P., Newman, R. A., Fischer, S. M. & Lippman, S. M. 2000. 15-Lipoxygenase-1 mediates nonsteroidal anti-inflammatory drug-induced apoptosis independently of cyclooxygenase-2 in colon cancer cells. *Cancer Research,* 60**,** 6846-6850.

Siddik, Z. H. 2003. Cisplatin: mode of cytotoxic action and molecular basis of resistance. *Oncogene,* 22**,** 7265-7279.

Siegel, R. L., Miller, K. D. & Jemal, A. 2016. Cancer statistics, 2016. *CA: a Cancer Journal for Clinicians,* 66**,** 7-30.

Silvani, A., Eoli, M., Salmaggi, A., Lamperti, E., Maccagnano, E., Broggi, G. & Boiardi, A. 2004. Phase II trial of cisplatin plus temozolomide, in recurrent and progressive malignant glioma patients. *Journal of Neuro-Oncology,* 66**,** 203-208.

Simões, R. V., Serganova, I. S., Kruchevsky, N., Leftin, A., Shestov, A. A., Thaler, H. T., Sukenick, G., Locasale, J. W., Blasberg, R. G. & Koutcher, J. A. 2015. Metabolic plasticity of metastatic breast cancer cells: adaptation to changes in the microenvironment. *Neoplasia,* 17**,** 671-684.

Simonnet, H., Vigneron, A. & Pouysségur, J. 2014. Conventional techniques to monitor mitochondrial oxygen consumption. *Methods in Enzymology. Elsevier*.542**,** 151-161.

Singh, B. & Bhaskar, S. 2018. Methods for Detection of Autophagy in Mammalian Cells. *Methods in Molecular Biology,* 2045**,** 245-258.

Singh, S., Okamura, T. & Ali-Osman, F. 2010. Serine phosphorylation of glutathione S-transferase P1 (GSTP1) by PKC alpha enhances GSTP1-dependent cisplatin metabolism and resistance in human glioma cells. *Biochemical Pharmacology,* 80**,** 1343-1355.

Singh, S. K., Clarke, I. D., Terasaki, M., Bonn, V. E., Hawkins, C., Squire, J. & Dirks, P. B. 2003. Identification of a cancer stem cell in human brain tumors. *Cancer Research,* 63**,** 5821-5828.

Sirover, M. A. 2011. On the functional diversity of glyceraldehyde-3-phosphate dehydrogenase: biochemical mechanisms and regulatory control. *Biochimica et Biophysica Acta (BBA)-General Subjects,* 1810**,** 741-751.

Sivak-Sears, N. R., Schwartzbaum, J. A., Miike, R., Moghadassi, M. & Wrensch, M. 2004. Case-control study of use of nonsteroidal antiinflammatory drugs and glioblastoma multiforme. *American Journal of Epidemiology,* 159**,** 1131-1139.

Sizoo, E. M., Braam, L., Postma, T. J., Pasman, H. R., Heimans, J. J., Klein, M., Reijneveld, J. C. & Taphoorn, M. J. 2010. Symptoms and problems in the end-of-life phase of high-grade glioma patients. *Journal of Neuro-Oncology,* 12**,** 1162-1166.

Slee, E. A., Adrain, C. & Martin, S. J. 2001. Executioner caspase-3,-6, and-7 perform distinct, non-redundant roles during the demolition phase of apoptosis. *Journal of biological Chemistry,* 276**,** 7320-7326.

Smith, M. L., Hawcroft, G. & Hull, M. A. 2000. The effect of non-steroidal anti-inflammatory drugs on human colorectal cancer cells: evidence of different mechanisms of action. *European Journal of Cancer,* 36**,** 664-674.

Smyth, E. M., Grosser, T., Wang, M., Yu, Y. & Fitzgerald, G. A. 2009. Prostanoids in health and disease. *Journal of Lipid Research,* 50**,** S423-S428.

Soda, Y., Myskiw, C., Rommel, A. & Verma, I. M. 2013. Mechanisms of neovascularization and resistance to anti-angiogenic therapies in glioblastoma multiforme. *Journal of Molecular Medicine,* 91**,** 439-448.

Soga, T. 2013. Cancer metabolism: key players in metabolic reprogramming. *Cancer Science,* 104**,** 275-281.

Soltany-Rezaee-Rad, M., Mottaghi-Dastjerdi, N., Setayesh, N., Roshandel, G., Ebrahimifard, F. & Sepehrizadeh, Z. 2014. Overexpression of FOXO3, MYD88, and GAPDH identified by suppression subtractive hybridization in esophageal cancer is associated with autophagy. *Gastroenterology Research and Practice,* 2014**,** 185035.

Søndergaard, K., Hilton, D., Penney, M., Ollerenshaw, M. & Demaine, A. 2002. Expression of hypoxia-inducible factor 1α in tumours of patients with glioblastoma. *Neuropathology and Applied Neurobiology,* 28**,** 210-217.

Song, Y.-D., Zhang, K.-F., Liu, D., Guo, Y.-Q., Wang, D.-Y., Cui, M.-Y., Li, G., Sun, Y.-X., Shen, J.-H. & Li, X.-G. 2014. Inhibition of EGFR-induced glucose metabolism sensitizes chondrosarcoma cells to cisplatin. *Tumor Biology,* 35**,** 7017-7024.

Sordella, R., Bell, D. W., Haber, D. A. & Settleman, J. 2004. Gefitinib-sensitizing EGFR mutations in lung cancer activate anti-apoptotic pathways. *Science,* 305**,** 1163-1167.

Sorenson, C. M., Barry, M. A. & Eastman, A. 1990. Analysis of Events Associated with Cell-Cycle Arrest at G2 Phase and Cell-Death Induced by Cisplatin. *Journal of the National Cancer Institute,* 82**,** 749-755.

Sousa, F., Moura, R. P., Moreira, E., Martins, C. & Sarmento, B. 2018. Therapeutic monoclonal antibodies delivery for the glioblastoma treatment. *Advances in protein chemistry and structural biology. Elsevier*.112**,** 61-80.

Sowers, J. L., Johnson, K. M., Conrad, C., Patterson, J. T. & Sowers, L. C. 2014. The role of inflammation in brain cancer. *Inflammation and Cancer. Springer*.2014**,** 75-105.

Spampatti, M., Vlotides, G., Spottl, G., Maurer, J., Goke, B. & Auernhammer, C. J. 2014. Aspirin inhibits cell viability and mTOR downstream signaling in gastroenteropancreatic and bronchopulmonary neuroendocrine tumor cells. *World Journal of Gastroenterology,* 20**,** 10038-49.

Spence, A. M., Muzi, M., Swanson, K. R., O'sullivan, F., Rockhill, J. K., Rajendran, J. G., Adamsen, T. C., Link, J. M., Swanson, P. E. & Yagle, K. J. 2008. Regional hypoxia in glioblastoma multiforme quantified with [18F] fluoromisonidazole positron emission tomography before radiotherapy: correlation with time to progression and survival. *Clinical Cancer Research,* 14**,** 2623-2630.

Spiegl-Kreinecker, S., Buchroithner, J., Elbling, L., Steiner, E., Wurm, G., Bodenteich, A., Fischer, J., Micksche, M. & Berger, W. 2002. Expression and functional activity of the ABC-transporter proteins P-glycoprotein and multidrug-resistance protein 1 in human brain tumor cells and astrocytes. *Journal of Neuro-Oncology,* 57**,** 27-36.

Spiro, T. P., Liu, L., Majka, S., Haaga, J., Willson, J. K. & Gerson, S. L. 2001. Temozolomide: the effect of once-and twice-a-day dosing on tumor tissue levels of the DNA repair protein O6-alkylguanine-DNA-alkyltransferase. *Clinical Cancer Research,* 7**,** 2309-2317.

Spitz, G. A., Furtado, C. M., Sola-Penna, M. & Zancan, P. 2009. Acetylsalicylic acid and salicylic acid decrease tumor cell viability and glucose metabolism modulating 6-phosphofructo-1-kinase structure and activity. *Biochemical Pharmacology,* 77**,** 46-53.

Stacpoole, P. W. 1989. The pharmacology of dichloroacetate. *Metabolism,* 38**,** 1124-1144.

Stankov, M., Panayotova-Dimitrova, D., Leverkus, M., Klusmann, J.-H. & Behrens, G. 2014. Flow Cytometric Analysis of Autophagic Activity with Cyto-ID Staining in Primary Cells. Bio-Protocol.

Stark, L. A., Din, F. V., Zwacka, R. M. & Dunlop, M. G. 2001. Aspirin-induced activation of the NF-kappaB signaling pathway: a novel mechanism for aspirin-mediated apoptosis in colon cancer cells. *FASEB Journal,* 15**,** 1273-1275.

Stine, Z. E., Walton, Z. E., Altman, B. J., Hsieh, A. L. & Dang, C. V. 2015. MYC, metabolism, and cancer. *Cancer Discovery,* 5**,** 1024-1039.

Storey, K. B. 2001. Molecular mechanisms of metabolic arrest, Journal of Experimental Biology *BIOS*.2002**,** 2955-2956.

Strese, S., Fryknas, M., Larsson, R. & Gullbo, J. 2013. Effects of hypoxia on human cancer cell line chemosensitivity. *Bmc Cancer,* 13**,** 331.

Strickland, M. & Stoll, E. A. 2017. Metabolic reprogramming in glioma. *Frontiers in Cell and Developmental Biology,* 5**,** 43.

Stupp, R., Hegi, M. E., Mason, W. P., Van Den Bent, M. J., Taphoorn, M. J., Janzer, R. C., Ludwin, S. K., Allgeier, A., Fisher, B. & Belanger, K. 2009. Effects of radiotherapy with concomitant and adjuvant temozolomide versus radiotherapy alone on survival in glioblastoma in a randomised phase III study: 5-year analysis of the EORTC-NCIC trial. *The Lancet oncology,* 10**,** 459-466.

Stupp, R., Mason, W. P., Van Den Bent, M. J., Weller, M., Fisher, B., Taphoorn, M. J., Belanger, K., Brandes, A. A., Marosi, C. & Bogdahn, U. 2005. Radiotherapy plus concomitant and adjuvant temozolomide for glioblastoma. *New England Journal of Medicine,* 352**,** 987-996.

Stupp, R., Taillibert, S., Kanner, A., Read, W., Steinberg, D. M., Lhermitte, B., Toms, S., Idbaih, A., Ahluwalia, M. S. & Fink, K. 2017. Effect of tumor-treating fields plus maintenance temozolomide vs maintenance temozolomide alone on survival in patients with glioblastoma: a randomized clinical trial. *Jama,* 318**,** 2306-2316.

Stupp, R., Taillibert, S., Kanner, A. A., Kesari, S., Steinberg, D. M., Toms, S. A., Taylor, L. P., Lieberman, F., Silvani, A. & Fink, K. L. 2015. Maintenance therapy with tumor-treating fields plus temozolomide vs temozolomide alone for glioblastoma: a randomized clinical trial. *Jama,* 314**,** 2535-2543.

Stupp, R., Wong, E. T., Kanner, A. A., Steinberg, D., Engelhard, H., Heidecke, V., Kirson, E. D., Taillibert, S., Liebermann, F. & Dbalý, V. 2012. NovoTTF-100A versus physician's choice chemotherapy in recurrent glioblastoma: a randomised phase III trial of a novel treatment modality. *European Journal of Cancer,* 48**,** 2192-2202.

Sturm, D., Witt, H., Hovestadt, V., Khuong-Quang, D.-A., Jones, D. T., Konermann, C., Pfaff, E., Tönjes, M., Sill, M. & Bender, S. 2012. Hotspot mutations in H3F3A and IDH1 define distinct epigenetic and biological subgroups of glioblastoma. *Cancer Cell,* 22**,** 425-437.

Su, M., Mei, Y. & Sinha, S. 2013. Role of the crosstalk between autophagy and apoptosis in cancer. *Journal of Oncology,* 2013**,** 102735.

Su, Y.-T., Chen, R., Wang, H., Song, H., Zhang, Q., Chen, L.-Y., Lappin, H., Vasconcelos, G., Lita, A. & Maric, D. 2018. Novel targeting of transcription and metabolism in glioblastoma. *Clinical Cancer Research,* 24**,** 1124-1137.

Subbaramaiah, K., Altorki, N., Chung, W. J., Mestre, J. R., Sampat, A. & Dannenberg, A. J. 1999. Inhibition of cyclooxygenase-2 gene expression by p53. *Journal of Biological Chemistry,* 274**,** 10911-10915.

Sullivan, R., Pare, G. C., Frederiksen, L. J., Semenza, G. L. & Graham, C. H. 2008. Hypoxia-induced resistance to anticancer drugs is associated with decreased senescence and requires hypoxia-inducible factor-1 activity. *Molecular Cancer Therapeutics,* 7**,** 1961-1973.

Sun, C. Y., Zhu, Y., Li, X. F., Wang, X. Q., Tang, L. P., Su, Z. Q., Li, C. Y., Zheng, G. J. & Feng, B. 2018. Scutellarin Increases Cisplatin-Induced Apoptosis and Autophagy to Overcome Cisplatin Resistance in Non-small Cell Lung Cancer via ERK/p53 and c-met/AKT Signaling Pathways. *Frontiers in Pharmacology,* 9**,** 92.

Sun, Q., Fan, W., Chen, K., Ding, X., Chen, S. & Zhong, Q. 2008. Identification of Barkor as a mammalian autophagy-specific factor for Beclin 1 and class III phosphatidylinositol 3-kinase. *Proceedings of the National Academy of Sciences,* 105**,** 19211-19216.

Sun, S., Xue, D., Chen, Z., Ou-Yang, Y., Zhang, J., Mai, J., Gu, J., Lu, W., Liu, X. & Liu, W. 2019. R406 elicits anti-Warburg effect via Syk-dependent and-independent mechanisms to trigger apoptosis in glioma stem cells. *Cell Death & Disease,* 10**,** 358.

Susin, S. A., Daugas, E., Ravagnan, L., Samejima, K., Zamzami, N., Loeffler, M., Costantini, P., Ferri, K. F., Irinopoulou, T. & Prévost, M.-C. 2000. Two distinct pathways leading to nuclear apoptosis. *Journal of Experimental Medicine,* 192**,** 571-580.

Sutendra, G. & Michelakis, E. D. 2013. Pyruvate dehydrogenase kinase as a novel therapeutic target in oncology. *Frontiers in Oncology,* 3**,** 38.

Sutherland, R., Carlsson, J., Durand, R. & Yuhas, J. 1981. Spheroids in cancer research. *Cancer Research,* 41**,** 2980-2984.

Suzuki, H., Aoki, K., Chiba, K., Sato, Y., Shiozawa, Y., Shiraishi, Y., Shimamura, T., Niida, A., Motomura, K. & Ohka, F. 2015. Mutational landscape and clonal architecture in grade II and III gliomas. *Nature Genetics,* 47**,** 458-468.

Suzuki, H., Tomida, A. & Tsuruo, T. 2001. Dephosphorylated hypoxia-inducible factor 1α as a mediator of p53-dependent apoptosis during hypoxia. *Oncogene,* 20**,** 5779-5788.

Suzuki, M., Nakamatsu, K., Kanamori, S., Okumra, M., Uchiyama, T., Akai, F. & Nishimura, Y. 2003. Feasibility study of the simultaneous integrated boost (SIB) method for malignant gliomas using intensity-modulated radiotherapy (IMRT). *Japanese Journal of Clinical Oncology,* 33**,** 271-277.

Suzuki, Y., Inoue, T. & Ra, C. 2010. NSAIDs, mitochondria and calcium signaling: special focus on aspirin/salicylates. *Pharmaceuticals,* 3**,** 1594-1613.

Swamy, M. V., Herzog, C. R. & Rao, C. V. 2003. Inhibition of COX-2 in colon cancer cell lines by celecoxib increases the nuclear localization of active p53. *Cancer Research,* 63**,** 5239-5242.

Swanson, R. A. 1992. Astrocyte glutamate uptake during chemical hypoxia *in vitro*. *Neuroscience Letters,* 147**,** 143-146.

Swietach, P., Patiar, S., Supuran, C. T., Harris, A. L. & Vaughan-Jones, R. D. 2009. The role of carbonic anhydrase 9 in regulating extracellular and intracellular ph in three-dimensional tumor cell growths. *Journal of Biological Chemistry,* 284**,** 20299-20310.

Syn, N. L., Lim, P. L., Kong, L. R., Wang, L., Wong, A. L.-A., Lim, C. M., Loh, T. K. S., Siemeister, G., Goh, B. C. & Hsieh, W.-S. 2018. Pan-CDK inhibition augments cisplatin lethality in nasopharyngeal carcinoma cell lines and xenograft models. *Signal Transduction and Targeted Therapy,* 3**,** 9.

Takahashi, H., Wilkinson, G. R., Padrini, R. & Echizen, H. 2004. CYP2C9 and oral anticoagulation therapy with acenocoumarol and warfarin: Similarities yet differences. *Clinical Pharmacology & Therapeutics,* 75**,** 376-380.

Takanashi, K., Tainaka, H., Kobayashi, K., Yasumori, T., Hosakawa, M. & Chiba, K. 2000. CYP2C9 Ile359 and Leu359 variants: enzyme kinetic study with seven substrates. *Pharmacogenetics and Genomics,* 10**,** 95-104.

Tan, S. K., Jermakowicz, A., Mookhtiar, A. K., Nemeroff, C. B., Schürer, S. C. & Ayad, N. G. 2018. Drug repositioning in glioblastoma: A pathway perspective. *Frontiers in Pharmacology,* 9**,** 218.

Tang, Z., Yuan, S., Hu, Y., Zhang, H., Wu, W., Zeng, Z., Yang, J., Yun, J., Xu, R. & Huang, P. 2012. Over-expression of GAPDH in human colorectal carcinoma as a preferred target of 3-bromopyruvate propyl ester. *Journal of Bioenergetics and Biomembranes,* 44**,** 117-125.

Tavares-Valente, D., Granja, S., Baltazar, F. & Queirós, O. 2018. Bioenergetic modulators hamper cancer cell viability and enhance response to chemotherapy. *Journal of Cellular and Molecular Medicine,* 22**,** 3782-3794.

Taylor, T. E., Furnari, F. B. & Cavenee, W. K. 2012. Targeting EGFR for treatment of glioblastoma: molecular basis to overcome resistance. *Current Cancer Drug Targets,* 12**,** 197-209.

Tchirkov, A., Khalil, T., Chautard, E., Mokhtari, K., Veronese, L., Irthum, B., Vago, P., Kémény, J. & Verrelle, P. 2007. Interleukin-6 gene amplification and shortened survival in glioblastoma patients. *British Journal of Cancer,* 96**,** 474-476.

Tesei, A., Zoli, W., Fabbri, F., Leonetti, C., Rosetti, M., Bolla, M., Amadori, D. & Silvestrini, R. 2008. NCX 4040, an NO-donating acetylsalicylic acid derivative: efficacy and mechanisms of action in cancer cells. *Nitric Oxide,* 19**,** 225-236.

Teslaa, T. & Teitell, M. A. 2014. Techniques to monitor glycolysis. *Methods in Enzymology. Elsevier*.542**,** 91-114.

Thaker, N. G. & Pollack, I. F. 2009. Molecularly targeted therapies for malignant glioma: rationale for combinatorial strategies. *Expert Review of Neurotherapeutics,* 9**,** 1815-1836.

Thiery, J. P. & Sleeman, J. P. 2006. Complex networks orchestrate epithelial–mesenchymal transitions. *Nature Reviews Molecular Cell Biology,* 7**,** 131-142.

Thomas, H. E., Zhang, Y., Stefely, J. A., Veiga, S. R., Thomas, G., Kozma, S. C. & Mercer, C. A. 2018. Mitochondrial complex I activity is required for maximal autophagy. *Cell Reports,* 24**,** 2404-2417.

Thoms, H. C., Dunlop, M. G. & Stark, L. A. 2007. p38-mediated inactivation of cyclin D1/cyclin-dependent kinase 4 stimulates nucleolar translocation of RelA and apoptosis in colorectal cancer cells. *Cancer Research,* 67**,** 1660-1669.

Thon, N., Kreth, S. & Kreth, F. W. 2013. Personalized treatment strategies in glioblastoma: MGMT promoter methylation status. *OncoTargets and Therapy,* 6**,** 1363-1372.

Thorat, M. A. & Cuzick, J. 2015. Prophylactic use of aspirin: systematic review of harms and approaches to mitigation in the general population. *European Journal of Epidemiology,* 30**,** 5-18.

Thun, M. J., Henley, S. J. & Patrono, C. 2002. Nonsteroidal anti-inflammatory drugs as anticancer agents: Mechanistic, pharmacologic, and clinical issues. *Journal of the National Cancer Institute,* 94**,** 252-266.

Thun, M. J., Namboodiri, M. M. & Heath Jr, C. W. 1991. Aspirin use and reduced risk of fatal colon cancer. *New England Journal of Medicine,* 325**,** 1593-1596.

Till, A., Lakhani, R., Burnett, S. F. & Subramani, S. 2012. Pexophagy: the selective degradation of peroxisomes. *International Journal of Cell Biology,* 2012**,** 512721.

Tisdale, E. J. 2001. Glyceraldehyde-3-phosphate dehydrogenase is required for vesicular transport in the early secretory pathway. *Journal of Biological Chemistry,* 276**,** 2480-2486.

Todoric, J., Antonucci, L. & Karin, M. 2016. Targeting inflammation in cancer prevention and therapy. *Cancer Prevention Research,* 9**,** 895-905.

Tokunaga, K., Nakamura, Y., Sakata, K., Fujimori, K., Ohkubo, M., Sawada, K. & Sakiyama, S. 1987. Enhanced expression of a glyceraldehyde-3-phosphate dehydrogenase gene in human lung cancers. *Cancer Research,* 47**,** 5616-5619.

Tomicic, M. T., Meise, R., Aasland, D., Berte, N., Kitzinger, R., Kramer, O. H., Kaina, B. & Christmann, M. 2015. Apoptosis induced by temozolomide and nimustine in glioblastoma cells is supported by JNK/c-Jun-mediated induction of the BH3-only protein BIM. *Oncotarget,* 6**,** 33755-33768.

Torre, L. A., Siegel, R. L., Ward, E. M. & Jemal, A. 2016. Global cancer incidence and mortality rates and trends—an update. *Cancer Epidemiology and Prevention Biomarkers,* 25**,** 16-27.

Trédan, O., Galmarini, C. M., Patel, K. & Tannock, I. F. 2007. Drug resistance and the solid tumor microenvironment. *Journal of the National Cancer Institute,* 99**,** 1441-1454.

Tsujii, M., Kawano, S., Tsuji, S., Sawaoka, H., Hori, M. & Dubois, R. N. 1998. Cyclooxygenase regulates angiogenesis induced by colon cancer cells. *Cell,* 93**,** 705-716.

Tucker, O. N., Dannenberg, A. J., Yang, F. K., Zhang, F., Teng, L. S., Daly, J. M., Soslow, R. A., Masferrer, J. L., Woerner, B. M., Koki, A. T. & Fahey, T. J. 1999. Cyclooxygenase-2 expression is up-regulated in human pancreatic cancer. *Cancer Research,* 59**,** 987-990.

Tung, Y.-C., Hsiao, A. Y., Allen, S. G., Torisawa, Y.-S., Ho, M. & Takayama, S. 2011. High-throughput 3D spheroid culture and drug testing using a 384 hanging drop array. *Analyst,* 136**,** 473-478.

Tyson, J. J., Csikasz-Nagy, A. & Novak, B. 2002. The dynamics of cell cycle regulation. *Bioessays,* 24**,** 1095-1109.

Urdiciain, A., Melendez, B., Rey, J. A., Idoate, M. A. & Castresana, J. S. 2018. Panobinostat Potentiates Temozolomide Effects and Reverses Epithelial-Mesenchymal Transition in Glioblastoma Cells. *Epigenomes,* 2**,** 5.

Van Den Bent, M. J., Carpentier, A. F., Brandes, A. A., Sanson, M., Taphoorn, M. J., Bernsen, H. J., Frenay, M., Tijssen, C. C., Grisold, W. & Sipos, L. 2006. Adjuvant procarbazine, lomustine, and vincristine improves progression-free survival but not overall survival in newly diagnosed anaplastic oligodendrogliomas and oligoastrocytomas: a randomized European Organisation for Research and Treatment of Cancer phase III trial. *Journal of Clinical Oncology,* 24**,** 2715-2722.

Van Engeland, M., Ramaekers, F. C., Schutte, B. & Reutelingsperger, C. P. 1996. A novel assay to measure loss of plasma membrane asymmetry during apoptosis of adherent cells in culture. *Cytometry: The Journal of the International Society for Analytical Cytology,* 24**,** 131-139.

Van Heerde, W. L., De Groot, P. G. & Reutelingsperger, C. P. 1995. The complexity of the phospholipid binding protein Annexin V. *Thrombosis and Haemostasis,* 74**,** 172-179.

Van Loo, G., Saelens, X., Van Gurp, M., Macfarlane, M., Martin, S. & Vandenabeele, P. 2002. The role of mitochondrial factors in apoptosis: a Russian roulette with more than one bullet. *Cell Death and Differentiation,* 9**,** 1031-1042.

Van Nifterik, K. A., Van Den Berg, J., Slotman, B. J., Lafleur, M. V. M., Sminia, P. & Stalpers, L. J. 2012. Valproic acid sensitizes human glioma cells for temozolomide and γ-radiation. *Journal of Neuro-Oncology,* 107**,** 61-67.

Van Oosterwijk, J. V., Herpers, B., Meijer, D., Briaire-De Bruijn, I., Cleton-Jansen, A., Gelderblom, H., Van De Water, B. & Bovée, J. 2011. Restoration of chemosensitivity for doxorubicin and cisplatin in chondrosarcoma in vitro: BCL-2 family members cause chemoresistance. *Annals of Oncology,* 23**,** 1617-1626.

Van Schaeybroeck, S., Karaiskou-Mccaul, A., Kelly, D., Longley, D., Galligan, L., Van Cutsem, E. & Johnston, P. 2005. Epidermal growth factor receptor activity determines response of colorectal cancer cells to gefitinib alone and in combination with chemotherapy. *Clinical Cancer Research,* 11**,** 7480-7489.

Van Uden, P., Kenneth, N. S. & Rocha, S. 2008. Regulation of hypoxia-inducible factor-1α by NF-κB. *Biochemical Journal,* 412**,** 477-484.

Vander Heiden, M. G., Cantley, L. C. & Thompson, C. B. 2009. Understanding the Warburg effect: the metabolic requirements of cell proliferation. *Science,* 324**,** 1029-1033.

Vander Heiden, M. G., Plas, D. R., Rathmell, J. C., Fox, C. J., Harris, M. H. & Thompson, C. B. 2001. Growth factors can influence cell growth and survival through effects on glucose metabolism. *Molecular and Cellular Biology,* 21**,** 5899-5912.

Vanlangenakker, N., Berghe, T. V., Krysko, D. V., Festjens, N. & Vandenabeele, P. 2008. Molecular mechanisms and pathophysiology of necrotic cell death. *Current Molecular Medicine,* 8**,** 207-220.

Vaupel, P. 2013. Tumor oxygenation: an appraisal of past and present concepts and a look into the future. *Oxygen Transport to Tissue. Springer*. XXXV**,** 229-236.

Vazquez, C. L. & Colombo, M. I. 2009. Assays to assess autophagy induction and fusion of autophagic vacuoles with a degradative compartment, using monodansylcadaverine (MDC) and DQ-BSA. *Methods in Enzymology,* 452**,** 85-95.

Véga, C., R. Sachleben Jr, L., Gozal, D. & Gozal, E. 2006. Differential metabolic adaptation to acute and long-term hypoxia in rat primary cortical astrocytes. *Journal of Neurochemistry,* 97**,** 872-883.

Velpula, K. K., Guda, M. R., Sahu, K., Tuszynski, J., Asuthkar, S., Bach, S. E., Lathia, J. D. & Tsung, A. J. 2017. Metabolic targeting of EGFRvIII/PDK1 axis in temozolomide resistant glioblastoma. *Oncotarget,* 8**,** 35639-35655.

Vengoji, R., Macha, M. A., Batra, S. K. & Shonka, N. A. 2018. Natural products: a hope for glioblastoma patients. *Oncotarget,* 9**,** 22194-22219.

Verhaak, R. G., Hoadley, K. A., Purdom, E., Wang, V., Qi, Y., Wilkerson, M. D., Miller, C. R., Ding, L., Golub, T. & Mesirov, J. P. 2010. Integrated genomic analysis identifies clinically relevant subtypes of glioblastoma characterized by abnormalities in PDGFRA, IDH1, EGFR, and NF1. *Cancer Cell,* 17**,** 98-110.

Veringa, S. J., Biesmans, D., Van Vuurden, D. G., Jansen, M. H., Wedekind, L. E., Horsman, I., Wesseling, P., Vandertop, W. P., Noske, D. P. & Kaspers, G. J. 2013. In vitro drug response and efflux transporters associated with drug resistance in

pediatric high grade glioma and diffuse intrinsic pontine glioma. *PloS One,* 8**,** e61512.

Vermeulen, K., Van Bockstaele, D. R. & Berneman, Z. N. 2003. The cell cycle: a review of regulation, deregulation and therapeutic targets in cancer. *Cell Proliferation,* 36**,** 131-149.

Von Minckwitz, G., Müller, B. M., Loibl, S., Budczies, J., Hanusch, C., Darb-Esfahani, S., Hilfrich, J., Weiss, E., Huober, J. & Blohmer, J. U. 2011. Cytoplasmic poly (adenosine diphosphate–ribose) polymerase expression is predictive and prognostic in patients with breast cancer treated with neoadjuvant chemotherapy. *Journal of Clinical Oncology,* 29**,** 2150-2157.

Vos, M. J., Zijlstra, M. P., Carra, S., Sibon, O. C. M. & Kampinga, H. H. 2011. Small heat shock proteins, protein degradation and protein aggregation diseases. *Autophagy,* 7**,** 101-103.

Vyas, S., Zaganjor, E. & Haigis, M. C. 2016. Mitochondria and cancer. *Cell,* 166**,** 555-566.

W. Humphrey, R., M. Brockway-Lunardi, L., T. Bonk, D., Dohoney, K. M., Doroshow, J. H., Meech, S. J., Ratain, M. J., Topalian, S. L. & M. Pardoll, D. 2011. Opportunities and challenges in the development of experimental drug combinations for cancer. *Journal of the National Cancer Institute,* 103**,** 1222-1226.

Wajant, H. 2002. The Fas signaling pathway: more than a paradigm. *Science,* 296**,** 1635-1636.

Walker, M. D., Strike, T. A. & Sheline, G. E. 1979. An analysis of dose-effect relationship in the radiotherapy of malignant gliomas. *International Journal of Radiation Oncology* Biology* Physics,* 5**,** 1725-1731.

Walmsley, S. R., Farahi, N., Peyssonnaux, C., Johnson, R. S., Cramer, T., Sobolewski, A., Condliffe, A. M., Cowburn, A. S., Johnson, N. & Chilvers, E. R. 2005. Hypoxia-induced neutrophil survival is mediated by HIF-1α–dependent NF-κB activity. *Journal of Experimental Medicine,* 201**,** 105-115.

Walsh, J. C., Lebedev, A., Aten, E., Madsen, K., Marciano, L. & Kolb, H. C. 2014. The clinical importance of assessing tumor hypoxia: relationship of tumor hypoxia to prognosis and therapeutic opportunities. *Antioxidants & Redox Signaling,* 21**,** 1516-1554.

Wang, D. & Lippard, S. J. 2005. Cellular processing of platinum anticancer drugs. *Nature Reviews Drug Discovery,* 4**,** 307-320.

Wang, H., Wang, H., Zhang, W., Huang, H. J., Liao, W. S. & Fuller, G. N. 2004. Analysis of the activation status of Akt, NFκB, and Stat3 in human diffuse gliomas. *Laboratory Investigation,* 84**,** 941-951.

Wang, J., Wang, Q., Cui, Y., Liu, Z. Y., Zhao, W., Wang, C. L., Dong, Y., Hou, L., Hu, G. & Luo, C. 2012. Knockdown of cyclin D1 inhibits proliferation, induces apoptosis, and attenuates the invasive capacity of human glioblastoma cells. *Journal of Neuro-Oncology,* 106**,** 473-484.

Wang, K., Kievit, F. M., Erickson, A. E., Silber, J. R., Ellenbogen, R. G. & Zhang, M. 2016. Culture on 3D chitosan-hyaluronic acid scaffolds enhances stem cell marker expression and drug resistance in human glioblastoma cancer stem cells. *Advanced Healthcare Materials,* 5**,** 3173-3181.

Wang, S., Xie, J., Li, J., Liu, F., Wu, X. & Wang, Z. 2016. Cisplatin suppresses the growth and proliferation of breast and cervical cancer cell lines by inhibiting integrin β5-mediated glycolysis. *American Journal of Cancer Research,* 6**,** 1108-1117.

Wang, X.-W., Labussière, M., Valable, S., Pérès, E. A., Guillamo, J.-S., Bernaudin, M. & Sanson, M. 2014. IDH1R132H Mutation Increases U87 Glioma Cell Sensitivity to Radiation Therapy in Hypoxia. *BioMed Research International,* 2014**,** 198697.

Wang, X. Q., Duan, X. M., Liu, L. H., Fang, Y. Q. & Tan, Y. 2005. Carboxyfluorescein diacetate succinimidyl ester fluorescent dye for cell Labeling. *Acta Biochimica Et Biophysica Sinica,* 37**,** 379-385.

Wang, Y., Roche, O., Xu, C., Moriyama, E. H., Heir, P., Chung, J., Roos, F. C., Chen, Y., Finak, G. & Milosevic, M. 2012. Hypoxia promotes ligand-independent EGF receptor signaling via hypoxia-inducible factor–mediated upregulation of caveolin-1. *Proceedings of the National Academy of Sciences,* 109**,** 4892-4897.

Wang, Y., Xie, Y., Li, J., Peng, Z.-H., Sheinin, Y., Zhou, J. & Oupický, D. 2017. Tumor-penetrating nanoparticles for enhanced anticancer activity of combined photodynamic and hypoxia-activated therapy. *ACS Nano,* 11**,** 2227-2238.

Wangpaichitr, M., Wu, C., Li, Y. Y., Nguyen, D. J., Kandemir, H., Shah, S., Chen, S., Feun, L. G., Prince, J. S. & Kuo, M. T. 2017. Exploiting ROS and metabolic differences to kill cisplatin resistant lung cancer. *Oncotarget,* 8**,** 49275-49292.

Waqas, M., Enam, S., Batool, M. & Rai, H. 2018. Basic Mechanisms of Glioblastoma Multiforme Cell Invasion: A Review Article. *Journal of Neurology and Neuroscience,* 9**,** 279.

Warburg, O. 1925. The metabolism of carcinoma cells. *The Journal of Cancer Research,* 9**,** 148-163.

Warburg, O. 1956. On the origin of cancer cells. *Science,* 123**,** 309-314.

Wartenberg, M., Ling, F. C., Muschen, M., Klein, F., Acker, H., Gassmann, M., Petrat, K., Putz, V., Hescheler, J. & Sauer, H. 2003. Regulation of the multidrug resistance transporter P-glycoprotein in multicellular tumor spheroids by hypoxiainducible factor-1 and reactive oxygen species. *FASEB Journal,* 17**,** 503-505.

Watson, J. A., Watson, C. J., Mccrohan, A.-M., Woodfine, K., Tosetto, M., Mcdaid, J., Gallagher, E., Betts, D., Baugh, J. & O'sullivan, J. 2009. Generation of an epigenetic signature by chronic hypoxia in prostate cells. *Human Molecular Genetics,* 18**,** 3594-3604.

Weidberg, H., Shvets, E. & Elazar, Z. 2011. Biogenesis and cargo selectivity of autophagosomes. *Annual Review of Biochemistry,* 80**,** 125-156.

Weihua, Z., Tsan, R., Huang, W.-C., Wu, Q., Chiu, C.-H., Fidler, I. J. & Hung, M.-C. 2008. Survival of cancer cells is maintained by EGFR independent of its kinase activity. *Cancer Cell,* 13**,** 385-393.

Weinberg, S. E. & Chandel, N. S. 2015. Targeting mitochondria metabolism for cancer therapy. *Nature Chemical Biology,* 11**,** 9-15.

Wen, P. Y. & Kesari, S. 2008. Malignant gliomas in adults. *New England Journal of Medicine,* 359**,** 492-507.

Wenger, R. H., Camenisch, G., Desbaillets, I., Chilov, D. & Gassmann, M. 1998. Up-regulation of hypoxia-inducible factor-1α is not sufficient for hypoxic/anoxic p53 induction. *Cancer Research,* 58**,** 5678-5680.

Wennogle, L. P., Liang, H., Quintavalla, J. C., Bowen, B. R., Wasvary, J., Miller, D. B., Allentoff, A., Boyer, W., Kelly, M. & Marshall, P. 1995. Comparison of recombinant cyclooxygenase-2 to native isoforms: aspirin labeling of the active site. *FEBS Letters,* 371**,** 315-320.

Wertz, I. E. & Dixit, V. M. 2000. Characterization of calcium release-activated apoptosis of LNCaP prostate cancer cells. *Journal of Biological Chemistry,* 275**,** 11470-11477.

Wheaton, W. W., Weinberg, S. E., Hamanaka, R. B., Soberanes, S., Sullivan, L. B., Anso, E., Glasauer, A., Dufour, E., Mutlu, G. M. & Budigner, G. S. 2014. Metformin inhibits mitochondrial complex I of cancer cells to reduce tumorigenesis. *Elife,* 3**,** e02242.

Wheelhouse, R. T. & Stevens, M. F. 1993. Decomposition of the antitumour drug temozolomide in deuteriated phosphate buffer: methyl group transfer is accompanied by deuterium exchange. *Journal of the Chemical Society, Chemical Communications***,** 1177-1178.

White, M., Johnson, G., Zhang, W., Hobrath, J., Piazza, G. & Grimaldi, M. 2013. Sulindac sulfide inhibits sarcoendoplasmic reticulum Ca2+ ATPase, induces endoplasmic reticulum stress response, and exerts toxicity in glioma cells: relevant similarities to and important differences from celecoxib. *Journal of Neuroscience Research,* 91**,** 393-406.

Whittle, I. R., Stavrinos, N., Akil, H., Yau, Y. & Lewis, S. C. 2010. Assessment of physiological parameters within glioblastomas in awake patients: a prospective clinical study. *British Journal of Neurosurgery,* 24**,** 447-453.

Williams, J. A., Zhao, K., Jin, S. & Ding, W.-X. 2017. New methods for monitoring mitochondrial biogenesis and mitophagy in vitro and in vivo. *Experimental Biology and Medicine,* 242**,** 781-787.

Wise, D. R., Ward, P. S., Shay, J. E., Cross, J. R., Gruber, J. J., Sachdeva, U. M., Platt, J. M., Dematteo, R. G., Simon, M. C. & Thompson, C. B. 2011. Hypoxia promotes isocitrate dehydrogenase-dependent carboxylation of α-ketoglutarate to citrate to support cell growth and viability. *Proceedings of the National Academy of Sciences,* 108**,** 19611-19616.

Wlodkowic, D., Telford, W., Skommer, J. & Darzynkiewicz, Z. 2011. Apoptosis and beyond: cytometry in studies of programmed cell death. *Methods in cell biology. Elsevier*.103**,** 55-98.

Wong, E. & Cuervo, A. M. 2010. Integration of clearance mechanisms: the proteasome and autophagy. *Cold Spring Harb Perspect Biology,* 2**,** a006734.

Wong, R. S. 2011. Apoptosis in cancer: from pathogenesis to treatment. *Journal of Experimental & Clinical Cancer Research,* 30**,** 87.

Wu, M., Neilson, A., Swift, A. L., Moran, R., Tamagnine, J., Parslow, D., Armistead, S., Lemire, K., Orrell, J. & Teich, J. 2007. Multiparameter metabolic analysis reveals a close link between attenuated mitochondrial bioenergetic function and enhanced glycolysis dependency in human tumor cells. *American Journal of Physiology-Cell Physiology,* 292**,** C125-C136.

Wu, Y., Deng, Y., Zhu, J., Duan, Y., Weng, W. & Wu, X. 2018. Pim1 promotes cell proliferation and regulates glycolysis via interaction with MYc in ovarian cancer. *OncoTargets and Therapy,* 11**,** 6647-6656.

Würstle, S., Schneider, F., Ringel, F., Gempt, J., Lämmer, F., Delbridge, C., Wu, W. & Schlegel, J. 2017. Temozolomide induces autophagy in primary and established glioblastoma cells in an EGFR independent manner. *Oncology Letters,* 14**,** 322-328.

Xie, T. X., Aldape, K. D., Gong, W. D., Kanzawa, T., Suki, D., Kondo, S., Lang, F., Ali-Osman, F., Sawaya, R. & Huang, S. Y. 2008. Aberrant NF-kappa B activity is critical in focal

necrosis formation of human glioblastoma by regulation of the expression of tissue factor. *International Journal of Oncology,* 33**,** 5-15.

Xing, F., Luan, Y., Cai, J., Wu, S., Mai, J., Gu, J., Zhang, H., Li, K., Lin, Y. & Xiao, X. 2017. The anti-warburg effect elicited by the cAMP-PGC1α pathway drives differentiation of glioblastoma cells into astrocytes. *Cell Reports,* 18**,** 468-481.

Xu, G. W., Mymryk, J. S. & Cairncross, J. G. 2005. Inactivation of p53 sensitizes astrocytic glioma cells to BCNU and temozolomide, but not cisplatin. *Journal of Neuro-Oncology,* 74**,** 141-149.

Xu, H., Zong, H., Ma, C., Ming, X., Shang, M., Li, K., He, X., Du, H. & Cao, L. 2017. Epidermal growth factor receptor in glioblastoma. *Oncology Letters,* 14**,** 512-516.

Xu, K., Wang, L. & Shu, H.-K. G. 2014. COX-2 overexpression increases malignant potential of human glioma cells through Id1. *Oncotarget,* 5**,** 1241-1252.

Xu, R.-H., Pelicano, H., Zhou, Y., Carew, J. S., Feng, L., Bhalla, K. N., Keating, M. J. & Huang, P. 2005. Inhibition of glycolysis in cancer cells: a novel strategy to overcome drug resistance associated with mitochondrial respiratory defect and hypoxia. *Cancer Research,* 65**,** 613-621.

Xu, X., Zhu, G.-Q., Zhang, K., Zhou, Y.-C., Li, X.-L., Xu, W., Zhang, H., Shao, Y., Zhang, Z.-Y. & Sun, W.-H. 2017. Cyclooxygenase-2 mediated synergistic effect of ursolic acid in combination with paclitaxel against human gastric carcinoma. *Oncotarget,* 8**,** 92770-92777.

Xu, Y., Li, Y., Pang, Y., Ling, M., Shen, L., Yang, X., Zhang, J., Zhou, J., Wang, X. & Liu, Q. 2012. EMT and stem cell-like properties associated with HIF-2α are involved in arsenite-induced transformation of human bronchial epithelial cells. *PLoS One,* 7**,** e37765.

Yamano, Y., Uzawa, K., Saito, K., Nakashima, D., Kasamatsu, A., Koike, H., Kouzu, Y., Shinozuka, K., Nakatani, K. & Negoro, K. 2010. Identification of cisplatin-resistance related genes in head and neck squamous cell carcinoma. *International Journal of Cancer,* 126**,** 437-449.

Yan, H., Parsons, D. W., Jin, G., Mclendon, R., Rasheed, B. A., Yuan, W., Kos, I., Batinic-Haberle, I., Jones, S. & Riggins, G. J. 2009. IDH1 and IDH2 mutations in gliomas. *New England Journal of Medicine,* 360**,** 765-773.

Yan, Y. L., Xu, Z. J., Dai, S., Qian, L., Sun, L. Q. & Gong, Z. C. 2016. Targeting autophagy to sensitive glioma to temozolomide treatment. *Journal of Experimental & Clinical Cancer Research,* 35**,** 23.

Yang, D. D., Kuan, C.-Y., Whitmarsh, A. J., Rinócn, M., Zheng, T. S., Davis, R. J., Rakic, P. & Flavell, R. A. 1997. Absence of excitotoxicity-induced apoptosis in the hippocampus of mice lacking the Jnk3 gene. *Nature,* 389**,** 865-870.

Yang, X., Chang, H. Y. & Baltimore, D. 1998. Autoproteolytic activation of pro-caspases by oligomerization. *Molecular Cell,* 1**,** 319-325.

Yang, Z. J., Chee, C. E., Huang, S. & Sinicrope, F. A. 2011. The role of autophagy in cancer: therapeutic implications. *Molecular Cancer Therapeutics,* 10**,** 1533-1541.

Yaniv, Y., Juhaszova, M., Nuss, H. B., Wang, S., Zorov, D. B., Lakatta, E. G. & Sollott, S. J. 2010. Matching ATP supply and demand in mammalian heart: in vivo, in vitro, and in silico perspectives. *The Annals of the New York Academy of Sciences,* 1188**,** 133-142.

Yao, K., Gietema, J. A., Shida, S., Selvakumaran, M., Fonrose, X., Haas, N. B., Testa, J. & O'dwyer, P. J. 2005. In vitro hypoxia-conditioned colon cancer cell lines derived

from HCT116 and HT29 exhibit altered apoptosis susceptibility and a more angiogenic profile in vivo. *British Journal of Cancer,* 93**,** 1356-1363.

Yarden, Y. 2001. The EGFR family and its ligands in human cancer: signalling mechanisms and therapeutic opportunities. *European Journal of Cancer,* 37**,** S3-S8.

Yin, M. J., Yamamoto, Y. & Gaynor, R. B. 1998. The anti-inflammatory agents aspirin and salicylate inhibit the activity of I(kappa)B kinase-beta. *Nature,* 396**,** 77-80.

Yip-Schneider, M. T., Sweeney, C. J., Jung, S. H., Crowell, P. L. & Marshall, M. S. 2001. Cell cycle effects of nonsteroidal anti-inflammatory drugs and enhanced growth inhibition in combination with gemcitabine in pancreatic carcinoma cells. *Journal of Pharmacology and Experimental Therapeutics,* 298**,** 976-985.

Yu, C., Li, W. B., Liu, J. B., Lu, J. W. & Feng, J. F. 2018. Autophagy: novel applications of nonsteroidal anti-inflammatory drugs for primary cancer. *Cancer Medicine,* 7**,** 471-484.

Yu, H., Pardoll, D. & Jove, R. 2009. STATs in cancer inflammation and immunity: a leading role for STAT3. *Nature Reviews Cancer,* 9**,** 798-809.

Yu, H. G., Huang, J. A., Yang, Y. N., Huang, H., Luo, H. S., Yu, J. P., Meier, J. J., Schrader, H., Bastian, A., Schmidt, W. E. & Schmitz, F. 2002. The effects of acetylsalicylic acid on proliferation, apoptosis, and invasion of cyclooxygenase-2 negative colon cancer cells. *The European Journal of Clinical Investigation,* 32**,** 838-846.

Yu, L., Chen, M. C. & Cheung, K. C. 2010. Droplet-based microfluidic system for multicellular tumor spheroid formation and anticancer drug testing. *Lab on a Chip,* 10**,** 2424-2432.

Yu, Y., Lou, L.-G., Liu, W.-P., Zhu, H.-J., Ye, Q.-S., Chen, X.-Z., Gao, W.-G. & Hou, S.-Q. 2008. Synthesis and anticancer activity of lipophilic platinum (II) complexes of 3, 5-diisopropylsalicylate. *European Journal of Medicinal Chemistry,* 43**,** 1438-1443.

Yuan, T. & Cantley, L. 2008. PI3K pathway alterations in cancer: variations on a theme. *Oncogene,* 27**,** 5497-5510.

Yue, W., Yang, C. S., Dipaola, R. S. & Tan, X.-L. 2014. Repurposing of metformin and aspirin by targeting AMPK-mTOR and inflammation for pancreatic cancer prevention and treatment. *Cancer Prevention Research,* 7**,** 388-397.

Yue, X., Lan, F., Yang, W., Yang, Y., Han, L., Zhang, A., Liu, J., Zeng, H., Jiang, T., Pu, P. & Kang, C. 2010. Interruption of beta-catenin suppresses the EGFR pathway by blocking multiple oncogenic targets in human glioma cells. *Brain Research,* 1366**,** 27-37.

Yueling, W., Hongmin, Z., Lin, L. & Jiangfen, W. 2010. Effect of aspirin alone or combined with cisplatin on human cervical carcinoma HeLa cells. *Journal of Medical Colleges of PLA,* 25**,** 11-18.

Yun, J., Mullarky, E., Lu, C., Bosch, K. N., Kavalier, A., Rivera, K., Roper, J., Chio, I. I. C., Giannopoulou, E. G. & Rago, C. 2015. Vitamin C selectively kills KRAS and BRAF mutant colorectal cancer cells by targeting GAPDH. *Science,* 350**,** 1391-1396.

Yung, W. K. A., Albright, R. E., Olson, J., Fredericks, R., Fink, K., Prados, M. D., Brada, M., Spence, A., Hohl, R. J., Shapiro, W., Glantz, M., Greenberg, H., Selker, R. G., Vick, N. A., Rampling, R., Friedman, H., Phillips, P., Bruner, J., Yue, N., Osoba, D., Zaknoen, S. & Levin, V. A. 2000. A phase II study of temozolomide vs. procarbazine in patients with glioblastoma multiforme at first relapse. *British Journal of Cancer,* 83**,** 588-593.

Zagzag, D., Zhong, H., Scalzitti, J. M., Laughner, E., Simons, J. W. & Semenza, G. L. 2000. Expression of hypoxia-inducible factor 1α in brain tumors: association with

angiogenesis, invasion, and progression. *Cancer: Interdisciplinary International Journal of the American Cancer Society,* 88**,** 2606-2618.

Zamzami, N., Larochette, N. & Kroemer, G. 2005. Mitochondrial permeability transition in apoptosis and necrosis. *Cell Death and Differentiation,* 12**,** 1478-1480.

Zamzami, N., Marchetti, P., Castedo, M., Decaudin, D., Macho, A., Hirsch, T., Susin, S. A., Petit, P. X., Mignotte, B. & Kroemer, G. 1995. Sequential Reduction of Mitochondrial Transmembrane Potential and Generation of Reactive Oxygen Species in Early Programmed Cell-Death. *Journal of Experimental Medicine,* 182**,** 367-377.

Zeng, W., Liu, P., Pan, W., Singh, S. R. & Wei, Y. 2015. Hypoxia and hypoxia inducible factors in tumor metabolism. *Cancer Letters,* 356**,** 263-267.

Zhang, C., Liu, J., Wu, R., Liang, Y., Lin, M., Liu, J., Chan, C. S., Hu, W. & Feng, Z. 2014. Tumor suppressor p53 negatively regulates glycolysis stimulated by hypoxia through its target RRAD. *Oncotarget,* 5**,** 5535-5546.

Zhang, C., Shi, J., Mao, S. Y., Xu, Y. S., Zhang, D., Feng, L. Y., Zhang, B., Yan, Y. Y., Wang, S. C., Pan, J. P., Yang, Y. P. & Lin, N. M. 2015. Role of p38 MAPK in enhanced human cancer cells killing by the combination of aspirin and ABT-737. *Journal of Cellular and Molecular Medicine,* 19**,** 408-417.

Zhang, D., Dai, D., Zhou, M., Li, Z., Wang, C., Lu, Y., Li, Y. & Wang, J. 2018. Inhibition of Cyclin D1 Expression in Human Glioblastoma Cells is Associated with Increased Temozolomide Chemosensitivity. *Cellular Physiology and Biochemistry,* 51**,** 2496-2508.

Zhang, H., Bosch-Marce, M., Shimoda, L. A., Tan, Y. S., Baek, J. H., Wesley, J. B., Gonzalez, F. J. & Semenza, G. L. 2008. Mitochondrial autophagy is an HIF-1-dependent adaptive metabolic response to hypoxia. *Journal of Biological Chemistry,* 283**,** 10892-10903.

Zhang, H. F., Gao, P., Fukuda, R., Kumar, G., Krishnamachary, B., Zeller, K. I., Dang, C. V. & Semenza, G. L. 2007. HIF-1 inhibits mitochondrial biogenesis and cellular respiration in VHL-deficient renal cell carcinoma by repression of C-MYC activity. *Cancer Cell,* 11**,** 407-420.

Zhang, J.-Y., Zhang, F., Hong, C.-Q., Giuliano, A. E., Cui, X.-J., Zhou, G.-J., Zhang, G.-J. & Cui, Y.-K. 2015. Critical protein GAPDH and its regulatory mechanisms in cancer cells. *Cancer Biology & Medicine,* 12**,** 10-22.

Zhang, J., Fg Stevens, M. & D Bradshaw, T. 2012. Temozolomide: mechanisms of action, repair and resistance. *Current Molecular Pharmacology,* 5**,** 102-114.

Zhang, J., Stevens, M. F. & Bradshaw, T. D. 2012. Temozolomide: mechanisms of action, repair and resistance. *Curr Mol Pharmacol,* 5**,** 102-14.

Zhang, L. R., Yang, X. F., Li, X., Li, C., Zhao, L., Zhou, Y. Y. & Hou, H. L. 2015. Butein sensitizes HeLa cells to cisplatin through the AKT and ERK/p38 MAPK pathways by targeting FoxO3a. *International Journal of Molecular Medicine,* 36**,** 957-966.

Zhang, R., Wang, R., Chen, Q. & Chang, H. 2015. Inhibition of autophagy using 3-methyladenine increases cisplatin-induced apoptosis by increasing endoplasmic reticulum stress in U251 human glioma cells. *Molecular Medicine Reports,* 12**,** 1727-1732.

Zhang, T., Yang, X., Liu, P., Zhou, J., Luo, J., Wang, H., Li, A. & Zhou, Y. 2017. Association between nonsteroidal anti-inflammatory drugs use and risk of central nervous system tumors: A dose-response meta analysis. *Oncotarget,* 8**,** 102486-102498.

Zhang, X., Lan, L., Niu, L., Lu, J., Li, C., Guo, M., Mo, S., Lu, J., Liu, Y. & Lu, B. 2017. Oxidative stress regulates cellular bioenergetics in esophageal squamous cell carcinoma cell. *Bioscience Reports,* 37**,** BSR20171006.

Zhang, X., Zhao, M., Huang, A.-Y., Fei, Z., Zhang, W. & Wang, X.-L. 2005. The effect of cyclin D expression on cell proliferation in human gliomas. *Journal of Clinical Neuroscience,* 12**,** 166-168.

Zhang, Y. & Barres, B. A. 2010. Astrocyte heterogeneity: an underappreciated topic in neurobiology. *Current Opinion in Neurobiology,* 20**,** 588-594.

Zhang, Z., Chen, F. & Shang, L. 2018. Advances in antitumor effects of NSAIDs. *Cancer Management and Research,* 10**,** 4631-4640.

Zhang, Z., Jin, F., Lian, X., Li, M., Wang, G., Lan, B., He, H., Liu, G.-D., Wu, Y. & Sun, G. 2018. Genistein promotes ionizing radiation-induced cell death by reducing cytoplasmic Bcl-xL levels in non-small cell lung cancer. *Scientific Reports,* 8**,** 328.

Zhao, J., Zhu, J., Lv, X., Xing, J., Liu, S., Chen, C. & Xu, Y. 2017. curcumin potentiates the potent antitumor activity of acnU against glioblastoma by suppressing the Pi3K/aKT and nF-κB/cOX-2 signaling pathways. *OncoTargets and Therapy,* 10**,** 5471-5482.

Zhao, T., Zhang, C. P., Liu, Z. H., Wu, L. Y., Huang, X., Wu, H. T., Xiong, L., Wang, X., Wang, X. M. & Zhu, L. L. 2008. Hypoxia-driven proliferation of embryonic neural stem/progenitor cells–role of hypoxia-inducible transcription factor-1α. *The FEBS Journal,* 275**,** 1824-1834.

Zhao, W., Shi, F., Guo, Z., Zhao, J., Song, X. & Yang, H. 2018. Metabolite of ellagitannins, urolithin A induces autophagy and inhibits metastasis in human sw620 colorectal cancer cells. *Molecular Carcinogenesis,* 57**,** 193-200.

Zhao, Y., Altman, B. J., Coloff, J. L., Herman, C. E., Jacobs, S. R., Wieman, H. L., Wofford, J. A., Dimascio, L. N., Ilkayeva, O. & Kelekar, A. 2007. Glycogen synthase kinase 3α and 3β mediate a glucose-sensitive antiapoptotic signaling pathway to stabilize Mcl-1. *Molecular and Cellular biology,* 27**,** 4328-4339.

Zhao, Y. W., Jing, Z. L., Li, Y. & Mao, W. F. 2016. Berberine in combination with cisplatin suppresses breast cancer cell growth through induction of DNA breaks and caspase-3-dependent apoptosis. *Oncology Reports,* 36**,** 567-572.

Zheng, L., Roeder, R. G. & Luo, Y. 2003. S phase activation of the histone H2B promoter by OCA-S, a coactivator complex that contains GAPDH as a key component. *Cell,* 114**,** 255-266.

Zhi, H., Wang, L., Zhang, J., Zhou, C., Ding, F., Luo, A., Wu, M., Zhan, Q. & Liu, Z. 2006. Significance of COX-2 expression in human esophageal squamous cell carcinoma. *Carcinogenesis,* 27**,** 1214-1221.

Zhong, Y., Wang, Q. J., Li, X., Yan, Y., Backer, J. M., Chait, B. T., Heintz, N. & Yue, Z. 2009. Distinct regulation of autophagic activity by Atg14L and Rubicon associated with Beclin 1–phosphatidylinositol-3-kinase complex. *Nature Cell Biology,* 11**,** 468-476.

Zhou, J., Liu, Z. & Li, F. 2012. Upconversion nanophosphors for small-animal imaging. *Chemical Society Reviews,* 41**,** 1323-1349.

Zhou, J., Patel, T. R., Sirianni, R. W., Strohbehn, G., Zheng, M.-Q., Duong, N., Schafbauer, T., Huttner, A. J., Huang, Y. & Carson, R. E. 2013. Highly penetrative, drug-loaded nanocarriers improve treatment of glioblastoma. *Proceedings of the National Academy of Sciences,* 110**,** 11751-11756.

Zhou, J., Schmid, T., Schnitzer, S. & Brüne, B. 2006. Tumor hypoxia and cancer progression. *Cancer Letters,* 237**,** 10-21.

Zimmermann, G. R., Lehar, J. & Keith, C. T. 2007. Multi-target therapeutics: when the whole is greater than the sum of the parts. *Drug Discovery Today,* 12**,** 34-42.

Zimmermann, K. C., Sarbia, M., Weber, A.-A., Borchard, F., Gabbert, H. E. & Schrör, K. 1999. Cyclooxygenase-2 expression in human esophageal carcinoma. *Cancer Research,* 59**,** 198-204.

Zirlik, K. & Duyster, J. 2018. Anti-angiogenics: Current situation and future perspectives. *Oncology Research and Treatment,* 41**,** 166-171.

Zolota, V., Tsamandas, A. C., Aroukatos, P., Panagiotopoulos, V., Maraziotis, T., Poulos, C. & Scopa, C. D. 2008. Expression of cell cycle inhibitors p21, p27, p14 and p16 in gliomas. Correlation with classic prognostic factors and patients' outcome. *Neuropathology,* 28**,** 35-42.

Zong, H., Parada, L. F. & Baker, S. J. 2015. Cell of origin for malignant gliomas and its implication in therapeutic development. *Cold Spring Harbor Perspectives in Biology,* 7**,** a020610.

Zong, H., Verhaak, R. G. & Canoll, P. 2012. The cellular origin for malignant glioma and prospects for clinical advancements. *Expert Review of Molecular Diagnostics,* 12**,** 383-394.

Zorov, D. B., Kinnally, K. W. & Tedeschi, H. 1992. Voltage Activation of Heart Inner Mitochondrial-Membrane Channels. *Journal of Bioenergetics and Biomembranes,* 24**,** 119-124.

Zorova, L. D., Popkov, V. A., Plotnikov, E. Y., Silachev, D. N., Pevzner, I. B., Jankauskas, S. S., Babenko, V. A., Zorov, S. D., Balakireva, A. V., Juhaszova, M., Sollott, S. J. & Zorov, D. B. 2018. Mitochondrial membrane potential. *Analytical Biochemistry,* 552**,** 50-59.

Zu, X. L. & Guppy, M. 2004. Cancer metabolism: facts, fantasy, and fiction. Biochemical and Biophysical Research Communications, 313, 459-465.

CHAPTER 9: APPENDICES

Table 9. 1. SDS-PAGE gel constituents for preparing four mini gels.

Constituent	Resolving Gel (30 ml)			Stacking Gel (10 ml)
	8%	10%	12%	
d.H_20	13.9 ml	11.9 ml	9.9 ml	6.8 ml
30%(w/v) Acrylamide mix	8 ml	10 ml	12 ml	1.7 ml
Tris buffer	7.5 ml 1.5M (PH8.8)	7.5 ml 1.5M (PH8.8)	7.5 ml 1.5M (PH8.8)	1.25 ml 1M (PH6.8)
10%(w/v) SDS	0.3 ml	0.3 ml	0.3 ml	0.1 ml
10%(w/v) Ammonium persulfate	0.3 ml	0.3 ml	0.3 ml	0.1 ml
TEMED	0.018 ml	0.012 ml	0.012 ml	0.01 ml

Table 9. 2. Specifications for the used primary antibodies and blotting conditions.

Antibody	Source	Molecular Wt. (KDa)	Resolving gel (final acrylamide concentration %)	Blotting membrane	Dilution	Diluting solution
Cyclin D1	Rabbit mAb	36	10	PVDF	1:2000	5%(w/v) BSA in PBS-T
p- Cyclin D1	Rabbit mAb	36	10	PVDF	1:2000	5%(w/v) BSA in PBS-T
PI3 Kinase Class III	Rabbit mAb	100	10	Nitrocellulose	1:1000	5%(w/v) milk in PBS-T
PIK3R4	Rabbit	153	8	Nitrocellulose	1:1000	5%(w/v) milk in PBS-T
ATG14	Rabbit	65	8	Nitrocellulose	1:1000	5%(w/v) BSA in PBS-T
HIF-1α	Mouse	120	8	PVDF, Nitrocellulose	1:500	5%(w/v) milk in PBS-T
HIF1β/ARNT1	Mouse	95	8	PVDF, Nitrocellulose	1:1000	5%(w/v) milk in PBS-T
p-c-Jun	Rabbit mAb	48	12	Nitrocellulose	1:1000	5%(w/v) milk in PBS-T
p-Hsp27	Rabbit mAb	27	12	Nitrocellulose	1:1000	5%(w/v) milk in PBS-T
β-actin	Mouse mAb	42	8-12	PVDF, Nitrocellulose	1:3000	5%(w/v) milk in PBS-T

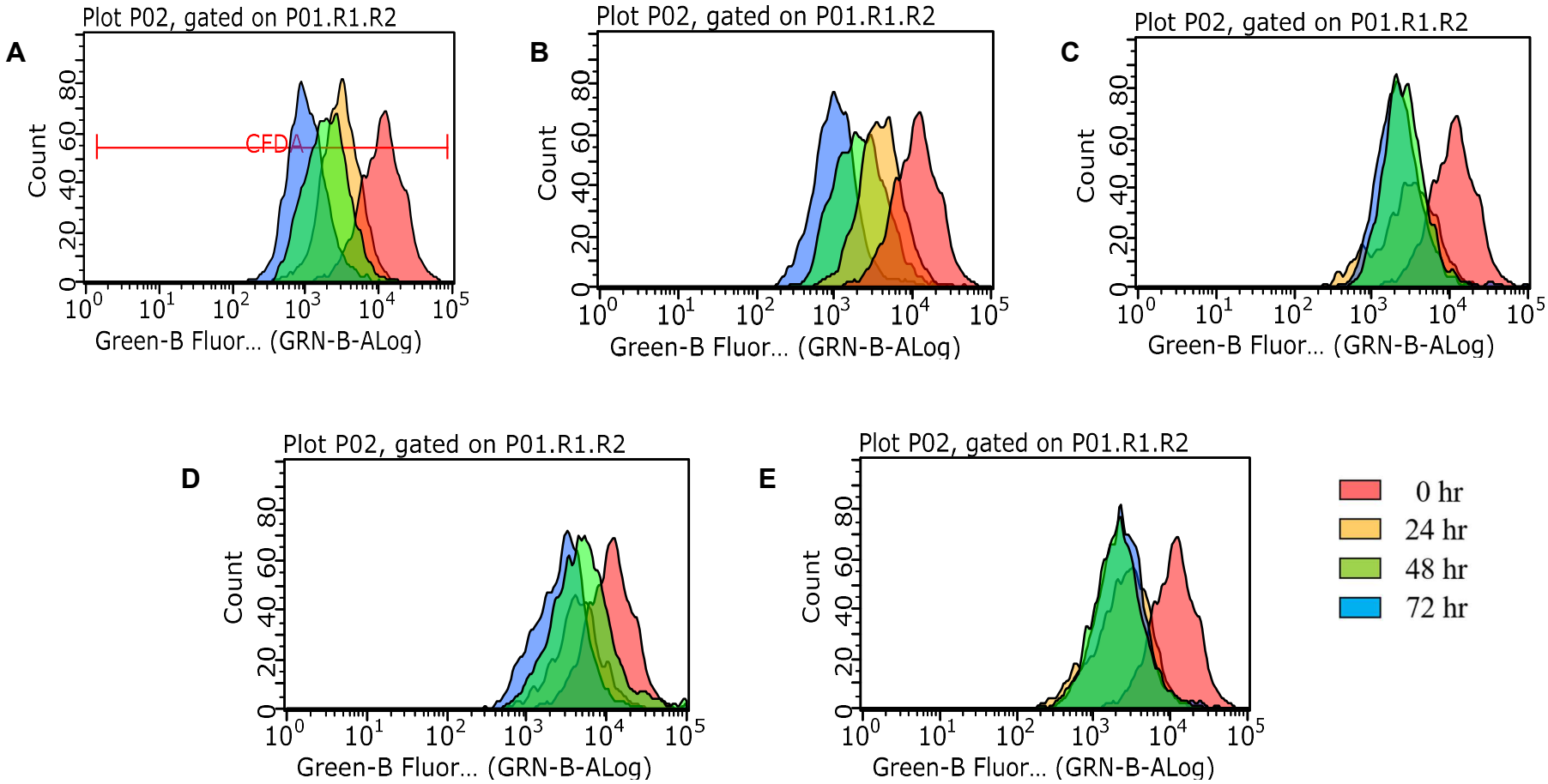

Figure 9. 1. Representative plots for cell proliferation following monotherapy in U87-MG cell line under normoxia. The data illustrates the effect following drug treatment over a period of three days, a leftward shift indicating cell proliferation. Red, yellow, green, and blue peaks represent the fluorescence of 0, 24, 48, and 72 hours, respectively. Panel A depicts control treatment, where a shift towards the left can be observed. Panel B and C are for Aspirin and PN517 treatments respectively, panel D shows effect following cisplatin treatment, where over lapping peaks suggest inhibition of proliferation. Panel E indicates TMZ treatment effects.

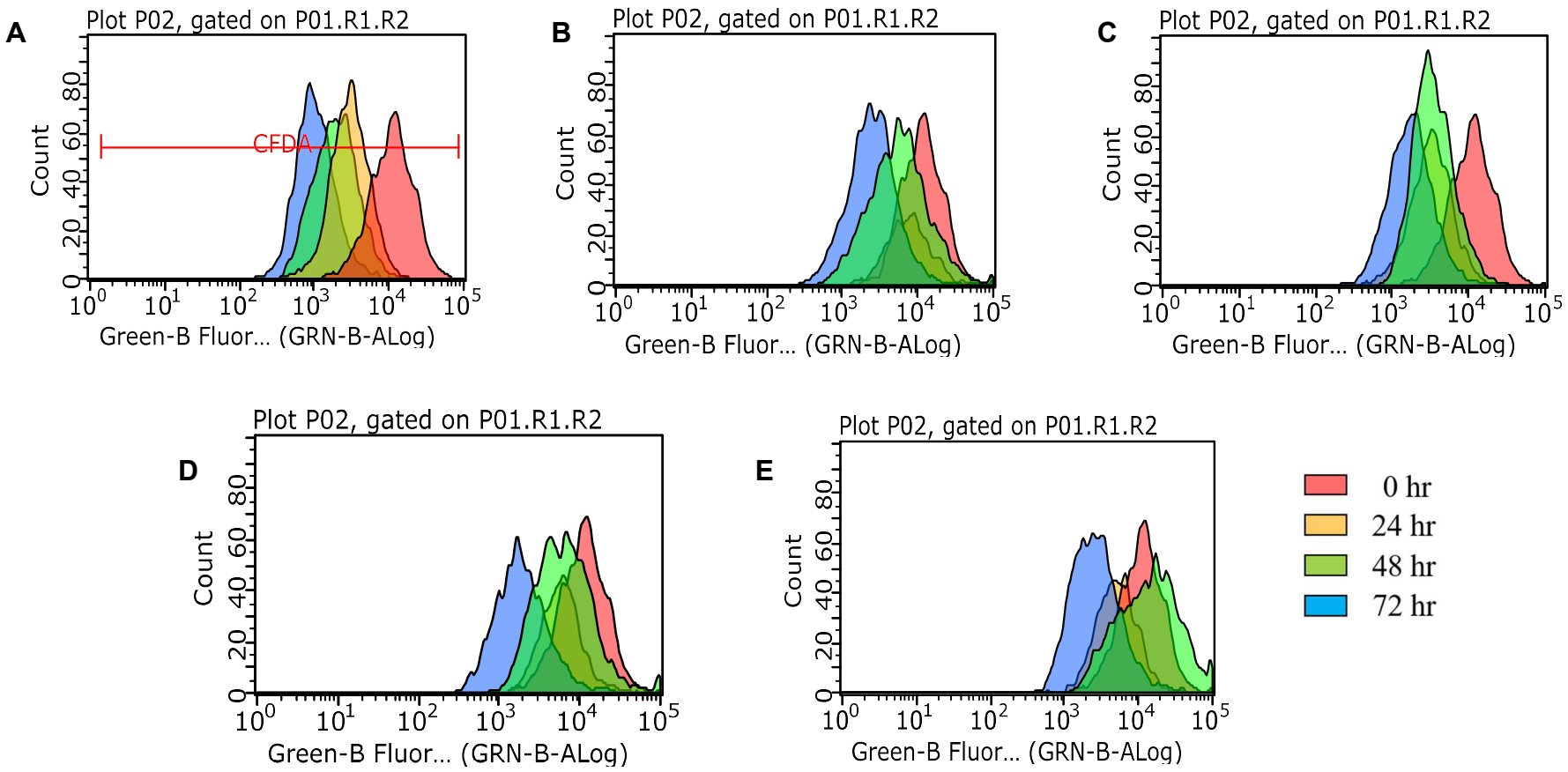

Figure 9. 2. Representative plots for cell proliferation following combined therapy in U87-MG cell line under normoxia. The data illustrates the effect following drug treatment over a period of three days, a leftward shift indicating cell proliferation. Red, yellow, green, and blue peaks represent the fluorescence of 0, 24, 48, and 72 hours, respectively. Panel A depicts control treatment, where a shift towards the left can be observed. Panel B and C are for Asp+Cis and Asp+TMZ treatments respectively. Panel D and E are for PN517+Cis and PN517+TMZ treatments respectively, where over lapping peaks suggest inhibition of proliferation.

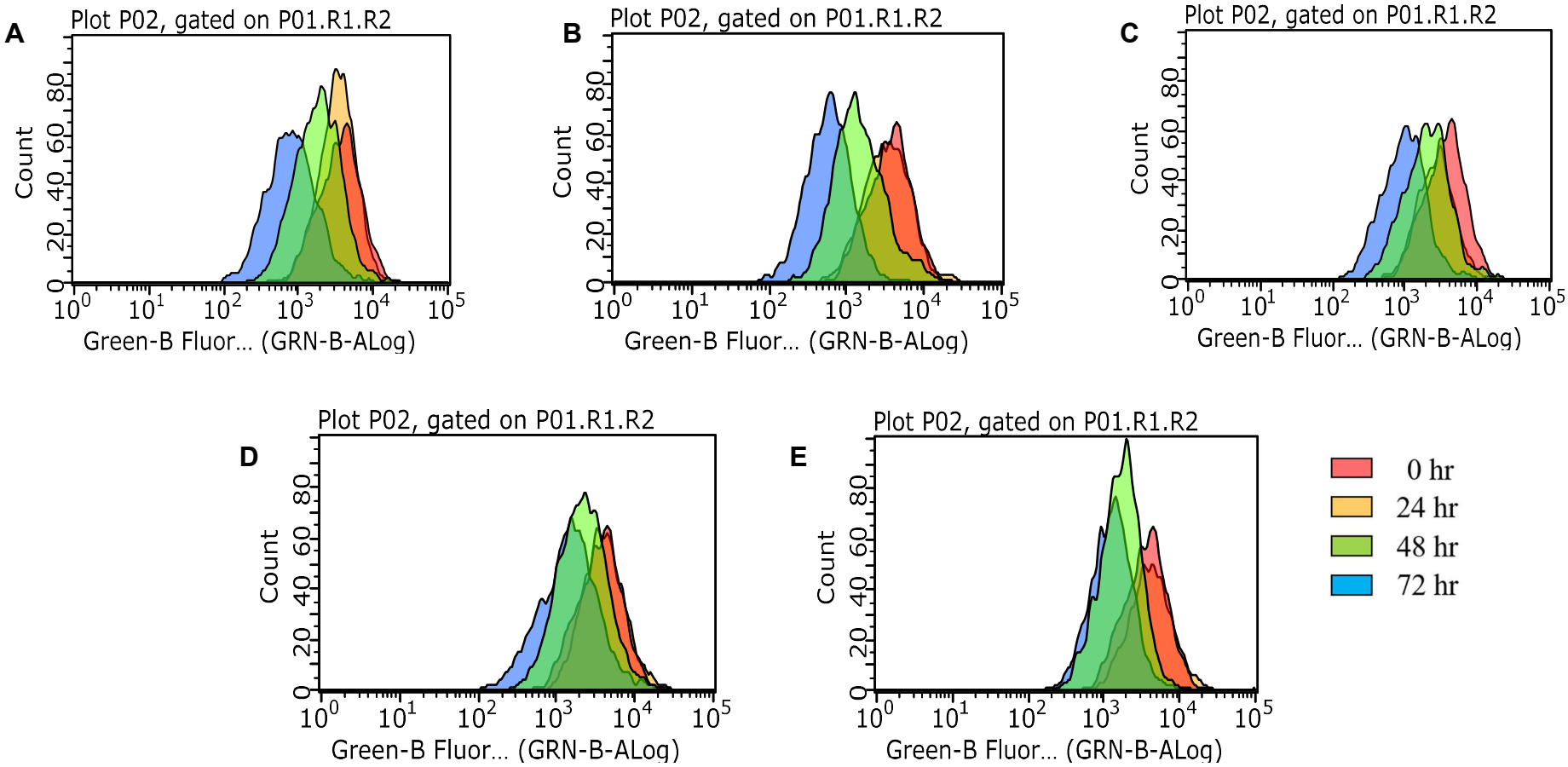

Figure 9. 3. Representative plots for cell proliferation following monotherapy in U87-MG cell line under hypoxia. The data illustrates the effect following drug treatment over a period of three days, a leftward shift indicating cell proliferation. Red, yellow, green, and blue peaks represent the fluorescence of 0, 24, 48, and 72 hours, respectively. Panel A depicts control treatment, where a shift towards the left can be observed. Panel B and C are for Aspirin and PN517 treatments respectively, panel D shows effect following cisplatin treatment, where over lapping peaks suggest inhibition of proliferation. Panel E indicates TMZ treatment effects.

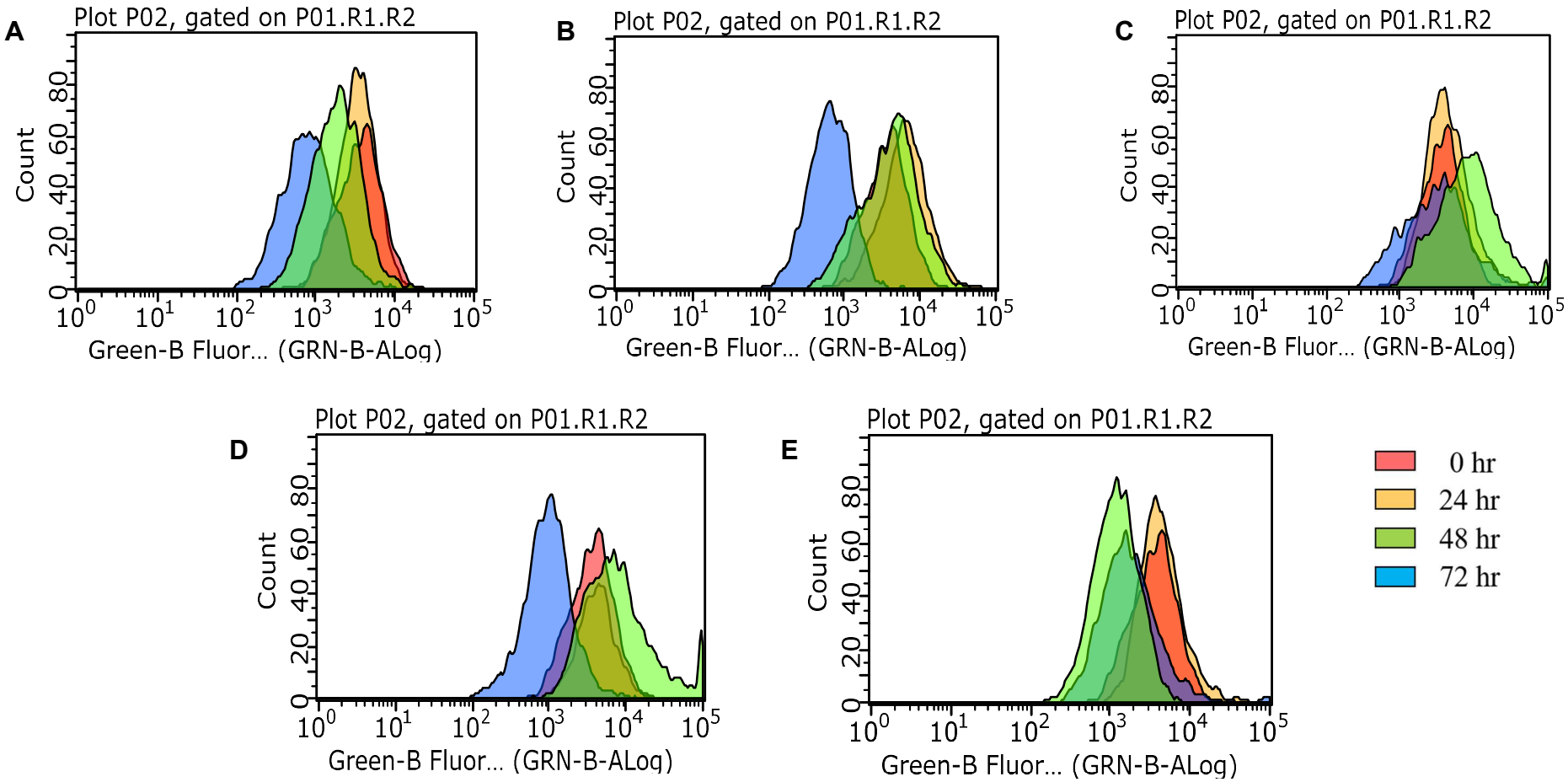

Figure 9. 4. Representative plots for cell proliferation following combined therapy in U87-MG cell line under hypoxia. The data illustrates the effect following drug treatment over a period of three days, a leftward shift indicating cell proliferation. Red, yellow, green, and blue peaks represent the fluorescence of 0, 24, 48, and 72 hours, respectively. Panel A depicts control treatment, where a shift towards the left can be observed. Panel B and C are for Asp+Cis and Asp+TMZ treatments respectively. Panel D and E are for PN517+Cis and PN517+TMZ treatments respectively, where over lapping peaks suggest inhibition of proliferation.

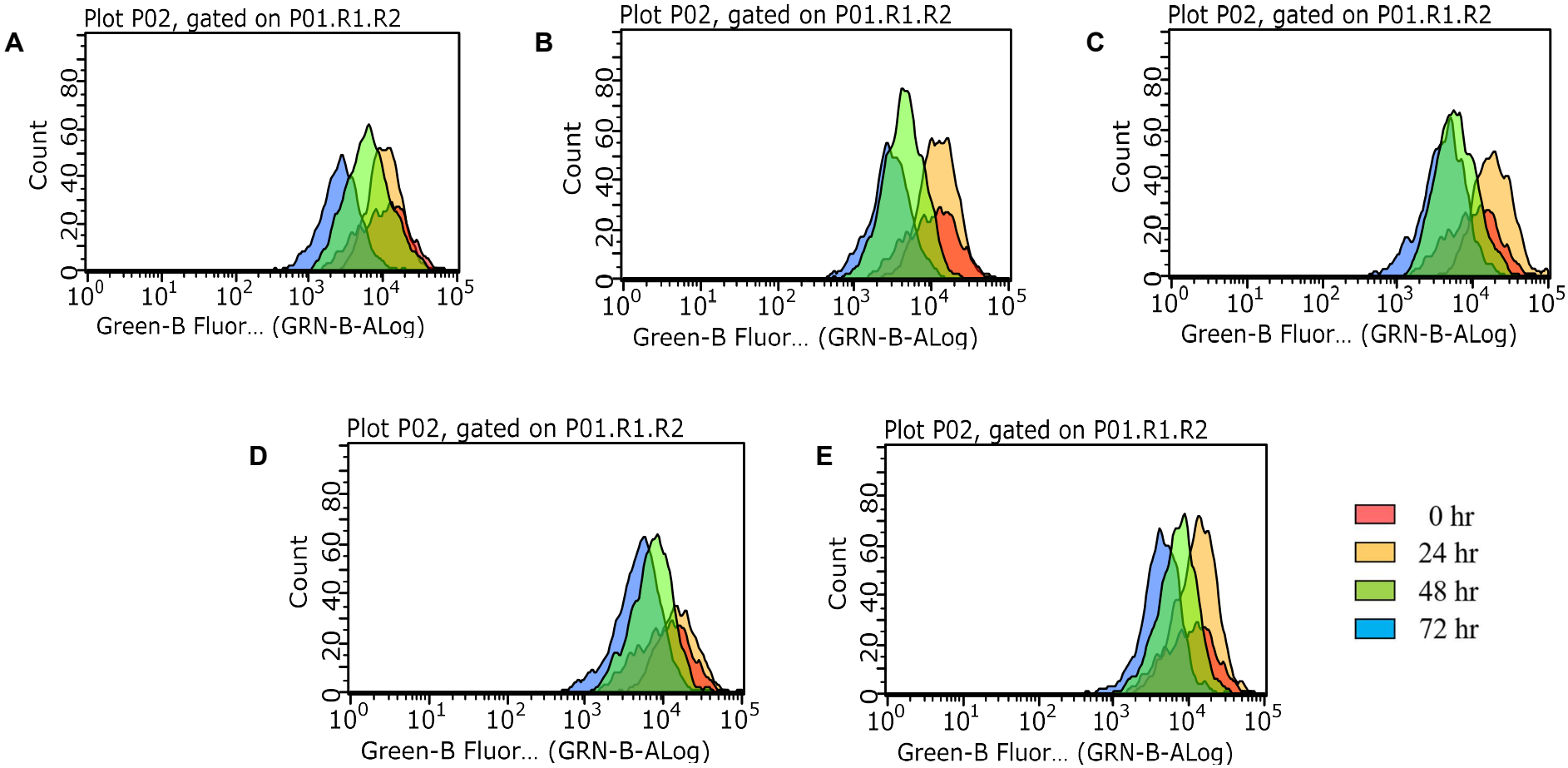

Figure 9. 5. Representative plots for cell proliferation following monotherapy in SVG-p12 cell line under normoxia. The data illustrates the effect following drug treatment over a period of three days, a leftward shift indicating cell proliferation. Red, yellow, green, and blue peaks represent the fluorescence of 0, 24, 48, and 72 hours, respectively. Panel A depicts control treatment, where a shift towards the left can be observed. Panel B and C are for Aspirin and PN517 treatments respectively, panel D shows effect following cisplatin treatment, where over lapping peaks suggest inhibition of proliferation. Panel E indicates TMZ treatment effects.

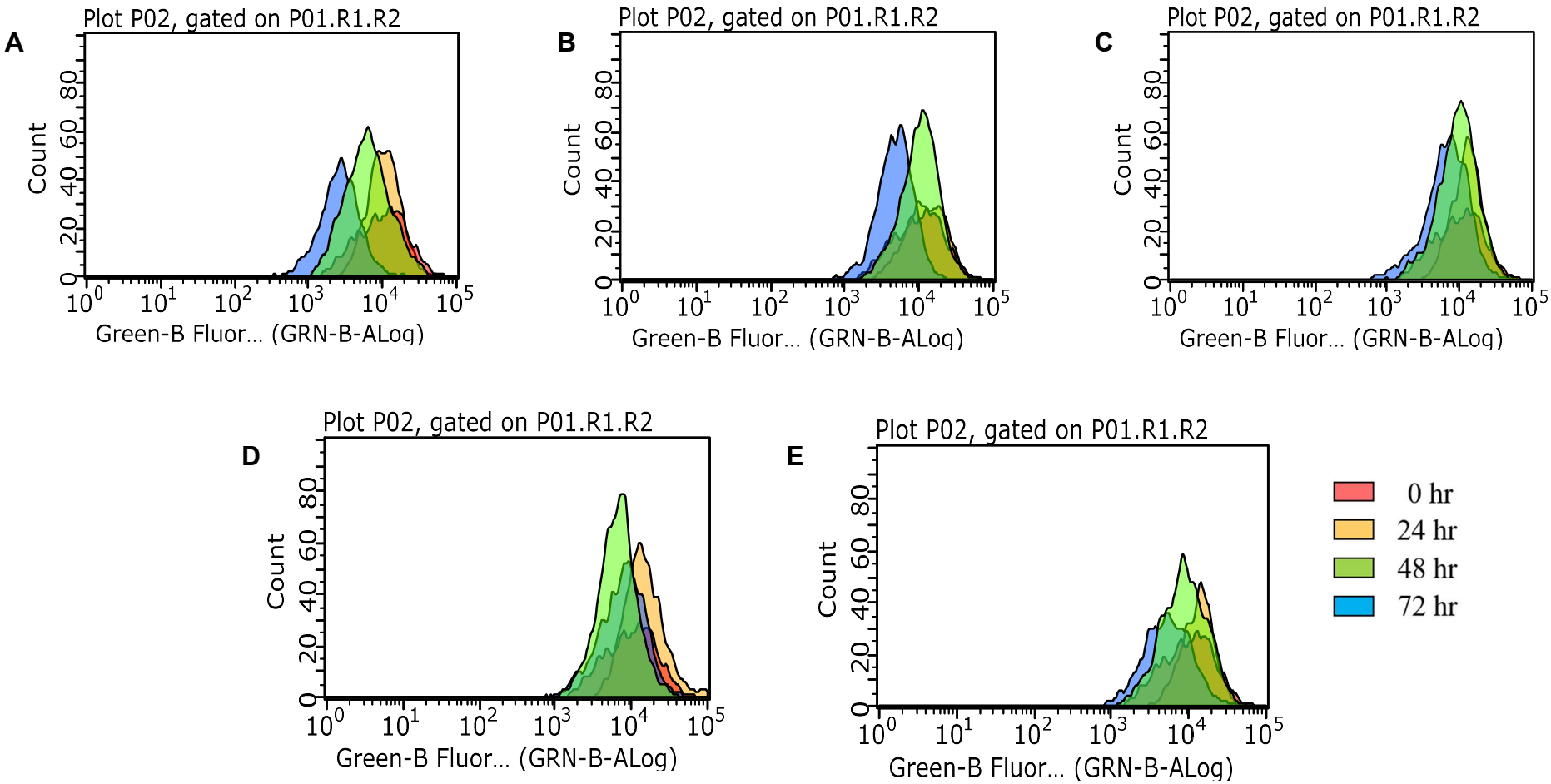

Figure 9. 6. Representative plots for cell proliferation following combined therapy in SVG-p12 cell line under normoxia. The data illustrates the effect following drug treatment over a period of three days, a leftward shift indicating cell proliferation. Red, yellow, green, and blue peaks represent the fluorescence of 0, 24, 48, and 72 hours, respectively. Panel A depicts control treatment, where a shift towards the left can be observed. Panel B and C are for Asp+Cis and Asp+TMZ treatments respectively. Panel D and E are for PN517+Cis and PN517+TMZ treatments respectively, where over lapping peaks suggest inhibition of proliferation.

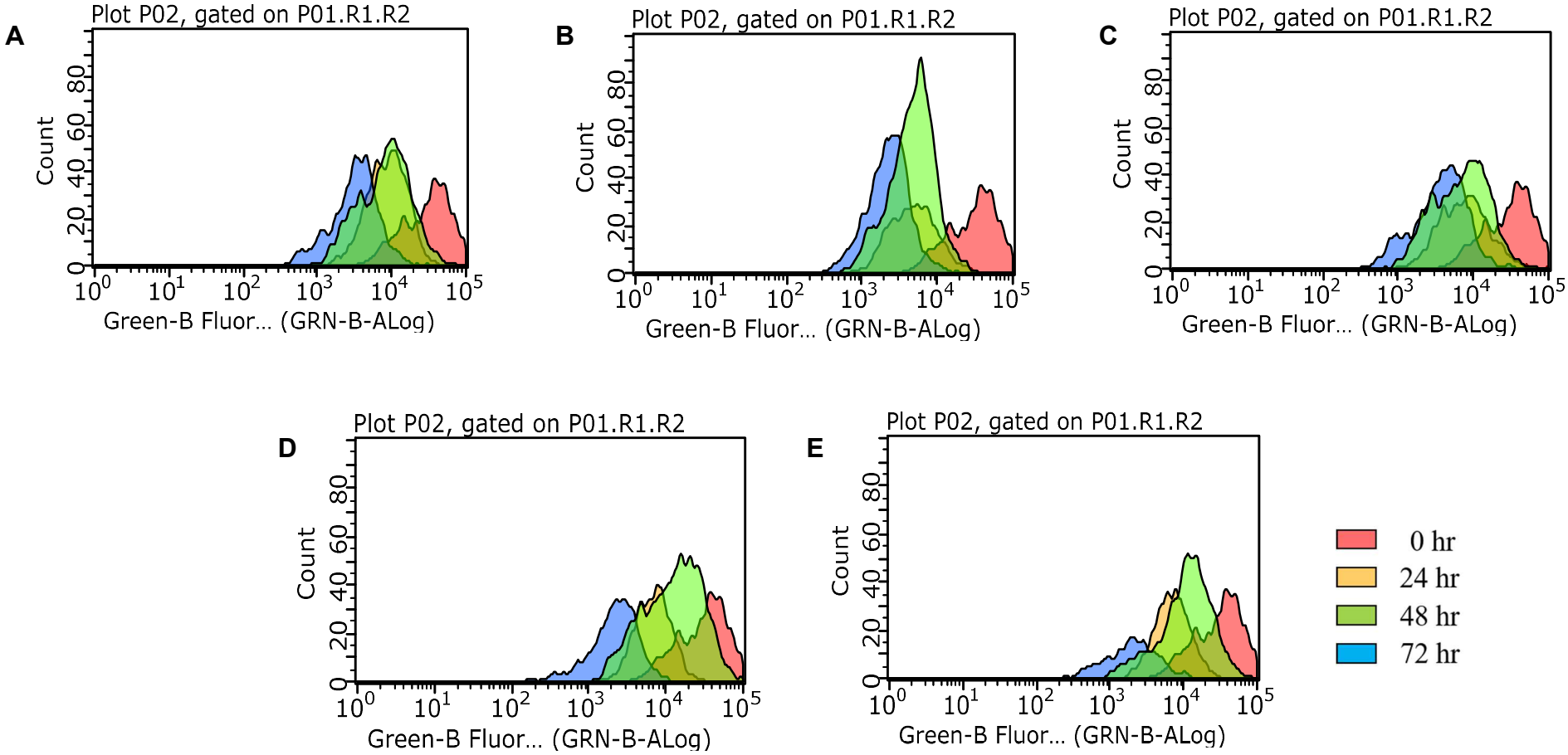

Figure 9. 7. Representative plots for cell proliferation following monotherapy in SVG-p12 cell line under hypoxia. The data illustrates the effect following drug treatment over a period of three days, a leftward shift indicating cell proliferation. Red, yellow, green, and blue peaks represent the fluorescence of 0, 24, 48, and 72 hours, respectively. Panel A depicts control treatment, where a shift towards the left can be observed. Panel B and C are for Aspirin and PN517 treatments respectively, panel D shows effect following cisplatin treatment, where over lapping peaks suggest inhibition of proliferation. Panel E indicates TMZ treatment effects.

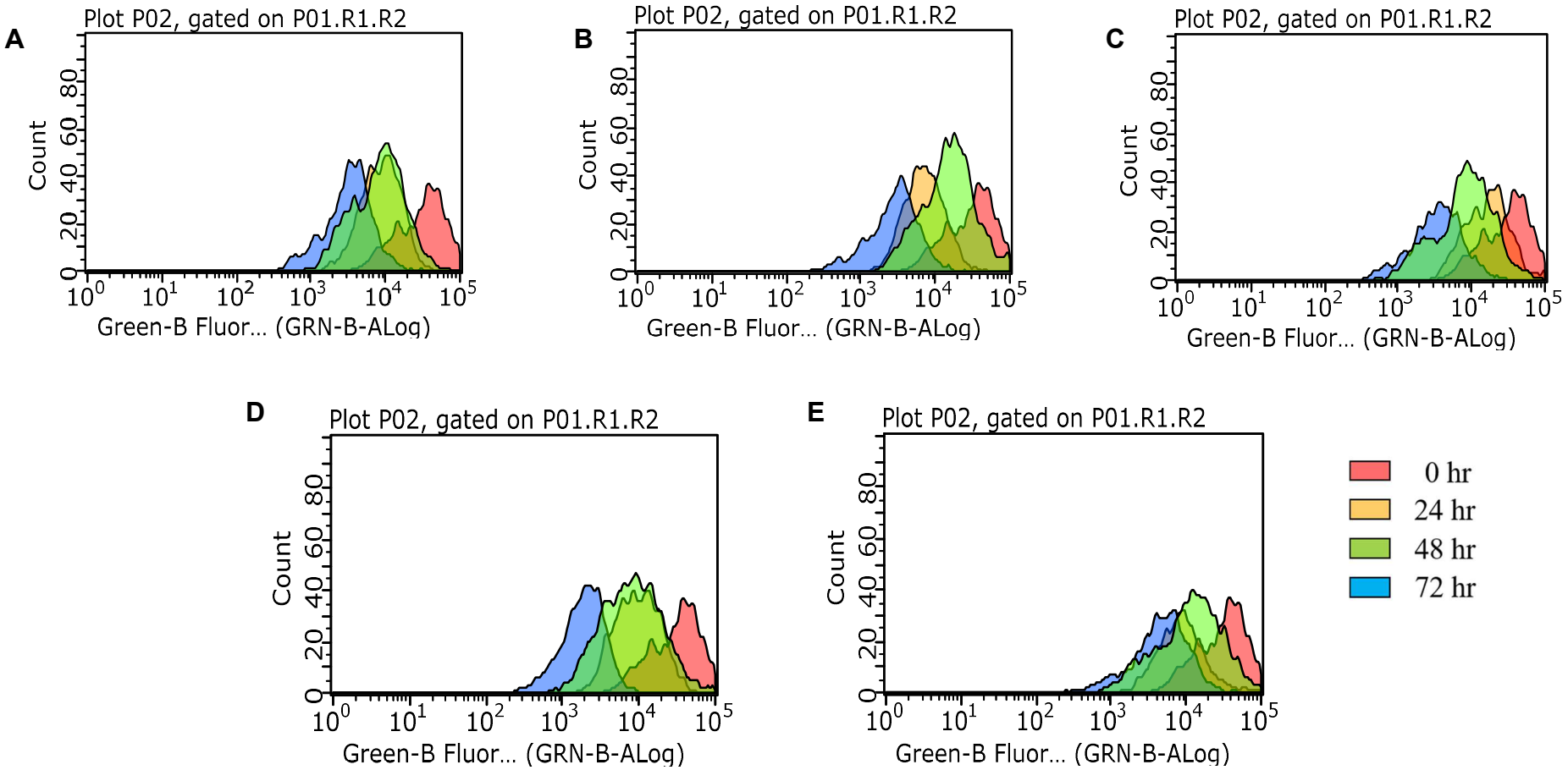

Figure 9. 8. Representative plots for cell proliferation following combined therapy in SVG-p12 cell line under hypoxia. The data illustrates the effect following drug treatment over a period of three days, a leftward shift indicating cell proliferation. Red, yellow, green, and blue peaks represent the fluorescence of 0, 24, 48, and 72 hours, respectively. Panel A depicts control treatment, where a shift towards the left can be observed. Panel B and C are for Asp+Cis and Asp+TMZ treatments respectively. Panel D and E are for PN517+Cis and PN517+TMZ treatments respectively, where over lapping peaks suggest inhibition of proliferation.

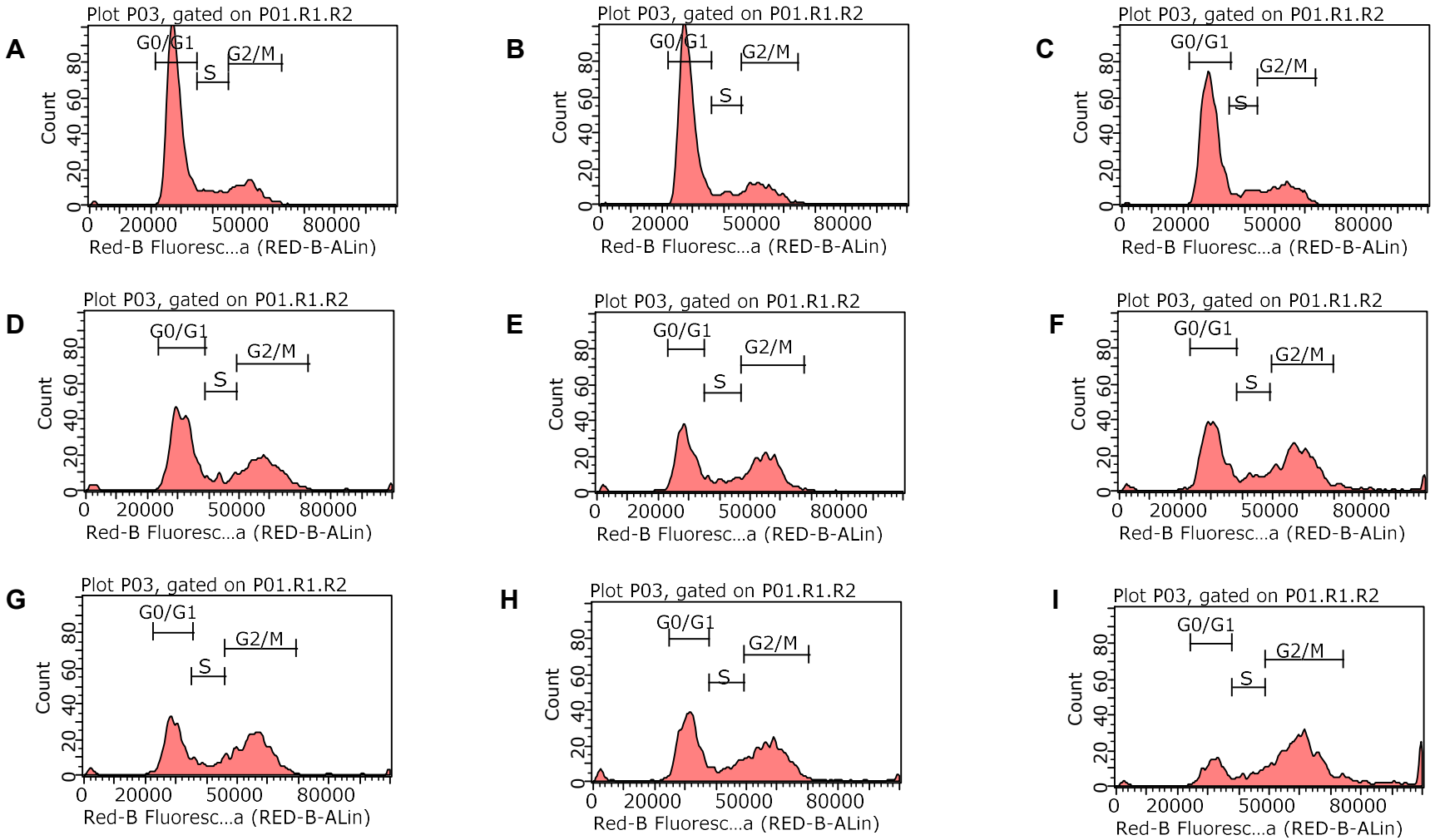

Figure 9. 9. Representative plots for cell cycle analysis following 72 hours of mono- and combined therapy in U87-MG cell line under normoxia. Data illustrates the effect on cell cycle phases using RNase and Propidium iodide. The treatments are as follows: A) Control, B) Aspirin, C) PN517, D) Cisplatin, E) TMZ, F) Aspirin+ cisplatin, G) Aspirin+ TMZ, H) PN517+ cisplatin, I) PN517+ TMZ.

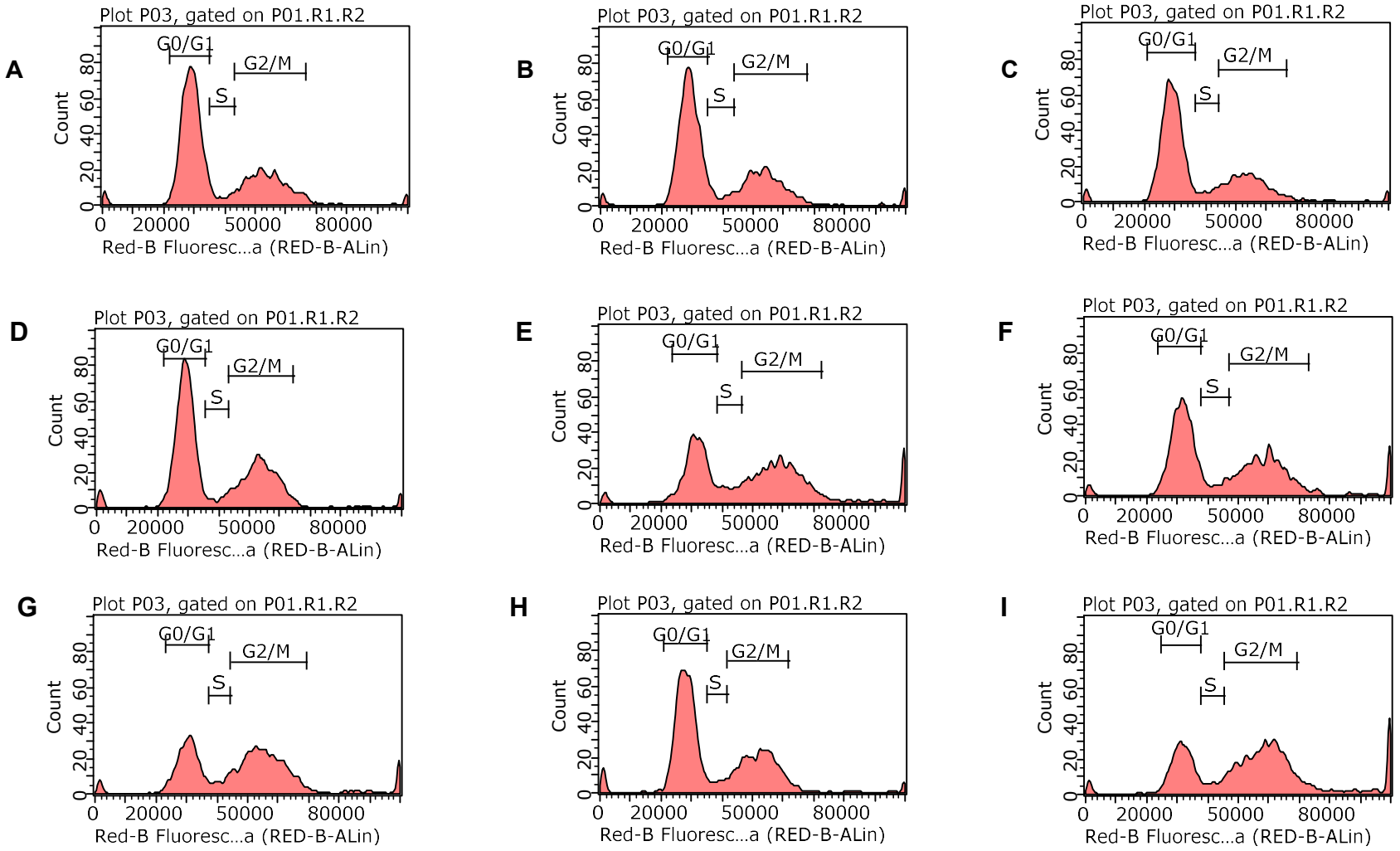

Figure 9. 10. Representative plots for cell cycle analysis following 72 hours of mono- and combined therapy in U87-MG cell line under hypoxia. Data illustrates the effect on cell cycle phases using RNase and Propidium iodide. The treatments are as follows: A) Control, B) Aspirin, C) PN517, D) Cisplatin, E) TMZ, F) Aspirin+ cisplatin, G) Aspirin+ TMZ, H) PN517+ cisplatin, I) PN517+ TMZ.

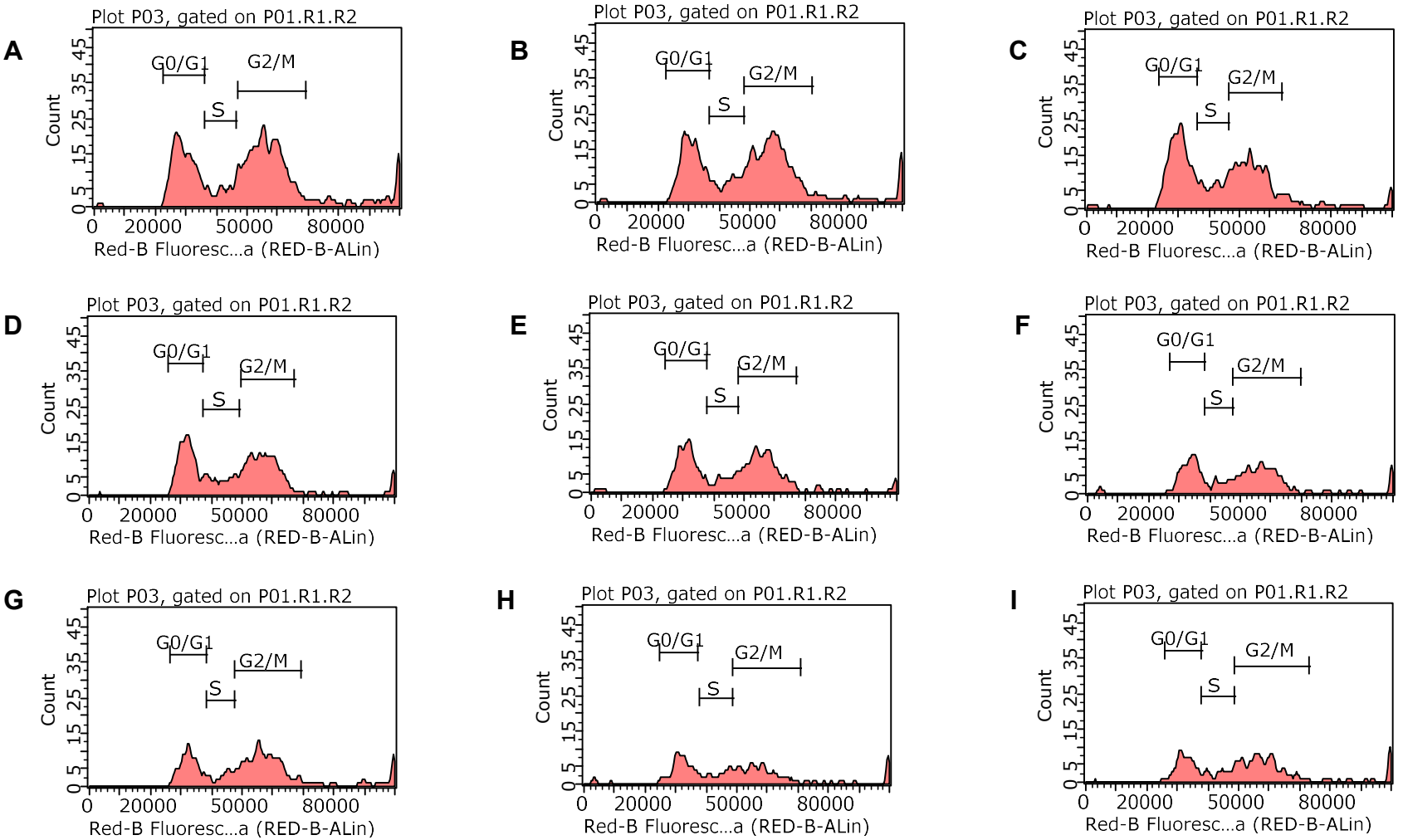

Figure 9. 11. Representative plots for cell cycle analysis following 72 hours of mono- and combined therapy in SVG-p12 cell line under normoxia. Data illustrates the effect on cell cycle phases using RNase and Propidium iodide. The treatments are as follows: A) Control, B) Aspirin, C) PN517, D) Cisplatin, E) TMZ, F) Aspirin+ cisplatin, G) Aspirin+ TMZ, H) PN517+ cisplatin, I) PN517+ TMZ.

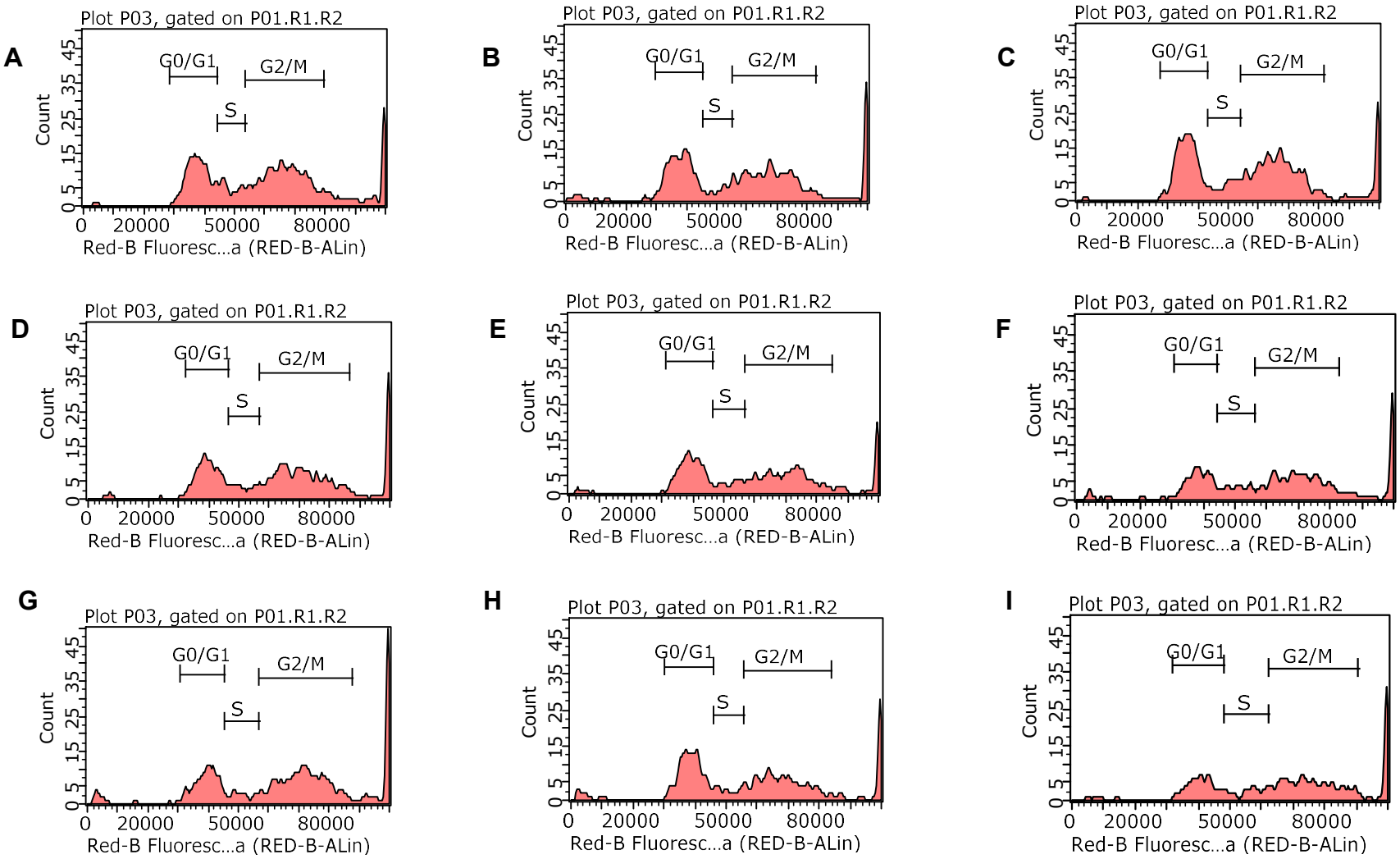

Figure 9. 12. Representative plots for cell cycle analysis following 72 hours of mono- and combined therapy in SVG-p12 cell line under hypoxia. Data illustrates the effect on cell cycle phases using RNase and Propidium iodide. The treatments are as follows: A) Control, B) Aspirin, C) PN517, D) Cisplatin, E) TMZ, F) Aspirin+ cisplatin, G) Aspirin+ TMZ, H) PN517+ cisplatin, I) PN517+ TMZ

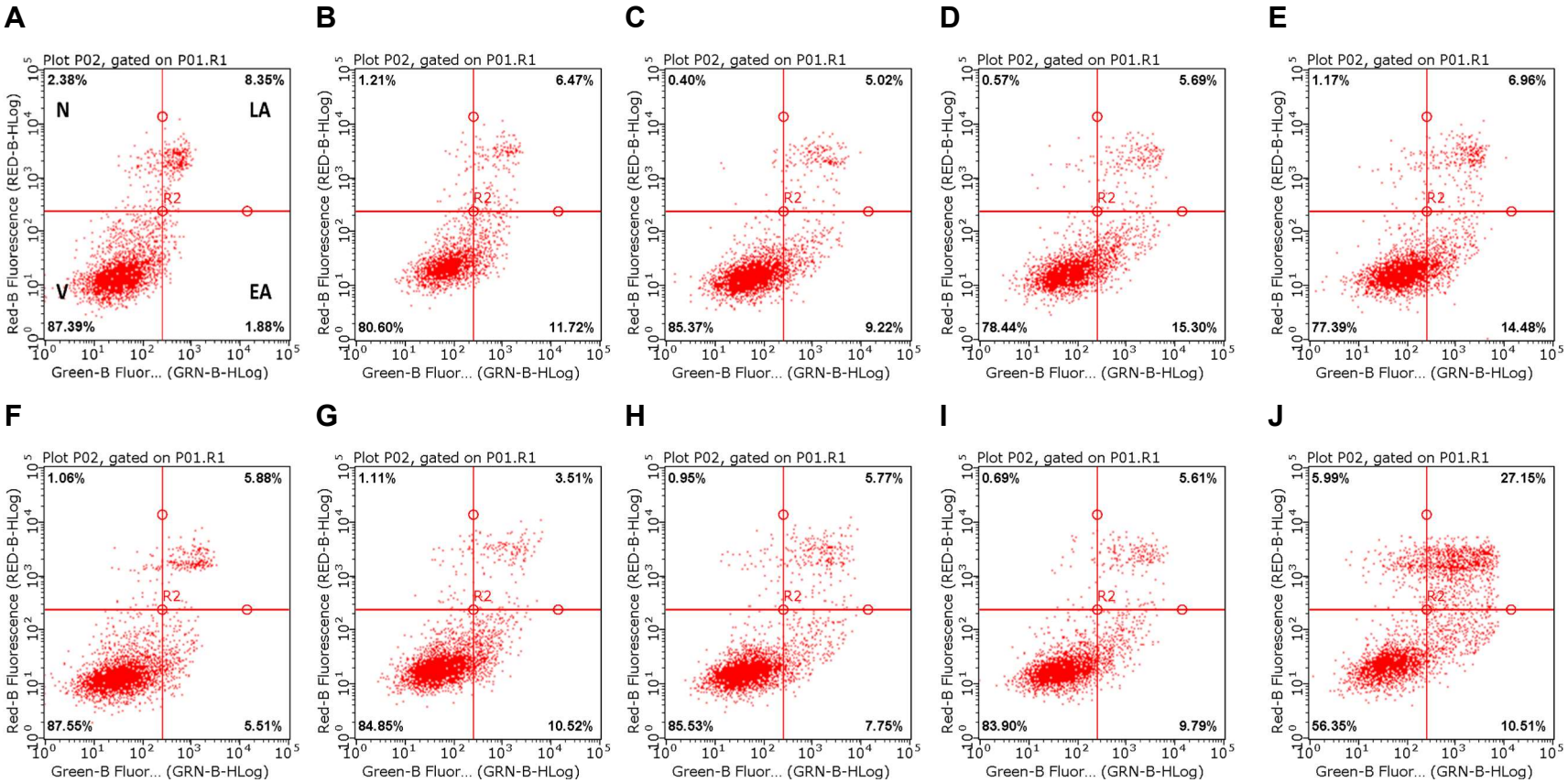

Figure 9. 13. Representative dot-plots for apoptosis assay following 72 hours of drug treatment in U87-MG cell line under normoxia. Images obtained from the flow-cytometer following analysis of the apoptosis assay using Annexin V/ PI staining at 72 hours. The treatments are as follows: A) Control, B) Cisplatin, C) Aspirin, D) PN517, E) TMZ, F) DMSO, G) Aspirin+ cisplatin, H) Aspirin+ TMZ, I) PN517+ cisplatin, J) PN517+ TMZ. Quadrant top-left indicates necrotic cells; quadrant top-right indicates late apoptosis; quadrant bottom-left depicts live cells whereas quadrant bottom-right indicates early apoptosis.

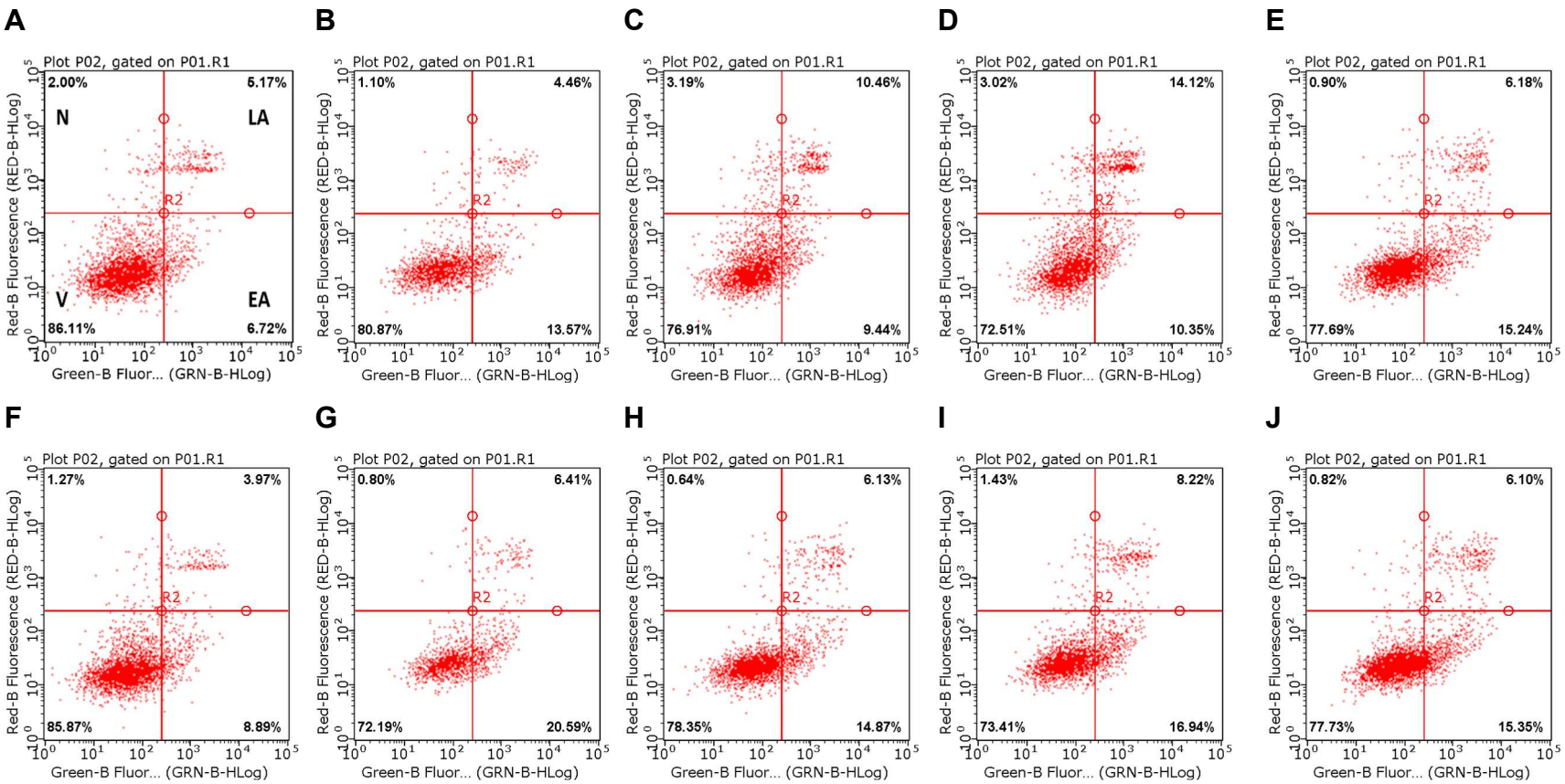

Figure 9. 14. Representative dot-plots for apoptosis assay following 72 hours of drug treatment in U87-MG cell line under hypoxia. Images obtained from the flow-cytometer following analysis of the apoptosis assay using Annexin V/ PI staining at 72 hours. The treatments are as follows: A) Control, B) Cisplatin, C) Aspirin, D) PN517, E) TMZ, F) DMSO, G) Aspirin+ cisplatin, H) Aspirin+ TMZ, I) PN517+ cisplatin, J) PN517+ TMZ. Quadrant top-left indicates necrotic cells; quadrant top-right indicates late apoptosis; quadrant bottom-left depicts live cells whereas quadrant bottom-right indicates early apoptosis.

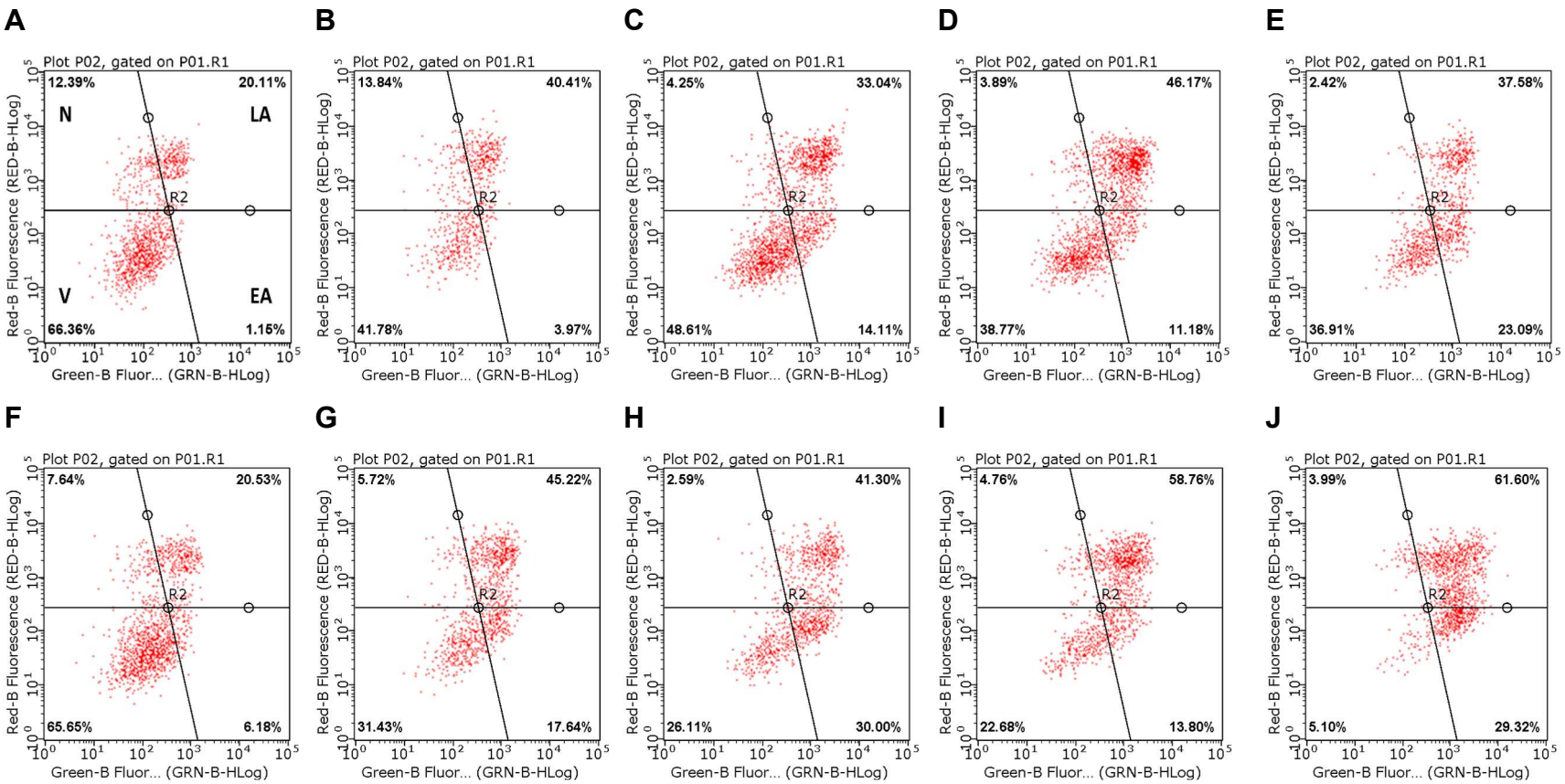

Figure 9. 15. Representative dot-plots for apoptosis assay following 72 hours of drug treatment in SVG-p12 cell line under normoxia. Images obtained from the flow-cytometer following analysis of the apoptosis assay using Annexin V/ PI staining at 72 hours. The treatments are as follows: A) Control, B) Cisplatin, C) Aspirin, D) PN517, E) TMZ, F) DMSO, G) Aspirin+ cisplatin, H) Aspirin+ TMZ, I) PN517+ cisplatin, J) PN517+ TMZ. Quadrant top-left indicates necrotic cells; quadrant top-right indicates late apoptosis; quadrant bottom-left depicts live cells whereas quadrant bottom-right indicates early apoptosis.

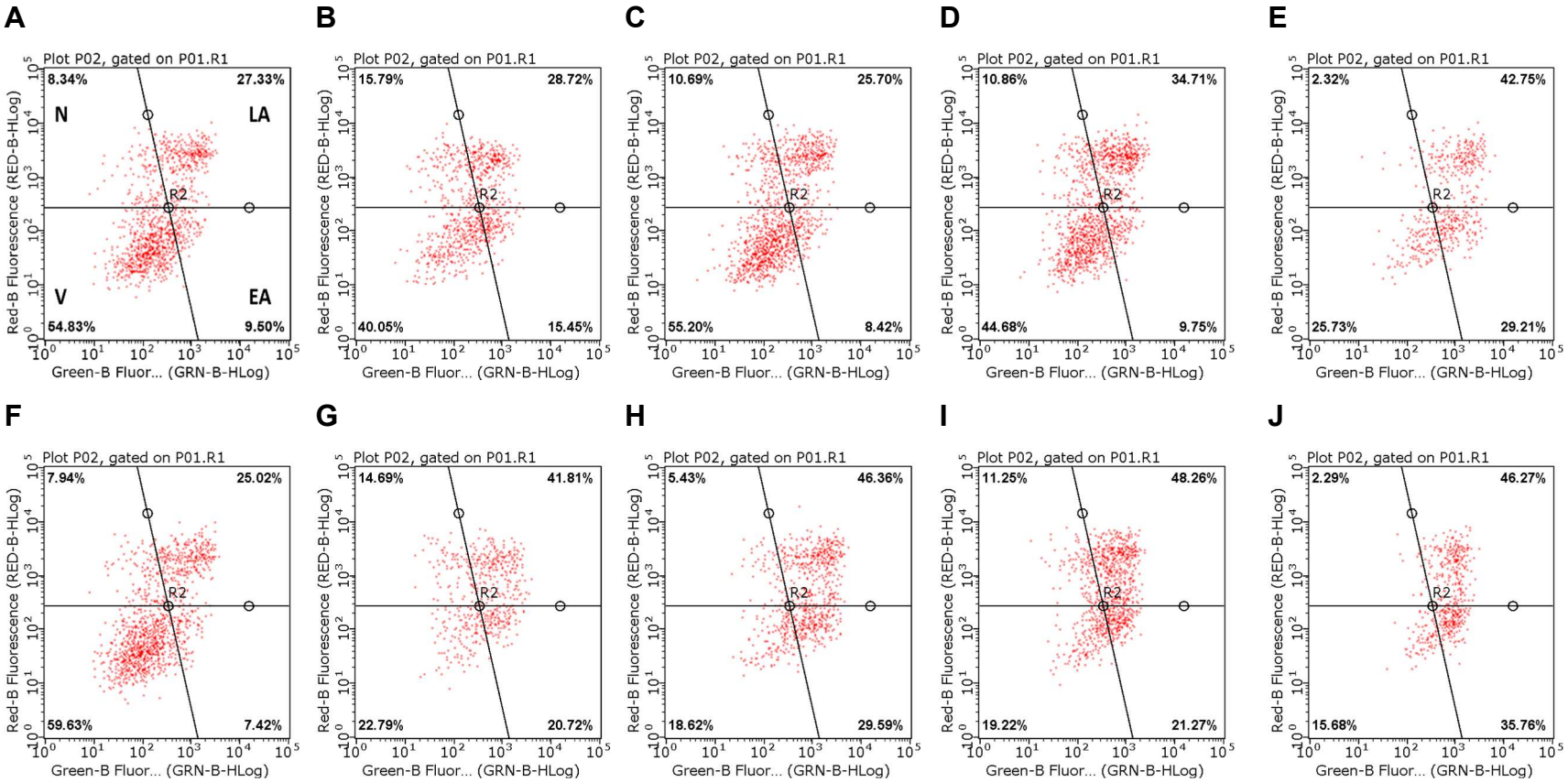

Figure 9. 16. Representative dot-plots for apoptosis assay following 72 hours of drug treatment in SVG-p12 cell line under hypoxia. Images obtained from the flow-cytometer following analysis of the apoptosis assay using Annexin V/ PI staining at 72 hours. The treatments are as follows: A) Control, B) Cisplatin, C) Aspirin, D) PN517, E) TMZ, F) DMSO, G) Aspirin+ cisplatin, H) Aspirin+ TMZ, I) PN517+ cisplatin, J) PN517+ TMZ. Quadrant top-left indicates necrotic cells; quadrant top-right indicates late apoptosis; quadrant bottom-left depicts live cells whereas quadrant bottom-right indicates early apoptosis**.**

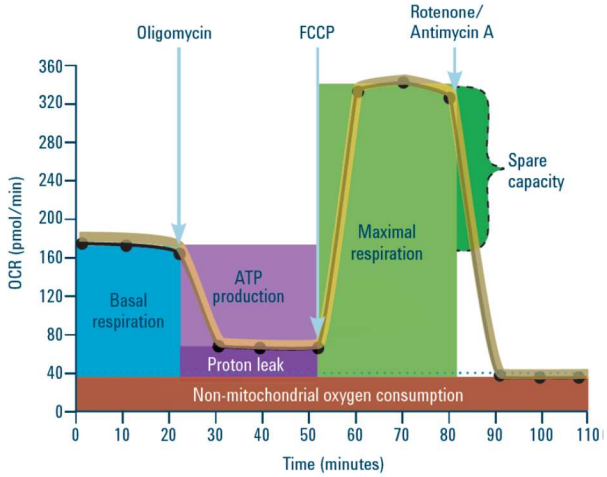

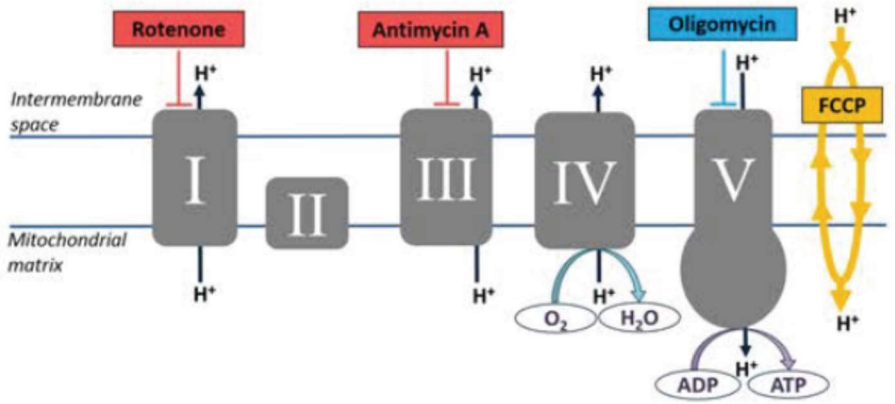

Parameter	Equation Used in Report Generator
Non-mitochondrial Respiration	Minimum rate measurement after Rotenone/antimycin A injection
Basal Respiration	(Last rate measurement before first injection) – (Non-Mitochondrial Respiration Rate)
Maximal Respiration	(Maximum rate measurement after FCCP injection) – (Non-Mitochondrial Respiration)
H+ (Proton) Leak	(Minimum rate measurement after Oligomycin injection) – (Non-Mitochondrial Respiration
ATP Production	(Last rate measurement before Oligomycin injection) – (Minimum rate measurement after Oligomycin injection)
Spare Respiratory Capacity	(Maximal Respiration) – (Basal Respiration)
Spare Respiratory Capacity as a %	(Maximal Respiration) / (Basal Respiration) × 100
Acute Response	(Last rate measurement before oligomycin Injection) – (Last rate measurement before acute injection)
Coupling Efficiency	ATP Production Rate) / (Basal Respiration Rate) × 100

Figure 9. 17. Seahorse XFp Cell Mito Stress Test Modulators of the ETC. The diagram illustrates the complexes of the ETC and the target of action of all of the compounds in the Seahorse XFp Cell Mito Stress Test Kit. Oligomycin inhibits ATP synthase (complex V), FCCP uncouples oxygen consumption from ATP production, and rotenone and antimycin A inhibit complexes I and III, respectively**.**

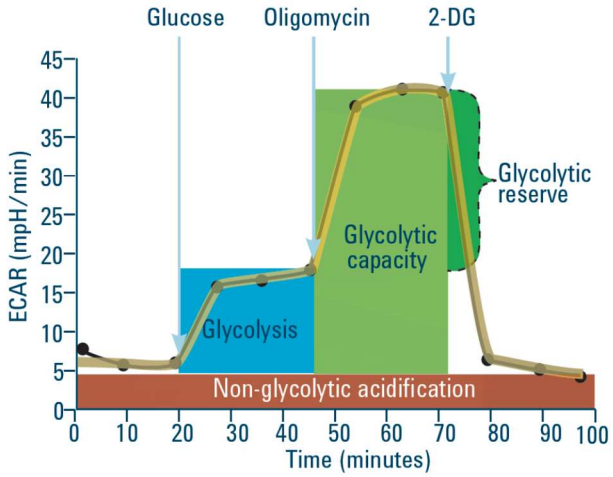

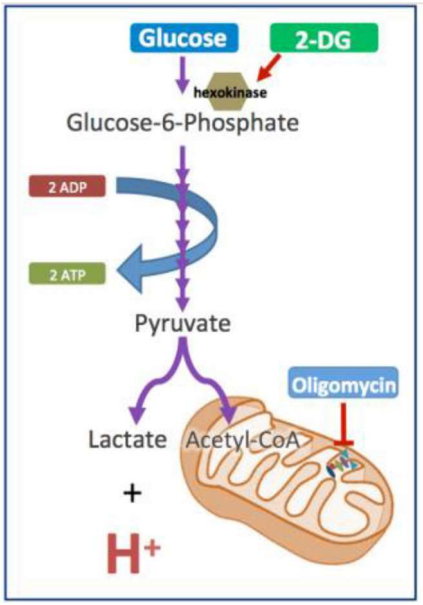

Parameter	Equation Used in Report Generator
Glycolysis	(Maximum rate measurement before Oligomycin injection) – (Last rate measurement before Glucose injection)
Glycolytic Capacity	(Maximum rate measurement after Oligomycin injection) – (Last rate measurement before Glucose injection)
Glycolytic Reserve	(Glycolytic Capacity) – (Glycolysis)
Glycolytic Reserve as a %	(Glycolytic Capacity Rate) /(Glycolysis) × 100
Non-glycolytic Acidification	Last rate measurement prior to glucose injection
Acute Response	(Last measurement rate before glucose injection – Last rate measurement before acute injection)

Figure 9. 18. Seahorse XFp Glycolysis Stress Test Modulators of Glycolysis. The diagram illustrates a simplified version of glycolysis and the sites of action of the kit components. Glucose fuels glycolysis. Oligomycin inhibits ATP synthase in the mitochondria resulting in an increased dependence on glycolysis. 2-DG is a competitive inhibitor of glucose, and functions to shut down glycolysis.